

**CARDIFF UNIVERSITY  
SCHOOL OF CHEMISTRY**



---

**Modular Metallodrug Antimicrobials**

---

**A thesis submitted for the degree of  
Doctor of Philosophy by:**

**Siôn Alun Edwards**

**December 2020**

CARDIFF UNIVERSITY  
SCHOOL OF CHEMISTRY

**Abstract**

Doctor of Philosophy

**Modular Metallodrug Antimicrobials**

By Siôn Alun Edwards

Metallodrugs, drugs that contain metals as an active ingredient, are a potent but underutilised class of drugs in modern medicine. Metals have been used in medicine since antiquity; however, the discovery of cisplatin in 1965 as a chemotherapeutic agent with anticancer properties and its subsequent introduction into the market lead to an increased interest in producing metallodrugs using modern chemical knowledge. Ligands are often a convenient starting point at which to modify the physicochemical properties of metallodrugs, and so a highly tuneable ligand architecture is beneficial when designing a metallodrug. Two such examples of highly tuneable ligands that are investigated in this thesis are N-heterocyclic carbenes (NHCs) and thiosemicarbazones (TSCs).

Chapter 1 introduces metallodrugs, including pertinent background information on the behaviour of surfactants, the use of NHC and TSC ligands in designing effective metal complexes with antimicrobial and/or anticancer activity, and briefly discusses silicone rubber medical devices. Chapter 2 focuses on the synthesis, characterisation, surface activity, and antibacterial activity against a panel of Gram positive and Gram negative bacteria of novel Ag-NHC complexes substituted with long alkyl chains and their precursor imidazolium bromide salts. A brief discussion of the thermodynamics of micellisation of some of the imidazolium salts is also presented. Chapter 3 describes the synthesis and characterisation of novel metal bithiosemicarbazone complexes (M-BTSCs) with long pendant alkyl chains and their anthelmintic activity against the larval and adult forms of the parasitic worm *Schistosoma mansoni*. The BTSC ligands are employed as tetradentate donors to coordinate Cu, Zn, Ni, Mn, and Co. Chapter 4 discusses the preparation of a novel silicone rubber formulation, and attempts to provide the silicone rubber with antimicrobial properties by doping with triclosan derivatives as well as Ag-NHCs and CuBTSCs previously described in Chapter 2 and Chapter 3 respectively. The physical properties and surface morphology of the produced silicones is also investigated, and compared to commercially relevant silicone rubber formulations.

## **Acknowledgements**

My first thanks have to go to my supervisors, Dr Ian Fallis and Prof David Williams. Ian, thank you for alerting me to the fact that this PhD was available and allowing me to undertake such a fascinating project. Your enthusiasm for the subject, and your knowledge, ideas, guidance, and patience have played a monumental part in allowing me to complete the work laid out in this thesis. Thank you for this opportunity. Thank you David for your support and guidance particularly in the early days of my doctoral studies, and for patiently introducing me to practical microbiology, of which I had no previous knowledge.

I would also like to thank the South West Bioscience Doctoral Training Partnership (SWBioDTP) and the BBSRC for funding this work. I would particularly like to thank Dr Sam Southern for the never-ending work she puts in to make the SWBio DTP the success that it is.

I am also very grateful to Prof Mark Waters and his team at Technovent Ltd in Bridgend. Thank you for letting me visit your lab and conduct my PIPS placement. I found the experience incredibly rewarding, and the warm and friendly welcome and work environment was far beyond anything I could have hoped for.

I also would like to thank Prof Karl Hoffmann and Dr Josephine Forde-Thomas of Aberystwyth University for conducting the antiparasitic screening found within this thesis, especially Jo for her hard work and lively correspondence. My thanks also go to my friend Jake Spencer of the EPR group at Cardiff University for lending me his potentiostat, which was an invaluable source of data for this thesis.

A huge part of what has made my experience conducting research in the School of Chemistry so memorable was my colleagues. I would like to thank the IAF group past and present whom I worked alongside: Andy, Seni, Mauro, Stokes, Adam, Gez, Nuha, Ibrahim, Reem, Bria, and Ash. I would like to offer particular thanks to Andy for his support, guidance, and pep talks, and to Bria who was there alongside me every step of the way. Thanks for making me laugh and putting up with me. I would also like to thank Gupps and Cécile, the undergraduate students whose hard work contributed to this thesis.

My thanks also go to all the members of the inorganic department past and present, particularly my jam buddy Sam, along with Andy, Mauro, and Gupps (again) for being such valuable drinking buddies. I would also like to thank Darren for his friendship and all the lunches we shared.

It would be remiss of me not to mention Ed, Alex, Jordan, and Al Mullins. I cannot picture my SWBio experience or what my PhD would have been like without your friendship, but it would have almost certainly been less rewarding. Thank you.

I would like to take this opportunity to also thank the School of Chemistry technical and support staff without whom the department would come grinding to a halt.

It would have been impossible to complete my studies without the support of my family and friends. I would like to thank my mum and dad, who have always believed in me and supported me. Thank you mum for your love, kindness, and understanding, and for all the homemade treats that kept me going. You were always had time to listen to me, and always made me believe I could achieve anything. Diolch yn fawr iawn Dad am fy nghefnogi i, ag am fod mor hael ym mhopeth rwyd ti'n wneud. Heb dy gefnogaeth di, ni fuaswn i byth wedi medru cyflawni cymaint. I would also like to thank my Nain for her constant love and support, and for always having a cup of tea and a biscuit ready when I visit. I'll have to come visit and have some chips again soon.

To my brother Brython, and my friends Geraint and Callum, thank you. Your friendship has been invaluable over the years, and I can always count on your support and wise counsel. To have such strong and long-lasting friendships as I have with you is a privilege.

I also owe an immense debt of gratitude to my wonderful girlfriend Shirley. You've been there by my side every step of the way, and put up with my stress with love and understanding. I could not have done this without your unending support.

Thank you everyone who made my PhD such a memorable experience.

## Contents

Chapter 1: Introduction .....	1
Surfactants.....	1
The CMC.....	2
Metallo drugs .....	5
Carbenes .....	6
Carbenes as ligands for transition metal complexes.....	8
Synthesis of metal NHC complexes .....	12
M-NHC complexes as metallo drugs .....	14
Thiosemicarbazones .....	23
Biological activity of metal-TSC complexes .....	25
Biomaterials .....	27
Silicone rubber medical devices .....	28
Summary.....	32
References.....	33
Chapter 2: Surface and antimicrobial activity of Ag-NHCs and imidazolium salts.....	42
Ionic liquids.....	42
Imidazolium salts .....	42
Antimicrobial effects of long chain imidazolium salts.....	43
Silver NHCs.....	44
Antimicrobial activity of Ag-NHCs .....	46
Aims .....	49
Experimental .....	50
Synthesis of benzimidazole .....	50
Enriched benzimidazole.....	51
Synthesis of 1-methylbenzimidazole.....	51
Enriched 1-methylbenzimidazole .....	52
Synthesis of 1-isopropylbenzimidazole .....	52
Synthesis of 1-isopropylimidazole.....	53
General synthesis of 3-alkyl-1-methylbenzimidazolium bromide salts.....	53
Synthesis of 3-alkyl-1-isopropylbenzimidazolium bromide salts .....	55
Synthesis of 1-methyl-3-octylimidazolium bromide.....	56
Synthesis of 3-alkyl-1-methylimidazolium bromide salts.....	57
Synthesis of 3-alkyl-1-isopropylimidazolium bromide .....	58
Preparation of silver oxide .....	59
Synthesis of Ag-NHCs .....	59
Determination of the critical micelle concentration by conductivity .....	65

Determination of Krafft temperature.....	65
MIC testing .....	65
Results and discussion.....	67
Synthesis of compounds.....	67
NHC precursor synthesis.....	68
Silver NHC complex synthesis.....	69
NMR spectroscopy .....	69
Mass spectrometry .....	72
Determination of CMC by conductivity .....	73
Determination of Krafft temperature.....	78
Thermodynamics of micellisation .....	79
The antimicrobial efficacy of Ag-NHCs and their parent salts.....	82
Antimicrobial efficacy of imidazolium and benzimidazolium bromide salts against Gram positive bacteria.....	83
Antimicrobial efficacy of imidazolium and benzimidazolium bromide salts against Gram negative bacteria .....	86
Antimicrobial efficacy of Ag-NHCs against Gram positive bacteria.....	87
Antimicrobial efficacy of Ag-NHCs against Gram negative bacteria .....	89
Conclusion .....	91
References.....	93
Chapter 3: Bisthiosemicarbazone complexes and their anthelmintic properties .....	98
CuATSM.....	98
MBTSC complexes .....	100
Schistosomiasis.....	104
Aims .....	109
Experimental .....	110
Synthesis of alkylisothiocyanates.....	110
Synthesis of 4-alkyl-3-thiosemicarbazide .....	111
Synthesis of H <sub>2</sub> GTSA ligands .....	112
Synthesis of H <sub>2</sub> GTSM.....	114
Synthesis of CuATSM and CuGTSM .....	115
Synthesis of ZnGTSA complexes .....	116
Synthesis of ZnATSM and ZnGTSM.....	117
Synthesis of NiGTSA complexes .....	118
Synthesis of MnGTSA complexes.....	119
Synthesis of CoGTSA complexes .....	120
Cyclic voltammetry.....	121
Determination of anthelmintic activity.....	122

Single-point adult worm screen.....	122
Results and discussion.....	123
Synthesis of ligands.....	123
Synthesis of complexes .....	124
NMR spectroscopy .....	125
Infrared spectroscopy .....	126
Electronic spectroscopy.....	128
Cyclic voltammetry.....	131
Anthelmintic properties of MGTSA complexes and their precursors.....	135
Schistosomula assay .....	135
Single-point adult worm screen.....	138
Conclusion .....	143
References.....	144
Chapter 4: Development of antimicrobial doped silicone rubbers.....	151
Antimicrobial silicone rubbers .....	151
Triclosan silicones .....	157
Aims .....	162
Experimental .....	163
Synthesis of triclosan acetate .....	164
Synthesis of triclosan benzoate .....	164
Synthesis of triclosan laurate .....	165
Synthesis of triclosan undecenoate .....	166
Synthesis of 3-decyl-1-vinylimidazolium bromide.....	166
Synthesis of 1-methyl-3-(undec-10-en-1-yl)imidazolium bromide.....	167
Preparation of polymer bases .....	167
V46 polymer base.....	167
V31 polymer base.....	168
V21 polymer base.....	168
Polymer Base X.....	168
Preparation of silicone rubber “TM1” .....	168
TM1 Part A .....	169
TM1 Part B .....	169
Determination of TM1 work time and room temperature cure time.....	169
Determination of TM1 heat cure time.....	170
Preparation of TM1 slab.....	170
Doping of silicones.....	170
The effect of 5 wt% doping on TM1 work time and room temperature cure time	170

The effect of 5 wt% doping on TM1 heat cure time .....	170
Preparation of 5 wt% doped TM1 slab .....	170
Determination of silicone hardness .....	171
Mechanical test – tensile strength.....	171
Mechanical test – tear resistance.....	171
Investigation into inhibition of silicone rubber curing .....	171
Transmetallation reaction to probe catalyst poisoning.....	172
Zone of inhibition assay (Kirby-Bauer method) .....	172
Results and discussion.....	174
Synthesis of compounds.....	174
NMR spectroscopy .....	176
Mass spectrometry .....	177
Silicone rubber development .....	177
Preparation of PDMS base mixes .....	178
Work time of TM1 .....	179
Cure time of TM1 .....	180
Preparation of TM1 slab.....	181
Physical properties of TM1 .....	182
Doping of silicones.....	183
Effect of 5 wt% doping on work time of TM1 .....	184
Effect of 5 wt% doping on cure time.....	185
Production of 5 wt% TM1 slabs.....	186
Physical properties of 5 wt% doped TM1 .....	188
Doped silicone hardness.....	188
Tensile strength of doped silicones .....	189
Tear resistance of doped silicones.....	191
Investigation into inhibition of curing by Ag-NHCs.....	192
Transmetallation reaction to probe catalyst poisoning.....	199
Surface morphology of silicone rubbers .....	200
Antimicrobial efficacy of doped silicones.....	204
Conclusion .....	210
References.....	212
Chapter 5: Concluding remarks .....	217
Surface and antimicrobial activity of Ag-NHCs and imidazolium salts.....	217
Bisthiosemicarbazone complexes and their anthelmintic properties .....	218
Development of antimicrobial doped silicone rubbers.....	218
References.....	220

Appendices.....	222
Molar concentrations of antimicrobial agents (Chapter 2).....	222
MIC testing of Ag-NHCs and (benz)imidazolium salts against bacteria (Chapter 2) .....	223
Square root of scan rates versus cathodic peak current (Chapter 3) .....	225
SEM/EDX of TM1 silicone rubbers (Chapter 4) .....	226

## **Abbreviations**

### **Spectroscopy and techniques**

CFU	Colony Forming Units
CMC	Critical Micelle Concentration
DFT	Density Functional Theory
EDX	Energy Dispersive X-ray spectroscopy
EI	Electron Ionisation
ESI	Electrospray Ionisation
FT-NMR	Fourier Transform Nuclear Magnetic Resonance spectroscopy
FTIR	Fourier Transform Infrared
GI <sub>50</sub>	Half-maximal growth inhibition concentration
HOMO	Highest Occupied Molecular Orbital
HRMS	High Resolution Mass Spectrometry
IC <sub>50</sub>	Half-maximal inhibitory concentration
IR	Infrared spectroscopy
LD <sub>50</sub>	Lethal dose
MIC	Minimum Inhibitory Concentration
MBC	Minimum Biocidal Concentration
MRI	Magnetic Resonance Imaging
MS	Mass Spectrometry
MTT assay	Cell viability test performed with the tetrazolium MTT
NMR	Nuclear Magnetic Resonance
PET	Positron Emission Tomography
SEM	Scanning Electron Microscopy
SOMO	Singly Occupied Molecular Orbital
SPECT	Single Photon Emission Computed Tomography

UV-vis Ultraviolet-visible spectroscopy

### **Miscellaneous**

ATCC The American Type Culture Collection

NCIMB The National Collection of Industrial, Food and Marine Bacteria

NCTC The National Collection of Type Cultures

RT Room temperature

WHO The World Health Organisation

### **Units**

A Amps

$\epsilon$  Extinction coefficient,  $\text{Lmol}^{-1}\text{cm}^{-1}$

eV Electron volts

K Kelvin

$\text{kNm}^{-1}$  Kilonewtons per metre,  $1 \times 10^3 \text{ Nm}^{-1}$

m/z Mass-to-charge ratio

mM Millimolar,  $1 \times 10^{-3}$  moles  $\text{L}^{-1}$

mmol Millimoles,  $1 \times 10^{-3}$  moles

MPa Megapascals,  $1 \times 10^6$  pascals

nm Nanometres,  $1 \times 10^{-9}$  metres

ppm Parts per million

$\mu\text{g}$  Micrograms,  $1 \times 10^{-6}$  grams

$\mu\text{L}$  Microliter,  $1 \times 10^{-6}$  litres

$\mu\text{M}$  Micromolar,  $1 \times 10^{-6}$  moles  $\text{L}^{-1}$

$\mu\text{S}$  Microsiemens,  $1 \times 10^{-6}$  siemens

wt% Weight percent

### **Solvents, chemicals, and compounds**

$\text{Boc}_2\text{O}$  Di-tert-butyl dicarbonate

CDCl <sub>3</sub>	Deuterated chloroform
COD	1,5-cyclooctadiene
CS <sub>2</sub>	Carbon disulphide
d <sub>6</sub> -DMSO	Deuterated dimethylsulfoxide
DCM	Dichloromethane
DMAP	4-dimethylaminopyridine
DMEM	Dulbecco's Modified Eagle Media
DMF	Dimethylformamide
DMSO	Dimethylsulfoxide
DNA	Deoxyribonucleic acid
Et <sub>2</sub> O	Diethyl ether
EtOH	Ethanol
H <sub>2</sub> O	Water
H <sub>2</sub> SO <sub>4</sub>	Sulphuric acid
HBF <sub>4</sub>	Tetrafluoroboric acid
HCl	Hydrochloric acid
KH	Potassium hydride
KOH	Potassium hydroxide
KOtBu	Potassium tert-butoxide
MeCN	Acetonitrile
n-BuLi	n-Butyl lithium
NaH	Sodium hydride
NaOH	Sodium hydroxide
NaOAc	Sodium acetate
NEt <sub>3</sub>	Triethylamine
NHC	Nucleophilic Heterocyclic Carbene

OAc <sup>-</sup>	Acetate anion
OTf <sup>-</sup>	Trifluoroacetate (or triflate) anion
PPh <sub>3</sub>	Triphenylphosphine
t-BuOH	tert-Butanol

## Chapter 1: Introduction

### Surfactants

The term surfactant is derived from the words “surface active agents”. Surfactants typically consist of 2 parts: the hydrophilic head group, and the hydrophobic ‘tail’ group. There are four classes into which surfactants are typically divided into: anionic, cationic, non-ionic, and zwitterionic. These classes are typically sorted based on the nature of the head group. These classes are summarised in Figure 1.

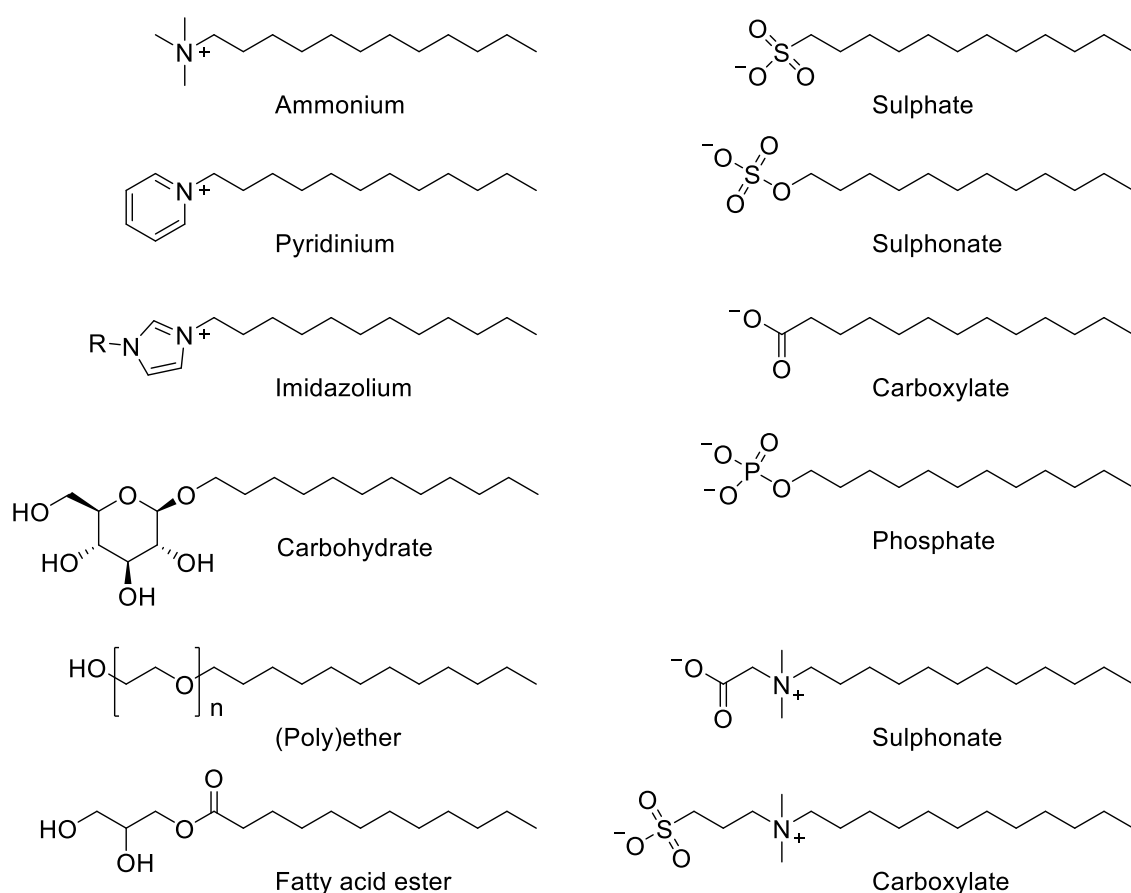


**Figure 1.** Structures of simple surfactants of the classes discussed below. The surfactants are separated into groups based on the charge associated with the head group: cationic, anionic, nonionic, and zwitterionic (surfactants with head groups containing cations and anions).

Cationic surfactants are typically based on amines: including tertiary alkylammonium cations,<sup>1</sup> pyridinium cations,<sup>2</sup> and imidazolium cations.<sup>3</sup> Examples of anionic surfactants are sulphates,<sup>4</sup> sulphonates,<sup>5</sup> carboxylates,<sup>6</sup> and phosphates.<sup>7</sup> Nonionic surfactants are afforded water solubility by hydrogen bonding from the water to covalently-bound oxygen atoms in the surfactant, and are typically based on carbohydrates,<sup>8</sup> (poly)ethers,<sup>9</sup> or fatty

acid esters.<sup>10</sup> Zwitterionic surfactants have an anionic and cationic component, and typically consist of amines and an anionic group such as a sulphonate or a carboxylate.<sup>11</sup> The hydrophobic component of the surfactant is often less varied, and typically consists of long alkyl chains, typically from  $-C_8H_{17}$  upwards.<sup>12-14</sup> Other examples include hydrophobic species such as perfluoroalkyl chains<sup>15</sup> or polysiloxane groups.<sup>16</sup> Surfactants may also contain bound metals as an integral part of their head groups. This subclass of surfactants are referred to as metallosurfactants.<sup>17-19</sup> Metallosurfactants allow for the introduction of the potential for chemical reactivity to a surfactant molecule, as traditional apo-surfactants are typically chemically “innocent”.<sup>20</sup>

An increase in the length of the hydrophobic component causes the solubility of the surfactant to decrease, and drives aggregation of the surfactant molecules at the surface. The longer the hydrophobic section of the surfactant the tighter they pack at the surface.<sup>15,21</sup> The thermodynamic reason for this aggregation at the surface is the preference of the head group to interact with water, and the preference of the hydrophobic section to avoid water, thus sticking out towards the air/water interface. The concentration of surfactants at a surface is termed absorption. The molecules at the surface of the interface are in constant exchange with those in the bulk. Brownian motion and the thermal energy of the solvent medium ensures that an equilibrium between the surface and the bulk occurs.<sup>22</sup> That the dissolution of surfactants causes a change in the surface tension of a solution is well known.<sup>23-25</sup> The dissolution of ionic surfactants in solution also affects the conductivity of the solution as it behaves as an electrolyte, meaning that measurement of ionic surfactant concentration is possible using conductivity.<sup>26-28</sup>

### **The CMC**

At a concentration individual to each surfactant, there is a thermodynamic drive for surfactants to aggregate together in the bulk solution instead of behaving as unimers. The aggregation of surfactants that forms is known as a micelle, and the concentration at which these aggregations form for each surfactant is known as the critical micelle concentration (CMC). The concentration is when there is no more room at the surface for additional surfactant molecules, and therefore surfactant molecules spontaneously self-assemble into micelles in order to satisfy the requirement of the hydrophilic head to interact with water, and the requirement of the hydrophobic chain to avoid contact with water molecules where possible. In water, a micelle consists of a hydrophilic surface, and a hydrophobic interior, whereupon the hydrophobic tail groups associate with each

other and are protected from interactions with water molecules by the outer layer of polar head groups.<sup>29</sup>

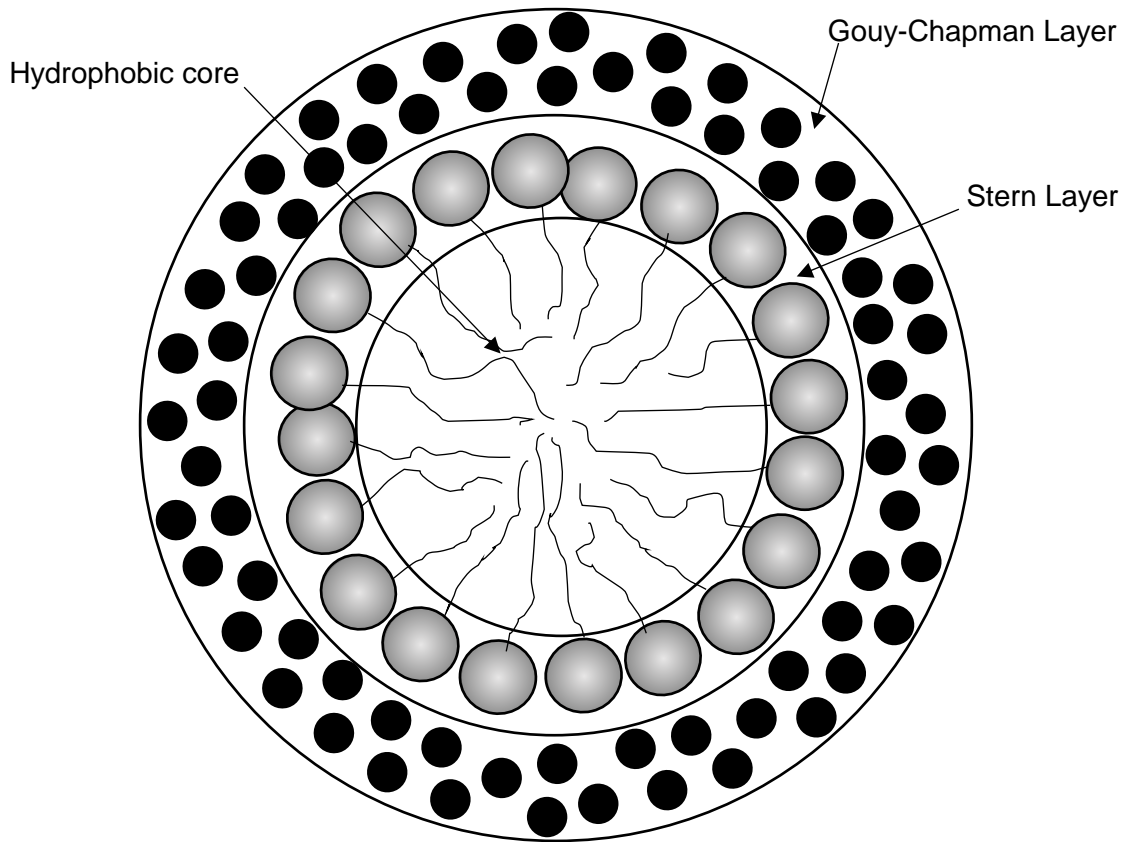


**Figure 2.** 2D illustration of the arrangement of individual surfactants molecules into a micelle in an aqueous environment.<sup>30,31</sup>

The free energy of micellisation ( $\Delta G_m^o$ ) can be simply related to the CMC via the following relation:

$$\Delta G_m^o = - RT \ln CMC \quad \text{Equation 1.}$$

There are three contributions to  $\Delta G_m^o$  from constituent parts of the surfactants which may be summarised in the following manner:

$$\Delta G_m^o = \Delta G_{HC} + \Delta G_{contact} + \Delta G_{packing} + \Delta G_{HG} \quad \text{Equation 2.}$$

Where  $\Delta G_{HC}$  is the free energy from the transport of the hydrophobic chain of the surfactant from bulk water to the micelle interior,  $\Delta G_{contact}$  is a surface free energy associated with solvent-hydrophobe interactions within the micelle's core,  $\Delta G_{packing}$  is

a free energy with a positive value associated with the restricted movement of the surfactant chain within the micelle, and  $\Delta G_{HG}$  is a positive contribution associated with electrostatic and conformation effects of the head group. Values of  $\Delta G_m^o$  may be rationalised through application of the Gibbs-Helmholtz equation:

$$\Delta G_m^o = \Delta H_m^o - T\Delta S_m^o \quad \text{Equation 3.}$$

Where  $\Delta G_m^o$  is the Gibbs free energy of micellisation,  $\Delta H_m^o$  is the enthalpy of micellisation, and  $\Delta S_m^o$  is the entropy of micellisation. There are three thermodynamic factors that may be rationalised in terms of entropy and enthalpy that contribute to the spontaneous self assembly of micelles. The first is the entropically favourable interaction between the hydrophobic chains vs their interaction with the surrounding water. The second is an antagonistic interaction due to electrostatic repulsion between the charged head groups at the surface, with the micelle offering a more thermodynamically favourable orientation. The last contribution is the entropically favourable expulsion of water and polar head groups from the core of the micelle.<sup>32</sup>

Micelles come in a variety of shapes and sizes, the simplest of which is the sphere. The minimum size of the sphere is determined by the all-trans length of the hydrophobic group.<sup>33</sup> More complex shapes exist, such as ellipsoids and rods, and the minimum sizes of these are similarly limited by the length of the hydrophobic group, the need for the hydrophobic group to remain in the interior of the micelle architecture, and the hydrophilic group to remain on the exterior. The shape that a micelle assumes is principally influenced by the packing of the polar head group.<sup>34</sup> Micellisation depends on a number of factors including pH, temperature, pressure and ionic strength of the surrounding environment.<sup>35</sup> Beyond the CMC, more micelles of the same size begin to form as opposed to the formation of larger micelles. This postulation holds true until a much higher concentration of surfactant, whereupon the micelles start to grow in size more rapidly.<sup>36</sup> Micelles are therefore typically fairly monodisperse in their sizes at low concentrations, although at extremes of concentration spherical micelles may begin to aggregate and form other micelle morphologies, or even form liquid crystals at even higher concentrations.<sup>37,38</sup> The above descriptions are described in relation to aqueous solution, however the formation of micelles is not just a phenomenon that occurs in water. The formation of micelles also occurs in organic solution, where the hydrophobic component of the micelle protrudes into the organic layer, and the interior of the micelle is composed of the hydrophilic head group. Micelles such as these are termed “reverse micelles”.<sup>39</sup> CMC values for some common surfactants are reported below in Table 1.

Compound	Abbreviation	Class	Head group	CMC (mM)
Sodium dodecylsulphate	SDS	Anionic	Sulphate	8.20
Dodecyltrimethylammonium bromide	DTAB	Cationic	Ammonium	14.6-16.0
Tetradecyltrimethylammonium bromide	TTAB	Cationic	Ammonium	3.60-3.72
Cetyltrimethylammonium bromide	CTAB	Cationic	Ammonium	0.92-1.00
Triton X-100	TX-100	Nonionic	(Poly)ether	0.24-0.27
Octaethylene glycol monododecyl ether	C <sub>12</sub> E <sub>8</sub>	Nonionic	(Poly)ether	0.11
Tetraethylene glycol monododecyl ether	C <sub>12</sub> E <sub>4</sub>	Nonionic	(Poly)ether	0.064

**Table 1.** CMC values of common surfactants adapted from the summary in work by Carnero Ruiz et al.<sup>40</sup>

### Metallo drugs

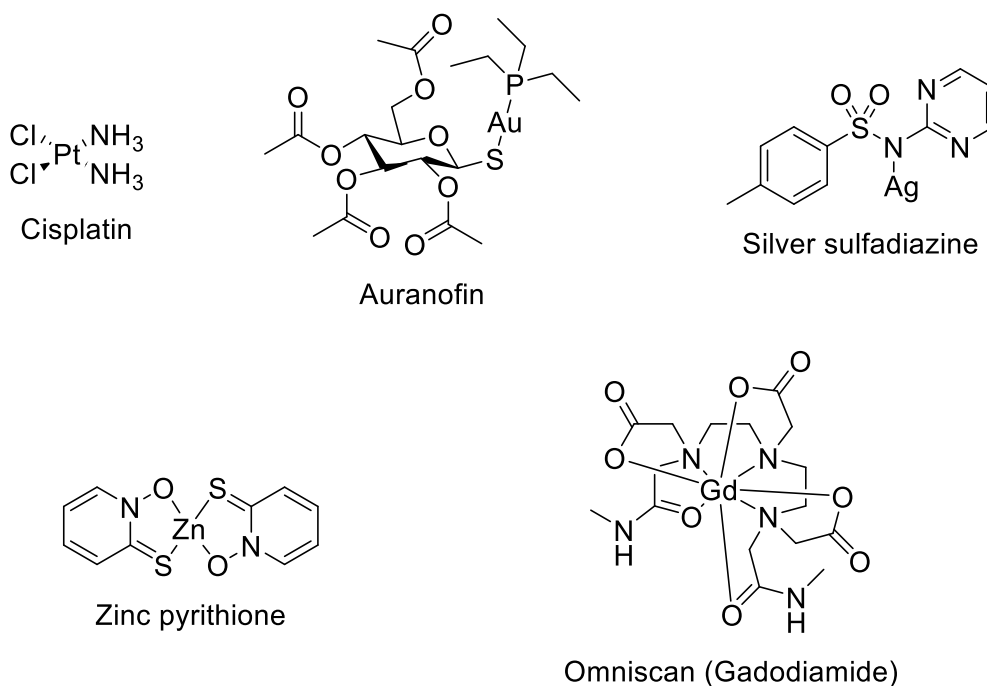


**Figure 3.** Examples of metallo drugs used in a clinical setting.<sup>41-51</sup>

Some surfactants have the potential to be used as ligands or ligand precursors for metals due to the presence of suitable donors within the surfactant structure. Many metals play important roles in biological processes, with many processes relying on said metals in

order for the correct chemistry to proceed.<sup>52,53</sup> Metallodrugs are drugs that contain metals as an active ingredient, be they used for therapeutic or diagnostic purposes.<sup>54</sup> Metallodrugs are an underrepresented component of modern medicine, making up a small number of the total drugs used in clinical settings.<sup>55</sup> However, a number of key medicines come from this class of compounds, such as: cisplatin and carboplatin,<sup>41-44</sup> which are commonly prescribed chemotherapy agents, auranofin,<sup>45</sup> an anti-inflammatory medicine used in the treatment of arthritis, silver sulfadiazine,<sup>46,47</sup> an antimicrobial agent typically used as a topical treatment for burns, and zinc pyrithione,<sup>48,49</sup> an antimicrobial and antifungal treatment. Examples of diagnostic metallodrugs include imaging agents such as the Gd(III)-based MRI contrast agent Omniscan,<sup>50,51</sup> or the variety of radioactive metal isotopes used in SPECT and PET scans.<sup>56</sup>

A key feature of any metallodrug is the ligand architecture used to stabilise the metal complex. There are a number of criteria a prospective metallodrug should meet:<sup>57-59</sup> suitable solubility within the desired medium, rate of release (related to ligand metal bond strength, taking into account phenomena such as the chelate effect and the macrocyclic effect), specificity (including appropriate membrane solubility), as well as any potentially deleterious side products that may form *in vivo*. It is therefore vitally important to have the option to tune these properties to ensure suitability of the agent. The easiest way to do this is by design of an appropriate ligand, modifying the pertinent physicochemical properties of the ligand by the selection of appropriate functional groups. A highly tuneable ligand scaffold that allows for wholesale modification of various positions of the ligand is therefore desirable. One such appropriate ligand type is the carbene.

### **Carbenes**

Carbenes are a particularly interesting class of organic compounds. A carbene is a neutral  $R_2C:$  compound, derived from methylene.<sup>60</sup> Carbenes consist of a divalent carbon with only 6 electrons, 4 of which are involved in bonding, leaving 2 non-bonding electrons available. The geometry of the RCR groups may be linear or bent, depending on the hybridisation of the central carbon.<sup>61</sup> An  $sp$ -hybridised carbon leaves 2 degenerate non-bonding  $p$ -orbitals, and therefore causes the carbene to adopt a linear geometry. By contrast, if the central carbon is  $sp^2$ -hybridised then the carbene undertakes a bent geometry. This is due to the hybridised  $s$  and  $p$  orbitals combining to form a bonding  $\sigma$  orbital, with the other  $p$  orbital remaining unchanged in energy defined as  $p_\pi$ . As the constituent  $p$  orbitals of the  $\sigma$  orbital gain some  $s$  character they decrease in energy, stabilising the  $\sigma$  orbital by comparison with the non-hybridised free carbon  $p$  orbitals.<sup>62,63</sup>

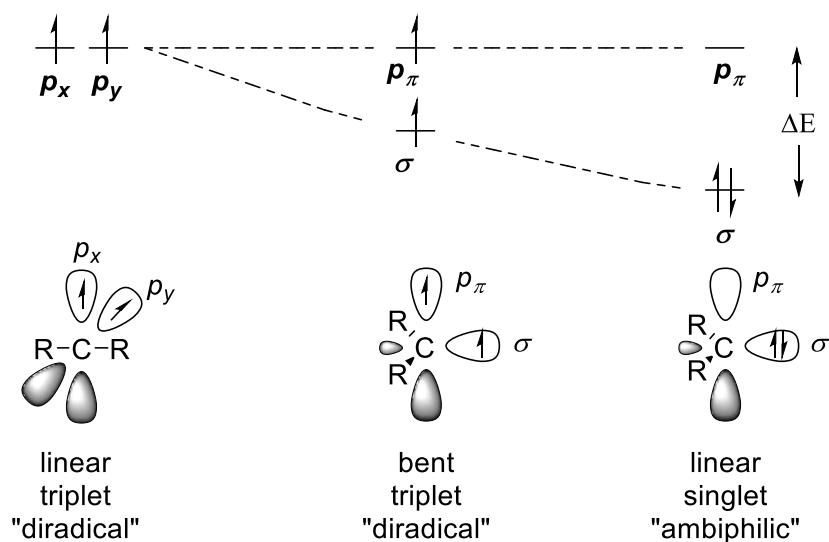


**Figure 4.** The ground state frontier orbitals of various carbene geometries, highlighting the difference in singlet-triplet separation with bond angle.

Bent carbenes are more common by far than linear carbenes. The distribution of the non-bonding electrons in linear carbenes is simple. If the  $sp$ -hybrid orbital is considered to be formed of the carbon  $s$  and  $p_z$  orbitals, then that leaves the remaining orbitals to be defined as  $p_x$  and  $p_y$ . The distribution of electrons between these  $p$  orbitals takes on a configuration of  $p_x^1 p_y^1$ , meaning one electron per  $p$  orbital, with the spins aligned parallel. The linear carbene therefore adopts a triplet ground state. The case of the bent carbene is far more complicated. A bent carbene may take a singlet ground state with the electrons paired in the  $\sigma$  orbital ( $\sigma^2 p_\pi^0$ ), or a triplet ground state, where one electron occupies the  $\sigma$  orbital, and one occupies the  $p_\pi$  orbital, with spins parallel to each other ( $\sigma^1 p_\pi^1$ ). Two other possible singlet states exist: where both electrons pair and occupy the  $p_\pi$  orbital ( $\sigma^0 p_\pi^2$ ), or where both electrons occupy different orbitals but have their spins antiparallel ( $\sigma^1 p_\pi^1$ ).<sup>62</sup> Both are energetically unfavourable however, meaning they are unlikely to occur, and therefore bear little relevance to the future discussion of the chemistry of carbenes that follows. This is due to the fact that the properties and reactivity of carbenes are typically determined by their ground state multiplicity.<sup>64</sup> Triplet carbenes are able to react as electrophiles, or in some cases as diradicals, whereas singlet carbenes are ambiphilic in nature due to their full  $\sigma$  orbitals allowing for them to react as nucleophiles, and their empty  $p_\pi$  orbitals allow for them to react as electrophiles.

The ground state a bent carbene adopts depends on the difference in energy between the  $\sigma$  and the  $p_\pi$  orbital. As a rule of thumb, a  $\Delta E$  value of greater than 2 eV causes the carbene to adopt a singlet ground state, as the spin pairing energy allowing for two electrons to occupy the  $\sigma$  orbital is more favourable than promoting an electron to the  $p_\pi$

orbital. By contrast, if  $\Delta E < 1.5$  eV, then the carbene adopts a triplet ground state, as the spin pairing energy is greater than the energy required to promote an electron to the  $p_{\pi}$  orbital.<sup>65</sup> The magnitude of  $\Delta E$  is determined by the nature of the R groups  $\alpha$  to the carbenic carbon.<sup>61</sup> The R groups influence the value of  $\Delta E$  by inductive and mesomeric means. Inductive electron withdrawing groups (-I) such as O, N, P etc. stabilise  $\sigma$  enriching its s character, leading to an increase in  $\Delta E$ , and therefore encouraging the carbene adopt a singlet ground state. By contrast, inductively electron donating groups (+I) increase the energy of  $\sigma$ , therefore decreasing  $\Delta E$ , and encouraging the carbene to adopt a triplet ground state. The mesomeric effects of each R substituent also need to be taken into account when predicting the degree of bending in a singlet carbene. If at least one of the associated R groups is a  $\pi$ -acceptor (-M, such as COR, CN etc.) then a linear or quasi-linear geometry is expected. This is due to  $\pi$ -interactions breaking the degeneracy of the  $p_x$  and  $p_y$  orbitals, and therefore forming a strange linear singlet carbene. If the R groups are  $\pi$ -donors instead (+M, e.g. O, N, P etc.) then the donation of electrons by the R groups into the carbene  $p_{\pi}$  orbital increases its energy, and therefore increases  $\Delta E$ , further stabilising the singlet ground state, and encouraging a bent geometry.

The unique chemistry of carbenes has seen application in a number of fields in chemistry such as in the synthesis of nanoparticles, as nucleophilic catalysts, scaffolds for the design of metal organic frameworks, and as Lewis bases.<sup>61</sup> The remainder of the discussion of carbenes in this thesis will focus on their role as ligands for transition metal complexes.

### Carbenes as ligands for transition metal complexes

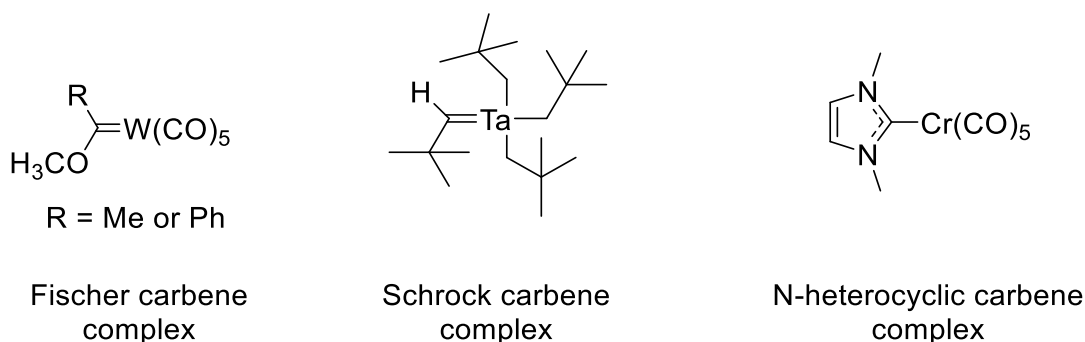


**Figure 5.** Early examples of Fischer carbenes, Schrock carbenes, and N-heterocyclic carbenes from the work of Fischer,<sup>66</sup> Schrock,<sup>67</sup> and Öfele<sup>68</sup> respectively.

The variance in ground states available mean that carbenes are incredibly versatile ligands for transition metals. In fact, much of the periodic table has at least one reported

instance of a carbene complex. Carbenes as ligands are typically classified into categories based on their reactivity towards a metal ion.<sup>61,69</sup> The three categories are typically defined as Fischer carbenes, Schrock carbenes (or Schrock alkylidenes), and N-heterocyclic carbenes (NHCs, sometimes referred to as Arduengo categories). The properties of each of these carbene types will be briefly outlined below.

Fischer carbene transition metal complexes were the first carbene complexes to be isolated. The complex was first described by Ernst Otto Fischer in 1964.<sup>66</sup> Tungsten hexacarbonyl was reacted with either phenyl lithium or methyl lithium. The charged complex was reacted with diazomethane to produce the first instances of transition metal carbene complexes, formally methyl- or phenylmethoxycarbene tungsten(0)pentacarbonyl complexes. Fischer carbenes are suitable ligands for middle to late transition metals in low oxidation states e.g, Fe(0), Mo(0), or Cr(0). Fischer carbene complexes typically have  $\pi$ -acceptor co-ligands attached to the metal centre. The carbene carbon is usually flanked by  $\pi$ -donors such as alkoxy or alkylamine groups. Fischer carbenes have a singlet ground state, and bind to the metal through donation of  $\sigma$  electrons into empty  $d$  orbitals on the metal. As the metals are low oxidation state electron-rich middle to late transition metals, there is significant  $\pi$ -backbonding through donation of metal  $d$  electrons into the empty  $p_{\pi}$  orbital of the carbene. Octahedral Fischer carbene complexes typically obey the 18-electron rule. Fischer carbenes react in a manner similar to carbonyls, as the carbene carbon is electrophilic due to the  $\sigma$ -donation being only partially compensated for by  $\pi$ -backbonding, and are therefore vulnerable to attack from nucleophiles.<sup>61,69</sup>

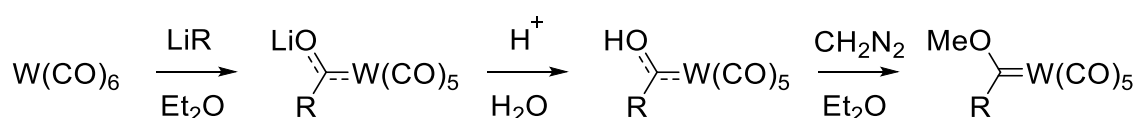


**Figure 6.** Preparation of the first Fischer carbene.<sup>66</sup>

By contrast, Schrock carbenes, a second class of carbene transition metal complexes, are based on a triplet ground state carbene ligand. First described in 1974 by Richard R. Schrock, the original Schrock carbene was prepared by reaction of dichlorotris(neopentyl)tantalum(V) with two equivalents of neopentyl lithium.<sup>67</sup> One of the neopentyl ligands underwent an  $\alpha$ -hydride abstraction leading to the isolation of the Schrock alkylidene complex. Schrock carbenes are suitable ligands for early transition metals in high oxidation states such as Ta(V) or Ti(IV). Unlike Fischer carbene complexes, Schrock carbene complexes do not exclusively have  $\pi$ -acceptor co-ligands. The carbene is not flanked by  $\pi$ -donors, with only hydrogen or alkyl substituents typical

of the groups  $\alpha$ -to the carbene carbon. As the Schrock carbene is in a triplet ground state, the carbene forms two covalent bonds by the pairing of the single electrons in the  $p_x$  and  $p_y$  orbitals with unpaired  $d$  electrons on the transition metal. As carbon is more electronegative than the early transition metals it complexes to, the covalent bonds formed are polarised towards the carbon atom. This leads to an electron rich and therefore nucleophilic carbene. Schrock carbenes are therefore vulnerable to electrophilic attack. Schrock carbenes can be considered to form “true” M-C double bonds according to valence bond theory due to their sharing of two triplet electrons with two unpaired metal electrons, whereas Fischer carbenes typically form M-C bonds with less than “true” double character due to the resonance structures afforded by the  $\pi$ -donating groups  $\alpha$ -to the carbene.

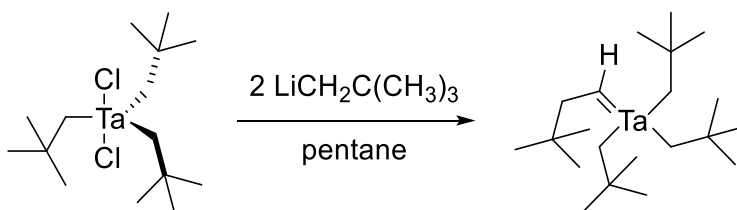


**Figure 7.** Preparation of the first example of a Schrock carbene.<sup>67</sup>

The third type of transition metal complexes discussed in this section are metal NHC complexes. NHCs are neutral cyclic organic compounds, typically with one or more heteroatom  $\alpha$ -to the carbene. NHCs, particularly free NHCs, are a relatively new subject in science. Despite free carbenes having been hypothesised in the 19<sup>th</sup> century in the work of Dumas,<sup>70</sup> Geuther,<sup>71</sup> Buchner and Kurtius,<sup>72</sup> and later work in the 1960s and 1970s by Wanzlick<sup>73</sup> and Lemal,<sup>74</sup> the first example of a free NHC was described in 1991 by Anthony J. Arduengo III,<sup>75</sup> when he and his group isolated a free imidazolin-2-ylidene NHC stabilised by bulky adamantyl R-groups attached to the nitrogen atoms  $\alpha$ -to the carbenic carbon. This discovery led to a substantial increase in the number of papers published on NHCs, which had previously been seen as only laboratory curiosities.

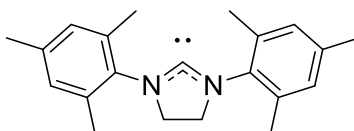


**Figure 8.** The structure of the first isolated free carbene, reported by Arduengo et al. in 1991.<sup>75</sup>

Transition metal NHC complexes however have been known for longer. In 1968, Öfele<sup>68</sup> and Wanzlick and Schöner<sup>76</sup> published separate works detailing the first examples of

transition metal NHC complexes. The complex described by Wanzlick and Schöner was formed upon the reaction of mercury(II) acetate with 1,3-diphenylimidazolium perchlorate forming a bisimidazol-2-ylidene mercury(II) complex with two perchlorate counter ions. The basic acetate counter ions facilitate the deprotonation of the imidazolium salt to allow for the formation of the NHC. At almost the same time, the group of Öfele produced a chromium NHC complex by heating a 1,3-dimethylimidazolium-pentacarbonylhydrido-chromate(0) complex salt, leading to the *in situ* deprotonation of the imidazolium cation and oxidative liberation of dihydrogen to produce the neutral chromium NHC complex: pentacarbonyl(1,3-dimethylimidazolin-2-ylidene)chromium(0).

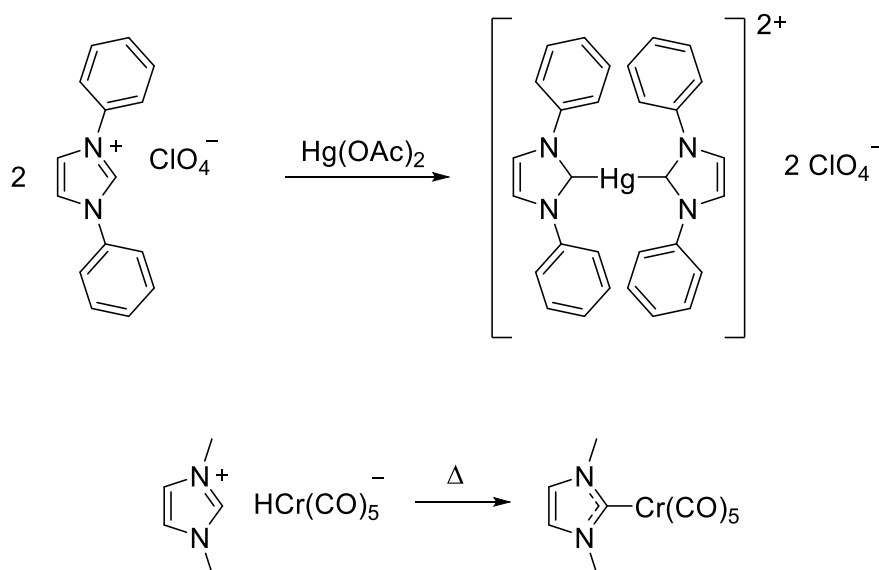


**Figure 9.** First examples of the preparation of metal-NHC complexes by Wanzlick and Schöner (top) and Öfele (bottom).

NHC transition metal complexes may be considered a special subclass of Fischer carbenes as they are singlet ground state carbenes that donate into metal  $d$  orbitals from their  $\sigma$  orbitals. However, there is limited  $\pi$ -backbonding into the NHC  $p_\pi$  orbital, meaning that M-NHC bonds are more similar to Lewis structure single bonds in character.<sup>77</sup> This unique behaviour is facilitated by the increased stability of the NHC singlet ground state due to a phenomenon referred to as the push-pull effect.<sup>78</sup> Most typical NHCs have an electronegative heteroatom either side of the carbene carbon. The  $\sigma$ -withdrawing effect (-I) due to the electronegativity of the heteroatom coupled with the mesomeric effect (+M) caused by the donation of the heteroatom's lone pair into the carbene  $p_\pi$  orbital results in the simultaneous decrease in the energy of the carbene  $\sigma$  orbital and increase in the energy of the carbene  $p_\pi$  orbital. The push-pull effect (-I,+M)

therefore leads to a double increase in  $\Delta E$ , resulting in a remarkably stable singlet ground state.

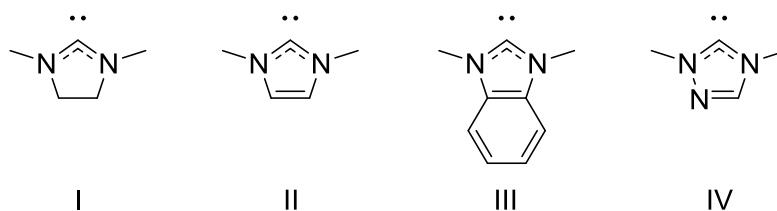


**Figure 10.** Example cyclic diamino carbenes derived from the following heterocycles: imidazoline (I), imidazole (II), benzimidazole (III), 1,2,4-triazine (IV).

The fact that NHCs bind to metals in an almost purely  $\sigma$ -fashion have led to comparisons between NHCs and phosphines as ligands, with NHCs in many cases surpassing phosphines in their  $\sigma$ -donating capabilities. Cyclic diaminocarbenes may be further classified into subclasses of NHC depending on the backbone of the cyclic system, which can further inform about the NHC's  $\sigma$ -donating capabilities. The four categories are: saturated backbone (I) as with NHCs derived from imidazoline, unsaturated backbone (II) as with NHCs derived from imidazole, benzannulated backbone (III) as with NHCs derived from benzimidazole, and a 3<sup>rd</sup> nitrogen on the backbone (IV) as with NHCs derived from 1,2,4-triazole. The  $\sigma$ -donor ability of the four types of ligands is in the order I > II > III > IV, with increasing backbone saturation increasing the strength of M-NHC bonds.<sup>79-81</sup> This can be rationalised due to a relatively large +I effect of the  $sp^3$  hybridised carbons in the saturated ligand, which is decreased by the change to  $sp^2$  carbons in unsaturated NHCs. The +I effect is weakened further by benzannulation. Finally, addition of an extra N atom (in 1,2,4-triazole derived NHCs) introduces a -I effect due to the electronegativity of the additional nitrogen, resulting in the weakest donors of the series. As NHCs gained recognition as versatile ligands, a variety of synthetic methods were developed in order to prepare transition metal NHC complexes.

### Synthesis of metal NHC complexes

Metal-NHC complexes have been synthesised in a variety of different manners, though typically there are 3 common routes which are employed to prepare the complexes. The 3 methods are: *in-situ* deprotonation of a precursor ligand in the presence of a metal source, preparation of a free NHC followed by reaction with a metal source, and transmetallation where a metal is displaced from a previously synthesised M-NHC complex with a new metal source. The groups of Öfele<sup>68</sup> and Wanzlick<sup>76</sup> reported the first examples of M-NHC complexes in separate works published in 1968. These

complexes were prepared via the *in situ* deprotonation method. The work of Öfele described a deprotonation via a decomposition due to heating, whereas the work of Wanzlick described the deprotonation of an imidazolium salt facilitated by the basic acetate counter ions of the mercury acetate salt employed as a metal source. This type of deprotonation via the bound counter ion is one mode by which to achieve *in situ* deprotonation. Examples of metal salts used in the literature include  $\text{Hg}(\text{OAc})_2$ ,<sup>76</sup>  $\text{Ag}_2\text{O}$ ,<sup>82–85</sup>  $\text{AgOAc}$ ,<sup>86–89</sup>  $\text{Ag}_2\text{CO}_3$ ,<sup>90–92</sup> and  $\text{Pd}(\text{OAc})_2$ .<sup>93–95</sup> The other mode employed involves using an external base to deprotonate the ligand precursor alongside a metal source. Reported bases employed to deprotonate imidazolium salts in the preparation of M-NHC complexes include: *n*-BuLi,<sup>96</sup> NaH,<sup>97</sup> KH,<sup>98</sup> KOtBu,<sup>99</sup> NaOH,<sup>100</sup> and NaOAc.<sup>101</sup> Synthesis of M-NHCs by the *in situ* deprotonation method is convenient as it does not require the isolation of the free carbene, allowing access to a variety of carbene ligands which would be too inherently unstable to isolate with ease. The use of silver salts, in particular  $\text{Ag}_2\text{O}$ , has become a ubiquitous method by which to prepare Ag-NHCs, which are either used as prepared for a particular function, or used as a gateway to prepare a wide variety of M-NHC complexes via transmetallation.

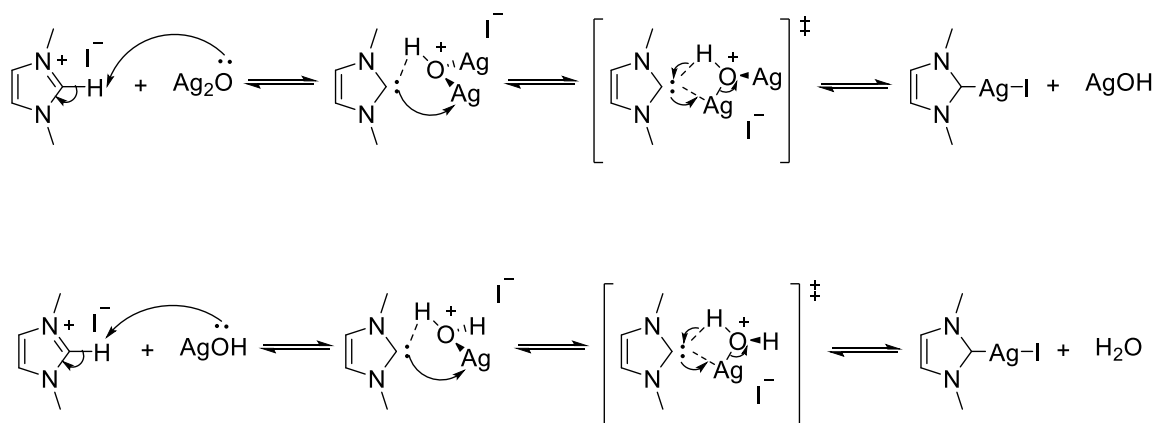


**Figure 11.** Sequential monomer mechanism for the synthesis of Ag-NHCs from two equivalents of imidazolium salt and one equivalent of  $\text{Ag}_2\text{O}$  as proposed by Lledós *et al.*<sup>102</sup>

Transmetallation is a common synthetic strategy employed in organometallic chemistry to prepare metal complexes. The preparation of M-NHCs via transmetallation most commonly occurs via an Ag-NHC intermediate.<sup>103,104</sup> The suitability of Ag-NHCs as transmetallation agents is based on the inherent lability and fluxionality of the Ag-carbene bond. The silver is therefore readily substituted by another metal that forms a less labile bond to the NHC ligand. The method was first reported by Wang *et al.* where 1,3-diethylbenzimidazol-2-ylidene silver(I) bromide was used as a precursor to synthesise

an Au(I)BrNHC (with Au(SMe<sub>2</sub>)Cl as the Au source) and a PdCl<sub>2</sub>(NHC)<sub>2</sub> complex (from PdCl<sub>2</sub>(MeCN)<sub>2</sub>).<sup>82</sup> Examples of M-NHCs containing Rh(I),<sup>105</sup> Cu(I),<sup>106</sup> Cu(II),<sup>107</sup> Au(I),<sup>108</sup> Au(III),<sup>109</sup> Ni(II),<sup>103</sup> Pd(II),<sup>110</sup> Pt(II),<sup>111</sup> Ir(III),<sup>112</sup> Re(I),<sup>113</sup> and Ru(II)<sup>114</sup> have been prepared by transmetalation. Preparing M-NHCs by transmetalation has much of the same benefits as the *in situ* deprotonation method, as it eliminates the need to prepare and handle free carbenes. An additional benefit is the fact that no base is required for the transmetalation reaction, therefore preserving any acidic protons in ligands present.

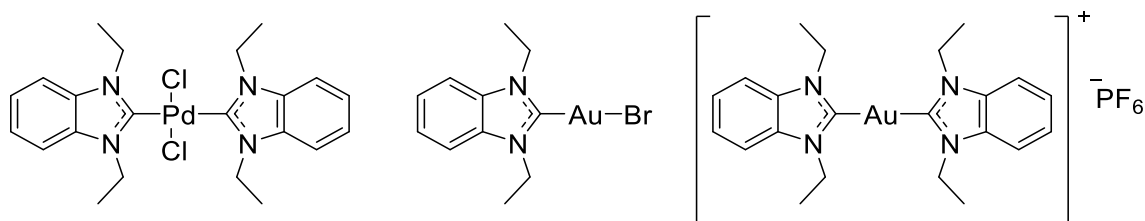


**Figure 12.** Complexes prepared by transmetalation from an Ag-NHC by Wang *et al.*<sup>82</sup>

The third strategy applied in the synthesis of M-NHC complexes is preparation via the free carbene. This method first became of interest when Arduengo *et al.* isolated the first stable free NHC in 1991.<sup>75</sup> The free carbenes are typically formed by reaction of an imidazolium salt or similar precursor with a strong base. Another method by which to prepare free carbenes is removal of small molecules such as removal of methanol from 5-methyltriazole by  $\alpha$ -elimination,<sup>115</sup> or the reduction of imidazole-2-thiones with potassium in boiling THF.<sup>116</sup> The preparation M-NHC complexes via free carbenes is the least common method seen in the literature due to the inherent instability of free carbenes to air and water. However, the inert atmosphere required for the preparation of M-NHCs via the free carbene route allows for the preparation of a wide variety of complexes which would not be stable under atmospheric conditions. With all the methods described, the formation of a carbene from a precursor complex is easily assessed by <sup>13</sup>C-NMR, as free carbenes typically have  $\delta > 200$  ppm, whereas the values for M-NHC carbenic carbons are typically slightly lower than that of the free carbene.<sup>61</sup> This is a drastic shift downfield on the spectrum by comparison with a precursor imidazolium salt, where the *sp*<sup>2</sup> NCN <sup>13</sup>C-NMR peak is found at  $\delta \approx 137$  ppm. The formation of a carbene can therefore cause a shift of at least 30 ppm in the <sup>13</sup>C-NMR spectrum, and is often accompanied with the loss of a proton signal from the <sup>1</sup>H-NMR of the ligand precursor.

### M-NHC complexes as metallodrugs

The variety of M-NHCs structures, wide range of their physicochemical properties, and relative stability has led to them being studied in the field of inorganic medicinal

chemistry. The enhanced strength of the metal-carbene bond by comparison with other ligands provides the complex with an enhanced stability under physiological conditions, which is of the utmost importance when designing metallodrugs. The first such example of research into the biological activity of M-NHC complexes is likely work by Çetinkaya *et al.*<sup>117</sup> which reported the antimicrobial efficacy of Ru(II)- and Rh(I)-NHC complexes against a variety of bacteria including: the Gram positive bacteria *Enterococcus faecalis* and *Staphylococcus aureus* and the Gram negative bacteria *Escherichia coli* and *Pseudomonas aeruginosa*. It was found that the most resistant of these organisms to the M-NHC complexes were the Gram negative bacteria, and that the Rh(I)-NHCs were far more effective against the Gram positive bacteria than the Ru(II)-NHCs tested. Further testing of Ru(II) complexes was conducted by Çetinkaya *et al* in order to probe their antimicrobial efficacy.<sup>118</sup> Ru(II) complexes based on imidazoline and a number of nitrogen heterocycles, some containing Ru-carbene bonds and some containing Ru-N bonds, were tested against the previously mentioned bacteria along with the fungi *Candida albicans* and *Candida tropicalis*. It was found that the carbene complexes of Ru(II) were far more effective against Gram positive bacteria and fungi than complexes containing Ru-N bonds only. Again, the complexes were seen to be far less effective against the Gram negative bacteria than the other organisms.

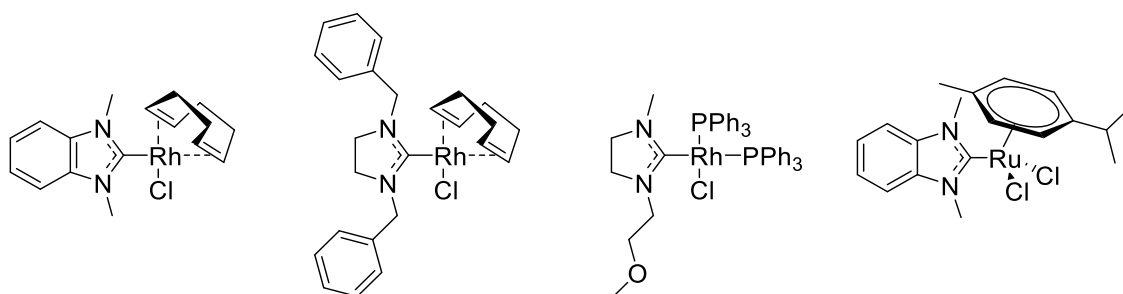


**Figure 13.** Some of the Rh- and Ru-NHCs tested by Çetinkaya *et al.*<sup>117</sup> against bacteria.

More recent work by Hartinger *et al.*<sup>119</sup> describes the preparation and anticancer activity of Ru-NHCs. These complexes were prepared from benzimidazolium salts, which formed Ag-NHCs by reaction with Ag<sub>2</sub>O. The complexes then underwent a transmetallation reaction with the dimeric [(η<sup>6</sup>-p-cymene)<sub>2</sub>RuX<sub>2</sub>]<sub>2</sub> (where X = Cl, Br, or I). The Ru-NHCs formed were RuX<sub>2</sub>(NHC)(η<sup>6</sup>-p-cymene) type complexes. The antiproliferative effects of these Ru-NHCs were tested against HCT116, SiHa, and NCI-H460 cancer cells, yielding low to middling IC<sub>50</sub> values typically between 6.2 μM and 173 μM, though a Ru-NHC with assymetric R groups on the benzimidazolium nitrogens (R' = methyl, R'' = benzyl, X = Cl) had an IC<sub>50</sub> value of 1212 μM against HCT116. A study by Lin *et al.*<sup>120</sup> focused on the specific mechanism of action of a similar RuX<sub>2</sub>(NHC)(η<sup>6</sup>-p-cymene) complex against

human oesophageal squamous carcinoma EC109 cells. It was found that the ruthenium complex halted cell proliferation by halting the cell cycle at the G2/M phase, indicating damage to the intracellular DNA that is difficult to repair. Another recent study by Hartinger *et al.*<sup>121</sup> on the interaction of a  $\text{RuX}_2(\text{NHC})(\eta^6\text{-p-cymene})$  complex with hen egg white lysozyme (HEWL) found that the Ru-NHC underwent ligand exchange with a site in the protein. It was found the complex underwent an unusual ligand exchange reaction, with the protein's His14 and Arg15 acting as a bidentate ligand and displacing the Ru-bound arene. The lability of the arene coupled with the stability of the Ru-carbene bond therefore likely allows the complex to diffuse into cells and interact with cellular components via ligand exchange reactions. Many additional biologically active examples in recent literature also contain complexes of Ru with both NHC and p-cymene ligands, highlighting the importance of this interplay.<sup>122–125</sup>

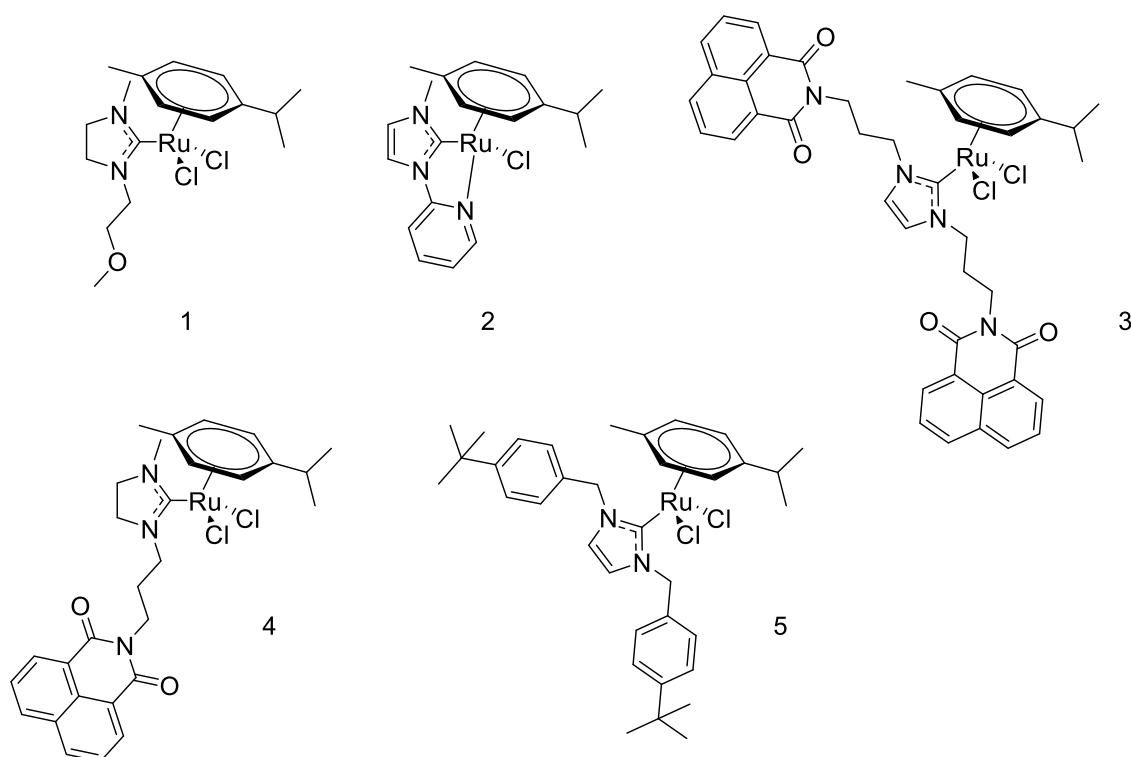


**Figure 14.** Anticancer Ru-NHC complexes with p-cymene ligands (1,<sup>118</sup> 2,<sup>122</sup> 3<sup>123</sup>, 4,<sup>124</sup> 5<sup>125</sup>).

The other metal employed in the work of Çetinkaya *et al.*<sup>117</sup> was rhodium. Rh(I) is isoelectronic with Pt(II), and was therefore swiftly studied for its anticancer activity due to the well-known activity of cisplatin.<sup>42</sup> As with ruthenium, where NHCs were typically paired with p-cymene ligands, NHCs are typically paired with cyclooctadiene (COD) in forming square planar Rh-NHC complexes. The literature has a number of examples of

RhXNHC(COD) complexes with strong antiproliferative effects against cancer cells.<sup>126–128</sup> A RhXNHC(COD) complex with a charged phosphonium side chain was also found to have antimicrobial effects against the Gram positive *S. aureus*, *Staphylococcus epidermidis*, *E. faecalis*, and *Enterococcus faecium*, as well as the Gram negative *E. coli*, *P. aeruginosa*, *Yersinia pseudotuberculosis*, and *Yersinia pestis*, though as reported previously with Ru-NHCs, the Rh-NHCs were more effective against the Gram positive bacteria than against the Gram negative bacteria.<sup>129</sup>

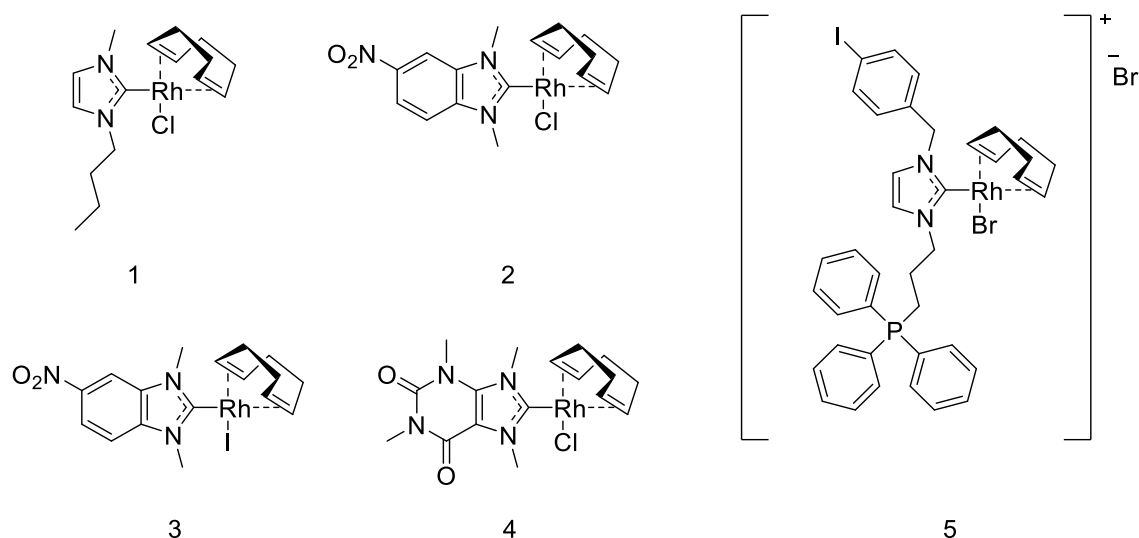


**Figure 15.** Biologically active Rh-NHCs. Compounds 1,<sup>126</sup> 2 and 3,<sup>127</sup> and 4<sup>128</sup> were reported with anticancer activity, whereas 5<sup>129</sup> was reported with antimicrobial activity.

As previously mentioned, Pt is the most studied metal in the field of inorganic medicinal chemistry, largely based on the success of the drug cisplatin. As such there are numerous cases in the literature of Pt-NHCs showing anticancer activity. An example of this comes from recent work by Schobert *et al.*<sup>130</sup> describing the antitumoral effects of a variety of *cis*[bis(benz)imidazole-2-ylidene(L')(L'')]Pt(II)NHCs. The highly active anticancer Pt-NHC complexes typically had micromolar IC<sub>50</sub> values. It was also found that the activity of the complex did not depend on the NHC ligand alone. Rather, the secondary ligands played an important role, as switching one chlorido ligand for triphenylphosphine resulted in IC<sub>50</sub> values on the nanomolar scale. Further work by Schobert *et al.*<sup>131</sup> focused on the role of overall charge and bulkiness of the secondary ligand on the localisation of Pt-NHCs in melanoma cells. For this purpose, complexes of the structure *cis*-[bis(1,3-di(4-ethynylbenzyl)imidazol-2-ylidene)(L')(L'')]platinum(II) were synthesised and tested alongside the previously described Pt-NHCs (*cis*-[bis(1,3-dibenzylimidazol-2-ylidene)(L')(L'')]. Complexes were synthesised starting from *cis*-[PtCl<sub>2</sub>(DMSO)<sub>2</sub>] and 1,3-di(4-ethynylbenzyl)imidazolium chloride, which was

deprotonated with tBuOK, forming the complex cis-[dichlorido-bis(1,3-di(4-ethynylbenzyl)imidazol-2-ylidene)]platinum(II). Some of the prepared complex was stirred in MeOH and DCM at room temperature in the presence of triphenylphosphine to form the positively charged cis-[Chlorido-bis(1,3-di(4-ethynylbenzyl)imidazole-2-ylidene)(triphenylphosphine)]platinum(II)<sup>+</sup> complex stabilised with a chloride counter ion. Both benzyl-substituted Pt-NHC complexes were found to interact with DNA *in vitro* to a greater extent than cisplatin, however uptake into melanoma cells occurred to a much greater degree for the complex where L' = Cl and L'' = PPh<sub>3</sub>, most likely due to active transport of the cationic complex into the cell. The ethenyl-tagged Pt-NHCs localised in the mitochondria of the cell. This advantage allows the ethenyl-tagged Pt-NHCs to bypass repair associated tumour resistance mechanisms which may occur when employing Pt-based treatments. A number of reviews into Pt-NHCs as anticancer agents are available for the interested reader. Further discussion of Pt-NHCs is beyond the scope of this thesis, however, a number of reviews describing Pt-NHC metallodrugs are available.<sup>132–134</sup>

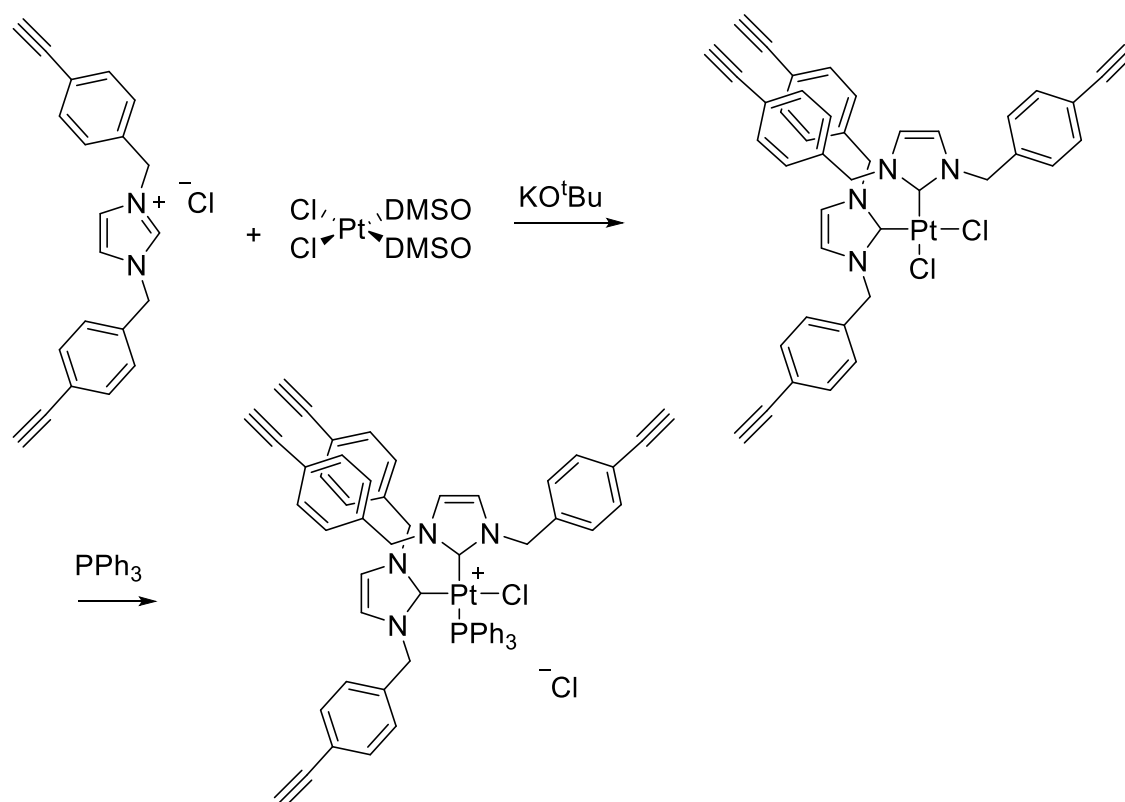


**Figure 16.** Preparation of ethenyl-tagged anticancer Pt-NHC for mitochondrial localisation, allowing efficacy against cells displaying repair associated tumour resistance.<sup>131</sup>

Beyond Pt(II), Ru(II), Rh(I), and Ir(III) (complexes of which have shown strong anticancer properties<sup>135–138</sup>), both Au(I)- and Ag(I)-NHCs have attracted much attention as potential metallodrugs. Much of the biological activity of these compounds is associated with their soft acid nature, allowing them to interact with free thiols and amines, which are abundant in living cells.<sup>139–142</sup> The interaction with these soft base donors has the potential to disrupt cellular activity.<sup>143,144</sup> Amongst a number of potential cellular targets, Au-NHCs were found to act on cancer cells by inhibition of thioredoxin reductase (TrxR)<sup>145–148</sup> and exhibit antimitochondrial activity.<sup>149–151</sup> Work by Ott *et al.*<sup>152</sup> described the preparation of neutral and cationic NHC-Au-L complexes, and found that TrxR inhibition is much more dependent on the identity of the L ligand rather than the NHC side chains.<sup>153</sup> Three NHC-Au-L complexes with 1,3-diethylbenzimidazol-2-ylidene NHC ligands were tested against MCF-7 (breast adenocarcinoma), HT-29 (colon carcinoma), and HEK-293 (human embryonic kidney) cells. One complex was a neutral complex where L = Cl, whereas the other complexes were cationic: one where L = PPh<sub>3</sub>, and one where L = NHC (of the structure previously described) therefore making it a bis(NHC)-Au complex. Both cationic complexes were stabilised by iodide ligands.

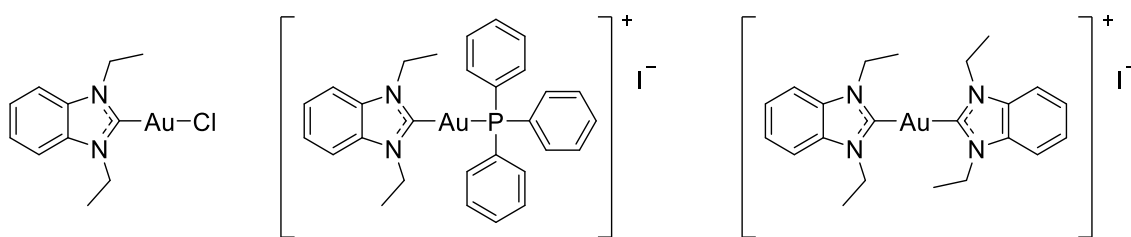


**Figure 17.** Au-NHC complexes described by Ott *et al.*<sup>152</sup> The complexes were prepared in order to probe the effect of the ancillary ligand on the biological activity of Au-NHCs.

It was found that the neutral Au-NHC had good cytotoxicity, but was surpassed by the cationic complexes. The neutral Au-NHC was however a more effective TrxR inhibitor than either of the cationic complexes. The differing selectivity of these complexes is rationalised by the bond dissociation energy of the Au-L bond, where the Au-Cl bond from the neutral complex has the lowest bond dissociation energy. The lower cytotoxicity of the neutral complex is linked to lower levels of gold uptake by comparison with that of the cationic species. The higher uptake of the cationic species is due to them being suitable substrates for membrane transport proteins. The protein binding of the 3 complexes was also studied by mass spectrometry using selenocysteine modified proteins.<sup>154</sup> As expected based on the TrxR inhibition of the three complexes, the neutral complex was confirmed to be the most effective selenocysteine binder of the three complexes. Further examination into the role of the bound phosphine determined that a

decrease in lipophilicity increased TrxR inhibition. Due to the success of the above Au-NHCs, Ott *et al.*<sup>155</sup> produced a large library of Au(I/III)-NHCs in an attempt to determine structure functionality relationships for Au-NHCs. No direct relationship could be drawn between cytotoxicity and TrxR inhibition, however it was found that most Au-NHCs had good values for both cytotoxicity and TrxR inhibition. The work therefore confirmed that TrxR inhibition was important for an Au-NHC's cytotoxicity but other factors such as lipophilicity, albumin binding, cellular uptake, and any additional modes of action provided by the ligand were also of import. Further study of the biscarbene iodide Au-NHC (Figure 17) found that the complex had a variety of effects on gemcitabine-resistant pancreatic cancer cells including: decreasing cell growth, arresting the cell cycle, apoptosis, alteration of the cell's redox homeostasis, and disruption of mitochondrial membrane potentials.<sup>156</sup>

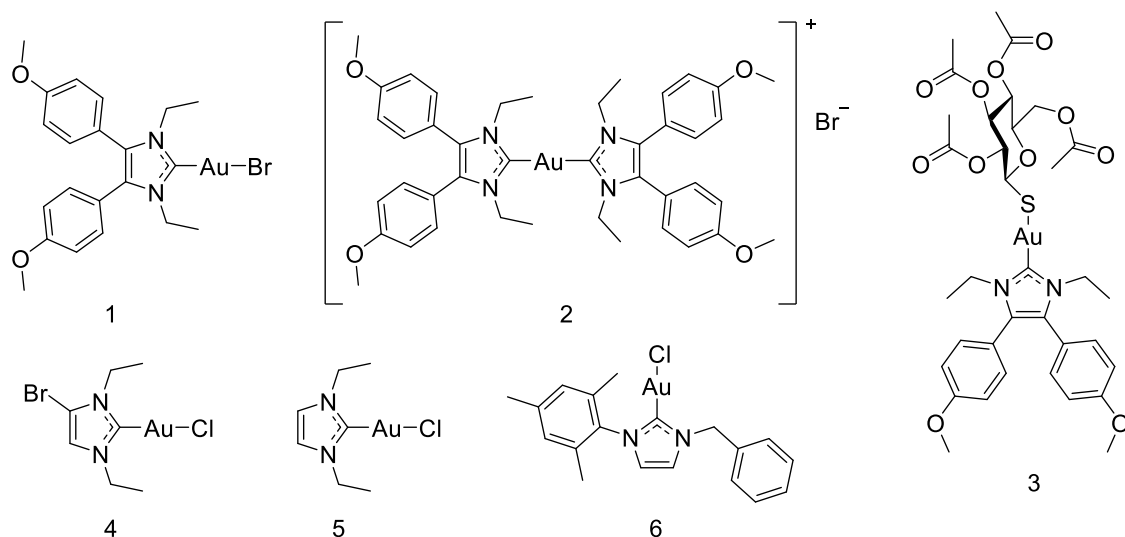


**Figure 18.** Selected anticancer (1-3),<sup>157</sup> antibacterial (4,5),<sup>158</sup> and antiparasitic (6)<sup>159</sup> Au-NHCs.

The spectrum of reported ancillary ligand for Au-NHCs is much broader than those reported for other metals (except silver and perhaps platinum). Au(I)-NHCs with anticancer activities have been reported with the following ancillary ligands: phosphines,<sup>157,160</sup> chloride,<sup>158,161,162</sup> bromide,<sup>157,163</sup> biscarbene,<sup>157,164–166</sup> thiols,<sup>157,161,162</sup> thiocyanate,<sup>161</sup> diphosphanes,<sup>167</sup> and dithiocarbamate,<sup>168</sup> amongst others. Au(III)-NHCs bearing N<sup>^</sup>N<sup>^</sup>N and N<sup>^</sup>C<sup>^</sup>N ligands have also been reported to have anticancer effects, and are readily reduced to Au(I) by glutathione to produce active Au(I)-glutathione complexes.<sup>109</sup> Au-NHCs have also been reported to have antibacterial qualities.<sup>158</sup> Ag(NHC)Cl complexes of imidazol-2-ylidene and benzimidazol-2-ylidene were tested against the Gram negative bacteria *E. coli*, *P. aeruginosa*, *Acinetobacter baumannii*,

*Enterobacter cloacae*, and *Klebsiella pneumoniae*, as well as the Gram positive *S. aureus* (2x methicillin-resistant *Staphylococcus aureus* (MRSA) strains) and *E. faecium*. As with other M-NHC complexes, it was found that the activity against Gram positive bacteria was much greater than against Gram negative bacteria. Overall, it was found that imidazole-2-ylidene Au complexes were slightly more effective than their counterpart benzimidazol-2-ylidene Au complexes. Au-NHCs have also been reported to display antiparasitic effects against *Leishmania infantum*<sup>159</sup> and *Plasmodium falciparum*.<sup>169</sup>

As with the previously described Au-NHCs, Ag-NHC metallodrugs have a much wider variety of ancillary ligands than Rh-, Ir- and Ru-NHC metallodrugs. Ag-NHCs are convenient to access synthetically due to their roles as precursors to other M-NHCs through transmetallation.<sup>103,104</sup> This allows for greater scope to build large libraries of Ag-NHCs which may be investigated. Unlike other M-NHCs, the majority of Ag-NHC literature (in inorganic medicinal chemistry) focuses on the potential of these compounds as antibacterial agents.<sup>170</sup> A discussion of the antibacterial applications of Ag-NHCs is presented in Chapter 2. Much in the manner that Au-NHCs are mainly anticancer agents with some reports of antimicrobial activity, Ag-NHCs are potent antibacterial agents with some anticancer activity. The first report of anticancer activity in Ag-NHCs was by Youngs *et al.* in 2008.<sup>171</sup> Three examples of 4,5-dichloroimidazol-2-ylidene based silver acetate complexes were found to be effective agents *in vitro* against ovarian cancer (OVCAR-3) and breast cancer (MB157) cells, however they had little activity against cervical cancer (Hela) cells. One complex, 1,3-dimethyl-4,5-dichloroimidazol-2-ylidene silver(I) acetate, was found to be active *in vivo* in an ovarian cancer xenograft mouse model.

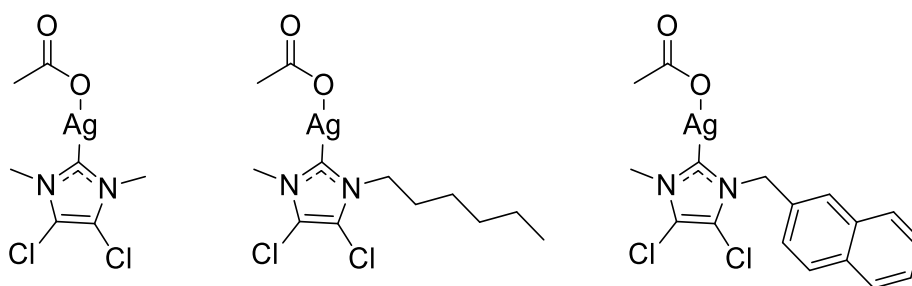


**Figure 19.** The first examples of anticancer Ag-NHCs reported by Youngs *et al.*<sup>171</sup>

Following the success of the work by the Youngs group, Tacke *et al.* described the synthesis of cyanobenzyl-substituted Ag-NHCs.<sup>172–174</sup> One example Ag-NHC (Figure 20, compound 1) from this work was found to have a roughly three-fold increase in activity against the renal cancer cell line Caki-1. The Ag-NHC was also found to have *in vitro*

efficacy against neuroblastoma cells (UKF-NB-3), colon cancer cells (HCT8), and paclitaxel-resistant prostate cancer cells (PC-3). The compound however failed to effect any tumour reduction *in vivo*.<sup>175</sup> Tacke and co-workers also investigated the anticancer activity of benzyl-substituted Ag-NHCs against the aforementioned Caki-1 cells and MCF-7 cells.<sup>176,177</sup> Of these a 4,5-di(p-tolyl)imidazole derivative with N-bound 4-methylbenzyl groups attached was found to be the most active (Figure 20, compound 2). Interestingly, the precursor imidazolium salt also showed anticancer activity, suggesting a possible synergistic effect between the ligand and the bound metal as a contributing factor to the complex's activity.

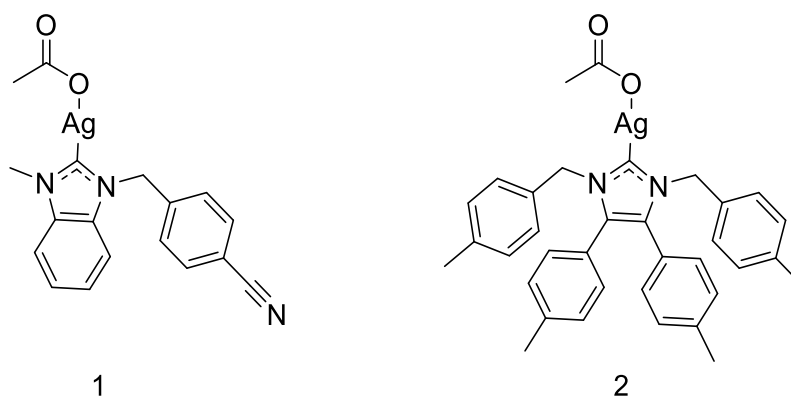


**Figure 20.** Anticancer Ag-NHCs reported by Tacke *et al* (1,<sup>175</sup> 2<sup>177</sup>).

The structural diversity of anticancer Ag-NHCs is much more varied than that of other M-NHCs (besides Au-NHC). LAg-NHC complexes with anticancer properties have been described with a variety of ancillary ligands other than the initially reported acetate including: other NHC ligands,<sup>178–182</sup> nitriles,<sup>178</sup> chloride,<sup>183–185</sup> bromide,<sup>186,187</sup> and iodide.<sup>188</sup> Non-imidazole based Ag-NHCs have also been reported to display anticancer activities including those derived from 1,2,4-triazine,<sup>186</sup> benzimidazole,<sup>175</sup> and xanthines.<sup>189</sup> More recent reports of the anticancer effects of Ag-NHCs come from the work of Budagumpi *et al.*<sup>190</sup> where asymmetric Ag-NHCs derived from 1,2,4-triazine with an N-bound coumarin moiety which showed strong anticancer activity against MCF-7 and HT-29 cells, though the complexes were more effective against the former cell line than the latter. Work by Şahin *et al.*<sup>191</sup> described two asymmetric 1-(2-methyl-2-propenyl)benzimidazole based Ag-NHCs substituted with N-bound 4-methylbenzyl or 4-isopropylbenzyl moieties which showed *in vitro* activity against prostate cancer cells (DU-145), MCF-7 cells, breast cancer cells (MDA-MB-231), and normal fibroblasts (L-929). The precursor imidazolium salts also showed activity, albeit less than the derived complex against the same cells. The compounds were also found to have less effect on the non-cancerous fibroblasts than on the cancer cells, whereas the increased

lipophilicity of the 4-isopropylbenzyl-substituted complex leant it an increased anticancer effect by comparison with the 4-methylbenzyl analogue. Majid *et al.*<sup>192</sup> also reported anticancer effects of bis-NHC 3-alkyl-1-propylbenzimidazol-2-ylidene Ag-NHCs with PF<sub>6</sub> counter ions against HCT 116, MCF-7, and K-562 cancer cell lines. The Ag-NHCs were also found to deposit “black blobs” of silver by use of microscopy, hinting at silver release as a mechanism for anticancer activity, as opposed to a previously suggested caspase-independently induced apoptosis. The complexes were also found to be non-toxic to female rats over 14 days by oral administration at a dose of 300 mg/kg. In all three recent examples decribed, the Ag-NHCs were prepared by reaction of an azolium salt with either Ag<sub>2</sub>O or AgOAc. The interested reader is directed to a number of recent review articles on the application of M-NHCs as metallodrugs.<sup>170,193–195</sup>

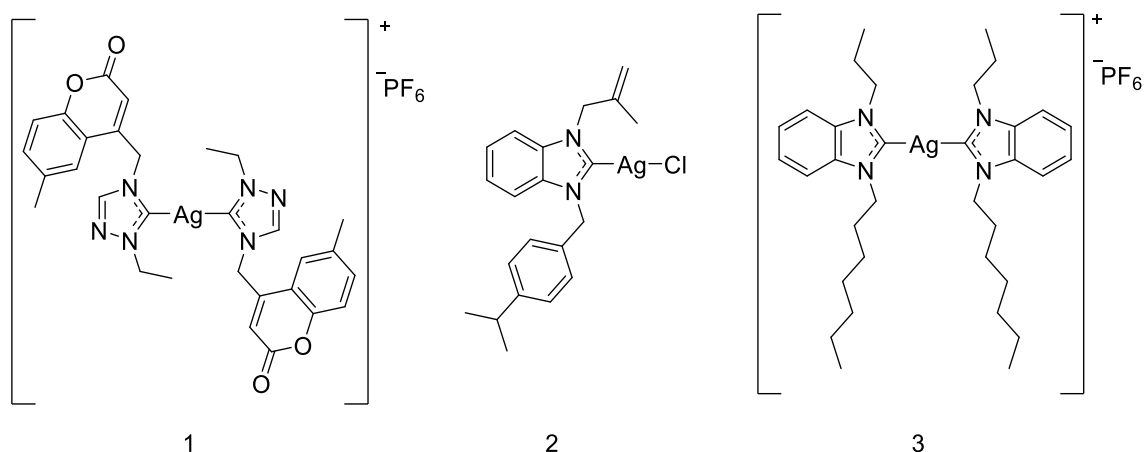


**Figure 21.** Recent examples of Ag-NHCs with anticancer activity (1,<sup>190</sup> 2,<sup>191</sup> 3<sup>192</sup>).

### Thiosemicarbazones

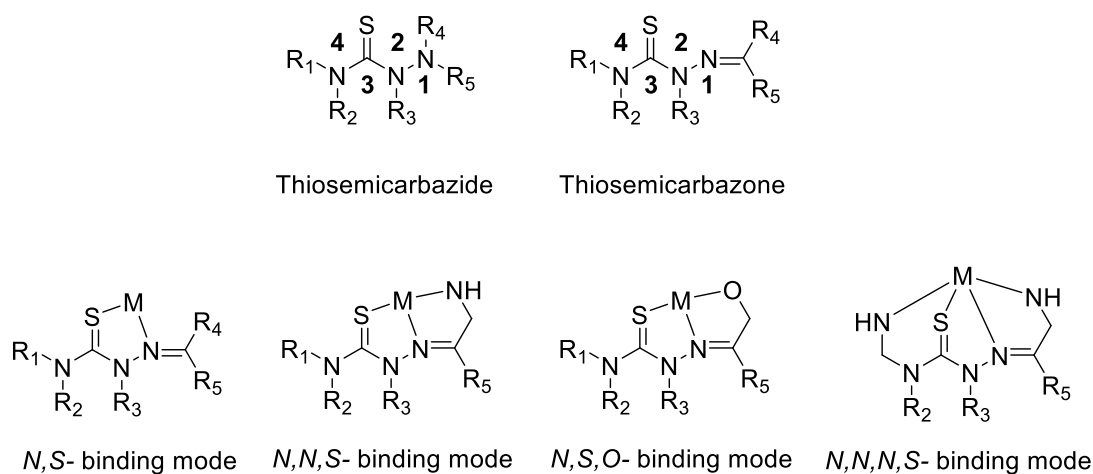


**Figure 22.** Thiosemicarbazone nomenclature, numbering, and exemplary metal-binding modes.<sup>196</sup>



## Biological activity of metal-TSC complexes

TSCs and their precursor thiosemicarbazides have been shown to have innate biological activity before binding metals. The biological activity of TSCs and thiosemicarbazones has been known since the early 20<sup>th</sup> century, with reports of the compounds being effective agents against bacteria<sup>199,200</sup> and mycobacteria (*Mycobacterium tuberculosis*,<sup>201,202</sup> *Mycobacterium leprae*,<sup>203</sup> *Mycobacterium bovis*<sup>204</sup>), parasites (*Trypanosoma cruzi*<sup>205</sup> and *P. falciparum*<sup>206</sup>), as well as viruses (*Variola major*<sup>207</sup>). Despite this, the antimicrobial mechanisms of action of TSCs and thiosemicarbazides are poorly understood. The mode of action may however match somewhat with that of TSCs and thiosemicarbazides against cancerous cells: acting as chelating agents for metals essential to biological functions such as iron and copper, and potentially inhibiting ribonucleotide reductase (an enzyme that is essential to DNA synthesis).<sup>208</sup> Binding metals to form metal TSC complexes (M-TSCs) has the potential to stifle the TSC's ability to bind to crucial cellular metals, but may introduce other modes of action derived from the bound metal. M-TSCs containing Co(II),<sup>209</sup> Co(III),<sup>210</sup> Ni(II),<sup>210,211</sup> Cu(II),<sup>210–213</sup> Zn(II),<sup>209,214</sup> V(V),<sup>211</sup> V(IV),<sup>215</sup> Mn(II),<sup>209</sup> Fe(III),<sup>216</sup> Ga(III),<sup>216</sup> and Pd(II)<sup>217</sup> have displayed antitumour efficacy amongst others, whereas other examples of M-TSCs have shown a range of antimicrobial activity against bacteria,<sup>196,218</sup> fungi,<sup>219,220</sup> viruses,<sup>221</sup> and protozoa,<sup>222</sup> whilst also showing enhanced antimicrobial activity by comparison with the parent TSC ligand.<sup>211,223,224</sup> As with the parent ligands, the mechanism of action of M-TSCs against microbes is poorly understood, and must also be approached on a metal-by-metal basis. Work by Djoko *et al.*<sup>225</sup> discussed the activity of a Cu(II) bithiosemicarbazone (BTSC a subclass of TSC) against *Neisseria gonorrhoeae*, suggesting that Cu(II) was released intracellularly by the TSC, whereupon the Cu(II) was reduced to the more biocidal Cu(I), which associates with membrane proteins crucial to cellular respiration, inhibiting the process. A more in-depth discussion of the chemistry and biological activity of M-BTSC complexes is presented in Chapter 3 of this work.

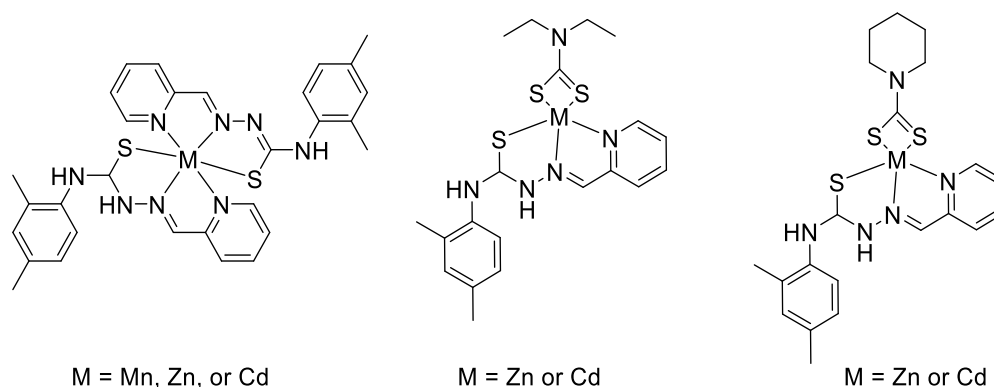


**Figure 24.** Recent antimicrobial M-TSC metallodrugs reported by Shalaby *et al.*<sup>226</sup>

A recent example from Shalaby *et al.*<sup>226</sup> focused on the preparation of a tridentate TSC containing a pyridine moiety and complexation of the aforementioned ligand to Mn, Zn, and Cd in a bis-*S,N,N*- motif. Complexes of Zn and Cd were also prepared using one equivalent of the tridentate TSC ligand, one of two N-bound dithiocarbamates, and an ancillary OH<sub>2</sub> ligand. The antifungal and antibacterial properties of the Zn and Mn complexes were tested against Gram positive *Bacillus cereus*, *Micrococcus luteus*, and *S. aureus*, Gram negative *E. coli*, *P. aeruginosa*, and *Serratia marcescens*, as well as the fungi *Aspergillus flavus*, *C. albicans*, *Fusarium oxysporum*, *Geotrichum candidum*, *Scopulariopsis brevicaulis*, and *Trichophyton rubrum*. The binary Mn complex inhibited the growth of all fungal species besides *T. rubrum*, but had no effect on the bacteria tested. The binary Zn complex on the other hand was only active against one fungus, *C. albicans*, but inhibited the growth of all bacterial species besides *S. marcescens* at a lower concentration than the control antibiotic chloramphenicol. The dithiocarbamate-containing complexes were only active against *S. brevicaulis* (though one example showed strong inhibition of *T. rubrum*), but were active against all bacteria. The minimum inhibitory concentration (MIC) of these complexes were higher than those found for the bivalent Zn complex (besides *S. marcescens*), and were typically higher than those reported for chloramphenicol (again, besides *S. marcescens*).

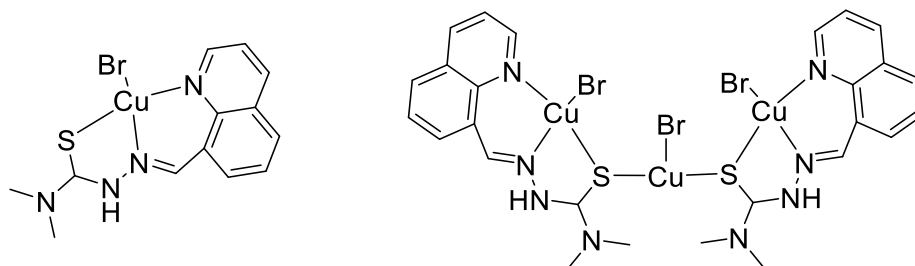


**Figure 25.** Varied anticancer Cu-TSC complexes prepared by Yang *et al.*<sup>227</sup> showing the influence of heating the same 1:1 mixture of metal salt and ligand. The left complex was produced at room temperature, whereas the right structure was produced by heating the components at reflux.

Another recent example of M-TSCs as metallodrugs describes the anticancer potential of a Cu(II)-TSC complex containing a tridentate TSC ligand derived from quinoline-8-carbaldehyde.<sup>227</sup> The complex either formed with a 1:1 ratio of ligand to metal when prepared at room temperature, or a 2:3 ratio of ligand to metal when prepared at reflux. The 1:1 ratio complex featured binding via the standard N1/S3 bidentate motif, with the additional N binding from the quinoline moiety. The coordination sphere of the Cu was satisfied by a Br ligand. The 2:3 ratio complex contained the same binding motif as the

1:1 complex, but featured a bridging CuBr moiety bound between two sulphur atoms (depicted in Figure 25). Both complexes showed remarkably low IC<sub>50</sub> values against MCF-7, Hela, A549, A549cisR, and MRC-5 cells. The complexes had lower IC<sub>50</sub> values than cisplatin against all cell lines, and in some cases (against A549cisR) the IC<sub>50</sub> values of the complexes were 150-300x less. A number of reviews describing the biological activity of M-TSC complexes and TSCs are available for further reading.<sup>196,228-231</sup>

## **Biomaterials**

Biomaterials are classified as any material that is used in a biological setting which interfaces with tissue, be they naturally derived substances or synthetic in nature.<sup>232-234</sup> Biomaterials are often used in order to repair or substitute body parts which may be missing due to birth defects or trauma. Biomaterials are therefore different to other forms of therapies as they often provide physical assistance rather than producing physiological or biochemical changes. For a material to be successfully employed as a biomaterial it must have suitable properties that allow for it to be interfaced with biological systems and minimise the chances of rejection from the host, and therefore cause damage or otherwise alter the host tissue. Potential biomaterials must therefore be as inert as possible, non-toxic, and as durable as possible.

One of the key applications of biomaterials is the design and production of medical devices. Medical devices may be internal, external, or a mixture of the two, and their main purpose is to increase quality of life for patients either by assisting patient treatment or patient function. Common medical devices used in a clinical setting include external devices such as artificial skin, dental fillings, and prostheses, internal devices such as pacemakers, artificial heart valves, artificial blood vessels, pins for bone repair, and artificial joint replacements, as well as medical devices that are both internal and external such as catheters.<sup>235-239</sup> The applications of biomaterials as medical devices are broad, and as such the required physicochemical properties for each of these applications varies. Whereas rigid, strong metals are required for pinning broken bones and filling dental cavities: orthopaedic pins are often made of stainless steel, and dental cavities are filled with gold, porcelain, composite resin, or historically silver amalgam, softer and more flexible materials are required to produce prostheses that match the firmness of tissue, or to ensure comfortable insertion of urinary catheters. Polymers such as polyurethanes and silicones are therefore more appropriate for such applications. Silicone rubber medical devices are particularly common. The chemistry of silicone rubbers is outlined briefly below.

## Silicone rubber medical devices

Silicone rubber is an excellent material with which to design medical devices due to its favourable and highly tuneable physicochemical properties: silicone rubber is inert, non-toxic, tasteless, hard-wearing, flexible/pliable, easy to manipulate, and has a low cost associated with its production.<sup>240</sup> Silicone rubber is a polymer that is typically comprised of many thousands of monomer units. The structure of silicones may be likened to ethers, with repeating  $[-SiR_2-O-]$  units throughout. Though there are many possible configurations for a silicone rubber, the simplest form is based on polydimethylsiloxane (PDMS), which is the material of choice for many medical devices. Most silicone rubber formulations include a PDMS base (with appropriate terminal functionality), a crosslinker: which is typically a PDMS derivative with many active sites where an appropriate reaction may take place, and a catalyst in order to allow the curing process to occur. Simple silicone rubber formulations may also include appropriate fillers (such as silica) and inhibitors. Appropriate fillers may be chosen based on the application of the designed device: silicone rubber in optical devices is often required to be transparent; as such the added mechanical strength afforded to the material by a filler such as silica is offset by the opacity lent to the material by silica doping. Appropriate crosslinker, PDMS base terminal functionalities, and catalysts are selected based on the curing system selected.<sup>240</sup>

One example curing system is free-radical peroxide-induced curing. For this, vinyl-terminated PDMS base polymers also act as crosslinkers, whereas the “catalyst” employed is typically an organic peroxide such as dicumyl peroxide or dichlorobenzoyl peroxide.<sup>241</sup> Vinyl termini allow for properties such as crosslinking density and maximum elongation to more easily be controlled<sup>242</sup>, therefore allowing for greater control of the properties of the final silicone material. Free-radical peroxide-induced curing is thought to occur via an initiation step whereupon the peroxide agent is homolytically split by heating producing a radical. The radical can then abstract an H atom from a methylsiloxane group in the propagation step, before two methylenesiloxane radicals couple in the termination step to form a new C-C bond (Figure 26).<sup>242,243</sup> Free-radical peroxide-induced curing is however an inefficient reaction, with high peroxide loading required, making it less favourable for industrial application than other curing systems employed.<sup>244</sup> The crosslinking produced is also inefficient in the presence of common high-surface area fillers such as silica.<sup>242</sup> Free-radical peroxide-induced curing is therefore not often used in the design of medical devices. Another less commonly used curing system is photoinitiated curing, where UV-light is used to produce radicals that act as a catalyst to crosslink PDMS which is functionalised with reactive groups such as

epoxide, acrylate, thiol, and vinyl.<sup>241</sup> Photoinitiated curing has the benefit of being conducted at room temperature, however the reaction is inhibited by oxygen. Oxygen inhibition may cause the silicone rubbers formed to be tacky and have poor structural consistency.<sup>245</sup>

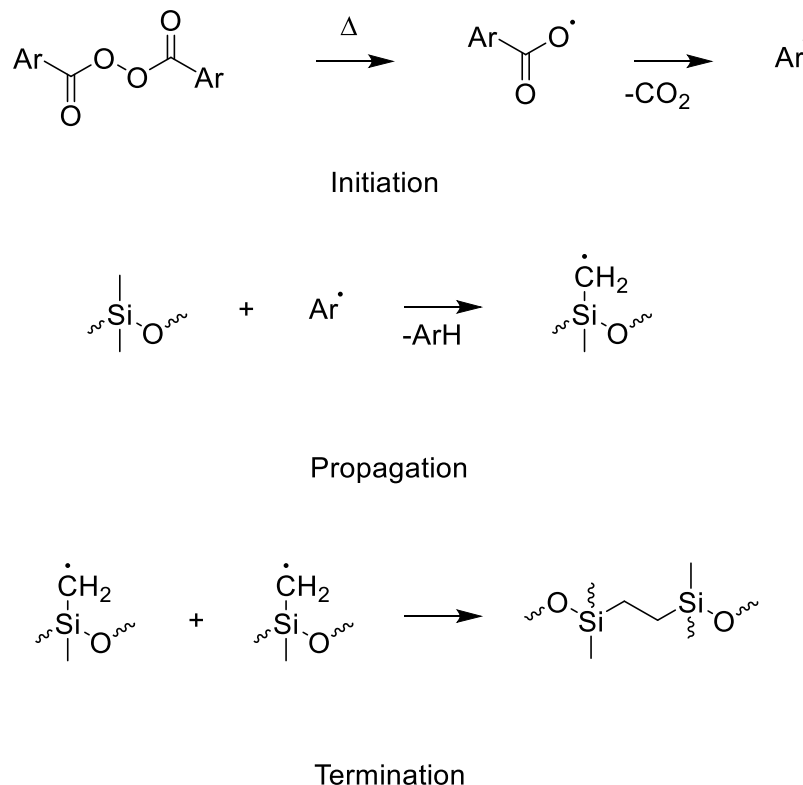


**Figure 26.** Mechanism for peroxide induced crosslinking of PDMS polymers.<sup>242</sup>

The two most common ways to produce silicone rubber are condensation curing and hydrosilylation. Condensation curing is conducted with silanol-terminated PDMS polymer bases, a PDMS crosslinker with hydrolysable functionalities and a catalyst. Historically, condensation curing was conducted with dialkyldicarbonyltin catalysts,<sup>246</sup> however due to tin's inherent toxicity and banning from European consumer products new systems such as titanium-based catalysts,<sup>247,248</sup> acidic catalysts such as sulfonic acids,<sup>249</sup> and nitrogen-containing bases such as DBU have been employed.<sup>250</sup> Titanium catalysts are now the most commonly used condensation cure catalysts in industry.<sup>251</sup> First generation titanium catalysts are titanium(IV) alkoxides, and have catalytic performance equivalent to the previously employed tin catalysts. They do however suffer from a number of drawbacks including short shelf lives, premature termination of catalytic activity and incompatibility with aminosiloxanes and other nucleophilic dopants, additives, and fillers due to the strongly Lewis acidic nature of the Ti(IV) centre and the easy hydrolysis of the Ti-alkoxide bond.<sup>252</sup> Second generation Ti(IV) catalysts are stabilised by acetylacetonate

(acac) ligands, leading to enhanced stability of the catalyst due to the chelate effect.<sup>253</sup> This enhanced stability leads is balanced by a decreased crosslinking kinetics, which in turn may lead to poor polymerisation selectivity further leading to gelation.<sup>254</sup> The mechanism of condensation curing with a Ti(IV) catalyst is shown in Figure 27.

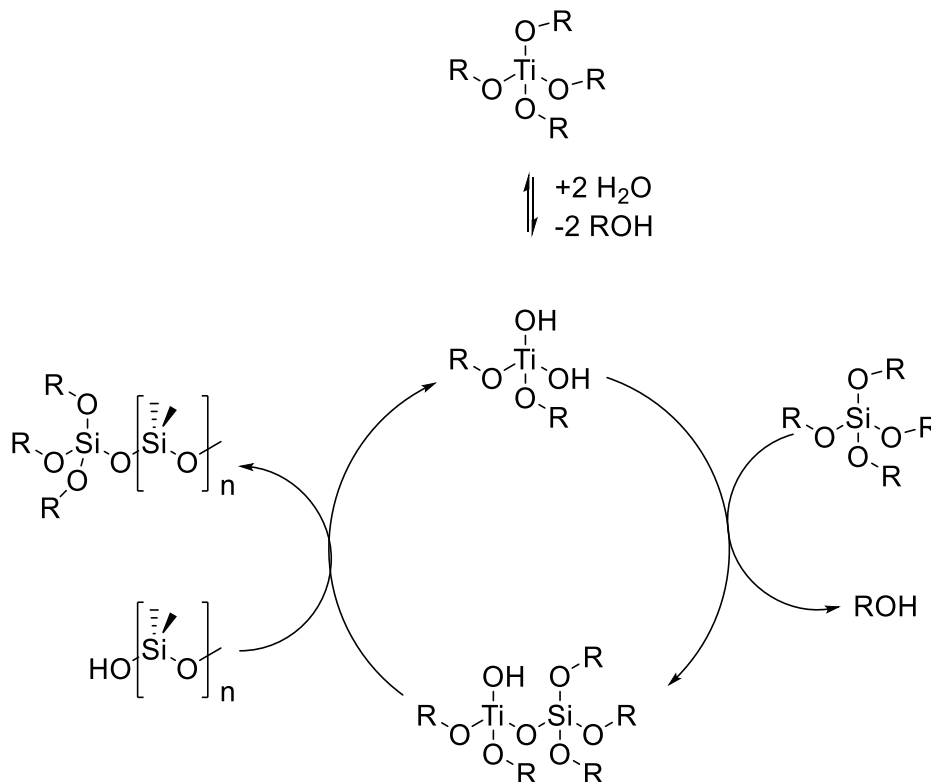


**Figure 27.** The mechanism of condensation curing of PDMS by Ti(IV) catalysts to produce silicone rubber.<sup>241</sup>

The other commonly used curing system in industry is Pt-cure hydrosilylation. The base polymer is typically a vinyl-terminated PDMS, with hydrosiloxane-containing crosslinkers and a Pt(0) catalyst. Speier's catalyst, Karstedt's catalyst, and platinum cyclovinylmethylsiloxane catalyst are all commonly used in industrial settings for the curing of silicone rubber.<sup>241</sup> Hydrosilylation is the addition of Si-H bonds across an unsaturated system, typically an alkene,<sup>255–259</sup> but also occurs in systems containing alkynes.<sup>260,261</sup> The catalytic cycle begins with the oxidative addition of a hydrosiloxane functionality to the Pt catalyst, followed by the association of the vinyl-terminated PDMS base polymer. The association of the vinyl-terminated PDMS allows for a 1,2-migratory insertion of the associated Pt hydride to form a new methylene bridge, followed by the reductive elimination of the newly crosslinked polymer, returning Pt(II) to Pt(0) and beginning the catalytic cycle anew. The Chalk-Harrod hydrosilylation mechanism described is illustrated below in Figure 28.<sup>262</sup> The alternative pathway (not illustrated in

Figure 28) where the migratory insertion is performed by the Pt-SiR<sub>3</sub> bond is not typically seen in Pt-catalysed hydrosilylation, but is the principal migratory insertion step observed in Rh-catalysed hydrosilylation.<sup>263</sup> Pt-catalysed curing is more popular in industry due to the cheap relative cost of Pt metal vs Rh. Hydrosilylation is unique amongst curing technologies in that it produces no side products.<sup>241</sup> This is of great advantage in an industrial setting due to the lack of potentially hazardous waste products produced and a 100% atom efficiency.

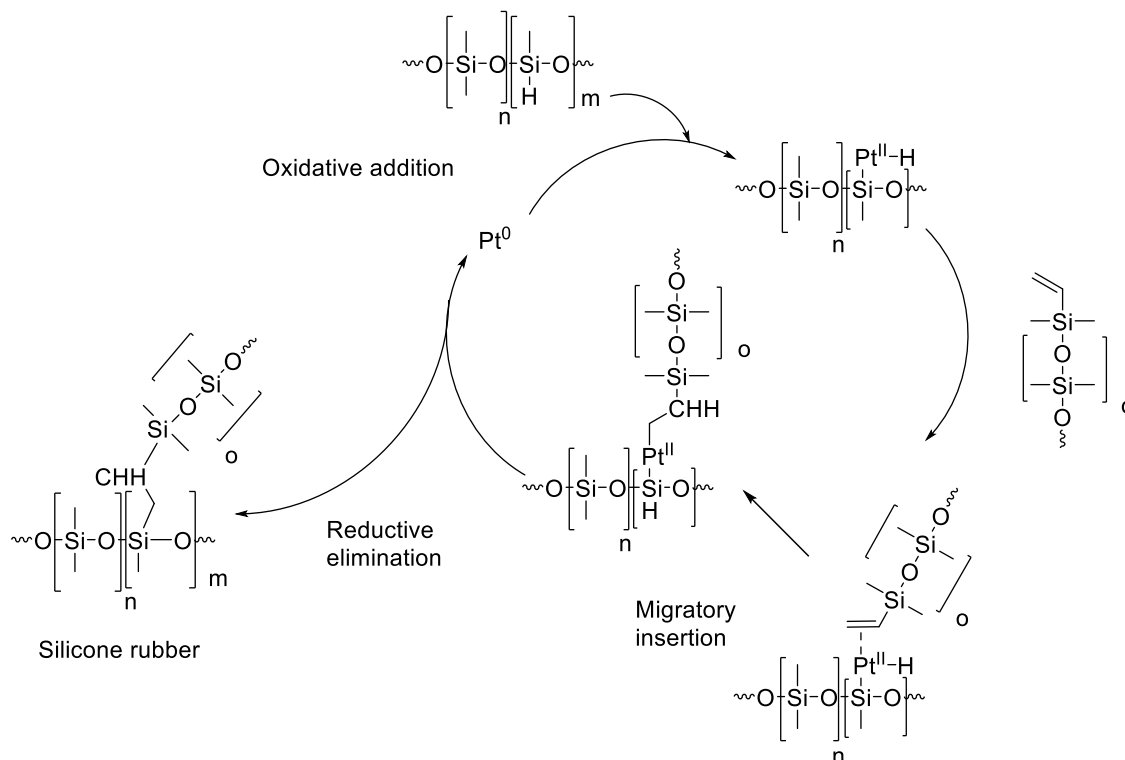


**Figure 28.** Catalytic cycle showing the Chalk-Harrod mechanism for hydrosilylation applied to silicone rubber components (alkene-terminated base polymer and hydride functionalised crosslinker). Mechanism adapted from Sugimoto et al.<sup>262</sup>

Silicone rubbers may be further functionalised with a variety of molecules depending on the desired application of the material.<sup>264–270</sup> This is particularly useful when designing medical devices, as despite the benefits of medical devices to patient health, they also present a route for opportunistic pathogens cause potentially life-threatening infections. Bacterial colonisation of medical devices can potentially lead to the formation of biofilms.<sup>271–276</sup> Despite the hydrophobic nature of silicone rubber, bacteria are able to associate with the surface. Once adhesion takes place, the adherent organisms may multiply, whilst also offering a route by which other microorganisms may more easily adhere, leading to the formation of mixed biofilms.<sup>277,278</sup> The eradication of mixed-species

biofilms is difficult via standard means due to the formation of a physical cellular matrix barrier and physiological interactions between the species. Preventing initial colonisation by bacteria is therefore vitally important. A discussion of doping silicone rubber with antimicrobial agents to prevent colonisation is presented in Chapter 4.

## Summary

The potential of NHCs and TSCs as ligands for the design of metallodrugs is highlighted above. The wide variety of structures and biological activities of the described complexes along with the seemingly endless potential ways in which to design ligand scaffolds to provide favourable biological interactions makes the usefulness of NHC- and TSC-based metallodrugs as potential future medicines clear. The ability to take a potentially biologically active ligand and afford it new properties by binding a therapeutic metal is invaluable, and may offer means by which to circumvent growing resistance to traditional antimicrobial agents amongst target organisms.

The work presented from hereon in will describe the design of novel antibacterial and antiparasitic metal complexes, and the later attempts to incorporate these to produce a novel biomaterial. Briefly, Chapter 2 will describe the synthesis and characterisation of novel long alkyl chain substituted Ag-NHCs, the surface activity of their precursor imidazolium salts, and the antibacterial activity of the Ag-NHC complexes and their precursors against a panel of Gram negative and Gram positive bacteria. Chapter 3 will discuss the synthesis and characterisation of first row transition metal M-BTSC complexes substituted with long alkyl chains. The activity of these complexes against the larval and adult stages of the parasitic worm *Schistosoma mansoni* is described. Chapter 4 will then focus on the development of a novel silicone rubber, and the attempts to incorporate Ag-NHCs, Cu-BTSCs, and esters of the ubiquitous antimicrobial triclosan into the material in order to produce biofouling resistant silicones which could potentially be applied to medical devices.

## References

- 1 G. Tsagkaropoulou, F. J. Allen, S. M. Clarke and P. J. Camp, *Soft Matter*, 2019, **15**, 8402–8411.
- 2 D. Fu, X. Gao, B. Huang, J. Wang, Y. Sun, W. Zhang, K. Kan, X. Zhang, Y. Xie and X. Sui, *RSC Adv.*, 2019, **9**, 28799–28807.
- 3 M. Kaur, G. Singh, A. Kaur, P. K. Sharma and T. S. Kang, *Langmuir*, 2019, **35**, 4085–4093.
- 4 K. Liu, L. Yang, X. Peng, H. Gong, J. Wang, J. R. Lu and H. Xu, *Langmuir*, 2020, **36**, 3531–3539.
- 5 J. M. Khan, A. Malik, M. Ahmad Khan, P. Sharma and P. Sen, *Colloids Surf. Physicochem. Eng. Asp.*, 2020, **586**, 124240.
- 6 Y. Huang, M. Guo, J. Tan and S. Feng, *Langmuir*, 2020, **36**, 2023–2029.
- 7 M. Yamada and K. Tanoue, *RSC Adv.*, 2019, **9**, 36416–36423.
- 8 J. E. Moore, T. M. McCoy, A. V. Sokolova, L. de Campo, G. R. Pearson, B. L. Wilkinson and R. F. Tabor, *J. Colloid Interface Sci.*, 2019, **547**, 275–290.
- 9 M. Poša and A. Pilipović, *J. Chem. Thermodyn.*, 2019, **138**, 167–178.
- 10 E. F. Busmann, D. G. Martínez, H. Lucas and K. Mäder, *Beilstein J. Nanotechnol.*, 2020, **11**, 213–224.
- 11 L. Ma, L. Bao, D. Hu, L. Zhao and T. Liu, *J. Supercrit. Fluids*, 2020, **158**, 104722.
- 12 Y. Gao, J. Chen, T. Zhang, J. E. S. Szymanowski, P. C. Burns and T. Liu, *Chem. – Eur. J.*, 2019, **25**, 15741–15745.
- 13 L. Wiehemeier, T. Brändel, Y. Hannappel, T. Kottke and T. Hellweg, *Soft Matter*, 2019, **15**, 5673–5684.
- 14 C. E. McNamee and H. Kawakami, *Langmuir*, 2020, **36**, 1887–1897.
- 15 C. A. Zentner, F. Anson, S. Thayumanavan and T. M. Swager, *J. Am. Chem. Soc.*, 2019, **141**, 18048–18055.
- 16 C. Yin, J. Fu and X. Lu, *Anal. Chim. Acta*, 2019, **1082**, 194–201.
- 17 T. Owen and A. Butler, *Coord. Chem. Rev.*, 2011, **225**, 678–687.
- 18 P. C. Griffiths, I. A. Fallis, C. James, I. R. Morgan, G. Brett, R. K. Heenan, R. Schweins, I. Grillo and A. Paul, *Soft Matter*, 2010, **6**, 1981–1989.
- 19 C. Schattschneider, S. Doniz Kettenmann, S. Hinojosa, J. Heinrich and N. Kulak, *Coord. Chem. Rev.*, 2019, **385**, 191–207.
- 20 P. C. Griffiths, I. A. Fallis, T. Chuenpratoom and R. Watanesk, *Adv. Colloid Interface Sci.*, 2006, **122**, 107–117.
- 21 J. N. Israelachvili, D. J. Mitchell and B. W. Ninham, *J. Chem. Soc. Faraday Trans. 2 Mol. Chem. Phys.*, 1976, **72**, 1525–1568.
- 22 J. Toro-Mendoza, G. Rodriguez-Lopez and O. Paredes-Altuve, *Phys. Chem. Chem. Phys.*, 2017, **19**, 9092–9095.
- 23 J. Xu, Y. Zhang, H. Chen, P. Wang, Z. Xie, Y. Yao, Y. Yan and J. Zhang, *J. Mol. Struct.*, 2013, **1052**, 50–56.
- 24 S. R. P. da Rocha, K. L. Harrison and K. P. Johnston, *Langmuir*, 1999, **15**, 419–428.
- 25 B. R. Bzdek, J. P. Reid, J. Malila and N. L. Prisle, *Proc. Natl. Acad. Sci.*, 2020, **117**, 8335–8343.
- 26 G. S. Aleiner and O. G. Us'yarov, *Colloid J.*, 2010, **72**, 588–594.
- 27 S. Mahbub, S. Akter, Luthfunnessa, P. Akter, M. A. Hoque, M. A. Rub, D. Kumar, Y. G. Alghamdi, A. M. Asiri and H. Džudžević-Čančar, *RSC Adv.*, 2020, **10**, 14531–14541.
- 28 B. Dong, N. Li, L. Zheng, L. Yu and T. Inoue, *Langmuir*, 2007, **23**, 4178–4182.
- 29 R. Nagarajan, *Langmuir*, 2002, **18**, 31–38.
- 30 O. G. Us'yarov, *Colloid J.*, 2007, **69**, 95–102.
- 31 D. Y. Pharr, *Phys. Sci. Rev.*, **2**, 7, id.6, 25pp.
- 32 J. Łuczak, C. Jungnickel, M. Joskowska, J. Thöming and J. Hupka, *J. Colloid Interface Sci.*, 2009, **336**, 111–116.
- 33 C. Tanford, *J. Phys. Chem.*, 1972, **76**, 3020–3024.

- 34 R. C. Oliver, J. Lipfert, D. A. Fox, R. H. Lo, S. Doniach and L. Columbus, *PLOS ONE*, 2013, **8**, e62488.
- 35 E. Mohajeri and G. Noudeh, *J. Chem.*, 2012, **9**, 2268–2274.
- 36 L. Magnus Bergström, *Curr. Opin. Colloid Interface Sci.*, 2016, **22**, 46–50.
- 37 J. Gao, W. Ge and J. Li, *Sci. China Ser. B Chem.*, 2005, **48**, 470–475.
- 38 P. Alexandridis, U. Olsson and B. Lindman, *Langmuir*, 1997, **13**, 23–34.
- 39 S. Jung, J. H. Kim, J. Kim, S. Choi, J. Lee, I. Park, T. Hyeon and D.-H. Kim, *Adv. Mater.*, 2014, **26**, 4825–4830.
- 40 J. Aguiar, P. Carpena, J. A. Molina-Bolívar and C. Carnero Ruiz, *J. Colloid Interface Sci.*, 2003, **258**, 116–122.
- 41 B. Rosenberg, L. Van Camp and T. Krigas, *Nature*, 1965, **205**, 698–699.
- 42 S. Dasari and P. B. Tchounwou, *Eur. J. Pharmacol.*, 2014, **0**, 364–378.
- 43 Chemical & Engineering News: Top Pharmaceuticals: Cisplatin, <http://pubs.acs.org/cen/coverstory/83/8325/8325cisplatin.html>, (accessed 13 April 2017).
- 44 G. Y. Ho, N. Woodward and J. I. G. Coward, *Crit. Rev. Oncol. Hematol.*, 2016, **102**, 37–46.
- 45 M. E. Suarez-Almazor, C. Spooner, E. Belseck and B. Shea, *Cochrane Database Syst. Rev.*, 2000, **2**, Art. No. CD002048. DOI:10.1002/14651858.CD002048.
- 46 C. L. Fox, *Arch. Surg. Chic. Ill 1960*, 1968, **96**, 184–188.
- 47 H. Khan, M. F. Khan and B. A. Khan, *Pharm. Chem. J.*, 2014, **48**, 269–272.
- 48 D. T. Ciccognani, G. Polson, D. Lei, K. DiNicola, R. Shalvoy, J. Arresse and G. Pierard, *J. Cosmet. Sci.*, 2004, **55**, 217–218.
- 49 M. Park, Y.-J. Cho, Y. W. Lee and W. H. Jung, *Sci. Rep.*, 2018, **8**, 12086.
- 50 E. Blumfield, D. W. Swenson, R. S. Iyer and A. L. Stanescu, *Pediatr. Radiol.*, 2019, **49**, 448–457.
- 51 D. Balériaux, C. Matos and D. De Greef, *Neuroradiology*, 1993, **35**, 490–494.
- 52 J. W. Copius Peereboom, *Sci. Total Environ.*, 1985, **42**, 1–27.
- 53 W. Maret, *Int. J. Mol. Sci.*, 2016, **17**, 66.
- 54 K. D. Mjos and C. Orvig, *Chem. Rev.*, 2014, **114**, 4540–4563.
- 55 E. J. Anthony, E. M. Bolitho, H. E. Bridgewater, O. W. L. Carter, J. M. Donnelly, C. Imberti, E. C. Lant, F. Lermyte, R. J. Needham, M. Palau, P. J. Sadler, H. Shi, F.-X. Wang, W.-Y. Zhang and Z. Zhang, *Chem. Sci.*, DOI:10.1039/D0SC04082G.
- 56 B. M. Zeglis, J. L. Houghton, M. J. Evans, N. Viola-Villegas and J. S. Lewis, *Inorg. Chem.*, 2014, **53**, 1880–1899.
- 57 R. K. Sodhi and S. Paul, *Cancer Ther. Oncol. Int. J.*, 2019, **14**, 1–8.
- 58 U. Ndagi, N. Mhlongo and M. E. Soliman, *Drug Des. Devel. Ther.*, 2017, **11**, 599–616.
- 59 C. Imberti and P. J. Sadler, in *Advances in Inorganic Chemistry*, eds. P. J. Sadler and R. van Eldik, Academic Press, 2020, vol. 75, pp. 3–56.
- 60 G. P. Moss, P. a. S. Smith and D. Tavernier, *Pure Appl. Chem.*, 1995, **67**, 1307–1375.
- 61 W. A. Herrmann and C. Köcher, *Angew. Chem. Int. Ed. Engl.*, 1997, **36**, 2162–2187.
- 62 F. E. Hahn and M. C. Jahnke, *Angew. Chem. Int. Ed.*, 2008, **47**, 3122–3172.
- 63 D. Bourissou, O. Guerret, F. P. Gabbaï and G. Bertrand, *Chem. Rev.*, 2000, **100**, 39–92.
- 64 G. B. Schuster, *Adv. Phys. Org. Chem.*, 1986, **22**, 311–361.
- 65 R. Hoffmann, *J. Am. Chem. Soc.*, 1968, **90**, 1475–1485.
- 66 E. O. Fischer and A. Maasböl, *Angew. Chem. Int. Ed. Engl.*, 1964, **3**, 580–581.
- 67 R. R. Schrock, *J. Am. Chem. Soc.*, 1974, **96**, 6796–6797.
- 68 K. Öfele, *J. Organomet. Chem.*, 1968, **12**, P42–P43.
- 69 P. de Frémont, N. Marion and S. P. Nolan, *Coord. Chem. Rev.*, 2009, **253**, 862–892.
- 70 J. B. Dumas and E. Péligot, *Ann Chim Phys*, 1835, **58**, 5.
- 71 A. Geuther, *Ann Chem Pharm*, 1862, **123**, 5.
- 72 E. Buchner and Th. Curtius, *Berichte Dtsch. Chem. Ges.*, 1885, **18**, 2377–2379.

- 73 H.-W. Wanzlick and E. Schikora, *Angew. Chem.*, 1960, **72**, 494–494.
- 74 D. M. Lemal, R. A. Lovald and K. I. Kawano, *J. Am. Chem. Soc.*, 1964, **86**, 2518–2519.
- 75 A. J. Arduengo, R. L. Harlow and M. Kline, *J. Am. Chem. Soc.*, 1991, **113**, 361–363.
- 76 H.-W. Wanzlick and H.-J. Schönherr, *Angew. Chem. Int. Ed. Engl.*, 1968, **7**, 141–142.
- 77 D. M. Khramov, V. M. Lynch and C. W. Bielawski, *Organometallics*, 2007, **26**, 6042–6049.
- 78 R. Sevinçek, H. Karabiyik and H. Karabiyik, *J. Mol. Model.*, 2013, **19**, 5327–5341.
- 79 H. V. Huynh, Y. Han, R. Jothibas and J. A. Yang, *Organometallics*, 2009, **28**, 5395–5404.
- 80 R. A. Kelly III, H. Clavier, S. Giudice, N. M. Scott, E. D. Stevens, J. Bordner, I. Samardjiev, C. D. Hoff, L. Cavallo and S. P. Nolan, *Organometallics*, 2008, **27**, 202–210.
- 81 S. Wolf and H. Plenio, *J. Organomet. Chem.*, 2009, **694**, 1487–1492.
- 82 H. M. J. Wang and I. J. B. Lin, *Organometallics*, 1998, **17**, 972–975.
- 83 F. Almalioti, J. MacDougall, S. Hughes, M. M. Hasson, R. L. Jenkins, B. D. Ward, G. J. Tizzard, S. J. Coles, D. W. Williams, S. Bamford, I. A. Fallis and A. Dervisi, *Dalton Trans.*, 2013, **42**, 12370–12380.
- 84 P. Marshall, R. L. Jenkins, W. Clegg, R. W. Harrington, S. K. Callear, S. J. Coles, I. A. Fallis and A. Dervisi, *Dalton Trans.*, 2012, **41**, 12839–12846.
- 85 M. Iglesias, D. J. Beetstra, J. C. Knight, L.-L. Ooi, A. Stasch, S. Coles, L. Male, M. B. Hursthouse, K. J. Cavell, A. Dervisi and I. A. Fallis, *Organometallics*, 2008, **27**, 3279–3289.
- 86 A. Kascatan-Nebioglu, A. Melaiye, K. Hindi, S. Durmus, M. J. Panzner, L. A. Hogue, R. J. Mallett, C. E. Hovis, M. Coughenour, S. D. Crosby, A. Milsted, D. L. Ely, C. A. Tessier, C. L. Cannon and W. J. Youngs, *J. Med. Chem.*, 2006, **49**, 6811–6818.
- 87 K. M. Hindi, T. J. Siciliano, S. Durmus, M. J. Panzner, D. A. Medvetz, D. V. Reddy, L. A. Hogue, C. E. Hovis, J. K. Hilliard, R. J. Mallett, C. A. Tessier, C. L. Cannon and W. J. Youngs, *J. Med. Chem.*, 2008, **51**, 1577–1583.
- 88 J. G. Leid, A. J. Ditto, A. Knapp, P. N. Shah, B. D. Wright, R. Blust, L. Christensen, C. B. Clemons, J. P. Wilber, G. W. Young, A. G. Kang, M. J. Panzner, C. L. Cannon, Y. H. Yun, W. J. Youngs, N. M. Seckinger and E. K. Cope, *J. Antimicrob. Chemother.*, 2012, **67**, 138–148.
- 89 M. J. Panzner, A. Deeraksa, A. Smith, B. D. Wright, K. M. Hindi, A. Kascatan-Nebioglu, A. G. Torres, B. M. Judy, C. E. Hovis, J. K. Hilliard, R. J. Mallett, E. Cope, D. M. Estes, C. L. Cannon, J. G. Leid and W. J. Youngs, *Eur. J. Inorg. Chem.*, 2009, **2009**, 1739–1745.
- 90 A. A. D. Tulloch, A. A. Danopoulos, S. Winston, S. Kleinhenz and G. Eastham, *J. Chem. Soc. Dalton Trans.*, 2000, 4499–4506.
- 91 A. Kunduracioğlu, Ö. Tamer, D. Avcı, İ. Kani, Y. Atalay and B. Çetinkaya, *Spectrochim. Acta. A. Mol. Biomol. Spectrosc.*, 2014, **121**, 35–45.
- 92 Y. Gök, S. Akkoç, Ö. Ö. Çelikal, İ. Özdemir and S. Günal, *Arab. J. Chem.*, 2019, **12**, 2513–2518.
- 93 S. Hohloch, N. Deibel, D. Schweinfurth, W. Frey and B. Sarkar, *Eur. J. Inorg. Chem.*, 2014, **2014**, 2131–2139.
- 94 Y. Li, J. Tang, J. Gu, Q. Wang, P. Sun and D. Zhang, *Organometallics*, 2014, **33**, 876–884.
- 95 A. J. Boydston, J. D. Rice, M. D. Sanderson, O. L. Dykhno and C. W. Bielawski, *Organometallics*, 2006, **25**, 6087–6098.
- 96 W. P. Fehlhammer, T. Bliss, U. Kernbach and I. Brüdgam, *J. Organomet. Chem.*, 1995, **490**, 149–153.
- 97 H. Schneider, D. Schmidt and U. Radius, *Chem. – Eur. J.*, 2015, **21**, 2793–2797.
- 98 A. J. Arduengo, R. Krafczyk, R. Schmutzler, H. A. Craig, J. R. Goerlich, W. J. Marshall and M. Unverzagt, *Tetrahedron*, 1999, **55**, 14523–14534.

- 99 A. J. Arduengo, H. V. R. Dias, R. L. Harlow and M. Kline, *J. Am. Chem. Soc.*, 1992, **114**, 5530–5534.
- 100 M. J. Saif and K. R. Flower, *Transit. Met. Chem.*, 2013, **38**, 113–118.
- 101 T. Scattolin, N. V. Tzouras, L. Falivene, L. Cavallo and S. P. Nolan, *Dalton Trans.*, 2020, **49**, 9694–9700.
- 102 J. M. Hayes, M. Viciano, E. Peris, G. Ujaque and A. Lledós, *Organometallics*, 2007, **26**, 6170–6183.
- 103 S. Hameury, P. de Fremont, P.-A. R. Breuil, H. Olivier-Bourbigou and P. Braunstein, *Dalton Trans.*, 2014, **43**, 4700–4710.
- 104 R. A. Haque, A. W. Salman, S. Budagumpi, A. A.-A. Abdullah and A. M. S. A. Majid, *Metallomics*, 2013, **5**, 760–769.
- 105 I. Benaissa, R. Taakili, N. Lugan and Y. Canac, *Dalton Trans.*, 2017, **46**, 12293–12305.
- 106 C. Gibard, D. Avignant, F. Cisnetti and A. Gautier, *Organometallics*, 2012, **31**, 7902–7908.
- 107 B. R. M. Lake and C. E. Willans, *Organometallics*, 2014, **33**, 2027–2038.
- 108 E. Schuh, C. Pflüger, A. Citta, A. Folda, M. P. Rigobello, A. Bindoli, A. Casini and F. Mohr, *J. Med. Chem.*, 2012, **55**, 5518–5528.
- 109 T. Zou, C. T. Lum, S. S.-Y. Chui and C.-M. Che, *Angew. Chem. Int. Ed.*, 2013, **52**, 2930–2933.
- 110 S. Y. Hussaini, R. A. Haque, T. Fatima, M. T. Agha, A. M. S. A. Majid and M. R. Razali, *J. Coord. Chem.*, 2018, **71**, 2787–2799.
- 111 J. C. Bernhammer and H. V. Huynh, *Organometallics*, 2014, **33**, 172–180.
- 112 A. Volpe, S. Baldino, C. Tubaro, W. Baratta, M. Basato and C. Graiff, *Eur. J. Inorg. Chem.*, 2016, **2016**, 247–251.
- 113 C. Y. Chan and P. J. Barnard, *Dalton Trans.*, 2015, **44**, 19126–19140.
- 114 L. Boubakri, A. Chakchouk-Mtibaa, A. S. Al-Ayed, L. Mansour, N. Abutaha, A. Halim Harrath, L. Mellouli, I. Özdemir, S. Yasar and N. Hamdi, *RSC Adv.*, 2019, **9**, 34406–34420.
- 115 D. Enders, K. Breuer, G. Raabe, J. Runsink, J. H. Teles, J.-P. Melder, K. Ebel and S. Brode, *Angew. Chem. Int. Ed. Engl.*, 1995, **34**, 1021–1023.
- 116 N. Kuhn and T. Kratz, *Synthesis*, 1993, **1993**, 561–562.
- 117 B. Çetinkaya, E. Çetinkaya, H. Küçükbay and R. Durmaz, *Arzneim.-Forschung Drug Res.*, 1996, **46**, 821–823.
- 118 B. Çetinkaya, I. Özdemir, B. Binbaşıoğlu, R. Durmaz and S. Günal, *Arzneim.-Forschung Drug Res.*, 1999, **49**, 538–540.
- 119 N. Y. S. Lam, D. Truong, H. Burmeister, M. V. Babak, H. U. Holtkamp, S. Movassaghi, D. M. Ayine-Tora, A. Zafar, M. Kubanik, L. Oehninger, T. Söhnel, J. Reynisson, S. M. F. Jamieson, C. Gaiddon, I. Ott and C. G. Hartinger, *Inorg. Chem.*, 2018, **57**, 14427–14434.
- 120 L. Guo, G. Lv, L. Qiu, H. Yang, L. Zhang, H. Yu, M. Zou and J. Lin, *Eur. J. Pharmacol.*, 2016, **786**, 60–71.
- 121 M. P. Sullivan, M. K. Nieuwoudt, G. A. Bowmaker, N. Y. S. Lam, D. Truong, D. C. Goldstone and C. G. Hartinger, *Chem. Commun.*, 2018, **54**, 6120–6123.
- 122 S. Movassaghi, S. Singh, A. Mansur, K. K. H. Tong, M. Hanif, H. U. Holtkamp, T. Söhnel, S. M. F. Jamieson and C. G. Hartinger, *Organometallics*, 2018, **37**, 1575–1584.
- 123 W. Streciwilk, A. Terenzi, R. Misgeld, C. Frias, P. G. Jones, A. Prokop, B. K. Keppler and I. Ott, *ChemMedChem*, 2017, **12**, 214–225.
- 124 W. Streciwilk, A. Terenzi, F. Lo Nardo, P. Prochnow, J. E. Bandow, B. K. Keppler and I. Ott, *Eur. J. Inorg. Chem.*, 2018, **2018**, 3104–3112.
- 125 G. Lv, L. Guo, L. Qiu, H. Yang, T. Wang, H. Liu and J. Lin, *Dalton Trans.*, 2015, **44**, 7324–7331.
- 126 J. R. McConnell, D. P. Rananaware, D. M. Ramsey, K. N. Buys, M. L. Cole and S. R. McAlpine, *Bioorg. Med. Chem. Lett.*, 2013, **23**, 2527–2531.

- 127L. Oehninger, S. Spreckelmeyer, P. Holenya, S. M. Meier, S. Can, H. Alborzina, J. Schur, B. K. Keppler, S. Wölfl and I. Ott, *J. Med. Chem.*, 2015, **58**, 9591–9600.
- 128J.-J. Zhang, J. K. Muenzner, M. A. A. el Maaty, B. Karge, R. Schobert, S. Wölfl and I. Ott, *Dalton Trans.*, 2016, **45**, 13161–13168.
- 129P. V. Simpson, C. Schmidt, I. Ott, H. Bruhn and U. Schatzschneider, *Eur. J. Inorg. Chem.*, 2013, **2013**, 5547–5554.
- 130T. Rehm, M. Rothemund, J. K. Muenzner, A. Noor, R. Kempe and R. Schobert, *Dalton Trans.*, 2016, **45**, 15390–15398.
- 131M. Rothemund, S. I. Bär, T. Rehm, H. Kostrhunova, V. Brabec and R. Schobert, *Dalton Trans.*, 2020, **49**, 8901–8910.
- 132S. B. Aher, P. N. Muskawar, K. Thenmozhi and P. R. Bhagat, *Eur. J. Med. Chem.*, 2014, **81**, 408–419.
- 133W. Liu and R. Gust, *Coord. Chem. Rev.*, 2016, **329**, 191–213.
- 134S. Bellemin-Laponnaz, *Eur. J. Inorg. Chem.*, 2020, **2020**, 10–20.
- 135Y. Han, X. Liu, Z. Tian, X. Ge, J. Li, M. Gao, Y. Li, Y. Liu and Z. Liu, *Chem. – Asian J.*, 2018, **13**, 3697–3705.
- 136H. Huang, S. Banerjee and P. J. Sadler, *ChemBioChem*, 2018, **19**, 1574–1589.
- 137Y. Gothe, T. Marzo, L. Messori and N. Metzler-Nolte, *Chem. – Eur. J.*, 2016, **22**, 12487–12494.
- 138C. Wang, J. Liu, Z. Tian, M. Tian, L. Tian, W. Zhao and Z. Liu, *Dalton Trans.*, 2017, **46**, 6870–6883.
- 139T.-L. Ho, H. C. Ho and L. D. Hamilton, *Chem. Biol. Interact.*, 1978, **23**, 65–84.
- 140K. L. Haas and K. J. Franz, *Chem. Rev.*, 2009, **109**, 4921–4960.
- 141A. Sasidharan, J. E. Riviere and N. A. Monteiro-Riviere, *J. Mater. Chem. B*, 2015, **3**, 2075–2082.
- 142H. J. Johnston, G. Hutchison, F. M. Christensen, S. Peters, S. Hankin and V. Stone, *Crit. Rev. Toxicol.*, 2010, **40**, 328–346.
- 143A. D. Russell and W. B. Hugo, *Prog. Med. Chem.*, 1994, **31**, 351–370.
- 144A. Giorgio and A. Merlino, *Coord. Chem. Rev.*, 2020, **407**, 213175.
- 145S. Gromer, L. D. Arscott, C. H. Williams Jr., R. H. Schirmer and K. Becker, *J. Biol. Chem.*, 1998, **273**, 20096–20101.
- 146K. Becker, S. Gromer, R. Heiner Schirmer and S. Müller, *Eur. J. Biochem.*, 2000, **267**, 6118–6125.
- 147Y. Cheng and Y. Qi, *Anticancer Agents Med. Chem.*, 2017, **17**, 1046–1069.
- 148V. Gandin and A. P. Fernandes, *Molecules*, 2015, **20**, 12732–12756.
- 149J. L. Hickey, R. A. Ruhayel, P. J. Barnard, M. V. Baker, S. J. Berners-Price and A. Filipovska, *J. Am. Chem. Soc.*, 2008, **130**, 12570–12571.
- 150P. J. Barnard, M. V. Baker, S. J. Berners-Price and D. A. Day, *J. Inorg. Biochem.*, 2004, **98**, 1642–1647.
- 151M. V. Baker, P. J. Barnard, S. J. Berners-Price, S. K. Brayshaw, J. L. Hickey, B. W. Skelton and A. H. White, *Dalton Trans.*, 2006, 3708–3715.
- 152R. Rubbiani, S. Can, I. Kitanovic, H. Alborzina, M. Stefanopoulou, M. Kokoschka, S. Mönchgesang, W. S. Sheldrick, S. Wölfl and I. Ott, *J. Med. Chem.*, 2011, **54**, 8646–8657.
- 153R. Rubbiani, I. Kitanovic, H. Alborzina, S. Can, A. Kitanovic, L. A. Onambele, M. Stefanopoulou, Y. Geldmacher, W. S. Sheldrick, G. Wolber, A. Prokop, S. Wölfl and I. Ott, *J. Med. Chem.*, 2010, **53**, 8608–8618.
- 154A. Pratesi, C. Gabbiani, E. Michelucci, M. Ginanneschi, A. M. Papini, R. Rubbiani, I. Ott and L. Messori, *J. Inorg. Biochem.*, 2014, **136**, 161–169.
- 155R. Rubbiani, L. Salassa, A. de Almeida, A. Casini and I. Ott, *ChemMedChem*, 2014, **9**, 1205–1210.
- 156X. Cheng, P. Holenya, S. Can, H. Alborzina, R. Rubbiani, I. Ott and S. Wölfl, *Mol. Cancer*, 2014, **13**, 1–15.
- 157W. Liu, K. Bendorf, M. Proetto, A. Hagenbach, U. Abram and R. Gust, *J. Med. Chem.*, 2012, **55**, 3713–3724.

- 158C. Schmidt, B. Karge, R. Misgeld, A. Prokop, R. Franke, M. Brönstrup and I. Ott, *Chem. – Eur. J.*, 2017, **23**, 1869–1880.
- 159C. Zhang, S. Bourgeade Delmas, Á. Fernández Álvarez, A. Valentin, C. Hemmert and H. Gornitzka, *Eur. J. Med. Chem.*, 2018, **143**, 1635–1643.
- 160P. Holenya, S. Can, R. Rubbiani, H. Alborzinia, A. Jünger, X. Cheng, I. Ott and S. Wölfl, *Metallomics*, 2014, **6**, 1591–1601.
- 161W. Walther, O. Dada, I. Ott, A. Prochnicka, B. Büttner, X. Zhu and M. Tacke, *Trends Cancer Res.*, 2018, **13**, 63.
- 162W. Walther, O. Dada, C. O’Beirne, I. Ott, G. Sánchez, C. Schmidt, C. Werner, X. Zhu and M. Tacke, *Lett. Drug Des. Discov.*, 2017, **14**, 2, 125–134.
- 163W. Liu, K. Bendorf, M. Proetto, U. Abram, A. Hagenbach and R. Gust, *J. Med. Chem.*, 2011, **54**, 8605–8615.
- 164L. Messori, L. Marchetti, L. Massai, F. Scaletti, A. Guerri, I. Landini, S. Nobili, G. Perrone, E. Mini, P. Leoni, M. Pasquali and C. Gabbiani, *Inorg. Chem.*, 2014, **53**, 2396–2403.
- 165D. Wragg, A. de Almeida, R. Bonsignore, F. E. Kühn, S. Leoni and A. Casini, *Angew. Chem. Int. Ed.*, 2018, **57**, 14524–14528.
- 166C. Schmidt, L. Albrecht, S. Balasupramaniam, R. Misgeld, B. Karge, M. Brönstrup, A. Prokop, K. Baumann, S. Reichl and I. Ott, *Metallomics*, 2019, **11**, 533–545.
- 167T. Zou, C. T. Lum, C.-N. Lok, W.-P. To, K.-H. Low and C.-M. Che, *Angew. Chem. Int. Ed.*, 2014, **53**, 5810–5814.
- 168R. W.-Y. Sun, M. Zhang, D. Li, Z.-F. Zhang, H. Cai, M. Li, Y.-J. Xian, S. W. Ng and A. S.-T. Wong, *Chem. – Eur. J.*, 2015, **21**, 18534–18538.
- 169C. Hemmert, A. P. Ramadani, L. Boselli, Á. Fernández Álvarez, L. Paloque, J.-M. Augereau, H. Gornitzka and F. Benoit-Vical, *Bioorg. Med. Chem.*, 2016, **24**, 3075–3082.
- 170N. A. Johnson, M. R. Southerland and W. J. Youngs, *Molecules*, 2017, **22**, 1263.
- 171D. A. Medvetz, K. M. Hindi, M. J. Panzner, A. J. Ditto, Y. H. Yun and W. J. Youngs, *Met.-Based Drugs*, 2008, **2008**, 384010.
- 172M. Tacke, *J. Organomet. Chem.*, 2015, **782**, 17–21.
- 173S. Patil, J. Claffey, A. Deally, M. Hogan, B. Gleeson, L. M. M. Mendez, H. Mueller-Bunz, F. Paradisi and M. Tacke, *Eur. J. Inorg. Chem.*, 2010, 1020–1031.
- 174F. Hackenberg and M. Tacke, *Dalton Trans.*, 2014, **43**, 8144–8153.
- 175I. Fichtner, J. Cinatl, M. Michaelis, L. Sanders, R. Hilger, B. Kennedy, A. Reynolds, F. Hackenberg, G. Lally, S. Quinn, I. McRae and M. Tacke, *Lett. Drug Des. Discov.*, 2012, **9**, 815–822.
- 176F. Hackenberg, G. Lally, H. Müller-Bunz, F. Paradisi, D. Quaglia, W. Streciwilk and M. Tacke, *Inorganica Chim. Acta*, 2013, **395**, 135–144.
- 177W. Streciwilk, J. Cassidy, F. Hackenberg, H. Müller-Bunz, F. Paradisi and M. Tacke, *J. Organomet. Chem.*, 2014, **749**, 88–99.
- 178H. Zetty Zulikha, R. A. Haque, S. Budagumpi and A. M. S. Abdul Majid, *Inorganica Chim. Acta*, 2014, **411**, 40–47.
- 179V. Gandin, M. Pellei, M. Marinelli, C. Marzano, A. Dolmella, M. Giorgetti and C. Santini, *J. Inorg. Biochem.*, 2013, **129**, 135–144.
- 180M. Pellei, V. Gandin, M. Marinelli, C. Marzano, M. Yousufuddin, H. V. R. Dias and C. Santini, *Inorg. Chem.*, 2012, **51**, 9873–9882.
- 181M. Marinelli, M. Pellei, C. Cimorelli, H. V. R. Dias, C. Marzano, F. Tisato, M. Porchia, V. Gandin and C. Santini, *J. Organomet. Chem.*, 2016, **806**, 45–53.
- 182C. R. Shahini, G. Achar, S. Budagumpi, M. Tacke and S. A. Patil, *Appl. Organomet. Chem.*, 2017, **31**, e3819.
- 183M. Monticelli, S. Bellemin-Laponnaz, C. Tubaro and M. Rancan, *Eur. J. Inorg. Chem.*, 2017, **2017**, 2488–2495.
- 184L. Eloy, A.-S. Jarrousse, M.-L. Teyssot, A. Gautier, L. Morel, C. Jolival, T. Cresteil and S. Roland, *ChemMedChem*, 2012, **7**, 805–814.

- 185A. Citta, E. Schuh, F. Mohr, A. Folda, M. L. Massimino, A. Bindoli, A. Casini and M. P. Rigobello, *Metallomics*, 2013, **5**, 1006–1015.
- 186M. Pellei, V. Gandin, M. Marinelli, A. Orsetti, F. D. Bello, C. Santini and C. Marzano, *Dalton Trans.*, 2015, **44**, 21041–21052.
- 187M. E. Garner, W. Niu, X. Chen, I. Ghiviriga, K. A. Abboud, W. Tan and A. S. Veige, *Dalton Trans.*, 2014, **44**, 1914–1923.
- 188A. H. Sandtorv, C. Leitch, S. L. Bedringaas, B. T. Gjertsen and H.-R. Bjørsvik, *ChemMedChem*, 2015, **10**, 1522–1527.
- 189H. A. Mohamed, B. R. M. Lake, T. Laing, R. M. Phillips and C. E. Willans, *Dalton Trans.*, 2015, **44**, 7563–7569.
- 190G. Achar, S. C. R, S. A. Patil, J. G. Małeckı and S. Budagumpi, *New J. Chem.*, 2019, **43**, 1216–1229.
- 191S. Şahin-Bölükbaşı and N. Şahin, *J. Organomet. Chem.*, 2019, **891**, 78–84.
- 192M. Atif, H. N. Bhatti, R. A. Haque, M. A. Iqbal, M. B. Ahamed Khadeer and A. M. S. A. Majid, *Appl. Biochem. Biotechnol.*, 2020, **191**, 1171–1189.
- 193X. Liang, S. Luan, Z. Yin, M. He, C. He, L. Yin, Y. Zou, Z. Yuan, L. Li, X. Song, C. Lv and W. Zhang, *Eur. J. Med. Chem.*, 2018, **157**, 62–80.
- 194T. Zou, C.-N. Lok, P.-K. Wan, Z.-F. Zhang, S.-K. Fung and C.-M. Che, *Curr. Opin. Chem. Biol.*, 2018, **43**, 30–36.
- 195S. A. Patil, S. A. Patil, R. Patil, R. S. Keri, S. Budagumpi, G. R. Balakrishna and M. Tacke, *Future Med. Chem.*, 2015, **7**, 1305–1333.
- 196E. Namiecinska, M. Sobiesiak, M. Malecka, P. Guga, B. Rozalska and E. Budzisz, *Curr. Med. Chem.*, 2019, **26**, 664–693.
- 197T. S. Lobana, S. Khanna, R. Sharma, G. Hundal, R. Sultana, M. Chaudhary, R. J. Butcher and A. Castineiras, *Cryst. Growth Des.*, 2008, **8**, 1203–1212.
- 198D. S. Kalinowski and D. R. Richardson, *Pharmacol. Rev.*, 2005, **57**, 547–583.
- 199Z. A. Kaplancıklı, M. D. Altıntop, B. Sever, Z. Cantürk and A. Özdemir, *Journal of Chemistry*, 2016, Article ID 1692540, 7 pages.
- 200M. Kalhor, M. Shabani, I. Nikokar and S. Reyhaneh Banisaeed, *Iran. J. Pharm. Res. IJPR*, 2015, **14**, 67–75.
- 201R. A. Rane, S. S. Naphade, P. K. Bangalore, M. B. Palkar, M. S. Shaikh and R. Karpoomath, *Bioorg. Med. Chem. Lett.*, 2014, **24**, 3079–3083.
- 202G. P. Volynets, M. A. Tukalo, V. G. Bdzhola, N. M. Derkach, M. I. Gumeniuk, S. S. Tarnavskiy, S. A. Starosyla and S. M. Yarmoluk, *J. Antibiot. (Tokyo)*, 2019, **72**, 218–224.
- 203Y. Matsuo, *Jpn. J. Microbiol.*, 1971, **15**, 93–94.
- 204S. Sardari, S. Feizi, A. H. Rezayan, P. Azerang, S. mohammad Shahcheragh, G. Ghavami and A. Habibi, *Iran. J. Pharm. Res. IJPR*, 2017, **16**, 1128–1140.
- 205B. Silva, P. Sales, A. José Romanha, S. Murta, C. Lima, M. Albuquerque, E. D'Elia, J. Aquino, V. Ferreira, F. Silva, A. Pinto and B. Silva, *Med. Chem.*, 2019, **15**, 240–256.
- 206R. Matsa, P. Makam, M. Kaushik, S. L. Hoti and T. Kannan, *Eur. J. Pharm. Sci.*, 2019, **137**, 104986.
- 207A. Rao, J. Mcfadzean and K. Kamalakshi, *Lancet*, 1966, **1**, 1068–1072.
- 208S. Arora, S. Agarwal and S. Singhal, *Int. J. Pharm. Pharm. Sci.*, 2014, **6**, 34–41.
- 209M. X. Li, C. L. Chen, D. Zhang, J. Y. Niu and B. S. Ji, *Eur. J. Med. Chem.*, 2010, **45**, 3169–3177.
- 210F. Bisceglie, M. Baldini, M. Belicchi-Ferrari, E. Buluggiu, M. Careri, G. Pelosi, S. Pinelli and P. Tarasconi, *Eur. J. Med. Chem.*, 2007, **42**, 627–634.
- 211E. Pahontu, F. Julea, T. Rosu, V. Purcarea, Y. Chumakov, P. Petrenco and A. Gulea, *J. Cell. Mol. Med.*, 2015, **19**, 865–878.
- 212M. Belicchi Ferrari, F. Bisceglie, G. Pelosi, P. Tarasconi, R. Albertini, P. P. Dall'Aglio, S. Pinelli, A. Bergamo and G. Sava, *J. Inorg. Biochem.*, 2004, **98**, 301–312.
- 213M. Baldini, M. Belicchi-Ferrari, F. Bisceglie, P. P. Dall'Aglio, G. Pelosi, S. Pinelli and P. Tarasconi, *Inorg. Chem.*, 2004, **43**, 7170–7179.

- 214M. Baldini, M. Belicchi-Ferrari, F. Bisceglie, S. Capacchi, G. Pelosi and P. Tarasconi, *J. Inorg. Biochem.*, 2005, **99**, 1504–1513.
- 215N. A. Lewis, F. Liu, L. Seymour, A. Magnusen, T. R. Erves, J. F. Arca, F. A. Beckford, R. Venkatraman, A. González-Sarrías, F. R. Fronczek, D. G. VanDerveer, N. P. Seeram, A. Liu, W. L. Jarrett and A. A. Holder, *Eur. J. Inorg. Chem.*, 2012, **2012**, 664–677.
- 216C. R. Kowol, R. Berger, R. Eichinger, A. Roller, M. A. Jakupec, P. P. Schmidt, V. B. Arion and B. K. Keppler, *J. Med. Chem.*, 2007, **50**, 1254–1265.
- 217E. Ramachandran, P. Kalaivani, R. Prabhakaran, N. P. Rath, S. Brinda, P. Poornima, V. V. Padma and K. Natarajan, *Metallomics*, 2012, **4**, 218–227.
- 218M. S. Hossain, P. K. Roy, C. M. Zakaria and M. Kudrat-E-Zahan, *Int. J. Chem. Stud.*, 2018, **6**, 19–31.
- 219D. Rogolino, A. Gatti, M. Carcelli, G. Pelosi, F. Bisceglie, F. M. Restivo, F. Degola, A. Buschini, S. Montalbano, D. Feretti and C. Zani, *Sci. Rep.*, 2017, **7**, 11214.
- 220P. Jain, D. Kumar, S. Chandra and N. Misra, *Appl. Organomet. Chem.*, 2020, **34**, e5371.
- 221L. de P. Fernandes, J. M. B. Silva, D. O. S. Martins, M. B. Santiago, C. H. G. Martins, A. C. G. Jardim, G. S. Oliveira, M. Pivatto, R. A. C. Souza, E. de F. Franca, V. M. Deflon, A. E. H. Machado and C. G. Oliveira, *Int. J. Mol. Sci.*, 2020, **21**, 8355.
- 222D. Bahl, F. Athar, M. B. P. Soares, M. S. de Sá, D. R. M. Moreira, R. M. Srivastava, A. C. L. Leite and A. Azam, *Bioorg. Med. Chem.*, 2010, **18**, 6857–6864.
- 223M. Haeili, C. Moore, C. J. C. Davis, J. B. Cochran, S. Shah, T. B. Shrestha, Y. Zhang, S. H. Bossmann, W. H. Benjamin, O. Kutsch and F. Wolschendorf, *Antimicrob. Agents Chemother.*, 2014, **58**, 3727–3736.
- 224K. Y. Djoko, M. M. Goytia, P. S. Donnelly, M. A. Schembri, W. M. Shafer and A. G. McEwan, *Antimicrob. Agents Chemother.*, 2015, **59**, 6444–6453.
- 225K. Y. Djoko, B. M. Paterson, P. S. Donnelly and A. G. McEwan, *Metallomics*, 2014, **6**, 854–863.
- 226A. B. M Ibrahim, M. K. Farh, J. R. Plaisier and E. M. Shalaby, *Future Med. Chem.*, 2018, **10**, 2507–2519.
- 227S. Gu, P. Yu, J. Hu, Y. Liu, Z. Li, Y. Qian, Y. Wang, Y. Gou and F. Yang, *Eur. J. Med. Chem.*, 2019, **164**, 654–664.
- 228N. P. Prajapati and H. D. Patel, *Synth. Commun.*, 2019, **49**, 2767–2804.
- 229B. Shakya and P. N. Yadav, *Mini Rev. Med. Chem.*, 2020, **20**, 638–661.
- 230H. A. El-Ghamry, M. Gaber and T. A. Farghaly, *Mini Rev. Med. Chem.*, 2019, **19**, 1068–1079.
- 231K. L. Summers, *Mini Rev. Med. Chem.*, 2019, **19**, 569–590.
- 232L. S. Nair and C. T. Laurencin, *Prog. Polym. Sci.*, 2007, **32**, 762–798.
- 233M. Long and H. J. Rack, *Biomaterials*, 1998, **19**, 1621–1639.
- 234R. Langer and D. A. Tirrell, *Nature*, 2004, **428**, 487–492.
- 235M. C. Hehemann, M. Towe, L. M. Huynh, F. M. El-Khatib and F. A. Yafi, *Sex. Med. Rev.*, 2019, **7**, 535–547.
- 236A. Xiao, C. Dhand, C. M. Leung, R. W. Beuerman, S. Ramakrishna and R. Lakshminarayanan, *J. Mater. Chem. B*, 2018, **6**, 2171–2186.
- 237A. Mitra, S. Choudhary, H. Garg and J. H.G., *J. Clin. Diagn. Res. JCDR*, 2014, **8**, ZE08-ZE13.
- 238F. G. Menezes, L. Corrêa, J. O. Medina-Pestana, W. F. Aguiar and L. F. A. Camargo, *Transpl. Infect. Dis.*, 2019, **21**, e13031.
- 239F. R. Jackaman, J. N. Francis and B. R. Hopkinson, *Ann. R. Coll. Surg. Engl.*, 1980, **62**, 386–387.
- 240P. Mazurek, S. Vudayagiri and A. L. Skov, *Chem. Soc. Rev.*, 2019, **48**, 1448–1464.
- 241D. Wang, J. Klein and E. Mejía, *Chem. – Asian J.*, 2017, **12**, 1180–1197.
- 242M. L. Dunham, D. L. Bailey and R. Y. Mixer, *Ind. Eng. Chem.*, 1957, **49**, 1373–1376.
- 243G. Baquey, L. Moine, O. Babot, M. Degueil and B. Maillard, *Polymer*, 2005, **46**, 6283–6292.

- 244A. M. Bueche, *Rubber Chem. Technol.*, 1955, **28**, 865–877.
- 245E. Blasco, M. Wegener and C. Barner-Kowollik, *Adv. Mater.*, 2017, **29**, 1604005.
- 246J. Cervantes, R. Zárraga and C. Salazar-Hernández, *Appl. Organomet. Chem.*, 2012, **26**, 157–163.
- 247R. Murai, S. Takahashi, S. Tanabe and I. Takeuchi, *Mar. Pollut. Bull.*, 2005, **51**, 940–949.
- 248A. C. A. Sousa, M. R. Pastorinho, S. Takahashi and S. Tanabe, *Environ. Chem. Lett.*, 2014, **12**, 117–137.
- 249United States, US5908909A, 1999.
- 250United States, US20140045969A1, 2014.
- 251World Intellectual Property Organization, WO2013036546A2, 2013.
- 252World Intellectual Property Organization, WO2005108498A1, 2005.
- 253A. Yamamoto and S. Kambara, *J. Am. Chem. Soc.*, 1957, **79**, 4344–4348.
- 254World Intellectual Property Organization, WO2009103894A1, 2009.
- 255G. Berthon-Gelloz, O. Buisine, J.-F. Brière, G. Michaud, S. Stérin, G. Mignani, B. Tinant, J.-P. Declercq, D. Chapon and I. E. Markó, *J. Organomet. Chem.*, 2005, **690**, 6156–6168.
- 256H. K. Carroll, F. G. L. Parlane, N. Reich, B. J. Jelier and C. D. Montgomery, *Inorganica Chim. Acta*, 2017, **465**, 78–83.
- 257J. J. Dunsford, K. J. Cavell and B. Kariuki, *J. Organomet. Chem.*, 2011, **696**, 188–194.
- 258T. Galeandro-Diamant, M.-L. Zanota, R. Sayah, L. Veyre, C. Nikitine, C. de Bellefon, S. Marrot, V. Meille and C. Thieuleux, *Chem. Commun.*, 2015, **51**, 16194–16196.
- 259T. Iimura, N. Akasaka and T. Iwamoto, *Organometallics*, 2016, **35**, 4071–4076.
- 260G. De Bo, G. Berthon-Gelloz, B. Tinant and I. E. Markó, *Organometallics*, 2006, **25**, 1881–1890.
- 261S. Dierick, E. Vercruyssen, G. Berthon-Gelloz and I. E. Markó, *Chem. – Eur. J.*, 2015, **21**, 17073–17078.
- 262S. Sakaki, N. Mizoe and M. Sugimoto, *Organometallics*, 1998, **17**, 2510–2523.
- 263S. Sakaki, M. Sumimoto, M. Fukuhara, M. Sugimoto, H. Fujimoto and S. Matsuzaki, *Organometallics*, 2002, **21**, 3788–3802.
- 264U. Ajdnik, L. F. Zemljič, M. Bračić, U. Maver, O. Plohl and J. Rebol, *Materials*, 2019, **12**, 847.
- 265T. Kawahara, Y. Takeuchi, G. Wei, K. Shirai, T. Yamauchi and N. Tsubokawa, *Polym. J.*, 2009, **41**, 744–751.
- 266Y. Jia, B. Xiang, W. Zhang, T. Liu and S. Luo, *Polym. J.*, 2020, **52**, 207–216.
- 267M. Akbar, R. Ullah and I. Qazi, *Eng. Fail. Anal.*, 2020, **110**, 104449.
- 268G. Sahal, H. J. Woerdenbag, W. L. J. Hinrichs, A. Visser, P. G. Tepper, W. J. Quax, H. C. van der Mei and I. S. Bilkay, *J. Ethnopharmacol.*, 2020, **246**, 112188.
- 269S. Ziraki, S. M. Zebarjad and M. J. Hadianfard, *J. Mech. Behav. Biomed. Mater.*, 2016, **57**, 289–296.
- 270A. L. R. Pires and Â. M. Moraes, *J. Appl. Polym. Sci.*, 2015, DOI:10.1002/app.41686.
- 271D. J. Stickler, *Nat. Clin. Pract. Urol.*, 2008, **5**, 598–608.
- 272D. J. Stickler, *J. Intern. Med.*, 2014, **276**, 120–129.
- 273R. P. C. Jordan, S. Malic, M. G. Waters, D. J. Stickler and D. W. Williams, *Microbiol. Discov.*, 2015, **3**, 1.
- 274D. W. Williams, T. Kuriyama, S. Silva, S. Malic and M. A. O. Lewis, *Periodontol. 2000*, 2011, **55**, 250–265.
- 275D. Morse, M. Wilson, X. qing Wei, D. Bradshaw, M. Lewis and D. Williams, *Lett. Appl. Microbiol.*, 2019, **68**, 337–343.
- 276A. Smith, S. Al Kutubi, D. Williams, D. Bradshaw, W. Rowe and P. Milward, *Dent. Oral Biol. Craniofacial Res.*, 2020, DOI:10.31487/j.DOB.2020.02.06.
- 277Y. Rao, W. Shang, Y. Yang, R. Zhou and X. Rao, *Front. Microbiol.*, 2020, **11**:1000. DOI:10.3389/fmicb.2020.01000.
- 278G. J. Williams and D. J. Stickler, *J. Med. Microbiol.*, 2008, **57**, 1135–1140.

## Chapter 2: Surface and antimicrobial activity of Ag-NHCs and imidazolium salts

### Ionic liquids

Some ionic surfactants are ionic liquids in their concentrated states. Ionic liquids are defined as salts that have a melting point of lower than 100 °C.<sup>1</sup> Room temperature ionic liquids are therefore those ionic liquids that have a melting point lower than room temperature, and are therefore liquids.<sup>2</sup> Ionic liquids have seen much use in chemical and engineering research, with current examples including: as solvents in synthesis,<sup>3</sup> catalysis,<sup>4</sup> or as materials for producing batteries.<sup>5</sup> There are many common structures in surfactants and ionic liquids in terms of speciation, with imidazolium salts particularly being one promising type of ionic liquid.<sup>6-8</sup>

### Imidazolium salts

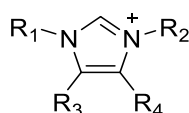


**Figure 1.** Basic structure of an imidazolium salt.

Imidazolium salts are cationic molecules, consisting of an imidazole heterocycle core with substitution on both nitrogen atoms. One of the nitrogen atoms is therefore formally a (delocalised) positively charged quaternary centre. Common counter-anion examples in the literature include halides,<sup>9</sup> tetrafluoroborates,<sup>10</sup> and hexafluorophosphates.<sup>11</sup> Imidazolium salts have a number of potential applications, including as N-heterocyclic carbene precursors. As such, a number of methods have been developed in order to synthesise imidazolium salts. Imidazolium salts offer a great deal of flexibility in terms of synthetic strategies. Imidazolium salts may be synthesised by alkylation of existing imidazoles, either symmetrically<sup>12</sup> or asymmetrically.<sup>13</sup> Imidazolium salts may also be synthesised by building the imidazolium ring from the respective carbonyl, amines, and dicarbonyl<sup>14</sup> or diimine<sup>15</sup> in a symmetric<sup>16,17</sup> manner, or asymmetrically by synthesis of the substituted imidazole and then alkylating with an electrophile.<sup>18,19</sup> While the above strategies are the most common, there is the possibility of synthesising imidazolium salts from other, precursors such as  $\alpha$ -hydroxyketones and bromoacetaldehyde diethylacetal.<sup>20</sup> The imidazolium salts described in this chapter are variations of di-alkylated benzimidazolium and imidazolium bromide salts. The synthesis of asymmetric imidazolium salts in this work typically proceeds via alkylation of the azolium ring, isolation of an N-alkylimidazole, then alkylation of the second nitrogen through reaction with a second alkyl bromide.

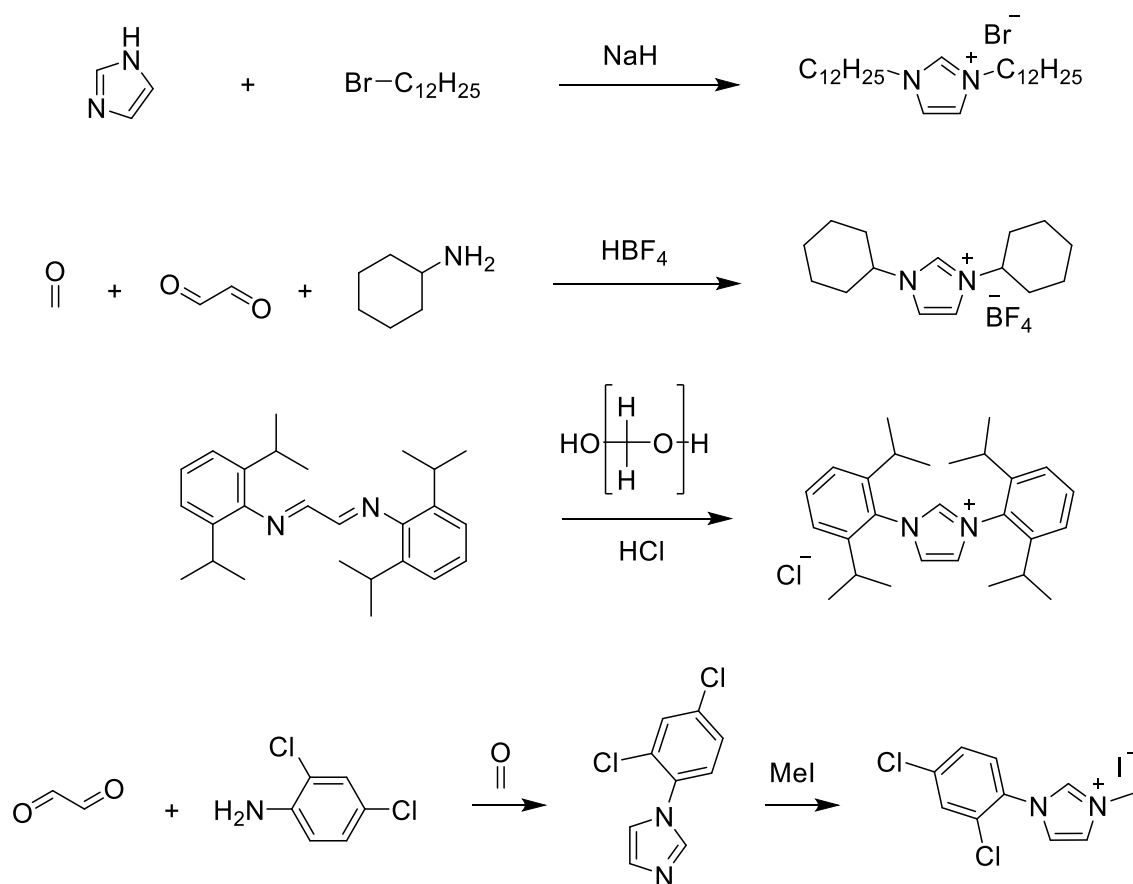


**Figure 2.** A selection of routes for synthesising imidazolium salts taken from the literature.<sup>12,14,15,19</sup>

### Antimicrobial effects of long chain imidazolium salts

Long chain imidazolium salts are likely to behave like other cationic surfactants in their interaction with cell membranes.<sup>21</sup> The cationic head group is attracted to the negatively charged phospholipids in the cell membrane of eukaryotic and prokaryotic cells. The association of a cationic surfactant to a cell membrane may interfere with its structural integrity potentially causing spontaneous monolayer curvature, leading to disordering of the phospholipid resulting in thinner and more flexible membranes. Surfactant association may also affect transport proteins within the membrane, therefore interfering with the cell's vital processes. The interference with the cell's membrane may go as far as to cause the membrane to rupture.<sup>22</sup> Cetyltrimethylammonium bromide (CTAB) has also been shown to induce oxidative stress in cells, potentially revealing other modes of action by which cationic surfactants have an antimicrobial effect. Traditional cationic surfactants such as CTAB have a higher activity against Gram positive bacteria than Gram negative bacteria, most likely due to lack of a secondary phospholipid membrane

in Gram positive bacteria.<sup>23</sup> A review on the antimicrobial efficacy of ionic liquids including imidazolium salts has been published.<sup>24</sup>

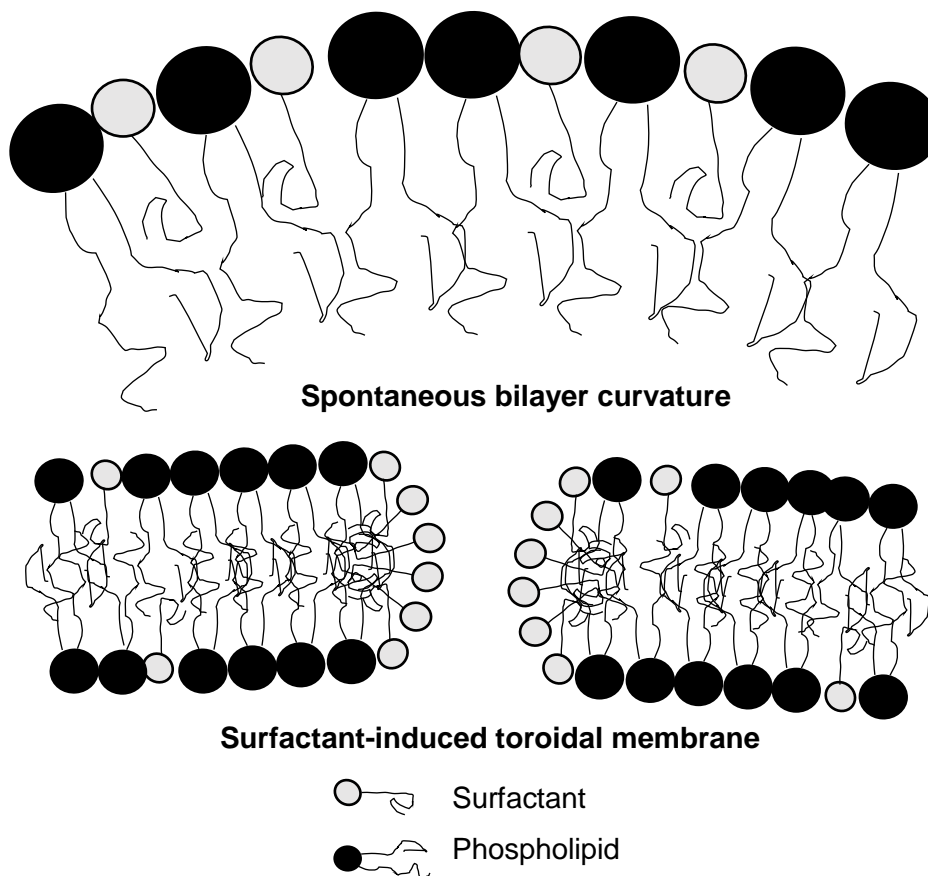


**Figure 3.** Interactions of surfactants with phospholipid membranes adapted from the literature.<sup>21</sup> Insertion of surfactants into a phospholipid bilayer can lead to spontaneous bilayer curvature (top) and potentially the formation of toroidal membrane pores (bottom) depending on the distribution and concentration of the surfactant.

### Silver NHCs

Imidazolium salts may be used as precursors in the synthesis of NHC complexes of a wide range of metal ion Lewis acids. Of particular interest in this work is their use as precursors in the synthesis of Ag-NHCs. The first Ag-NHC was reported in the work of Arduengo *et al.* who synthesised their Ag-NHC via a free carbene route.<sup>25</sup> 1,3-dimesitylimidazol-2-ylidene was reacted with silver triflate at room temperature under an inert atmosphere of dry nitrogen, to produce the respective homoleptic imidazole-2-ylidene silver(I) complex with an 80% yield. The issue with producing Ag-NHCs by this route is due to the sensitivity of the free NHC (see chapter 1). This approach was used to produce Ag-NHCs in a limited number of cases due to this inherent sensitivity.

Following this, a new approach was used by Bertrand *et al.* to synthesise Ag-NHCs using silver(I) acetate.<sup>26</sup> The basic silver source was used to deprotonate a triazolium salt in THF at reflux for 2 hours in order to produce a polymeric linear Ag-NHC. The complex was then stabilised by addition of silver(I) triflate. This use of a basic silver source in order to produce Ag-NHCs was also conducted by Wang and Lin,<sup>27</sup> who used silver(I) oxide to produce an Ag-NHC. The reaction was conducted at room temperature in DCM, with 1,3-diethylbenzimidazolium bromide as a ligand precursor. The Ag-NHC produced was a homoleptic positively charged Ag-NHC, with argentophilic interactions between NHC silver atom and an  $\text{AgBr}_2^-$  counter ion in the solid state. The method is currently the *de facto* manner in which to prepare Ag-NHCs due to its simplicity and the mild conditions employed.<sup>28–30</sup>

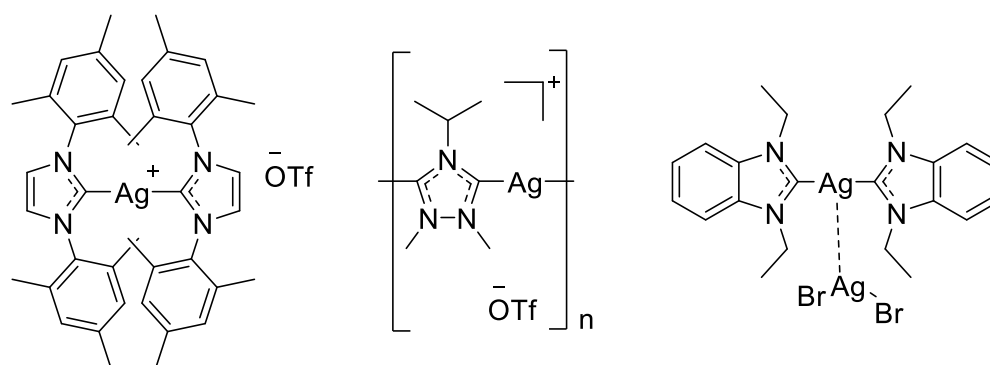


**Figure 4.** Early examples of Ag-NHCs reported by Arduengo *et al.*,<sup>25</sup> Bertrand *et al.*,<sup>26</sup> and Wang and Lin.<sup>27</sup>

The above solid state structure (Figure 4) described in the work by Wang and Lin gives some insight into the structural diversity of simple Ag-NHCs produced with halide counter ions.  $[\text{Ag}(\text{NHC})_2][\text{AgBr}_2]$  has a simplified empirical formula of  $[\text{AgBr}(\text{NHC})]$ , but the solid state structure depends on a number of factors. Work by Nolan and coworkers shows the variety of solid state structures achieved through reaction of  $\text{Ag}_2\text{O}$  and 2 equivalents of imidazolium chloride salt in dichloromethane.<sup>31</sup> A change in the flanking substituents of the imidazolium salt had a large effect on the solid state structure, with examples of  $[\text{AgCl}(\text{NHC})]$ ,  $[\text{AgCl}(\text{NHC})][\text{AgCl}(\text{NHC})]$  dimers with argentophilic interactions,  $[\text{Ag}(\text{NHC})_2][\text{AgCl}_2]$  dimers, and polymers containing argentophilic interactions and bridging chlorine atoms, all share the same empirical formula of  $[\text{AgCl}(\text{NHC})]$ . The situation is no less complicated in the solution phase, with many examples showing the fluxional nature of AgNHCs in solution between the neutral  $[\text{AgX}(\text{NHC})]$  and the  $[\text{Ag}(\text{NHC})_2][\text{AgX}_2]$  dimer. An increase in solvent polarity favours the formation of the dimeric species due to its ionic nature. The solvents tested were chloroform, acetonitrile, and DMSO, with DMSO containing the most dimeric Ag-NHC, and chloroform containing

the lowest. Different structures may be crystallised depending on solvent polarity. The existence of an equilibrium between the two forms is evidenced by Caytan and Roland.<sup>32</sup> The work also shows that the equilibrium rate between the two states is determined by the steric bulk of the pendant groups, with isopropylimidazol-2-ylidene complexes exchanging between the two forms at a far slower rate than methylbenzimidazol-2-ylidene complexes in DMSO. Nolan *et al.*<sup>31</sup> also showed that larger anions are more easily influenced by solvent polarity. They were able to form an iodide species  $[\text{Ag}(\text{NHC})_2]_2[\text{Ag}_4\text{I}_6]$  containing an  $[\text{Ag}_4\text{I}_6]^{2-}$  cluster in acetonitrile, whereas Zhang *et al.*<sup>33</sup> reported the formation of only the monomeric neutral  $[\text{Ag}(\text{NHC})]$  in dichloromethane. For simplicity, this work will describe all Ag-NHCs in their monomeric forms, though the truth is more than likely far more complicated.

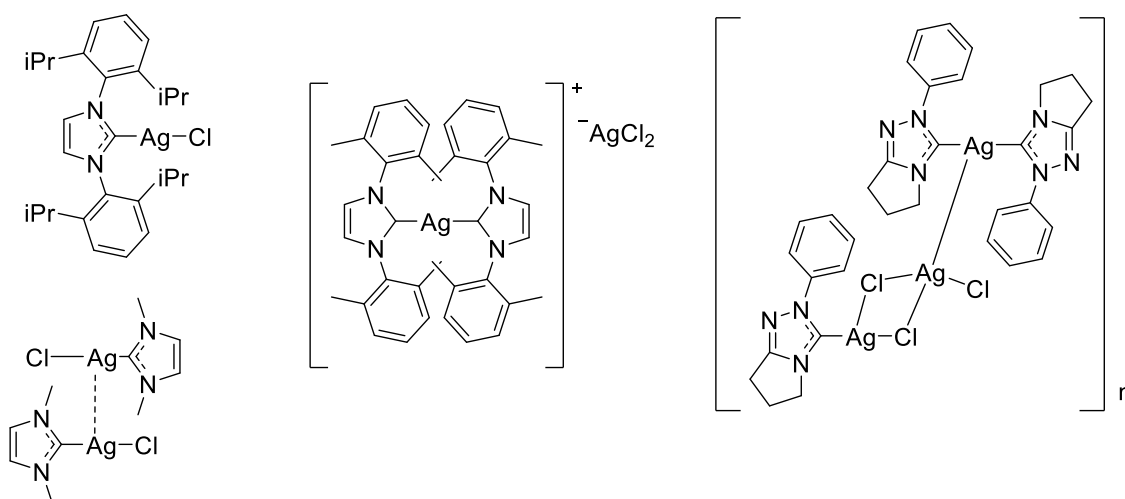


**Figure 5.** Solid state structures of  $\text{AgCl}(\text{NHC})$  complexes reported by Nolan *et al.*<sup>31</sup> Note the stoichiometry of all complexes depicted is 1:1:1 NHC:Ag:Cl.

### Antimicrobial activity of Ag-NHCs

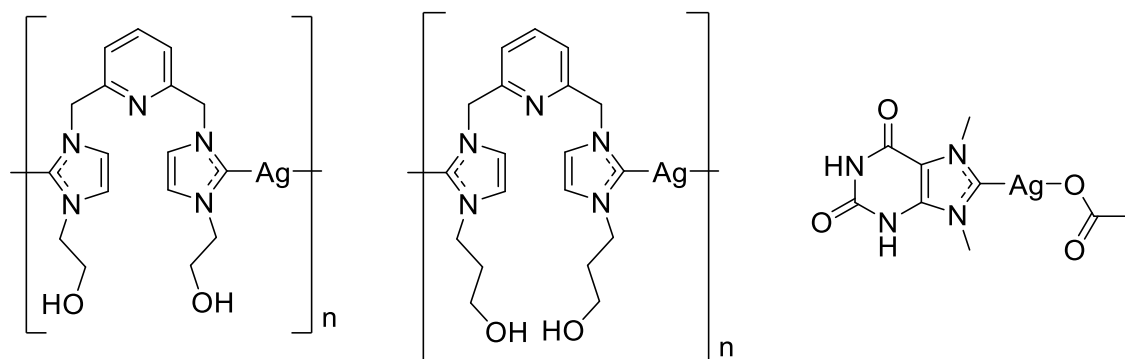


**Figure 6.** The first example of antimicrobial pincer Ag-NHCs reported by Youngs *et al.*<sup>34</sup> (left), and an antimicrobial Ag-NHC derived from caffeine (right).<sup>35</sup>

The first examples of the use of Ag-NHCs as antimicrobials were reported by Youngs *et al.* in 2004.<sup>34</sup> The complexes were based on pincer-like NHC ligands bridged by a substituted pyridine, and were synthesised using Ag<sub>2</sub>O in dichloromethane. The three complexes produced were tested to try and establish their minimum inhibitory concentration (MIC) against *Staphylococcus aureus*, *Pseudomonas aeruginosa*, and *Escherichia coli*. Two of the three complexes produced were more effective against the bacteria tested than AgNO<sub>3</sub>, showing some enhancement of the inherent antimicrobial activity of the Ag(I) cation by the NHC ligand. Youngs *et al.* then went on to develop a number of Ag-NHCs based on natural products such as caffeine and xanthine, making use of the methylimidazole moiety and methylating the other nitrogen to produce an imidazolium salt.<sup>35</sup> The complexes were tested against a number of Gram positive and Gram negative bacteria, and was found to be exceptionally effective, with MIC values of between 1 and 8 µg/mL in all cases except one strain of *E. coli*: *J53* (5000 µg/mL). *E. coli J53* contained the silver resistance plasmid pMG101, conferring resistance against the deleterious effects of Ag(I) by coding for the silver resistance genes silP, silA, silB, silC, silR, silS, and silE, which were retrieved from a silver nitrate-resistant *Salmonella* isolate recovered from a burn ward.<sup>36</sup> From these findings, it was concluded that the Ag(I) species played a crucial role in the antimicrobial effect of this complex. It was also shown that the complex was effective against a number of *Burkholderia spp.*, which are known as highly resistant respiratory pathogens.<sup>35</sup> The success of these compounds lead to the development of 4,5-dichloroimidazol-2-ylidene Ag-NHCs in an attempt to synthesise Ag-NHCs that were robust enough to withstand systemic delivery due to the electron-withdrawing groups on the imidazole backbone.<sup>37-39</sup> The dichloro-complexes are also cytotoxic,<sup>38</sup> which raises concerns as to their application as antimicrobial agents, along with the well-documented toxicity of some halogenated aromatic compounds.<sup>40</sup>

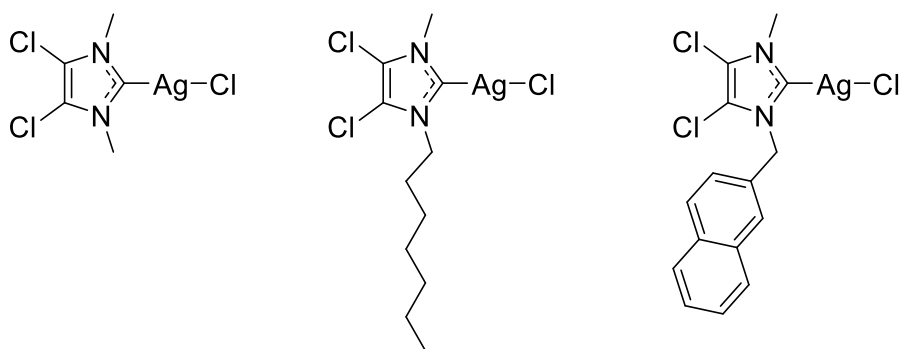


**Figure 7.** Antimicrobial 4,5-dichloroimidazol-2-ylidene Ag-NHCs described by Youngs *et al.*<sup>37-39</sup>

Tacke *et al.*<sup>41-47</sup> produced a large number of lipophilic Ag-NHCs, and tested their antimicrobial efficacy by means of a Kirby-Bauer disk diffusion test: a simple assay where discs impregnated with antimicrobial agent is placed on a lawn of bacteria swabbed on agar in order to determine a “zone of inhibition” which informs to an antimicrobial agent’s efficacy. Many of the Ag-NHCs showed a moderate efficacy, with the zone of inhibition being between 5-7 mm distance away from the compound. Again, the efficacy of the Ag(I) species was shown, as the parent imidazolium salts had smaller zones by comparison with their Ag-NHC counterpart. The most effective compounds (zone of inhibition of 10-11 mm) were those that were most lipophilic, suggesting that lipophilicity is also an important factor, due to the ability of lipophilic molecules to penetrate more deeply into the lipid membrane.

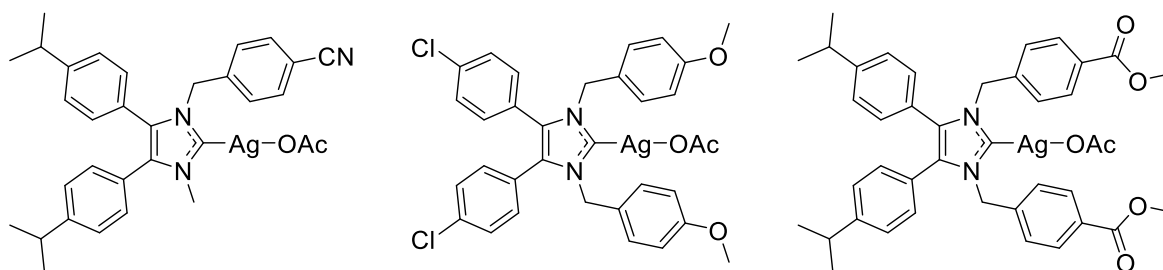


**Figure 8.** Examples of antimicrobial Ag-NHCs based on 4,5,-diphenylimidazole reported by Tacke *et al.*<sup>46</sup>

More recent examples have shown the synthesis of a number Ag-NHC species based on imidazole<sup>48-50</sup> and benzimidazole.<sup>50-53</sup> Ag-NHCs have shown a wide range of activity when tested against Gram positive and Gram negative bacteria *in vitro*. Work by Budagumpi *et al.*<sup>50</sup> in particular highlights the role of the N-bound groups pendant to the NHC ligand is of vital import to the activity of Ag-NHCs. It was found that Ag-NHCs with N-bound coumarin groups were far more effective against Gram negative *E. coli* than against Gram positive *S. aureus*. Ag-NHCs have even shown activity in some cases against organisms that have the potential to be used in bioterrorism such as *Burkholderia mallei*, *Burkholderia pseudomallei*, and *Yersinia pestis*.<sup>39</sup> The first glimpses of the use of Ag-NHCs *in vivo* are promising, with improved survival rates shown in infected *Galleria mellonella* larvae<sup>54</sup> and even infected mice.<sup>55</sup> For the most part, the literature appears to be in agreement that the efficacy of Ag-NHCs is dependent on their lipophilicity.<sup>56,57</sup> Other effects such as release rate of Ag(I) from the supporting ligand based on the donor strength of the attached Ag-NHC along with complex stability, and low cytotoxicity are also of import when designing a novel antimicrobial Ag-NHC. The reader’s attention is directed to a number of review articles with a more complete view of the application of Ag-NHCs as antimicrobial agents.<sup>58-61</sup>

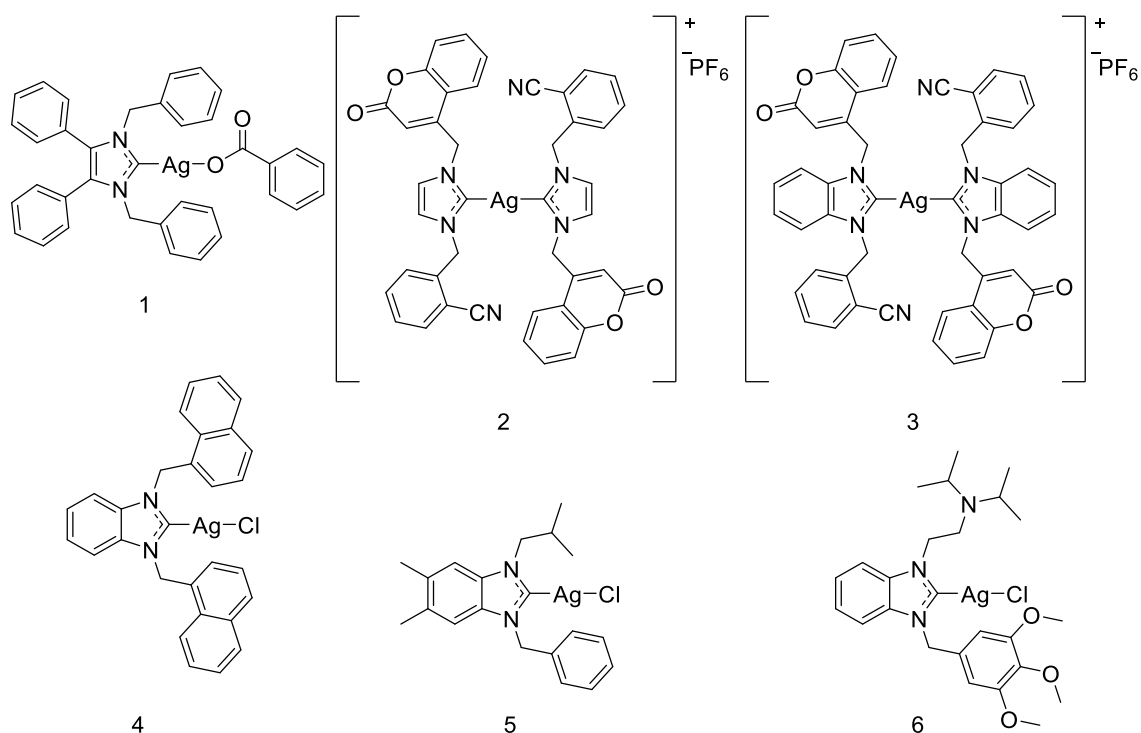


**Figure 9.** Recently reported antimicrobial Ag-NHCs: 1,<sup>49</sup> 2 and 3,<sup>50</sup> 4,<sup>51</sup> 5,<sup>52</sup> 6.<sup>53</sup>

## Aims

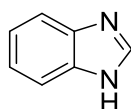
The purpose of the work described below is to present the synthesis of novel long-chain-containing Ag-NHCs by means of preparing their parent imidazolium bromide salts. The structures described are systematically varied with methyl, isopropyl, octyl, dodecyl, and hexadecyl groups used in order to produce a library of similar compounds to examine the differences in the physicochemical properties of the compounds in an iterative manner. The compounds synthesised were fully characterised by NMR spectroscopy, mass spectrometry, and infrared spectroscopy where appropriate. The behaviour of the imidazolium salts as surfactants will be examined, with emphasis on the effects of temperatures between room temperature and incubation/physiological temperatures on the behaviour of each salt. The antimicrobial effects of the synthesised Ag-NHCs is discussed, with their antimicrobial efficacy tested against Gram positive and Gram negative bacteria. Through this, the influence of the Ag(I) species as an antimicrobial agent will be explored, with each carbene's parent imidazolium salt also tested in order to ascertain whether there is a difference in efficacy between the two species. Producing a library of compounds also allows the examination of structure property relationships, such as the effect of small changes to the structure of the compound on its surface activity and antimicrobial properties.

## Experimental

All compounds used were commercial grade and used as provided unless stated otherwise.  $^1\text{H-NMR}$  and  $^{13}\text{C}\{^1\text{H}\}\text{-NMR}$  spectra were recorded in either  $\text{CDCl}_3$ ,  $d_6\text{-DMSO}$ , or  $(\text{CD}_3)_2\text{CO}$  using Bruker Ultrashield FT-NMR spectrometers with a field strength of either 500, 400, or 300 MHz. Spectra were analysed by MestReNova software version 6.0.2-5475 and digitally referenced to the residual solvent signal. Low and high resolution mass spectra were produced on a Waters LCT Premier XE spectrometer by Cardiff University School of Chemistry Analytical Services. Infra-red spectra were recorded using a Shimadzu IR-Affinity-1S FTIR. Conductivity measurements were performed using a Mettler Toledo portable conductivity meter. The conductivity meter was calibrated using a Mettler Toledo 1413  $\mu\text{S}$  conductivity standard before each experiment. Temperatures were kept consistent using a 1 L water bath using an electronic contact thermometer.

Broths and agars were supplied by Fisher. The bacteria used to conduct MIC testing were reference strains: *Staphylococcus epidermidis* (ATCC 35984/RP62A), *Staphylococcus epidermidis* (ATCC 14990), *Staphylococcus aureus* (NCTC 6571), *Staphylococcus aureus* (NCIMB 9518), *Pseudomonas aeruginosa* (ATCC 15692), and *Escherichia coli* (NCTC 12923). Stock cultures were maintained on Microbank™ plastic beads at  $-80\text{ }^\circ\text{C}$ . Working cultures were maintained on tryptone soy agar (TSA, Sigma Aldrich) at  $4\text{ }^\circ\text{C}$ . Before each experiment, a single colony was transferred to 10 mL of Mueller-Hinton broth (MHB) and incubated at  $37\text{ }^\circ\text{C}$  overnight. The concentrated inoculum was diluted approximately 1:10 in fresh broth to produce a suspension with equivalent turbidity to a 0.5 MacFarland standard (absorbance of 0.08 - 0.1 at 600 nm ( $\sim 1 \times 10^8$  CFU/mL)) using a micro spectrophotometer. The standardised solution was then diluted 1:100 to produce a test inoculum containing  $\sim 1 \times 10^6$  CFU/mL. MIC testing results were recorded using a BMG LabTech FLUOstar Omega plate reader, with optical density measurements recorded at 600 nm wavelength.

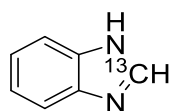
## Synthesis of benzimidazole



Benzimidazole was prepared on a small scale as a test in order to facilitate preparation of  $^{13}\text{C-C2}$ -labelled benzimidazole and derivative NHCs. Formic acid (90%, 3.2 mL, 75 mmol) and *o*-phenylenediamine (5.4g, 50 mmol) were added to a flask and heated to reflux for 2 hours. The mixture was then allowed to cool to room temperature. The

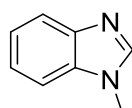
contents were then carefully neutralised with a sodium hydroxide solution (10% w/w). The solid precipitate was then collected on a Buchner funnel and washed with water. The crude solid was then added to water (75 mL) containing activated charcoal (0.2 g). The solution was then heated to boiling and allowed to stir for 15 minutes. The hot solution was then rapidly filtered through a hot sinter and allowed to cool. At this point, off-white, needle-like crystals formed. These were then collected on a Buchner funnel and washed with cold water (5 mL), yielding the product, benzimidazole (4.1 g, 69%). **<sup>1</sup>H-NMR** (300 MHz, *d*<sub>6</sub>-DMSO, 298K): δ (ppm): 8.26 (s, 1H, NCHN), 7.62 (m, 2H, aromatic), 7.20 (m, 2H, aromatic). **<sup>13</sup>C-NMR** (75 MHz, *d*<sub>6</sub>-DMSO, 298K): δ (ppm): 142.35 (NCHN), 138.27 (CCHCH), 122.29 (CHCH), 115.65 (CCHCH). **MS (EI)** 118.05 [M + H<sup>+</sup>]. This data matches that of a commercially sourced sample.

### Enriched benzimidazole



o-phenylenediamine (0.169 mL, 4.25 mmol), <sup>13</sup>C-enriched formic acid (0.459g, 4.25 mmol), and phosphoric acid (1 mL, conc.) were added to a vessel. The mixture was heated at reflux for 2 hours. The reaction was allowed to cool to room temperature, then water was added. The pH of the solution was carefully adjusted to 7 by dropwise addition of a sodium hydroxide solution (1 M). Upon neutralisation, a precipitate developed. The precipitate was then recrystallized by heating the reaction mixture to boiling, then allowing it to cool to room temperature. The crystals were then gathered on a Buchner funnel, and washed with ice-water. The product, <sup>13</sup>C-enriched benzimidazole, was obtained as off-white, needles (0.372 g, 74%). **<sup>1</sup>H-NMR** (400 MHz, CDCl<sub>3</sub>, 298K): δ (ppm): 8.09 (d, 1H, <sup>1</sup>J = 206.0 Hz, NCHN), 7.67 (s, 2H, CCHCH), 7.30 (dd, 2H, <sup>3</sup>J = 6.1 Hz, <sup>4</sup>J = 3.2 Hz, CHCH). **<sup>13</sup>C-NMR** (101 MHz, CDCl<sub>3</sub>, 298K): δ (ppm): 140.59 (NCHN). **HRMS (ESI)** found m/z 120.0646, calculated m/z 120.0643 for [C<sub>6</sub><sup>13</sup>CH<sub>7</sub>N<sub>2</sub>] (M+H<sup>+</sup>) (+2.5 ppm).

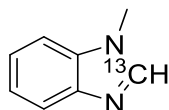
### Synthesis of 1-methylbenzimidazole



To a flask equipped with a magnetic stirrer, benzimidazole (2.36 g, 20 mmol) was added, followed by THF (20 mL), and potassium hydroxide (2.24 g, 40 mmol). To this solution, methyl iodide (1.25 mL, 20 mmol) was added. Stirring was maintained at room

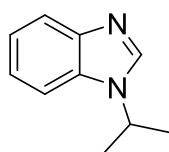
temperature for 3 hours. Distilled water (10 mL) was then added to the reaction medium. The mixture was then extracted with chloroform (6 x 10 mL), washed with brine (10 mL), then dried over magnesium sulphate. The suspension was then filtered, and the volatiles were removed *in vacuo*. The oil obtained was recrystallised with hexane, then isolated on a Buchner funnel under vacuum. The solid was then washed with hexane (10 mL) to give the desired product, 1-methylbenzimidazole, as off-white crystals (1.82 g, 69%). **<sup>1</sup>H-NMR** (400 MHz, d<sub>6</sub>-DMSO, 298K): δ (ppm): 8.17 (s, 1H, NCHN), 7.65 (dd, <sup>3</sup>J = 7.9 Hz, <sup>4</sup>J = 0.8 Hz, 1H, aromatic), 7.55 (dd, <sup>3</sup>J = 7.9 Hz, <sup>4</sup>J = 0.8 Hz, 1H, aromatic), 7.23 (m, 2H, aromatic), 3.83 (s, 3H, NCH<sub>3</sub>). **<sup>13</sup>C-NMR** (101 MHz, d<sub>6</sub>-DMSO, 298K): δ (ppm): 144.51 (NCHN), 143.33 (CCHCH), 134.55 (CCHCH), 122.16 (CHCH), 121.35 (CHCH), 119.25 (CCHCH), 110.10 (CCHCH), 30.59 (NCH<sub>3</sub>). **MS (ESI)** 133.06 [M + H<sup>+</sup>]. This data matches that of a commercially sourced sample.

### Enriched 1-methylbenzimidazole



<sup>13</sup>C-enriched benzimidazole (0.2 g, 1.67 mmol) was dissolved in THF (2 mL). To this solution KOH (0.38 g, 6.8 mmol) was added, followed by methyl iodide (0.21 mL, 3.37 mmol). The suspension was stirred at room temperature for 3 hours. Distilled water (5 mL) was then added, and the reaction mixture extracted with chloroform (3 x 5 mL). The organic layers were then washed with brine (10 mL), then dried over magnesium sulphate. The volatiles were then removed *in vacuo*. The resultant oil was then placed in a freezer to solidify. Once solid, the mixture was triturated with hexane under sonication. The resultant solid was collected on a Buchner funnel and washed with hexane to yield <sup>13</sup>C-enriched 1-methylbenzimidazole as a beige powder (0.14 g, 63.1%). **<sup>1</sup>H-NMR** (400 MHz, CDCl<sub>3</sub>, 298K): δ (ppm): 7.86 (d, 1H, <sup>1</sup>J = 204.2 Hz, NCHN), 7.65 (ddd, 2H, CCHCH), 7.30 (qd, 2H, <sup>3</sup>J = 7.1 Hz, <sup>4</sup>J = 1.4 Hz, CHCH), 3.84 (d, 3H, <sup>3</sup>J = 3.5 Hz, NCH<sub>3</sub>). **<sup>13</sup>C-NMR** (100 MHz, CDCl<sub>3</sub>, 298K): δ (ppm): 143.65 (NCHN). **MS (ESI)** 134.08 [M<sup>+</sup>].

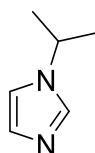
### Synthesis of 1-isopropylbenzimidazole



Potassium hydroxide (0.84 g, 15 mmol) and benzimidazole (1.4 g, 11.8 mmol) were added to DMSO (20 mL). The mixture was allowed to stir for 30 minutes at room

temperature, and then 2-bromopropane (1.11 mL, 11.8 mmol) was added. The reaction was then stirred at room temperature for 3 hours. Once the reaction was complete, water (200 mL) was added. The product was then extracted with chloroform (3 x 30 mL) and then dried over MgSO<sub>4</sub>. The solvent was then removed *in vacuo* to yield the product, 1-isopropylbenzimidazole, as a yellowish oil (1.24g, 65%). **<sup>1</sup>H-NMR** (300 MHz, CDCl<sub>3</sub>, 298K): δ (ppm): 7.94 (s, 1H, NCHN), 7.81 (m, 1H, aromatic), 7.36 (m, 1H, aromatic), 7.24 (m, 2H, aromatic), 4.56 (sep, <sup>3</sup>J = 6.8 Hz, 1H, (CH<sub>3</sub>)<sub>2</sub>CH), 1.52 (d, 6H, <sup>3</sup>J = 6.8 Hz, (CH<sub>3</sub>)<sub>2</sub>CH). **<sup>13</sup>C-NMR** (75 MHz, CDCl<sub>3</sub>, 298K): δ (ppm): 143.84 (NCHN), 140.18 (CCHCH), 133.24 (CCHCH), 122.72 (CHCH), 122.15 (CCHCH), 120.24 (CCHCH), 110.20 (CCHCH), 47.73 (NCH(CH<sub>3</sub>)<sub>2</sub>), 22.56 (NCH(CH<sub>3</sub>)<sub>2</sub>). **MS(ESI)** 161.11 [M + H<sup>+</sup>]. This matches data reported by Lopyrev *et al.*<sup>62</sup>

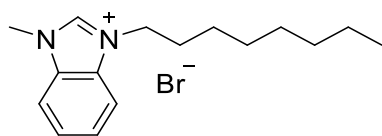
### Synthesis of 1-isopropylimidazole



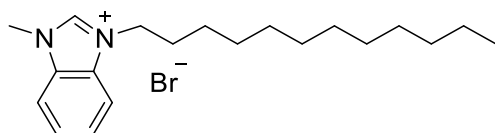
Dry acetonitrile (10 mL) was added to sodium hydride (0.8 g, 60% in mineral oil, 20 mmol) and imidazole (1.36 g, 20 mmol) under a nitrogen atmosphere at 0 °C. The mixture was allowed to heat to room temperature and stirred for 2 hours. The reaction was then cooled again to 0 °C, and 2-bromopropane (4.79 mL, 50 mmol) was added. The reaction was allowed to stir overnight, then the solvent was removed *in vacuo*. Water (100 mL) was then added to the reaction mixture, and the product was extracted using dichloromethane (3 x 10 mL) then dried over MgSO<sub>4</sub>. The dichloromethane was then removed *in vacuo* to yield 1-isopropylimidazole as a yellowish oil (1.40 g, 63%). **<sup>1</sup>H-NMR** (300 MHz, CDCl<sub>3</sub>, 298K): δ (ppm): 7.47 (s, 1H, NCHN), 6.99 (broad s, 1H, NCHCHN), 6.90 (broad s, 1H, NCHCHN), 4.28 (sep, <sup>3</sup>J = 6.7 Hz, 1H, (CH<sub>3</sub>)<sub>2</sub>CH), 1.42 (d, <sup>3</sup>J = 6.7 Hz, 6H, (CH<sub>3</sub>)<sub>2</sub>CH). **<sup>13</sup>C-NMR** (75 MHz, CDCl<sub>3</sub>, 298K): δ (ppm): 135.18 (NCHN), 129.12 (NCHCHN), 116.59 (NCHCHN), 49.11 (NCH(CH<sub>3</sub>)<sub>2</sub>), 23.75 (NCH(CH<sub>3</sub>)<sub>2</sub>). **MS (EI)** 110.0837 [M<sup>+</sup>]. This matches data reported by Ruhland *et al.*<sup>63</sup>

### General synthesis of 3-alkyl-1-methylbenzimidazolium bromide salts

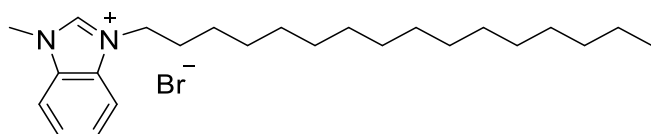
1-methylbenzimidazole (0.572 g, 4 mmol) was dissolved in toluene (10 mL). Alkyl bromide (6 mmol) was added to the reaction and stirred overnight at reflux. Volatiles were then removed *in vacuo* to yield a pale brown oil. The oil was stored at -30 °C, then triturated under sonication with diethyl ether. The white powder yielded was the product, 1-methyl-3-alkylbenzimidazolium bromide:



**1-methyl-3-octylbenzimidazolium bromide (1)** (1.226 g, 82%).  $^1\text{H-NMR}$  (400 MHz,  $\text{CDCl}_3$ , 298 K):  $\delta$  (ppm): 11.16 (s, 1H,  $\text{NCHN}$ ), 7.65 (m, 4H, aromatic), 4.56 (t, 2H,  $^3J = 7.5$  Hz,  $\text{NCH}_2\text{CH}_2$ ), 4.29 (s, 3H,  $\text{NCH}_3$ ), 2.01 (quin, 2H,  $^3J = 7.5$  Hz,  $\text{NCH}_2\text{CH}_2\text{CH}_2$ ), 1.20 (m, 10H,  $\text{CH}_2$ ), 0.82 (t, 3H,  $^3J = 7.0$  Hz,  $\text{CH}_2\text{CH}_3$ ).  $^{13}\text{C-NMR}$  (101 MHz,  $\text{CDCl}_3$ , 298 K)  $\delta$  (ppm): 143.29 ( $\text{NCHN}$ ), 132.18 ( $\text{CCHCH}$ ), 131.24 ( $\text{CCHCH}$ ), 127.38 ( $\text{CCHCH}$ ), 127.35 ( $\text{CCHCH}$ ), 113.00 ( $\text{CHCH}$ ), 47.86 ( $\text{NCH}_2$ ), 33.85 ( $\text{NCH}_3$ ), 31.77 ( $\text{CH}_2$ ), 29.66 ( $\text{CH}_2$ ), 29.12 ( $\text{CH}_2$ ), 29.09 ( $\text{CH}_2$ ), 26.69 ( $\text{CH}_2$ ), 22.67 ( $\text{CH}_2$ ), 14.16 ( $\text{CH}_3$ ). **IR** (ATR,  $\text{cm}^{-1}$ ): 3477, 3411, 3142, 3044, 2946, 2922, 2857, 1616, 1567, 1462, 1429, 1374, 1356, 1274, 1216, 1143, 1102, 1013, 875, 768, 743, 670, 613, 548, 458, 425. **HRMS (ES+)** found  $m/z$  245.2018, calculated  $m/z$  245.2018 for  $[\text{C}_{16}\text{H}_{25}\text{N}_2]$  ( $\text{M}^+ - \text{Br}^-$ ) ( $\pm 0.00$  ppm).



**3-dodecyl-1-methylbenzimidazolium bromide (2)** (1.480 g, 97 %).  $^1\text{H-NMR}$  (400 MHz,  $\text{CDCl}_3$ , 298 K):  $\delta$  (ppm): 11.09 (s, 3H,  $\text{NCHN}$ ), 7.68 (m, 4H, aromatic), 4.55 (s, 2H,  $\text{NCH}_2\text{CH}_2$ ) 4.28 (s, 3H,  $\text{NCH}_3$ ), 2.00 (quin, 2H,  $^3J = 7.0$  Hz,  $\text{NCH}_2\text{CH}_2\text{CH}_2$ ), 1.18 (m, 18H,  $\text{CH}_2$ ) 0.81 (t, 3H,  $^3J = 6.9$  Hz,  $\text{CH}_2\text{CH}_3$ ).  $^{13}\text{C-NMR}$  (101 MHz,  $\text{CDCl}_3$ , 298 K)  $\delta$  (ppm): 142.87 ( $\text{NCHN}$ ), 132.08 ( $\text{CCHCH}$ ), 131.13 ( $\text{CCHCH}$ ), 127.27 ( $\text{CHCH}$ ), 127.23 ( $\text{CHCH}$ ), 113.09 ( $\text{CCHCH}$ ), 112.92 ( $\text{CCHCH}$ ), 47.76 ( $\text{NCH}_2$ ), 33.92 ( $\text{NCH}_3$ ), 31.87 ( $\text{CH}_2$ ), 29.56 ( $\text{CH}_2$ ), 29.49 ( $\text{CH}_2$ ), 29.36 ( $\text{CH}_2$ ), 29.30 ( $\text{CH}_2$ ), 29.05 ( $\text{CH}_2$ ), 26.58 ( $\text{CH}_2$ ), 22.66 ( $\text{CH}_2$ ), 14.11 ( $\text{CH}_3$ ). **MS (ESI)** 301.26 [ $\text{M}^+ - \text{Br}^-$ ]. This matches data reported by Chen *et al.*<sup>64</sup>

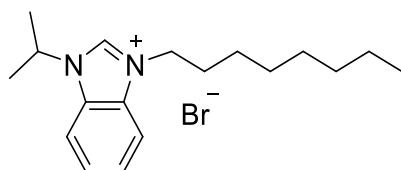


**3-hexadecyl-1-methylbenzimidazolium bromide (3)** (1.638 g, 94%).  $^1\text{H-NMR}$  (400 MHz,  $\text{CDCl}_3$ , 298 K):  $\delta$  (ppm): 11.43 (s, 1H,  $\text{NCHN}$ ), 7.68 (m, 4H, aromatic), 4.57 (t, 2H,  $^3J = 7.5$  Hz,  $\text{NCH}_2\text{CH}_2$ ), 4.31 (s, 3H,  $\text{NCH}_3$ ), 2.04 (quin, 2H,  $^3J = 7.6$  Hz,  $\text{NCH}_2\text{CH}_2\text{CH}_2$ ), 1.22 (m, 26H,  $\text{CH}_2$ ), 0.86 (t, 3H,  $^3J = 6.9$  Hz,  $\text{CH}_2\text{CH}_3$ ).  $^{13}\text{C-NMR}$  (101 MHz,  $\text{CDCl}_3$ , 298 K)  $\delta$  (ppm): 143.30 ( $\text{NCHN}$ ), 132.18 ( $\text{CCHCH}$ ), 131.24 ( $\text{CCHCH}$ ), 127.37 ( $\text{CHCH}$ ), 127.35 ( $\text{CHCH}$ ), 113.00 (broad,  $\text{CCHCH}$ ), 47.86 ( $\text{NCH}_2$ ), 33.86 ( $\text{NCH}_3$ ), 32.02 ( $\text{CH}_2$ ), 29.80 ( $\text{CH}_2$ ), 29.77 ( $\text{CH}_2$ ), 29.76 ( $\text{CH}_2$ ), 29.74 ( $\text{CH}_2$ ), 29.68 ( $\text{CH}_2$ ), 29.61 ( $\text{CH}_2$ ), 29.48

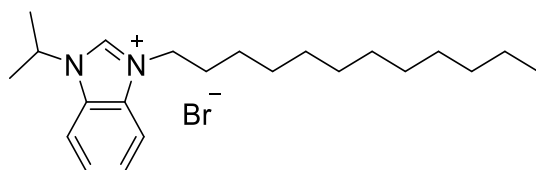
(CH<sub>2</sub>), 29.46 (CH<sub>2</sub>), 29.15 (CH<sub>2</sub>), 26.70 (CH<sub>2</sub>), 22.79 (CH<sub>2</sub>), 14.24 (CH<sub>3</sub>). **MS (ESI)** 357.31 [M<sup>+</sup> - Br<sup>-</sup>]. This matches data reported by Doroshkevich *et al.*<sup>65</sup>

### Synthesis of 3-alkyl-1-isopropylbenzimidazolium bromide salts

1-isopropylbenzimidazole (0.64 g, 4 mmol) and alkyl bromide (4.8 mmol) were dissolved in acetonitrile (10 mL) and heated at reflux overnight. The reaction mixture was allowed to cool and the solvent removed *in vacuo* to yield a yellowish-brown oil. The oil was then dissolved in minimum dichloromethane, and triturated with diethyl ether under sonication to yield the product as an off-white powder.

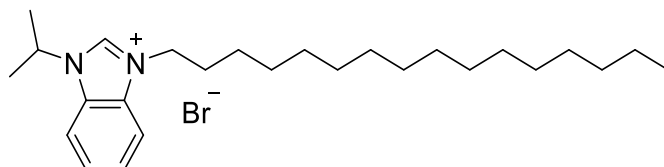


**1-isopropyl-3-octylbenzimidazolium bromide (4)** (1.17 g, 83%). **<sup>1</sup>H-NMR** (400 MHz, CDCl<sub>3</sub>, 298K): δ (ppm): 11.42 (s, 1H, NCHN), 7.79 (m, 1H, aromatic), 7.70 (m, 1H, aromatic), 7.62 (m, 2H, aromatic), 5.03 (sep, 1H, <sup>3</sup>J = 6.7 Hz, (CH<sub>3</sub>)<sub>2</sub>CH), 4.68 (t, 2H, <sup>3</sup>J = 7.6 Hz, NCH<sub>2</sub>), 2.00 (quin, 2H, <sup>3</sup>J = 7.6 Hz, NCH<sub>2</sub>CH<sub>2</sub>), 1.80 (d, 6H, <sup>3</sup>J = 6.8 Hz, CH(CH<sub>3</sub>)<sub>2</sub>), 1.26 (broad m, 10H, CH<sub>2</sub>), 0.80 (t, 3H, <sup>3</sup>J = 7.0 Hz, CH<sub>3</sub>). **<sup>13</sup>C-NMR** (101 MHz, CDCl<sub>3</sub>, 298 K) δ (ppm): 141.51 (NCHN), 131.64 (CCHCH), 130.61 (CCHCH), 127.16 (CHCH), 127.09 (CHCH), 113.70 (CCHCH), 113.24 (CCHCH), 51.90 (NCH(CH<sub>3</sub>)<sub>2</sub>), 47.73 (NCH<sub>2</sub>), 31.69 (CH<sub>2</sub>), 29.72 (CH<sub>2</sub>), 29.03 (CH<sub>2</sub>), 26.58 (CH<sub>2</sub>), 22.56 (CH<sub>2</sub>), 22.41 (CH<sub>2</sub>), 14.05 (CH<sub>3</sub>). **IR** (ATR, cm<sup>-1</sup>): 3104, 3012, 2954, 2922, 2857, 1559, 1462, 1429, 1372, 1323, 1257, 1216, 1143, 1102, 980, 954, 874, 760, 719, 662, 613, 564, 537, 425. **HRMS (ES<sup>+</sup>)** found m/z 273.2343, calculated m/z 273.2331 for [C<sub>18</sub>H<sub>29</sub>N<sub>2</sub>] (M<sup>+</sup> - Br<sup>-</sup>) (+4.4 ppm).



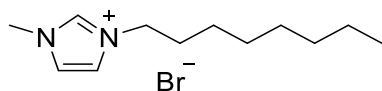
**3-dodecyl-1-isopropylbenzimidazolium bromide (5)** (1.03 g, 62%). **<sup>1</sup>H-NMR** (400 MHz, CDCl<sub>3</sub>, 298K): δ (ppm): 11.46 (s, 1H, NCHN), 7.75 (m, 1H, aromatic), 7.70 (m, 1H, aromatic), 7.63 (m, 2H, aromatic), 5.03 (sep, 1H, <sup>3</sup>J = 6.7 Hz, (CH<sub>3</sub>)<sub>2</sub>CH), 4.71 (t, 2H, <sup>3</sup>J = 7.6 Hz, NCH<sub>2</sub>), 2.03 (quin, 2H, <sup>3</sup>J = 7.6 Hz, NCH<sub>2</sub>CH<sub>2</sub>), 1.84 (d, 6H, <sup>3</sup>J = 6.8 Hz, CH(CH<sub>3</sub>)<sub>2</sub>), 1.22 (broad m, 18H, CH<sub>2</sub>), 0.86 (t, 3H, <sup>3</sup>J = 6.9 Hz, CH<sub>3</sub>). **<sup>13</sup>C-NMR** (101 MHz, CDCl<sub>3</sub>, 298 K) δ (ppm): 141.86 (NCHN), 131.84 (CCHCH), 130.69 (CCHCH), 127.15 (CHCH), 127.04 (CHCH), 113.64 (CCHCH), 113.34 (CCHCH), 52.10 (NCH(CH<sub>3</sub>)<sub>2</sub>),

47.86 (NCH<sub>2</sub>), 32.01 (CH<sub>2</sub>), 29.84 (CH<sub>2</sub>), 29.69 (CH<sub>2</sub>), 29.62 (CH<sub>2</sub>), 29.49 (CH<sub>2</sub>), 29.43 (CH<sub>2</sub>), 29.21 (CH<sub>2</sub>), 26.71 (CH<sub>2</sub>), 22.79 (CH<sub>2</sub>), 22.43 (CH<sub>2</sub>), 14.23 (CH<sub>3</sub>). **IR** (ATR, cm<sup>-1</sup>): 3460, 3403, 3126, 3020, 2946, 2913, 2857, 2359, 1616, 1559, 1465, 1425, 1371, 1318, 1265, 1211, 1185, 1145, 1094, 997, 866, 776, 719, 662, 621, 548, 475, 442. **HRMS (ES+)** found m/z 329.2965, calculated m/z 329.2957 for [C<sub>22</sub>H<sub>37</sub>N<sub>2</sub>] (M<sup>+</sup> - Br) (+2.4 ppm)..



**3-hexadecyl-1-isopropylbenzimidazolium bromide (6)** (1.22 g, 66%). **<sup>1</sup>H-NMR** (400 MHz, CDCl<sub>3</sub>, 298K): δ (ppm): 11.41 (s, 1H, NCHN), 7.78 (m, 1H, aromatic), 7.73 (m, 1H, aromatic), 7.66 (m, 2H, aromatic), 5.05 (sep, 1H, <sup>3</sup>J = 6.8 Hz, (CH<sub>3</sub>)<sub>2</sub>CH), 4.73 (t, 2H, <sup>3</sup>J = 7.6 Hz, NCH<sub>2</sub>), 2.06 (quin, 2H, <sup>3</sup>J = 7.6 Hz, NCH<sub>2</sub>CH<sub>2</sub>), 1.86 (d, 6H, <sup>3</sup>J = 6.8 Hz, CH(CH<sub>3</sub>)<sub>2</sub>), 1.24 (broad m, 26H, CH<sub>2</sub>), 0.88 (t, 3H, <sup>3</sup>J = 6.8 Hz, CH<sub>3</sub>). **<sup>13</sup>C-NMR** (101 MHz, CDCl<sub>3</sub>, 298 K) δ (ppm): 141.76 (NCHN), 131.82 (CCHCH), 130.68 (CCHCH), 127.14 (CHCH), 127.04 (CHCH), 113.65 (CCHCH), 113.34 (CCHCH), 52.07 (NCH(CH<sub>3</sub>)<sub>2</sub>), 47.86 (NCH<sub>2</sub>), 32.01 (CH<sub>2</sub>), 29.82 (CH<sub>2</sub>), 29.78 (CH<sub>2</sub>), 29.76 (CH<sub>2</sub>), 29.75 (CH<sub>2</sub>), 29.73 (CH<sub>2</sub>), 29.69 (CH<sub>2</sub>), 29.61 (CH<sub>2</sub>), 29.49 (CH<sub>2</sub>), 29.45 (CH<sub>2</sub>), 29.20 (CH<sub>2</sub>), 26.70 (CH<sub>2</sub>), 22.78 (CH<sub>2</sub>), 22.42 (CH<sub>2</sub>), 14.22 (CH<sub>3</sub>). **IR** (ATR, cm<sup>-1</sup>): 3452, 3385, 3126, 2995, 2913, 2849, 2359, 1641, 1567, 1470, 1429, 1388, 1339, 1307, 1257, 1211, 1135, 1094, 1013, 939, 875, 848, 752, 719, 556, 516, 483, 417. **HRMS (ES+)** found m/z 385.3586, calculated m/z 385.3583 for [C<sub>18</sub>H<sub>29</sub>N<sub>2</sub>] (M<sup>+</sup> - Br) (+0.8 ppm).

### Synthesis of 1-methyl-3-octylimidazolium bromide (7)

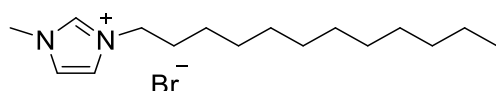


1-methylimidazole (1 mL, 12.5 mmol) and 1-bromooctane (2.15 mL, 12.5 mmol) were added to toluene (10 mL). The mixture was heated to reflux, and left to react overnight. The reaction was allowed to then cool to room temperature, and the solvent removed *in vacuo*. The resultant oil was then washed thrice with hexane (3 x 10 mL) to yield the imidazolium salt as a pale yellow, almost colourless oil. 1-methyl-3-octylimidazolium bromide (2.85 g, 83%). **<sup>1</sup>H-NMR** (400 MHz, CDCl<sub>3</sub>, 298K): δ (ppm): 9.79 (s, 1H, NCHN), 7.54 (t, 1H, <sup>4</sup>J = 1.8 Hz, NCHCHN), 7.36 (t, 1H, <sup>4</sup>J = 1.8 Hz, NCHCHN), 4.14 (t, 2H, <sup>3</sup>J = 7.4 Hz, NCH<sub>2</sub>CH<sub>2</sub>), 3.93 (s, 3H, NCH<sub>3</sub>), 1.72 (quin, 2H, <sup>3</sup>J = 7.4 Hz, NCH<sub>2</sub>CH<sub>2</sub>CH<sub>2</sub>), 1.08 (broad m, 10H, CH<sub>2</sub>), 0.68 (t, 3H, <sup>3</sup>J = 6.9 Hz, CH<sub>2</sub>CH<sub>3</sub>). **<sup>13</sup>C-NMR** (101 MHz, CDCl<sub>3</sub>, 298K): δ (ppm): 136.54 (NCHN), 123.65 (NCHCHN), 121.85 (NCHCHN), 49.75 (NCH<sub>2</sub>),

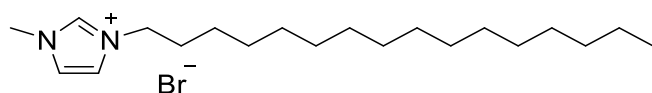
36.47 (N-CH<sub>3</sub>), 31.34 (CH<sub>2</sub>), 29.99 (CH<sub>2</sub>), 28.70 (CH<sub>2</sub>), 28.63 (CH<sub>2</sub>), 25.91 (CH<sub>2</sub>), 22.24 (CH<sub>2</sub>), 13.76 (CH<sub>3</sub>). **MS (ESI)** 195.18 [M<sup>+</sup> - Br<sup>-</sup>]. This matches data reported by Wilding *et al.*<sup>66</sup>

### Synthesis of 3-alkyl-1-methylimidazolium bromide salts

1-methylimidazole (1 mL, 12.5 mmol) and either 1-bromododecane or 1-bromohexadecane (12.5 mmol) were added to toluene (10 mL). The mixture was heated to reflux, and left to react overnight. The reaction was allowed to then cool to room temperature, and the white precipitate that formed was collected on a Büchner funnel under suction. The white solid was washed with hexane (10 mL) to yield the product:



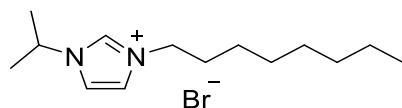
**3-dodecyl-1-methylimidazolium bromide (8)** (3.89 g, 94%). **<sup>1</sup>H-NMR** (400 MHz, CDCl<sub>3</sub>, 298K): δ (ppm): 9.85 (s, 1H, NCHN), 7.56 (t, 1H, <sup>4</sup>J = 1.7 Hz, NCHCHN), 7.37 (t, 1H, <sup>4</sup>J = 1.8 Hz, NCHCHN), 4.16 (t, 2H, <sup>3</sup>J = 7.4 Hz, NCH<sub>2</sub>CH<sub>2</sub>), 3.96 (s, 3H, NCH<sub>3</sub>), 1.74 (quin, 2H, <sup>3</sup>J = 7.1 Hz, NCH<sub>2</sub>CH<sub>2</sub>CH<sub>2</sub>), 1.11 (broad m, 18H, CH<sub>2</sub>), 0.71 (t, 3H, <sup>3</sup>J = 6.9 Hz, CH<sub>2</sub>CH<sub>3</sub>). **<sup>13</sup>C-NMR** (101 MHz, CDCl<sub>3</sub>, 298K): δ (ppm): 136.65 (NCHN), 123.70 (NCHCHN), 121.86 (NCHCHN), 49.82 (NCH(CH<sub>3</sub>)<sub>2</sub>), 36.53 (NCH<sub>3</sub>), 31.62 (CH<sub>2</sub>), 30.07 (CH<sub>2</sub>), 29.33 (CH<sub>2</sub>), 29.32 (CH<sub>2</sub>), 29.26 (CH<sub>2</sub>), 29.14 (CH<sub>2</sub>), 29.05 (CH<sub>2</sub>), 28.77 (CH<sub>2</sub>), 26.00 (CH<sub>2</sub>), 22.40 (CH<sub>2</sub>), 13.87 (CH<sub>3</sub>). **MS (ESI)** 251.24 [M<sup>+</sup> - Br<sup>-</sup>]. This matches data reported by Garcia *et al.*<sup>67</sup>



**3-hexadecyl-1-methylimidazolium bromide (9)** (4.35 g, 90%). **<sup>1</sup>H-NMR** (400 MHz, CDCl<sub>3</sub>, 298K): δ (ppm): 10.36 (s, 1H, NCHN), 7.46 (t, 1H, <sup>4</sup>J = 1.7 Hz, NCHCHN), 7.32 (t, 1H, <sup>4</sup>J = 1.8 Hz, NCHCHN), 4.29 (t, 2H, <sup>3</sup>J = 7.5 Hz, NCH<sub>2</sub>CH<sub>2</sub>...), 4.11 (s, 3H, NCH<sub>3</sub>), 1.89 (quin, 2H, <sup>3</sup>J = 7.2 Hz, NCH<sub>2</sub>CH<sub>2</sub>CH<sub>2</sub>), 1.24 (broad m, 26H, CH<sub>2</sub>), 0.85 (t, 3H, <sup>3</sup>J = 6.9 Hz, CH<sub>2</sub>CH<sub>3</sub>). **<sup>13</sup>C-NMR** (101 MHz, CDCl<sub>3</sub>, 298K): δ (ppm): 137.77 (NCHN), 123.51 (NCHCHN), 121.78 (NCHCHN), 50.30 (NCH(CH<sub>3</sub>)<sub>2</sub>), 36.89 (NCH<sub>3</sub>), 32.01 (CH<sub>2</sub>), 30.40 (CH<sub>2</sub>), 29.78 (CH<sub>2</sub>), 29.74 (CH<sub>2</sub>), 29.69 (CH<sub>2</sub>), 29.60 (CH<sub>2</sub>), 29.47 (CH<sub>2</sub>), 29.45 (CH<sub>2</sub>), 29.09 (CH<sub>2</sub>), 26.36 (CH<sub>2</sub>), 22.78 (CH<sub>2</sub>), 14.22 (CH<sub>3</sub>). **MS (ESI)** 307.29 [M<sup>+</sup> - Br<sup>-</sup>]. This matches data reported by Anderson *et al.*<sup>68</sup>

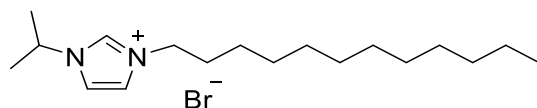
## Synthesis of 3-alkyl-1-isopropylimidazolium bromide

1-isopropylimidazole (1.36 g, 12 mmol) and alkyl bromide (12 mmol) were dissolved in acetonitrile (10 mL). The volatiles were then removed under reduced pressure and the oil produced was triturated with hexane (3 x 10 mL) to yield the product.



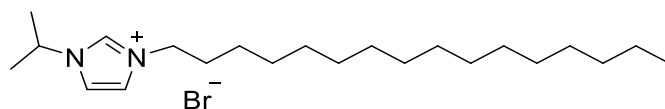
**1-isopropyl-3-octylimidazolium bromide (10)** as a pale yellow oil (3.62 g, quantitative).

**<sup>1</sup>H-NMR** (400 MHz, CDCl<sub>3</sub>, 298K): δ (ppm): 10.34 (s, 1H, NCHN), 7.58 (t, 1H, <sup>4</sup>J = 1.8 Hz, NCHCHN), 7.45 (t, 1H, <sup>4</sup>J = 1.8 Hz, NCHCHN), 4.84 (sep, 1H, <sup>3</sup>J = 6.7 Hz, (CH<sub>3</sub>)<sub>2</sub>CH), 4.28 (t, 2H, <sup>3</sup>J = 7.4 Hz, NCH<sub>2</sub>CH<sub>2</sub>), 1.84 (quin, 2H, <sup>3</sup>J = 7.3 Hz, NCH<sub>2</sub>CH<sub>2</sub>CH<sub>2</sub>), 1.54 (d, 6H, <sup>3</sup>J = 6.7 Hz, (CH<sub>3</sub>)<sub>2</sub>CH), 1.17 (broad m, 10H, CH<sub>2</sub>), 0.78 (t, 3H, <sup>3</sup>J = 6.7 Hz, CH<sub>2</sub>CH<sub>3</sub>). **<sup>13</sup>C-NMR** (101 MHz, CDCl<sub>3</sub>, 298K): δ (ppm): 135.86 (NCHN), 122.15 (NCHCHN), 120.19 (NCHCHN), 53.24 (NCH(CH<sub>3</sub>)<sub>2</sub>), 50.04 (NCH<sub>2</sub>), 31.63 (CH<sub>2</sub>), 30.31 (CH<sub>2</sub>), 28.98 (CH<sub>2</sub>), 28.92 (CH<sub>2</sub>), 26.23 (CH<sub>2</sub>), 23.18 (CH<sub>2</sub>), 22.53 (CH<sub>2</sub>), 14.02 (CH<sub>2</sub>CH<sub>3</sub>). **IR** (ATR, cm<sup>-1</sup>): 3408, 3128, 3056, 2954, 2925, 2853, 1560, 1458, 1375, 1333, 1312, 1267, 1178, 1149, 1036, 1002, 881, 759, 721, 654. **HRMS (ES<sup>+</sup>)** found m/z 223.2170, calculated m/z 223.2174 for [C<sub>14</sub>H<sub>27</sub>N<sub>2</sub>] (M<sup>+</sup> - Br<sup>-</sup>) (-1.8 ppm).



**3-dodecyl-1-isopropylimidazolium bromide (11)** as a viscous yellow oil (2.86 g, 66%).

**<sup>1</sup>H-NMR** (400 MHz, CDCl<sub>3</sub>, 298K): δ (ppm): 10.39 (s, 1H, NCHN), 7.58 (t, 1H, <sup>4</sup>J = 1.8 Hz, NCHCHN), 7.43 (t, 1H, <sup>4</sup>J = 1.8 Hz, NCHCHN), 4.83 (sep, 1H, <sup>3</sup>J = 6.7 Hz, (CH<sub>3</sub>)<sub>2</sub>CH), 4.26 (t, 2H, <sup>3</sup>J = 7.4 Hz, NCH<sub>2</sub>CH<sub>2</sub>), 1.82 (quin, 2H, <sup>3</sup>J = 7.1 Hz, NCH<sub>2</sub>CH<sub>2</sub>CH<sub>2</sub>), 1.53 (d, 6H, <sup>3</sup>J = 6.7 Hz, (CH<sub>3</sub>)<sub>2</sub>CH), 1.17 (broad m, 18H, CH<sub>2</sub>), 0.77 (t, 3H, <sup>3</sup>J = 6.8 Hz, CH<sub>2</sub>CH<sub>3</sub>). **<sup>13</sup>C-NMR** (101 MHz, CDCl<sub>3</sub>, 298K): δ (ppm): 135.73 (NCHN), 122.08 (NCHCHN), 120.21 (NCHCHN), 53.12 (NCH(CH<sub>3</sub>)<sub>2</sub>), 49.90 (NCH<sub>2</sub>), 31.77 (CH<sub>2</sub>), 30.24 (CH<sub>2</sub>), 29.55 (CH<sub>2</sub>), 29.47 (CH<sub>2</sub>), 29.39 (CH<sub>2</sub>), 29.27 (CH<sub>2</sub>), 29.21 (CH<sub>2</sub>), 28.91 (CH<sub>2</sub>), 26.15 (CH<sub>2</sub>), 23.64 (CH<sub>2</sub>), 23.09 (CH<sub>2</sub>), 22.54 (CH<sub>2</sub>), 14.00 (CH<sub>3</sub>). **IR** (ATR, cm<sup>-1</sup>): 3395, 3134, 3068, 2922, 2857, 1620, 1559, 1462, 1379, 1339, 1266, 1176, 1150, 1005, 863, 752, 719, 654. **HRMS (ES<sup>+</sup>)** found m/z 279.2792, calculated m/z 279.2800 for [C<sub>18</sub>H<sub>35</sub>N<sub>2</sub>] (M<sup>+</sup> - Br<sup>-</sup>) (-2.9 ppm).



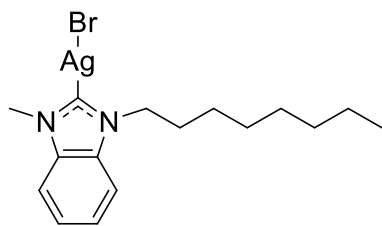
**3-hexadecyl-1-isopropylimidazolium bromide (12)** as a white solid (4.33 g, 87%). **<sup>1</sup>H-NMR** (400 MHz, CDCl<sub>3</sub>, 298K): δ (ppm): 10.58 (s, 1H, NCHN), 7.55 (t, 1H, <sup>4</sup>J = 1.8 Hz, NCHCHN), 7.42 (t, 1H, <sup>4</sup>J = 1.8 Hz, NCHCHN), 4.90 (sep, 1H, <sup>3</sup>J = 6.7 Hz, (CH<sub>3</sub>)<sub>2</sub>CH), 4.33 (t, 2H, <sup>3</sup>J = 7.4 Hz, NCH<sub>2</sub>CH<sub>2</sub>), 1.88 (quin, 2H, <sup>3</sup>J = 7.2 Hz, NCH<sub>2</sub>CH<sub>2</sub>CH<sub>2</sub>), 1.59 (d, 6H, <sup>3</sup>J = 6.7 Hz, (CH<sub>3</sub>)<sub>2</sub>CH), 1.17 (broad m, 26H, CH<sub>2</sub>), 0.83 (t, 3H, <sup>3</sup>J = 6.9 Hz, CH<sub>2</sub>CH<sub>3</sub>). **<sup>13</sup>C-NMR** (101 MHz, CDCl<sub>3</sub>, 298K): δ (ppm): 136.26 (NCHN), 122.05 (NCHCHN), 120.08 (NCHCHN), 53.33 (NCH(CH<sub>3</sub>)<sub>2</sub>), 50.13 (NCH<sub>2</sub>), 31.95 (CH<sub>2</sub>), 30.42 (CH<sub>2</sub>), 29.72 (CH<sub>2</sub>), 29.69 (CH<sub>2</sub>), 29.64 (CH<sub>2</sub>), 29.56 (CH<sub>2</sub>), 29.44 (CH<sub>2</sub>), 29.39 (CH<sub>2</sub>), 29.08 (CH<sub>2</sub>), 26.34 (CH<sub>2</sub>), 23.27 (CH<sub>2</sub>), 22.72 (CH<sub>2</sub>), 14.16 (CH<sub>3</sub>). **IR** (ATR, cm<sup>-1</sup>): 3395, 3134, 3060, 2913, 2849, 1633, 1567, 1543, 1478, 1372, 1331, 1266, 1176, 1143, 1013, 825, 760, 719, 638. **HRMS (ES<sup>+</sup>)** found m/z 335.3427, calculated m/z 335.3426 for [C<sub>22</sub>H<sub>43</sub>N<sub>2</sub>] (M<sup>+</sup> - Br<sup>-</sup>) (+0.3 ppm).

### Preparation of silver oxide

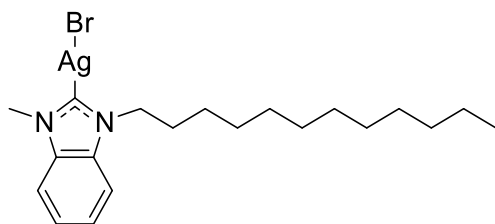
Silver oxide was prepared by way of a simple precipitation from the reaction of silver nitrate and base. Sodium hydroxide (0.66 g, 16.5 mmol), was dissolved in water (20 mL). The sodium hydroxide solution was added to a solution of silver nitrate (2.74 g, 16.1 mmol) in water (5 mL). The dark brown/black precipitate that immediately formed was separated on a Büchner funnel, and washed with water (2 x 10 mL), ethanol (2 x 10 mL), and diethyl ether (2 x 10 mL). The product was then sucked to dryness on the filter paper before being used immediately.

### Synthesis of Ag-NHCs

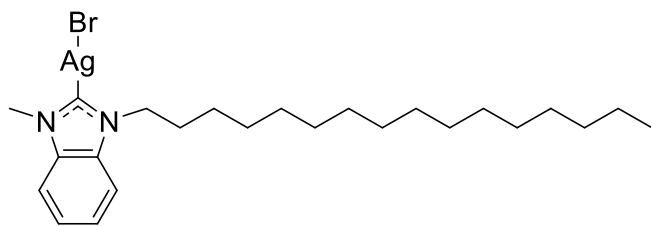
Fresh silver oxide (0.3 g, 1.3 mmol) was added to a solution of imidazolium/benzimidazolium salt (1.2 mmol) in dichloromethane (20 mL). The reaction vessel was covered in foil, and left to stir in the dark overnight at room temperature. The dichloromethane was reduced *in vacuo* in order to concentrate the solution (~2 mL). Hexane (10 mL) was then added in order to precipitate the silver NHC complex as a white solid. The solid white carbene was then collected on a Büchner funnel and stored in the darkness wrapped in foil.



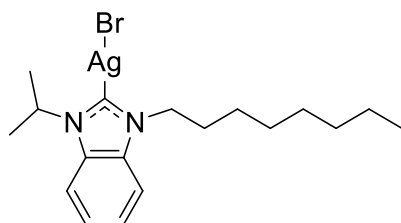
**1-methyl-3-octylbenzimidazol-2-ylidene silver(I) bromide (1Ag)** (0.283 g, 54%). **<sup>1</sup>H-NMR** (500 MHz, *d*<sub>6</sub>-DMSO, 298K): δ (ppm): 7.83 (m, 1H, aromatic), 7.77 (m, 1H, aromatic), 7.46 (m, 2H, aromatic), 4.47 (t, 2H, <sup>3</sup>*J* = 6.9 Hz, NCH<sub>2</sub>CH<sub>2</sub>), 4.05 (s, 1H, NCH<sub>3</sub>), 1.85 (quin, 2H, <sup>3</sup>*J* = 6.7 Hz, NCH<sub>2</sub>CH<sub>2</sub>CH<sub>2</sub>), 1.24 (m, 10H, CH<sub>2</sub>), 0.80 (t, 3H, <sup>3</sup>*J* = 6.8 Hz, CH<sub>2</sub>CH<sub>3</sub>). **<sup>13</sup>C-NMR** (126 MHz, *d*<sub>6</sub>-DMSO, 298K): δ (ppm): 189.01 (CAg), 134.02 (CCHCH), 133.16 (CCHCH), 123.96 (CHCH), 123.94 (CHCH), 112.14 (CCHCH), 111.95 (CCHCH), 48.38 (NCH<sub>2</sub>), 35.57 (NCH<sub>3</sub>), 31.25 (CH<sub>2</sub>), 30.00 (CH<sub>2</sub>), 28.67 (CH<sub>2</sub>), 28.63 (CH<sub>2</sub>), 26.17 (CH<sub>2</sub>), 22.11 (CH<sub>2</sub>), 14.00 (CH<sub>3</sub>). **IR** (ATR, cm<sup>-1</sup>): 2954, 2920, 2848, 2360, 2341, 1483, 1456, 1442, 1396, 1375, 1348, 1228, 1138, 1095, 1012, 927, 788, 746, 669, 578, 549, 418. **HRMS (ES<sup>+</sup>)** found *m/z* 595.2933, calculated *m/z* 595.2930 for [C<sub>32</sub>H<sub>48</sub>N<sub>4</sub><sup>107</sup>Ag] (NHC-Ag-NHC<sup>+</sup>) (+0.5 ppm).



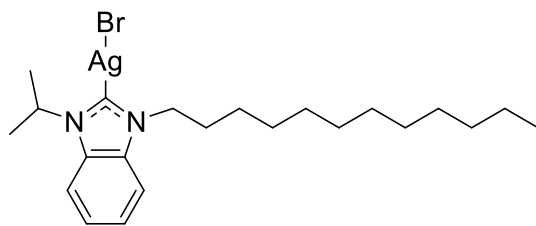
**3-dodecyl-1-methylbenzimidazol-2-ylidene silver(I) bromide (2Ag)** (0.418 g, 71%). **<sup>1</sup>H-NMR** (500 MHz, *d*<sub>6</sub>-DMSO, 298K): δ (ppm): 7.84 (m, 1H, aromatic), 7.78 (m, 1H, aromatic), 7.47 (m, 2H, aromatic), 4.48 (t, 2H, <sup>3</sup>*J* = 7.0 Hz, NCH<sub>2</sub>CH<sub>2</sub>), 4.06 (s, 3H, NCH<sub>3</sub>), 1.86 (quin, 2H, <sup>3</sup>*J* = 6.9 Hz, NCH<sub>2</sub>CH<sub>2</sub>CH<sub>2</sub>), 1.25 (m, 18H, CH<sub>2</sub>), 0.84 (t, 3H, <sup>3</sup>*J* = 7.0 Hz, CH<sub>2</sub>CH<sub>3</sub>). **<sup>13</sup>C-NMR** (126 MHz, *d*<sub>6</sub>-DMSO, 298K): δ (ppm): 188.93 (CAg), 134.03 (CCHCH), 133.15 (CCHCH), 123.95 (CHCH), 112.15 (CCHCH), 111.96 (CCHCH), 48.37 (NCH<sub>2</sub>), 35.57 (NCH<sub>3</sub>), 31.35 (CH<sub>2</sub>), 29.97 (CH<sub>2</sub>), 29.08 (CH<sub>2</sub>), 29.06 (CH<sub>2</sub>), 29.02 (CH<sub>2</sub>), 28.76 (CH<sub>2</sub>), 28.65 (CH<sub>2</sub>), 26.14 (CH<sub>2</sub>), 22.16 (CH<sub>2</sub>), 14.04 (CH<sub>3</sub>). **IR** (ATR, cm<sup>-1</sup>): 3062, 2916, 2848, 2360, 2330, 1734, 1541, 1458, 1400, 1355, 1215, 1138, 1091, 1031, 1012, 929, 788, 748, 719, 669, 650, 565, 472, 418. **HRMS (ES<sup>+</sup>)** found *m/z* 707.4196, calculated *m/z* 707.4182 for [C<sub>40</sub>H<sub>64</sub>N<sub>4</sub><sup>107</sup>Ag] (NHC-Ag-NHC<sup>+</sup>) (+1.4 ppm).



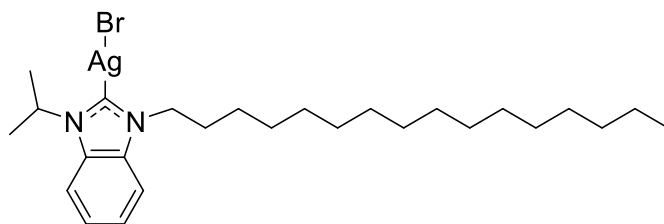
**3-hexadecyl-1-methylbenzimidazol-2-ylidene (3Ag)** (0.378 g, 58%). **<sup>1</sup>H-NMR** (500 MHz, *d*<sub>6</sub>-DMSO, 298K): δ (ppm): 8.10 (m, 1H, aromatic), 8.03 (m, 1H, aromatic), 7.71 (m, 2H, aromatic), 4.48 (t, 2H, <sup>3</sup>*J* = 7.1 Hz, NCH<sub>2</sub>CH<sub>2</sub>), 4.08 (s, 3H, NCH<sub>3</sub>), 1.88 (quin, 2H, <sup>3</sup>*J* = 6.5 Hz, NCH<sub>2</sub>CH<sub>2</sub>CH<sub>2</sub>), 1.24 (m, 26H, CH<sub>2</sub>), 0.85 (t, 3H, <sup>3</sup>*J* = 6.3 Hz, CH<sub>2</sub>CH<sub>3</sub>). **<sup>13</sup>C-NMR** (126 MHz, *d*<sub>6</sub>-DMSO, 298K): δ (ppm): 189.59 (CAg), 123.87 (CHCH), 113.56 (CCHCH), 111.85 (CCHCH), 48.37 (NCH<sub>2</sub>), 35.52 (NCH<sub>3</sub>), 31.28 (CH<sub>2</sub>), 30.04 (CH<sub>2</sub>), 28.98 (CH<sub>2</sub>), 28.69 (CH<sub>2</sub>), 26.16 (CH<sub>2</sub>), 22.08 (CH<sub>2</sub>), 13.94 (CH<sub>3</sub>). **IR** (ATR, cm<sup>-1</sup>): 2918, 2848, 2362, 2339, 1869, 1734, 1697, 1683, 1647, 1558, 1541, 1508, 1489, 1473, 1396, 1373, 1363, 1217, 788, 748, 719, 669, 516, 418. **HRMS (ES<sup>+</sup>)** found *m/z* 819.5448, calculated *m/z* 819.5434 for [C<sub>48</sub>H<sub>80</sub>N<sub>4</sub><sup>107</sup>Ag] (NHC-Ag-NHC<sup>+</sup>) (+1.7 ppm).



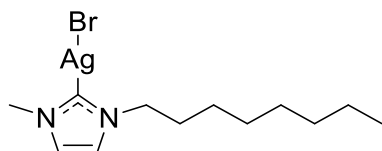
**1-isopropyl-3-octyl-benzimidazol-2-ylidene silver(I) bromide (4Ag)** (0.177 g, 32%). **<sup>1</sup>H-NMR** (500 MHz, *d*<sub>6</sub>-DMSO, 298K): δ (ppm): 7.94 (m, 1H, aromatic), 7.82 (m, 1H, aromatic), 7.43 (m, 2H, aromatic), 5.09 (m, 1H, <sup>3</sup>*J* = 6.9 Hz, (CH<sub>3</sub>)<sub>2</sub>CH), 4.46 (t, 2H, <sup>3</sup>*J* = 7.1 Hz, NCH<sub>2</sub>CH<sub>2</sub>), 1.84 (quin, 2H, <sup>3</sup>*J* = 6.9 Hz, NCH<sub>2</sub>CH<sub>2</sub>CH<sub>2</sub>), 1.67 (d, 6H, <sup>3</sup>*J* = 6.9 Hz, (CH<sub>3</sub>)<sub>2</sub>CH), 1.24 (m, 10H, CH<sub>2</sub>), 0.81 (t, 3H, <sup>3</sup>*J* = 6.9 Hz, CH<sub>2</sub>CH<sub>3</sub>). **<sup>13</sup>C-NMR** (126 MHz, *d*<sub>6</sub>-DMSO, 298K): δ (ppm): 185.29 (CAg), 133.44 (CCHCH), 132.28 (CCHCH), 124.00 (CHCH), 123.72 (CHCH), 112.69 (CCHCH), 112.22 (CCHCH), 51.98 (NCH(CH<sub>3</sub>)<sub>2</sub>), 48.97 (NCH<sub>2</sub>), 31.13 (CH<sub>2</sub>), 29.80 (CH<sub>2</sub>), 28.52 (CH<sub>2</sub>), 28.49 (CH<sub>2</sub>), 26.09 (CH<sub>2</sub>), 22.48 (CH<sub>2</sub>), 22.01 (CH<sub>2</sub>), 13.91 (CH<sub>3</sub>). **IR** (ATR, cm<sup>-1</sup>): 2926, 2852, 2214, 1737, 1652, 1604, 1556, 1477, 1462, 1408, 1390, 1371, 1296, 1228, 1217, 1203, 1168, 1141, 1087, 1016, 918, 750, 725, 644, 611, 570, 528, 432. **HRMS (ES<sup>+</sup>)** found *m/z* 651.3552, calculated *m/z* 651.3556 for [C<sub>36</sub>H<sub>56</sub>N<sub>4</sub><sup>107</sup>Ag] (NHC-Ag-NHC<sup>+</sup>) (-0.6 ppm).



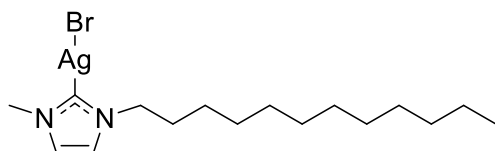
**3-dodecyl-1-isopropylbenzimidazol-2-ylidene silver(I) bromide (5Ag)** (0.390 g, 63%). .  $^1\text{H-NMR}$  (500 MHz,  $d_6$ -DMSO, 298K):  $\delta$  (ppm): 7.92 (m, 1H, aromatic), 7.81 (m, 1H, aromatic), 7.42 (m, 2H, aromatic), 5.13 (sep, 1H,  $^3J = 6.6$  Hz,  $(\text{CH}_3)_2\text{CH}$ ), 4.48 (t, 2H,  $^3J = 6.8$  Hz,  $\text{NCH}_2\text{CH}_2$ ), 1.84 (quin, 2H,  $^3J = 6.8$  Hz,  $\text{NCH}_2\text{CH}_2\text{CH}_2$ ), 1.67 (d, 6H,  $^3J = 6.7$  Hz,  $(\text{CH}_3)_2\text{CH}$ ), 1.24 (m, 18H,  $\text{CH}_2$ ), 0.80 (t, 3H,  $^3J = 7.0$  Hz,  $\text{CH}_2\text{CH}_3$ ).  $^{13}\text{C-NMR}$  (126 MHz,  $d_6$ -DMSO, 298K):  $\delta$  (ppm): 186.59, 133.54 (CCHCH), 132.38 (CCHCH), 124.12 (CHCH), 123.86 (CHCH), 112.78 (CCHCH), 112.28 (CCHCH), 52.01 ( $\text{NCH}(\text{CH}_3)_2$ ), 49.04 ( $\text{NCH}_2$ ), 31.35 ( $\text{CH}_2$ ), 29.06 ( $\text{CH}_2$ ), 28.98 ( $\text{CH}_2$ ), 28.74 ( $\text{CH}_2$ ), 26.21 ( $\text{CH}_2$ ), 22.16 ( $\text{CH}_2$ ), 14.02 ( $\text{CH}_3$ ). **IR** (ATR,  $\text{cm}^{-1}$ ): 2922, 2850, 1737, 1477, 1458, 1409, 1388, 1365, 1294, 1228, 1217, 1136, 1089, 1016, 931, 887, 790, 742, 528. **HRMS (ES+)** found  $m/z$  765.4813, calculated  $m/z$  765.4805 for  $[\text{C}_{44}\text{H}_{72}\text{N}_4^{109}\text{Ag}]$  ( $\text{NHC-Ag-NHC}^+$ ) (+1.0 ppm).



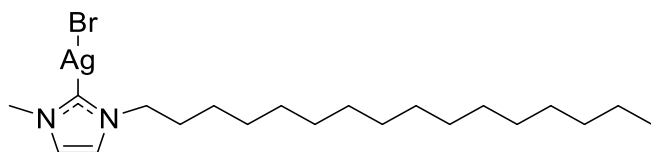
**3-hexadecyl-1-isopropylbenzimidazol-2-ylidene silver(I) bromide (6Ag)** (0.467 g, 68%). .  $^1\text{H-NMR}$  (500 MHz,  $d_6$ -DMSO, 298K):  $\delta$  (ppm): 7.93 (m, 1H, aromatic), 7.82 (m, 1H, aromatic), 7.44 (m, 2H, aromatic), 5.12 (sep, 1H,  $^3J = 6.8$  Hz,  $(\text{CH}_3)_2\text{CH}$ ), 4.48 (t, 2H,  $^3J = 7.1$  Hz,  $\text{NCH}_2\text{CH}_2$ ), 1.84 (quin, 2H,  $^3J = 7.0$  Hz,  $\text{NCH}_2\text{CH}_2\text{CH}_2$ ), 1.68 (d, 6H,  $^3J = 6.9$  Hz,  $(\text{CH}_3)_2\text{CH}$ ), 1.24 (m, 26H,  $\text{CH}_2$ ), 0.82 (t, 3H,  $^3J = 6.9$  Hz,  $\text{CH}_2\text{CH}_3$ ).  $^{13}\text{C-NMR}$  (126 MHz,  $d_6$ -DMSO, 298K):  $\delta$  (ppm): 186.23 (CAg), 133.50 (CCHCH), 132.37 (CCHCH), 124.10 (CHCH), 123.85 (CHCH), 112.76 (CCHCH), 112.26 (CCHCH), 51.97 ( $\text{NCH}(\text{CH}_3)_2$ ), 49.04 ( $\text{NCH}_2$ ), 31.35 ( $\text{CH}_2$ ), 29.95 ( $\text{CH}_2$ ), 29.09 ( $\text{CH}_2$ ), 29.07 ( $\text{CH}_2$ ), 29.05 ( $\text{CH}_2$ ), 29.02 ( $\text{CH}_2$ ), 28.95 ( $\text{CH}_2$ ), 28.93 ( $\text{CH}_2$ ), 28.76 ( $\text{CH}_2$ ), 28.64 ( $\text{CH}_2$ ), 26.20 ( $\text{CH}_2$ ), 22.59 ( $\text{CH}_2$ ), 22.15 ( $\text{CH}_2$ ), 13.99 ( $\text{CH}_3$ ). **IR** (ATR,  $\text{cm}^{-1}$ ): 2918, 2850, 1739, 1463, 1386, 1369, 1294, 1228, 1203, 1136, 1087, 1016, 918, 738, 642, 509, 445. **HRMS (ES+)** found  $m/z$  877.6069, calculated  $m/z$  877.6057 for  $[\text{C}_{52}\text{H}_{88}\text{N}_4^{109}\text{Ag}]$  ( $\text{NHC-Ag-NHC}^+$ ) (+1.4 ppm).



**1-methyl-3-octylimidazol-2-ylidene silver(I) bromide (7Ag)** (0.316 g, 69%). **<sup>1</sup>H-NMR** (500 MHz, d<sub>6</sub>-DMSO, 298K): δ (ppm): 7.48 (d, 1H, <sup>4</sup>J = 1.6 Hz, NCHCHN), 7.42 (d, 1H, <sup>4</sup>J = 1.6 Hz, NCHCHN), 4.07 (t, 2H, <sup>3</sup>J = 7.1 Hz, NCH<sub>2</sub>CH<sub>2</sub>), 3.78 (s, 3H, NCH<sub>3</sub>), 1.75 (m, 2H, <sup>3</sup>J = 7.1 Hz, NCH<sub>2</sub>CH<sub>2</sub>CH<sub>2</sub>), 1.23 (m, 10H, CH<sub>2</sub>), 0.84 (t, 3H, J = 6.9 Hz, CH<sub>2</sub>CH<sub>3</sub>). **<sup>13</sup>C-NMR** (126 MHz, d<sub>6</sub>-DMSO, 298K): δ (ppm): 179.19 (C-Ag), 122.93 (NCHCHN), 121.77 (NCHCHN), 50.71 (NCH<sub>2</sub>), 38.09 (NCH<sub>3</sub>), 31.22 (CH<sub>2</sub>), 30.96 (CH<sub>2</sub>), 28.62 (CH<sub>2</sub>), 28.49 (CH<sub>2</sub>), 25.81 (CH<sub>2</sub>), 22.10 (CH<sub>2</sub>), 13.99 (CH<sub>3</sub>). MS (ESI) 495.24 [NHC-Ag-NHC<sup>+</sup>]. This matches data reported by Che *et al.*<sup>69</sup>

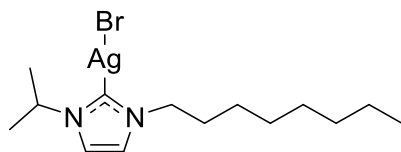


**3-dodecyl-1-methylimidazol-2-ylidene silver(I) bromide (8Ag)** (0.399 g, 76%). **<sup>1</sup>H-NMR** (500 MHz, d<sub>6</sub>-DMSO, 298K): δ (ppm): 7.48 (d, 1H, <sup>4</sup>J = 1.7 Hz, NCHCHN), 7.42 (d, 1H, <sup>4</sup>J = 1.6 Hz, NCHCHN), 4.07 (t, 2H, <sup>3</sup>J = 7.0 Hz, NCH<sub>2</sub>CH<sub>2</sub>), 3.78 (s, 3H, NCH<sub>3</sub>), 1.75 (quin, 2H, <sup>3</sup>J = 7.1 Hz, NCH<sub>2</sub>CH<sub>2</sub>CH<sub>2</sub>), 1.24 (m, 18H, CH<sub>2</sub>), 0.85 (t, 3H, <sup>3</sup>J = 6.9 Hz, CH<sub>2</sub>CH<sub>3</sub>). **<sup>13</sup>C-NMR** (126 MHz, d<sub>6</sub>-DMSO, 298K): δ (ppm): 179.37 (C-Ag), 122.92 (NCHCHN), 121.76 (NCHCHN), 50.70 (NCH<sub>2</sub>), 38.09 (NCH<sub>3</sub>), 31.33 (CH<sub>2</sub>), 30.96 (CH<sub>2</sub>), 29.05 (CH<sub>2</sub>), 29.00 (CH<sub>2</sub>), 28.96 (CH<sub>2</sub>), 28.75 (CH<sub>2</sub>), 28.54 (CH<sub>2</sub>), 25.81 (CH<sub>2</sub>), 22.14 (CH<sub>2</sub>), 14.00 (CH<sub>3</sub>). **MS (ESI)** 607.35 [NHC-Ag-NHC<sup>+</sup>]. This matches data reported by Çetinkaya *et al.*<sup>70</sup>

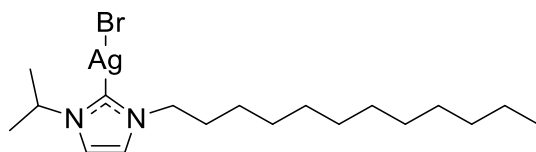


**3-hexadecyl-1-methylimidazol-2-ylidene silver(I) bromide (9Ag)** (0.480 g, 81%). **<sup>1</sup>H-NMR** (500 MHz, d<sub>6</sub>-DMSO, 298K): δ (ppm): 7.50 (s, 1H, NCHCHN), 7.44 (s, 1H, NCHCHN), 4.09 (t, 2H, J = 6.9 Hz, NCH<sub>2</sub>CH<sub>2</sub>), 3.80 (s, 3H, NCH<sub>3</sub>), 1.77 (quin, 2H, <sup>3</sup>J = 6.8 Hz, NCH<sub>2</sub>CH<sub>2</sub>CH<sub>2</sub>), 1.23 (m, 26H, CH<sub>2</sub>), 0.86 (t, 3H, J = 6.9 Hz, CH<sub>2</sub>CH<sub>3</sub>). **<sup>13</sup>C-NMR** (126 MHz, d<sub>6</sub>-DMSO, 298K): δ (ppm): 122.96 (NCHCHN), 121.81 (NCHCHN), 50.73 (NCH<sub>2</sub>), 38.10 (NCH<sub>3</sub>), 31.34 (CH<sub>2</sub>), 31.01 (CH<sub>2</sub>), 29.08 (CH<sub>2</sub>), 29.05 (CH<sub>2</sub>), 29.01 (CH<sub>2</sub>),

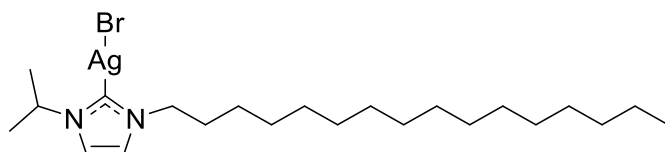
28.97 (CH<sub>2</sub>), 28.76 (CH<sub>2</sub>), 28.56 (CH<sub>2</sub>), 25.84 (CH<sub>2</sub>), 22.14 (CH<sub>2</sub>), 14.01 (CH<sub>3</sub>). **MS (ESI)** 719.53 [NHC-Ag-NHC<sup>+</sup>]. This matches data reported by Che *et al.*<sup>69</sup>



**1-isopropyl-3-octylimidazol-2-ylidene silver(I) bromide (10Ag)** (0.162 g, 33%). **<sup>1</sup>H-NMR** (500 MHz, d<sub>6</sub>-DMSO, 298K): δ (ppm): 7.58 (d, 1H, <sup>4</sup>J = 1.8 Hz, NCHCHN), 7.50 (d, 1H, <sup>4</sup>J = 1.8 Hz, NCHCHN), 4.64 (sep, 1H, <sup>3</sup>J = 6.7 Hz, (CH<sub>3</sub>)<sub>2</sub>CH), 4.07 (t, 2H, J = 7.1 Hz, NCH<sub>2</sub>CH<sub>2</sub>), 1.76 (quin, 2H, <sup>3</sup>J = 6.8 Hz, NCH<sub>2</sub>CH<sub>2</sub>CH<sub>2</sub>), 1.43 (d, 6H, <sup>3</sup>J = 6.7 Hz, (CH<sub>3</sub>)<sub>2</sub>CH), 1.23 (m, 10H, CH<sub>2</sub>), 0.83 (t, 3H, J = 7.0 Hz, CH<sub>2</sub>CH<sub>3</sub>). **<sup>13</sup>C-NMR** (126 MHz, d<sub>6</sub>-DMSO, 298K): δ (ppm): 177.44 (C-Ag), 121.87 (NCHCHN), 118.56 (NCHCHN), 53.40 (NCH(CH<sub>3</sub>)<sub>2</sub>), 51.00 (NCH<sub>2</sub>), 31.14 (CH<sub>2</sub>), 30.86 (CH<sub>2</sub>), 28.54 (CH<sub>2</sub>), 28.41 (CH<sub>2</sub>), 25.80 (CH<sub>2</sub>), 23.40 (CH<sub>2</sub>), 22.04 (CH<sub>2</sub>), 13.94 (CH<sub>3</sub>). **HRMS (ES<sup>+</sup>)** found m/z 553.3240 calculated m/z 553.3241 for [C<sub>28</sub>H<sub>52</sub>N<sub>4</sub><sup>109</sup>Ag] (NHC-Ag-NHC<sup>+</sup>) (+0.2 ppm).



**3-dodecyl-1-isopropylimidazol-2-ylidene silver(I) bromide (11Ag)** (0.361 g, 64%). **<sup>1</sup>H-NMR** (500 MHz, d<sub>6</sub>-DMSO, 298K): δ (ppm): 7.58 (d, 1H, <sup>4</sup>J = 1.2 Hz, NCHCHN), 7.50 (s, 1H, NCHCHN), 4.63 (sep, 1H, <sup>3</sup>J = 6.7 Hz, (CH<sub>3</sub>)<sub>2</sub>CH), 4.07 (t, 2H, <sup>3</sup>J = 7.0 Hz, NCH<sub>2</sub>CH<sub>2</sub>), 1.77 (quin, 2H, <sup>3</sup>J = 6.7 Hz, NCH<sub>2</sub>CH<sub>2</sub>CH<sub>2</sub>), 1.43 (d, 6H, <sup>3</sup>J = 6.7 Hz, (CH<sub>3</sub>)<sub>2</sub>CH), 1.21 (m, 18H, CH<sub>2</sub>), 0.84 (t, 3H, <sup>3</sup>J = 6.8 Hz, CH<sub>2</sub>CH<sub>3</sub>). **<sup>13</sup>C-NMR** (126 MHz, d<sub>6</sub>-DMSO, 298K): δ (ppm): 177.42 (C-Ag), 121.88 (NCHCHN), 118.58 (NCHCHN), 53.42 (NCH(CH<sub>3</sub>)<sub>2</sub>), 51.02 (NCH<sub>2</sub>), 31.30 (CH<sub>2</sub>), 30.88 (CH<sub>2</sub>), 29.02 (CH<sub>2</sub>), 28.92 (CH<sub>2</sub>), 28.90 (CH<sub>2</sub>), 28.70 (CH<sub>2</sub>), 28.46 (CH<sub>2</sub>), 25.80 (CH<sub>2</sub>), 23.41 (CH<sub>2</sub>), 22.10 (CH<sub>2</sub>), 13.96 (CH<sub>3</sub>). **IR** (ATR, cm<sup>-1</sup>): 3140, 3089, 2916, 2846, 2357, 2339, 1463, 1425, 1373, 1232, 1213, 1136, 1110, 887, 835, 752, 725, 677, 551, 530, 418. **HRMS (ES<sup>+</sup>)** found m/z 663.4490, calculated m/z 663.4495 for [C<sub>36</sub>H<sub>68</sub>N<sub>4</sub><sup>107</sup>Ag] (NHC-Ag-NHC<sup>+</sup>) (-0.8 ppm).



**3-hexadecyl-1-isopropylimidazol-2-ylidene silver(I) bromide (12Ag)** (0.457 g, 73%). **<sup>1</sup>H-NMR** (500 MHz, (CD<sub>3</sub>)<sub>2</sub>CO, 298K): 7.49 (d, 1H, <sup>4</sup>J = 1.8 Hz, NCHCHN), 7.44 (d, 1H,

$^4J = 1.8$  Hz, NCHCHN), 4.79 (sep, 1H,  $^3J = 6.8$  Hz,  $(\text{CH}_3)_2\text{CH}$ ), 4.21 (t, 2H,  $^3J = 7.2$  Hz,  $\text{NCH}_2\text{CH}_2$ ), 1.84 (quin, 2H,  $^3J = 7.2$  Hz,  $\text{NCH}_2\text{CH}_2\text{CH}_2$ ), 1.53 (d, 6H,  $^3J = 6.8$  Hz,  $(\text{CH}_3)_2\text{CH}$ ), 1.33 (m, 26H,  $\text{CH}_2$ ), 0.88 (t, 3H,  $J = 6.9$  Hz,  $\text{CH}_2\text{CH}_3$ ).  **$^{13}\text{C-NMR}$**  (126 MHz,  $\text{d}_6\text{-DMSO}$ , 298K):  $\delta$  (ppm): 177.36 (C-Ag), 121.87 (NCHCHN), 118.58 (NCHCHN), 53.41 (NCH $(\text{CH}_3)_2$ ), 50.99 (NCH $_2$ ), 31.28 ( $\text{CH}_2$ ), 30.84 ( $\text{CH}_2$ ), 29.02 ( $\text{CH}_2$ ), 28.99 ( $\text{CH}_2$ ), 28.89 ( $\text{CH}_2$ ), 28.87 ( $\text{CH}_2$ ), 28.69 ( $\text{CH}_2$ ), 28.43 ( $\text{CH}_2$ ), 25.78 ( $\text{CH}_2$ ), 23.39 ( $\text{CH}_2$ ), 22.08 ( $\text{CH}_2$ ), 13.94 ( $\text{CH}_3$ ). **IR** (ATR,  $\text{cm}^{-1}$ ): 3145, 3116, 3089, 2916, 2848, 2360, 2330, 1558, 1471, 1425, 1375, 1217, 1180, 1134, 883, 846, 754, 719, 677, 549, 418. **HRMS (ES+)** found  $m/z$  775.5735, calculated  $m/z$  775.5747 for  $[\text{C}_{44}\text{H}_{84}\text{N}_4^{107}\text{Ag}]$  (NHC-Ag-NHC $^+$ ) (-1.5 ppm).

### Determination of the critical micelle concentration by conductivity

The critical micelle concentration of long-chain benzimidazolium salts and imidazolium salts was elucidated by conductimetry. Stock solutions of the (benz)imidazolium bromide salt were serially diluted using distilled water, and each solution was in turn added to a vessel in the water bath and allowed to equilibrate for 5 minutes. The specific conductivity of each solution was measured thrice at 25 °C. This process was repeated at 30, 35, and 40 °C. Average specific conductivities were plotted against salt concentration in order to determine the CMC.

### Determination of Krafft temperature

The Krafft temperature of each long chain imidazolium/benzimidazolium was determined by conductivity measurements in a manner similar to that reported by El-Dossoki.<sup>71</sup> Briefly, (benz)imidazolium bromide salts were suspended in water at a concentration 10 times their CMC. The suspensions were then left at 4 °C overnight. The temperature of the suspension was then raised slowly in a water bath, with conductivity measurements being taken three times per degree Celsius. The suspension was measured until it was determined that it had turned clear.

### MIC testing

A (benz)imidazolium salt or Ag-NHC of interest were dissolved to a final concentration of 10 mg/mL in DMSO. The salt/NHC was then serially diluted by half seven times to produce 8 test solutions. The test solutions were then diluted further into Mueller-Hinton broth (MHB) (980  $\mu\text{L}$ ). The test solution (100  $\mu\text{L}$ ) was pipetted into a single well on a 96-well plate tissue culture plate. An inoculum of a test organism in broth (either: *S. epidermidis* (ATCC 35984/RP62A), *S. epidermidis* (ATCC 14990), *S. aureus* (NCTC 6571), *S. aureus* (NCIMB 9518), *P. aeruginosa* (ATCC 15692), or *E. coli* (NCTC 12923)) in MHB (100  $\mu\text{L}$ ,  $1 \times 10^6$  CFU/mL) was added to the test solution. The final DMSO

concentration in the well was 1% v/v. Each concentration was repeated in triplicate. Positive controls for each compound were added in triplicate containing  $5 \times 10^5$  CFU/mL of the appropriate test organism in MHB spiked with 1% v/v DMSO. Negative controls in triplicate, broth containing 1% v/v DMSO). The plates were then incubated for 24 hours at 37 °C. Bacterial growth in each well was then assessed by optical density measurement. The lowest concentration displaying an 80% or greater reduction in growth is the MIC value for the compound against the organism. Each test was conducted in duplicate (except where noted with “\*”) to give a total of 6 values per concentrations per organism. The species and strain numbers of the test organisms used in the MIC testing of Ag-NHCs and their precursors, along with the clinical interest in particular strains are summarised below in Table 1.

Organism	Shape	Gram stain	Notes
<i>Staphylococcus epidermidis</i> (ATCC 35984/RP62A)	Spherical	+	Not typically pathogenic. Grows on skin and is associated with infections via catheters or implants. This strain is able to form biofilms and is methicillin resistant. <sup>72</sup>
<i>Staphylococcus epidermidis</i> (ATCC 14990)	Spherical	+	Not typically pathogenic. Grows on skin and is associated with infections via catheter or implants. Type strain. <sup>73</sup>
<i>Staphylococcus aureus</i> (NCTC 6571)	Spherical	+	Opportunistic pathogen. Common bacterial species in humans. Some strains are particularly resistant to antibiotics (MRSA). Antimicrobial testing control strain. <sup>74</sup>
<i>Staphylococcus aureus</i> (NCIMB 9518)	Spherical	+	Opportunistic pathogen. Common bacterial species in humans. Some strains are particularly resistant to antibiotics (MRSA). Antimicrobial testing control strain. <sup>74</sup> NCIMB quality control strain.
<i>Pseudomonas aeruginosa</i> (ATCC 15692)	Rod	-	Multidrug resistant pathogen, associated with hospital-acquired infections such as ventilator-acquired pneumonia. <sup>75</sup>
<i>Escherichia coli</i> (NCTC 12923)	Rod	-	Coliform bacteria. Most strains are harmless, however some strains may cause food poisoning. This strain has an insertion element within ompC, meaning ompF is expressed as the sole outer membrane porin. <sup>76</sup>

**Table 1.** Organisms used in the MIC testing of (benz)imidazolium salts and Ag-NHCs.

## Results and discussion

### Synthesis of compounds

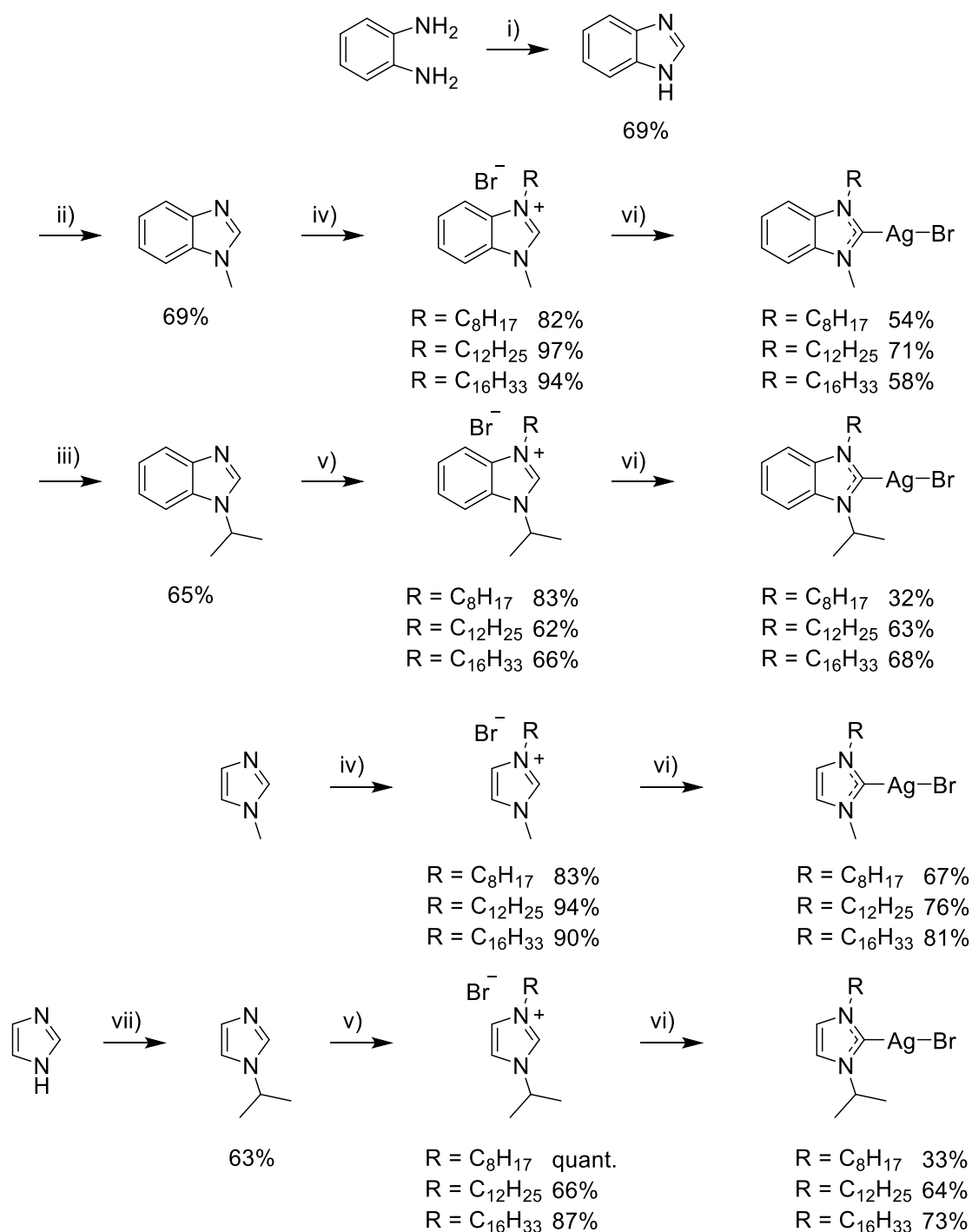


**Figure 10.** Synthetic scheme for the preparation of described compounds. i) formic acid, 2 h, reflux. ii) MeI, KOH, THF, RT, 3 h. iii) Isopropyl bromide, KOH, DMSO, RT, 3.5 hr. iv) RBr, toluene, reflux, overnight. v) RBr, MeCN, reflux, overnight. vi) Ag<sub>2</sub>O, DCM, RT, overnight. vii) Isopropyl bromide, NaH, MeCN, N<sub>2</sub> atmosphere, 0 °C, 30 min, RT, 2 h, 0 °C to RT, overnight.

### **NHC precursor synthesis.**

Benzimidazole was prepared by reaction of formic acid and *o*-phenylenediamine under reflux in a manner similar to that reported in the literature.<sup>77</sup> 1-alkyl benzimidazole and imidazoles were prepared by simple reaction of the azole with a slight excess of alkyl halide, with slight variation for each, except 1-methylimidazole, which was purchased from commercial sources. From these initial experiments it was possible to synthesise <sup>13</sup>C-enriched benzimidazole. This was then alkylated in the same manner as the non-enriched compounds, however no further work was done with these compounds due to time constraints.

Four similar methods were used in the synthesis of long chain imidazolium and benzimidazolium salts, with slight variations. In all cases, the alkylating agent was either 1-bromooctane, 1-bromododecane, or 1-bromohexadecane, and the reactions were heated at reflux overnight. The 3-alkyl-1-methylbenzimidazolium bromide salts (**1-3**) were prepared by reaction of 1-methylbenzimidazole with 1.5 equivalents of alkylating agent in toluene. Upon removal of the solvent the oil produced could be frozen then triturated with diethyl ether to precipitate the product as a white powder. 3-alkyl-1-isopropylbenzimidazolium bromide salts (**4-6**) were similarly prepared but with acetonitrile as the solvent and a smaller excess: 1.2 equivalents of alkyl bromide. The oil produced had to be dissolved in minimal dichloromethane and precipitated with diethyl ether, as the isopropylbenzimidazolium salts were soluble in hexane, and remained an oil in neat diethyl ether, requiring addition of a suitable solvent to disperse the product and impurities before precipitation. 3-alkyl-1-methylimidazolium bromide salts (**7-9**) were prepared in toluene, with a 1:1 ratio of methylimidazole to alkylating agent, but the work up was different for the shorter octyl-substituted salt. 1-methyl-3-octylimidazolium bromide was worked up by removal of solvent, and washing thrice with hexane to yield the product as an oil, whereas the reactions containing the 1-bromododecane and 1-bromohexadecane were allowed to cool to room temperature, whereupon the product precipitated from toluene as a white powder. By contrast, the 3-alkyl-1-isopropylimidazolium bromide salts (**10-12**) were prepared in acetonitrile. The acetonitrile was removed, and the oil triturated with hexane to yield the product. By comparison with the methyl substituted imidazolium salts, where the C<sub>8</sub>-chain produced an oil and the longer chain produced a solid, the C<sub>8</sub> and C<sub>12</sub>-chain substituted isopropylimidazolium salts were oils, and only the C<sub>16</sub>-substituted salt was a solid. It is also worth noting that addition of the fused benzene ring to the benzimidazolium salts gave them greater solubility in hexane, so diethyl ether was chosen as the triturating agent. Diethyl ether's high vapour pressure was also a helpful factor in purifying the

benzimidazolium salts as it readily evaporated. An excess of alkyl bromide was used in the reaction with 1-alkylbenzimidazole by comparison with 1-alkylimidazole due to the decreased nucleophilicity of the benzimidazole lone pair by comparison with the imidazole.

### **Silver NHC complex synthesis.**

Ag-NHCs were prepared in a manner derived from the literature with slight modifications.<sup>78-80</sup> Fresh silver oxide was prepared before each reaction to act as both the silver source and a weak base. Aged silver oxide was found to decompose slowly to yield silver metal, and thus caused the reactions to have lower yields. An excess of silver oxide was used in the reaction in order to encourage the formation of the [AgBr(NHC)] species. The reaction was conducted in DCM so that the equilibrium between the monomeric carbene and its dimeric [Ag(NHC)<sub>2</sub>][AgBr<sub>2</sub>] ionic species would favour the monomer due to DCM being non-polar.<sup>31</sup> The reactions were conducted at room temperature overnight and were wrapped in foil in order to exclude light due to the inherent light sensitivity of silver coordination complexes in solution.<sup>81</sup> The Ag-NHCs were all white to off-white powders, regardless of whether the parent imidazolium or benzimidazolium salt was a liquid or a solid. The Ag-NHCs were prepared in poor to good yields (32-81 % yield), with most examples exhibiting yields of greater than 55%. One factor that greatly affected yield was the exposure of the Ag-NHC reaction mixture to light during the work up process, as it was observed that the white precipitate forming would grey and then darken when exposed to light for too long, forming silver metal. This had the potential to severely decrease yields, and make the work up challenging. Those complexes of the type 3-alkyl-1-isopropylbenzimidazol-2-ylidene silver(I) bromide (**4Ag--6Ag**) appeared to be more sensitive than the others, and had to be handled under red light only during purification.

### **NMR spectroscopy**

The NMR spectra of all compounds synthesised were measured in either CDCl<sub>3</sub>, d<sub>6</sub>-DMSO, or d<sub>6</sub>-acetone. The NMR spectra of Ag-NHCs was typically measured in d<sub>6</sub>-DMSO due to a lack of solubility in other commonly available solvents. Known compounds matched well with the spectra already reported in the literature.<sup>64-70</sup> The formation of a (benz)imidazolium salt from a 1-alkyl(benz)imidazole was easily characterised by the formation of a large, broad multiplet around 1.2-1.3 ppm derived from the methylene protons in the alkyl chain. The accompanying terminal methyl group is found at typically 0.68-0.85 ppm, and is more easily used to assess whether there is any excess alkyl bromide left in solution by comparison of its integration to that of the

imidazole/benzimidazole protons. A new signal arises between 4.1 and 4.8 ppm, typically split into a triplet, signifying the alpha methylene protons of the alkyl chain upon quaternisation of the nitrogen by the alkylating agent. The position of the C2-proton on the spectrum is also much further downfield (roughly 2 ppm) indicating that the proton environment is far more deshielded as a result of the quaternisation of the second nitrogen. The formation of an imidazolium salt is also clear in the  $^{13}\text{C}$ -NMR due to the evolution of a new shift around 45-50 ppm: the  $\alpha$ -methylene group of the newly bound alkyl chain. Assignment of the alkyl carbons alpha to each nitrogen is possible with a fair amount of certainty due to comparison with literature values.<sup>64-68</sup> The unambiguous assignment of each methylene in the alkyl chain is beyond the scope of this work, as it does not provide any value to the determination of the effects of alkyl chain length on the surface activity or antimicrobial efficacy of the salts described. The assignment of which backbone carbon corresponds to which shift in the asymmetric imidazolium salts is also difficult. The assignment of the aromatic benzimidazole carbon shifts was done based on literature precedence for other known benzimidazolium salts.<sup>62,64,65</sup>

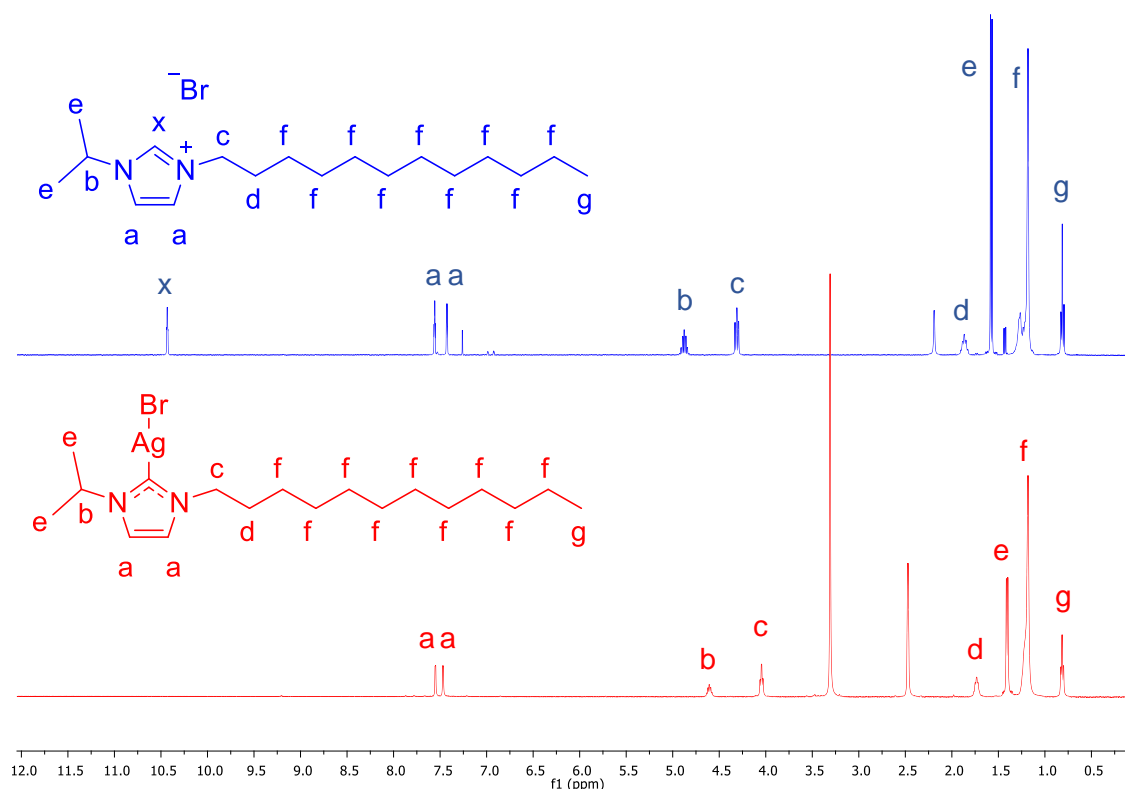


**Figure 11.** Example  $^1\text{H}$ -NMR spectra of the formation of an Ag-NHC (**11Ag**, red) from an imidazolium salt (**11**, blue). Imidazolium salt spectrum recorded in  $\text{CDCl}_3$ , Ag-NHC spectrum recorded in  $d_6$ -DMSO. The disappearance of the shift at 10.39 ppm signifies the deprotonation of the imidazolium salt upon formation of the Ag-NHC.

The formation of Ag-NHCs from an imidazolium salt is clear in both  $^1\text{H}$ - and  $^{13}\text{C}\{^1\text{H}\}$ -NMR spectroscopy. This is in part due to the key C2 carbon that is deprotonated by  $\text{Ag}_2\text{O}$ . There are no longer shifts present from the acidic C2-bonded proton as it has been removed in the  $^1\text{H}$ -NMR (Figure 11), leading to the loss of the furthest downfield signal in all the above reported imidazolium salts upon formation of the Ag-NHC. There is also a slight change in the other aromatic protons, with the backbone protons in methylimidazol-2-ylidene Ag(I)Br species being shifted slightly upfield by comparison with their parent salts. This phenomenon is not seen in their isopropyl-substituted counterparts, where there is no change in the backbone proton shifts. The small changes observed during complexation may be artefacts of the change in solvent in most cases from  $\text{CDCl}_3$  to  $d_6$ -DMSO, but the absence of the furthest downfield proton shift is clear to observe.

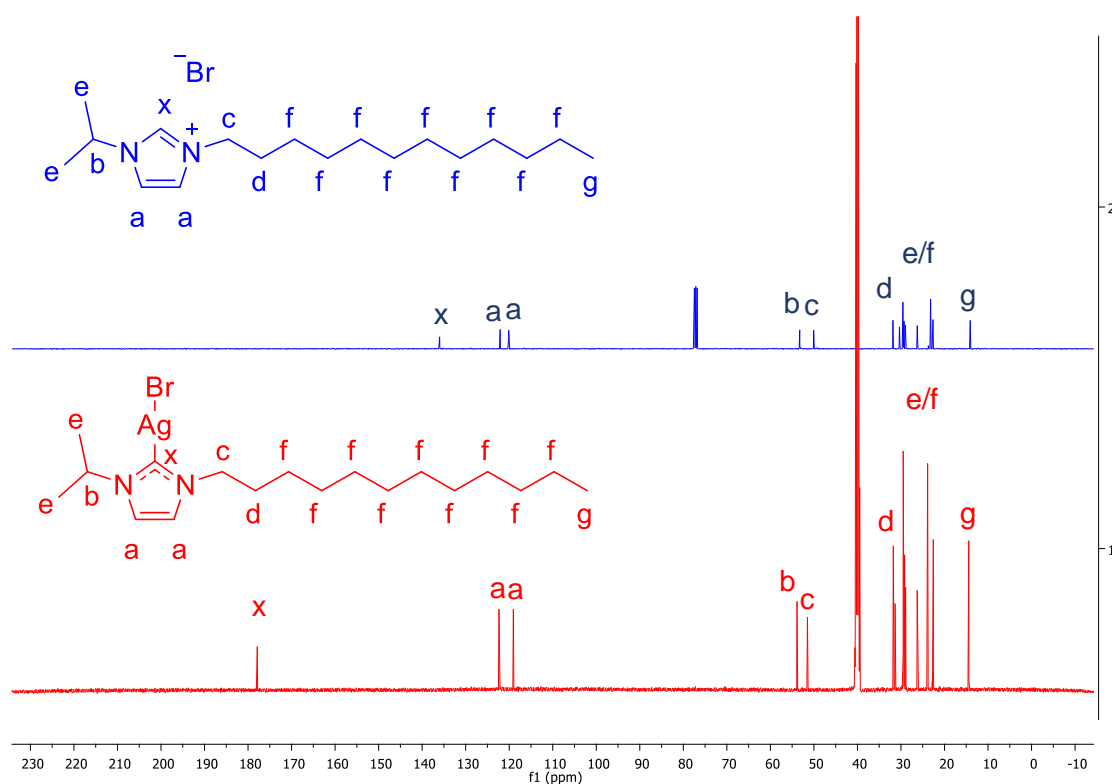


**Figure 12.** Example of  $^{13}\text{C}\{^1\text{H}\}$ -NMR spectra of the formation of an Ag-NHC (**11Ag**, red) from an imidazolium salt (**11**, blue). Imidazolium salt spectrum recorded in  $\text{CDCl}_3$ , Ag-NHC spectrum recorded in  $d_6$ -DMSO. A large shift downfield of the C2- carbon signal upon complexation is observed. Note that  $^{107/109}\text{Ag}$  satellites are not observed.

Another key indicator of the formation of an Ag-NHC from its parent salt is the large downfield shift in the signal attributable to the C2-carbon in  $^{13}\text{C}\{^1\text{H}\}$ -NMR upon complexation. In almost all cases, as shift downfield of greater than 30 ppm is observed,

with the new CAg carbene signal appearing between 170 and 190 ppm where present. In some cases (such as 3-hexadecyl-1-methylimidazol-2-ylidene silver(I) bromide) this shift downfield is not observed, but rather the furthest downfield shift belonging to the C2 carbon in the parent salt is no longer present. This potentially suggests that the carbene has formed but there is a dynamic equilibrium present faster than NMR timescale. This is consistent with the literature, where reports of “scrambling” of Ag-NHCs between a monomeric and dimeric species are known,<sup>32,82</sup> and where it is common that the C2 CAg signal may not be observed.<sup>83–85</sup>

### Mass spectrometry

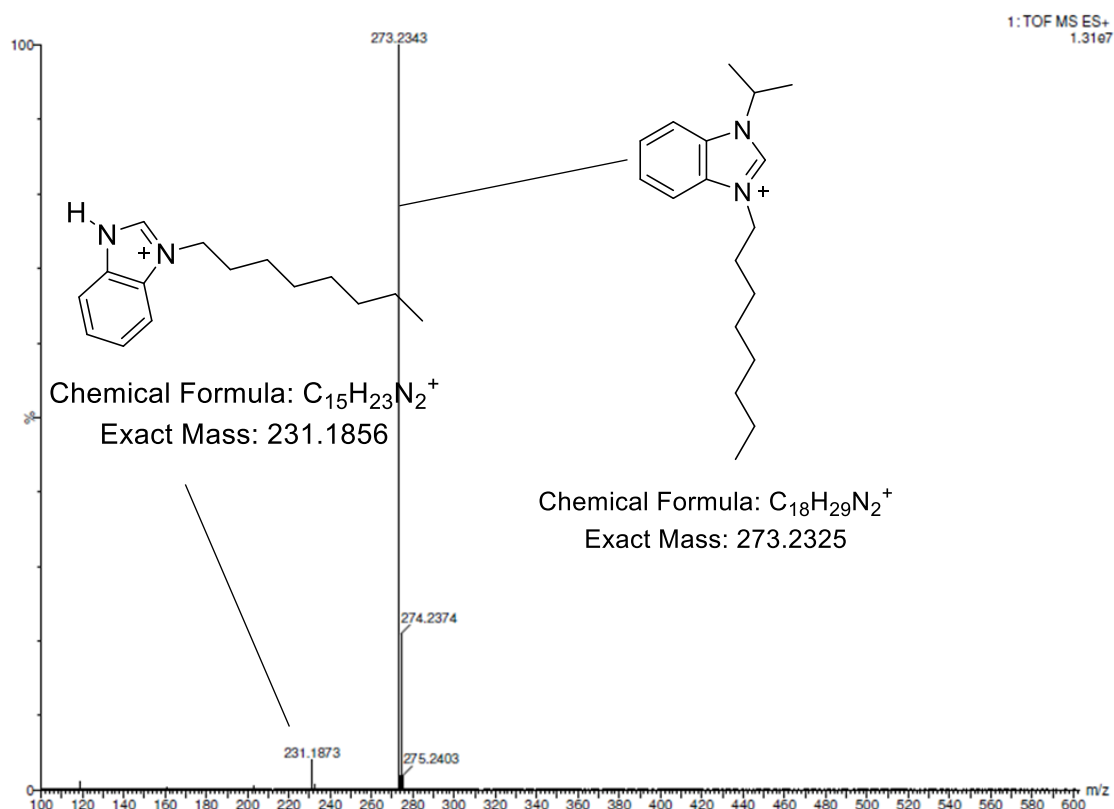


**Figure 13.** Exemplary high resolution mass spectrum of an imidazolium salt: 4.

The mass spectra for all imidazolium/benzimidazolium salts were recorded in positive mode electrospray ionisation. In all cases the principal peak belongs to the  $[M - Br]^-$  peak. In the case of Ag-NHCs, the mass spectra have a principal peak belonging to the  $[Ag(NHC)_2]^+$  cation. This species is the cationic component of the dimeric form observed in the dynamic equilibrium of Ag-NHCs observed in solution, which is discussed above. The appearance of this species is likely to be the observable species under ionisation when detected in positive mode. The mass spectra of all Ag-NHCs show good agreement with the predicted values for the  $[Ag(NHC)_2]^+$  cation, and all spectra contain the distinct isotope pattern of Ag, with principal peaks in the pattern caused by  $^{107}Ag$

([M]<sup>+</sup>) and <sup>109</sup>Ag ([M]<sup>+</sup> + 2). In some cases, peaks belonging to the parent imidazolium salt are observed, but it is unclear whether this is decomposition of the Ag-NHC under ionisation or trace levels of impurity not detected by NMR spectroscopy.

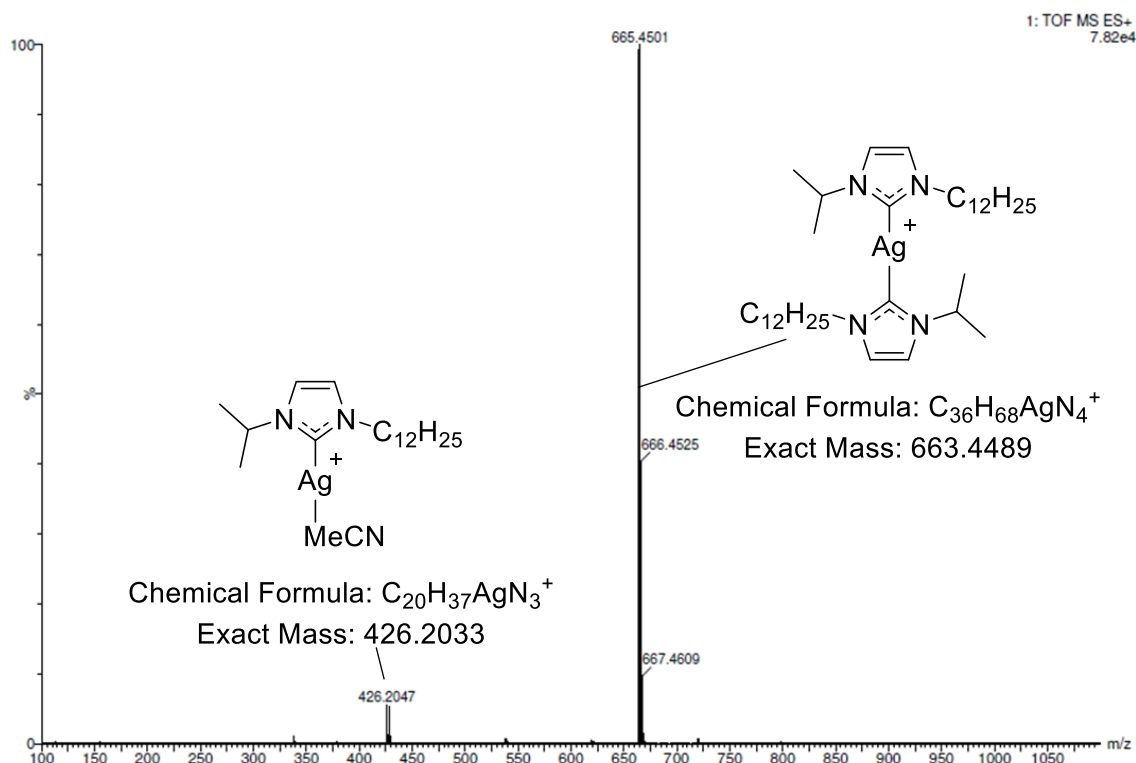
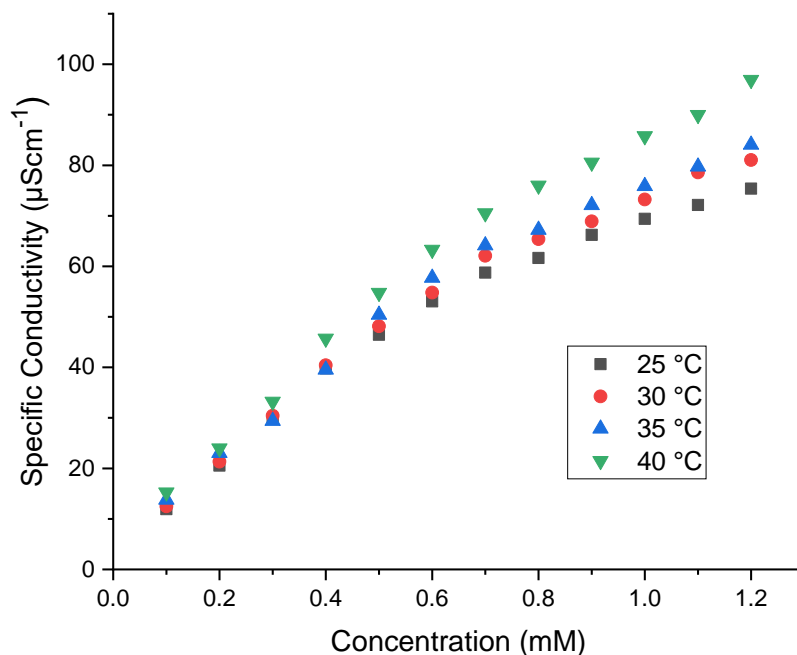


**Figure 14.** Exemplary high resolution mass spectrum of an Ag-NHC: **11Ag** containing a bis(3-dodecyl-1-isopropylimidazol-2-ylidene)silver(I) cation: the dimeric  $[Ag(NHC)_2]^+$  form of **11Ag**. Also observed is the  $[AgNHC + MeCN]$  adduct.

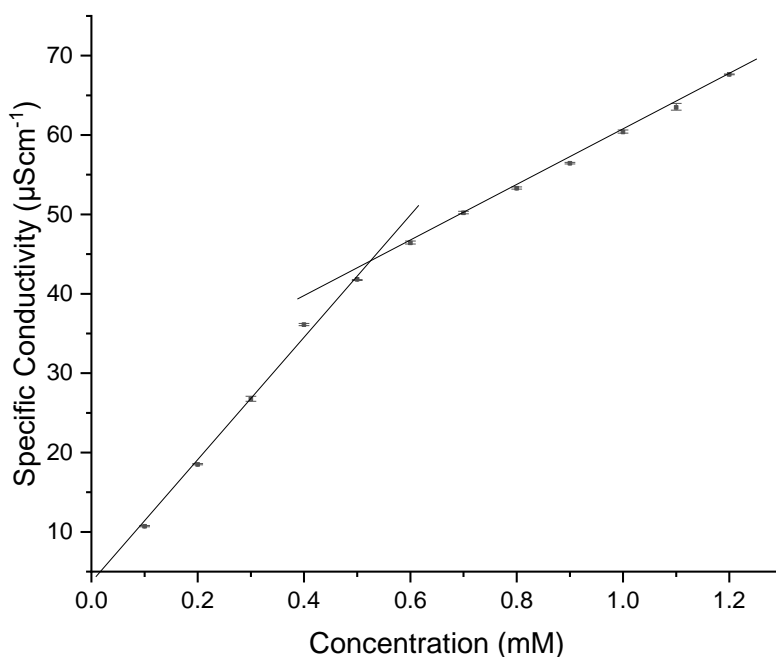
### Determination of CMC by conductivity

The determination of the critical micelle concentration of the synthesised imidazolium bromide salts in aqueous media was assessed using conductivity based on methodologies employed in the literature.<sup>71,86,87</sup> Conductimetry was chosen as the method of CMC determination due to it being an appropriate method for ionic surfactants such as imidazolium salts,<sup>67,71,86</sup> the ease of use vs a tensiometer,<sup>88,89</sup> and due to the fact that it does not introduce additional components that may influence the CMC i.e., pyrene or similar.<sup>90,91</sup> A concentrated solution of each imidazolium salt was prepared based on literature knowledge of the CMC of similar compounds and within the limits of the solubility of each salt.<sup>67,68,87,92,93</sup> Some of the benzimidazolium salts were not soluble at room temperature due to their Krafft temperatures being higher than room temperature (*vide infra*). With a decrease of concentration comes a decrease in conductivity. The increase in conductivity with the increase in concentration is coupled with a decrease in

the viscosity of the solvent with increasing temperature, leading to an overall increase in specific conductivity with temperature.<sup>86</sup>

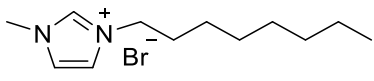
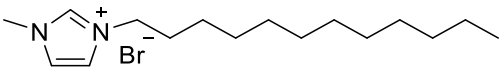
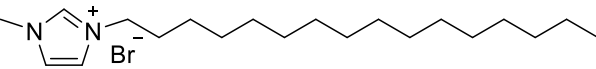
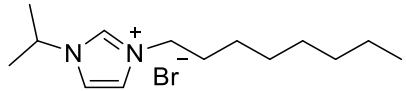
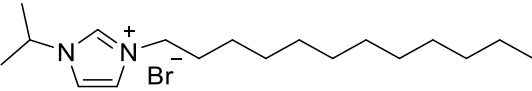


**Figure 15.** Plot of specific conductivity of a solution vs concentration of **9** recorded at 25 °C, 30°C, 35°C, and 40 °C. Error bars are removed for clarity.

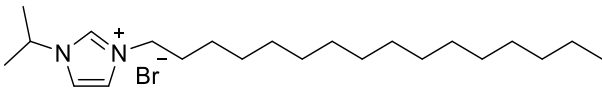
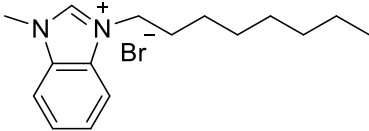
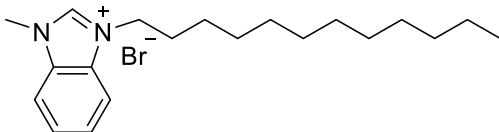
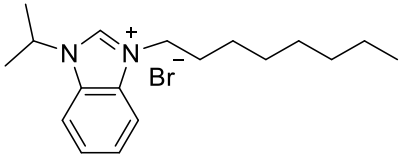


**Figure 16.** Plot of specific conductivity of a solution vs concentration of **12** recorded at 25 °C. The plot illustrates the two linear regimes discussed that are observed for the free surfactant unimers and the micellar form. Data points are from the mean of 3 values recorded, whereas errors are based on the conductivity extremes of each concentration.

As can be seen from the example graph of **12** (Figure 16), when the average specific conductivity is plotted against concentration two linear regimes emerge. The two separate regimes indicate two species in the solution as expected: the change in conductivity with concentration for free surfactant in the lower concentrations, and a more gradual change in conductivity with concentration following the formation and aggregation of micelles. This is due to micelles being less mobile than their constituent unimers in solution, with the decrease in the rate of change in the conductivity of micelles vs free surfactant being based on the association of counter ions in solution to the micelle, leaving less free anions in solution to support current.<sup>86</sup> The CMC of a particular surfactant may be determined by acquiring the formulae for both linear relationships between the average specific conductivity and concentration and finding the point of intersection. The plots also allow for the estimation of the degree of counter ion binding ( $\beta$ ) to be calculated from the slope of the linear regime above the CMC (described later).<sup>71,94,95</sup> The experimentally determined CMCs and estimated  $\beta$  values are reported below in Table 2.

Salt	Temperature (°C)	CMC (mM)	$\beta$
1-methyl-3-octylimidazolium bromide ( <b>7</b> ) 	25	178	0.43
	30	186	0.46
	35	192	0.47
	40	196	0.43
3-dodecyl-1-methylimidazolium bromide ( <b>8</b> ) 	25	10.5	0.67
	30	11.0	0.67
	35	11.6	0.65
	40	11.7	0.62
3-hexadecyl-1-methylimidazolium bromide ( <b>9</b> ) 	25	0.62	0.60
	30	0.63	0.54
	35	0.66	0.55
	40	0.68	0.47
1-isopropyl-3-octylimidazolium bromide ( <b>10</b> ) 	25	157	0.60
	30	154	0.57
	35	153	0.55
	40	151	0.50
3-dodecyl-1-isopropylimidazolium bromide ( <b>11</b> ) 	25	8.26	0.7
	30	8.19	0.67
	35	8.12	0.64
	40	7.99	0.61

**Table 2.** CMC determined by conductivity over a range of temperatures for various long-chain (benz)imidazolium bromide salts and calculated  $\beta$  values (1/2).

3-hexadecyl-1-isopropylimidazolium bromide (12) 	25 30 35 40	0.50 0.50 0.49 0.48	0.57 0.61 0.52 0.51
1-methyl-3-octylbenzimidazolium bromide (1) 	25 30 35 40	102 103 106 108	0.59 0.57 0.57 0.55
3-dodecyl-1-methylbenzimidazolium bromide (2) 	35 40	5.80 6.26	0.57 0.57
1-isopropyl-3-octylbenzimidazolium bromide (4) 	25 30 35 40	90.1 90.5 92.9 90.7	0.55 0.55 0.54 0.56
3-dodecyl-1-methylimidazolium bromide (tensiometry) <sup>92</sup>	25	10.6	-
1-methyl-3-octylimidazolium bromide (tensiometry) <sup>67</sup>	25	170	-
3-hexadecyl-1-methylimidazolium bromide (tensiometry) <sup>87</sup>	25	0.51	-

**Table 2 cont.** CMCs determined by conductivity over a range of temperatures for various long-chain (benz)imidazolium bromide salts and calculated  $\beta$  values (2/2).

As can be seen from the above, the relationship of the CMC with temperature varies by salt. All 3-alkyl-1-methylimidazolium bromide salts show an increase in the CMC with temperature, while all 3-alkyl-1-isopropylimidazolium salts show the inverse; a decrease in their CMCs with an increase in temperature. The benzimidazolium salts which were soluble at the range of temperatures reported show an increase in their CMCs with temperature, besides a decrease in CMC for 1-isopropyl-3-octylbenzimidazolium bromide between 35 °C and 40 °C. The CMCs, particularly those at room temperature, of the literature known 3-alkyl-1-methylimidazolium bromide salts match closely with those reported, and also match with the CMCs derived by different methods other than determination by conductivity.<sup>67,68,87,92,93</sup> The variation of the CMC with temperature is

based on two opposing factors. The first factor is that hydration of the polar cationic head group decreases with an increase in temperature, driving aggregation and the formation of micelles. The second factor is the breakdown of the solvating water around the hydrophobic tail, which opposes aggregation, as the low entropy of these surrounding water molecules is a key driving force of aggregation.

The relationship between the CMC of salts in a set may be plotted as a logarithm of the CMC against the number of carbons in the pendant alkyl chain. In the cases where this is possible (imidazolium salts), the relationship between the two factors is inversely linear, as the CMC is seen to decrease with an increase in the number of carbons in the associated chain. This relationship is rationalised in equation 1:<sup>96</sup>

$$\log CMC = A - BN_c \quad \text{Equation 1.}$$

The value for  $\log CMC$  therefore depends on two constants A and B. A is the contribution of the polar head group to micelle formation, whereas B is the contribution of the non-polar tail group to micelle formation, modulated by the number of methylene groups present ( $N_c$ ). Micelle formation in aqueous solution is more likely when values of A are small and the B term are large, in agreement with the experimental observation that the longer the carbon chain present, the lower the salt's CMC. The value for  $\beta$  is seen to increase with alkyl chain length, as described in the literature.<sup>97</sup>

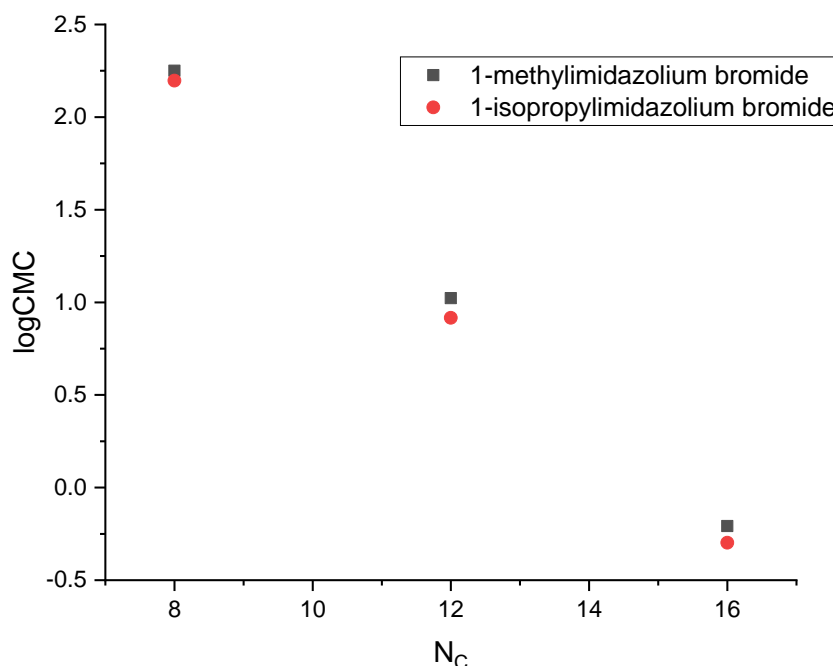


**Figure 17.**  $\log CMC$  vs number of carbons in the pendant alkyl chain of 1-methylimidazolium and 1-isopropylimidazolium bromide salts recorded at 25 °C.

## Determination of Krafft temperature

The Krafft temperature of each salt was explored using conductivity.<sup>71,98</sup> The Krafft temperature is the temperature at which the solubility of a surfactant matches its CMC in a particular solvent.<sup>99</sup> In the cases described, the Krafft temperature is determined in aqueous conditions. Below the Krafft temperature micelles will not form due to the surfactant only being soluble at concentrations lower than its CMC. Above the CMC there is a sharp spike in solubility due to the formation of micelles. This means that measurement of the Krafft is relatively simple by conductivity, as plotting the conductivity of a concentrated surfactant solution versus temperature should reveal the previously described sharp increase in conductivity upon micelle formation, and by extension allow for the Krafft temperature to be determined. The Krafft temperature is known to increase with additional methylene groups in alkyl-substituted surfactants, due to an increase in Van der Waals interactions between the carbon chains.<sup>100</sup> In the cases of a number of the longer chain-substituted benzimidazolium salts, the solutions remain opaque at room temperature due to their greater than room temperature Krafft temperatures, but become fully transparent when heated above room temperature.

The plots of surfactants with a measurable Krafft temperature take on a distinctive sigmoidal-like shape, starting with a steady increase of low conductivity with low temperatures where the surfactant is insoluble, a sharp increase in conductivity as micelles begin to form, and a steady plateauing of high conductivity values with a gradual increase with temperature once micelles have formed. This phenomenon is due to the initially poorly solubilised surfactant poorly conducting due to their relatively low concentration in solution, to the much higher conductivity achieved when micelles form due to the large number of surfactants in solution due to the formation micelles allowing for greater solvation.<sup>86</sup> The Krafft temperatures of all salts increase with carbon chain length as is expected. For imidazolium salts, the only salts in this study with a measurable Krafft temperature are those with hexadecyl groups. The Krafft temperature is roughly 25 °C for the 3-hexadecyl-1-methylimidazolium bromide, which matches with the literature,<sup>86</sup> whereas it is lower for its novel isopropyl counterpart at 18 °C. Krafft temperatures of 35 °C and 49 °C. are observed for 3-dodecyl- and 3-hexadecyl-1-methylbenzimidazolium bromide respectively, illustrating why it was not possible to assess the CMC of these surfactants. Conversely, the octyl-substituted counterpart has a lower than measurable CMC by the conductivity method. The Krafft temperatures for 3-alkyl-1-isopropylbenzimidazolium bromide salts tell a similar story, with Krafft temperatures of 22 °C and 42 °C for the dodecyl- and hexadecyl-substituted salts.

(Benz)imidazolium salt	Krafft temperature (°C)
1	Not measureable by conductivity
2	35
3	49
4	Not measureable by conductivity
5	22
6	42
7	Not measureable by conductivity
8	Not measureable by conductivity
9	25
10	Not measureable by conductivity
11	Not measureable by conductivity
12	18

**Table 3.** Krafft temperatures of (benz)imidazolium salts established by conductivity measurements.

### Thermodynamics of micellisation

The calculations in this section are based on the mass action model<sup>101</sup> and the analysis of Inoue *et al.*<sup>87</sup> The standard Gibbs free energy of micellisation ( $\Delta G_m^o$ ) may be calculated for standard surfactants with monovalent counter ions using the following equation for a 1:1 surfactant such as an imidazolium salt:<sup>102</sup>

$$\Delta G_m^o = (1 + \beta)RT \ln x_{CMC} \quad \text{Equation 2.}$$

Where  $\beta$  is the degree of counter ion binding, and  $x_{CMC}$  is the mole fraction of surfactant in solution. The above equation may be expressed in the following manner taking the concentration of water to be 55.4 M:

$$\Delta G_m^o = (1 + \beta)RT \ln \frac{c_{CMC}}{55.4} \quad \text{Equation 3.}$$

The degree of counter ion binding  $\beta$  may be derived from  $\alpha$ : the degree of ionisation, which is found by taking the ratio of the gradients of the specific conductivity vs concentration above ( $S_2$ ) and below the CMC ( $S_1$ ), by the simple relation below:<sup>92,103</sup>

$$\alpha = S_2/S_1 \quad \text{Equation 4.}$$

$$\beta = 1 - \alpha \quad \text{Equation 5.}$$

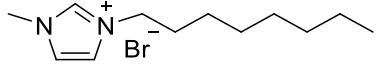
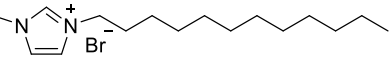
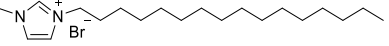
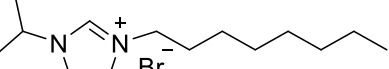
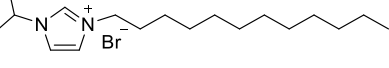
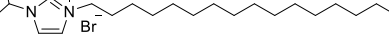
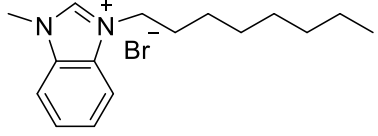
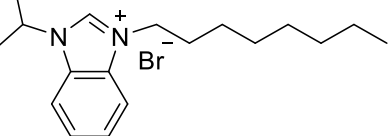
The relationship between the Gibbs free energy and the increase in carbon chain length is linear when plotted, in agreement with the literature. The enthalpy of micellisation ( $\Delta H_m^o$ ) may be calculated by the following relationship from the Gibbs free energy by application of a derived form of the Gibbs-Helmholtz equation (Equation 6):

$$\frac{\partial(\frac{\Delta G_m^o}{T})}{\partial(\frac{1}{T})} = \Delta H_m^o \quad \text{Equation 6.}$$

This in turn allows the entropy of micellisation to be calculated using the Gibbs-Helmholtz equation:

$$\Delta G_m^o = \Delta H_m^o - T\Delta S_m^o \quad \text{Equation 7.}$$

The trends shown in the plotted thermodynamic parameters matches closely with those seen in the literature for reported imidazolium salts.<sup>87</sup> The calculated thermodynamic parameters are shown in Table 4 below for salts where 4 temperatures were recorded. It can be seen that the values for the free energy of micellisation are fairly consistent across the range of temperature measured for all salts, and it should be noted that the free energy of micellisation is always negative, and therefore indicates that micellisation is a thermodynamically favourable process. The contributions to a negative free energy of micellisation rely on a negative enthalpic contribution and a positive entropic contribution. At lower temperatures, it can be seen that the positive entropic contribution is largely responsible for the negative value seen for the free energy of micellisation, and therefore entropy dominates the micellisation process. However, as the temperature increases, the enthalpic contribution to the free energy of micellisation becomes more important in providing a negative value. This is likely at least in part to do with the decrease in the entropy of the ordered water around the hydrophobic tails of the surfactant as the temperature increases as described previously, and in most cases, the entropic contribution to the free energy of micellisation becomes negative by 40 °C. The increased enthalpic contribution is also likely due to the thermal energy provided to the surfactant monomers, encouraging micellisation. The plot below (Figure 18) shows the values for  $\Delta G_m^o$ ,  $\Delta H_m^o$ , and  $-T\Delta S_m^o$  for micellisation in  $\text{kJ mol}^{-1}$  versus temperature for an example imidazolium salt (**8**).

Salt	Temperature (°C)	$\Delta G_m^0$ (kJ mol <sup>-1</sup> )	$\Delta H_m^0$ (kJ mol <sup>-1</sup> )	$\Delta S_m^0$ (J mol <sup>-1</sup> )
<b>7</b> 	25	-20.3	40.7	205
	30	-21.0	7.86	95.2
	35	-21.3	-23.9	-8.4
	40	-20.9	-54.6	-108
<b>8</b> 	25	-35.5	-8.61	90.1
	30	-35.8	-24.2	38.4
	35	-35.8	-39.3	-11.2
	40	-35.7	-53.9	-58.1
<b>9</b> 	25	-45.2	-37.1	27.2
	30	-44.2	-66.3	-73.1
	35	-44.9	-94.6	-161
	40	-43.0	-122	-253
<b>10</b> 	25	-23.2	-14.5	29.4
	30	-23.2	-21.5	5.49
	35	-23.3	-28.4	-16.3
	40	-23.1	-35.0	-38.0
<b>11</b> 	25	-37.1	-35.3	6.04
	30	-37.1	-38.5	-4.58
	35	-37.1	-41.6	-14.6
	40	-37.0	-44.5	-24.2
<b>12</b> 	25	-45.2	25.4	237
	30	-46.9	-23.6	77.1
	35	-45.3	-71.0	-83.3
	40	-45.7	-117	-228
<b>1</b> 	25	-24.8	-10.4	48.4
	30	-24.9	-15.6	30.7
	35	-25.1	-20.6	14.6
	40	-25.1	-25.5	-1.43
<b>4</b> 	25	-24.8	-21.4	10.8
	30	-24.9	-6.4	61.5
	35	-25.1	8.0	108
	40	-25.1	22.	154

**Table 4.** Calculated micellisation thermodynamic parameters based on conductivity data recorded for imidazolium and benzimidazolium bromide salts in aqueous solution at a given temperature.

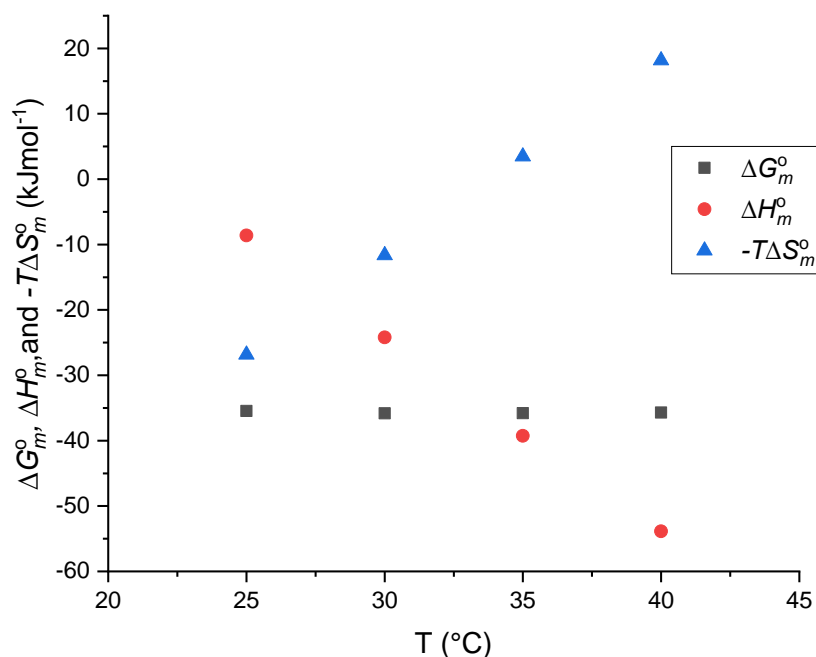


**Figure 18.** Calculated thermodynamic parameters for 3-dodecyl-1-methylimidazolium bromide vs temperature  $\Delta G_m^o$  values are plotted as squares,,  $\Delta H_m^o$  as circles, and  $-T\Delta S_m^o$  as triangles

### The antimicrobial efficacy of Ag-NHCs and their parent salts

The antimicrobial efficacy of the Ag-NHCs and their precursors was assessed by the broth microdilution method.<sup>104–107</sup> The microdilution method is a known and well reported protocol for establishing the minimum inhibitory concentration (MIC) of a compound and should be seen as an essential part of establishing the antimicrobial efficacy of a new agent.<sup>58–61</sup> The compounds were tested against a selection of Gram positive and Gram negative bacteria consisting of: *Staphylococcus aureus* NCIMB 9518, *Staphylococcus aureus* NCTC 6571, *Staphylococcus epidermidis* ATCC 14990, *Staphylococcus epidermidis* RP62A, *Pseudomonas aeruginosa* ATCC 15692, and *Escherichia coli* NCTC 12923 in order to provide a variety of potential susceptibilities to the tested antimicrobial agent, and to establish the spectrum of antimicrobial efficacy. The bacterial strains selected are all known reference strains.

A range of 8 concentrations of compound from 100  $\mu\text{g/mL}$  to 0.78125  $\mu\text{g/mL}$  were employed, with serial dilution from a 10 mg/mL stock solution in DMSO. The equivalent molarities per compound are summarised in the appendices. The concentrations are achieved via dilution in half every time. This is effective in determining whether an agent

is effective or not, due to the concentration values converging and becoming closer together at lower concentrations therefore allowing determination of the MIC of an effective antimicrobial agent, while efficiently detecting the activity of moderately active compounds that are not suitable for proceeding with as potential antimicrobial agents. The cut-off for an effective agent in this work is considered to be 5 µg/mL based on typical MIC breakpoints for effective antimicrobial agents against test strains.<sup>104</sup> Each MIC value was derived from triplicate plating of the test plates repeated on two separate occasions. The layout of a example experimental plate is illustrated below in Figure 19.

	1	2	3	4	5	6	7	8	9	10	
<b>A</b>	100	50	25	12.5	6.25	3.125	1.5625	0.78125	+	-	O1
<b>B</b>	100	50	25	12.5	6.25	3.125	1.5625	0.78125	+	-	
<b>C</b>	100	50	25	12.5	6.25	3.125	1.5625	0.78125	+	-	
<b>D</b>											
<b>E</b>	100	50	25	12.5	6.25	3.125	1.5625	0.78125	+	-	O2
<b>F</b>	100	50	25	12.5	6.25	3.125	1.5625	0.78125	+	-	
<b>G</b>	100	50	25	12.5	6.25	3.125	1.5625	0.78125	+	-	
<b>H</b>											

**Figure 19.** Layout of a prepared 96-well test plate. Outer numbers and letters are for grid coordinates. Values within the grid are concentrations of test compound (in µg/mL) and also contain a test organism. Organism 1 (O1) and Organism 2 (O2) are the two bacterial strains tested against on this plate. + and – are the positive and negative controls, containing no bacteria and no test compound, and bacteria but no test compound respectively. Column 11 and 12 of the 96-well plate are omitted as they contain no solution. Blank areas within the grid also contain no solution.

### **Antimicrobial efficacy of imidazolium and benzimidazolium bromide salts against Gram positive bacteria**

The antimicrobial efficacy of the Ag-NHC's precursor salts against two *S. aureus* and two *S. epidermidis* species are described in Table 5 below.

Salt	MIC Value ( $\mu\text{g/mL}$ )			
	<i>S. aureus</i> NCIMB 9518	<i>S. aureus</i> NCTC 6571	<i>S. epidermidis</i> RP62A	<i>S. epidermidis</i> ATCC 14990
1	50	25	25	12.5
2	3.125	3.125	1.5625	1.5625
3	1.5625	1.5625	0.78125	0.78125
4	50*	50*	25*	25*
5	3.125*	3.125*	1.5625*	1.5625*
6	1.5625*	1.5625*	0.78125*	0.78125*
7	R	R	R	100
8	3.125	3.125	1.5625	1.5625
9	0.78125	0.78125	0.78125	0.78125
10	100	100	100	50
11	1.5625	1.5625	0.78125	0.78125
12	0.78125	0.78125	0.78125	0.78125

**Table 5.** Minimum inhibitory concentrations (MICs) of imidazolium salts tested against 4 Gram positive bacteria in  $\mu\text{g/mL}$ . Values of "R" show the strain is resistant to the compound at 100  $\mu\text{g/mL}$  and below (\* = single triplicate repeat).

As can be seen, the general trend is that the long chain imidazolium and benzimidazolium salts are effective antibacterial agents, with some moderate activity from the octyl-substituted salts to exceptionally low MIC values for the longer chain-substituted salts. Salt **1** is the most effective octyl-substituted salt against *S. aureus* species, followed by **4**, then **10**, and then **7**, which is resisted by both *S. aureus* species tested. The lowest MIC seen in this set is 25  $\mu\text{g/mL}$  recorded by **1** against *S. aureus* NCTC 6571, which indicates that the octyl-substituted salts are not suitable as antimicrobials against *S. aureus* species. The susceptibility of *S. epidermidis* species follows the same trend as the susceptibility of *S. aureus* species, with the most effective being **1**, then **4**, then **10**, then **7**. The strain *S. epidermidis* ATCC 14990 shows susceptibility to **7** in the tested range, with an MIC of 100  $\mu\text{g/mL}$ , unlike the other Gram positive strains tested. In the case of all three octyl-substituted salts, the strain *S. epidermidis* ATCC 14990 shows a greater susceptibility to the antimicrobial agents than its counterpart *S. epidermidis* RP62A. The enhanced activity of the 1-methylbenzimidazolium bromide salt by comparison with the other salts may be due to its enhanced lipophilicity afforded by the fused benzene ring not present in the other salts, as lipophilicity has been previously described as a potential factor in increasing the efficacy of antimicrobials, as the compound is more able to cross and interact with the bacterial membrane.<sup>42–46,108</sup>

The order of effectiveness of the dodecyl-substituted salts against the Gram positive bacteria is different to that of the octyl-substituted salts, with the most effective against all strains being **11**, with an MIC of 0.78125 µg/mL against *S. epidermidis* strains, the lowest measurable concentration in this assay. **11** also has an MIC of 1.5625 µg/mL against both *S. aureus* strains. The other 3 salts are tied with MICs of 1.5625 µg/mL against both *S. epidermidis* strains, and 3.125 µg/mL against both *S. aureus* strains. It is clear that the MIC values for the dodecyl-substituted salts are far superior to those of the octyl-substituted salts, highlighting increasing chain length as a potent factor in increasing the antimicrobial activity of a compound. The additional efficacy of **11** vs **2** and particularly **5** in this case may indicate an interaction not accounted for when solely ascribing lipophilicity as the important factor in the antimicrobial efficacy of the salts described, as the benzimidazolium salts are more lipophilic than the isopropylimidazolium salt.

The efficacy of the hexadecyl-substituted salts is not greater than the dodecyl-substituted salts to the same magnitude as the dodecyl salts' efficacy is greater than the efficacy of the octyl salts. The efficacy of **3** against *S. aureus* and *S. epidermidis* species is one concentration more effective than its 3-dodecyl counterpart, with inhibition at even the lowest concentration against *S. epidermidis* species. The efficacy of **12** against Gram positive bacteria is exceptional, with the salt registering the lowest possible MIC for this assay of 0.78125 µg/mL against all species tested. **9** also however has an MIC of 0.78125 µg/mL against all Gram positive species. The fact that the hexadecyl-substituted imidazolium salts are more effective than their benzimidazolium counterparts is counter to the previous arguments regarding lipophilicity's relationship to antimicrobial efficacy, as the benzimidazolium salts are more lipophilic than their imidazolium counterparts.

It can be seen from the above findings that the principal factor that affects the efficacy of the above imidazolium salts against Gram positive bacteria is the length of the pendant alkyl chain. There are however differences amongst the efficacy of salts with the same alkyl chains, and these differences would need further examination in order to determine the reasoning behind this observation. The literature states that the efficacy of alkylimidazolium salts depends on a number of factors including: hydrophobicity, adsorption, CMC, and solubility and transport in the test medium, and is unlikely to be affected by the nature of the polar head group.<sup>22,23,67,97,109</sup>

**Antimicrobial efficacy of imidazolium and benzimidazolium bromide salts against Gram negative bacteria**

Salt	MIC Value ( $\mu\text{g/mL}$ )	
	<i>Escherichia coli</i> NCTC 12923	<i>Pseudomonas aeruginosa</i> ATCC 15692
1	R	R
2	25	R
3	50	R
4	R*	R*
5	25*	R*
6	50*	R*
7	R	R
8	25	R
9	25	100
10	R	R
11	50	R
12	50	R

**Table 6.** Minimum inhibitory concentrations (MICs) of imidazolium salts tested against 2 Gram negative bacteria in  $\mu\text{g/mL}$ . Values of "R" show the strain is resistant to the compound at 100  $\mu\text{g/mL}$  and below (\* = single triplicate repeat).

The efficacy of the tested imidazolium salts against Gram negative bacteria is far different than their efficacy against Gram positive bacteria. In the case of the octyl-substituted salts, there is no activity seen against the *P. aeruginosa* or *E. coli* strains tested, with resistance above the highest concentration seen in all cases. There is some activity seen in the case of the dodecyl-substituted salts, with values of 25, 25, 25 and 50  $\mu\text{g/mL}$  seen for the **2**, **5**, **8**, and **11** against *E. coli*. By contrast, no dodecyl-substituted salts show any activity against *P. aeruginosa* in the range of concentrations tested. The efficacy of the salts against *E. coli* is different to the activity seen against the Gram positive *Staphylococcus* species, with the **11** being the least active against *E. coli*, while being the most active against the Gram positive bacteria tested. In the case of the hexadecyl-substituted salts, the MIC values are as follows against *E. coli*: 50  $\mu\text{g/mL}$  for **3**, 50  $\mu\text{g/mL}$  for **6**, 25  $\mu\text{g/mL}$  for **9**, and 50  $\mu\text{g/mL}$  for **12**. Again, the harder *P. aeruginosa* shows resistance against all salts besides **9**, for which an MIC value of 100  $\mu\text{g/mL}$  was found.

The immediate difference in efficacy of the tested salts against Gram negative and Gram positive bacteria can be partially explained by the difference in the types of cell wall each type of bacterium has. Gram positive bacteria have a simple structure, with a single thick

layer of peptidoglycan surrounding the plasma membrane. Gram negative bacteria have a more complicated structure, with an outer lipopolysacharride layer, an impermeable secondary plasma membrane, a thinner layer of peptidoglycan than Gram positive bacteria, then the internal plasma membrane. If the mode of action of the imidazolium salts against bacteria is indeed the disruption of the plasma membrane, then association of the salt to the secondary plasma membrane without disrupting the internal plasma membrane of Gram negative bacteria may go some way to explaining the decreased activity of the salt against Gram negative bacteria by comparison with their Gram positive counterparts. If the effect of the imidazolium salt is by disruption of the intracellular processes, then the lower permeability of the secondary membrane is also likely to have an effect.<sup>110</sup> The difference between the activity of the salts against *E. coli* v *P. aeruginosa* is also of interest. *P. aeruginosa* are renowned for their resistance to a wide variety of antimicrobial agents. The inherent resistance in *P. aeruginosa* strains is typically conferred by a mixture of multidrug efflux pumps with chromosomally encoded antimicrobial resistance genes, a membrane with low permeability, and the typically low permeability of the species' cell envelope.<sup>111,112</sup> These factors may go some way to explaining the difference in efficacy of the salts against *P. aeruginosa* and *E. coli*, and in the case of **9** shows a potential start point from which to develop treatments for hardy multidrug-resistant Gram negative bacteria.

#### Antimicrobial efficacy of Ag-NHCs against Gram positive bacteria

Salt	MIC Value (µg/mL)			
	<i>S. aureus</i> NCIMB 9518	<i>S. aureus</i> NCTC 6571	<i>S. epidermidis</i> RP62A	<i>S. epidermidis</i> ATCC 14990
<b>1Ag</b>	25	25	3.125	3.125
<b>2Ag</b>	1.5625	1.5625	0.78125	0.78125
<b>3Ag</b>	1.5625	1.5625	0.78125	0.78125
<b>4Ag</b>	25*	25*	50*	25*
<b>5Ag</b>	1.5625*	1.5625*	0.78125*	0.78125*
<b>6Ag</b>	1.5625*	1.5625*	0.78125*	0.78125*
<b>7Ag</b>	25	25	25	25
<b>8Ag</b>	3.125	3.125	1.5625	0.78125
<b>9Ag</b>	0.78125	0.78125	0.78125	0.78125
<b>10Ag</b>	50	100	100	50
<b>11Ag</b>	1.5625	1.5625	0.78125	0.78125
<b>12Ag</b>	0.78125	1.5625	0.78125	0.78125

**Table 7.** Minimum inhibitory concentrations (MICs) of Ag-NHCs tested against 4 Gram positive bacteria in ug/mL. Values of "R" show the strain is resistant to the compound at 100 µg/mL and below. (\* = single triplicate repeat)

The octyl-substituted Ag-NHCs have an activity of 25 µg/mL for **1Ag**, **4Ag**, and **7Ag**. The activity of **10Ag** is 50 µg/mL against *S. aureus* NCIMB 9518, and 100 µg/mL against *S. aureus* NCTC 6571. The MIC values are decreased for **1Ag**, **4Ag**, and **10Ag** against *S. aureus* NCIMB 9518 by comparison with the parent imidazolium salt, and decrease for **4Ag** but remain the same for the other two complexes against the other *S. aureus* strain. The activity of **7Ag** is greatly increased against both *S. aureus* strains by comparison with its parent salt, to which both species were resistant.

The same pattern is seen in activity for both *S. epidermidis* species, with the most active species being those with methyl substituents, then the isopropyl species. An activity of 3.125 µg/mL is registered for **1Ag** against both strains, then 25 µg/mL for **7Ag** against both species, then two values for both **4Ag** and **10Ag**: 50 µg/mL and 100 µg/mL against *S. epidermidis* RP62A, and 25 µg/mL and 50 µg/mL respectively against *S. epidermidis* ATCC 14990. The activity of the **1Ag** species is greatly increased, as is that of the methylimidazol-2-ylidene species by comparison with their parent salts. The activity of the **10Ag** is much the same as that of the parent salt. The release rate of Ag(I) from the ligand may account for the difference in the difference in activity between the isopropyl- and methyl-substituted species, with exchange rates between the monomeric neutral and dimeric cationic Ag-NHC species varying drastically based on the steric bulk of the coordinated ligand.<sup>31,82</sup> This increase in steric bulk may therefore have a significant impact on the release rate of Ag(I) from the Ag-NHC, meaning that methyl-substituted Ag-NHCs may have a much higher release rate of Ag(I), accounting for the increase in activity between the ligand and the salt.<sup>113,114</sup> The release rate is also likely affected by the strength of the NHC-Ag bond, with the great increase in activity of the benzimidazol-2-ylidene species potentially being caused by a faster rate of Ag(I) release by comparison with its imidazole-2-ylidene counterparts due to the lower  $\delta$ -donor strength of the benzimidazol-2-ylidene ligand by comparison with the imidazole-2-ylidene ligand.<sup>115</sup>

The above postulation for the increased release rate of Ag(I) from benzimidazol-2-ylidene by comparison with imidazole-2-ylidene is further supported by the trends observed in the activity of the dodecyl-substituted Ag-NHCs, with an MIC of 1.5625 µg/mL for **2Ag** against both *S. aureus* species, lower than its precursor salt. This efficacy is matched by the isopropyl counterpart **5Ag**. This is by comparison with the MICs of the imidazole-2-ylidene Ag(I) bromide NHCs against *S. aureus* species: 3.125 µg/mL for **8Ag**, and 1.5625 µg/mL for **11Ag**, both of which are the same value as their parent salts' MICs against the *S. aureus* species tested. The same pattern is mostly reflected in the

MIC values for the dodecyl-substituted Ag-NHCs against *S. epidermidis* species: 0.78125 µg/mL for **1Ag** and **4Ag** against both strains, a decrease in MIC by comparison with the salt, 1.5625 and 0.78125 µg/mL against *S. epidermidis* RP62A and *S. epidermidis* ATCC 14990 respectively for **8Ag**, a decrease in MIC against the ATCC 14990 strain by comparison with the ligand, and 0.78125 µg/mL against both strains for **11Ag**, the same MIC as its parent salt, though it should be noted that this is the lowest concentration tested, therefore either could be more potent. Again, it is seen that the Ag(I) increases the activity of the benzimidazol-2-ylidene by comparison with its parent salt, with the influence of the low steric hindrance allowing for **8Ag** to release Ag(I) at a greater rate, allowing for an increase in activity by comparison with its parent salt.

The MIC values for the hexadecyl-substituted Ag-NHCs do not provide any further insight as to the effects of the donor strength of the ligand and sterics on a complex's antimicrobial efficacy. The values for all Ag-NHCs remain the same as those for their parent salts against all Gram positive species, with the exception of **12Ag** against *S. aureus* NCTC 6571, where the MIC is higher than its salt counterpart. This may be due to the decreased solubility of the C<sub>16</sub>-chain Ag-NHC in aqueous media by comparison with its parent imidazolium bromide salt. There is therefore no additional information on the effect of structure on activity that may be gleaned from the above information.

#### Antimicrobial efficacy of Ag-NHCs against Gram negative bacteria

Salt	MIC Value (µg/mL)	
	<i>Escherichia coli</i> NCTC 12923	<i>Pseudomonas aeruginosa</i> ATCC 15692
<b>1Ag</b>	12.5	6.25
<b>2Ag</b>	6.25	6.25
<b>3Ag</b>	12.5	6.25
<b>4Ag</b>	25*	25*
<b>5Ag</b>	12.5*	25*
<b>6Ag</b>	25*	25*
<b>7Ag</b>	50	25
<b>8Ag</b>	25	25
<b>9Ag</b>	25	50
<b>10Ag</b>	100	100
<b>11Ag</b>	12.5	25
<b>12Ag</b>	6.25	12.5

**Table 8.** Minimum inhibitory concentrations (MICs) of imidazolium Ag-NHCs tested against 2 Gram negative bacteria in µg/mL. Values of "R" show the strain is resistant to the compound at 100 µg/mL and below (\* = single triplicate repeat).

The antimicrobial efficacy of the Ag-NHCs tested is markedly different from that of their parent salts. In most cases, the MIC for the Ag-NHCs is lower than that of the precursor, and only occasionally is it equal (in the case of the longer chain imidazole-2-ylidene species against the tested *E. coli* strain). The MIC of the octyl-substituted Ag-NHCs against *P. aeruginosa* is 6.25, 25, 12.5, and 100 µg/mL for **1Ag**, **4Ag**, **7Ag**, and **10Ag** respectively. The MIC values for the above species against *E. coli* are 12.5, 12.5, 50, and 100 µg/mL respectively, all of which are lower than their precursors. The MIC values for the dodecyl-substituted Ag-NHCs against *P. aeruginosa* are as follows: 6.25 µg/mL for **2Ag**, 25 µg/mL for **5Ag**, 25 µg/mL for **8Ag**, and 25 µg/mL for **11Ag**, all of which are lower than their precursors. The MIC values are all lower for the Ag-NHCs besides **2Ag** and **3Ag** against *E.coli*. This suggests a more prominent role for Ag(I) in the efficacy of Ag-NHCs against Gram negative bacteria than against Gram positive bacteria, as the precursor salt is already particularly effective against Gram positive organisms.<sup>116–119</sup>

## Conclusion

Novel imidazolium and benzimidazolium salts were prepared via substitution reactions of 1-alkylated imidazole and benzimidazole with long-chain 1-bromoalkanes. The imidazolium salts were prepared in good yields either as white powders, or ionic liquids in the case of those containing shorter alkyl groups. The salts prepared were reacted with  $\text{Ag}_2\text{O}$  to produce Ag-NHCs in moderate yields, all of which were solid. The preparation of these Ag-NHCs was mostly confirmed by analysis of the C2 carbon on the imidazole ring and its attached proton by NMR spectroscopy. Upon formation of the Ag-NHC, it was found that the signal belonging to the proton attached to the C2 carbon visible in the  $^1\text{H}$ -NMR of the precursor salt was not present in the spectrum of the Ag-NHC. It was also found that complexation of Ag caused a dramatic shift downfield of roughly 30 ppm of the signal belonging to the C2 carbon in the  $^{13}\text{C}\{^1\text{H}\}$ -NMR spectrum of the Ag-NHC compared to the imidazolium or benzimidazolium bromide. All species were also characterised with mass spectrometry, with low resolution spectra prepared for literature known compounds and high resolution spectra for novel compounds. Mass spectra of Ag-NHCs revealed only the dimeric  $[\text{Ag}(\text{NHC})_2][\text{AgX}_2]$  form, though this may be a function of the ionisation mode. Novel compounds were also characterised with infrared spectroscopy.

The surface activity of the synthesised amphiphilic salts was assessed using conductivity. The critical micelle concentration of a salt in an aqueous environment was derived from a plot of the specific conductivity of a range of concentrations. The plot formed two linear regimes in all cases, and the point at which these lines crossed was taken as the CMC. The CMCs of the literature known 1-methylimidazolium bromide salts matched closely with the values reported. CMCs of novel 3-alkyl-1-isopropylimidazolium bromide salts were found to be 157 mM, 8.26 mM, and 0.504 mM at 25 °C where alkyl groups were octyl, dodecyl, and hexadecyl respectively. The values determined by conductivity for literature known salts matched closely even with the CMCs determined by other methods such as drop volume tensiometry or NMR spectroscopy. The CMC values typically increased between 25 °C and 40 °C for all salts besides those of the 1-isopropylimidazolium bromide class, which showed a steady decrease with the increase of temperature. The Krafft temperatures of each salt was determined, with values far in excess of room temperature found for dodecyl- and hexadecyl-substituted benzimidazolium bromide salts, making them impractical for application as room temperature surfactants. The Krafft temperature of all other species were assessed to be below 4 °C besides hexadecyl-substituted imidazolium bromide salts which had a measurable sub-20 °C Krafft temperature. The values obtained from conductivity

measurements were employed to estimate the thermodynamics of the micellisation process for those salts for which 4 CMCs vs temperature could be obtained. At lower temperatures a positive entropic contribution is largely responsible for the negative value seen for the free energy of micellisation, so micellisation is entropically driven. However, as the temperature increases, the enthalpic contribution to the free energy of micellisation becomes more important in providing a negative value, meaning the micellisation is enthalpically driven.

The salts and Ag-NHCs synthesised showed moderate to excellent activity against a panel of 6 Gram positive and Gram negative bacteria, with the exception of the imidazolium and benzimidazolium bromide salts against *P. aeruginosa*, which was resistant to all but one of the salts tested. The tested compounds were far more effective against Gram positive organisms than Gram negative organisms, but showed good activity against even the hardy *P. aeruginosa* in the cases of some Ag-NHCs. The MIC value of the compounds tested typically decreased with the increase in alkyl-chain length, with MIC values of typically 3.125 µg/mL or less observed for compounds with pendant alkyl chains of  $-C_{12}H_{25}$  or longer. Alkyl-chain length therefore appeared to be the principal factor in determining the antimicrobial efficacy of a compound. The introduction of Ag to the salts to form Ag-NHCs typically improved upon the antimicrobial activity of the salts, but the increase in efficacy was usually modest. The antimicrobial efficacy of the parent imidazolium or benzimidazolium salt is therefore important in the prediction of the activity of the derivative Ag-NHC. Nevertheless, the incorporation of Ag(I) to form antimicrobial complexes has shown to be effective in increasing the efficacy of an antimicrobial compound, and therefore highlights the potential of incorporation of metals to improve the activity of antimicrobial agents.

## References

- 1 P. Wasserscheid and W. Keim, *Angew. Chem. Int. Ed.*, 2000, **39**, 3772–3789.
- 2 T. Welton, *Chem. Rev.*, 1999, **99**, 2071–2084.
- 3 G. Carrasco-Huertas, R. J. Jiménez-Riobóo, M. C. Gutiérrez, M. L. Ferrer and F. del Monte, *Chem. Commun.*, 2020, **56**, 3592–3604.
- 4 X. Lv, C. Liu, Z. Shao, S. Song and S. Sun, *ACS Sustain. Chem. Eng.*, 2020, **8**, 5975–5984.
- 5 A. Su, P. Guo, J. Li, D. Kan, Q. Pang, T. Li, J. Sun, G. Chen and Y. Wei, *J. Mater. Chem. A*, 2020, **8**, 4775–4783.
- 6 B. Pawłowska, A. Telesiński and R. Biczak, *Chemosphere*, 2019, **237**, 124436.
- 7 A. Boruń, *J. Mol. Liq.*, 2019, **276**, 214–224.
- 8 J. Tang, H. Song, X. Feng, A. Yohannes and S. Yao, *Curr. Med. Chem.*, 2019, **26**, 5947–5967.
- 9 W. Zhang, X. Liu, B. He, Z. Gong, J. Zhu, Y. Ding, H. Chen and Q. Tang, *ACS Appl. Mater. Interfaces*, 2020, **12**, 4540–4548.
- 10 L. Tan, J. Zhu, M. Zhou, X. He and S. Zhang, *J. Mol. Liq.*, 2020, **298**, 112054.
- 11 O. A. Al-Rashed and A. A. Nazeer, *J. Mol. Liq.*, 2019, **288**, 111015.
- 12 X. Frogneux, L. Hippolyte, D. Mercier, D. Portehault, C. Chanéac, C. Sanchez, P. Marcus, F. Ribot, L. Fensterbank and S. Carenco, *Chem. – Eur. J.*, 2019, **25**, 11481–11485.
- 13 P. Marshall, R. L. Jenkins, W. Clegg, R. W. Harrington, S. K. Callear, S. J. Coles, I. A. Fallis and A. Dervisi, *Dalton Trans.*, 2012, **41**, 12839–12846.
- 14 J. H. Kim, R. T. Mertens, A. Agarwal, S. Parkin, G. Berger and S. G. Awuah, *Dalton Trans.*, 2019, **48**, 6273–6282.
- 15 B.-C. Liu, N. Ge, Y.-Q. Zhai, T. Zhang, Y.-S. Ding and Y.-Z. Zheng, *Chem. Commun.*, 2019, **55**, 9355–9358.
- 16 M. H. Dunn, N. Konstandaras, M. L. Cole and J. B. Harper, *J. Org. Chem.*, 2017, **82**, 7324–7331.
- 17 Q. Yao, X. Lu, K. Liu, C. Ma, J. Su, C. Lin, D. Li, J. Dou, J. Sun and W. Duan, *Dalton Trans.*, 2019, **48**, 5144–5148.
- 18 F. Willig, J. Lang, A. C. Hans, M. R. Ringenberg, D. Pfeffer, W. Frey and R. Peters, *J. Am. Chem. Soc.*, 2019, **141**, 12029–12043.
- 19 B. D. Stringer, L. M. Quan, P. J. Barnard, D. J. D. Wilson and C. F. Hogan, *Organometallics*, 2014, **33**, 4860–4872.
- 20 A. Fürstner, M. Alcarazo, V. César and C. W. Lehmann, *Chem. Commun.*, 2006, 2176–2178.
- 21 H. Heerklotz, *Q. Rev. Biophys.*, 2008, **41**, 205–264.
- 22 N. A. Falk, *J. Surfactants Deterg.*, 2019, **22**, 1119–1127.
- 23 C. Zhou and Y. Wang, *Curr. Opin. Colloid Interface Sci.*, 2020, **45**, 28–43.
- 24 J. N. Pendleton and B. F. Gilmore, *Int. J. Antimicrob. Agents*, 2015, **46**, 131–139.
- 25 A. J. Arduengo, H. V. R. Dias, J. C. Calabrese and F. Davidson, *Organometallics*, 1993, **12**, 3405–3409.
- 26 O. Guerret, S. Solé, H. Gornitzka, M. Teichert, G. Trinquier and G. Bertrand, *J. Am. Chem. Soc.*, 1997, **119**, 6668–6669.
- 27 H. M. J. Wang and I. J. B. Lin, *Organometallics*, 1998, **17**, 972–975.
- 28 N. R. Naz, G. Schnakenburg, A. Mikeházi, Z. Kelemen, L. Nyulászi, R. T. Boéré and R. Streubel, *Chem. Commun.*, 2020, **56**, 2646–2649.
- 29 U. F. M. Haziz, R. A. Haque, S.-Z. Zhan and M. R. Razali, *J. Organomet. Chem.*, 2020, **910**, 121137.
- 30 M. R. Nocol, M. S. Vela Gurovic, S. Ruiz Díaz and G. F. Silbestri, *Carbohydr. Res.*, 2019, **471**, 6–12.
- 31 P. de Frémont, N. M. Scott, E. D. Stevens, T. Ramnial, O. C. Lightbody, C. L. B. Macdonald, J. A. C. Clyburne, C. D. Abernethy and S. P. Nolan, *Organometallics*, 2005, **24**, 6301–6309.

- 32 E. Caytan and S. Roland, *Organometallics*, 2014, **33**, 2115–2118.
- 33 Q.-X. Liu, F.-B. Xu, Q.-S. Li, X.-S. Zeng, X.-B. Leng, Y. L. Chou and Z.-Z. Zhang, *Organometallics*, 2003, **22**, 309–314.
- 34 A. Melaiye, R. S. Simons, A. Milsted, F. Pingitore, C. Wesdemiotis, C. A. Tessier and W. J. Youngs, *J. Med. Chem.*, 2004, **47**, 973–977.
- 35 A. Kascatan-Nebioglu, A. Melaiye, K. Hindi, S. Durmus, M. J. Panzner, L. A. Hogue, R. J. Mallett, C. E. Hovis, M. Coughenour, S. D. Crosby, A. Milsted, D. L. Ely, C. A. Tessier, C. L. Cannon and W. J. Youngs, *J. Med. Chem.*, 2006, **49**, 6811–6818.
- 36 S. Silver, *FEMS Microbiol. Rev.*, 2003, **27**, 341–353.
- 37 K. M. Hindi, T. J. Siciliano, S. Durmus, M. J. Panzner, D. A. Medvetz, D. V. Reddy, L. A. Hogue, C. E. Hovis, J. K. Hilliard, R. J. Mallett, C. A. Tessier, C. L. Cannon and W. J. Youngs, *J. Med. Chem.*, 2008, **51**, 1577–1583.
- 38 D. A. Medvetz, K. M. Hindi, M. J. Panzner, A. J. Ditto, Y. H. Yun and W. J. Youngs, *Met.-Based Drugs*, 2008, **2008**, 1–7.
- 39 M. J. Panzner, A. Deeraksa, A. Smith, B. D. Wright, K. M. Hindi, A. Kascatan-Nebioglu, A. G. Torres, B. M. Judy, C. E. Hovis, J. K. Hilliard, R. J. Mallett, E. Cope, D. M. Estes, C. L. Cannon, J. G. Leid and W. J. Youngs, *Eur. J. Inorg. Chem.*, 2009, **2009**, 1739–1745.
- 40 A. E. Vickers, T. C. Sloop and G. W. Lucier, *Environ. Health Perspect.*, 1985, **59**, 121–128.
- 41 S. Patil, K. Dietrich, A. Deally, B. Gleeson, H. Müller-Bunz, F. Paradisi and M. Tacke, *Helv. Chim. Acta*, 2010, **93**, 2347–2364.
- 42 S. Patil, J. Claffey, A. Deally, M. Hogan, B. Gleeson, L. M. M. Mendez, H. Mueller-Bunz, F. Paradisi and M. Tacke, *Eur. J. Inorg. Chem.*, 2010, 1020–1031.
- 43 S. Patil, A. Deally, B. Gleeson, F. Hackenberg, H. Müller-Bunz, F. Paradisi and M. Tacke, *Z. Für Anorg. Allg. Chem.*, 2011, **637**, 386–396.
- 44 F. Hackenberg, G. Lally, H. Müller-Bunz, F. Paradisi, D. Quaglia, W. Streciwilk and M. Tacke, *J. Organomet. Chem.*, 2012, **717**, 123–134.
- 45 F. Hackenberg, G. Lally, H. Müller-Bunz, F. Paradisi, D. Quaglia, W. Streciwilk and M. Tacke, *Inorganica Chim. Acta*, 2013, **395**, 135–144.
- 46 W. Streciwilk, J. Cassidy, F. Hackenberg, H. Müller-Bunz, F. Paradisi and M. Tacke, *J. Organomet. Chem.*, 2014, **749**, 88–99.
- 47 S. Patil, A. Deally, B. Gleeson, H. Mueller-Bunz, F. Paradisi and M. Tacke, *Metallomics*, 2011, **3**, 74–88.
- 48 A. Pöthig, S. Ahmed, H. C. Winther-Larsen, S. Guan, P. J. Altmann, J. Kudermann, A. M. Santos Andresen, T. Gjøen and O. A. Høgmoen Åstrand, *Front. Chem.*, , DOI:10.3389/fchem.2018.00584.
- 49 C. O’Beirne, N. F. Alhamad, Q. Ma, H. Müller-Bunz, K. Kavanagh, G. Butler, X. Zhu and M. Tacke, *Inorganica Chim. Acta*, 2019, **486**, 294–303.
- 50 G. Achar, P. P. Hokrani, K. N. Brinda, J. G. Małecki and S. Budagumpi, *J. Mol. Struct.*, 2019, **1196**, 627–636.
- 51 Y. Gök, S. Akkoç, Ö. Ö. Çelikal, İ. Özdemir and S. Günal, *Arab. J. Chem.*, 2019, **12**, 2513–2518.
- 52 I. Slimani, L. Mansour, N. Abutaha, A. H. Harrath, J. Al-Tamimi, N. Gürbüz, I. Özdemir and N. Hamdi, *J. King Saud Univ. - Sci.*, 2020, **32**, 1544–1554.
- 53 Ü. Kızrak, O. Çiftçi, İ. Özdemir, N. Gürbüz, S. D. Düşünceli, M. Kaloğlu, L. Mansour, F. Zaghrouba, N. Hamdi and İ. Özdemir, *J. Organomet. Chem.*, 2019, **882**, 26–32.
- 54 N. Browne, F. Hackenberg, W. Streciwilk, M. Tacke and K. Kavanagh, *Biomaterials Int. J. Role Met. Ions Biol. Biochem. Med.*, 2014, **27**, 745–752.
- 55 C. L. Cannon, L. A. Hogue, R. K. Vajravelu, G. H. Capps, A. Ibricevic, K. M. Hindi, A. Kascatan-Nebioglu, M. J. Walter, S. L. Brody and W. J. Youngs, *Antimicrob. Agents Chemother.*, 2009, **53**, 3285–3293.
- 56 Y. Gök, S. Akkoç, S. Albayrak, M. Akkurt and M. N. Tahir, *Appl. Organomet. Chem.*, 2014, **28**, 244–251.

- 57 M. Kaloğlu, N. Kaloğlu, İ. Özdemir, S. Günal and İ. Özdemir, *Bioorg. Med. Chem.*, 2016, **24**, 3649–3656.
- 58 M. Tacke, *J. Organomet. Chem.*, 2015, **782**, 17–21.
- 59 N. A. Johnson, M. R. Southerland and W. J. Youngs, *Molecules*, 2017, **22**, 1263.
- 60 X. Liang, S. Luan, Z. Yin, M. He, C. He, L. Yin, Y. Zou, Z. Yuan, L. Li, X. Song, C. Lv and W. Zhang, *Eur. J. Med. Chem.*, 2018, **157**, 62–80.
- 61 S. Y. Hussaini, R. A. Haque and M. R. Razali, *J. Organomet. Chem.*, 2019, **882**, 96–111.
- 62 O. V. Starikova, G. V. Dolgushin, L. I. Larina, P. E. Ushakov, T. N. Komarova and V. A. Lopyrev, *Russ. J. Org. Chem.*, 2003, **39**, 1467–1470.
- 63 A. Brück and K. Ruhland, *Organometallics*, 2009, **28**, 6383–6401.
- 64 L. Wang and E. Y.-X. Chen, *Green Chem.*, 2015, **17**, 5149–5153.
- 65 A. N. Shendrik, O. V. Baranova and V. S. Doroshkevich, *Russ. J. Org. Chem.*, 2012, **48**, 663–666.
- 66 M. A. Ab Rani, A. Brant, L. Crowhurst, A. Dolan, M. Lui, N. H. Hassan, J. P. Hallett, P. A. Hunt, H. Niedermeyer, J. M. Perez-Arlandis, M. Schrems, T. Welton and R. Wilding, *Phys. Chem. Chem. Phys.*, 2011, **13**, 16831.
- 67 A. Cornellias, L. Perez, F. Comelles, I. Ribosa, A. Manresa and M. T. Garcia, *J. Colloid Interface Sci.*, 2011, **355**, 164–171.
- 68 Q. Q. Baltazar, J. Chandawalla, K. Sawyer and J. L. Anderson, *Colloids Surf. Physicochem. Eng. Asp.*, 2007, **302**, 150–156.
- 69 T. Zou, C. T. Lum, S. S.-Y. Chui and C.-M. Che, *Angew. Chem. Int. Ed.*, 2013, **52**, 2930–2933.
- 70 Z. Taşçı, A. Kunduracioğlu, İ. Kani and B. Çetinkaya, *ChemCatChem*, 2012, **4**, 831–835.
- 71 F. I. El-Dossoki, *J. Solut. Chem.*, 2013, **42**, 125–135.
- 72 S. R. Gill, D. E. Fouts, G. L. Archer, E. F. Mongodin, R. T. DeBoy, J. Ravel, I. T. Paulsen, J. F. Kolonay, L. Brinkac, M. Beanan, R. J. Dodson, S. C. Daugherty, R. Madupu, S. V. Angiuoli, A. S. Durkin, D. H. Haft, J. Vamathevan, H. Khouri, T. Utterback, C. Lee, G. Dimitrov, L. Jiang, H. Qin, J. Weidman, K. Tran, K. Kang, I. R. Hance, K. E. Nelson and C. M. Fraser, *J. Bacteriol.*, 2005, **187**, 2426–2438.
- 73 D. Jones, R. H. Deibel and C. F. Niven, *J. Bacteriol.*, 1963, **85**, 62–67.
- 74 N. G. Heatley, *Biochem. J.*, 1944, **38**, 61–65.
- 75 D. Nathwani, G. Raman, K. Sulham, M. Gavaghan and V. Menon, *Antimicrob. Resist. Infect. Control*, DOI:10.1186/2047-2994-3-32.
- 76 U. Choi and C.-R. Lee, *Front. Microbiol.*, 2019, 10:953, DOI:10.3389/fmicb.2019.00953.
- 77 E. C. Wagner and W. H. Millett, *Org. Synth.*, 1939, **19**, 12.
- 78 F. Quintin, J. Pinaud, F. Lamaty and X. Bantreil, *Organometallics*, 2020, **39**, 636–639.
- 79 F. Almalioti, J. MacDougall, S. Hughes, M. M. Hasson, R. L. Jenkins, B. D. Ward, G. J. Tizzard, S. J. Coles, D. W. Williams, S. Bamford, I. A. Fallis and A. Dervisi, *Dalton Trans.*, 2013, **42**, 12370–12380.
- 80 D. S. McGuinness and K. J. Cavell, *Organometallics*, 2000, **19**, 741–748.
- 81 G. Calzaferri, *Catal. Today*, 1997, **39**, 145–157.
- 82 H.-L. Su, L. M. Pérez, S.-J. Lee, J. H. Reibenspies, H. S. Bazzi and D. E. Bergbreiter, *Organometallics*, 2012, **31**, 4063–4071.
- 83 M. Iglesias, D. J. Beetstra, J. C. Knight, L.-L. Ooi, A. Stasch, S. Coles, L. Male, M. B. Hursthouse, K. J. Cavell, A. Dervisi and I. A. Fallis, *Organometallics*, 2008, **27**, 3279–3289.
- 84 N. Kaloğlu, İ. Özdemir, S. Günal and İ. Özdemir, *Appl. Organomet. Chem.*, 2017, **31**, e3803.
- 85 S. Wei, X. Li, Z. Yang, J. Lan, G. Gao, Y. Xue and J. You, *Chem. Sci.*, 2012, **3**, 359–363.

- 86 J. Łuczak, C. Jungnickel, M. Joskowska, J. Thöming and J. Hupka, *J. Colloid Interface Sci.*, 2009, **336**, 111–116.
- 87 T. Inoue, H. Ebina, B. Dong and L. Zheng, *J. Colloid Interface Sci.*, 2007, **314**, 236–241.
- 88 M. Anouti, J. Jones, A. Boisset, J. Jacquemin, M. Caillon-Caravanier and D. Lemordant, *J. Colloid Interface Sci.*, 2009, **340**, 104–111.
- 89 A. Fluksman and O. Benny, *Anal. Methods*, 2019, **11**, 3810–3818.
- 90 J. Aguiar, P. Carpena, J. A. Molina-Bolívar and C. Carnero Ruiz, *J. Colloid Interface Sci.*, 2003, **258**, 116–122.
- 91 Z. Wei, D. Yi, X. Hu, C. Sun, Y. Long and H. Zheng, *Colloids Surf. Physicochem. Eng. Asp.*, 2020, **595**, 124698.
- 92 M. Ao and D. Kim, *J. Chem. Eng. Data*, 2013, **58**, 1529–1534.
- 93 F. Geng, J. Liu, L. Zheng, L. Yu, Z. Li, G. Li and C. Tung, *J. Chem. Eng. Data*, 2010, **55**, 147–151.
- 94 J. M. del Rio, G. Prieto, F. Sarmiento and V. Mosquera, *Langmuir*, 1995, **11**, 1511–1514.
- 95 A. Di Michele, L. Brinchi, P. Di Profio, R. Germani, G. Savelli and G. Onori, *J. Colloid Interface Sci.*, 2011, **358**, 160–166.
- 96 L. Shi, N. Li, H. Yan, Y. Gao and L. Zheng, *Langmuir*, 2011, **27**, 1618–1625.
- 97 M. T. Garcia, I. Ribosa, L. Perez, A. Manresa and F. Comelles, *Colloids Surf. B Biointerfaces*, 2014, **123**, 318–325.
- 98 A. Ohta, Y. Hata, Y. Mizuno, T. Asakawa and S. Miyagishi, *J. Phys. Chem. B*, 2004, **108**, 12204–12209.
- 99 S. Liu, X. Wang, L. Chen, L. Hou and T. Zhou, *Soft Matter*, 2014, **10**, 9177–9186.
- 100 L. G. Chen and H. Bermudez, *Langmuir*, 2012, **28**, 1157–1162.
- 101 R. F. Kamrath and E. I. Franses, *J. Phys. Chem.*, 1984, **88**, 1642–1648.
- 102 R. Zana, *Langmuir*, 1996, **12**, 1208–1211.
- 103 D. Fu, X. Gao, B. Huang, J. Wang, Y. Sun, W. Zhang, K. Kan, X. Zhang, Y. Xie and X. Sui, *RSC Adv.*, 2019, **9**, 28799–28807.
- 104 J. M. Andrews, *J. Antimicrob. Chemother.*, 2001, **48**, 5–16.
- 105 K. A. Hammer, C. F. Carson and T. V. Riley, *J. Appl. Microbiol.*, 1999, **86**, 985–990.
- 106 A. Espinel-Ingroff, *J. Clin. Microbiol.*, 1998, **36**, 2950–2956.
- 107 L. B. Reller, M. Weinstein, J. H. Jorgensen and M. J. Ferraro, *Clin. Infect. Dis.*, 2009, **49**, 1749–1755.
- 108 F. Hackenberg, A. Deally, G. Lally, S. Malenke, H. Müller-Bunz, F. Paradisi, S. Patil, D. Quaglia and M. Tacke, *Int. J. Inorg. Chem.*, 2012, Article ID 121450, 13 pages, DOI: 10.1155/2012/121450.
- 109 M. T. Garcia, I. Ribosa, L. Perez, A. Manresa and F. Comelles, *Langmuir*, 2013, **29**, 2536–2545.
- 110 A. H. Delcour, *Biochim. Biophys. Acta*, 2009, **1794**, 808–816.
- 111 N. Mesaros, P. Nordmann, P. Plésiat, M. Roussel-Delvallez, J. Van Eldere, Y. Glupczynski, Y. Van Laethem, F. Jacobs, P. Lebecque, A. Malfroot, P. M. Tulkens and F. Van Bambeke, *Clin. Microbiol. Infect.*, 2007, **13**, 560–578.
- 112 K. Poole, *Clin. Microbiol. Infect.*, 2004, **10**, 12–26.
- 113 H. Zetty Zulikha, R. A. Haque, S. Budagumpi and A. M. S. Abdul Majid, *Inorganica Chim. Acta*, 2014, **411**, 40–47.
- 114 H. A. Mohamed, B. R. M. Lake, T. Laing, R. M. Phillips and C. E. Willans, *Dalton Trans.*, 2015, **44**, 7563–7569.
- 115 H. V. Huynh, Y. Han, R. Jothibas and J. A. Yang, *Organometallics*, 2009, **28**, 5395–5404.
- 116 S. Silver, L. T. Phung and G. Silver, *J. Ind. Microbiol. Biotechnol.*, 2006, **33**, 627–634.
- 117 J. A. Lemire, J. J. Harrison and R. J. Turner, *Nat. Rev. Microbiol.*, 2013, **11**, 371–384.
- 118 R. B. Thurman and C. P. Gerba, *Crit. Rev. Environ. Control*, 1989, **18**, 295–315.

119A. B. G. Lansdown, *J. Wound Care*, 2002, **11**, 125–130.

### Chapter 3: Bisthiosemicarbazone complexes and their anthelmintic properties

Bisthiosemicarbazone metal complexes are a subclass of thiosemicarbazone metal complexes. Bisthiosemicarbazones consist of two semithiocarbazone moieties within the structure of the ligand, and therefore contain two Schiff base donors and two thiolate donors.<sup>1</sup> Bisthiosemicarbazone ligands are therefore typically tetradentate, and are therefore form many stable complexes due to the chelate effect. In complexes of these ligands the ligand is usually dianionic, which extends the conjugation of the ligand  $\pi$ -system, leading to dramatic changes in the colour of the complex by comparison with its parent ligand.<sup>2</sup> The literature related to bisthiosemicarbazones is dominated by CuATSM, a hypoxia selective positron emission tomography (PET) contrast agent. Any discussion of the literature surrounding bisthiosemicarbazone metal complexes would be inadequate without first discussing CuATSM.

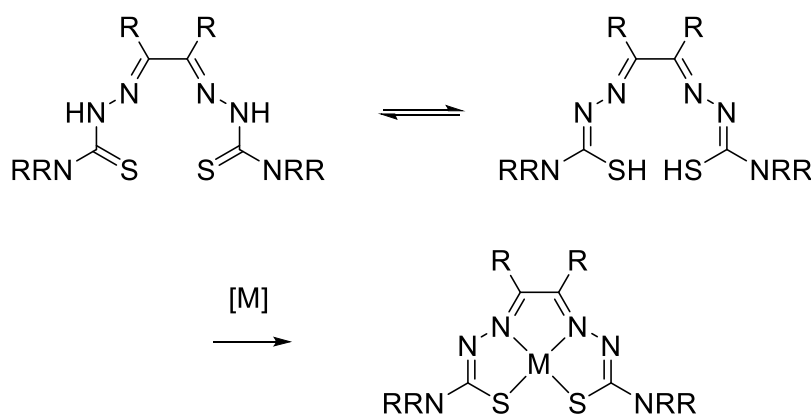


**Figure 1.** Complexation of a metal by an example bisthiosemicarbazone complex. Note the deprotonation of the hydrazinic nitrogens upon formation of the metal complex. R-groups are varied throughout the literature, and may lead to symmetric or asymmetric examples.

#### **CuATSM**

CuATSM is a bisthiosemicarbazone metal complex consisting of an diacetyl backbone forming the imine components of the ligand, and two N-methyl-substituted thiosemicarbazone moieties.<sup>3</sup> CuATSM has a square-planar geometry, similar to other bisthiosemicarbazone complexes.<sup>4</sup> This is partly due to the planar ATSM ligand providing 4 suitable donors (2x N, 2x S), and partially due to the Jahn-Teller distortion that occurs in  $d^9$  Cu(II) in an octahedral ligand field. This distortion leads to unequal occupation of  $d_z^2$  and  $d_{x^2-y^2}$  orbitals that contribute to the  $e_g$  molecular orbital, forming what is known as 4+2 coordination (2 long bonds, 4 short bonds) when the Cu  $d_z^2$  orbital is filled and the  $d_{x^2-y^2}$  orbital is half occupied. In extreme cases, the axial ligands attached by the long

bonds may dissociate entirely, leaving a square-planar complex. When employed as a PET contrast agent the ligand architecture surrounds a positron emitting isotope of copper, the most common of which is  $^{64}\text{Cu}$ , forming  $^{64}\text{CuATSM}$ .<sup>5-7</sup> CuATSM has many benefits by comparison with other hypoxia selective contrast agents due to excellent localisation times and tumour-to-background contrast ratios, along with a much longer radioactive half-life than the typically used clinical isotopes. This allows more time for additional manipulation and handling of the agent and allows for the patient to be scanned in facilities that do not have access to a cyclotron.<sup>8</sup>

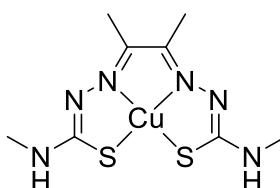


**Figure 2.** Structure of CuATSM.

The complex is formed quickly in part due to the excellent Cu(II) binding afforded by the mixed hard/soft Schiff base/thiolate donors on the ligand.<sup>9</sup> This allows for a minimum of manipulation and purification, which makes  $^{64}\text{CuATSM}$  beneficial by comparison with organic agents such as fluorinated imidazoles, for which the preparation is invariably more involved.<sup>10</sup> Half-lives of some isotopes relevant to medicine are summarised below (Table 1).  $^{64}\text{CuATSM}$  has been shown to be selective for hypoxic tissue, in part due to the reduction potential of the bound metal.<sup>4,11,12</sup> This has led to  $^{64}\text{CuATSM}$  being employed *in vivo* as a hypoxia selective agent,<sup>5,13-15</sup> and human clinical trials for CuATSM with a variety of Cu isotopes for imaging have been in progress since the year 2000.<sup>16-19</sup>

Isotope	Half-life
$^{68}\text{Ga}$	68 minutes
$^{18}\text{F}$	109.8 minutes
$^{99\text{m}}\text{Tc}$	6 hours
$^{64}\text{Cu}$	12.2 hours
$^{86}\text{Y}$	14.7 hours
$^{111}\text{In}$	2.8 days
$^{89}\text{Zr}$	3.2 days

**Table 1.** Selected half-lives of radioactive isotopes employed in medicine.<sup>10</sup>

CuATSM has in recent years been shown to positively affect neurodegenerative conditions such as Parkinson's disease<sup>20</sup> (where the complex is also in phase 1 clinical

trials as of 2020)<sup>21</sup>, Alzheimer's disease,<sup>22,23</sup> as well as improving amyotrophic lateral sclerosis (ALS), for which ATSM is also in phase 1 clinical trials,<sup>24</sup> by interrupting the activity of mutant superoxide dismutase enzymes.<sup>25–27</sup> The neuroprotective nature of CuATSM in ALS models is also seen in the Zn analogue, ZnATSM.<sup>28</sup>

### MBTSC complexes

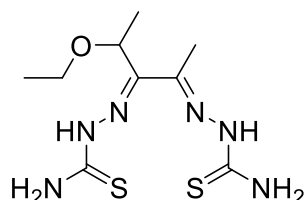


**Figure 3.** The structure of the bithiosemicarbazone ligand  $H_2KTS$ .

The biological effects of MBTSC complexes were first reported in the 1950s, with initial publications focusing on the antitumour activities against a variety of cell lines.<sup>29,30</sup> Examples continued to crop up throughout the 1960s<sup>31–33</sup> and 1970s<sup>34–36</sup>, with examples containing primarily Zn and Cu. These early examples of MBTSC complexes were based on the 3-ethoxy-2-oxobutylaldehyde bis(thiosemicarbazone) ligand, known as  $H_2KTS$ .<sup>35–38</sup> Issues with the toxicity of MKTS complexes however,<sup>38</sup> particularly the ability of the complexes to inhibit DNA synthesis,<sup>36</sup> prevented progress towards clinical trials. In recent literature CuATSM, and its glyoxal backbone counterpart CuGTSM, have risen to prominence as promising complexes.<sup>4,39–45</sup> In contrast with CuKTS derivatives, both CuGTSM and CuATSM were shown to cause no deleterious effects in mice at significant doses over significant periods of time (10–30 mg/kg/day for >6 weeks).<sup>20,46</sup>

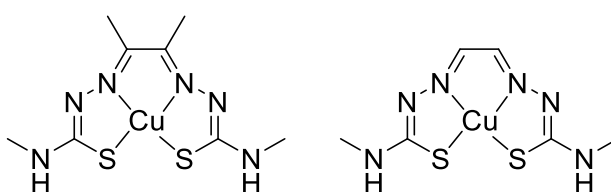


**Figure 4.** The structures of the bithiosemicarbazone complexes CuATSM (left) and CuGTSM (right).

Despite their very similar structures (comparison in Figure 4), the mode of action of these complexes is significantly different. CuATSM is more difficult than CuGTSM to reduce (0.6 V for CuATSM vs 0.44 V for CuGTSM referenced against Ag/AgCl) which contributes to CuATSM's selectivity for hypoxic tissue.<sup>44</sup> The difference in reduction potential allows CuATSM to diffuse readily in and out of normoxic tissue, but it is selectively reduced in hypoxic tissue, which produces an even more extreme reducing

environment than normal tissue. CuGTSM however is nonselectively reduced in all tissue.<sup>4,11,12</sup> Upon reduction to Cu(I), copper may then be released from the ligand in an irreversible reduction process.<sup>47-53</sup> This informs that slight modifications to the ligand structure of an MBTSC can cause drastic changes in the reduction potential of the associated metal, and therefore change the suitability of a complex to a certain application. CuGTSM's lack of selectivity for hypoxic tissue due to its relatively positive reduction potential leads to other potential uses as a source of Cu(I). Cu(I) is readily oxidised to produce Cu<sup>2+</sup> ions, which is known to interact with nucleic acids,<sup>54</sup> alter the activity of enzymes,<sup>25,26</sup> and cause oxidative damage to cell membranes, and cause free radicals and reactive oxygen species (ROS) to form, which further damages the viability of the cell.<sup>55-58</sup> CuGTSM's ability to readily release biocidal copper therefore makes it a promising candidate as an antimicrobial and anticancer reagent.

Work by Haupt *et al.*<sup>59</sup> described the activity of CuGTSM and CuATSM against prostate cancer cells. Both compounds were shown to have activity against human prostate carcinoma PC3 cells, however the easier reduction of CuGTSM vs CuATSM allowed for an increase in comparative bioavailable copper. The LD<sub>50</sub> for CuGTSM was reported as 1.7 µM, vs 7 µM for CuATSM. The efficacy of CuGTSM and CuATSM with an additional 20 µM of copper (physiological copper concentration) against PC3 cells was also compared to that of clioquinol with the same concentration of additional copper. Clioquinol is a copper ionophore that at the time was being assessed in phase 1 clinical trials as a treatment for patients with advanced haematological malignancies.<sup>60,61</sup> CuGTSM was found to be 100x more efficient at killing PC3 cells in the presence of physiological copper than clioquinol. It was also seen that H<sub>2</sub>GTSM and H<sub>2</sub>ATSM exhibited no toxicity in the absence of copper.

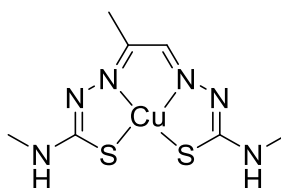


**Figure 5.** The structure of CuPTSM.

Work by Richardson *et al.*<sup>62</sup> described the activity of CuBTSC complexes, including CuATSM, CuGTSM, and the monomethyl backbone CuPTSM (Figure 5) against SK-N-MC neuroepithelioma cells and mortal human MRC5 fibroblasts. Of the BTSC ligands and MBTSC complexes tested, CuGTSM was the most effective against both cell lines. These values are lower than those reported for CuATSM and the intermediate CuPTSM. The IC<sub>50</sub> values are shown below in Table 2.

Compound	IC <sub>50</sub> (μM)	
	SK-N-MC	MRC5
H <sub>2</sub> GTSM	0.02 ± 0.004	6.15 ± 0.66
H <sub>2</sub> PTSM	0.017 ± 0.003	4.73 ± 0.75
H <sub>2</sub> ATSM	> 12.5	> 12.5
CuGTSM	0.009 ± 0.001	0.27 ± 0.05
CuPTSM	0.016 ± 0.001	0.65 ± 0.08
CuATSM	0.46 ± 0.17	2.13 ± 0.11
DFO	22.7 ± 1.6	> 12.5
Dp44mT	0.004 ± 0.001	2.19 ± 0.07
3-AP	0.36 ± 0.03	> 12.5

**Table 2.** IC<sub>50</sub> values of selected CuBTSC complexes, H<sub>2</sub>BTSC ligands, and controls against SK-N-MC and MRC5 cells.

CuGTSM was also more effective against the tested cells than 2/3 of the positive controls employed: desferrioxamine (DFO), a compound used for the treatment of iron overload,<sup>63</sup> and 3-AP: a thiosemicarbazone which was being investigated in clinical trials as an anticancer agent.<sup>64</sup> CuGTSM was also seen to have similar but significantly less efficacy by comparison with the third positive control Dp44mT, a thiosemicarbazone with known anti-proliferative activity and well-studied chelating agent that has been employed many times as an anticancer agent.<sup>65–67</sup>

CuGTSM was the only CuBTSC shown to have a statistically significant increase in its anti-proliferative effects by comparison with its parent ligand. Another key aspect of the anti-proliferative effects of CuGTSM is the difference in activity against the malignant neuroepithelioma cells than the healthy fibroblasts, with CuGTSM displaying increased activity against the neoplastic cells than against the mortal cells. The increased release of Cu from the most antiproliferative compounds was assessed by synthesis of <sup>64</sup>CuBTSC analogues. These compounds caused a decreased <sup>64</sup>Cu release from cancer cells than from control cells, suggesting that CuGTSM and other unsubstituted/monosubstituted CuBTSC release Cu and lead to Cu accumulation in cells. Further work by the group of Richardson *et al.*<sup>68</sup> highlighted the anticancer efficacy of CuGTSM, this time showing a greater efficacy than even Dp44mT against SK-N-MC cells.

The accumulation of intracellular Cu by release from CuGTSM was further confirmed in work by Donnelly *et al.*<sup>69</sup> where the copper levels in SKOV-3, HEK293, and HEK293 P-

gp cell lines were investigated. It was found that treatment of the cells with CuGTSM and other glyoxal-based backbone CuBTSC complexes increased the intracellular copper concentration and increased levels of p-ERK (phosphorylated extracellular signal-regulated kinase), an indirect indicator of increased bioavailable copper due to activation of the Ras-Raf-MEK-ERK pathway.<sup>70-72</sup> It was also found that adding low concentrations of the CuBTSCs to the SKOV-3 cells led to ATP7A (an endogenous copper transporter) from the Golgi network of the cell being trafficked to a more diffuse dispersion throughout the cell in order to aid with efflux of copper. The response was equivalent to treatment with a much higher concentration CuCl<sub>2</sub>, indicating that CuGTSM delivers copper to a cell then releases it.

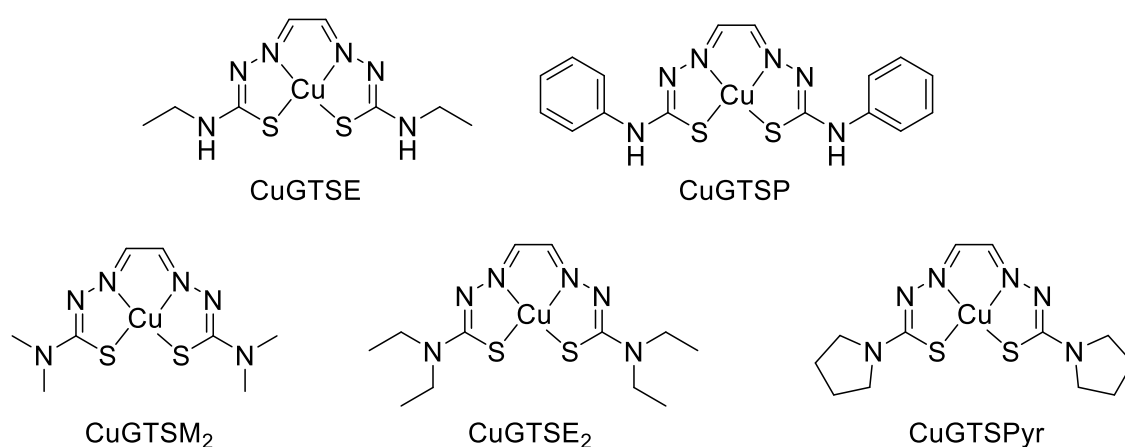


**Figure 6.** Glyoxal-based backbone CuBTSC complexes studied by Donnelly *et al.*<sup>69</sup>

Whereas previously it was thought that the copper is released due to reduction as Cu(I), recent work by Hurst *et al.*<sup>73</sup> has suggested that previously unreported oxidative mechanisms of copper release may also take place, as CuBTSCs and ZnATSM have one-electron oxidations that can occur within the range of physical oxidants such as H<sub>2</sub>O<sub>2</sub> catalysed by horseradish peroxidase (HRP) or myeloperoxidase, by the biological chlorinating agents HOCl and taurine chloramine, and peroxyxynitrite species. The oxidation is ligand-centred, and leads to the release of Cu<sup>2+</sup> ions.

A recent example from the work of Grapperhaus *et al.*<sup>74</sup> describes the anticancer effects of Cu, Zn, and Ni complexes of 3 different ligand architectures. The ligands described are thiosemicarbazone-alkylthiocarbamate hybrid structures (shown below) which form complexes analogous to MBTSC complexes (structures shown in Figure 7). The anticancer effects of the complexes were assessed by MTT assay against an adenocarcinoma cell line and a nonmalignant lung fibroblast cell line. GI<sub>50</sub> values (the concentration at which 50% of maximal inhibition of cell proliferation has occurred) were typically low for the copper complexes, with GI<sub>50</sub> concentrations of less than 0.29 μM in

all cases against the adenocarcinoma cell line, with 2 of the Cu complexes having  $GI_{50}$  concentrations of less than 0.1  $\mu\text{M}$ . The complexes were also seen to be more effective than CuATSM, which had a value of 0.48  $\mu\text{M}$ , but were not as effective as CuGTSM, which had a  $GI_{50}$  of 0.02  $\mu\text{M}$  against the adenocarcinoma cells. These values are very low by comparison with cisplatin, which is a widely used chemotherapy agent, which had a  $GI_{50}$  value of 10.9  $\mu\text{M}$  against the adenocarcinoma cells.

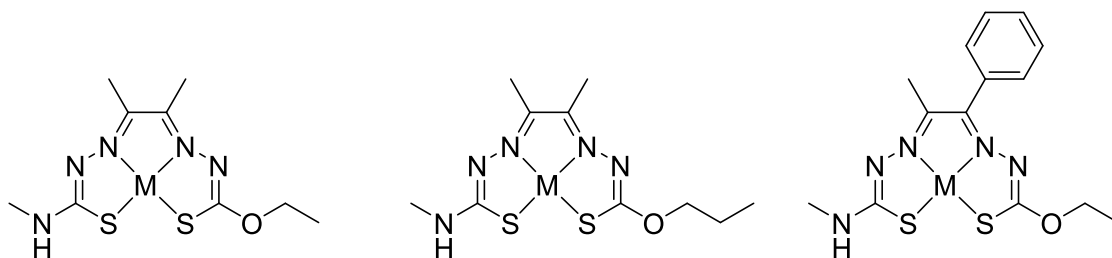


**Figure 7.** Hybrid thiosemicarbazone-alkylthiocarbamate metal complexes described in the work of Grapperhaus et al. where  $M = \text{Cu}, \text{Zn}, \text{or Ni}$ .<sup>74</sup>

CuGTSM has been shown to have an antibacterial effect against a wide range of clinically important bacteria including *Neisseria gonorrhoeae*,<sup>45</sup> *Mycobacterium tuberculosis*,<sup>75</sup> *Staphylococcus aureus*,<sup>76</sup> and *Chlamydia trachomatis*.<sup>77</sup> The mechanism of action is thought to mirror that described for the anticancer properties of CuGTSM, based on the release of bioavailable copper, which is known to be toxic to bacteria.<sup>58</sup> The literature is also rife with publications describing the neuroprotective properties of CuGTSM,<sup>23,46,78,79</sup> similar to those described for CuATSM. CuBTSCs have been designed in order to improve on the hypoxia selectivity or specific organ targeting of CuATSM as a PET contrast agent,<sup>80</sup> CuPTSM has been shown to improve symptoms in mouse models of Menkes disease,<sup>81</sup> a ZnBTSC acts as an antidiabetic compound due to its high hypoglycaemic activity and improves glucose intolerance in KK-A<sup>y</sup> mice,<sup>82</sup> and CuBTSCs are also reported to have antiprotozoan activity.<sup>83</sup> The potent bioactivity and versatility of MBTSC complexes, coupled with previous unpublished results from within the group lead to interest in developing MBTSC complexes as antischistosomal agents.

### Schistosomiasis

Schistosomiasis is a chronic helminthiasis (worm infection) that occurs in human beings in tropical areas of the world.<sup>84</sup> Schistosomiasis is caused by 6 clinically relevant trematode worm parasites of the genus *Schistosoma*: *Schistosoma mansoni*, *Schistosoma haematobium*, *Schistosoma japonicum*, *Schistosoma intercalatum*, *Schistosoma mekongi*, and *Schistosoma guineensis*.<sup>85,86</sup> The latter 3 species are less significant in human disease due to narrow geographic distribution or low infection rates.

*S. mansoni* and *S. haematobium* are ubiquitous in many of the tropical areas of the planet, and are responsible for the majority of cases of schistosomiasis in Africa, the Arabian peninsula, and South America (where *S. mansoni* is responsible for the majority of cases of schistosomiasis), whereas *S. japonicum* is responsible for cases of the disease in China, the Philippines, and Indonesia.<sup>84</sup> Schistosomiasis is considered the most deadly of the neglected tropical diseases (NTDs) and is responsible for over 300,000 deaths a year.<sup>87,88</sup> Schistosomiasis also disproportionately affects children, who are more likely to develop severe infections, which is characterised by a high number of eggs and a high number of adult worms.<sup>89</sup> This increased infection rate is largely due to children spending more time in contaminated bodies of water than adults, though common infection routes in adults include those who work in water such as fishermen<sup>90</sup> and rice farmers.<sup>91</sup>

Schistosomiasis prevalence (2012): ▲ ≥50% (high), ▲ 10-49% (moderate), ▲ <10% (low), ▲ countries requiring evaluation, ▲ N/A, ▲ non-endemic countries.

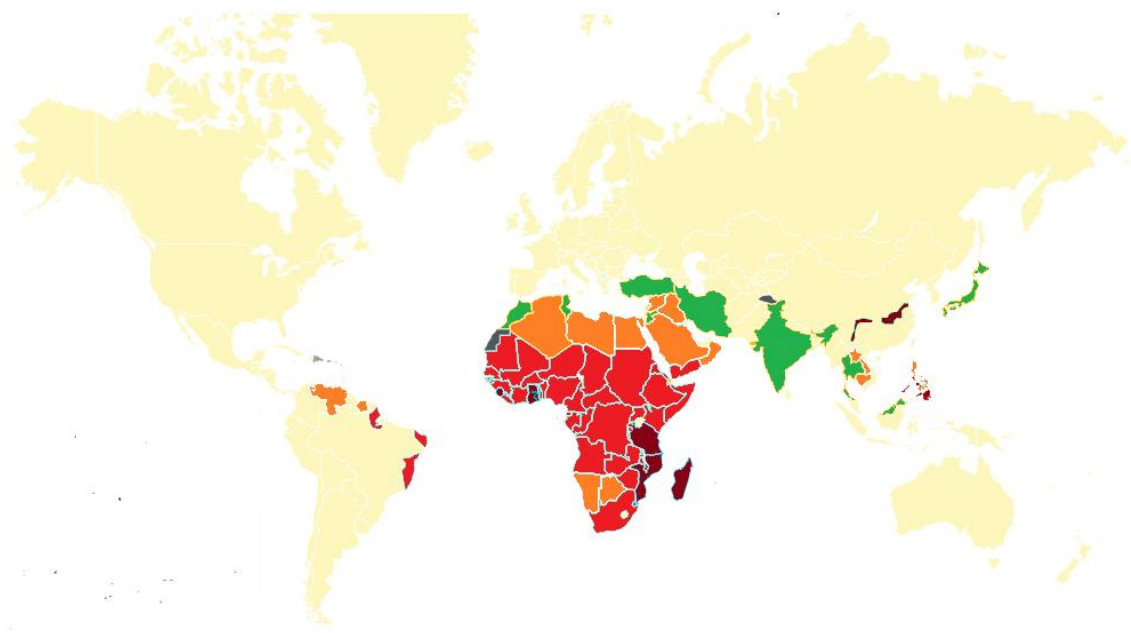


**Figure 8.** Worldwide distribution of Schistosomiasis in 2012. Figure adapted from the work of McManus et al.<sup>89</sup> based on Map: Distribution of schistosomiasis, worldwide, 2012, WHO, © 2012. Countries requiring evaluation are those which may have interrupted the transmission of schistosomiasis, but needed verification as of 2012.

Infection occurs through cercariae (the free-swimming larval life stage of trematodes released from infected snails) penetrating the skin of a human host. The initial infection stage is often characterised by a rash. After a few weeks to months of exposure, acute schistosomiasis (AS), also known as Katayama fever, sets in.<sup>92</sup> Those experiencing AS

express general symptoms such as fever, coughing, headaches, and the development of hives.<sup>93</sup> The symptoms are caused by the host's immune response to the migration of schistosomula (the life stage of the parasite upon entry to the vertebrate host).<sup>92</sup> The migrating schistosomula migrate to the liver, where they form adult pairs and migrate to either the bowels (in the case of *S. mansoni*<sup>94</sup> and *S. japonicum*<sup>95</sup>) or the bladder (*S. haematobium*<sup>96</sup>) where they produce eggs that are excreted by the host to restart the life cycle of the parasite. The immune response in later stages of schistosomiasis is caused by the host's reaction to proteolytic enzymes released by the schistosome's eggs rather than any direct mechanism involving the adult worms.<sup>85</sup> The immune response to these eggs signifies the chronic schistosomiasis (CS) stage of the disease, and is characterised by the formation of granulomas in the host tissue, which progress to the formation of pseudopolyps, ulcers, and bleeding.<sup>84</sup> Other symptoms of CS depend on the location of the eggs in the host (bladder or bowel) and may include: blood in the urine, hydronephrosis, hydronephrosis, diarrhea with or without blood, abdominal pain, and loss of appetite, and can lead to secondary infections of the liver, spleen, lungs, genitals, and even the brain.<sup>85</sup>

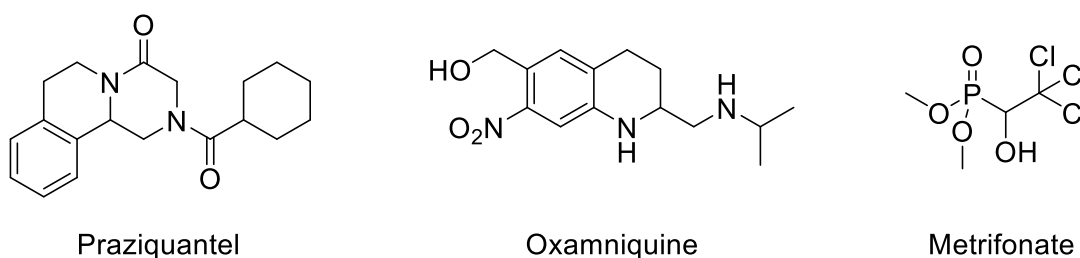


**Figure 9.** The structures of the antischistosomal drugs praziquantel (PZQ), oxamniquine (OXA), and metrifonate.

There is no vaccine available to prevent schistosomiasis, with the control of *Schistosoma* infections in humans typically managed by one drug, the pyrazinoisoquinolone praziquantel (PZQ).<sup>84,88,97,98</sup> While PZQ is active against the adult life stages of all *Schistosoma spp.* it is ineffective against immature forms such as schistosomules. Infections are therefore managed over a period of time with repeated administrations of PZQ in the hope of killing mature schistosomes whenever they develop in the host.<sup>99</sup> The repeat doses of PZQ may also lead to the additional negative of selecting for PZQ-resistant adult schistosomes, potentially allowing the population to develop a resistance to PZQ. This lack of suitable candidate drugs lead to a revival of antischistosome drug discovery in the early 20<sup>th</sup> century, including examples such as the previously examined oxamniquine (OXA, effective on *S. mansoni* only)<sup>100</sup>, metrifonate (effective on *S. haematobium* only).<sup>101</sup> PZQ derivatives such as substituted pyrazino[2, 1-a]isoquinoline

derivatives showed some efficacy against juvenile *S. mansoni* and *S. japonicum in vitro*. The acyl and oxo groups at positions 2 and 4 on PZQ was found to be essential to schistosomicidal activity, as was the pendant cyclohexyl group.<sup>102</sup> Modification of the 10-position on the phenyl ring with an amino group, or replacing 3- or 4-aminophenyl groups with PZQ's cyclohexyl group leads to a 4 fold decrease in schistosomicidal activity.<sup>103</sup> Addition of a hydroxy group to the 10-position of the phenyl ring lead to improved *ex-vivo* efficacy by comparison with PZQ, and also showed activity against juvenile worms (unlike PZQ), but the *in vivo* activity of the derivative was less than that of the parent PZQ.<sup>104</sup>

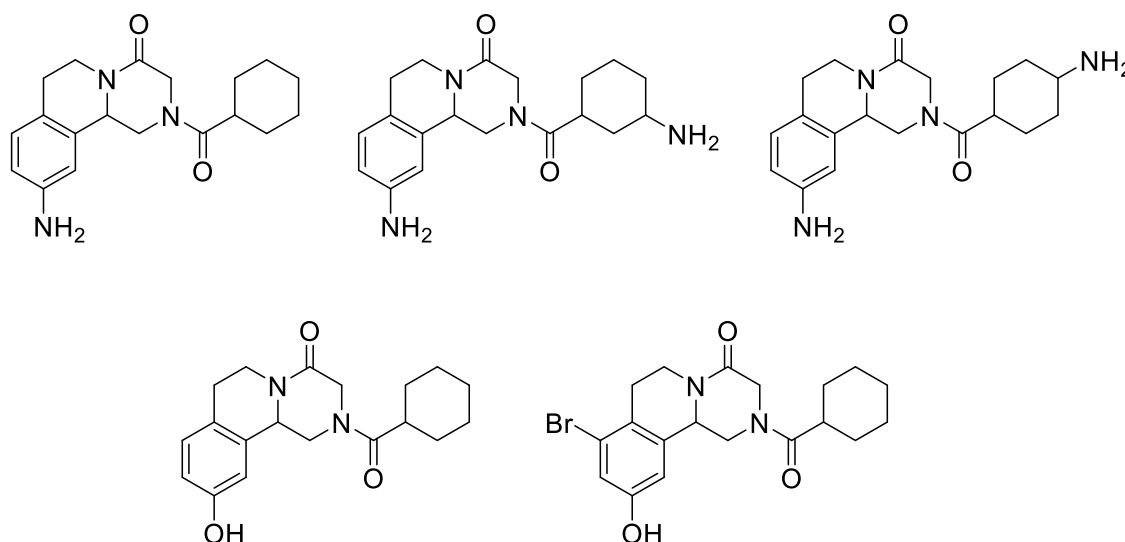


**Figure 10.** Substituted PZQ derivatives.<sup>102-104</sup>

Replacement of the phenyl ring in the compounds for thiophene resulted in similar efficacy as the parent PZQ against *S. mansoni* adults, whereas a chloroacetyl derivative of the same thiophene-based compound showed improved efficacy against *S. japonicum* vs PZQ *in vitro*.<sup>105</sup> Work by Patra *et al.* lead to incorporation of ferrocene<sup>106</sup> into PZQ derivatives (by reaction of PZQ and mono-carboxylic acid substituted ferrocene species with DIPEA and HATU in DMF), and using PZQ as an  $\eta^6$ -donor to  $\text{Cr}(\text{CO})_3$ <sup>107</sup> (prepared by reaction of PZQ with dibutyl ether in THF at reflux) showed comparable, and in some cases improved results by comparison with PZQ against adult worms *in vitro*. These complexes were however significantly less effective than PZQ when tested in an *S. mansoni* mouse model.<sup>108</sup> Ferrocenyl and ruthenocenyl derivatives were prepared by reaction of OXA with  $\text{K}_2\text{CO}_3$  and a metallocene source ((ferrocenylmethyl)-trimethylammonium iodide or trimethylammoniomethylruthenocene iodide respectively) in acetonitrile at reflux. The OXA-based complexes showed activity against adult and

juvenile *S. mansoni* and *S. haematobium*, though the *in vivo* efficacy against adult worms was decreased in comparison with the parent compound.<sup>109,110</sup> The efficacy of this metal-OXA derivative against *S. haematobium* and against juvenile worms, which differs from the parent compound, potentially suggests an additional/different mechanism of action due to the addition of the metallocene.<sup>109</sup>

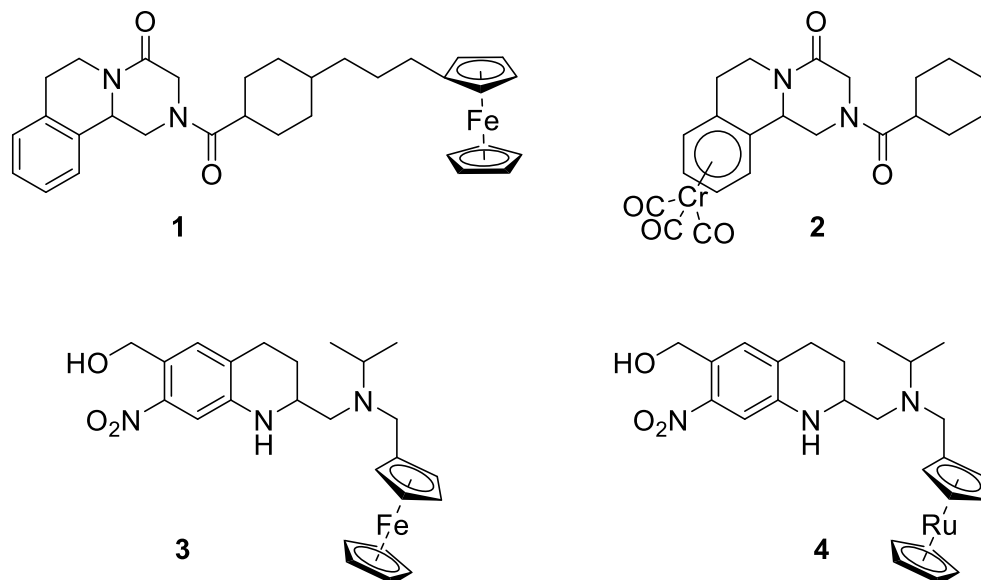


**Figure 11.** Antischistosomal metal complexes reported by Patra et al. (**1**<sup>106</sup> and **2**<sup>107</sup>) and Hess et al.<sup>109</sup> (**3** and **4**).

Derivatives of the antimalarials artemisinin, trioxaquinolines,<sup>111,112</sup> tetraoxolanes,<sup>113–115</sup> and mefloquine<sup>116–118</sup> have also been reported as having activity against the various life stages of *Schistosoma spp.*,<sup>119</sup> as well as the repurposing of drugs such as the hydantoin Ro 13-3978, meclonazepam, and Ro 15-5458 (all of which are benzodiazepines), the latter two compounds of which have shown good activity against all life stages against all immature life stages of schistosomes.<sup>101</sup> Reports of schistosomicidal metal complexes are few, and reports of effective agents are even less common. Ferrocenyl and ruthenocenyl derivatives of mefloquine have been reported, but exhibited poor schistosomicidal activity.<sup>116,119</sup> Bisquinoline-based tetraazamacrocyclic complexes of Fe(II) and Mn(II) showed good antischistosomal activity against *S. mansoni in vitro* and *in vivo*, however both complexes were found to be moderately cytotoxic.<sup>120</sup> The main issue is that in most cases the *in vitro* activity of the tested compounds does not lead to *in vivo* efficacy, and therefore no true successor for PZQ has been found and implemented.

More recent examples of antischistosomal compounds have focused on new compound classes including: ureas,<sup>121</sup> aminopyrazinamides,<sup>122</sup> pyrazolopyrimidine-5-carboxamides,<sup>122</sup> biarylsulfonamides,<sup>122</sup> hydroxamic acids,<sup>123</sup> pyrimidopyrimidines,<sup>124</sup>

thiazoles, thiosemicarbazones<sup>125</sup>, and their pthalyl derivatives,<sup>126</sup> imidazole derivatives,<sup>127</sup> oxadiazoles,<sup>128</sup> carbazole aminoalcohols,<sup>129</sup> biarylalkyl carboxylic acids (BACADs),<sup>130</sup> chalcones,<sup>131</sup> diterpenes,<sup>97</sup> lignans,<sup>132</sup> and cryptolepines.<sup>133</sup> Besides the work of Patra *et al.*,<sup>106–109</sup> Hess *et al.*,<sup>109</sup> Gasser *et al.*,<sup>116,119</sup> and Hubin *et al.*,<sup>120</sup> there have been no reports of metal complexes being implemented as treatments for schistosomiasis, despite reports of increased schistosomicidal activity by comparison with the parent compound, a potential new mechanism of action, and a low toxicity.<sup>109</sup>

## Aims

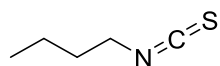
The purpose of the work described below is to present the synthesis of novel long-chain containing MG TSA (glyoxal-bis[N4-alkylthiosemicarbazonato]M<sup>II</sup>) by preparation of the ligands from their long-chain primary amines. The compounds described are a variation on a theme, with butyl, hexyl, and octyl groups used to produce symmetrical ligands forming a library of similar compounds to examine the differences in the physicochemical properties of the compounds in an iterative manner. The compounds synthesised will be fully characterised by NMR spectroscopy, mass spectrometry, UV-visible spectroscopy, infrared spectroscopy, and elemental analysis where NMR is not possible. The electrochemical behaviour of the synthesised MG TSA complexes will be examined, by cyclic voltammetry to probe whether the length of the pendant alkyl chains affect the redox potential of the bound metal. The anthelmintic effects of the prepared MG TSA complexes will be assessed against *S. mansoni* via high throughput screening and assays against both schistosomula and adult schistosomes. Through this, the influence of the bound metal and the lipophilicity of the ligand on antischistosomal activity will be assessed.

## Experimental

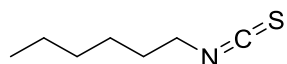
All compounds used were commercial grade and used as provided unless stated otherwise.  $^1\text{H-NMR}$  and  $^{13}\text{C}\{^1\text{H}\}\text{-NMR}$  spectra were recorded in either  $\text{CDCl}_3$  or  $\text{d}_6\text{-DMSO}$ , using Bruker Ultrashield FT-NMR spectrometers with a field strength of either 400 or 300 MHz. Spectra were analysed by MestReNova software version 6.0.2-5475 and digitally referenced using to the residual solvent signal. Low and high resolution mass spectra were produced on a Waters LCT Premier XE spectrometer by Cardiff University School of Chemistry Analytical Services. Infra-red spectra were recorded using a Shimadzu IR-Affinity-1S FTIR. UV-Vis studies were conducted on a Shimadzu UV-1800 spectrophotometer as acetonitrile solutions ( $5 \times 10^{-5}$  M). Voltammograms were measured using an Autolab PGSTAT204 potentiostat/galvanostat running Nova 2.1.4 software. Microanalyses were performed by the Elemental Analysis Service at London Metropolitan University, UK. Anti-parasitic assays were performed by Dr Josephine Forde-Thomas and Prof Karl Hoffmann, Parasitology and Epidemiology Group, Aberystwyth University, UK.

### Synthesis of alkylisothiocyanates

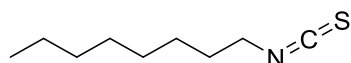
1-alkylamine (4.4 mmol) was added to ethanol (3 mL). Triethylamine (0.612 mL, 4.4 mmol) and carbon disulphide (3 mL, 50 mmol) were added to the solution, then the mixture was allowed to stir for 30 minutes at room temperature. The reaction was then cooled in an ice bath. To the cooled solution,  $\text{Boc}_2\text{O}$  (0.95 g, 4.35 mmol) in ethanol (1 mL) was added, followed immediately by catalytic DMAP ( $\sim 5$  mg,  $\sim 0.04$  mmol) in ethanol (1 mL). The reaction was then allowed to proceed for a further 30 minutes at room temperature. Volatiles were then removed under reduced pressure (CAUTION,  $\text{CS}_2$  is highly flammable), leaving behind a yellowish oil, the product, which was used without further purification.



**n-butylisothiocyanate (1).**  $^1\text{H-NMR}$  (300 MHz,  $\text{CDCl}_3$ , 298K):  $\delta$  (ppm): 3.49 (t, 2H,  $^3J = 6.6$  Hz,  $\text{NCH}_2$ ), 1.66 (m, 2H,  $\text{NCH}_2\text{CH}_2$ ), 1.43 (m, 2H,  $\text{CH}_2\text{CH}_3$ ), 0.93 (t, 3H,  $^3J = 7.3$  Hz,  $\text{CH}_2\text{CH}_3$ ).  $^{13}\text{C-NMR}$  (75 MHz,  $\text{CDCl}_3$ , 298K):  $\delta$  (ppm): 44.83 ( $\text{NCH}_2$ ), 31.97 ( $\text{NCH}_2\text{CH}_2$ ), 19.85 ( $\text{CH}_2\text{CH}_3$ ), 13.36 ( $\text{CH}_2\text{CH}_3$ ). This data matches that of a commercially sourced sample.



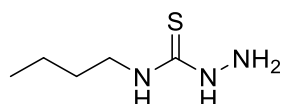
**n-hexylisothiocyanate (2).** **<sup>1</sup>H-NMR** (300 MHz, CDCl<sub>3</sub>, 298K): δ (ppm): 3.46 (t, 2H, <sup>3</sup>J = 6.6 Hz, NCH<sub>2</sub>), 1.64 (m, 2H, NCH<sub>2</sub>CH<sub>2</sub>), 1.31 (m, 6H, CH<sub>2</sub>), 0.84 (t, 2H, <sup>3</sup>J = 6.4 Hz, CH<sub>2</sub>CH<sub>3</sub>). **<sup>13</sup>C-NMR** (75 MHz, CDCl<sub>3</sub>, 298K): δ (ppm): 129.24 (SCN), 45.05 (NCH<sub>2</sub>), 30.95 (NCH<sub>2</sub>CH<sub>2</sub>), 26.21 (CH<sub>2</sub>), 22.44 (CH<sub>2</sub>), 18.33 (CH<sub>2</sub>), 13.94 (CH<sub>3</sub>). This data matches that of a commercially sourced sample.



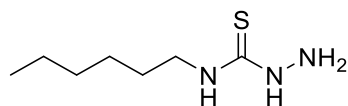
**n-octylisothiocyanate (3).** **<sup>1</sup>H-NMR** (300 MHz, CDCl<sub>3</sub>, 298K): δ (ppm): 3.49 (t, 2H, <sup>3</sup>J = 6.6 Hz, NCH<sub>2</sub>), 1.68 (m, 2H, NCH<sub>2</sub>CH<sub>2</sub>), 1.35 (m, 10H, CH<sub>2</sub>), 0.87 (t, 2H, <sup>3</sup>J = 6.4 Hz, CH<sub>2</sub>CH<sub>3</sub>). **<sup>13</sup>C-NMR** (75 MHz, CDCl<sub>3</sub>, 298K): δ (ppm): 45.17 (NCH<sub>2</sub>), 31.82 (NCH<sub>2</sub>CH<sub>2</sub>), 30.06 (CH<sub>2</sub>), 29.17 (CH<sub>2</sub>), 26.67 (CH<sub>2</sub>), 22.72 (CH<sub>2</sub>), 22.50 (CH<sub>2</sub>), 14.19 (CH<sub>3</sub>). This data matches that of a commercially sourced sample.

#### Synthesis of 4-alkyl-3-thiosemicarbazide

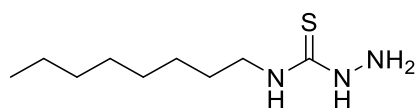
Crude alkylisothiocyanate (4.4 mmol) was dissolved in ethanol (10 mL). Hydrazine hydrate (0.257 mL, 5.3 mmol) in ethanol (5 mL) was added slowly to the reaction vessel over a period of 30 minutes at 0 °C. The reaction was then allowed to stir at 0 °C for 30 minutes, followed by a further 30 minutes at room temperature. The reaction was then stored overnight in a freezer. The white precipitate that formed was collected by filtration, then recrystallized from hot methanol to yield the product as a white powder:



**4-butyl-3-thiosemicarbazide (4)** (0.414 g, 58%). **<sup>1</sup>H-NMR** (400 MHz, d<sub>6</sub>-DMSO, 298K): δ (ppm): 8.54 (s, 1H, NH<sub>2</sub>NH), 7.78 (s, 1H, NHCH<sub>2</sub>), 4.43 (s, 2H, NH<sub>2</sub>NH), 3.43 (m, 2H, NCH<sub>2</sub>), 1.47 (quin, 2H, <sup>3</sup>J = 7.5 Hz, NCH<sub>2</sub>CH<sub>2</sub>), 1.27 (m, 2H, CH<sub>2</sub>CH<sub>3</sub>), 0.88 (t, 3H, <sup>3</sup>J = 7.3 Hz, CH<sub>2</sub>CH<sub>3</sub>). **<sup>13</sup>C-NMR** (101 MHz, d<sub>6</sub>-DMSO, 298K): δ (ppm): 181.10 (CS), 42.55 (NHCH<sub>2</sub>), 31.26 (NCH<sub>2</sub>CH<sub>2</sub>), 19.52 (CH<sub>2</sub>CH<sub>3</sub>), 13.79 (CH<sub>2</sub>CH<sub>3</sub>). **MS (ESI)** 148.09 [M + H<sup>+</sup>]. This data matches that of a commercially sourced sample.



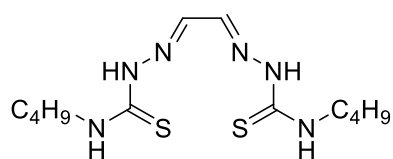
**4-hexyl-3-thiosemicarbazide (5)** (0.461 g, 55%). **<sup>1</sup>H-NMR** (400 MHz, d<sub>6</sub>-DMSO, 298K): δ (ppm): 8.54 (s, 1H, NH<sub>2</sub>NH), 7.78 (s, 1H, NHCH<sub>2</sub>), 4.42 (s, 2H, NH<sub>2</sub>NH), 3.41 (m, 2H, NCH<sub>2</sub>), 1.47 (m, 2H, NCH<sub>2</sub>CH<sub>2</sub>), 1.28 (m, 6H, CH<sub>2</sub>), 0.85 (t, 3H, <sup>3</sup>J = 6.7 Hz, CH<sub>2</sub>CH<sub>3</sub>). **<sup>13</sup>C-NMR** (101 MHz, d<sub>6</sub>-DMSO, 298K): δ (ppm): 181.12 (CS), 42.88 (NHCH<sub>2</sub>), 31.10 (NCH<sub>2</sub>CH<sub>2</sub>), 29.11 (CH<sub>2</sub>), 26.05 (CH<sub>2</sub>), 22.13 (CH<sub>2</sub>), 13.94 (CH<sub>3</sub>). **MS (ESI)** 176.12 [M + H<sup>+</sup>]. This data matches that of a commercially sourced sample.



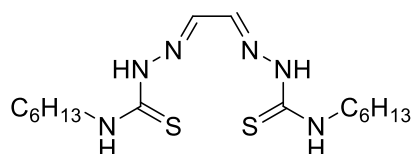
**4-octyl-3-thiosemicarbazide (6)** (0.605 g, 63%). **<sup>1</sup>H-NMR** (400 MHz, d<sub>6</sub>-DMSO, 298K): δ (ppm): 8.54 (s, 1H, NH<sub>2</sub>NH), 7.78 (s, 1H, NHCH<sub>2</sub>), 4.42 (s, 2H, NH<sub>2</sub>NH), 3.41 (m, 2H, NCH<sub>2</sub>), 1.47 (m, 2H, NCH<sub>2</sub>CH<sub>2</sub>), 1.28 (m, 6H, CH<sub>2</sub>), 0.85 (t, 3H, <sup>3</sup>J = 6.7 Hz, CH<sub>2</sub>CH<sub>3</sub>). **<sup>13</sup>C-NMR** (101 MHz, d<sub>6</sub>-DMSO, 298K): δ (ppm): 177.54 (CS), 43.34 (NHCH<sub>2</sub>), 31.26 (NCH<sub>2</sub>CH<sub>2</sub>), 28.80 (CH<sub>2</sub>), 26.33 (CH<sub>2</sub>), 25.03 (CH<sub>2</sub>), 22.10 (CH<sub>2</sub>), 17.57 (CH<sub>2</sub>), 13.97 (CH<sub>3</sub>). **MS (ESI)** 204.16 [M + H<sup>+</sup>]. This data matches that of a commercially sourced sample.

### Synthesis of H<sub>2</sub>GTSA ligands

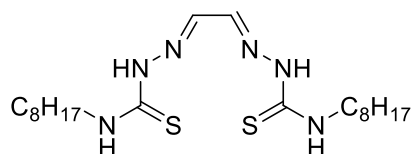
4-alkyl-3-thiosemicarbazide (10 mmol) and glyoxal solution (40 wt% in H<sub>2</sub>O, 0.544 mL, 5 mmol) were added to ethanol (20 mL). Sulphuric acid (1-3 drops) was added, and the reaction mixture was allowed to stir at room temperature for 4 hours. The resultant pale yellow solid was collected by filtration to yield the product:



**H<sub>2</sub>GTSA** (glyoxal-bis[N4-butylthiosemicarbazone]) (**7**) (1.20 g, 76%). **<sup>1</sup>H-NMR** (400 MHz, d<sub>6</sub>-DMSO, 298K): δ (ppm): 11.71 (s, 2H, NNHCS), 8.51 (t, 2H, <sup>3</sup>J = 5.9 Hz, NHCH<sub>2</sub>), 7.72 (s, 2H, NCHCHN), 3.50 (m, 4H, NHCH<sub>2</sub>), 1.52 (m, 4H, NCH<sub>2</sub>CH<sub>2</sub>), 1.27 (m, 4H, CH<sub>2</sub>CH<sub>3</sub>), 0.88 (t, 6H, <sup>3</sup>J = 7.4 Hz, CH<sub>2</sub>CH<sub>3</sub>). **<sup>13</sup>C-NMR** (101 MHz, d<sub>6</sub>-DMSO, 298K): δ (ppm): 176.68 (CS), 140.06 (NCHCHN), 43.27 (NCH<sub>2</sub>CH<sub>2</sub>), 30.81 (NCH<sub>2</sub>CH<sub>2</sub>), 19.55 (CH<sub>2</sub>CH<sub>3</sub>), 13.80 (CH<sub>2</sub>CH<sub>3</sub>). **MS (ESI)** 317.15 [M + H<sup>+</sup>]. This matches data reported by Barrett *et al.*<sup>134</sup>

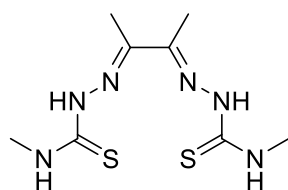


**H<sub>2</sub>GTSH** (glyoxal-bis[N4-hexylthiosemicarbazone]) (**8**) (1.45 g, 78%). **<sup>1</sup>H-NMR** (400 MHz, d<sub>6</sub>-DMSO, 298K): δ (ppm): 11.69 (s, 2H, NNHCS), 8.50 (t, 2H, <sup>3</sup>J = 5.8 Hz, NHCH<sub>2</sub>), 7.72 (s, 2H, NCHCHN), 3.48 (m, 4H, NHCH<sub>2</sub>), 1.54 (m, 4H, NCH<sub>2</sub>CH<sub>2</sub>), 1.26 (s, 12H, CH<sub>2</sub>), 0.86 (t, 6H, <sup>3</sup>J = 6.6 Hz, CH<sub>2</sub>CH<sub>3</sub>). **<sup>13</sup>C-NMR** (101 MHz, d<sub>6</sub>-DMSO, 298K): δ (ppm): 176.66 (CS), 140.05 (NCHCHN), 43.56 (NCH<sub>2</sub>CH<sub>2</sub>), 31.03 (CH<sub>2</sub>), 28.58 (CH<sub>2</sub>), 25.99 (CH<sub>2</sub>), 22.05 (CH<sub>2</sub>), 13.93 (CH<sub>3</sub>). **MS (ESI)** 373.22 [M + H<sup>+</sup>]. This matches data reported by Barrett *et al.*<sup>134</sup>



**H<sub>2</sub>GTSO** (glyoxal-bis[N4-octylthiosemicarbazone]) (**9**) (1.89 g, 88%). **<sup>1</sup>H-NMR** (400 MHz, d<sub>6</sub>-DMSO, 298K): δ (ppm): 11.70 (s, 2H, NNHCS), 8.51 (t, 2H, <sup>3</sup>J = 5.9 Hz, NHCH<sub>2</sub>), 7.72 (s, 2H, NCHCHN), 3.48 (m, 4H, NHCH<sub>2</sub>), 1.53 (m, 4H, NCH<sub>2</sub>CH<sub>2</sub>), 1.27 (m, 20H, CH<sub>2</sub>), 0.85 (t, 6H, <sup>3</sup>J = 6.8 Hz, CH<sub>2</sub>CH<sub>3</sub>). **<sup>13</sup>C-NMR** (101 MHz, d<sub>6</sub>-DMSO, 298K): δ (ppm): 176.66 (CS), 140.05 (NCHCHN), 43.56 (NCH<sub>2</sub>CH<sub>2</sub>), 31.28 (CH<sub>2</sub>), 28.78 (CH<sub>2</sub>), 28.66 (CH<sub>2</sub>), 28.62 (CH<sub>2</sub>), 26.33 (CH<sub>2</sub>), 22.12 (CH<sub>2</sub>), 13.99 (CH<sub>3</sub>). **MS (ESI)** 429.27 [M + H<sup>+</sup>]. This matches data reported by Barrett *et al.*<sup>134</sup>

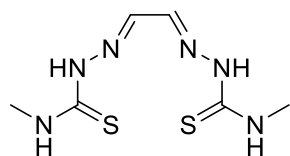
### Synthesis of H<sub>2</sub>ATSM



4-methyl-3-thiosemicarbazide (**10**) (1.262 g, 12 mmol) and 2,3-butanedione (0.527 mL, 6 mmol) were dissolved in ethanol (20 mL). Catalytic concentrated sulphuric acid (1-3 drops) was added, and the reaction was allowed to reflux for 4 hours. The resultant precipitate was collected on a Büchner funnel, and washed with cold ethanol (2 x 10 mL) to yield diacetyl-bis[N4-methylthiosemicarbazone] (H<sub>2</sub>ATSM) as a pale yellow powder (1.470 g, 94%). **<sup>1</sup>H-NMR** (400 MHz, d<sub>6</sub>-DMSO, 298K): δ (ppm): 10.19 (s, 2H, NNHCS), 8.35 (m, 2H, NHCH<sub>3</sub>), 3.02 (d, 6H, <sup>3</sup>J = 4.6 Hz, NHCH<sub>3</sub>), 2.20 (s, 6H, NC(CH<sub>3</sub>)). **<sup>13</sup>C-NMR** (101 MHz, d<sub>6</sub>-DMSO, 298K): δ (ppm): 178.47 (CS), 147.94 (NC(CH<sub>3</sub>)), 31.19 (NCH<sub>3</sub>),

11.65 (NC(CH<sub>3</sub>)). **MS (ESI)** 261.10 [M + H<sup>+</sup>]. This matches data reported by Holland *et al.*<sup>135</sup>

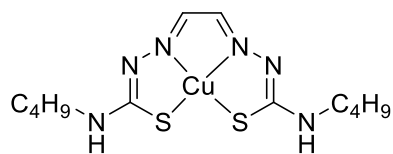
### Synthesis of H<sub>2</sub>GTSM



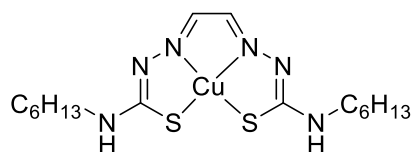
4-methyl-3-thiosemicarbazide (**11**) (0.631 g, 6 mmol) and glyoxal solution (40 wt% in H<sub>2</sub>O, 0.344 mL, 3 mmol) were dissolved in ethanol (10 mL). Concentrated sulphuric acid (1-3 drops) was added to the mixture, and the reaction was allowed to proceed at reflux for 4 hours. The precipitate that formed was isolated on a Büchner funnel, and then washed with cold ethanol (2 x 5 mL) to yield glyoxal-bis[N4-methylthiosemicarbazone] (H<sub>2</sub>GTSM) as a pale yellow powder (0.689 g, 99%). **<sup>1</sup>H-NMR** (400 MHz, d<sub>6</sub>-DMSO, 298K): δ (ppm): 11.74 (s, 2H, NNHCS), 8.48 (m, 2H, NHCH<sub>3</sub>), 7.72 (s, 2H, NCHCHN), 2.96 (d, 6H, <sup>3</sup>J = 4.5 Hz, NHCH<sub>3</sub>). **<sup>13</sup>C-NMR** (101 MHz, d<sub>6</sub>-DMSO, 298K): δ (ppm): 177.55 (CS), 140.01 (NCHCHN), 30.89 (NCH<sub>3</sub>). **MS (ESI)** 231.05 [M – H<sup>+</sup>]. This matches data reported by Stefani *et al.*<sup>62</sup>

### Synthesis of CuGTSA complexes

The parent H<sub>2</sub>GTSA ligand (1 mmol) and Cu(OAc)<sub>2</sub>·H<sub>2</sub>O (0.199 g, 1 mmol) were added to ethanol (20 mL) and stirred at room temperature for 4 hours. The solvent was then removed under reduced pressure to yield the respective complex as a deep red powder:

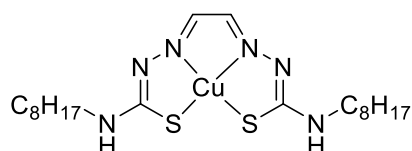


**CuGTSA** (glyoxal-bis[N4-butylthiosemicarbazone]copper(II)) (**7Cu**) (0.265 g, 70%). **Elemental analysis** Calculated (%) for [C<sub>12</sub>H<sub>22</sub>CuN<sub>6</sub>S<sub>2</sub>]: C, 38.13, H, 5.87, N, 22.23; found: C, 38.59, H, 5.6, 21.54. **IR** (ATR, cm<sup>-1</sup>): 3415, 3302, 2954, 2929, 2872, 1693, 1543, 1521, 1494, 1429, 1363, 1267, 1224, 1188, 1172, 1006, 958, 871, 812, 790, 734, 688, 623, 518, 466. **UV-Vis** (MeCN): λ<sub>max</sub> (ε / L mol<sup>-1</sup> cm<sup>-1</sup>) 544 (5300), 494 (8200), 370 (10300), 312 (18620), 260 (15400). **HRMS (ES+)** found m/z 378.0736, calculated m/z 378.0722 for [C<sub>12</sub>H<sub>23</sub>N<sub>6</sub>S<sub>2</sub><sup>63</sup>Cu] (+3.7 ppm).



**CuGTSH** (glyoxal-bis[N4-hexylthiosemicarbazonato]copper(II)) (**8Cu**) (0.333 g, 77%).

**Elemental analysis** Calculated (%) for  $[C_{16}H_{30}CuN_6S_2]$ : C, 44.27, H, 6.97, N, 19.36; found C, 42.00, H, 6.56, N, 15.98. **IR** (ATR,  $cm^{-1}$ ): 3415, 3373, 3300, 3118, 2960, 2926, 2852, 1697, 1683, 1614, 1519, 1429, 1363, 1317, 1267, 1217, 1188, 1157, 1095, 1068, 921, 871, 846, 796, 734, 688, 626, 578, 543, 447. **UV-Vis** (MeCN):  $\lambda_{max}$  ( $\epsilon / L mol^{-1} cm^{-1}$ ) 544 (3200), 492 (4900), 375 (6000), 315 (10520), 262 (8280). **HRMS (ES+)** found  $m/z$  434.1346, calculated  $m/z$  434.1348 for  $[C_{16}H_{31}N_6S_2^{63}Cu]$  (-0.55 ppm).

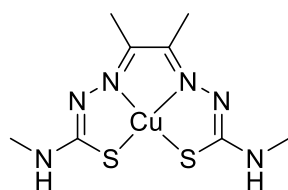


**CuGTSO** (glyoxal-bis[N4-octylthiosemicarbazonato]copper(II)) (**9Cu**) (0.314 g, 64%).

**Elemental analysis** Calculated (%) for  $[C_{20}H_{38}CuN_6S_2]$ : C, 49.00, H, 7.81, N, 17.14; found: C, 46.72, H, 7.36, N, 16.81. **IR** (ATR,  $cm^{-1}$ ): 3417, 3375, 3298, 2958, 2926, 2852, 1697, 1683, 1517, 1490, 1423, 1363, 1338, 1265, 1222, 1207, 1174, 1093, 1072, 1006, 966, 921, 871, 846, 808, 734, 686, 624, 516, 449. **UV-Vis** (MeCN):  $\lambda_{max}$  ( $\epsilon / L mol^{-1} cm^{-1}$ ) 546 (3620), 492 (5700), 372 (7520), 316 (13300), 254 (7840). **HRMS (ES+)** found  $m/z$  490.1976, calculated  $m/z$  490.1974 for  $[C_{20}H_{39}N_6S_2^{63}Cu]$  (+0.4 ppm).

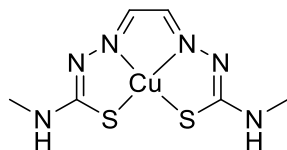
### Synthesis of CuATSM and CuGTSM

The respective ligand (1 mmol) and  $Cu(OAc)_2 \cdot H_2O$  (0.199 g, 1 mmol) were combined in ethanol (20 mL), then heated to reflux for 4 hours. The volatiles were removed *in vacuo*, and the resultant residue was dissolved in dichloromethane (20 mL). The mixture was washed with water (3 x 20 mL), then brine (20 mL). The DCM solution was then dried over sodium sulphate. The sodium sulphate was removed by filtration, and the dichloromethane removed *in vacuo* to yield the a deep red powder.



**CuATSM** (diacetyl-bis[N4-methylthiosemicarbazonato]copper(II)) (**10Cu**) (0.216 g, 66%). **Elemental analysis** Calculated (%) for  $[C_8H_{14}CuN_6S_2]$ : C, 29.85, H, 4.38, N,

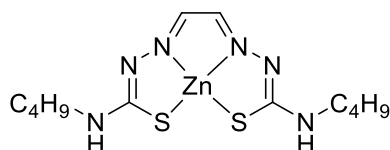
26.11; found: C, 29.76, H, 4.17, N, 26.00. **MS (ESI)** 322.01 [M + H<sup>+</sup>]. This matches data reported by Betts *et al.*<sup>136</sup>



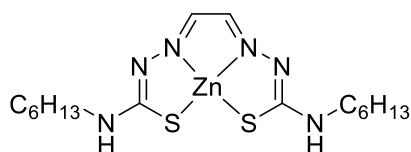
**CuGTSM** (glyoxal-bis[N4-methylthiosemicarbazonato]copper(II)) (**11Cu**) (0.197 g, 67%). **Elemental analysis** Calculated (%) for [C<sub>6</sub>H<sub>10</sub>CuN<sub>6</sub>S<sub>2</sub>]: C, 24.52, H, 3.43, N, 28.60; found: C, 24.40, H, 3.50, N, 28.51. **MS (ESI)** 293.98 [M + H<sup>+</sup>]. This matches data reported by Stefani *et al.*<sup>62</sup>

### Synthesis of ZnGTSA complexes

The respective H<sub>2</sub>GTSA ligand (0.5 mmol) and Zn(OAc)<sub>2</sub>·2H<sub>2</sub>O (0.11 g, 0.5 mmol) were added to ethanol (10 mL) and stirred at room temperature for 4 hours. The solvent was then removed under reduced pressure to yield the ZnGTSA complex as a golden yellow powder:

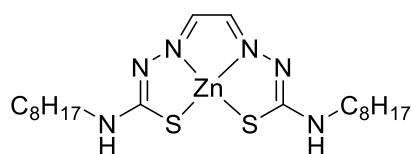


**ZnGTSB** (glyoxal-bis[N4-butylthiosemicarbazonato]zinc(II)) (**7Zn**) (0.108 g, 57%). **<sup>1</sup>H-NMR** (400 MHz, d<sub>6</sub>-DMSO, 298K): δ (ppm): 7.53 (s, 2H, NCHCHN), 3.32 (m, 4H, obscured by H-OD signal in solvent, NHCH<sub>2</sub>), 1.49 (m, 4H, NCH<sub>2</sub>CH<sub>2</sub>), 1.29 (m, 4H, CH<sub>2</sub>CH<sub>3</sub>), 0.87 (t, 6H, <sup>3</sup>J = 7.3 Hz, CH<sub>2</sub>CH<sub>3</sub>). **<sup>13</sup>C-NMR** (101 MHz, d<sub>6</sub>-DMSO, 298K): δ (ppm): 41.83 (NCH<sub>2</sub>CH<sub>2</sub>), 31.04 (NCH<sub>2</sub>CH<sub>2</sub>), 19.67 (CH<sub>2</sub>CH<sub>3</sub>), 13.75 (CH<sub>2</sub>CH<sub>3</sub>). **IR** (ATR, cm<sup>-1</sup>): 3444, 3265, 3196, 2954, 2927, 2866, 1550, 1494, 1471, 1440, 1394, 1309, 1267, 1251, 1215, 1153, 1093, 1062, 1044, 1022, 979, 952, 925, 904, 860, 804, 773, 628, 561, 457, 418. **UV-Vis** (MeCN): λ<sub>max</sub> (ε / L mol<sup>-1</sup> cm<sup>-1</sup>). 445 (12200), 332 (9880), 266 (10380). **HRMS (ES<sup>+</sup>)** found m/z 379.0724, calculated m/z 379.0717 for [C<sub>12</sub>H<sub>23</sub>N<sub>6</sub>S<sub>2</sub><sup>64</sup>Zn] (+1.8 ppm).



**ZnGTSH** (glyoxal-bis[N4-hexylthiosemicarbazonato]zinc(II)) (**8Zn**) (0.158 g, 73%). **<sup>1</sup>H-NMR** (400 MHz, d<sub>6</sub>-DMSO, 298K): δ (ppm): 7.52 (s, 2H, NCHCHN), 3.32 (m, 4H,

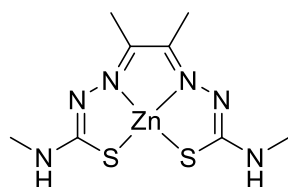
obscured by H-OD signal in solvent,  $\text{NHCH}_2$ ), 1.49 (m, 4H,  $\text{NCH}_2\text{CH}_2$ ), 1.26 (m, 12H,  $\text{CH}_2$ ), 0.86 (t, 6H,  $^3J = 6.5$  Hz,  $\text{CH}_2\text{CH}_3$ ).  $^{13}\text{C-NMR}$  (101 MHz,  $\text{d}_6\text{-DMSO}$ , 298K):  $\delta$  (ppm): 42.33 ( $\text{NCH}_2\text{CH}_2$ ), 31.02 ( $\text{CH}_2$ ), 25.95 ( $\text{CH}_2$ ), 22.07 ( $\text{CH}_2$ ), 21.49 ( $\text{CH}_2$ ), 13.93 ( $\text{CH}_2$ ), 12.65 ( $\text{CH}_3$ ). **IR** (ATR,  $\text{cm}^{-1}$ ): 3186, 2980, 2954, 2922, 2854, 1558, 1541, 1489, 1456, 1386, 1338, 1305, 1251, 1149, 1097, 1037, 1012, 935, 806, 763, 723, 628, 599, 563, 416. **UV-Vis** (MeCN):  $\lambda_{\text{max}}$  ( $\epsilon / \text{L mol}^{-1} \text{cm}^{-1}$ ). 442 (7660), 336 (12920), 271 (22200). **HRMS (ES+)** found  $m/z$  435.1352, calculated  $m/z$  435.1343 for  $[\text{C}_{16}\text{H}_{31}\text{N}_6\text{S}_2^{64}\text{Zn}]$  (+2.1 ppm).



**ZnGTSO** (glyoxal-bis[N4-octylthiosemicarbazonato]zinc(II)) (**9Zn**) (0.116 g, 47%).  $^1\text{H-NMR}$  (400 MHz,  $\text{d}_6\text{-DMSO}$ , 298K):  $\delta$  (ppm): 7.52 (s, 2H,  $\text{NCHCHN}$ ), 3.32 (m, 4H, obscured by H-OD signal in solvent,  $\text{NHCH}_2$ ), 1.49 (m, 4H,  $\text{NCH}_2\text{CH}_2$ ), 1.25 (m, 20H,  $\text{CH}_2$ ), 0.86 (t, 6H,  $^3J = 6.7$  Hz,  $\text{CH}_2\text{CH}_3$ ).  $^{13}\text{C-NMR}$  (101 MHz,  $\text{d}_6\text{-DMSO}$ , 298K):  $\delta$  (ppm): 43.27 ( $\text{NCH}_2\text{CH}_2$ ), 31.25 ( $\text{CH}_2$ ), 28.76 ( $\text{CH}_2$ ), 28.68 ( $\text{CH}_2$ ), 26.52 ( $\text{CH}_2$ ), 22.09 ( $\text{CH}_2$ ), 13.96 ( $\text{CH}_3$ ). **IR** (ATR,  $\text{cm}^{-1}$ ): 3186, 2954, 2918, 2852, 1550, 1489, 1456, 1386, 1305, 1257, 1224, 1149, 1103, 1020, 904, 806, 763, 721, 609, 561, 406. **UV-Vis** (MeCN):  $\lambda_{\text{max}}$  ( $\epsilon / \text{L mol}^{-1} \text{cm}^{-1}$ ). 448 (2620) 335 (1380), 273 (10020). **HRMS (ES+)** found  $m/z$  491.1981, calculated  $m/z$  491.1969 for  $[\text{C}_{20}\text{H}_{39}\text{N}_6\text{S}_2^{64}\text{Zn}]$  (+2.4 ppm).

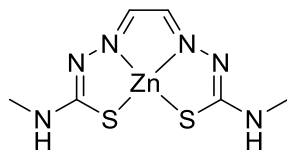
### Synthesis of ZnATSM and ZnGTSM

The relevant ligand (1 mmol) and  $\text{Zn}(\text{OAc})_2 \cdot 2\text{H}_2\text{O}$  (0.22 g, 1 mmol) were added to ethanol (20 mL). The mixture was then refluxed for 4 hours. The reaction was then allowed to cool to room temperature, upon which a golden yellow precipitate formed. The precipitate was then collected on a filter paper, and washed with cold ethanol (2 x 5 mL) to yield the product:



**ZnATSM** (diacetyl-bis[N4-methylthiosemicarbazonato]zinc(II)) (**10Zn**) (0.241g, 75%).  $^1\text{H-NMR}$  (400 MHz,  $\text{d}_6\text{-DMSO}$ , 298K):  $\delta$  (ppm): 7.19 (m, 2H,  $\text{NHCH}_3$ ), 2.83 (m, 6H,  $\text{NHCH}_3$ ), 2.20 (s, 6H,  $\text{NC}(\text{CH}_3)$ ).  $^{13}\text{C-NMR}$  (101 MHz,  $\text{d}_6\text{-DMSO}$ , 298K):  $\delta$  (ppm): 29.22

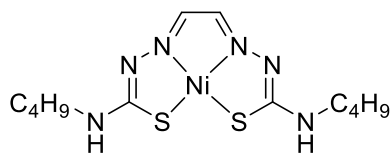
(NCH<sub>3</sub>), 13.88 (NC(CH<sub>3</sub>)). **MS (ESI)** 323.01 [M + H<sup>+</sup>]. This matches data reported by Betts *et al.*<sup>136</sup>



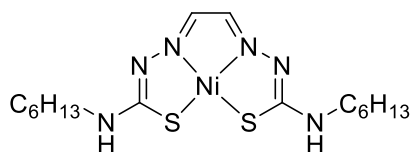
**ZnGTSM** (glyoxal-bis[N4-methylthiosemicarbazonato]zinc(II)) (**11Zn**) (0.183 g, 62%). **<sup>1</sup>H-NMR** (400 MHz, d<sub>6</sub>-DMSO, 298K): δ (ppm): 7.57 (s, 2H, NCHCHN), 2.81 (s, 6H, NHCH<sub>3</sub>). **<sup>13</sup>C-NMR** (101 MHz, d<sub>6</sub>-DMSO, 298K): δ (ppm): 18.54 (NCH<sub>3</sub>). **MS (ESI)** 294.98 [M + H<sup>+</sup>]. This matches data reported by Donnelly *et al.*<sup>137</sup>

### Synthesis of NiGTSA complexes

Ni(OAc)<sub>2</sub>·4H<sub>2</sub>O (0.124g, 0.5 mmol) and a H<sub>2</sub>GTSA ligand (0.5 mmol) were added to ethanol (10 mL). The reaction mixture was then stirred for 4 hours at room temperature. The complex was isolated by removal of volatiles under reduced pressure as a brown powder.

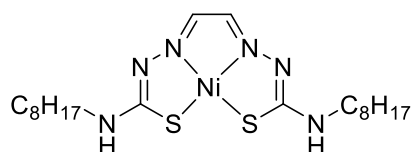


**NiGTSA** (glyoxal-bis[N4-butylthiosemicarbazonato]nickel(II)) (**7Ni**) (0.116g, 62%). **<sup>1</sup>H-NMR** (400 MHz, d<sub>6</sub>-DMSO, 298K): δ (ppm): 8.06 (m, 2H, NHCH<sub>2</sub>), 7.00 (s, 2H, NCHCHN), 3.19 (m, 4H, NHCH<sub>2</sub>), 1.43 (m, 4H, NCH<sub>2</sub>CH<sub>2</sub>), 1.25 (m, 4H, CH<sub>2</sub>CH<sub>3</sub>), 0.85 (t, 6H, <sup>3</sup>J = 7.5 Hz, CH<sub>2</sub>CH<sub>3</sub>). **<sup>13</sup>C-NMR** (101 MHz, d<sub>6</sub>-DMSO, 298K): δ (ppm): 177.13 (CS), 143.83 (NCHCHN), 45.45 (NCH<sub>2</sub>CH<sub>2</sub>), 30.75 (NCH<sub>2</sub>CH<sub>2</sub>), 19.47 (CH<sub>2</sub>CH<sub>3</sub>), 13.59 (CH<sub>2</sub>CH<sub>3</sub>). **IR** (ATR, cm<sup>-1</sup>): 3325, 3207, 2980, 2926, 1683, 1558, 1523, 1506, 1489, 1454, 1392, 1361, 1282, 1251, 1184, 1165, 1057, 956, 844, 815, 736, 659, 621, 532, 509, 486, 451, 426. **UV-Vis** (MeCN): λ<sub>max</sub> (ε / L mol<sup>-1</sup> cm<sup>-1</sup>). 442 (13460), 420 (13280), 334 (4800), 258 (25200). **HRMS (ES<sup>+</sup>)** found m/z 373.0789, calculated m/z 373.0779 for [C<sub>12</sub>H<sub>23</sub>N<sub>6</sub>S<sub>2</sub><sup>58</sup>Ni] (+2.7 ppm).



**NiGTSH** (glyoxal-bis[N4-hexylthiosemicarbazonato]nickel(II)) (**8Ni**) (0.115 g, 54%). **<sup>1</sup>H-NMR** (400 MHz, d<sub>6</sub>-DMSO, 298K): δ (ppm): 8.06 (m, 2H, NHCH<sub>2</sub>), 6.99 (s, 2H,

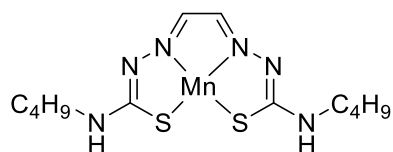
NCHCHN), 3.18 (m, 4H, NHCH<sub>2</sub>), 1.44 (m, 4H, NCH<sub>2</sub>CH<sub>2</sub>), 1.23 (m, 12H, CH<sub>2</sub>) 0.86 (m, 6H, CH<sub>3</sub>). <sup>13</sup>C-NMR (101 MHz, d<sub>6</sub>-DMSO, 298K): δ (ppm): 177.08 (CS), 143.80 (NCHCHN), 45.72 (NCH<sub>2</sub>CH<sub>2</sub>), 30.86 (NCH<sub>2</sub>CH<sub>2</sub>), 28.60 (CH<sub>2</sub>), 25.92 (CH<sub>2</sub>), 21.99 (CH<sub>2</sub>), 13.87 (CH<sub>3</sub>). IR (ATR, cm<sup>-1</sup>): 3672, 3649, 3325, 3211, 2980, 2926, 1695, 1683, 1558, 1523, 1506, 1489, 1456, 1394, 1361, 1300, 1251, 1188, 1166, 1058, 954, 842, 817, 761, 736, 659, 621, 536, 509, 484, 451, 426. UV-Vis (MeCN): λ<sub>max</sub> (ε / L mol<sup>-1</sup> cm<sup>-1</sup>). 441 (12140), 418 (12140), 334 (5680), 260 (23980). HRMS (ES<sup>+</sup>) found m/z 429.1411, calculated m/z 429.1405 for [C<sub>16</sub>H<sub>31</sub>N<sub>6</sub>S<sub>2</sub><sup>58</sup>Ni] (+1.4 ppm).



**NiGTSO** (glyoxal-bis[N4-octylthiosemicarbazonato]nickel(II)) (**9Ni**) (0.120 g, 50%). <sup>1</sup>H-NMR (400 MHz, d<sub>6</sub>-DMSO, 298K): δ (ppm): 8.05 (m, 2H, NHCH<sub>2</sub>), 6.98 (s, 2H, NCHCHN), 3.17 (m, 4H, NHCH<sub>2</sub>), 3.16 (m, 4H, NHCH<sub>2</sub>), 1.42 (m, 4H, NCH<sub>2</sub>CH<sub>2</sub>), 1.23 (m, 20H, CH<sub>2</sub>), 0.85 (t, 6H, <sup>3</sup>J = 6.5 Hz, CH<sub>2</sub>CH<sub>3</sub>). <sup>13</sup>C-NMR (101 MHz, d<sub>6</sub>-DMSO, 298K): δ (ppm): 176.93 (CS), 143.60 (NCHCHN), 45.54 (NCH<sub>2</sub>), 31.01 (CH<sub>2</sub>), 28.41 (CH<sub>2</sub>), 26.08 (CH<sub>2</sub>), 21.87 (CH<sub>2</sub>), 13.75 (CH<sub>3</sub>). IR (ATR, cm<sup>-1</sup>): 3670, 3649, 3332, 3205, 3116, 2980, 2916, 2852, 1697, 1683, 1587, 1558, 1510, 1489, 1440, 1386, 1336, 1307, 1267, 1166, 1080, 1028, 966, 956, 852, 810, 758, 723, 650, 609, 590, 518, 495, 468, 426. UV-Vis (MeCN): λ<sub>max</sub> (ε / L mol<sup>-1</sup> cm<sup>-1</sup>). 440 (10580), 418 (10560), 334 (4280), 260 (27960). HRMS (ES<sup>+</sup>) found m/z 485.2028, calculated m/z 485.2031 for [C<sub>20</sub>H<sub>39</sub>N<sub>6</sub>S<sub>2</sub><sup>58</sup>Ni] (-0.6 ppm).

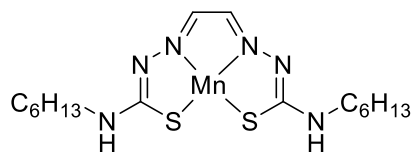
### Synthesis of MnGTSA complexes

Mn(OAc)<sub>2</sub>·4H<sub>2</sub>O (0.087 g, 0.5 mmol) was dissolved in ethanol (10 mL). To this solution, a parent H<sub>2</sub>GTSA ligand was added (0.5 mmol). The complex was then allowed to form at room temperature for 4 hours with stirring. The resultant solution with a cream-coloured precipitate was concentrated *in vacuo* to yield more precipitate, which was then further dried under reduced pressure to produce the complex:

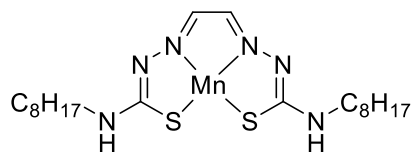


**MnGTSA** (glyoxal-bis[N4-butylthiosemicarbazonato]manganese(II)) (**7Mn**) (0.176g, 95%). **Elemental analysis** Calculated (%) for [C<sub>12</sub>H<sub>22</sub>MnN<sub>6</sub>S<sub>2</sub>]: C, 39.02, H, 6.00, N,

22.75; found: C, 40.02, H, 6.24, 18.52. **IR** (ATR,  $\text{cm}^{-1}$ ): 3670, 3647, 3365, 3122, 2980, 1558, 1514, 1471, 1450, 1394, 1325, 1269, 1207, 1136, 1087, 1053, 952, 914, 840, 748, 698, 659, 624, 543, 449. **UV-Vis** (MeCN):  $\lambda_{\text{max}}$  ( $\epsilon / \text{L mol}^{-1} \text{cm}^{-1}$ ) 348 (37020). **HRMS (ES+)** found  $m/z$  370.0816, calculated  $m/z$  370.0806 for  $[\text{C}_{12}\text{H}_{23}\text{N}_6\text{S}_2^{55}\text{Mn}]$  (+2.7 ppm).



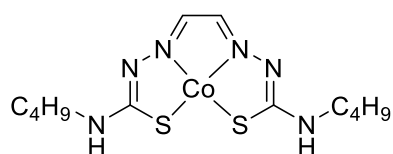
**MnGTSH** (glyoxal-bis[N4-hexylthiosemicarbazonato]manganese(II)) (**8Mn**) (0.160 g, 75%). **Elemental analysis** Calculated (%) for  $[\text{C}_{16}\text{H}_{30}\text{MnN}_6\text{S}_2]$ : C, 45.16, H, 7.11, N, 19.75; found C, 42.80, H, 6.77, N, 16.33. **IR** (ATR,  $\text{cm}^{-1}$ ): 3674, 3649, 3365, 3120, 2980, 2889, 1516, 1509, 1471, 1456, 1394, 1338, 1269, 1209, 1157, 1087, 956, 914, 842, 829, 813, 746, 698, 624, 545, 447, 418. **UV-Vis** (MeCN):  $\lambda_{\text{max}}$  ( $\epsilon / \text{L mol}^{-1} \text{cm}^{-1}$ ). 450 (1180), 352 (38680), 349 (38840), 342 (38300). **HRMS (ES+)** found  $m/z$  426.1438, calculated  $m/z$  426.1432 for  $[\text{C}_{16}\text{H}_{31}\text{N}_6\text{S}_2^{55}\text{Mn}]$  (+1.4 ppm).



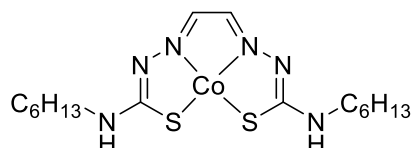
**MnGTSO** (glyoxal-bis[N4-octylthiosemicarbazonato]manganese(II)) (**9Mn**) (0.134 g, 56%). **Elemental analysis** Calculated (%) for  $[\text{C}_{20}\text{H}_{38}\text{MnN}_6\text{S}_2]$ : C, 49.88, H, 7.95, N, 17.45; found: C, 43.16, H, 7.22, N, 14.58. **IR** (ATR,  $\text{cm}^{-1}$ ): 3670, 3649, 3358, 3136, 2980, 2914, 2848, 1539, 1519, 1462, 1394, 1338, 1317, 1274, 1247, 1219, 1207, 1184, 1159, 1091, 1058, 966, 914, 864, 825, 754, 725, 624, 607, 576, 457, 441, 418. **UV-Vis** (MeCN):  $\lambda_{\text{max}}$  ( $\epsilon / \text{L mol}^{-1} \text{cm}^{-1}$ ) 350 (16000), 276 (23620). **HRMS (ES+)** found  $m/z$  482.2062, calculated  $m/z$  482.2058 for  $[\text{C}_{20}\text{H}_{39}\text{N}_6\text{S}_2^{55}\text{Mn}]$  (+0.8 ppm).

### Synthesis of CoGTSA complexes

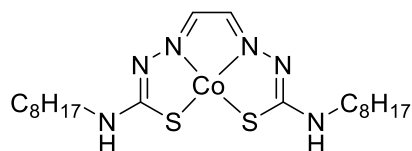
$\text{H}_2\text{GTSA}$  (0.5 mmol) was mixed with  $\text{Co}(\text{OAc})_2 \cdot 2\text{H}_2\text{O}$  (0.121 g, 0.5 mmol) in ethanol (10 mL). The mixture was then allowed to stir at room temperature for 4 hours. The volatiles were then removed using a rotary evaporator to yield the respective CoGTSA complex as a black powder.



**CoGTSB** (glyoxal-bis[N4-butylthiosemicarbazonato]cobalt(II)) (**7Co**) (0.173 g, 93%).  
**Elemental analysis** Calculated (%) for [C<sub>12</sub>H<sub>22</sub>CoN<sub>6</sub>S<sub>2</sub>]: C, 38.60, H, 5.94, N, 22.51; found C, 35.61, H, 5.15, N, 16.1. **IR** (ATR, cm<sup>-1</sup>): 3676, 3649, 3365, 3319, 3209, 3122, 2981, 2929, 1697, 1683, 1652, 1635, 1560, 1541, 1508, 1490, 1473, 1459, 1394, 1340, 1313, 1250, 1221, 1165, 1087, 1016, 966, 927, 842, 813, 746, 721, 663, 609, 447, 420. **UV-Vis** (MeCN): λ<sub>max</sub> (ε / L mol<sup>-1</sup> cm<sup>-1</sup>) 392 (6360), 336 (7020), 260 (13860). **HRMS (ES<sup>+</sup>)** found m/z 373.0683, calculated m/z 373.0679 for [C<sub>12</sub>H<sub>23</sub>N<sub>6</sub>S<sub>2</sub><sup>59</sup>Co] (+1.1 ppm).



**CoGTSH** (glyoxal-bis[N4-hexylthiosemicarbazonato]cobalt(II)) (**8Co**) (0.09 g, 42%).  
**Elemental analysis** Calculated (%) for [C<sub>16</sub>H<sub>30</sub>CoN<sub>6</sub>S<sub>2</sub>]: C, 44.74, H, 7.04, N, 19.57; found C, 40.83, H, 6.00, N, 15.83. **IR** (ATR, cm<sup>-1</sup>): 3668, 3649, 3209, 2980, 2927, 2870, 1699, 1683, 1558, 1541, 1507, 1458, 1396, 1340, 1307, 1259, 1226, 1166, 1080, 1043, 1016, 966, 829, 815, 725, 663, 605, 501, 486, 447, 418. **UV-Vis** (MeCN): λ<sub>max</sub> (ε / L mol<sup>-1</sup> cm<sup>-1</sup>) 394 (6140), 337 (7660), 270 (40540). **HRMS (ES<sup>+</sup>)** found m/z 429.1306, calculated m/z 429.1305 for [C<sub>16</sub>H<sub>31</sub>N<sub>6</sub>S<sub>2</sub><sup>59</sup>Co] (+0.2 ppm).



**CoGTSO** (glyoxal-bis[N4-octylthiosemicarbazonato]cobalt(II)) (**9Co**) (0.152 g, 63%).  
**Elemental analysis** Calculated (%) for [C<sub>20</sub>H<sub>38</sub>CoN<sub>6</sub>S<sub>2</sub>]: C, 49.47, H, 7.89, N, 17.31; found: C, 38.67, H, 6.04, N, 11.63. **IR** (ATR, cm<sup>-1</sup>): 3674, 3649, 3213, 2980, 2926, 2854, 1699, 1683, 1558, 1539, 1506, 1456, 1396, 1338, 1251, 1157, 1072, 1016, 966, 831, 721, 671, 665, 611, 472, 457, 418. **UV-Vis** (MeCN): λ<sub>max</sub> (ε / L mol<sup>-1</sup> cm<sup>-1</sup>) 396 (3920), 334, (4340), 260 (19260). **HRMS (ES<sup>+</sup>)** found m/z 485.1939, calculated m/z 485.1931 for [C<sub>20</sub>H<sub>38</sub>N<sub>6</sub>S<sub>2</sub><sup>59</sup>Co] (+1.6 ppm).

### Cyclic voltammetry

The cell was equipped with a MW2013 Pt working electrode, a Pt wire auxiliary electrode and a Ag pseudo-reference electrode. Scans were measured at 500, 250, and 100 mV/s. MGTSAs complexes were dissolved in anhydrous, degassed DMF, and contained nBu<sub>4</sub>PF<sub>6</sub> (0.1 M) as a supporting electrolyte. Voltages were referenced against an

internal ferrocene/ferrocenium<sup>+</sup> redox couple. The redox potentials of each complex were reported as the mid-point between the reduction and oxidation current peaks.

### **Determination of anthelmintic activity**

Samples of **10**, **11**, and their Cu and Zn complexes, along with **7**, **8**, **9**, their complexes containing Cu, Zn, Ni, Mn, and Co, and precursors (**4-6**, 2,3-butanedione, and glyoxal) were assessed for their anthelmintic efficacy against *Schistosoma mansoni* in the schistosomule larval form using the high throughput Roboworm drug-discovery platform, Parasitology and Epidemiology Group, Aberystwyth University, Wales, UK. Schistosomules were incubated at 37 °C under 5% CO<sub>2</sub> enriched atmosphere for 72 hours with a test compound (10 µM). The compounds were provided as pre-prepared stock solutions in DMSO. Following incubation the effect of the compounds on the phenotype and motility of the schistosomules was estimated by bright field imaging analysis. Values for each compound were recorded in duplicate. The limits set below which a compound was considered a “hit” was a value of -0.15 for phenotype and -0.35 for motility. Auranofin and praziquantel were used as positive controls; DMSO was used as a negative control.

### **Single-point adult worm screen**

*S. mansoni* adult worms were collected from hepatic portal veins by perfusion<sup>138</sup> 3 weeks after percutaneous exposure to ~4000 *S. mansoni* cercariae of TO mice (Harlan, UK). Adult worms were moved into 50 mL falcon tubes and subjected to three rounds of centrifugation at 300g for 2 minutes, followed by washing in phenol-red free DMEM. The washed parasites were then pelleted by gravity. A 96-well tissue culture plate (Fisher Scientific, Loughborough, UK) was then loaded with between 10 and 15 worms per well. Each experimental well contained 200 µL of modified DMEM (Gibco, Paisley, UK) enriched with 10% v/v HEPES (Sigma-Aldrich, Gillingham, UK), 10% v/v fetal calf serum (Gibco, Paisley, UK), 0.7% v/v 200 mM L-glutamine (Gibco, Paisley, UK), and 1% v/v antibiotic/antimycotic (Gibco, Paisley, UK). The worms were then incubated for 2 hours at 37 °C in a humidified atmosphere enriched with 5% CO<sub>2</sub>. MG-TSA complexes, their ligands, and precursors in DMSO were loaded to each well at a final concentration of 20 µM (with a final 0.3% DMSO final concentration). The worms were then scored by eye using microscopic methods.<sup>139</sup> Scores were assigned between 0-4 for each compound against the schistosomes: 4 = normal movement, 3 = full body movement but sluggish, 2 = movement at the anterior and posterior regions only, 1 = movement of the suckers only and slight contraction of the body, 0 = dead.

## Results and discussion

### Synthesis of ligands

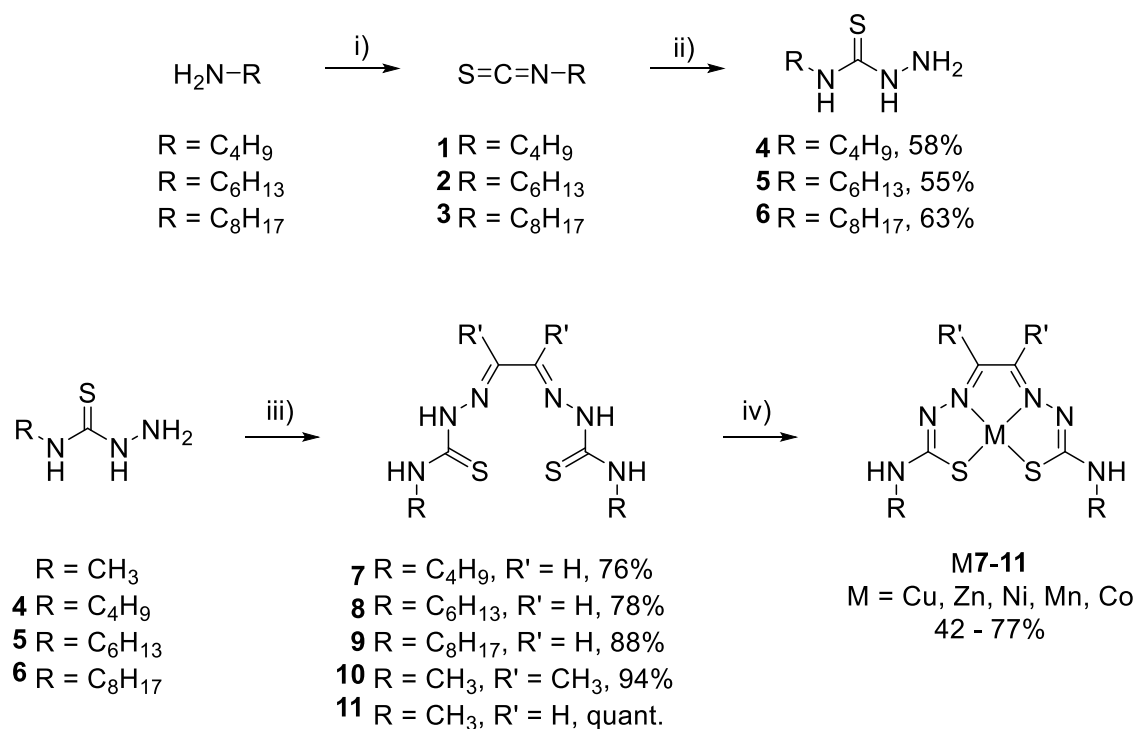


**Figure 12.** Synthetic scheme for the preparation of MBTSC complexes, their ligands, and precursors. i)  $\text{NEt}_3$ ,  $\text{CS}_2$ , EtOH, 30 min,  $\text{Boc}_2\text{O}$ , DMAP, 30 min. ii) EtOH, hydrazine hydrate, 1.5 h. iii) Dicarboxyl, EtOH, conc.  $\text{H}_2\text{SO}_4$ , 4 h. iv)  $\text{M}(\text{OAc})_2 \cdot x\text{H}_2\text{O}$ , EtOH, 4 h (where  $\text{M} = \text{Cu, Zn, Ni, Mn, or Co}$ ).

Alkyl isothiocyanates (**1-3**, Figure 12) were prepared in a manner similar to known literature methods.<sup>140,141</sup> Carbon disulphide is well established in the literature as a sulphur source for the synthesis of alkyl isothiocyanates.<sup>142-144</sup> The reaction of the alkylamine with an excess of carbon disulphide in the presence of base produces a triethylammonium N-alkyldithiocarbamate salt. This stable intermediate is then decomposed with a desulfurylation agent to produce the isothiocyanate functionality. The use of boc anhydride is preferred other desulfurylation agents<sup>145</sup> since the side products formed are readily removed ( $\text{CO}_2$ ,  $\text{CSO}$ ,  $\text{t-BuOH}$ ).<sup>146</sup> The use of carbon disulphide as a source of sulphur was preferred to another common sulphur source, thiosphosgene,<sup>147-149</sup> due to the latter's relative toxicity and cost by comparison with the former.  $\text{Boc}_2\text{O}$  was used in nearly stoichiometric amounts (0.99 equivalents) in order to ensure almost complete reaction of the dithiocarbamate salt without leaving any residual anhydride as an impurity. The alkyl isothiocyanates were of sufficient purity to be used directly in the next step. The 4-alkyl-3-thiosemicarbazides were prepared in a manner

similar to the literature,<sup>150–152</sup> by reaction of 1 equivalent of crude alkylisothiocyanate with 1.2 equivalents of hydrazine hydrate in ethanol. After an hour and a half of reaction, the solution was placed in a freezer, causing the desired product to precipitate allowing for separation by filtration from the reaction mixture. The product was then recrystallized to yield the 4-alkyl-3-thiosemicarbazide product in moderate yields of 50-60%. The yield could potentially be improved upon if required with longer reaction times and purification of the alkylisothiocyanate.

Bis(thiosemicarbazone) ligands were produced in a manner typical for similar ligands.<sup>62,153,154</sup> H<sub>2</sub>ATSM and H<sub>2</sub>GTSM were prepared in refluxing ethanol, with the reaction duration being 4 hours. The formation of a yellowish precipitate was observed immediately upon addition of sulphuric acid and appeared to continue to evolve for the duration of the reaction. H<sub>2</sub>GTSB was initially prepared in a similar manner, but a darkening of the precipitate was observed over time when heat was applied, suggesting some potential decomposition of the bithiosemicarbazone ligand formed. H<sub>2</sub>GTSB prepared at room temperature had a paler yellow colouration by comparison with its counterpart prepared at reflux, and the <sup>1</sup>H-NMR analysis conducted contained less impurity peaks. H<sub>2</sub>GTSB along with the other long-chain-bearing bithiosemicarbazone ligands were therefore prepared at room temperature. The increased reactivity of the dialdehyde by comparison with a dione, coupled with the precipitation of the product signifying the completion of the reaction make conducting the reaction at room temperature a viable option. As with the reactions above that were conducted at reflux, the formation of a yellowish precipitate was observed immediately upon addition of sulphuric acid. The long alkyl chain-substituted bithiosemicarbazone ligands (H<sub>2</sub>GTSA) were prepared in good yields of 76% or greater.

### **Synthesis of complexes**

Metal complexes were prepared using a 1:1 molar ratio of H<sub>2</sub>GTSA ligand and metal acetate salt in ethanol in a manner derived from the literature.<sup>153,155,156</sup> The salts used to prepare MG TSA complexes included: copper(II) acetate, zinc(II) acetate, nickel(II) acetate, manganese(II) acetate, and cobalt(II) acetate as their hydrates. Use of metal acetate salts is advantageous in the complexation reaction as the acetate counter ion facilitates the ligand deprotonation. (the use of metal salts without basic ligands has the potential to lead to the formation of charged bithiosemicarbazone metal complexes).<sup>157,158</sup> A distinctive colour change (except in the case of manganese) was seen within 10 minutes of the addition of a metal salt, with the colour often appearing immediately.



**Figure 13.**  $H_2GTSB$  and its metal complexes as solids and in DMSO solution: (L-R) **7**, **7Cu**, **7Zn**, **7Ni**, **7Mn**, and **7Co**.

The identity of ligands and precursors synthesised was confirmed by  $^1H$ -NMR,  $^{13}C\{^1H\}$ -NMR, mass spectrometry, with novel compounds being additionally analysed with high resolution mass spectrometry and infrared spectroscopy. Complexes of copper, manganese, and cobalt were characterised using elemental analysis, mass spectrometry, infrared spectroscopy, and UV-visible spectroscopy where appropriate, but were not analysed using NMR spectroscopy due to the paramagnetic nature of the metal centres. Complexes of zinc and nickel, which include diamagnetic metal centres, were analysed by  $^1H$ -NMR,  $^{13}C\{^1H\}$ -NMR, mass spectrometry, infrared spectroscopy, and UV-visible spectroscopy. High resolution mass spectrometry was employed to characterise all novel complexes. Complexes were analysed by cyclic voltammetry where possible. Ligands and complexes showed similar physical characteristics for the most part, and were typically insoluble in water, sparingly soluble in chloroform, and soluble in DMSO and DMF. The exception to this is the cobalt complexes, which were partially soluble in DMSO and DMF, and zinc complexes, which were poorly soluble in DMSO and DMF.

### **NMR spectroscopy**

$^1H$ -NMR and  $^{13}C\{^1H\}$ -NMR spectra were typical of those reported for the literature known alkyl isothiocyanate precursors (**1-3**).<sup>159-161</sup> Despite being a crude product (no work up other than removal of volatiles *in vacuo*) the spectra typically included only relatively small impurity peaks by comparison. The  $^{13}C\{^1H\}$ -NMR spectra matched well with that seen for commercial samples. Precursors **4-6** were submitted for analysis in  $d_6$ -DMSO, which allowed for the observation of amine and hydrazinic protons in each molecule. This is due to the lack of deuterium exchange in the aprotic  $d_6$ -DMSO allowing for the typically exchangeable (in protic solvents) amine and hydrazinic protons to remain in

place, producing broad singlets at roughly 8.5, 7.8, and 4.5 ppm. The  $^{13}\text{C}\{^1\text{H}\}$ -NMR spectra showed the development of a shift at roughly 180 ppm, indicative of the formation of a thiocarbonyl moiety, suggesting the reaction had proceeded as expected. The NMR spectra of the bithiosemicarbazone ligands were recorded in  $d_6$ -DMSO for similar reasons as their thiosemicarbazide precursors. The remaining hydrazinic proton environment on the  $\text{H}_2\text{BTSC}$  is shifted drastically downfield to 10 ppm (**10**) or greater (**7-9,11** ligands) due to the loss of the shielding provided by the protons on terminal hydrazinic nitrogen, and the formation of an electron rich imine  $\pi$ -bond in their place. The  $^{13}\text{C}\{^1\text{H}\}$ -NMR spectra are similar to those of the precursor, but feature additional environments for the tertiary diimine carbons (~140 ppm), and an additional methyl environment at 11.65 ppm in the case of **10**.

The paramagnetic nature of Cu(II), Mn(II), and Co(II) prevent the simple NMR analysis of the synthesised BTSC complexes. The low solubility of the Zn(II)BTSC complexes presented a challenge in acquiring detailed spectra except in the cases of **10Zn** and **11Zn**. A BTSC ligand is doubly deprotonated when exposed to a metal(II) acetate salt, leading to the loss of signals above 8.51 ppm in all  $^1\text{H}$ -NMR spectra, signifying the removal of the hydrazinic protons and formation of the complex. The *NH* protons alpha to the alkyl chains are not observed in the Zn(II)BTSC complexes,<sup>137</sup> but are present at roughly 8.1 ppm in the three Ni(II) complexes reported. The spectra for Ni(II) complexes show broadening suggesting some transience in the complex, potentially due to coordination of solvent molecules causing a switching in the geometry of the complex between the expected square planar geometry and an octahedral geometry on an NMR-observable timescale.<sup>2</sup> Octahedral Ni(II) complexes are paramagnetic, resulting in broadening of the NMR signals. Good quality  $^{13}\text{C}\{^1\text{H}\}$ -NMR spectra of the Zn(II)BTSC complexes were difficult to obtain due to their inherently low solubility.

### Infrared spectroscopy

The infrared spectra for many of the GTSA complexes display common features. All complexes show bands between 3400 and 3200  $\text{cm}^{-1}$  indicative of aliphatic NH stretching. In most all cases, these are single bands suggesting these are secondary amines. Typically bands present between 3370-3290  $\text{cm}^{-1}$  are indicative of secondary amines, which are present in all complexes in the form of amine groups  $\alpha$ -to the alkyl substituents in the molecule. This is in agreement with literature values for such stretches.<sup>162,163</sup> Stretches corresponding to  $\text{sp}^3$  C-H stretching are seen in all complexes between 3000 and 2880  $\text{cm}^{-1}$  caused by the pendant alkyl groups of varying lengths  $\alpha$ -to the secondary amines previously discussed. The values for free C=N imine stretching

is typically 1690-1640  $\text{cm}^{-1}$ . The value is expected to be different in GTSA ligands due to the imine forming part of a semithiocarbazone moiety. The value for free GTSM C=N stretching is given as 1560  $\text{cm}^{-1}$ , with the values for C=N stretching reported as 1540  $\text{cm}^{-1}$  and 1555  $\text{cm}^{-1}$  for CuGTSM and NiGTSM respectively.<sup>2</sup> Bands corresponding to C=N stretching may be seen between 1558 and 1519  $\text{cm}^{-1}$  in all CuGTSA and NiGTSA complexes. Bands between 1558 and 1506  $\text{cm}^{-1}$  are also observed in ZnGTSA, MnGTSA, and CoGTSA complexes which may also correspond to C=N stretching, though it is worth noting that all GTSA complexes have a dense collection of peaks between 1500-1000  $\text{cm}^{-1}$  making unambiguous speciation difficult.

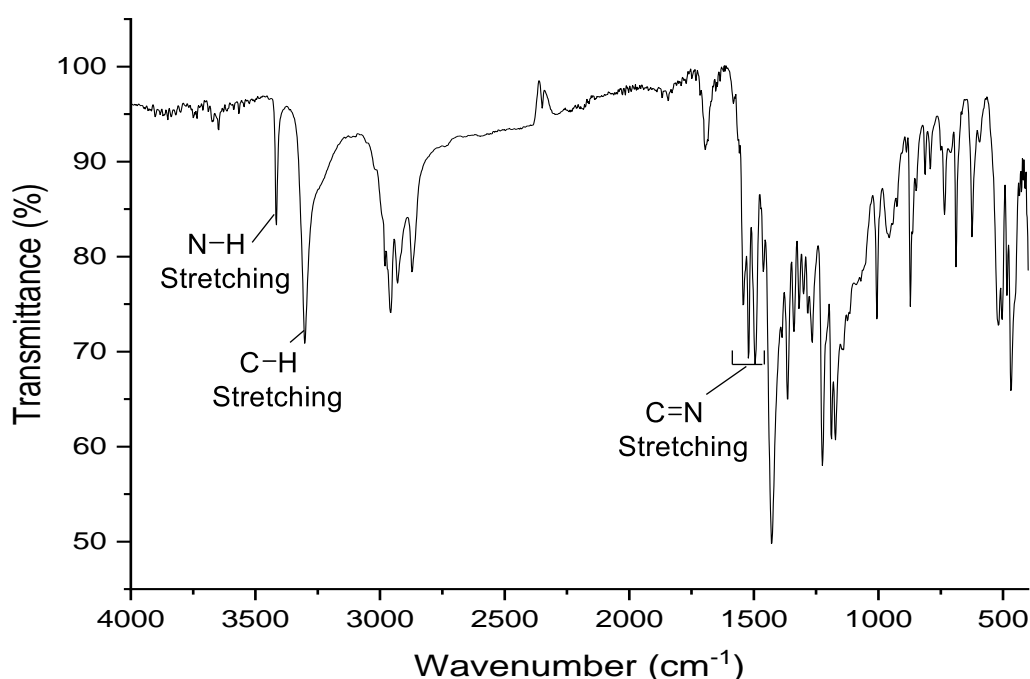


**Figure 14.** Example IR spectrum of an MBTSC complex, specifically **7Cu**.

Thiocarbonyl C=S stretches are more difficult to observe than carbonyl C=O stretches due to their occurrence at lower wavenumbers comparatively. This decrease in frequency is due to the increased atomic mass of sulphur by comparison with oxygen. Thiocarbonyl based stretches and bends are typically found at 1550  $\text{cm}^{-1}$  and below,<sup>164</sup> and therefore have many potential functional groups that may also occur in the same area of an infrared spectrum, obscuring the band, and making it difficult to assign species in this area of the spectrum with absolute certainty. All GTSA complexes show strong absorptions between 1250  $\text{cm}^{-1}$  and 750  $\text{cm}^{-1}$  that may account for the C=S stretches and bends of the thiourea-like donor on the ligand, with C=S stretching in free

thiosemicarbazones observed between 1275-1300  $\text{cm}^{-1}$ , whereas the band at 750  $\text{cm}^{-1}$  may occur due to C=S bending.

### Electronic spectroscopy

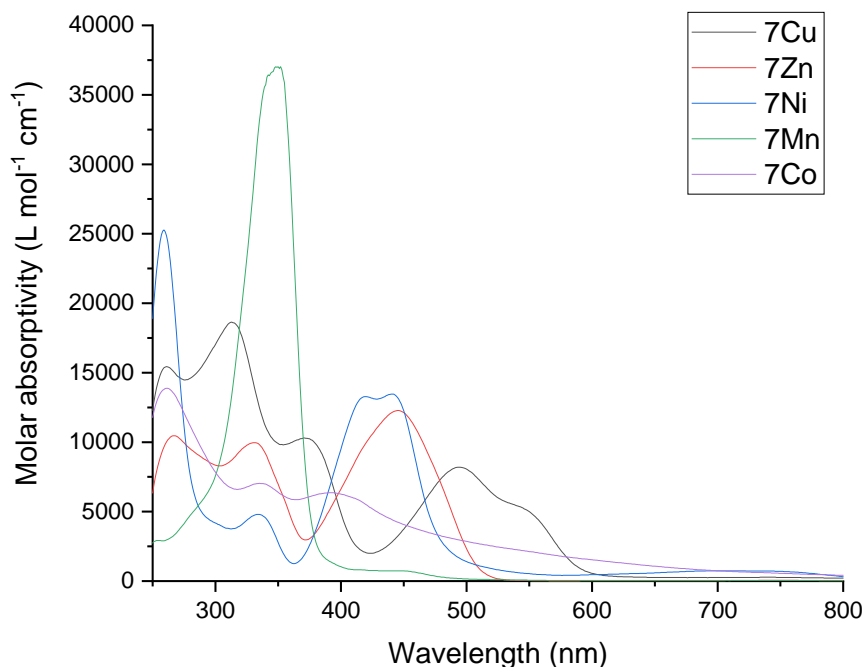


**Figure 15.** UV-vis spectra **7M** complexes: **7Cu**, **7Zn**, **7Ni**, **7Mn**, and **7Co** as  $5 \times 10^{-5}$  M solutions in acetonitrile.

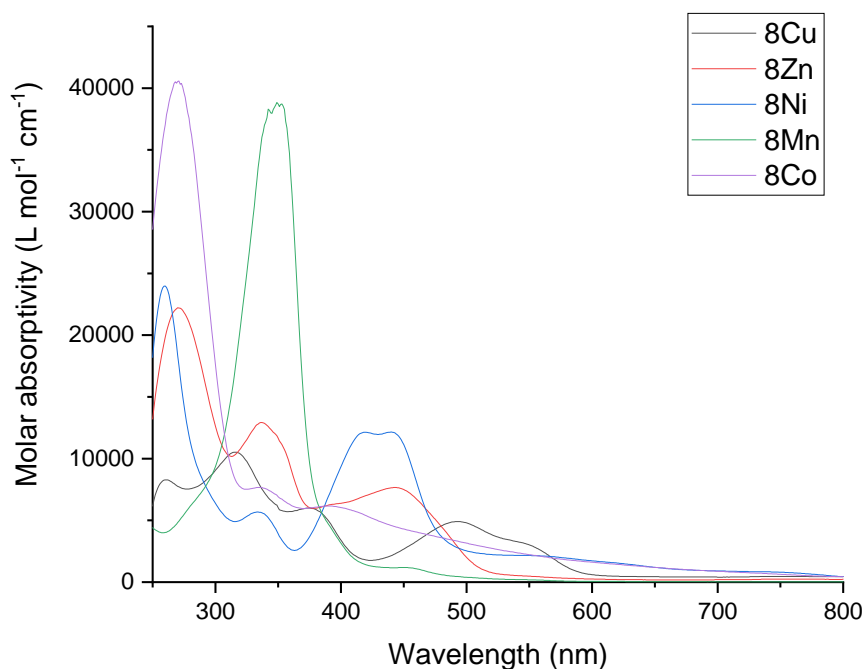


**Figure 16.** UV-vis spectra **8M** complexes: **8Cu**, **8Zn**, **8Ni**, **8Mn**, and **8Co** as  $5 \times 10^{-5}$  M solutions in acetonitrile.

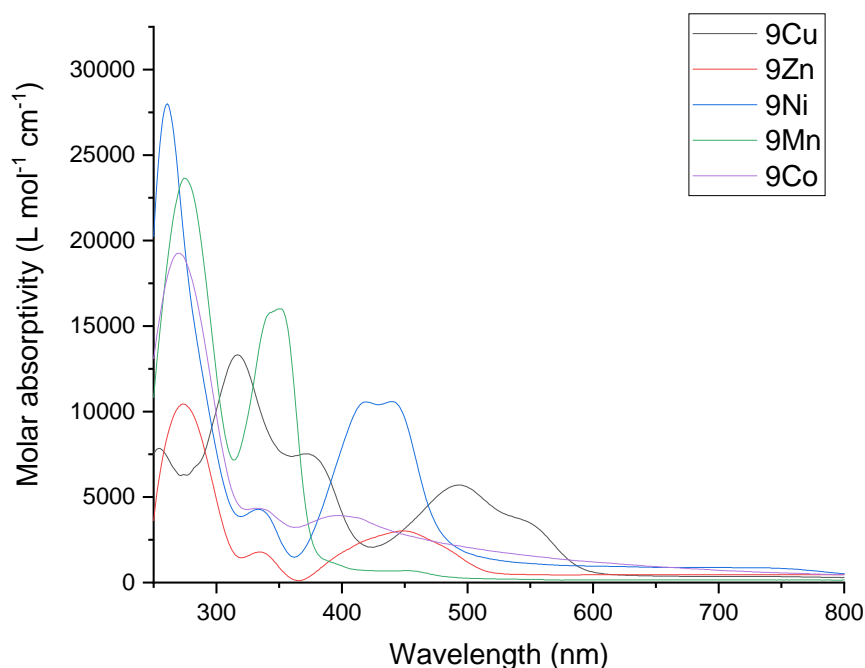


**Figure 17.** UV-vis spectra **9M** complexes: **9Cu**, **9Zn**, **9Ni**, **9Mn**, and **9Co** as  $5 \times 10^{-5} M$  solutions in acetonitrile.

The complexes were also characterised by electronic spectroscopy. The transitions observed are summarised below in Table 3.

BTSC	Transition							
	$\lambda_{\max}$ (nm)	$\epsilon$ ( $L \text{ mol}^{-1} \text{ cm}^{-1}$ )	$\lambda_{\max}$ (nm)	$\epsilon$ ( $L \text{ mol}^{-1} \text{ cm}^{-1}$ )	$\lambda_{\max}$ (nm)	$\epsilon$ ( $L \text{ mol}^{-1} \text{ cm}^{-1}$ )	$\lambda_{\max}$ (nm)	$\epsilon$ ( $L \text{ mol}^{-1} \text{ cm}^{-1}$ )
<b>7Cu</b>	312	18620	370	10300	494	8200	544	5300
<b>8Cu</b>	315	13280	375	7480	492	4900	544	3200
<b>9Cu</b>	316	13300	372	7520	492	5700	546	3620
<b>7Zn</b>	266	10380	332	9880	445	12200		
<b>8Zn</b>	272	22180	336	12920	442	7660		
<b>9Zn</b>	276	9780	335	1380	448	2620		
<b>7Ni</b>	334	4800	420	13280	442	13460		
<b>8Ni</b>	334	5680	418	12140	441	12140		
<b>9Ni</b>	334	4280	418	10560	440	10580		
<b>7Mn</b>	348	37020						
<b>8Mn</b>	342	38300	349	38840	352	38680		
<b>9Mn</b>	350	16000						
<b>7Co</b>	334	7020	392	6360				
<b>8Co</b>	337	7660	394	6140				
<b>9Co</b>	334	4340	396	3920				

**Table 3.** Summarised electronic transitions observed for MG TSA complexes (**7-9M**).

Despite the simplicity of the GTSA framework, there are few studies into the electronic properties of these complexes. Analogous complexes with methyl-substituted backbones (such as ZnATSM) show that the ligand centred transitions consist of  $\pi$ - $\pi^*$

transitions from the sulphur up to the carbonyl carbon backbone.<sup>165</sup> The  $\epsilon$  values recorded suggest that the transitions observed are charge transfers in nature. The transitions are not d-d transitions, as d-d transitions have relatively low extinction coefficients by comparison with charge transfer bands, due to the fact that d-d transitions are Laporte forbidden transitions (and may also be spin forbidden depending on the number of d-electrons). Charge transfer bands on the other hand are selection rule allowed, and therefore produce much more intense bands. The observation of the d-d transitions in the MG TSA complexes may potentially be possible in more concentrated solution, but this is limited by the limited solubility of the complexes, particularly those derived from the ligand H<sub>2</sub>GTSA.

The spectra of all CuGTSA complexes are similar to each other. There are two main bands in each spectrum, each of which has a shoulder peak. The bands are similar in shape and intensity to CuATSM, but show a red shift of roughly 20 nm in three of the transitions. The low energy band is likely due to an n- $\pi^*$  transition from the sulphur based lone pairs whereas the higher energy band is likely due to  $\pi$ - $\pi^*$  transitions.<sup>165</sup> Only the shoulder is bathochromically shifted by comparison with CuATSM in the higher energy band. This is as expected with regard to the transitions calculated by Holland *et al.*<sup>166</sup> for CuATSM, where it is shown that the molecular orbitals involved in the transition caused by an absorbance at 314 nm have no contribution from the backbone carbonyl groups, and therefore the substitution of methyl for proton in CuGTSA ligands would have no effect on the energy of this transition.

The transitions reported for ZnGTSA are similar to those reported for ZnATSM, but are red shifted as with the CuGTSA complexes.<sup>165</sup> The molecular orbital contributions are potentially similar to ZnATSM, but likely differ due to the additional flexibility afforded to the ZnGTSA complexes by the lack of methyl groups on the carbonyl backbone. The additional flexibility afforded allows the zinc complex to distort away from a square planar geometry in a number of cases,<sup>156,167</sup> and may result in “significant” intermolecular interactions.<sup>4</sup> There does appear to be a difference in between the ratio of intensities between the three bands in each complex. The difference in intensity between **7Zn**, **8Zn**, and **9Zn** appears to vary dependent on the length of the pendant alkyl chain, in contrast with the literature, which states a lack of variation in electron density at the terminal nitrogen atoms.<sup>165</sup>

The UV-vis spectra of each NiGTSA complex is similar to the other, consisting of two major bands, the lower energy of which consists of two overlapping peaks. A similar set of two overlapping low energy peaks are observed in the UV-visible spectrum of

NiATSM<sub>2</sub> (bisdiacetyl-bis[N4-dimethylthiosemicarbazonato]nickel(II)), but are not seen in NiATSM, where the low energy band only contains one peak.<sup>162</sup> This may suggest a non-negligible contribution from the pendant amines to the molecular orbitals in which the transitions occur. MnGTSA complexes typically exhibit less complicated spectra than their previously described counterparts, but the most variance within this compound class. This is due to d<sup>5</sup> Mn(II)-based transitions being spin forbidden, leading to weak ( $\epsilon \sim 0.01 \text{ L mol}^{-1} \text{ cm}^{-1}$ ) transitions that are not observable in dilute solution. This suggests that only ligand centred  $\pi$ - $\pi^*$  transition may occur. CoGTSA complexes contain high energy transitions of equal heights, corresponding to d- $\pi^*$  and n- $\pi^*$  based on similar square planar Co(II) complexes containing Schiff base donors.<sup>168-170</sup> All spectra contain broad peaks between 260-270 nm corresponding to the DMSO used to solubilise the complexes (Co and other MGTA complexes). The decrease transition intensity for CoGTSA may be due to a lack of solubility, and may therefore not truly reflect the extinction coefficient.

### **Cyclic voltammetry**

Cyclic voltammograms of some of the non-H<sub>2</sub>GTSM-based MGTA complexes were recorded to determine whether additional methylene groups pendant to the terminal amines on the complexes affected the ligand geometry, and therefore affected the redox potential of the bound metal centre. The redox potentials described below were referenced to an internal ferrocene/ferrocenium redox couple. The voltammograms of all complexes were recorded in DMF with (n-Bu)<sub>4</sub>NPF<sub>6</sub> as a supporting electrolyte. The use of a non-aqueous environment was necessitated by the complexes' lack of solubility in aqueous media. The electrochemical behaviour of the MGTA complexes is summarised below in Table 4.

All three Cu complexes showed two quasi-reversible redox couples. The peak separations for the anodic and cathodic peaks on all shifts typically matched similarly to that of the ferrocene standard, and varied dependant on the scan rate as expected, with a decrease in the peak currents observed with a decrease in scan rate. A plot of the square root of the scan rate vs anodic peak current showed an almost linear relationship (appendices), indicating that the electrochemical reactions are mostly reversible. The quasi-reversible nature of these redox couples may be attributed to the ligand.<sup>12,166</sup> In order to accommodate the new oxidation state, the ligand most likely twists in order to satisfy optimal geometrical and ligand donor requirements of the metal. This electrochemical behaviour matches closely with that of CuATSM and CuGTSM, as well as their derivatives in the literature.<sup>12,166</sup>

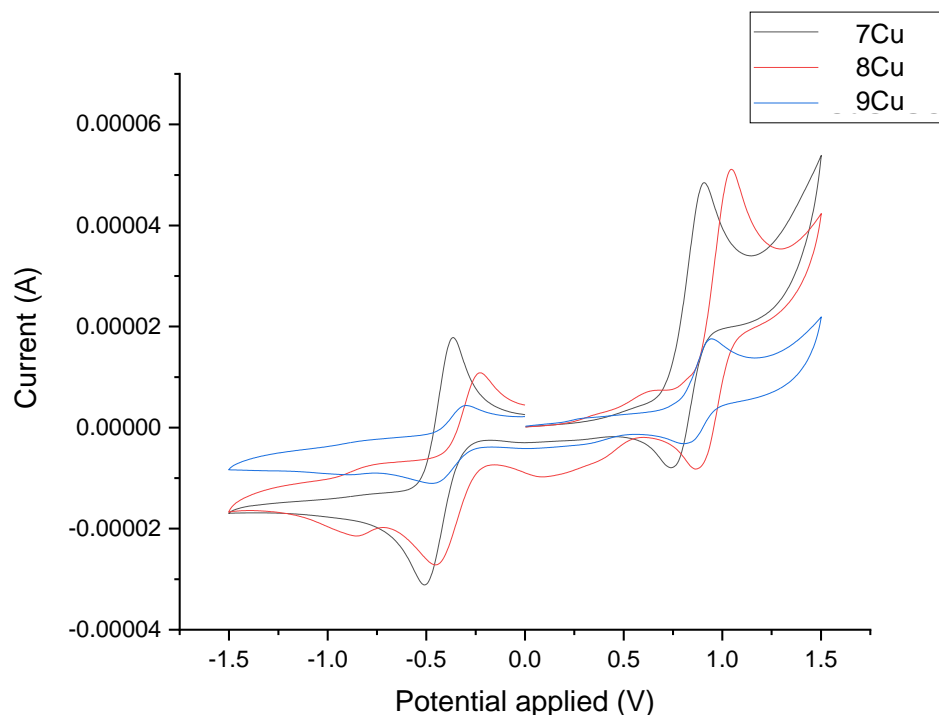


**Figure 18.** Cyclic voltammograms of **7Cu**, **8Cu**, and **9Cu** at 250 mV/s scan rate, showing two distinct redox couples:  $Cu^I/Cu^{II}$  at negative potentials and  $Cu^{II}/Cu^{III}$  at positive potentials.

The voltammograms of the nickel complexes also contain two redox events, both occurring at negative potentials of lower than -1.5 V by comparison with ferrocene. The peaks are close together in potential, and therefore may be interpreted as a two-electron transfer reaction. The event that occurs at the more positive of the two potentials is most likely a ligand-centred reduction, whereas the event at the more negative potential most likely corresponds to the Ni(I)/Ni(II) redox couple.<sup>171,172</sup> This two-electron transfer reaction is similar to that reported in the literature for similar NiBTSC complexes. DFT of a similar NiBTSC complex by Straistari *et al.*<sup>172</sup> suggests the first redox event leads to the formation of a  $[Ni^{II}L^{\bullet}]^{-}$  with  $S = 1/2$ , a delocalised ligand-based radical species where the electron density of the SOMO is spread throughout the hydrazine bridge. Further reduction occurs at more negative voltage to a  $[Ni^IL^{\bullet}]^{-}$  with  $S = 1$ , split between two orthogonal SOMOs. This process is unlikely to be affected greatly by the difference in pendant groups as the SOMOs and HOMO used to assign these processes are spread over the same functional groups in the literature NiBTSC and the NiGTSA complexes previously described. A plot of the square root of the scan rate  $v$  anodic peak current showed an almost linear relationship (appendices), suggesting that the electrochemical reactions are most likely quasi-reversible in nature.

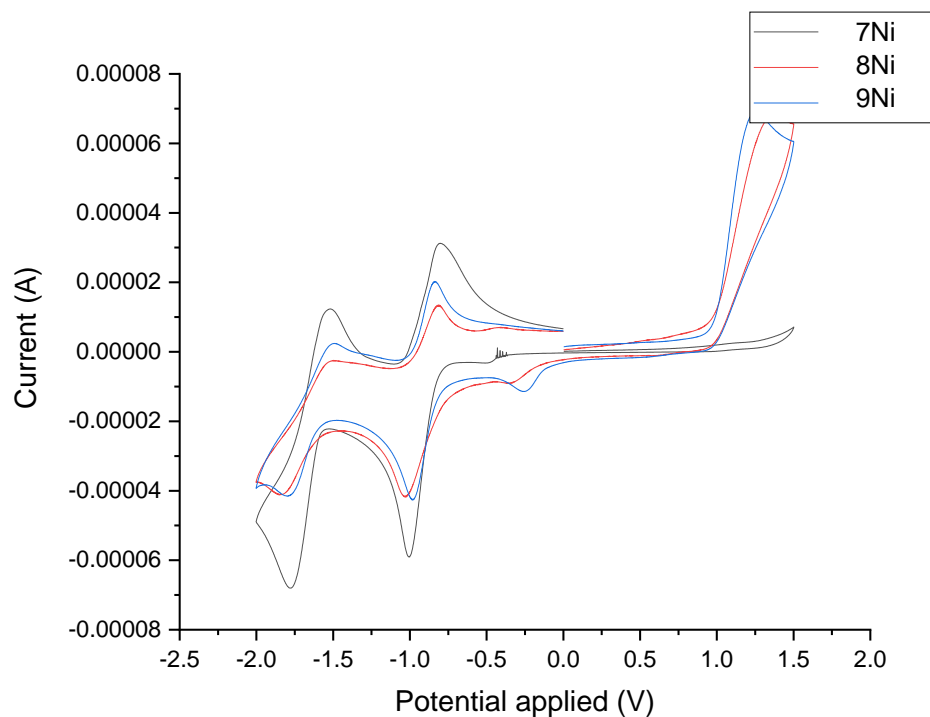


**Figure 19.** Cyclic voltammograms of **7Ni**, **8Ni**, and **9Ni** at 250 mV/s scan rate, showing a potential two-electron transfer reaction.

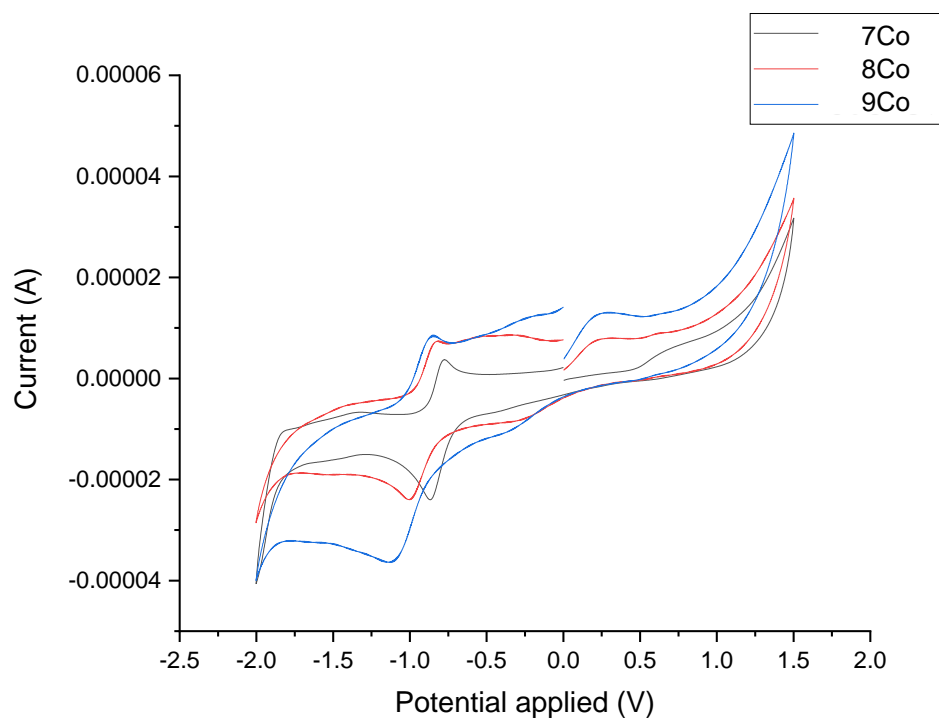


**Figure 20.** Cyclic voltammograms of CoGTSB, CoGTSH, and CoGTSO at 250 mV/s scan rate, showing the Co<sup>I</sup>/Co<sup>II</sup> redox couple.

The CoGTSA complexes show one reversible redox couple centred between -1.441 V to -1.526 V vs ferrocene. The redox couple is likely reversible, as a plot of the square root of the scan rate vs the cathodic peak current yields a linear relationship (appendices). The nature of the redox couple is likely to be  $\text{Co}^{\text{II}}/\text{Co}^{\text{I}}$  based on the assignment of this redox couple to the CVs observed for  $\text{Co}(\text{II})\text{BTSC}$  complexes and related  $\text{Co}(\text{II})$  complexes with tetradentate mixed hard/soft donors.<sup>173–175</sup> The literature described  $\text{Co}^{\text{III}}/\text{Co}^{\text{II}}$  anodic peak that occurs prior to the reversible  $\text{Co}^{\text{II}}/\text{Co}^{\text{I}}$  redox couple is not observed, suggesting that the complex is in the assigned  $\text{Co}(\text{II})$  oxidation state.<sup>174</sup>

The cyclic voltammograms for the MnGTSA and ZnGTSA complexes do not appear to contain any reversible or quasi-reversible redox events. This is not particularly surprising for the ZnGTSA complexes due to the fact that Zn has a full 3d shell, and is renowned for being redox inert. The lack of distinguishable redox couples for Mn is more surprising as Mn is known to have very rich redox chemistry. The apparent lack of redox events may therefore be due to the limits imposed by the solvent/electrolyte system chosen, which has a solvent window between -2 V and 1.5 V.

	$E_{1/2}$ $\text{Cu}^{\text{II}}/\text{Cu}^{\text{I}}$ (V)	$\Delta E$ (V)	$i_a/i_c$	$E_{1/2}$ $\text{Cu}^{\text{III}}/\text{Cu}^{\text{II}}$ (V)	$\Delta E$ (V)	$i_a/i_c$
<b>7Cu</b>	-1.031	0.119	0.941	0.266	0.1	1
<b>8Cu</b>	-1.054	0.164	1.31	0.253	0.185	0.833
<b>9Cu</b>	-1.023	0.205	1.05	0.221	0.154	0.933
CuATSM <sup>12</sup>	-0.83			0.32		
	$E_{1/2}$ $[\text{Ni}^{\text{II}}\text{L}^{\bullet}]/\text{Ni}^{\text{I}}\text{L}$ (V)	$\Delta E$ (V)	$i_a/i_c$	$E_{1/2}$ $\text{Ni}^{\text{III}}/[\text{Ni}^{\text{II}}\text{L}^{\bullet}]$ (V)	$\Delta E$ (V)	$i_a/i_c$
<b>7Ni</b>	-2.244	0.124	0.800	-1.5665	0.107	1.429
<b>8Ni</b>	-2.3505	0.263	0.938	-1.6245	0.163	1.692
<b>9Ni</b>	-2.3775	0.281	0.857	-1.6385	0.161	1.071
NiATSM <sup>171</sup>	-2.45			-1.64		
	$E_{1/2}$ $\text{Co}^{\text{II}}/\text{Co}^{\text{I}}$ (V)	$\Delta E$ (V)	$i_a/i_c$			
<b>7Co</b>	-1.5145	0.181	1.23E+00			
<b>8Co</b>	-1.5305	0.171	1.18E+00			
<b>9Co</b>	-1.5345	0.188	1.43E+00			
CoGTSH <sub>2</sub> <sup>175</sup>	-1.85					

**Table 4.** Electrochemical behaviour of MGTSA complexes. Potentials were referenced against an in-situ ferrocene/ferrocenium couple. Assignments of the electrochemical reactions occurring are based on literature findings for similar complexes.<sup>12,166,172–175</sup>

## Anthelmintic properties of MGTA complexes and their precursors

### Schistosomula assay

The test GTSA complexes, their parent ligands, and their precursors were tested for anthelmintic activity against schistosomules. Schistosomules are the larval form of *Schistosoma spp.* parasites which develop to allow the organism to survive in a host's bloodstream. The activity of the compounds was assessed by the automated Roboworm platform, which assigned a value to the schistosomules in each treatment condition for the effect of the compounds on the phenotype and mobility of the organism.<sup>97</sup> For a compound to be considered a "hit", a value of -0.15 or less had to be achieved for the phenotype score, and a value of -0.35 or less for the motility score. The results of the schistosomula assay are listed in Figure 21 and Table 5.

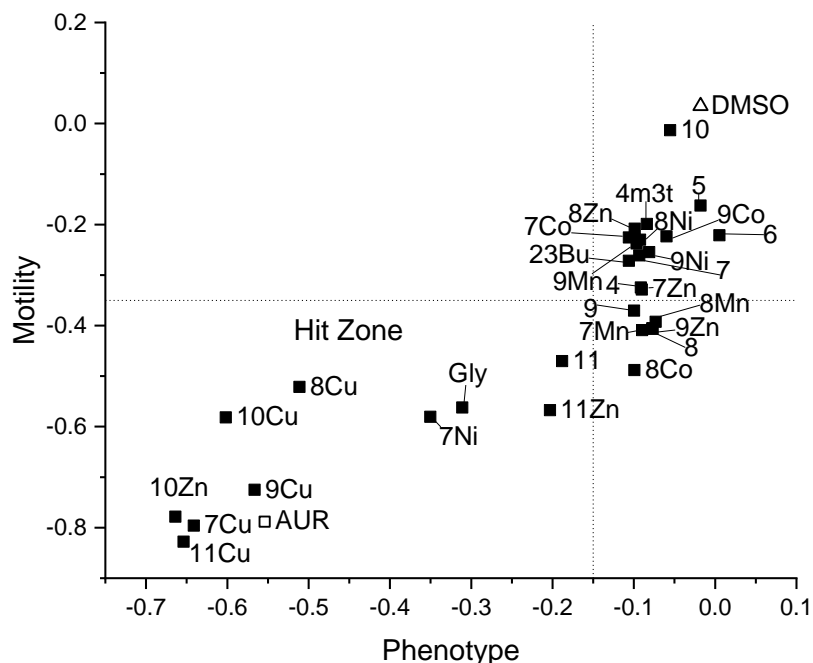


**Figure 21.** Graphical depiction shows the average scores from all compounds screened, average scores for DMSO and auranofin (AUR) are also included. Dotted gridlines highlight the boundary between a compound being considered a hit for phenotype (< -0.15) and motility (< -0.35). Complexes and ligands are referred to by name. Non-synthesised precursors are given the following designations: Gly = glyoxal, 23Bu = 2,3-butanedione, and 4m3t = 4-methyl-3-thiosemicarbazide.

Compound (10 $\mu$ M)	Average phenotype score	Average motility score	Hit status
<b>10</b>	-0.06	-0.422	Non-hit
<b>11</b>	-0.19	-0.549	Hit
<b>7</b>	-0.09	-0.188	Non-hit
<b>8</b>	-0.08	-0.455	Non-hit
<b>9</b>	-0.10	-0.340	Non-hit
<b>10Cu</b>	-0.60	-0.529	Hit
<b>11Cu</b>	-0.65	-0.865	Hit
<b>7Cu</b>	-0.64	-0.772	Hit
<b>8Cu</b>	-0.51	-0.498	Hit
<b>9Cu</b>	-0.57	-0.740	Hit
<b>10Zn</b>	-0.66	-0.755	Hit
<b>11Zn</b>	-0.20	-0.597	Hit
<b>7Zn</b>	-0.09	-0.416	Non-hit
<b>8Zn</b>	-0.10	-0.206	Non-hit
<b>9Zn</b>	-0.08	-0.329	Non-hit
<b>7Ni</b>	-0.35	-0.537	Hit
<b>8Ni</b>	-0.09	-0.232	Non-hit
<b>9Ni</b>	-0.08	-0.162	Non-hit
<b>7Mn</b>	-0.09	-0.312	Non-hit
<b>8Mn</b>	-0.07	-0.343	Non-hit
<b>9Mn</b>	-0.10	-0.146	Non-hit
<b>7Co</b>	-0.11	-0.250	Non-hit
<b>8Co</b>	-0.10	-0.317	Non-hit
<b>9Co</b>	-0.06	-0.281	Non-hit
Glyoxal	-0.31	-0.530	Hit
2,3-butanedione	-0.11	-0.202	Non-hit
4-methyl-3-thiosemicarbazone	-0.08	-0.123	Non-hit
<b>4</b>	-0.09	-0.299	Non-hit
<b>5</b>	-0.02	-0.079	Non-hit
<b>6</b>	0.01	-0.287	Non-hit

**Table 5.** Anthelmintic screening results for MGTSA complexes, ligands, and precursors against schistosomula.

As can be seen from the data, all CuBTSC complexes tested, including the control **10Cu** and **11Cu** complexes were considered hits. Historically, copper oleate was used as an ointment to protect against infection by *S. japonicum*.<sup>176</sup> The values for **11Cu** and **7Cu** surpassed those of Auranofin in both phenotype and motility scores, which has been shown have a 100% mortality rate in schistosomula treated at a concentration of 10  $\mu$ M following 24 hours incubation as a result of enzyme inhibition and increased oxidative

stress.<sup>177</sup> The mechanism of action of copper against schistosomules is as of yet unknown, but based on its mechanism of action against the simpler bacteria, copper's toxicity to schistosomules may be due to a number of causes. Copper is known to interact with nucleic acids, alter the active sites of enzymes, and oxidise membrane components, leading to the formation of free radicals and reactive oxygen species (ROS).<sup>58</sup> The increasing lipophilicity of the CuGTSA complexes yields a pattern that is not easily explained in terms of its relationship to the compound's efficacy. The most effective CuGTSA complex in terms of combined phenotype and motility score is **11Cu**, followed by **7Cu**, **9Cu**, then **8Cu**. The increasing number of methylene groups appears to decrease the efficacy of the complexes up to -C<sub>4</sub>H<sub>9</sub>, however **9Cu** is more effective than **8Cu**, suggesting that an upturn in efficacy in line with an increase in lipophilicity may occur once the pendant alkyl chains are sufficiently long. Verification of this observation would require the preparation of further CuGTSA complexes with even longer pendant alkyl groups.

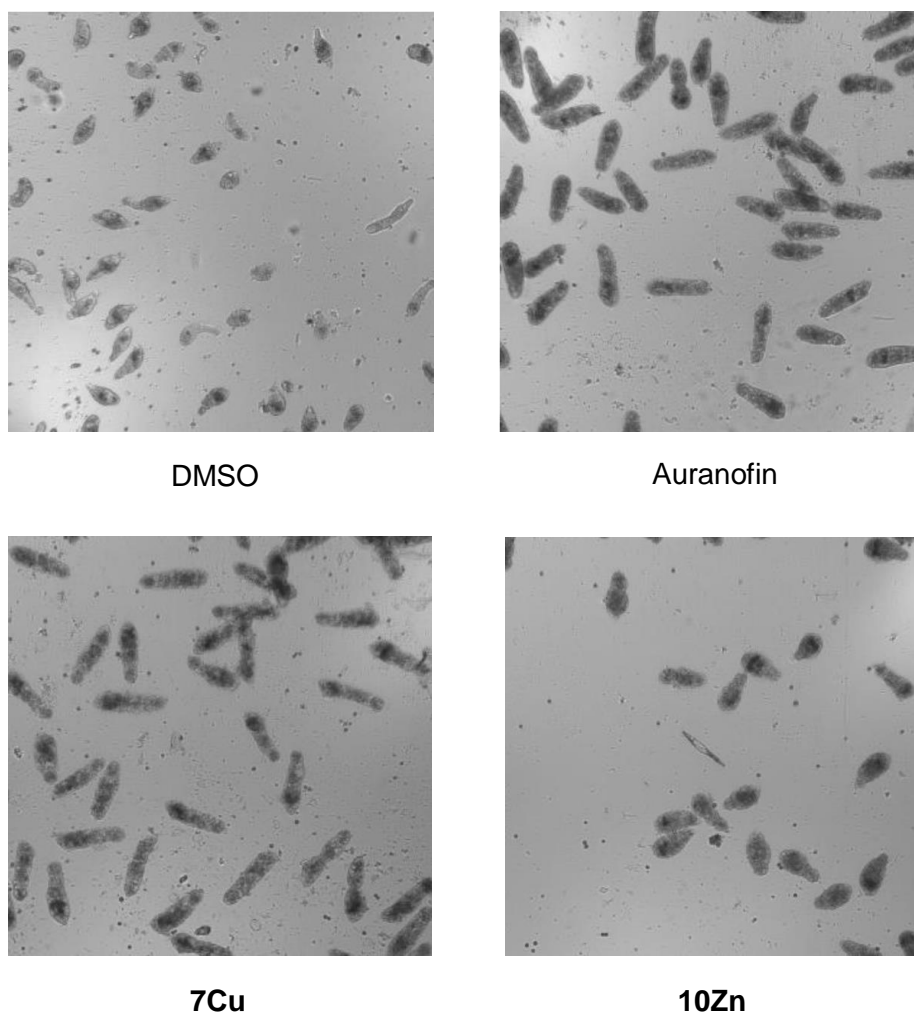


**Figure 22.** Schistosomules treated with DMSO (positive control), Auranofin (negative control), 7Cu, and 10Zn.

Unexpected hits were recorded by **10Zn** and **11Zn**, of which **10Zn** was seen to be in the same realms of efficacy as **11Cu**, **7Cu**, and Auranofin. This is an unexpected result, as the suspected mechanism of action of the effective agents (including Auranofin) is suspected based on the redox chemistry of the bound metal, or redox reactions caused by the metal once it is released from the ligand architecture. In fact, the decreased activity of **10Cu** by comparison with the similar **11Cu** may be down to the decreased ability of the ATSM ligand to twist due to its dimethyl backbone, therefore making release of the bound Cu or access to the bound Cu more difficult.<sup>4</sup> The exceptional efficacy of **10Zn**, and to a lesser degree **11Zn**, is therefore surprising due to the redox inert nature of Zn. Further research must be conducted in order to establish whether **10Zn** is therefore the active species behind the effect observed. There is however some suggestion in the literature that ZnBTSC complexes may become transmetallated with Cu(II) under biological conditions to produce the active CuBTSC complex,<sup>13,166,178</sup> a reaction which does not occur with the other metal BTSC complexes and Cu(II), so this may also account for the apparent activity of the ZnBTSC complexes.

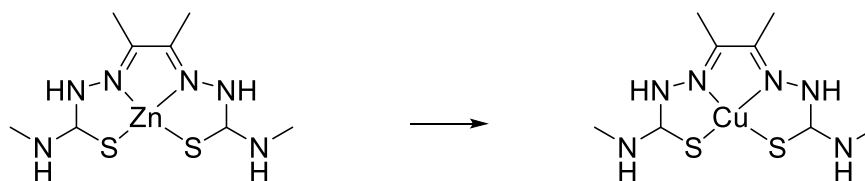


**Figure 23.** Transmetallation of ZnATSM (**10Zn**) to form CuATSM (**10Cu**).<sup>74,166</sup>

Hits were also observed for NiGTSB and the ligand H<sub>2</sub>GTSM. The efficacy of H<sub>2</sub>GTSM may be related to the efficacy of its precursor, glyoxal, which was the only precursor considered a hit. The phenotype and motility scores caused by treatment with NiGTSB are higher than those recorded against CuGTSA complexes. Coupled with the increased mammalian toxicity of Ni by comparison with Cu, **7Ni** is a less likely candidate to be used in a therapeutic manner than the Cu or Zn complexes. Whereas most of the non-Cu MGTSAs were not considered hits on schistosomules at a 10 μM concentration, the complexes **8Co**, as well as **7Mn** and **8Mn**, along with the ligands **8** and **9** were found to affect the motility of the schistosomules within the hit threshold. All other complexes, ligands, and precursors were found to be ineffective against schistosomules.

### Single-point adult worm screen

Following identification of hit compounds against schistosomules, the compounds that were found to have anthelmintic activity were tested against adult *S. mansoni* pairs by a single point titration of compound at 20 μM. Compounds were ran in triplicate, and the

effects on the adult schistosomes were scored by eye at 24 and 72 hours. The viability of the worms was scored from 0-4 by the following scale: 0 – dead, 1 – movement of the suckers only and slight contraction of the body, 2 – movement at the anterior and posterior regions only, 3 – full body movement but sluggish, 4 – normal movement.<sup>97</sup> The scores assigned to the effect of each compound against adult schistosomes is summarised in Table 6 and Figures 24-27. The statistical significance of each result was assessed by one-way ANOVA followed by Dunnetts multiple comparisons test.

Compound	Immediately effective (males and females assessed collectively)	Effective at 24 hours		Effective at 72 hours		Precipitate observed in well
		Males	Females	Males	Females	
11	NO	NO	NO	NO	NO	YES
10Cu	NO	YES*	YES*	YES*	YES*	YES
11Cu	YES	YES*	YES*	YES*	YES*	NO
7Cu	YES	YES*	YES*	YES*	YES*	NO
8Cu	NO	YES*	YES*	YES	YES*	YES
9Cu	NO	NO	NO	NO	NO	YES
7Ni	NO	YES*	YES*	NO	NO	YES
10Zn	NO	YES*	YES*	YES*	YES*	NO
11Zn	NO	YES***	N/A	YES***	N/A	YES
Glyoxal	NO	NO	N/A	NO	N/A	NO

**Table 6.** Summary of adult worm screening against compounds that displayed antischistosomule activity. Statistical significance was assessed by one-way ANOVA followed by Dunnetts multiple comparisons test. \* $P < 0.0001$ , \*\* $P < 0.001$ , \*\*\* $P < 0.01$ .

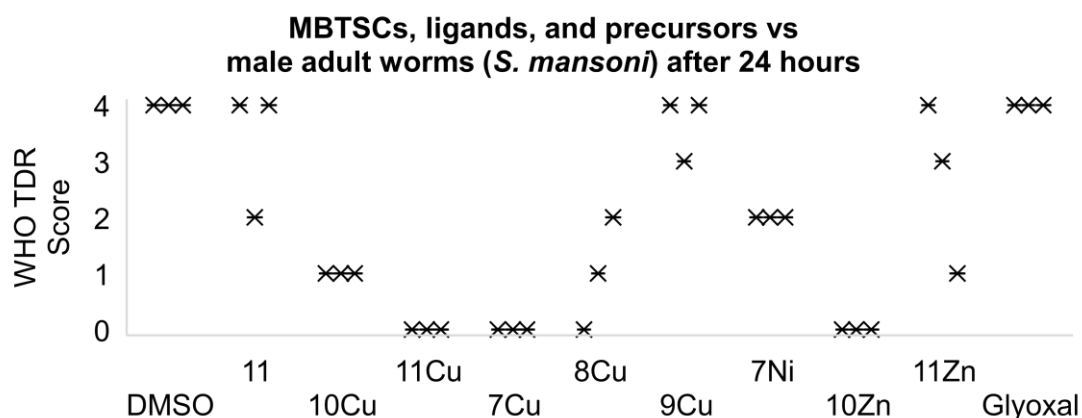


**Figure 24.** Antischistosomal activity of selected compounds against adult male schistosomes after 24 hours. Scores were recorded in triplicate. Each point represents a single worm.

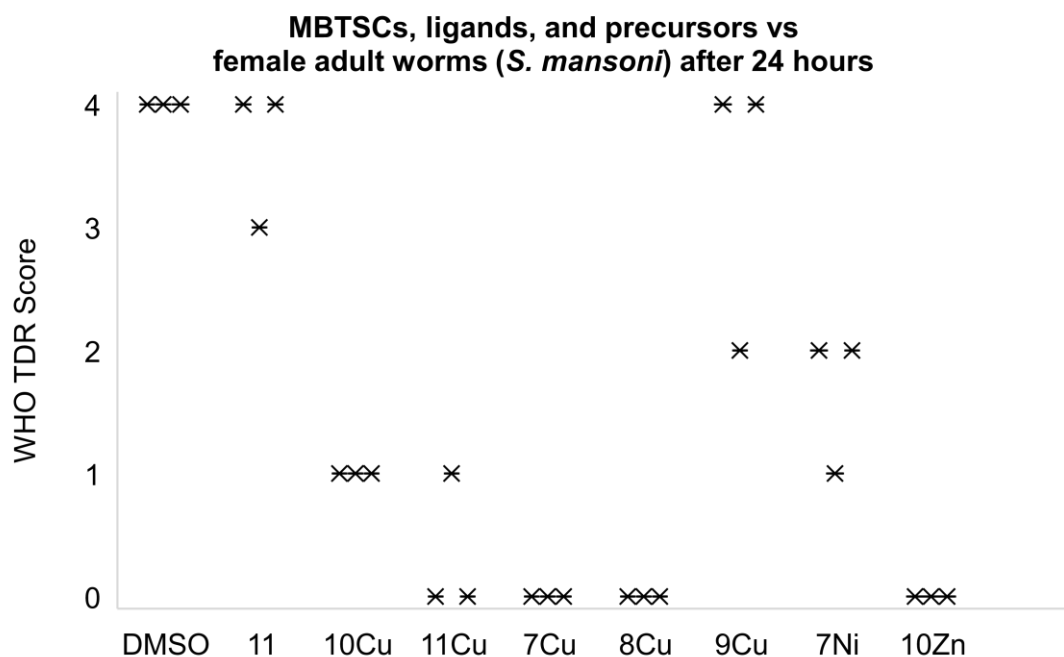


**Figure 25.** Antischistosomal activity of selected compounds against adult female schistosomes after 24 hours. Scores were recorded in triplicate. Each point represents a single worm.

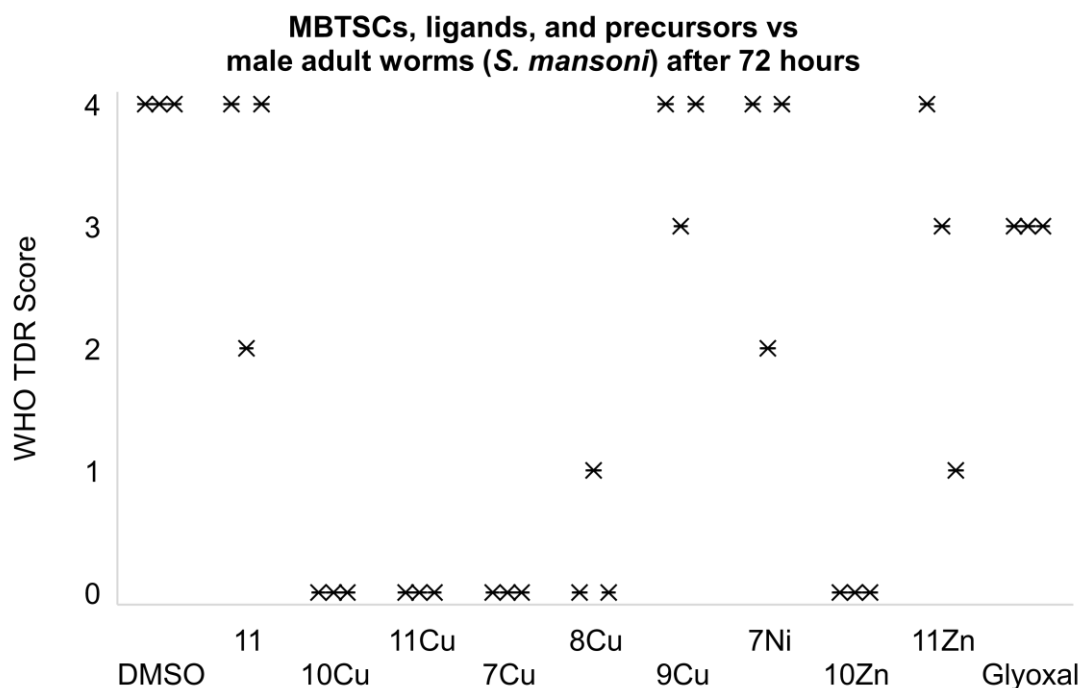


**Figure 26.** Antischistosomal activity of selected compounds against adult male schistosomes after 72 hours. Scores were recorded in triplicate. Each point represents a single worm.

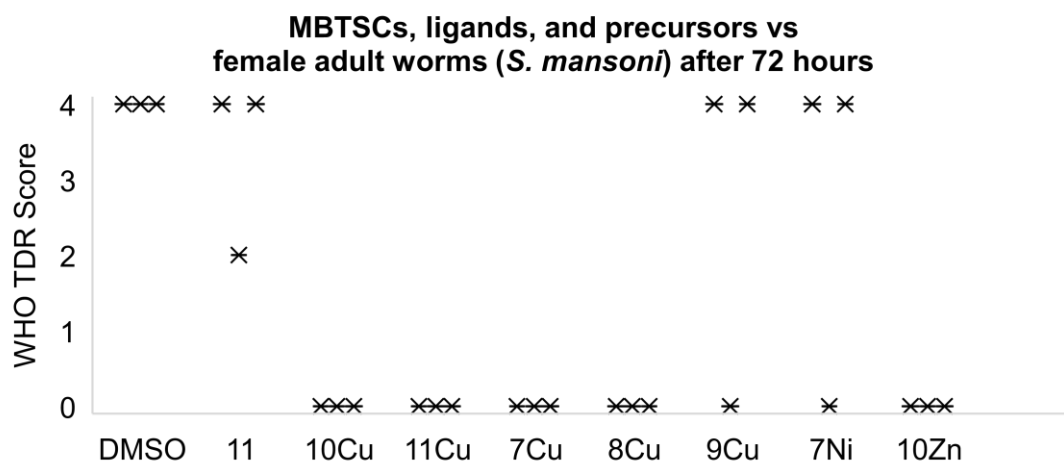


**Figure 27.** Antischistosomal activity of selected compounds against adult female schistosomes after 72 hours. Scores were recorded in triplicate. Each point represents a single worm.

As can be seen, all CuBTSC complexes except **9Cu** are effective against the adult schistosomes after 24 and 72 hours. Of these complexes, **11Cu** and **7Cu** were seen to be immediately effective. Immediate efficacy was established by a visual check of the schistosome pairs upon addition of the compound. The two immediately effective compounds, along with **10Zn** were the only compounds that had no precipitate present in the wells. **10Zn**, along with **11Zn** were found to be effective after 24 and 72 hours, though **11Zn** was not tested against female schistosomes due to a lack of suitable females available. The efficacy of **11Zn** was also only significant at a lower confidence interval than the other compounds. **11** was found to be ineffective against adult schistosomes, whereas **7Ni** was found to be effective against both sexes after 24 hours, but was found to no longer be effective after 72 hours. There are clear differences in the assigned scores of male and female schistosomes against the same compounds in some cases, with the males appearing to generally more resistant to the test compounds, and particularly after only 24 hours.

There is a clear difference between the physiology and phenotype of male and female schistosomes, with females typically being longer and thinner than the males.<sup>179</sup> The susceptibility of schistosomes, and the role which gender plays in susceptibility is poorly understood. In the case of Praziquantel, one of the most commonly used anthelmintic treatments, early work on *S. mansoni* suggested contrary to the above findings with MGTSA complexes. Male worms were typically found to be more susceptible than females.<sup>180-183</sup> In the case of primate chemotherapy studies into schistosomiasis, it was found that female worms of the species *Schistosoma haematobium* were more

susceptible to treatment with praziquantel than male worms.<sup>184</sup> The inverse was reported with *S. mansoni*, where it was found that the male worms were more susceptible to Praziquantel than females.<sup>185</sup> The same results were then observed in mice.<sup>102</sup> There is no simple explanation for the above observation of the greater susceptibility of females than males to MBTSC complexes. More work will therefore be required in order to understand the mechanism of action of the agents before drawing any theories as to why female schistosomes appear to be more sensitive to treatment with MBTSC complexes than males.

## Conclusion

Novel MBTSC complexes were synthesised starting from primary alkylamines. Isothiocyanates were prepared by reaction of a primary amine with CS<sub>2</sub>, then reacted immediately with hydrazine hydrate to produce 4-alkyl-3-thiosemicarbazides in good yields. The thiosemicarbazides were then reacted with a dicarbonyl (glyoxal for H<sub>2</sub>GTSA, and 2,3-butanedione for H<sub>2</sub>ATSM) producing H<sub>2</sub>BTSC ligands with excellent yields. These ligands were then complexed to Cu (all H<sub>2</sub>BTSCs), Zn (all H<sub>2</sub>BTSCs), Ni (H<sub>2</sub>GTSB, H<sub>2</sub>GTSH, and H<sub>2</sub>GTSO), Mn (H<sub>2</sub>GTSB, H<sub>2</sub>GTSH, and H<sub>2</sub>GTSO), and Co (H<sub>2</sub>GTSB, H<sub>2</sub>GTSH, and H<sub>2</sub>GTSO). The compounds were found to be spectroscopically and electrochemically similar to similar literature compounds.

The anthelmintic activity of the produced MBTSC complexes, their parent ligands, and precursors was tested against the parasite *S. mansoni* in two separate stages of its life cycle: the larval schistosomula stage, and as adult schistosomes. It was found that CuBTSCs were effective against schistosomula, with the least effective being CuGTSH. Of these, CuGTSM and CuGTSB were found to be more effective than auranofin, which has a well-reported anthelmintic activity. CuGTSO was ineffective against adult schistosomes, whereas all other CuBTSC complexes were found to be effective anthelmintic agents after 24 and 72 hours in culture. Of these, CuGTSM and CuGTSB, those complexes with short to medium alkyl chains, were found to be immediately effective when applied to the worms in the well plates used. ZnGTSM and ZnATSM were also found to be effective against schistosomula, a surprise result due to zinc's lack of redox chemistry, as CuBTSCs are thought to be effective anthelmintic agents due to the redox activity of the bound Cu. One theory is that the ZnBTSCs react with biologically available copper to produce an active CuBTSC *in situ*. ZnATSM was also found to be active against adult schistosomes. NiGTSB was also found to be effective against schistosomula, though its scores were not as negative as those recorded for CuBTSCs. NiGTSB's efficacy against adult schistosomes appeared to decrease between 24 and 72 hours. The efficacy of the synthesised CuBTSCs and ZnBTSCs against schistosomula and adult schistosomes highlights the potential of Cu- and ZnBTSCs as agents that may aid the management of schistosomiasis worldwide.

## References

- 1 M. Christlieb and J. R. Dilworth, *Chem. – Eur. J.*, 2006, **12**, 6194–6206.
- 2 H. Beraldo, L. P. Boyd and D. X. West, *Transit. Met. Chem.*, 1997, **23**, 67–71.
- 3 I. N. Fleming, R. Manavaki, P. J. Blower, C. West, K. J. Williams, A. L. Harris, J. Domarkas, S. Lord, C. Baldry and F. J. Gilbert, *Br. J. Cancer*, 2015, **112**, 238–250.
- 4 P. J. Blower, T. C. Castle, A. R. Cowley, J. R. Dilworth, P. S. Donnelly, E. Labisbal, F. E. Sowrey, S. J. Teat and M. J. Went, *Dalton Trans.*, 2003, 4416–4425.
- 5 J. S. Lewis, D. W. McCarthy, T. J. McCarthy, Y. Fujibayashi and M. J. Welch, *J. Nucl. Med.*, 1999, **40**, 177–183.
- 6 J. S. Lewis, R. Laforest, T. L. Buettner, S.-K. Song, Y. Fujibayashi, J. M. Connett and M. J. Welch, *Proc. Natl. Acad. Sci. U. S. A.*, 2001, **98**, 1206–1211.
- 7 J. A. O'Donoghue, P. Zanzonico, A. Pugachev, B. Wen, P. Smith-Jones, S. Cai, E. Burnazi, R. D. Finn, P. Burgman, S. Ruan, J. S. Lewis, M. J. Welch, C. C. Ling and J. L. Humm, *Int. J. Radiat. Oncol. Biol. Phys.*, 2005, **61**, 1493–1502.
- 8 A. L. Vāvere and J. S. Lewis, *Dalton Trans.*, 2007, 4893–4902.
- 9 B. Modéc, N. Podjed and N. Lah, *Molecules*, 2020, **25**, 1573.
- 10 B. M. Zeglis, J. L. Houghton, M. J. Evans, N. Viola-Villegas and J. S. Lewis, *Inorg. Chem.*, 2014, **53**, 1880–1899.
- 11 J. L. J. Dearling and P. J. Blower, *Chem. Commun.*, 1998, 2531–2532.
- 12 J. L. Dearling, J. S. Lewis, G. E. Mullen, M. J. Welch and P. J. Blower, *JBIC J. Biol. Inorg. Chem.*, 2002, **7**, 249–259.
- 13 K.-I. Matsumoto, L. Szajek, M. C. Krishna, J. A. Cook, J. Seidel, K. Grimes, J. Carson, A. L. Sowers, S. English, M. V. Green, S. L. Bacharach, W. C. Eckelman and J. B. Mitchell, *Int. J. Oncol.*, 2007, **30**, 873–881.
- 14 M. Colombié, S. Gouard, M. Frindel, A. Vidal, M. Chérel, F. Kraeber-Bodéré, C. Rousseau and M. Bourgeois, *Front. Med.*, 2015, 2:58, DOI:10.3389/fmed.2015.00058.
- 15 E. A. Pérès, J. Toutain, L.-P. Paty, D. Divoux, M. Ibazizène, S. Guillouet, L. Barré, A. Vidal, M. Cherel, M. Bourgeois, M. Bernaudin and S. Valable, *EJNMMI Res.*, 2019, **9**, 114.
- 16 N. Takahashi, Y. Fujibayashi, Y. Yonekura, M. J. Welch, A. Waki, T. Tsuchida, N. Sadato, K. Sugimoto and H. Itoh, *Ann. Nucl. Med.*, 2000, **14**, 323–328.
- 17 N. Takahashi, Y. Fujibayashi, Y. Yonekura, M. J. Welch, A. Waki, T. Tsuchida, N. Sadato, K. Sugimoto, A. Nakano, J.-D. Lee and H. Itoh, *Ann. Nucl. Med.*, 2001, **15**, 293–296.
- 18 K. Tateishi, U. Tateishi, M. Sato, S. Yamanaka, H. Kanno, H. Murata, T. Inoue and N. Kawahara, *Am. J. Neuroradiol.*, 2013, **34**, 92–99.
- 19 S. E. Lapi, J. S. Lewis and F. Dehdashti, *Semin. Nucl. Med.*, 2015, **45**, 177–185.
- 20 L. W. Hung, V. L. Villemagne, L. Cheng, N. A. Sherratt, S. Ayton, A. R. White, P. J. Crouch, S. Lim, S. L. Leong, S. Wilkins, J. George, B. R. Roberts, C. L. L. Pham, X. Liu, F. C. K. Chiu, D. M. Shackelford, A. K. Powell, C. L. Masters, A. I. Bush, G. O'Keefe, J. G. Culvenor, R. Cappai, R. A. Cherny, P. S. Donnelly, A. F. Hill, D. I. Finkelstein and K. J. Barnham, *J. Exp. Med.*, 2012, **209**, 837–854.
- 21 Collaborative Medicinal Development Pty Limited, *A Phase 1 Dose Escalation Study of Cu(II)ATSM Administered Orally to Patients With Early Idiopathic Parkinson's Disease*, clinicaltrials.gov, 2020.
- 22 X. Y. Choo, J. R. Liddell, M. T. Huuskonen, A. Grubman, D. Moujalled, J. Roberts, K. Kysenius, L. Patten, H. Quek, L. E. Oikari, C. Duncan, S. A. James, L. E. McInnes, D. J. Hayne, P. S. Donnelly, E. Pollari, S. Vähätalo, K. Lejavová, M. I. Kettunen, T. Malm, J. Koistinaho, A. R. White and K. M. Kanninen, *Front. Neurosci.*, 2018, 12:668, DOI:10.3389/fnins.2018.00668.
- 23 S. McKenzie-Nickson, J. Chan, K. Perez, L. W. Hung, L. Cheng, A. Sedjahtera, L. Gunawan, P. A. Adlard, D. J. Hayne, L. E. McInnes, P. S. Donnelly, D. I. Finkelstein, A. F. Hill and K. J. Barnham, *ACS Chem. Neurosci.*, 2018, **9**, 2731–2740.

- 24 Collaborative Medicinal Development Pty Limited, *A Phase 1 Single and Multiple Dose Escalation and Pharmacokinetic Study of Cu(II)ATSM Administered Orally to Patients With Amyotrophic Lateral Sclerosis/Motor Neuron Disease*, clinicaltrials.gov, 2020.
- 25 J. C. Meeuwssen, J. J. Sirois, C. Samuel Bradford, E. M. Labut, N. I. Lopez, J. K. Hurst and J. S. Beckman, *Free Radic. Biol. Med.*, 2016, **100**, S105.
- 26 F. G. Vieira, T. Hatzipetros, K. Thompson, A. J. Moreno, J. D. Kidd, V. R. Tassinari, B. Levine, S. Perrin and A. Gill, *IBRO Rep.*, 2017, **2**, 47–53.
- 27 M. T. H. Kuo, J. S. Beckman and C. A. Shaw, *Neurobiol. Dis.*, 2019, **130**, 104495.
- 28 E. J. McAllum, B. R. Roberts, J. L. Hickey, T. N. Dang, A. Grubman, P. S. Donnelly, J. R. Liddell, A. R. White and P. J. Crouch, *Neurobiol. Dis.*, 2015, **81**, 20–24.
- 29 G. Bähr and E. Hess, *Z. Für Anorg. Allg. Chem.*, 1952, **268**, 351–363.
- 30 G. Bähr, E. Hess, E. Steinkopf and G. Schleitzer, *Z. Für Anorg. Allg. Chem.*, 1953, **273**, 325–332.
- 31 B. A. Gingras, T. Suprunchuk, O. Bernardini and C. H. Bayley, *Can. J. Chem.*, 1963, **41**, 1629-1632.
- 32 C. G. D. Brown, J. K. H. Wilde and J. Berger, *Br. Vet. J.*, 1968, **124**, 325–334.
- 33 T. O. Roby, T. E. Amerault and L. A. Spindler, *Res. Vet. Sci.*, 1968, **9**, 494–499.
- 34 D. Kessel and R. Stanley McElhinney, *Biochem. Pharmacol.*, 1975, **24**, 133–137.
- 35 D. T. Minkel, C. Chan-Stier and D. H. Petering, *Mol. Pharmacol.*, 1976, **12**, 1036–1044.
- 36 D. T. Minkel, L. A. Saryan and D. H. Petering, *Cancer Res.*, 1978, **38**, 124–129.
- 37 H. G. Petering, H. H. Buskirk and G. E. Underwood, *Cancer Res.*, 1964, **24**, 367–372.
- 38 H. G. Petering, H. H. Buskirk and J. A. Crim, *Cancer Res.*, 1967, **27**, 1115–1121.
- 39 N. Majerníková, J. J. Yu and A. B. Maier, *Clin. Transl. Imaging*, 2020, **8**, 449-460.
- 40 Y. Fujibayashi, H. Taniuchi, Y. Yonekura, H. Ohtani, J. Konishi and A. Yokoyama, *J. Nucl. Med.*, 1997, **38**, 1155–1160.
- 41 K. A. Krohn, J. M. Link and R. P. Mason, *J. Nucl. Med.*, 2008, **49**, 129S-148S.
- 42 K. S. C. Chao, W. R. Bosch, S. Mutic, J. S. Lewis, F. Dehdashti, M. A. Mintun, J. F. Dempsey, C. A. Perez, J. A. Purdy and M. J. Welch, *Int. J. Radiat. Oncol.*, 2001, **49**, 1171–1182.
- 43 C. J. Anderson and R. Ferdani, *Cancer Biother. Radiopharm.*, 2009, **24**, 379–393.
- 44 Z. Xiao, P. S. Donnelly, M. Zimmermann and A. G. Wedd, *Inorg. Chem.*, 2008, **47**, 4338–4347.
- 45 K. Y. Djoko, B. M. Paterson, P. S. Donnelly and A. G. McEwan, *Metallomics*, 2014, **6**, 854–863.
- 46 P. J. Crouch, L. W. Hung, P. A. Adlard, M. Cortes, V. Lal, G. Filiz, K. A. Perez, M. Nurjono, A. Caragounis, T. Du, K. Laughton, I. Volitakis, A. I. Bush, Q.-X. Li, C. L. Masters, R. Cappai, R. A. Cherny, P. S. Donnelly, A. R. White and K. J. Barnham, *Proc. Natl. Acad. Sci.*, 2009, **106**, 381–386.
- 47 Y. Yoshii, M. Yoneda, M. Ikawa, T. Furukawa, Y. Kiyono, T. Mori, H. Yoshii, N. Oyama, H. Okazawa, T. Saga and Y. Fujibayashi, *Nucl. Med. Biol.*, 2012, **39**, 177–185.
- 48 T. Liu, M. Karlsen, A. M. Karlberg and K. R. Redalen, *EJNMMI Res.*, 2020, **10**, 33.
- 49 J. L. J. Dearling and A. B. Packard, *Nucl. Med. Biol.*, 2010, **37**, 237–243.
- 50 D. Schilter, *Nat. Rev. Chem.*, 2017, **1**, 1–1.
- 51 N. Haugaard, *Ann. N. Y. Acad. Sci.*, 2000, **899**, 148–158.
- 52 R. Requejo, T. R. Hurd, N. J. Costa and M. P. Murphy, *FEBS J.*, 2010, **277**, 1465–1480.
- 53 K. Y. Djoko, P. S. Donnelly and A. G. McEwan, *Metallomics*, 2014, **6**, 2250–2259.
- 54 B. Lippert, *Biometals*, 1992, **5**, 195–208.
- 55 J. A. Simpson, K. H. Cheeseman, S. E. Smith and R. T. Dean, *Biochem. J.*, 1988, **254**, 519–523.
- 56 S. Kobayashi, K. Ueda and T. Komano, *Agric. Biol. Chem.*, 1990, **54**, 69–76.

- 57 J. L. Stauber and T. M. Florence, *Mar. Biol.*, 1987, **94**, 511–519.
- 58 C. Cervantes and F. Gutierrez-Corona, *FEMS Microbiol. Rev.*, 1994, **14**, 121–137.
- 59 M. A. Cater, H. B. Pearson, K. Wolyniec, P. Klaver, M. Bilandzic, B. M. Paterson, A. I. Bush, P. O. Humbert, S. La Fontaine, P. S. Donnelly and Y. Haupt, *ACS Chem. Biol.*, 2013, **8**, 1621–1631.
- 60 M. A. Cater and Y. Haupt, *Biochem. J.*, 2011, **436**, 481–491.
- 61 D. Chen, Q. C. Cui, H. Yang, R. A. Barrea, F. H. Sarkar, S. Sheng, B. Yan, G. P. V. Reddy and Q. P. Dou, *Cancer Res.*, 2007, **67**, 1636–1644.
- 62 C. Stefani, Z. Al-Eisawi, P. J. Jansson, D. S. Kalinowski and D. R. Richardson, *J. Inorg. Biochem.*, 2015, **152**, 20–37.
- 63 D. S. Kalinowski and D. R. Richardson, *Pharmacol. Rev.*, 2005, **57**, 547–583.
- 64 J. E. Karp, F. J. Giles, I. Gojo, L. Morris, J. Greer, B. Johnson, M. Thein, M. Sznol and J. Low, *Leuk. Res.*, 2008, **32**, 71–77.
- 65 M. Whitnall, J. Howard, P. Ponka and D. R. Richardson, *Proc. Natl. Acad. Sci.*, 2006, **103**, 14901–14906.
- 66 J. Yuan, D. B. Lovejoy and D. R. Richardson, *Blood*, 2004, **104**, 1450–1458.
- 67 P. Li, X. Zheng, K. Shou, Y. Niu, C. Jian, Y. Zhao, W. Yi, X. Hu and A. Yu, *Am. J. Transl. Res.*, 2016, **8**, 5370–5385.
- 68 R. Anjum, D. Palanimuthu, D. S. Kalinowski, W. Lewis, K. C. Park, Z. Kovacevic, I. U. Khan and D. R. Richardson, *Inorg. Chem.*, 2019, **58**, 13709–13723.
- 69 K. M. Acevedo, D. J. Hayne, L. E. McInnes, A. Noor, C. Duncan, D. Moujalled, I. Volitakis, A. Rigopoulos, K. J. Barnham, V. L. Villemagne, A. R. White and P. S. Donnelly, *J. Med. Chem.*, 2018, **61**, 711–723.
- 70 L. Li, G.-D. Zhao, Z. Shi, L.-L. Qi, L.-Y. Zhou and Z.-X. Fu, *Oncol. Lett.*, 2016, **12**, 3045–3050.
- 71 M. L. Turski, D. C. Brady, H. J. Kim, B.-E. Kim, Y. Nose, C. M. Counter, D. R. Winge and D. J. Thiele, *Mol. Cell. Biol.*, 2012, **32**, 1284–1295.
- 72 D. C. Brady, M. S. Crowe, M. L. Turski, G. A. Hobbs, X. Yao, A. Chaikuad, S. Knapp, K. Xiao, S. L. Campbell, D. J. Thiele and C. M. Counter, *Nature*, 2014, **509**, 492–496.
- 73 J. J. Sirois, L. Padgitt-Cobb, M. A. Gallegos, J. S. Beckman, C. M. Beaudry and J. K. Hurst, *Inorg. Chem.*, 2018, **57**, 8923–8932.
- 74 S. A. Andres, K. Bajaj, N. S. Vishnosky, M. A. Peterson, M. S. Mashuta, R. M. Buchanan, P. J. Bates and C. A. Grapperhaus, *Inorg. Chem.*, 2020, **59**, 4924–4935.
- 75 A. Speer, T. B. Shrestha, S. H. Bossmann, R. J. Basaraba, G. J. Harber, S. M. Michalek, M. Niederweis, O. Kutsch and F. Wolschendorf, *Antimicrob. Agents Chemother.*, 2013, **57**, 1089–1091.
- 76 M. Haeili, C. Moore, C. J. C. Davis, J. B. Cochran, S. Shah, T. B. Shrestha, Y. Zhang, S. H. Bossmann, W. H. Benjamin, O. Kutsch and F. Wolschendorf, *Antimicrob. Agents Chemother.*, 2014, **58**, 3727–3736.
- 77 J. W. Marsh, K. Y. Djoko, A. G. McEwan and W. M. Huston, *Pathog. Dis.*, 2017, **75**, ftx084.
- 78 P. J. Crouch and K. J. Barnham, *Acc. Chem. Res.*, 2012, **45**, 1604–1611.
- 79 S. J. Parker, J. Meyerowitz, J. L. James, J. R. Liddell, T. Nonaka, M. Hasegawa, K. M. Kanninen, S. Lim, B. M. Paterson, P. S. Donnelly, P. J. Crouch and A. R. White, *PLoS ONE*, 2012, **7**(8), e42277, DOI:10.1371/journal.pone.0042277.
- 80 M. A. Green, C. J. Mathias, L. R. Willis, R. K. Handa, J. L. Lacy, M. A. Miller and G. D. Hutchins, *Nucl. Med. Biol.*, 2007, **34**, 247–255.
- 81 M. Munakata, H. Kodama, C. Fujisawa, T. Hiroki, K. Kimura, M. Watanabe, M. Nishikawa and S. Tsuchiya, *Pediatr. Res.*, 2012, **72**, 270–276.
- 82 S. Kadowaki, M. Munekane, Y. Kitamura, M. Hiromura, S. Kamino, Y. Yoshikawa, H. Saji and S. Enomoto, *Biol. Trace Elem. Res.*, 2013, **154**, 111–119.
- 83 J. R. Ames, M. D. Ryan and P. Kovacic, *Life Sci.*, 1987, **41**, 1895–1902.
- 84 G. A. Dziwornu, H. D. Attram, S. Gachuhi and K. Chibale, *RSC Med. Chem.*, 2020, **11**, 455–490.

- 85 B. Gryseels, K. Polman, J. Clerinx and L. Kestens, *Lancet Lond. Engl.*, 2006, **368**, 1106–1118.
- 86 D. G. Colley, A. L. Bustinduy, W. E. Secor and C. H. King, *Lancet Lond. Engl.*, 2014, **383**, 2253–2264.
- 87 M. A. Verjee, *Res. Rep. Trop. Med.*, 2019, **10**, 153–163.
- 88 A. Crusco, H. Whiteland, R. Baptista, J. E. Forde-Thomas, M. Beckmann, L. A. J. Mur, R. J. Nash, A. D. Westwell and K. F. Hoffmann, *ACS Infect. Dis.*, 2019, **5**, 1188–1199.
- 89 D. P. McManus, D. W. Dunne, M. Sacko, J. Utzinger, B. J. Vennervald and X.-N. Zhou, *Nat. Rev. Dis. Primer*, 2018, **4**, 1–19.
- 90 A. Olsen, S. Kinung'hi and P. Magnussen, *Am. J. Trop. Med. Hyg.*, 2015, **92**, 1240–1244.
- 91 E. J. Carlton, Y. Liu, B. Zhong, A. Hubbard and R. C. Spear, *PLoS Negl. Trop. Dis.*, 2015, **9**, e0003444.
- 92 A. G. Ross, D. Vickers, G. R. Olds, S. M. Shah and D. P. McManus, *Lancet Infect. Dis.*, 2007, **7**, 218–224.
- 93 S. Jauréguiberry, L. Paris and E. Caumes, *Clin. Microbiol. Infect.*, 2010, **16**, 225–231.
- 94 J. Cao, W.-J. Liu, X.-Y. Xu and X.-P. Zou, *World J. Gastroenterol.*, 2010, **16**, 723–727.
- 95 M. Chen, *Infect. Dis. Poverty*, 2014, **3**, 6.
- 96 D. J. Gray, A. G. Ross, Y.-S. Li and D. P. McManus, *BMJ*, 2011, 342:d2651 DOI:10.1136/bmj.d2651.
- 97 A. Crusco, C. Bordoni, A. Chakraborty, K. C. L. Whatley, H. Whiteland, A. D. Westwell and K. F. Hoffmann, *Eur. J. Med. Chem.*, 2018, **152**, 87–100.
- 98 J. Edwards, M. Brown, E. Peak, B. Bartholomew, R. J. Nash and K. F. Hoffmann, *PLoS Negl. Trop. Dis.*, 2015, **9**, e0003604.
- 99 N. Vale, M. J. Gouveia, G. Rinaldi, P. J. Brindley, F. Gärtner and J. M. Correia da Costa, *Antimicrob. Agents Chemother.*, 2017, **61**, e02582-16.
- 100 H. C. Richards and R. Foster, *Nature*, 1969, **222**, 581–582.
- 101 D. Cioli, L. Pica-Mattoccia and S. Archer, *Pharmacol. Ther.*, 1995, **68**, 35–85.
- 102 P. Andrews, H. Thomas, R. Pohlke and J. Seubert, *Med. Res. Rev.*, 1983, **3**, 147–200.
- 103 F. Ronketti, A. Ramana, C.-M. Xia, L. Pica-Mattoccia, D. Cioli and M. Todd, *Bioorg. Med. Chem. Lett.*, 2007, **17**, 4154–4157.
- 104 W. Duan, S. Qiu, Y. Zhao, H. Sun, C. Qiao and C. Xia, *Bioorg. Med. Chem. Lett.*, 2012, **22**, 1587–1590.
- 105 W.-L. Wang, L.-J. Song, X. Chen, X.-R. Yin, W.-H. Fan, G.-P. Wang, C.-X. Yu and B. Feng, *Molecules*, 2013, **18**, 9163–9178.
- 106 M. Patra, K. Ingram, V. Pierroz, S. Ferrari, B. Spingler, J. Keiser and G. Gasser, *J. Med. Chem.*, 2012, **55**, 8790–8798.
- 107 M. Patra, K. Ingram, V. Pierroz, S. Ferrari, B. Spingler, R. B. Gasser, J. Keiser and G. Gasser, *Chem. – Eur. J.*, 2013, **19**, 2232–2235.
- 108 M. Patra, K. Ingram, A. Leonidova, V. Pierroz, S. Ferrari, M. N. Robertson, M. H. Todd, J. Keiser and G. Gasser, *J. Med. Chem.*, 2013, **56**, 9192–9198.
- 109 J. Hess, G. Panic, M. Patra, L. Mastrobuoni, B. Spingler, S. Roy, J. Keiser and G. Gasser, *ACS Infect. Dis.*, 2017, **3**, 645–652.
- 110 V. Buchter, J. Hess, G. Gasser and J. Keiser, *Parasit. Vectors*, 2018, **11**, 580.
- 111 J. Boissier, F. Coslédan, A. Robert and B. Meunier, *Antimicrob. Agents Chemother.*, 2009, **53**, 4903–4906.
- 112 V. Pradines, J. Portela, J. Boissier, F. Coslédan, B. Meunier and A. Robert, *Antimicrob. Agents Chemother.*, 2011, **55**, 2403–2405.
- 113 K. Ingram, I. A. Yaremenko, I. B. Krylov, L. Hofer, A. O. Terent'ev and J. Keiser, *J. Med. Chem.*, 2012, **55**, 8700–8711.

- 114 T. Taniguchi, T. Kumagai, R. Shimogawara, S. Ichinose, A. Hiramoto, A. Sato, M. Morita, M. Nojima, H.-S. Kim, Y. Wataya and N. Ohta, *Parasitol. Int.*, 2011, **60**, 231–236.
- 115 M. Yamabe, T. Kumagai, R. Shimogawara, E. A. Blay, A. Hino, K. Ichimura, A. Sato, H.-S. Kim and N. Ohta, *Parasitol. Int.*, 2017, **66**, 917–924.
- 116 F. d'Orchymont, J. Hess, G. Panic, M. Jakubaszek, L. Gemperle, J. Keiser and G. Gasser, *MedChemComm*, 2018, **9**, 1905–1909.
- 117 K. Ingram, W. Ellis and J. Keiser, *Antimicrob. Agents Chemother.*, 2012, **56**, 3207–3215.
- 118 J. Keiser, J. Chollet, S.-H. Xiao, J.-Y. Mei, P.-Y. Jiao, J. Utzinger and M. Tanner, *PLoS Negl. Trop. Dis.*, 2009, **3**(1), e350. DOI:10.1371/journal.pntd.0000350.
- 119 J. Keiser and J. Utzinger, *Curr. Pharm. Des.*, 2012, **18**, 3531–3538.
- 120 M. O. F. Khan, J. Keiser, P. N. A. Amoyaw, M. F. Hossain, M. Vargas, J. G. Le, N. C. Simpson, K. D. Roewe, T. N. C. Freeman, T. R. Hasley, R. D. Maples, S. J. Archibald and T. J. Hubin, *Antimicrob. Agents Chemother.*, 2016, **60**, 5331–5336.
- 121 V. Pasche, B. Laleu and J. Keiser, *Parasit. Vectors*, 2018, **11**, 298.
- 122 V. Pasche, B. Laleu and J. Keiser, *ACS Infect. Dis.*, 2019, **5**, 102–110.
- 123 T. Bayer, A. Chakrabarti, J. Lancelot, T. B. Shaik, K. Hausmann, J. Melesina, K. Schmidtkunz, M. Marek, F. Erdmann, M. Schmidt, D. Robaa, C. Romier, R. J. Pierce, M. Jung and W. Sippl, *ChemMedChem*, 2018, **13**, 1517–1529.
- 124 D. Monaldi, D. Rotili, J. Lancelot, M. Marek, N. Wössner, A. Lucidi, D. Tomaselli, E. Ramos-Morales, C. Romier, R. J. Pierce, A. Mai and M. Jung, *J. Med. Chem.*, 2019, **62**, 8733–8759.
- 125 E. de F. Santiago, S. A. de Oliveira, G. B. de Oliveira Filho, D. R. M. Moreira, P. A. T. Gomes, A. L. da Silva, A. F. de Barros, A. C. da Silva, T. A. R. dos Santos, V. R. A. Pereira, G. G. A. Gonçalves, F. A. Brayner, L. C. Alves, A. G. Wanderley and A. C. L. Leite, *Antimicrob. Agents Chemother.*, 2014, **58**, 352–363.
- 126 M. de Oliveira Barbosa, S. A. de Oliveira, C. A. L. M. Filho, A. R. Oliveira, C. J. B. Fernandes, J. P. Lucena, F. A. de Sousa, M. C. H. de Barros Dias, F. A. Brayner, L. C. Alves and A. C. L. Leite, *Eur. J. Pharm. Sci. Off. J. Eur. Fed. Pharm. Sci.*, 2019, **133**, 15–27.
- 127 S. S. Botros, S. William, A.-N. A. Sabra, N. M. El-Lakkany, S. H. Seif el-Din, A. García-Rubia, V. Sebastián-Pérez, A. R. Blaazer, E. de Heuvel, M. Sijm, Y. Zheng, I. G. Salado, J. C. Munday, L. Maes, I. J. P. de Esch, G. J. Sterk, K. Augustyns, R. Leurs, C. Gil and H. P. De Koning, *Int. J. Parasitol. Drugs Drug Resist.*, 2019, **9**, 35–43.
- 128 A. A. Sayed, A. Simeonov, C. J. Thomas, J. Inglese, C. P. Austin and D. L. Williams, *Nat. Med.*, 2008, **14**, 407–412.
- 129 W. Wang, Q. Li, Y. Wei, J. Xue, X. Sun, Y. Yu, Z. Chen, S. Li and L. Duan, *Int. J. Parasitol. Drugs Drug Resist.*, 2017, **7**, 191–199.
- 130 A. M. Peter Ventura, S. Haeberlein, K. Lange-Grünweller, A. Grünweller, R. K. Hartmann, C. G. Grevelding and M. Schlitzer, *ChemMedChem*, 2019, **14**, 1856–1862.
- 131 V. R. D. Pereira, I. J. A. Junior, L. S. da Silveira, R. B. Geraldo, P. de F. Pinto, F. S. Teixeira, M. C. Salvadori, M. P. Silva, L. A. Alves, P. V. S. Z. Capriles, A. das C Almeida, E. S. Coimbra, P. L. S. Pinto, M. R. C. Couri, J. de Moraes and A. A. Da Silva Filho, *Chem. Biodivers.*, 2018, **15**, e1800398.
- 132 R. L. T. Parreira, E. S. Costa, V. C. G. Heleno, L. G. Magalhães, J. M. Souza, P. M. Pauletti, W. R. Cunha, A. H. Januário, G. V. Símaro, J. K. Bastos, R. S. Laurentiz, T. Kar, G. F. Caramori, D. F. Kawano and M. L. Andrade E Silva, *Chem. Biodivers.*, 2019, **16**, e1800305.
- 133 S. El Bardicy, I. El Sayed, F. Yousif, P. Van der Veken, A. Haemers, K. Augustyns and L. Pieters, *Pharm. Biol.*, 2012, **50**, 134–140.
- 134 GB966849A, 1964.

- 135 J. P. Holland, J. A. Hickin, E. Grenville-Mathers, T. Nguyen and J. M. Peach, *J. Chem. Res.*, 2008, **2008**, 702–703.
- 136 H. M. Betts, P. J. Barnard, S. R. Bayly, J. R. Dilworth, A. D. Gee and J. P. Holland, *Angew. Chem. Int. Ed.*, 2008, **47**, 8416–8419.
- 137 P. S. Donnelly, A. Caragounis, T. Du, K. M. Laughton, I. Volitakis, R. A. Cherny, R. A. Sharples, A. F. Hill, Q.-X. Li, C. L. Masters, K. J. Barnham and A. R. White, *J. Biol. Chem.*, 2008, **283**, 4568–4577.
- 138 S. R. Smithers and R. J. Terry, *Parasitology*, 1965, **55**, 695–700.
- 139 B. Ramirez, Q. Bickle, F. Yousif, F. Fakorede, M.-A. Mouries and S. Nwaka, *Expert Opin. Drug Discov.*, 2007, **2**, S53–61.
- 140 M. Stein, A. Breit, T. Fehrentz, T. Gudermann and D. Trauner, *Angew. Chem. Int. Ed.*, 2013, **52**, 9845–9848.
- 141 W. Huang, Z. Zhang, X. Barros-Álvarez, C. Y. Koh, R. M. Ranade, J. R. Gillespie, S. A. Creason, S. Shibata, C. L. M. J. Verlinde, W. G. J. Hol, F. S. Buckner and E. Fan, *Eur. J. Med. Chem.*, 2016, **124**, 1081–1092.
- 142 D. Li, Y. Shu, P. Li, W. Zhang, H. Ni and Y. Cao, *Med. Chem. Res.*, 2013, **22**, 3119–3125.
- 143 D. Dolles, M. Nimczick, M. Scheiner, J. Ramler, P. Stadtmüller, E. Sawatzky, A. Drakopoulos, C. Sotriffer, H.-J. Wittmann, A. Strasser and M. Decker, *ChemMedChem*, 2016, **11**, 1270–1283.
- 144 S. L. Nowotarski, B. Pachaiyappan, S. L. Holshouser, C. J. Kutz, Y. Li, Y. Huang, S. K. Sharma, R. A. Casero and P. M. Woster, *Bioorg. Med. Chem.*, 2015, **23**, 1601–1612.
- 145 N. Sun, B. Li, J. Shao, W. Mo, B. Hu, Z. Shen and X. Hu, *Beilstein J. Org. Chem.*, 2012, **8**, 61–70.
- 146 H. Munch, J. S. Hansen, M. Pittelkow, J. B. Christensen and U. Boas, *Tetrahedron Lett.*, 2008, **49**, 3117–3119.
- 147 M. T. Robak, M. Trincado and J. A. Ellman, *J. Am. Chem. Soc.*, 2007, **129**, 15110–15111.
- 148 Y. He, J. Li, S. Luo, J. Huang and Q. Zhu, *Chem. Commun.*, 2016, **52**, 8444–8447.
- 149 E. I. Jiménez, W. E. Vallejo Narváez, C. A. Román-Chavarría, J. Vazquez-Chavez, T. Rocha-Rinza and M. Hernández-Rodríguez, *J. Org. Chem.*, 2016, **81**, 7419–7431.
- 150 F. Vandresen, H. Falzirolli, S. A. Almeida Batista, A. P. B. da Silva-Giardini, D. N. de Oliveira, R. R. Catharino, A. L. T. G. Ruiz, J. E. de Carvalho, M. A. Foglio and C. C. da Silva, *Eur. J. Med. Chem.*, 2014, **79**, 110–116.
- 151 M. D. Altıntop, Ö. Atli, S. Ilgin, R. Demirel, A. Özdemir and Z. A. Kaplancikli, *Eur. J. Med. Chem.*, 2016, **108**, 406–414.
- 152 E. J. Jacobsen, M. A. Mitchell, S. K. Hendges, K. L. Belonga, L. L. Skaletzky, L. S. Stelzer, Thomas. J. Lindberg, E. L. Fritzen, H. J. Schostarez, T. J. O'Sullivan, L. L. Maggiora, C. W. Stuchly, A. L. Laborde, M. F. Kubicek, R. A. Poorman, J. M. Beck, H. R. Miller, G. L. Petzold, P. S. Scott, S. E. Truesdell, T. L. Wallace, J. W. Wilks, C. Fisher, L. V. Goodman, P. S. Kaytes, S. R. Ledbetter, E. A. Powers, G. Vogeli, J. E. Mott, C. M. Trepod, D. J. Staples, E. T. Baldwin and B. C. Finzel, *J. Med. Chem.*, 1999, **42**, 1525–1536.
- 153 P. A. Waghorn, M. W. Jones, M. B. M. Theobald, R. L. Arrowsmith, S. I. Pascu, S. W. Botchway, S. Faulkner and J. R. Dilworth, *Chem. Sci.*, 2013, **4**, 1430–1441.
- 154 C. González-García, A. Mata, F. Zani, M. A. Mendiola and E. López-Torres, *J. Inorg. Biochem.*, 2016, **163**, 118–130.
- 155 T. A. Su, D. S. Shihadih, W. Cao, T. C. Detomasi, M. C. Heffern, S. Jia, A. Stahl and C. J. Chang, *J. Am. Chem. Soc.*, 2018, **140**, 13764–13774.
- 156 B. M. Paterson, K. F. White, J. M. White, B. F. Abrahams and P. S. Donnelly, *Angew. Chem. Int. Ed.*, 2017, **56**, 8370–8374.
- 157 J. P. Holland, P. J. Barnard, D. Collison, J. R. Dilworth, R. Edge, J. C. Green, J. M. Heslop, E. J. L. McInnes, C. G. Salzmann and A. L. Thompson, *Eur. J. Inorg. Chem.*, 2008, **2008**, 3549–3560.

- 158E. López-Torres, M. A. Mendiola, J. Rodríguez-Procopio, M. T. Sevilla, E. Colacio, J. Ma Moreno and I. Sobrados, *Inorganica Chim. Acta*, 2001, **323**, 130–138.
- 159H. Ghosh, R. Yella, J. Nath and B. K. Patel, *Eur. J. Org. Chem.*, 2008, **2008**, 6189–6196.
- 160Ł. Janczewski, A. Gajda and T. Gajda, *Eur. J. Org. Chem.*, 2019, **2019**, 2528–2532.
- 161M. T. C. Ang, L. Phan, A. K. Alshamrani, J. R. Harjani, R. Wang, G. Schatte, N. J. Mosey and P. G. Jessop, *Eur. J. Org. Chem.*, 2015, **2015**, 7334–7343.
- 162A. J. Gupta, N. S. Vishnosky, O. Hietsoi, Y. Losovyj, J. Strain, J. Spurgeon, M. S. Mashuta, R. Jain, R. M. Buchanan, G. Gupta and C. A. Grapperhaus, *Inorg. Chem.*, 2019, **58**, 12025–12039.
- 163E. Palma, F. Mendes, G. R. Morais, I. Rodrigues, I. C. Santos, M. P. C. Campello, P. Raposinho, I. Correia, S. Gama, D. Belo, V. Alves, A. J. Abrunhosa, I. Santos and A. Paulo, *J. Inorg. Biochem.*, 2017, **167**, 68–79.
- 164D. M. Wiles, B. A. Gingras and T. Suprunchuk, *Can. J. Chem.*, 1967, **45**, 469–473.
- 165M. Christlieb, J. P. Holland and J. R. Dilworth, *Inorganica Chim. Acta*, 2010, **363**, 1133–1139.
- 166J. P. Holland, F. I. Aigbirhio, H. M. Betts, P. D. Bonnitcha, P. Burke, M. Christlieb, G. C. Churchill, A. R. Cowley, J. R. Dilworth, P. S. Donnelly, J. C. Green, J. M. Peach, S. R. Vasudevan and J. E. Warren, *Inorg. Chem.*, 2007, **46**, 465–485.
- 167D. Dayal, D. Palanimuthu, S. V. Shinde, K. Somasundaram and A. G. Samuelson, *JBIC J. Biol. Inorg. Chem.*, 2011, **16**, 621–632.
- 168C. J. Hipp and W. A. Baker, *J. Am. Chem. Soc.*, 1970, **92**, 792–798.
- 169B. Ortiz and S. M. Park, *Bull. Korean Chem. Soc.*, 2000, **21**, 405–411.
- 170P. K. Sonkar, V. Ganesan and A. Prajapati, *Ionics*, 2016, **22**, 1741–1749.
- 171R. Jain, A. A. Mamun, R. M. Buchanan, P. M. Kozlowski and C. A. Grapperhaus, *Inorg. Chem.*, 2018, **57**, 13486–13493.
- 172T. Straistari, J. Fize, S. Shova, M. Réglie, V. Artero and M. Orio, *ChemCatChem*, 2017, **9**, 2262–2268.
- 173A. A. Isse, A. Gennaro and E. Vianello, *J. Chem. Soc. Dalton Trans.*, 1993, 2091–2096.
- 174A. P. King, H. A. Gellineau, J.-E. Ahn, S. N. MacMillan and J. J. Wilson, *Inorg. Chem.*, 2017, **56**, 6609–6623.
- 175M. Cañadas, E. López-Torres, A. Martínez-Arias, M. Antonia Mendiola and M. Teresa Sevilla, *Polyhedron*, 2000, **19**, 2059–2068.
- 176G. W. Hunter, E. H. Kaufman Jr. and C. Pan, *Exp. Parasitol.*, 1952, **1**, 168–175.
- 177E. Peak, I. W. Chalmers and K. F. Hoffmann, *PLoS Negl. Trop. Dis.*, 2010, **4**, e759.
- 178H. Saji, A. Saiga, Y. Iida, Y. Magata and A. Yokoyama, *J. Label. Compd. Radiopharm.*, 1993, **33**, 127–135.
- 179Z. Lu, F. Sessler, N. Holroyd, S. Hahnel, T. Quack, M. Berriman and C. G. Grevelding, *Sci. Rep.*, 2016, **6**, 31150.
- 180R. Gönnert and P. Andrews, *Z. Für Parasitenkd.*, 1977, **52**, 129–150.
- 181B. Becker, H. Mehlhorn, P. Andrews, H. Thomas and J. Eckert, *Z. Für Parasitenkd.*, 1980, **63**, 113–128.
- 182Y. S. Liang, G. C. Coles, M. J. Doenhoff and V. R. Southgate, *Int. J. Parasitol.*, 2001, **31**, 1227–1235.
- 183Y.-S. Liang, G. C. Coles, J.-R. Dai, Y.-C. Zhu and M. J. Doenhoff, *J. Helminthol.*, 2002, **76**, 327–333.
- 184G. Webbe, C. James, G. S. Nelson and R. F. Sturrock, *Arzneimittelforschung.*, 1981, **31**, 542–544.
- 185V. S. Delgado, D. P. Suárez, I. M. Cesari and R. N. Incani, *Parasitol. Res.*, 1992, **78**, 648–654.

## Chapter 4: Development of antimicrobial doped silicone rubbers

### Antimicrobial silicone rubbers

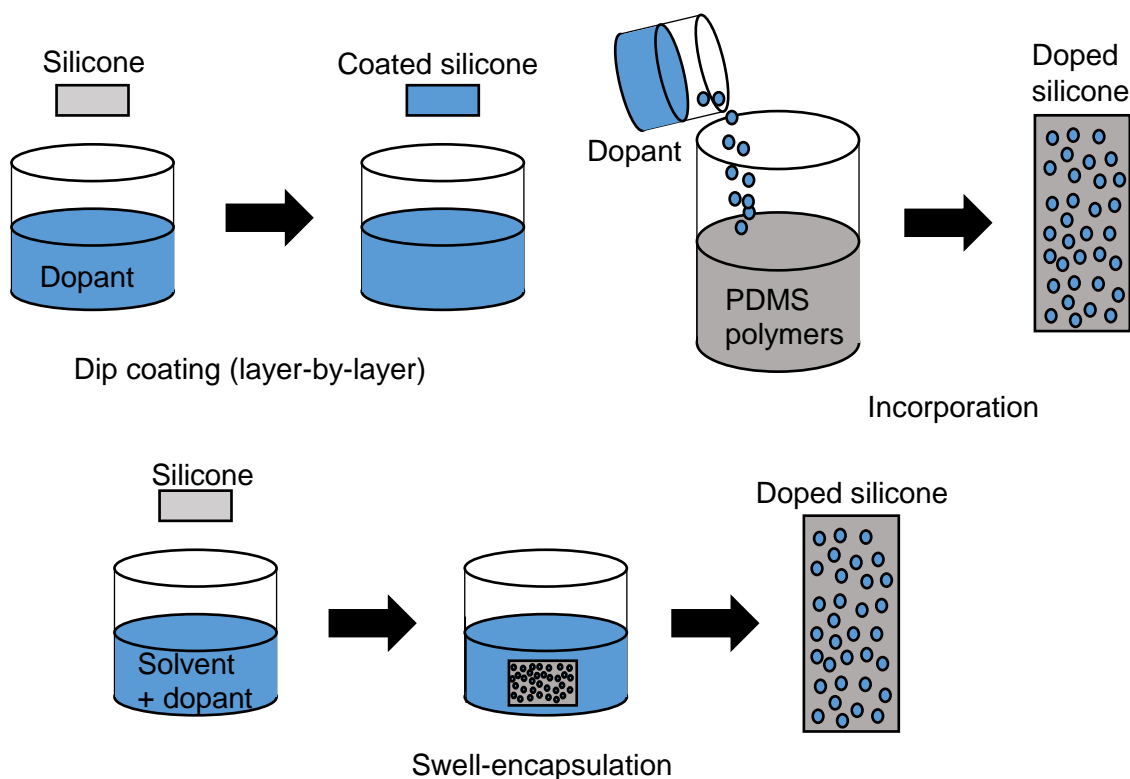


**Figure 1.** Physical doping methods employed to prepare doped silicones: layer-by-layer dip coating, incorporation, and swell-encapsulation.

The preparation of silicone rubber often involves a catalysed reaction of terminal functionalised polydimethylsiloxanes (PDMS) and a crosslinking agent. Silicone rubbers are exceptional materials suitable for use as medical devices due to their high strength, and the large range of favourable properties such as elasticity and hardness available.<sup>1</sup> Silicone rubbers, as with many other medical devices, suffer due to colonisation of pathogenic microorganisms.<sup>2-5</sup> One method for preventing this colonisation is the incorporation of antimicrobial agents into silicone.<sup>6-8</sup> This has been achieved by various methods which may be split into physical functionalisation and chemical functionalisation. One physical method is the layer-by-layer approach: where a surface is coated by a thin film of active material that may then have a second layer added that adheres by electrostatic interactions or hydrogen bonding.<sup>9-11</sup> Layer-by-layer functionalisation is achieved by dip, spin, or spray coating. Another method is the incorporation of antimicrobial agents into the bulk of the material, so that the antimicrobial agent is slowly released over time through diffusion-controlled release.<sup>12-15</sup> As with the layer-by-layer method, the incorporation method for the inclusion of antimicrobial agents

in silicone is a physical rather than a chemical process, involving just intermolecular interactions such as van der Waals forces and hydrogen bonding, and involves the addition of the antimicrobial agent into the liquid polymers before the curing of the silicone takes place.<sup>16</sup> The third commonly employed physical method for producing doped silicones is swell-encapsulation, where a cured silicone rubber is dipped into an antimicrobial-enriched solvent which can swell the silicone matrix. The solvent is then left to evaporate, at which point the silicone returns to its original size encapsulating the antimicrobial agent.<sup>17-19</sup> Chemical doping of silicones may be achieved in a number of ways dependent on the functionalities introduced to the PDMS/silicone rubber and the functionalities on the antimicrobial agent. Silicone rubbers have been doped chemically with antimicrobial agents by hydrosilylation,<sup>20</sup> ring-opening polymerisation (ROP),<sup>21</sup> condensation,<sup>22</sup> plasma treatment,<sup>23</sup> as well as producing antimicrobial silicone copolymers.<sup>24</sup>

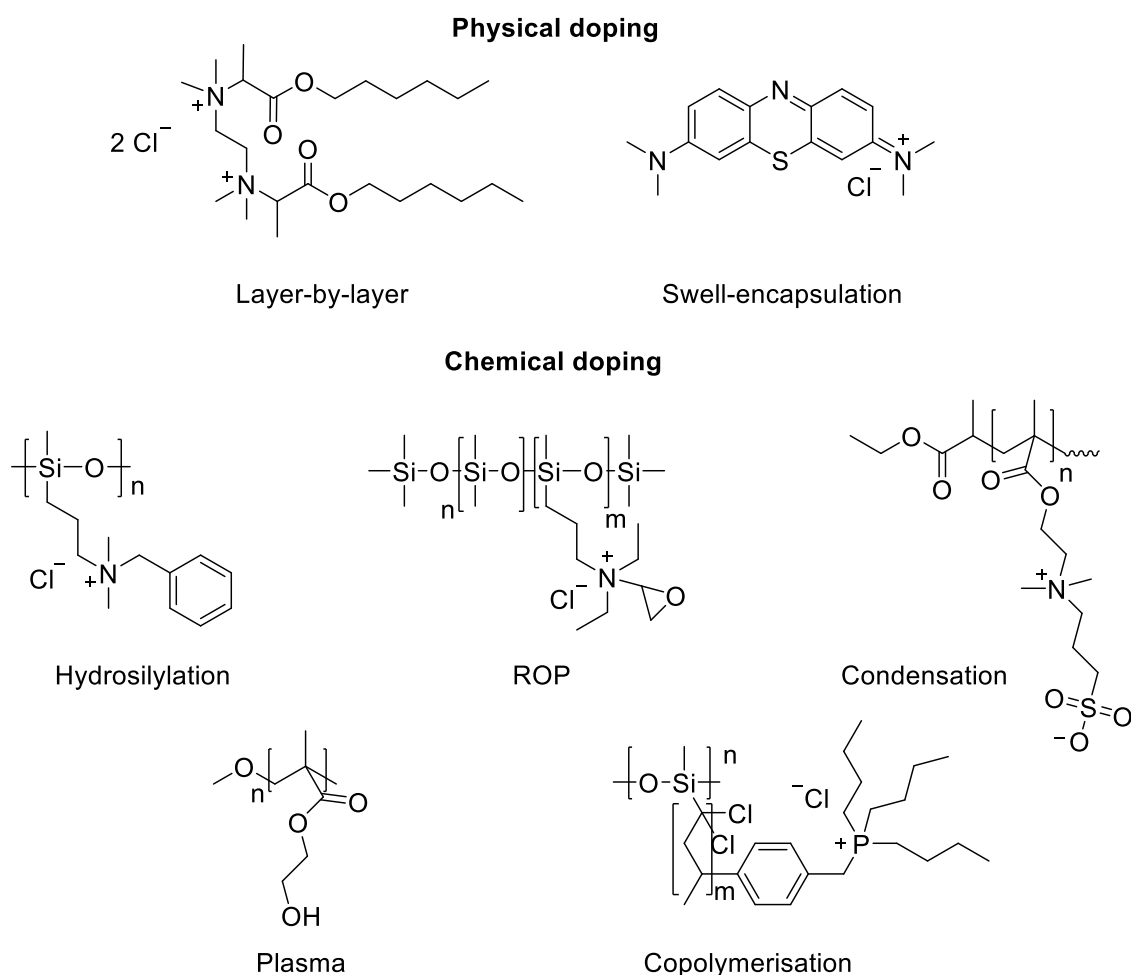


**Figure 2.** Antimicrobial agents incorporated into silicone rubber by layer-by-layer addition,<sup>11</sup> swell-encapsulation,<sup>17</sup> hydrosilylation,<sup>20</sup> ROP,<sup>21</sup> condensation,<sup>22</sup> plasma treatment,<sup>23</sup> and copolymerisation.<sup>24</sup>

The incorporation method is simple to conduct, requiring less effort than chemical modification of the silicone, and require less specialised equipment needed than the layer-by-layer method. The incorporation method allows for more accurate addition of dopant than the layer by layer process or the swelling process as those methods rely on the addition of antimicrobial agent to cured silicone rubber. The work in this chapter is based on the incorporation method, examples of which will now be described in more detail.

A wide variety of antimicrobial agents have been incorporated into silicone, including: antimicrobial acryl monomers with a norfloxacin moiety into silicone azobisisobutyronitrile,<sup>25</sup> Ag, Ag-based zeolite, and piperazine-containing components,<sup>26</sup> benzoic acid and sodium benzoate,<sup>27</sup> filastatin,<sup>28</sup> miconazole and trimethylsilyl-nystatin,<sup>29</sup> cranberry derived materials,<sup>30</sup> and natamycin.<sup>31</sup> Silver in particular has been employed by a number of research groups, typically as nanoparticulate silver.<sup>32–36</sup> Attempts to improve the inherent antimicrobial activity of silver have been made, with examples such as the work by Gosau et al.,<sup>37</sup> where copper additives were used as a complement to the activity of silver.

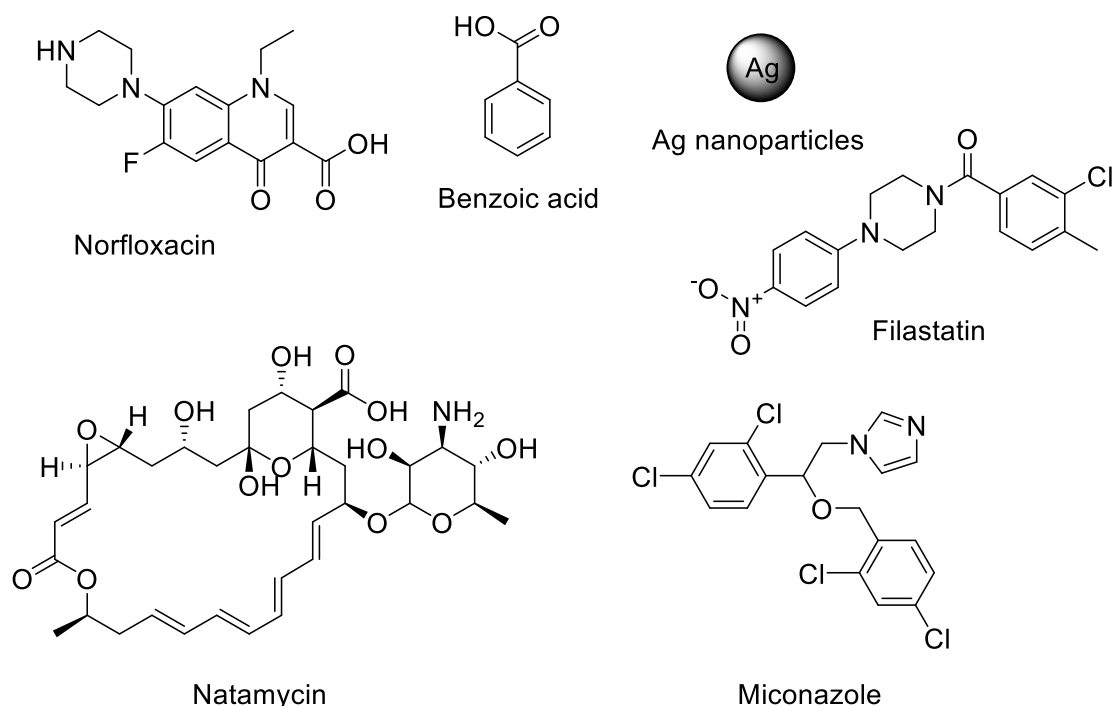


**Figure 3.** Antimicrobial agents incorporated into silicone. Norfloxacin,<sup>25</sup> benzoic acid,<sup>27</sup> Ag nanoparticles,<sup>36</sup> filastatin,<sup>28</sup> miconazole,<sup>29</sup> and natamycin.<sup>31</sup>

Work by Ghamrawi *et al.*<sup>38,39</sup> features the incorporation of cationic biocides: polyhexamethylene guanidine dodecylbenzenesulfonate (PHMG-DBS), 1-octyl-3-

methylimidazolium tetrafluoroborate (OMIM-BF<sub>4</sub>) and 1-dodecyl-3-methylimidazoliumtetrafluoroborate (DMIM-BF<sub>4</sub>). The silicones produced were PDMS-based with an ethyl silicate curing agent in the absence of a catalyst.<sup>38</sup> The cationic biocides were doped into the silicones at 2 and 5 wt% via the incorporation method via a room temperature condensation curing process. The antimicrobial properties afforded to the silicones by the dopants was assessed against a panel of 8 bacteria and 5 yeasts.

Species	Bacteria /yeast	Antibacterial activity (R (rounded))					
		PHMG-DBS 2%	PHMG-DBS 2%	OMIM-BF <sub>4</sub> 2%	OMIM-BF <sub>4</sub> 5%	DMIM-BF <sub>4</sub> 2%	DMIM-BF <sub>4</sub> 5%
<i>Staphylococcus aureus</i> ATCC 25923	Bacteria (+)	3	3	3	3	3	3
<i>Staphylococcus epidermidis</i> DSM 18857	Bacteria (+)	3	3	3	3	3	3
<i>Escherichia coli</i> ATCC 8739	Bacteria (-)	4	5	5	5	5	5
<i>Pseudomonas aeruginosa</i> ATCC 25375	Bacteria (-)	1	5	1	1	5	5
<i>Enterobacter cloacae</i> DSM 30054	Bacteria (-)	7	7	5	7	7	7
<i>Enterococcus faecalis</i> ATCC 29212	Bacteria (+)	1	3	1	4	3	4
<i>Klebsiella pneumonia</i> DSM 16609	Bacteria (-)	<1	4	3	3	5	5
<i>Acinetobacter baumannii</i> ATCC 19606	Bacteria (-)	5	5	1	5	5	5
<i>Candida albicans</i> IHEM 14796	Yeast	4	5	1	3	5	5
<i>Candida glabrata</i> IHEM 9556	Yeast	4	4	1	3	4	4
<i>Candida krusei</i> IHEM 14534	Yeast	5	5	3	2	5	5
<i>Candida parapsilosis</i> IHEM 4223	Yeast	2	4	1	3	4	4
<i>Candida tropicalis</i> IHEM 21234	Yeast	3	4	1	2	4	4

**Table 1.** Antimicrobial activity (R) of different dopings of cationic biocide against Gram positive (+) and negative (-) bacteria and yeasts from the work of Ghamrawi et al.<sup>38</sup>

The antimicrobial activity was evaluated by an “R” value, a logarithmic scale measuring the decrease in viable bacterial or yeast cells based on enumeration of viable cells per cm<sup>2</sup> against a control silicone with no biocide. The most effective biocide employed was 2 wt% and 5 wt% DMIM-BF<sub>4</sub>, along with 5 wt% PHMG-DBS, which had R values of greater than 3 for all species tested. 5 wt% OMIM-BF<sub>4</sub> and 2 wt% PHMG-DBS were less effective, but still showed a >99.9% reduction in bacterial growth, whereas 2 wt% OMIM only had a 99% reduction in bacterial growth.

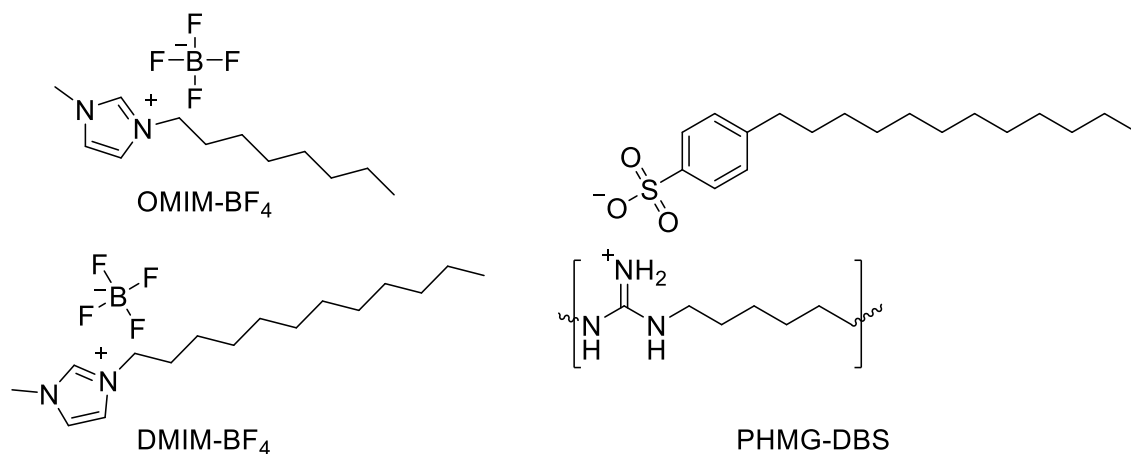


**Figure 4.** Compounds discussed in papers by Ghamrawi *et al.*<sup>27,28</sup>

The second paper by Ghamrawi *et al.*<sup>39</sup> employs the same procedure and dopant weights for preparation of the antimicrobial silicone, but this time discusses the antimicrobial activity afforded by the dopants against non-*Candida* fungi. The study focused on the resistance to colonisation by 8 species of filamentous fungi of the previously described doped silicones. Zones of inhibition are summarised in Table 2 below. The antimicrobial efficacy of the silicones was assessed by the Kirby Bauer disc diffusion method.<sup>29,40–47</sup> The results against filamentous fungi were different to those observed with bacteria and *Candida spp.* as 5 wt% PHMG-DBS provided the largest zones of inhibition with zones of inhibition that measure ≥20 mm against all filamentous fungi. The next most effective doped silicone was 2 wt% PHMG-DBS. The PHMG-DBS-doped silicones were the only ones to show any zone of inhibition against *T. reesei*. This highlights the effectiveness of PHMG-DBS against filamentous fungi, as 2 wt% PHMG-DBS had larger zones of inhibition than either of the silicones with 5 wt% imidazolium salt. The least effective were OMIM-BF<sub>4</sub>-doped silicones, with only the 5 wt% OMIM-BF<sub>4</sub> showing small zones of inhibition against *T. pinophilus* and *P. chrysogenum*. The zones observed for DMIM-BF<sub>4</sub>-doped silicones were moderate in size, and only reached zones of greater than 20 mm for both weights against *B. spectabilis*, and greater than 20 mm against *T. pinophilus*. In

all cases the antimicrobial efficacy of the silicones increased with increased dopant weight.

Species	Zone of inhibition (mm)					
	PHMG-DBS 2%	PHMG-DBS 2%	OMIM-BF <sub>4</sub> 2%	OMIM-BF <sub>4</sub> 5%	DMIM-BF <sub>4</sub> 2%	DMIM-BF <sub>4</sub> 5%
<i>Alternaria alternata</i> IHEM 18586	6.7 ± 11.5	24.7 ± 3.8	0	0	13.3 ± 11.5	1.7 ± 2.9
<i>Aspergillus niger</i> IHEM 5296	20.0	20.0	0	0	2.7 ± 4.6	6.7 ± 5.5
<i>Byssochlamys spectabilis</i> CBS 628.66	20.0	24.7 ± 0.6	0	0	20.0	29.3 ± 0.6
<i>Cladosporium sphaerospermum</i> IHEM 18883	22 ± 1.0	25.7 ± 0.6	0	0	3.3 ± 5.8	13.3 ± 11.5
<i>Penicillium chrysogenum</i> IHEM 20859	24 ± 1.0	27 ± 1.7	0	1.0	0	11.7 ± 2.1
<i>Stachybotrys chartarum</i> IHEM 20352	14 ± 12.3	25.7 ± 0.6	0	0	0	2.3 ± 4.0
<i>Talaromyces pinophilus</i> IHEM 5847	20.0	28 ± 2.6	0	6.7 ± 11.5	17.3 ± 2.1	24.7 ± 1.7
<i>Trichoderma reesei</i> IHEM 5651	22.3 ± 0.6	21.7 ± 1.5	0	0	0	0

**Table 2.** Antibacterial activities of cationic biocide-doped silicones against filamentous fungi.<sup>39</sup>

Although the increase of dopant weight increases the antimicrobial activity of doped silicones, the effects of increasing the dopant weight on the silicone material's other properties should be considered. The addition of a greater weight of dopant may effect the elongation at breakage, tensile strength, tear resistance, and surface roughness of a material, among other properties, and may therefore affect the material's suitability for use in certain applications. A current example from the literature where the physical properties of doped silicone materials prepared by the incorporation method comes from the work of Herla *et al.*<sup>48</sup> Two different types of soft denture liner were doped with chitosan salts: chitosan hydrochloride and chitosan glutamate at weights of 0.1 wt%, 0.2 wt%, 0.4 wt%, and 1 wt%. Chitosan salts have been shown to have been shown to have antimicrobial effects against Gram positive and Gram negative bacteria, as well as fungi, and are therefore suitable dopants for producing antimicrobial materials. The study tested two physical properties: Shore A hardness, and surface roughness. It was shown that the Shore A hardness of the material was not affected by increasing weight of

dopant, whereas the surface roughness was impacted negatively, producing a more rough surface. The Shore hardness was assessed by use of a durometer, as standard, whereas the roughness was assessed by contact profilometry. The surface roughness typically increased with increased dopant weight. This suggests certain physical properties are more affected by the addition of dopants than others.

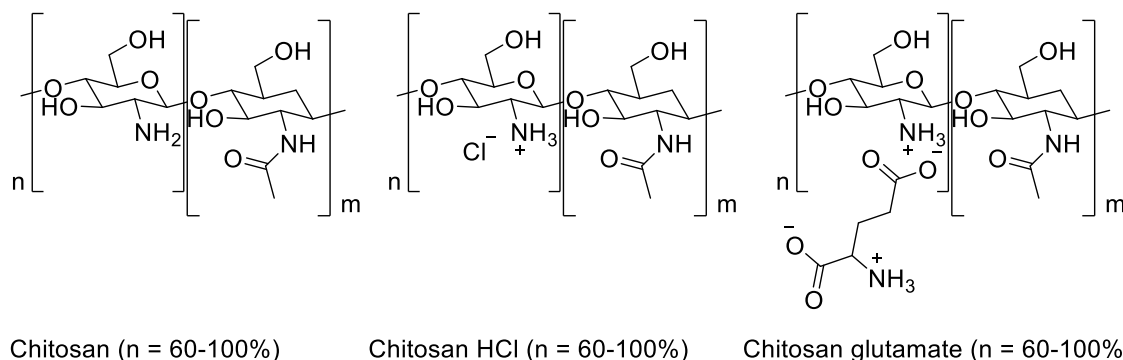


**Figure 5.** Chitosan-based dopants employed by Herla et al.<sup>48</sup> to form antimicrobial soft silicones.

Another article in the recent literature focuses on the incorporation of fucose-functionalised silver nanoparticles into the matrix of silicone rubber in order to provide urinary catheters with a resistance to colonisation by the multidrug resistant *Pseudomonas aeruginosa*.<sup>49</sup> Fucose-functionalised silver nanoparticles were chosen due to the known efficacy of silver nanoparticles against *P. aeruginosa*, and the decrease in biofilm viability observed when treated with fucose-functionalised silver nanoparticles by comparison with bare silver nanoparticles by promoting increased formation of reactive oxygen species (ROS) within the bacteria. The incorporation of fucose-functionalised nanoparticles into model urinary catheters was observed to decrease the colonisation of the silicone by *P. aeruginosa* significantly by comparison with the blank and control non-functionalised silver nanoparticle-doped silicone by SEM.

### Triclosan silicones

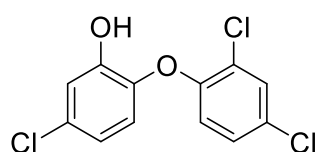


**Figure 6.** The structure of the antimicrobial agent Triclosan.

Triclosan is a common antimicrobial agent, and is found in toothpaste, soaps, and detergents, as well as a number of other domestic and medical applications.<sup>50–52</sup> It is a phenyl ether with sparing solubility in water, and it freely soluble in organic solvents. The

first reported use of triclosan as an antimicrobial agent for medical silicones was reported in 2003 by Stickler *et al.*,<sup>53</sup> where triclosan was loaded as a 10 g/L solution in 5% weight/volume polyethylene glycol into the balloon of a Foley catheter in order to allow for the triclosan to diffuse through the silicone of the catheter. The test catheter and a control consisting of a Foley catheter where the balloon was loaded with water were infected with a 4 h urine culture of *Proteus mirabilis*, and a cross-section of the catheter incubated overnight on tryptone soy agar plates inoculated with *P. mirabilis*. The incubated catheters were then examined by SEM. The control showed a clear blockage due to biofilm formation, whereas the triclosan-treated catheter was shown to resist catheter colonisation for at least 7 days without visible biofilm development. Triclosan is able to control the urinary pH,<sup>54</sup> stopping the increase in pH that leads to encrustation of the catheter due to precipitation of magnesium and calcium phosphates.<sup>55–59</sup> It was also found that the triclosan becomes impregnated throughout the catheter, leading to complete inhibition of crystalline biofilm formation. The *in situ* model appeared to retain triclosan within the catheter for at least 7 days.

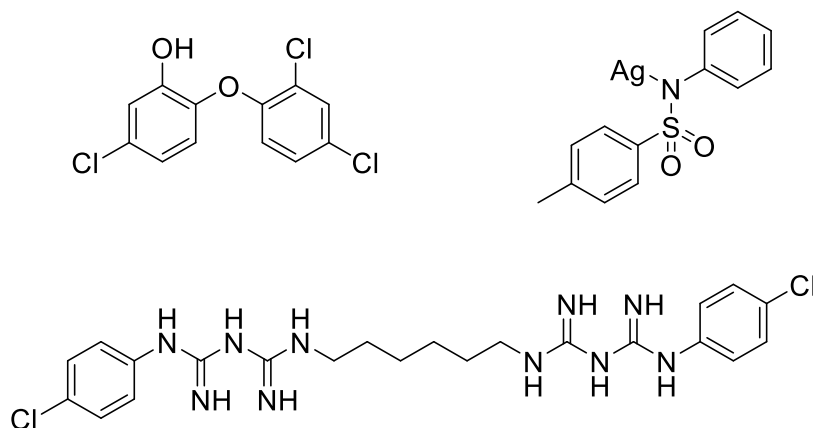


**Figure 7.** Compounds doped into silicone by Modak *et al.*<sup>39</sup> including: triclosan, silver sulfadiazene, and chlorhexidine.

Work in 2003 by Modak *et al.*<sup>60</sup> focused on the impregnation of model catheters with antimicrobial agents, employing a cocktail of triclosan, silver sulfadiazine, and chlorhexidine. The antimicrobial activity of these compounds was assessed by the Kirby Bauer disk diffusion test. Three samples were prepared as chlorhexidine and silver sulfadiazine-doped catheter, chlorhexidine, silver sulfadiazine, and triclosan-doped catheter, as well as a commercially available nitrofurazone-doped catheter test materials. The antimicrobial susceptibility of a number of organisms was tested, including: *S. aureus*, *S. epidermidis*, *E. coli*, *E. faecalis*, *P. aeruginosa*, *C. albicans*, as well as clinical isolates of Methicillin-resistant *Staphylococcus aureus* (MRSA),

Vancomycin-resistant *Enterococcus faecium* (VREF), *P. mirabilis*, *Enterobacter aerogens*, and *K. pneumoniae*. The antimicrobial efficacy of these silicones is summarised in Table 3. The mean zone of inhibition for the silver hydrogel-doped silicone was unobservable in most cases due to resistance by the test bacteria. The two component-doped catheter had a mean effective zone of inhibition between 1.5-8.5 mm against all organisms. The addition of triclosan to form a three component-doped catheter increased the mean zone of inhibition against most organisms, with zones of 4-18.6 mm observed, with only the zone of inhibition of VREF remaining the same as with the two component-doped catheter. This enhanced antimicrobial efficacy against most species suggests the suitability of triclosan as a broad-spectrum dopant in the production of microbial colonisation-resistant silicone materials.

	Zone of inhibition (mm)		
	Chlorhexidine + silver sulfadiazine	Chlorhexidine + silver sulfadiazine + triclosan	Nitrofurazone
<b>Uropathogen</b>			
<i>S. aureus</i>	6	13	11.5
<i>S. epidermidis</i>	8.5	18.6	17.5
<i>E. coli</i>	5	9.3	12.2
<i>E. faecalis</i>	3.7	3.5	0
<i>P. aeruginosa</i>	5.2	6.4	0
<i>C. albicans</i>	6.3	7.6	0
<b>Clinical isolate</b>			
MRSA	7.2	13.6	13
VREF	4	4	0
<i>P. mirabilis</i>	5.5	9	0
<i>E. aerogenes</i>	1.5	7.3	8
<i>K. pneumoniae</i>	4.3	9.8	9

**Table 3.** Zones of inhibition recorded by doped silicone catheters from the work of Modak *et al.*<sup>60</sup>

McBride *et al.*<sup>61</sup> reported the incorporation of triclosan into silicones by combining the triclosan and the silicone elastomer before curing. The study also featured a triclosan-doped silicone modified by polyethylene glycol allyl methyl ether (AMPEG), in an attempt to alter the release rate of triclosan from the silicone matrix. Triclosan was doped into silicone at 0.1, 0.25, 0.50, 0.75, 1.0 wt%. The rate of release was found to increase relative to the wt% doping, with a greater wt% releasing more triclosan cm<sup>-2</sup>day<sup>-0.5</sup>. Triclosan-doped silicone was seen to resist *S. epidermidis* colonisation after 24 hours at concentrations of 0.25 wt% or greater, whereas a concentration of 1 wt% was needed to resist colonisation by *E. coli* after 24 hours. The release rate of 1 wt% triclosan from doped silicone and doped silicone modified with 2 and 4 wt% AMPEG was also



form the titanium coated poly(N-hydroxyethylactylamide) “brushes”. Triclosan was then grafted to these brushes by the 1:1 reaction of triclosan with oxalyl chloride to form the triclosan oxalyl chloride ester, which was then subsequently reacted in situ with the poly(N-hydroxyethylactylamide) “brushes” to form a triclosan-ester-modified silica-based surface. Then, in 2019, Xie *et al.*<sup>70</sup> reported the first application of triclosan ester polymerised into silicone rubber to be applied to marine anti-biofouling. PFTA telomeres consisting of 4:4:1 dodecafluoroheptyl methacrylate (DFMA), triclosan acrylate, and 3-mercaptopropyl trimethoxysilane (KH590) were synthesised in an inert atmosphere by radical polymerisation catalysed by azobisisobutyronitrile (AIBN). These PFTA telomeres were then mixed with bis-silanol terminated PDMS and condensation cured with a tin catalyst. Samples containing 4, 8, and 12 wt% PFTA telomeres were prepared, as well as silicones with telomeres containing no triclosan acrylate, and control silicones with no grafted telomeres. The antimicrobial activity of the silicones produced were tested against *P. aeruginosa* via antibiofilm formation test by submerging silicones in a *P. aeruginosa* inoculated broth, washing away unattached organisms, staining the attached biofilm with crystal violet, then measuring absorbance at 589 nm . It was found that triclosan ester doped silicones visually were stained much less than silicones lacking triclosan ester. The absorbance values for PFTA telomere-doped silicone also showed a much lower absorbance at 589 nm than non-triclosan ester-doped silicones. This suggests a much lower concentration of *P. aeruginosa* biofilm present on the surface of triclosan ester-doped silicones.

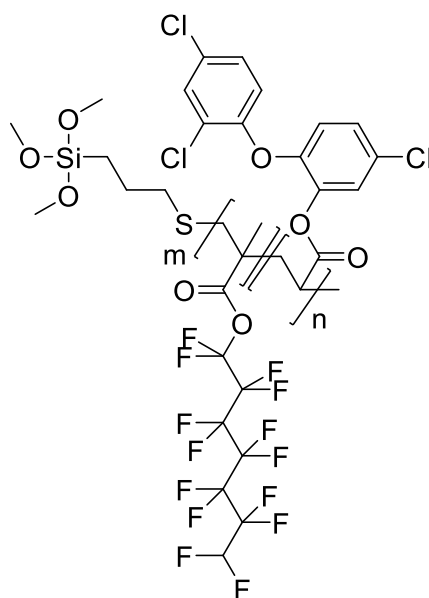


**Figure 9.** Siloxane-based triclosan ester reported by Xie *et al.*<sup>70</sup>

## **Aims**

The aim of this chapter is to produce a novel silicone rubber formulation suitable for use as a material to produce medical devices. The physical properties of this silicone will be tested to determine its suitability for medical applications. The silicone rubber produced will be doped with a variety of dopants ranging from triclosan and its esters to successful antimicrobial agents previously described (see previous chapters) in order to produce antimicrobial silicone materials resistant to bacterial colonisation. The effects of doping the silicone rubber formulation with antimicrobial agents on the physical properties of the silicone will be investigated, as well as the antimicrobial efficacy of the novel materials against a range of Gram positive and Gram negative organisms.

## Experimental

All compounds used were commercial grade and used as provided unless stated otherwise.  $^1\text{H}$ -NMR and  $^{13}\text{C}\{^1\text{H}\}$ -NMR spectra were recorded in  $\text{CDCl}_3$  using Bruker Ultrashield FT-NMR spectrometers with a field strength of either 400 or 300 MHz. Spectra were analysed by MestReNova software version 6.0.2-5475 and digitally referenced to the residual solvent signal. Low and high resolution mass spectra were produced on a Waters LCT Premier XE spectrometer by Cardiff University School of Chemistry Analytical Services. Infra-red spectra were recorded using a Shimadzu IR-Affinity-1S FTIR.

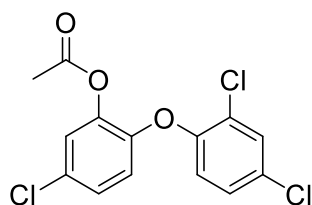
Silicone rubber production and associated physical testing was conducted at Technovent Ltd, Bridgend, UK with the kind permission of Professor Mark Waters. M511 Rubber HEAT Platinum Catalyst Concentrate was prepared by staff at Technovent Ltd. Mechanical testing was conducted using a Mecmesin MultiTest-d motorised test stand equipped with a Mecmesin AFG 500N digital force gauge. The Shore A Hardness of TM1 samples was measured according to ASTM D 2240-2005 method using a Rex H-1000 Mini-Dial durometer (Shore A). Scanning Electron Microscopy (SEM) was conducted with a Tescan MAIA3 field emission gun scanning electron microscope equipped with an Oxford Instruments X-ray MaxN 80 detector. Test silicones were mounted on adhesive carbon tape. Silicone samples were sputter coated with Au/Pd in order to help prevent charging on the sample surface. GC-MS analysis was conducted using a Waters GCT Time of flight mass spectrometer (TOF) with an Agilent 6980 GC interface. 5  $\mu\text{L}$  of sample was added using a split/splitless inlet with 20% split with a 190  $^\circ\text{C}$  inlet temperature. The temperature was programmed to 40  $^\circ\text{C}$ , and the temperature held for 5 minutes. The temperature was then ramped at a rate of 5  $^\circ\text{C}/\text{min}$  until 300  $^\circ\text{C}$ , then held at the maximum temperature for 5 minutes. A 30 m, 35% phenyl, 65% methyl polysiloxane capillary column was used in order to distinguish the sample's constituent parts. The system was calibrated using heptacosafuorotributylamine. The limit of detection of the apparatus was determined using an EPA Volatile Organic Compounds Mix 2, and found to be between 1 to 5  $\mu\text{g}/\text{mL}$ .

Broths and agars were supplied by Fisher. The bacteria used to conduct testing were reference strains: *Staphylococcus epidermidis* (ATCC 35984/RP62A), *Staphylococcus epidermidis* (ATCC 14990), *Staphylococcus aureus* (NCTC 6571), *Staphylococcus aureus* (NCIMB 9518), *Pseudomonas aeruginosa* (ATCC 15692), *Escherichia coli* (NCTC 12923). Stock cultures were maintained on Microbank™ plastic beads at -80  $^\circ\text{C}$ . Working cultures were maintained on tryptone soy agar (TSA, Sigma Aldrich) at 4  $^\circ\text{C}$ .

Before each experiment, a single colony was transferred to 10 mL of Mueller-Hinton broth (MHB) and incubated at 37 °C overnight. The concentrated inoculum was diluted approximately 1:10 in fresh broth to produce a suspension with equivalent turbidity to a 0.5 MacFarland standard (absorbance of 0.08 - 0.1 at 600 nm ( $\sim 1 \times 10^8$  CFU/mL)) using a micro spectrophotometer. The standardised solution was then diluted 1:100 to produce a test inoculum containing  $\sim 1 \times 10^6$  CFU/mL.

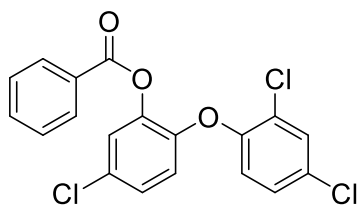
Please see previous chapters for the synthesis of: 3-dodecyl-1-methylbenzimidazolium bromide, 3-dodecyl-1-methylimidazolium bromide, 3-dodecyl-1-methylbenzimidazol-2-ylidene silver(I) bromide, 3-dodecyl-1-methylimidazol-2-ylidene silver(I) bromide, CuGTSB, CuGTSH, and CuGTSO.

### Synthesis of triclosan acetate



Triclosan (16.21 g, 56 mmol) and acetic anhydride (7 mL, 74 mmol) were added to cold pyridine (100 mL). The mixture was then stirred at room temperature for 24 hours. Ice (300 mL) was then added producing a white precipitate. The mixture was then placed in a refrigerator, and the ice was allowed to melt. The white precipitate was then collected on a Büchner funnel. The solid was then recrystallized from hot methanol to produce white needles of triclosan acetate (5-chloro-2-(2,4-dichlorophenoxy)phenyl acetate) (15.46 g, 83%). **<sup>1</sup>H-NMR** (400 MHz, CDCl<sub>3</sub>, 298K):  $\delta$  (ppm): 7.35 (s, 1H, aromatic), 7.07 (m, 3H, aromatic), 6.75 (m, 2H, aromatic), 2.12 (s, 3H, CH<sub>3</sub>). **<sup>13</sup>C-NMR** (101 MHz, CDCl<sub>3</sub>, 298K):  $\delta$  (ppm): 168.34 (OCOCH<sub>3</sub>), 151.05, 146.79, 141.79, 130.45, 129.60, 129.28, 128.24, 127.05, 126.02, 124.49, 120.51, 120.22, 20.48 (CH<sub>3</sub>). **MS(ESI)** 330.96 [M<sup>+</sup> + H<sup>+</sup>]. This matches data reported by Lourens.<sup>71</sup>

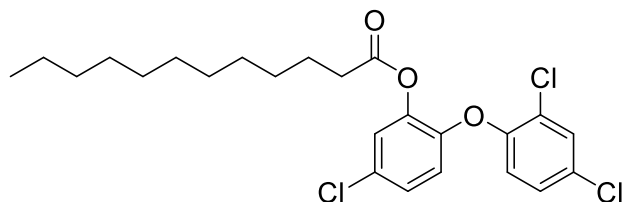
### Synthesis of triclosan benzoate



Triclosan (16.21 g, 56 mmol) was dissolved in cold pyridine (100 mL). Benzoic anhydride (16.7 g, 74 mmol) was then added, and the mixture was allowed to warm up to room

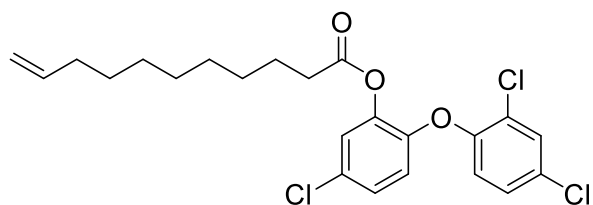
temperature. The mixture was then stirred for 24 hours. Ice (300 mL) was then added, and the mixture was placed in a refrigerator. Once all the ice had melted the remaining solid was separated by filtration. The crude white powder was recrystallized from minimal hot methanol to yield the product, triclosan benzoate (5-chloro-2-(2,4-dichlorophenoxy)phenyl benzoate) (20.67 g, 94%). **<sup>1</sup>H-NMR** (400 MHz, CDCl<sub>3</sub>, 298K): δ (ppm): 8.05 (m, 2H, aromatic), 7.62 (m, 1H, aromatic), 7.46 (m, 2H, aromatic), 7.34 (m, 2H, aromatic), 7.22 (m, 1H, aromatic), 7.16 (m, 1H, aromatic), 6.91 (m, 2H, aromatic). **<sup>13</sup>C-NMR** (101 MHz, CDCl<sub>3</sub>, 298K): δ (ppm): 164.18 (OCO), 151.26, 146.97, 142.01, 134.05, 130.45, 130.38, 129.55, 129.45, 128.68, 128.54, 128.21, 127.19, 126.09, 124.80, 120.55, 120.52. **MS (ESI)** 414.97 [M + Na<sup>+</sup>]. This matches data reported by Model and Bindler.<sup>72</sup>

### Synthesis of triclosan laurate



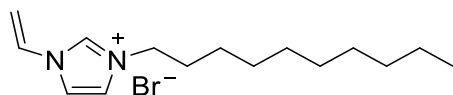
Triclosan (16.21 g, 56 mmol) was added to cold pyridine (100 mL) followed by lauroyl chloride (16.18 mL, 70 mmol). The mixture was then allowed to stir for 24 hours. HCl solution (1M, 50 mL) was added to the reaction and stirred briefly before the addition of dichloromethane (40 mL). The organic layer was then removed, and the aqueous layer further extracted with dichloromethane (2 x 30 mL). The organic extracts were washed with brine (50 mL), then further dried over sodium sulphate. The sodium sulphate was then removed by filtration, and the solvent reduced under reduced pressure. The concentrate was then purified by column chromatography to yield the purified product as an oil. Triclosan laurate (5-chloro-2-(2,4-dichlorophenoxy)phenyl dodecanoate) (22.26 g, 84%). **<sup>1</sup>H-NMR** (300 MHz, CDCl<sub>3</sub>, 298K): δ (ppm): 7.45 (m, 1H, aromatic), 7.19 (m, 2H, aromatic), 7.15 (m, 1H, aromatic), 6.85 (m, 1H, aromatic), 2.47 (t, 2H, <sup>3</sup>J = 7.1 Hz, (CO)CH<sub>2</sub>), 1.64 (m, 2H, (CO)CH<sub>2</sub>CH<sub>2</sub>), 1.27 (m, 16H, CH<sub>2</sub>), 0.88 (t, 3H, <sup>3</sup>J = 6.3 Hz, CH<sub>2</sub>CH<sub>3</sub>). **<sup>13</sup>C-NMR** (101 MHz, CDCl<sub>3</sub>, 298K): δ (ppm): 171.20 (OCO), 151.13, 146.61, 142.01, 130.38, 129.37, 129.36, 128.13, 126.90, 125.79, 124.51, 120.34, 120.12, 33.88 (CH<sub>2</sub>), 31.94 (CH<sub>2</sub>), 29.63 (CH<sub>2</sub>), 29.61 (CH<sub>2</sub>), 29.44 (CH<sub>2</sub>), 29.35 (CH<sub>2</sub>), 29.24 (CH<sub>2</sub>), 28.97 (CH<sub>2</sub>), 24.82 (CH<sub>2</sub>), 22.71 (CH<sub>2</sub>), 14.14 (CH<sub>3</sub>). **MS (ESI)** 471.12 [M<sup>+</sup>]. This matches data reported by Ochs et al.<sup>73</sup>

### Synthesis of triclosan undecenoate



Undec-10-enoic acid (18.4 g, 100 mmol) and thionyl chloride (20 mL, 270 mmol) were mixed together and refluxed for 4 hours under a nitrogen atmosphere. The reaction was allowed to cool to room temperature, then excess thionyl chloride was removed under reduced pressure (CAUTION!). The resultant brown oil was dissolved in cold pyridine (100 mL). Triclosan (16.21 g, 56 mmol) was added to the pyridine solution, and the mixture was allowed to stir for 24 hours at room temperature. The mixture was then diluted with HCl solution (1M, 50 mL) and extracted with dichloromethane (100 mL). The dichloromethane was concentrated under reduced pressure. The product was then purified by column chromatography. Triclosan undecenoate (5-chloro-2-(2,4-dichlorophenoxy)phenyl undec-10-enoate) was yielded as a pale yellow oil (16.94 g, 66%). **<sup>1</sup>H-NMR** (300 MHz, CDCl<sub>3</sub>, 298K): δ (ppm): 7.31 (m, 1H, aromatic), 7.04 (m, 3H, aromatic), 6.70 (m, 2H, aromatic), 5.68 (m, 1H, H<sub>2</sub>C=CHCH<sub>2</sub>), 4.85 (m, 2H, H<sub>2</sub>C=CHCH<sub>2</sub>), 2.35 (t, 2H, <sup>3</sup>J = 7.4 Hz, (CO)CH<sub>2</sub>), 1.91 (m, 2H, H<sub>2</sub>C=CHCH<sub>2</sub>), 1.52 (m, 2H, (CO)CH<sub>2</sub>CH<sub>2</sub>), 1.20 (m, 10H, CH<sub>2</sub>). **<sup>13</sup>C-NMR** (75 MHz, CDCl<sub>3</sub>, 298K): δ (ppm): 180.01, 171.26 (OCO), 151.09, 146.58, 141.95, 139.18, 130.35, 129.35, 128.14, 126.93, 125.75, 124.48, 120.34, 120.12, 114.20 (H<sub>2</sub>C=CHCH<sub>2</sub>), 33.80 (CH<sub>2</sub>), 29.26 (CH<sub>2</sub>), 29.17 (CH<sub>2</sub>), 29.06 (CH<sub>2</sub>), 28.90 (CH<sub>2</sub>), 24.79 (CH<sub>2</sub>). **HRMS (ES+)** found m/z 455.0948, calculated m/z 455.0948 for [C<sub>23</sub>H<sub>26</sub>O<sub>3</sub>Cl<sub>3</sub>] (M<sup>+</sup>) (±0.00 ppm).

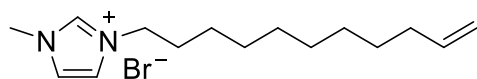
### Synthesis of 3-decyl-1-vinylimidazolium bromide



1-vinylimidazole (1.35 mL, 14.9 mmol) and 1-bromodecane (3.1 mL, 14.9 mmol) were added to acetonitrile (10 mL). The mixture was then refluxed overnight. The acetonitrile was then removed *in vacuo* to yield the product as a crude oil. The crude oil was triturated with hexane in order to remove any remaining impurities, yielding pure 3-decyl-1-vinylimidazolium bromide as an oil (4.36 g, 89%). **<sup>1</sup>H-NMR** (400 MHz, CDCl<sub>3</sub>, 298K): δ (ppm): 10.47 (s, 1H, NCHN), 7.94 (d, 1H, <sup>4</sup>J = 1.8 Hz, NCHCHN), 7.56 (d, 1H, <sup>4</sup>J = 1.7 Hz, NCHCHN), 7.23 (dd, <sup>3</sup>J = 15.7 Hz, <sup>3</sup>J = 8.7 Hz, HHC=CHN), 5.86 (dd, 1H, <sup>3</sup>J = 15.7, <sup>2</sup>J = 2.9 Hz, trans HHC=CHN), 5.12 (dd, 1H, <sup>3</sup>J = 8.7, <sup>2</sup>J = 2.9 Hz, cis HHC=CHN), 4.17

(t, 2H,  $^3J = 7.4$  Hz,  $\text{NCH}_2$ ), 1.70 (m, 2H,  $\text{NCH}_2\text{CH}_2$ ), 0.98 (m, 14H,  $\text{CH}_2$ ), 0.60 (t, 3H,  $^3J = 6.8$  Hz,  $\text{CH}_2\text{CH}_3$ ).  $^{13}\text{C-NMR}$  (101 MHz,  $\text{CDCl}_3$ , 298K):  $\delta$  (ppm): 134.81 (NCHN), 127.76 ( $\text{H}_2\text{C}=\text{CHCH}_2$ ), 122.55 (NCHCHN), 119.38 (NCHCHN), 109.17 ( $\text{H}_2\text{C}=\text{CHCH}_2$ ), 49.80 ( $\text{NCH}_2$ ), 31.24 ( $\text{NCH}_2\text{CH}_2$ ), 29.71 ( $\text{CH}_2$ ), 28.87 ( $\text{CH}_2$ ), 28.80 ( $\text{CH}_2$ ), 28.65 ( $\text{CH}_2$ ), 28.43 ( $\text{CH}_2$ ), 25.64 ( $\text{CH}_2$ ), 22.06 ( $\text{CH}_2$ ), 13.54 ( $\text{CH}_3$ ). **MS (ESI)** 235.22 [ $\text{M}^+ - \text{Br}^-$ ]. This matches data reported by El Seoud *et al.*<sup>74</sup>

### Synthesis of 1-methyl-3-(undec-10-en-1-yl)imidazolium bromide



1-methylimidazole (5.28 g, 64.3 mmol), and undec-10-enyl bromide (15.00 g, 64.3 mmol) were added to a round bottom flask and refluxed for 72 hours to produce a viscous orangey-brown oil. The oil was cooled at  $-20$  °C overnight, to give crude 1-methyl-3-(undec-10-en-1-yl)imidazolium bromide as a dark orange solid, which was then triturated with hexane. The product was yielded as soft dark orange crystals in a viscous dark orange oil. The crystals melted back to oil when removed from the surrounding oil. 1-methyl-3-(undec-10-en-1-yl)imidazolium bromide (20.28 g, quant.).  $^1\text{H-NMR}$  (400 MHz,  $\text{CDCl}_3$ , 298K):  $\delta$  (ppm): 10.10 (s, 1H, NCHN), 7.59 (t, 1H,  $^4J = 1.7$  Hz, NCHCHN), 7.40 (t, 1H,  $^4J = 1.7$  Hz, NCHCHN), 5.62 (ddt,  $^3J = 16.9$  Hz,  $^3J = 10.2$  Hz,  $^3J = 6.7$  Hz,  $\text{CH}_2\text{CH}=\text{CH}_2$ ), 4.81 (m, 1H,  $^3J = 17.1$  Hz, trans  $\text{HHC}=\text{CHCH}_2$ ), 4.74 (m, 1H,  $^3J = 10.2$  Hz, cis  $\text{HHC}=\text{CHCH}_2$ ), 4.16 (t,  $^3J = 7.4$  Hz, 2H,  $\text{NCH}_2$ ), 3.96 (s, 3H,  $\text{NCH}_3$ ), 1.85 (m, 2H,  $\text{CH}_2\text{CH}=\text{CH}_2$ ), 1.74 (t, 2H,  $^3J = 7.0$  Hz,  $\text{NCH}_2\text{CH}_2$ ), 1.13 (m, 12H,  $\text{CH}_2$ ).  $^{13}\text{C-NMR}$  (101 MHz,  $\text{CDCl}_3$ , 298K):  $\delta$  (ppm): 138.83 (NCHN), 136.80 ( $\text{CH}_2\text{CH}=\text{CH}_2$ ), 123.66 (NCHCHN), 121.90 (NCHCHN), 113.89 ( $\text{CH}_2\text{CH}=\text{CH}_2$ ), 49.79 ( $\text{NCH}_2$ ), 36.43 ( $\text{NCH}_3$ ), 33.45 ( $\text{CH}_2$ ), 30.05 ( $\text{CH}_2$ ), 29.00 ( $\text{CH}_2$ ), 28.71 ( $\text{CH}_2$ ), 28.67 ( $\text{CH}_2$ ), 28.54 ( $\text{CH}_2$ ), 25.93 ( $\text{CH}_2$ ). **MS (ESI)** 235.21 [ $\text{M}^+ - \text{Br}^-$ ]. This matches data reported by King *et al.*<sup>75</sup>

### Preparation of polymer bases

#### V46 polymer base

Hexamethyldisilazane-treated silica (448.8 g) was added slowly in 2 portions to DMS-V46 Vinyl Terminated Polydimethylsiloxane (1514 g, 60,000 sCt,  $117,000$  g  $\text{mol}^{-1}$ , 0.04-0.06 wt% vinyl). The components were mixed by hand until homogeneous. Silica (107.2 g) was added, and mixed by hand until homogeneous. The base mixture was then stirred mechanically for 2 hours using a mixer.

### V31 polymer base

Hexamethyldisilazane-treated silica (548.8 g) was added slowly in 2 portions to DMS-V31 Vinyl Terminated Polydimethylsiloxane (1514 g, 1,000 cSt, 28,000 g mol<sup>-1</sup>, 0.18-0.26 wt% vinyl). The components were mixed by hand until homogeneous. Silica (117.2 g) was added, and mixed by hand until homogeneous. The base mixture was then stirred mechanically for 2 hours using a mixer.

### V21 polymer base

Hexamethyldisilazane-treated silica (588.8 g) was added slowly in 2 portions to DMS-V21 Vinyl Terminated Polydimethylsiloxane (1514 g, 100 cSt, 6,000 g mol<sup>-1</sup>, 0.8-1.2 wt% vinyl). The components were mixed by hand until homogeneous. Silica (117.2 g) was added, and mixed by hand until homogeneous. The base mixture was then stirred mechanically for 2 hours using a mixer.

Commercial PDMS polymers used to prepare polymer bases are summarised below in Table 4.

PDMS polymer	Molecular weight (g mol <sup>-1</sup> )	Viscosity (cSt)	Vinyl content (wt%)
V46	117000	60000	0.04-0.06
V31	28000	1000	0.18-0.26
V21	6000	100	0.8-1.2

**Table 4.** Commercial PDMS polymers used to prepare silicone rubber base polymers.

### Polymer Base X

V21 polymer base (50 g) and V31 polymer base (150 g) was added to V46 polymer base (800 g). The mixture of bases was mixed by hand until evenly distributed, then stirred mechanically for 20 minutes until homogeneous.

### Preparation of silicone rubber “TM1”

RTV (Room-Temperature Vulcanizing) silicones are prepared by mixing a two-component system of base and curative (A + B). In the below described system, Part A corresponds to the Pt-containing curing agent, while Part B corresponds to the crosslinking component that provides the rigidity to the material once cured.

### TM1 Part A

M511 Rubber HEAT Platinum Catalyst Concentrate (40 g, Technovent Ltd.) was folded into Polymer Base X (360 g). The components were then mechanically mixed for 20 minutes.

### TM1 Part B

H-301 methylhydrosiloxane-dimethylsiloxane copolymer (40 g, trimethylsiloxane terminated, 25-35 cSt, 1,900-2000 g mol<sup>-1</sup>, 25-35 wt% hydride) was mixed with Polymer Base X (360 g). The components were then mechanically mixed for 20 minutes.

A summary of the components used to prepare silicone rubber is provided below.

Component	Notes
V21 polymer base	Prepared from V21 polymer (1514 g), silica (117.2 g), and hexamethyldisilazane-treated silica (588.8 g).
V31 polymer base	Prepared from V31 polymer (1514 g), silica (117.2 g), and hexamethyldisilazane-treated silica (548.8 g).
V46 polymer base	Prepared from V46 polymer (1514 g), silica (107.2 g), and hexamethyldisilazane-treated silica (448.8 g).
Polymer Base X	Mixed base prepared from 5 wt% V21 polymer base, 15 wt% V31 polymer base, and 80 wt% V46 polymer base.
TM1 Part A	Pt-containing part of the 2-component system. Prepared from 10 wt% M511 Rubber HEAT Platinum Catalyst Concentrate (a mixture of base polymer and Pt catalyst prepared by Technovent Ltd.) and 90 wt% Polymer Base X.
TM1 Part B	Crosslinker-containing part of the 2-component system. Prepared from 10 wt% H-301 methylhydrosiloxane-dimethylsiloxane copolymer (trimethylsiloxane terminated, 25-35 sCt, 1,900-2000 g mol <sup>-1</sup> , 25-35 wt% hydride) and 90 wt% Polymer Base X.

**Table 5.** A summary of components used to prepare silicone rubber in this work.

### Determination of TM1 work time and room temperature cure time

TM1 Part A (5 g) and TM1 Part B (5 g) were combined. The mixture was checked *ad hoc*, with the work time determined as the point where the mixture no longer flowed freely. The mixture was then checked periodically to see if it had set.

### **Determination of TM1 heat cure time**

TM1 Part A (5 g) and TM1 Part B (5 g) were combined. The mixture was placed in an oven set to 100 °C. The mixture was checked once every 10 minutes to determine whether the silicone had set.

### **Preparation of TM1 slab**

TM1 Part A (40 g) and TM1 Part B (40 g) were combined. The components were mixed in a vacuum mixer for 2 minutes in order to mix the components homogeneously and remove air bubbles. The polymer mix was transferred in an aluminium mould (2.5 mm x 150 mm x 100 mm) previously sprayed with a release agent (MediMould\* Wax Mould Sealant and Release Agent) in order to facilitate the release of the silicone, and compressed in a vice for 1 hour at room temperature. The mould was then clamped and transferred to an oven set at 100 °C. The slab was then left in the oven to cure for 15 minutes. The solid slab of TM1 silicone rubber was then removed from the mould once it had cooled to room temperature.

### **Doping of silicones**

TM1 silicone was doped to 5 wt% using a number of triclosan derivatives, imidazolium salts, and Cu-TSM compounds, including: triclosan, triclosan acetate, triclosan laurate, triclosan undec-10-enoate, triclosan benzoate, 1-methyl-3-dodecylimidazolium bromide, 1-methyl-3-dodecylbenzimidazolium bromide.

### **The effect of 5 wt% doping on TM1 work time and room temperature cure time**

TM1 Part A (4.75 g) and TM1 Part B (4.75 g) were combined along with dopant (0.5 g). The mixture was checked *ad hoc*, with the work time determined as the point where the mixture no longer flowed freely. The mixture was then checked periodically to see if it had set.

### **The effect of 5 wt% doping on TM1 heat cure time**

TM1 Part A (4.75 g) and TM1 Part B (4.75 g) were combined along with dopant (0.5 g). The mixture was placed in an oven set to 100 °C. The mixture was checked once every 10 minutes to determine whether the silicone had set.

### **Preparation of 5 wt% doped TM1 slab**

TM1 Part A (28.5 g), TM1 Part B (28.5 g) and dopant (3 g) were combined. The components were mixed in a vacuum mixer for 2 minutes in order to mix the components homogeneously and remove air bubbles. The polymer mix was transferred in an

aluminium mould (2.5 mm x 150 mm x 100 mm) previously sprayed with a release agent (MediMould\* Wax Mould Sealant and Release Agent) in order to facilitate the release of the silicone, and compressed in a vice for 1 hour at room temperature. The mould was then clamped and transferred to an oven set at 100 °C. The slab was then left in the oven to cure for 15 minutes. The solid slab of TM1 silicone rubber was then removed from the mould once it had cooled to room temperature.

### **Determination of silicone hardness**

The hardness of 10 random points on the slab were determined using a durometer. The mean value taken and the standard deviation was calculated.

### **Mechanical test – tensile strength**

The tensile strength of each silicone sample was determined according ASTM D 412-16 standard for determination of tensile strength.<sup>76</sup> Samples were cut into dumbbell shapes using a vice and a mould, and stress was applied using clamps attached to the motorised test stand. The force applied to elongate the silicone sample, along with its displacement (in mm) was measured up until breakage. The dimensions of the narrow section of the dumbbell were 25 mm x 4 mm x 2 mm.

### **Mechanical test – tear resistance**

The ability of the silicones to resist the propagation of a tear was tested in line with the ASTM D 624-00 (2020) standard.<sup>77</sup> Silicone slabs were cut into 2 mm x 49 mm x 10 mm portions. A 4 mm incision was made into the material in the 10 mm direction, starting 24.5 mm (half way) into the slab. Stress was applied using clamps attached to the motorised test stand. The force applied to elongate the silicone sample, along with its displacement (in mm) was measured up until breakage.

### **Investigation into inhibition of silicone rubber curing**

A test reaction was conducted in order to determine whether Ag-NHCs could affect the activity of a Pt-based hydrosilylation catalyst. Briefly 1,1,1,3,5,5,5-heptamethyltrisiloxane (2.716 mL, 10 mmol) and styrene (1.150 mL, 10 mmol), 3-dodecyl-1-methylimidazol-2-ylidene silver(I) bromide (0.438 g, 1 mmol), and a dodecane internal standard (1.136 mL, 5 mmol) were added to *o*-xylene (15 mL). The mixture was heated to 70 °C, and then allowed to thermally equilibrate for 2 hours. Karstedt's catalyst (1 µmol/mL, 0.5 mL, 0.005 mol%) was added to the mixture. A sample (1-3 drops) was taken from the reaction mixture before the addition of the catalyst, and every 15 minutes subsequently for 3 hours. The sample was immediately dropped onto a charcoal column in order to remove

metals, and eluted with HPLC-grade dichloromethane. A control reaction was also conducted in the above manner in the absence of an Ag-NHC.

### Transmetalation reaction to probe catalyst poisoning

Platinum cyclovinylmethoxysiloxane complex (0.487 g, 2-2.3 wt% Pt in cyclovinylmethoxysiloxane, 0.05 mmol Pt) and 3-dodecyl-1-methylimidazol-2-ylidene silver(I) bromide (0.044 g, 0.1 mmol) were dissolved in toluene (1 mL). The reaction was then covered in foil and heated at 100 °C for 12 hours. The brown mixture was then filtered through celite, then volatiles were removed *in vacuo*. The mixture was then analysed by mass spectrometry.

### Zone of inhibition assay (Kirby-Bauer method)

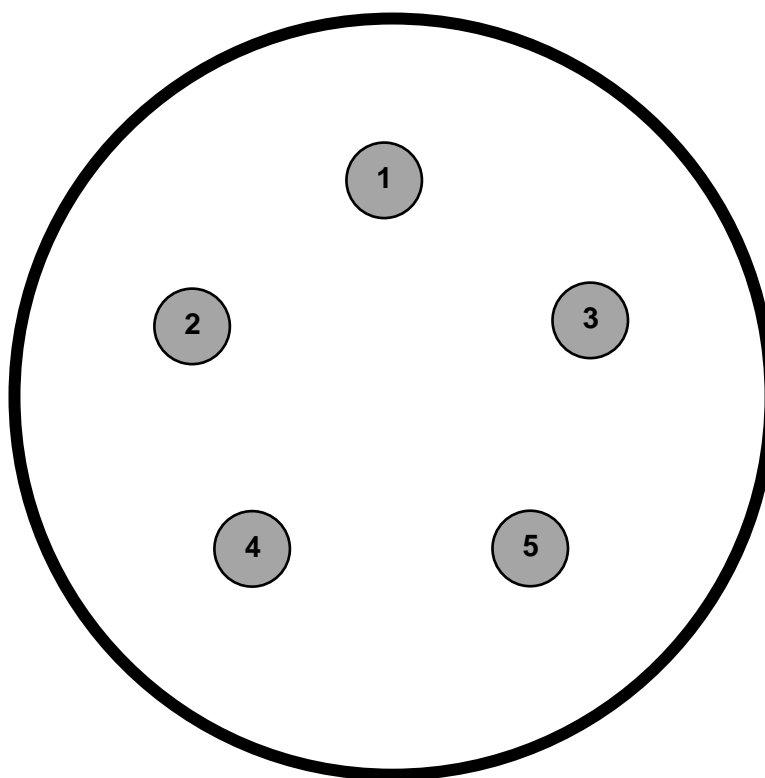


**Figure 10.** The basic layout of an agar plate used to conduct a Kirby-Bauer disc diffusion zone of inhibition assay with 5 antimicrobial agents tested (1-5). The agar is seeded with a "lawn" of bacteria prior to placement of the discs.

A sterile cotton swab was used to inoculate a Mueller-Hinton agar plate by streaking a swab dipped in a test inoculum of a single organism thrice over the whole agar surface area, taking care to rotate the plate approximately 60 degrees after each swab to ensure the inoculum covers the entire surface in a uniform manner. The inoculated plate was then allowed to dry partially covered for roughly 5 minutes. A 6 mm disc of 5 wt% doped test silicone was placed gently on the surface of the inoculated agar using a set of

sterilised forceps. This was repeated 2 or 3 more times with a different 5 wt% doped test silicone, followed by the addition of a single undoped control silicone disc (6 mm). The finished test plate therefore contained one test organism, 3 or 4 different 5 wt% doped test silicone discs, and a single control silicone disc. The finished test plate was then placed in an incubator set at 37 °C for 24 hours. The zone of inhibition was then measured using a ruler. A zone of inhibition that did not extend beyond the limits of the silicone disc was defined as 6 mm. Each zone of inhibition for each 5 wt% doped silicone against each organism was assessed in triplicate, with a mean value taken as the effective zone of inhibition.

## Results and discussion

### Synthesis of compounds

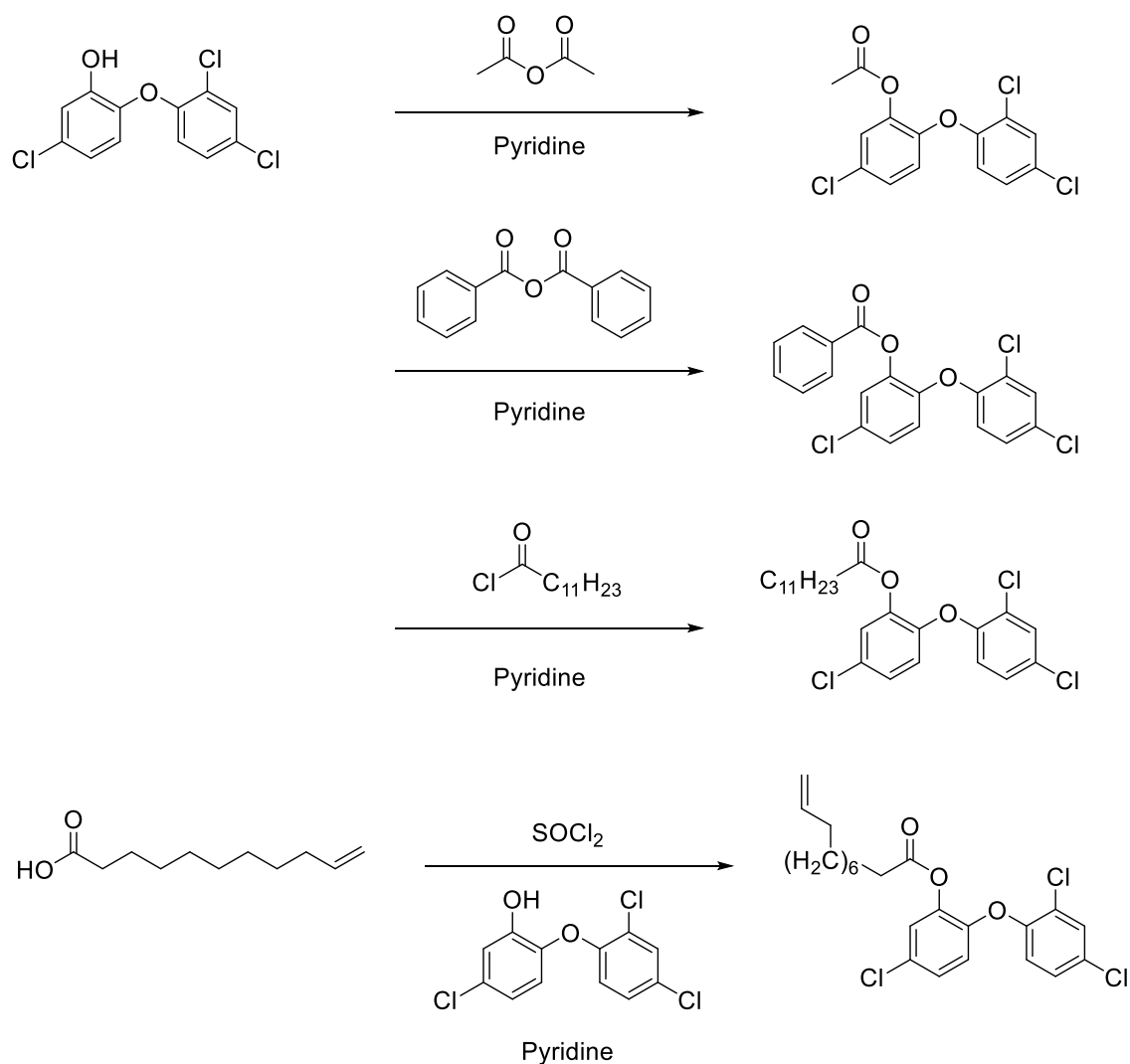


**Figure 11.** Synthetic scheme for the preparation of triclosan ester dopants.

Esters of triclosan were prepared in pyridine using anhydrides or acyl chlorides of the appropriate acid. In the synthesis of triclosan undecenoate, the electrophile, undec-10-en-1-oyl chloride, is prepared and used *in-situ* from the reaction of the parent carboxylic acid and thionyl chloride to avoid hydrolysis of the synthesised compound and to conduct the reaction in a timelier manner. The compounds prepared by use of an anhydride as the source of the ester, triclosan acetate and triclosan benzoate, were solids, whereas the compounds prepared with acyl chlorides as ester sources, triclosan undecenoate and triclosan laurate, were oils. This is of course not a function of the carbonyl used, and is instead based on the pendant R-group. In the case of the acyl chlorides a long chain R-group was employed, which causes the compound to form an oil, whereas the anhydrides used had shorter R groups such as methyl or phenyl, tending towards the

formation of a solid in a compound that already contains an aromatic ether. Triclosan acetate and triclosan benzoate readily precipitated from pyridine upon the reaction's completion. The triclosan esters with long chains attached were more difficult to isolate than their peers due to an increased solubility in pyridine afforded by the R-groups. The prepared triclosan ester could however be simply separated from the crude reaction mixture of excess acyl chloride and pyridine by use of a short silica column with DCM as an eluent, whereupon the first few fractions all contained the desired triclosan ester. The 4 triclosan esters described were then employed as dopants, along with samples of the parent triclosan. Samples of imidazolium and benzimidazolium bromide salts (3-dodecyl-1-methylimidazolium bromide and 3-dodecyl-1-methylbenzimidazolium bromide), and their related Ag-NHCs previously described in this thesis were also employed as dopants.

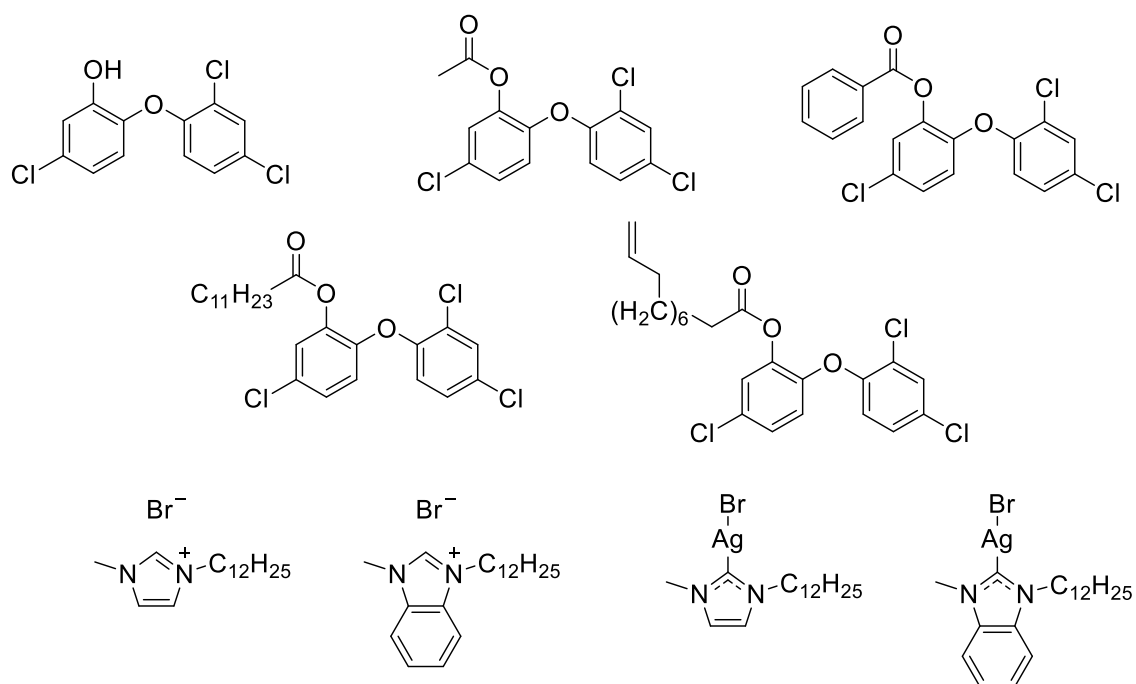


**Figure 12.** Constituent compounds of the first phase employed as TM1 dopants: triclosan, triclosan acetate, triclosan benzoate, triclosan laurate, triclosan undecyloate, 3-dodecyl-1-methylimidazolium bromide, 3-dodecyl-1-methylbenzimidazolium bromide, 3-dodecyl-1-methylimidazol-2-ylidene silver(I) bromide, and 3-dodecyl-1-methylbenzimidazol-2-ylidene silver(I) bromide.

Following the initial preparation of doped silicones and their subsequent testing, CuGTSB, CuGTSH, CuGTSO, 3-decyl-1-vinylimidazolium bromide and 1-methyl-3-(undec-10-en-1-yl)imidazolium bromide were prepared as potential dopants. The imidazolium salts were prepared in a manner similar to that described in previous

chapters. 1-methyl-3-(undec-10-en-1-yl)imidazolium bromide was prepared neat to remove the production of waste solvent on a large scale due to the increased scale of the reaction. The neat reaction proceeded more slowly, but produced pure imidazolium salt in quantitative yield upon freezing and trituration. This second batch of dopants was then were then taken forward to the silicone development stage.

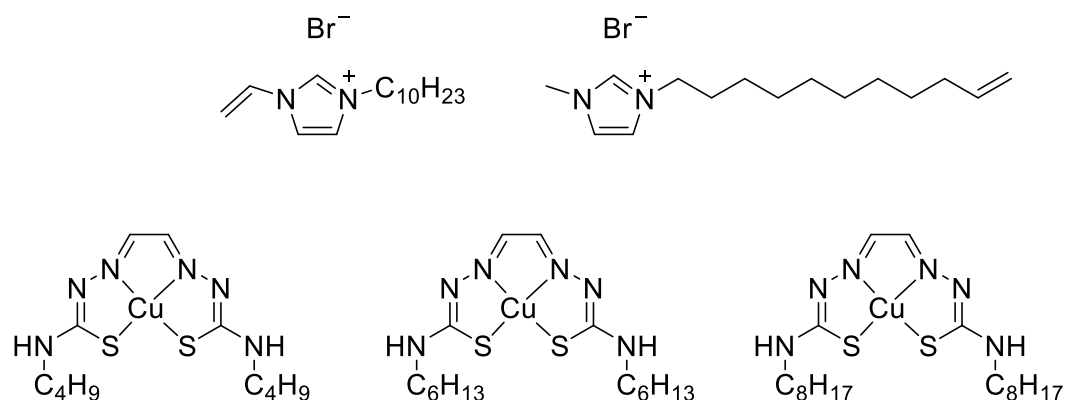


**Figure 13.** Constituent compounds of the second phase employed as TM1 dopants: 3-decyl-1-vinylimidazolium bromide, 1-methyl-3-(undec-10-enyl)imidazolium bromide, CuGTSB, CuGTSH, and CuGTSO.

### NMR spectroscopy

The NMR spectra in this chapter were all conducted in CDCl<sub>3</sub>. The spectra of all literature known species matched well with those reported.<sup>65,71,73,78–83</sup> The unambiguous assignment of the triclosan-based aromatic shifts in the <sup>1</sup>H and <sup>13</sup>C{<sup>1</sup>H}-NMR of triclosan species was challenging, particularly those from triclosan benzoate due to the similarity of the aromatic shifts.<sup>64,68,84</sup> In many cases, the environments overlap, convoluting the spectra and preventing the simple assignment of the aromatic shifts in the <sup>13</sup>C{<sup>1</sup>H}-NMR even through application of HSQC spectroscopy. The integration in <sup>1</sup>H-NMR of the total aromatic environments seen could be used however to determine whether the compound was synthesised by comparing the integration of the aromatic area with the integration of the R-groups, the distinctive features of which were easy to assign in most cases besides triclosan benzoate. The assignment of triclosan benzoate was assessed by integration of the peaks in the aromatic region and comparison with the other triclosan esters to remove common peaks in order to assign each of the phenyl proton environments. The <sup>13</sup>C{<sup>1</sup>H}-NMR spectra of all triclosan esters contain the correct number of carbon environments expected. The unambiguous assignment of aromatic carbon environments is difficult as described for the <sup>1</sup>H-NMR spectra due to the similarity in the environments' chemical shifts.<sup>64,68,84</sup> It is however possible to pick out the clearly defined carbonyl carbon for all triclosan esters with values of 168.34 ppm for triclosan

acetate, 164.18 ppm for triclosan benzoate, 171.20 for triclosan laurate, and 171.26 ppm for triclosan undecenoate. The  $^1\text{H}$ -NMR spectra of 3-decyl-1-vinylimidazolium bromide and 1-methyl-3-(undec-10-en-1-yl)imidazolium bromide are similar to other imidazolium species reported in this thesis in the literature.<sup>74,78</sup> The  $^{13}\text{C}\{^1\text{H}\}$ -NMR spectra of both species are similar to those discussed previously in this thesis, with imidazole ring shifts of 134.81 ppm for the C2 carbon and 122.55 ppm and 119.38 ppm for the backbone carbons in the vinyl species, and shifts of 138.83 ppm (C2), 123.66 ppm (backbone), and 121.90 ppm (backbone) for the undec-10-enyl species.

### Mass spectrometry

The mass spectra of all species synthesised were recorded in positive mode with electrospray ionisation. The triclosan esters produced the expected  $[\text{M} + \text{H}^+]$  peak, whereas the imidazolium salts produced an  $[\text{M} - \text{Br}^-]$  peak. As the mass spectra were recorded in positive mode, the appearance of the imidazolium salt without the bromide counter ion is likely to be the observable species under ionisation.

### Silicone rubber development



**Figure 14.** Mixers and extractors used in the preparation of PDMS base mixtures (Technovent Ltd, Bridgend, Wales, UK).

The physical properties of a silicone elastomer depend on a number of factors. One of the main factors is the molecular weight of the polymers used in the hydrosilylation reaction.<sup>85</sup> When attempting to design new medical devices, it is important for the rubber produced to have some elasticity and flexibility, but be tough enough to be hard-wearing.<sup>86,87</sup> Higher molecular weight polymers of PDMS provide elasticity and high viscosity, whereas lower molecular weight polymers provide a low viscosity material with strong plastic-like behaviour or rigidity.<sup>85,88</sup> Silica filler is also used to increase tensile strength of the rubber, and the ratio of silica to methylated silica must be taken into consideration with regard to properties such as water absorption.<sup>85,89,90</sup> A new formulation based on standard polymers and formulations at Technovent Ltd (Bridgend, Wales, UK) was designed, with the aim of making an industrially relevant and accessible material. The material produced was dubbed TM1 (for Test Material 1), and its properties were investigated for its suitability in medical devices.

### **Preparation of PDMS base mixes**

The preparation of TM1 requires the preparation of a Part A and Part B as the technology employed is a two component system.<sup>1</sup> The preparation of Part A and Part B requires the preparation of a number of different PDMS base mixes. The base mixes typically consist of PDMS of varying molecular weights and silica (natural and methylated) fillers. Both Part A and Part B consisted of 90% w/w PDMS Polymer Base X, which in turn was prepared from 80% w/w V46 polymer base, 15% w/w V31 polymer base, and 5% w/w V21 polymer base. Each of the foundation polymer bases were prepared following standard procedures at Technovent Ltd.

The foundation polymer bases consist of 1514 g of a vinyl-terminated PDMS with no less than 448.8 g of hexamethyldisilazane-treated silica and no less than 107.2 g of silica. The foundation polymer bases were named based on the Gelest product code of the PDMS polymer, with V46 being the highest molecular weight and most viscous polymer used (60,000 sCt, 117,000 g mol<sup>-1</sup>, 0.04-0.06 wt% vinyl), followed by V31 (1,000 sCt, 28,000 g mol<sup>-1</sup>, 0.18-0.26 wt% vinyl), and then finally V21 (100 sCt, 6,000 g mol<sup>-1</sup>, 0.8-1.2 wt% vinyl). As can be seen, the high molecular weight V46 polymer is far more viscous and contains far fewer vinyl groups per weight than the lower molecular weight polymers. This is due to the fact that the vinyl group on each end of a long chain contributes less to the total mass of the polymer than in a lower molecular weight polymer. The amount of hexamethyldisilazane-treated silica used increased with a decrease in the molecular weight, with 448.8 g used in the V46 polymer base, 548.8 g used in the V31 polymer base, and 588.8 g used in the V21 base. A reduced amount of

silica was also used in the preparation of V46 polymer base, with 107.2 g used by comparison with the 117.2 g used in the V31 and V21 polymer bases. The reasoning for this is due to the increase of tensile strength afforded by an increase in silica weight used coinciding with an increase in viscosity. Less silica was used in the preparation of V46 polymer base due to its already high viscosity. The methylated silica was added in two portions to the polymer base in order to ensure less wastage and better incorporation of the silica into the polymer. Each polymer base was mixed mechanically for 2 hours to ensure homogeneity and consistency throughout the formulation.

The mixture of 80 wt% V46 polymer base, 15 wt% V31 polymer base, and 5 wt% V21 polymer base making Base X was chosen as a starting point for TM1 due to the elasticity provided by using mostly V46 polymer base plus the additional rigidity and strength provided by the lower molecular weight polymers.<sup>85</sup> Base X was used to prepare Part A and Part B of the two component system. As previously discussed, the active component, constituting 10% wt% of Part A or Part B, was the only difference between the two parts, with the remainder of the mass of both consisting of Polymer Base X. The catalyst component, Part A, contains 10 wt% of M511 Rubber HEAT Platinum Catalyst Concentrate, a mixture of 99 wt% M511 Polymer Base and 1 wt% of Pt cyclovinylmethylsiloxane complex (2-2.3 wt% in cyclovinylmethylsiloxane). The crosslinker component, Part B, contains 10 wt% H-301 methylhydrosiloxane-dimethylsiloxane copolymer (trimethylsiloxane terminated, 25-35 sCt, 1,900-2000 g mol<sup>-1</sup>, 25-35 wt% hydride), which acts as the hydride source in the hydrosilylation reaction catalysed by the platinum catalyst in Part A. The source of the unsaturated bonds for the hydrosilylation reaction are the termini of the PDMS polymers constituting Base X,<sup>1</sup> necessitating the separation of Part A and Part B until curing is desired in order to prevent the reaction from occurring.<sup>91</sup>

### **Work time of TM1**

The work time of a new silicone formulation is a property that must be considered. The work time is essentially for how long the mixed Part A and Part B remain malleable once mixed.<sup>92,93</sup> The work time was assessed by *ad-hoc* checks roughly every five minutes, increasing in frequency as the viscosity of the material appeared to be increasing. The viscosity of the Part A and Part B 1:1 mixture was checked by moving and spreading the material within a test cup in order to see whether the silicone would tear due to the material having partially cured to the point where it could no longer be reshaped. The work time is an important factor, as enough time is needed to move the silicone to an appropriate mould before it sets. The work time of the TM1 sample was found to be 26

minutes. The mixture was then set aside, and checked on an *ad-hoc* basis to determine a rough room temperature cure time.

### **Cure time of TM1**

The cure time of TM1 was assessed at room temperature and at 100 °C. The 10 g sample used in the assessment of the work time was set aside in order to assess the rough room temperature cure time. The cure time was assessed as the time it took so that the silicone rubber was no longer tacky to the touch, and had set completely into a solid. The room temperature curing of TM1 was 3 hours. The cure time at 100 °C was far faster than that at room temperature, as expected. The 10 g 1:1 mixture of Part A and Part B was checked every 10 minutes to determine whether the silicone had set. The 100 °C cure time was found to be 10 minutes.



**Figure 15.** TM1 silicone rubber after curing at 100 °C for 10 minutes.

## Preparation of TM1 slab



**Figure 16.** Aluminium mould used to cure slabs of silicone rubber.

The preparation of a homogenous slab of silicone rubber is an important step in the determination of the mechanical properties of a new silicone formulation, as it must be possible to prepare uniform silicone samples for physical testing. An 80 g 1:1 mixture of Part A and Part B were folded together by hand then vacuum mixed for 2 minutes in an attempt to remove air from the mixture, as bubbles of air in the rubber once it has set will affect the mechanical properties of the rubber, weakening it. The vacuum mixed liquid Part A and Part B are then removed carefully from the vessel with a spatula in order to avoid re-aerating the mixture and introducing bubbles, and smoothly spread onto an aluminium mould prepared with a release agent. The use of a release agent is important, as the silicone rubber formed upon curing may stick to the mould, and may therefore tear upon any attempt to remove the material. The mould is then clamped in a vice and allowed to settle at room temperature for an hour so that any unevenness caused by spreading the silicone mixture is mitigated before rapid curing at high temperature. The vice is then moved to an oven set to 100 °C for an hour in order to cure the mixture into a solid slab of silicone rubber. The vice was then removed from the oven and allowed to cool to room temperature so that the slab could be removed. The mould requires gentle persuasion with a screwdriver or similar implement to open initially but then freely released the silicone rubber once the initial seal was broken. The silicone slab was then taken to test its physical properties.

## Physical properties of TM1

The three initial derived physical properties determined for TM1 are shown below in Table 6.

Sample	Hardness (Durometer)	Tensile strength (MPa)	Maximum elongation (%)	Tear resistance (kNm <sup>-1</sup> )
TM1	25.6 (± 2.55)	1.78 (± 0.263)	1016 (± 129)	12.3 (± 2.34)
M511 Maxillofacial Rubber (Technovent Ltd, Bridgend, Wales, UK) <sup>94</sup>	14.2 (± 0.83)	3.13 (± 0.313)	758.3 (± 100)	5.63 (± 1.88)
A-2186 Platinum RTV Silicone Elastomer (Factor II Inc., Lakeside, AZ, USA) <sup>95</sup>	30.7 (± 1.72)	4.89 (± 0.45)	-	20.77 (± 2.41)
RT Vulcanized VST-30 silicone (Factor II Inc. Lakeside, AZ, USA) <sup>96</sup>	31.3	4.38	931	16.55
Cosmesil Z004 (Principality Medical Ltd, Newport, Wales, UK) <sup>97</sup>	36.44 (± 1.81)	3.86 (± 0.41)	608.6 (± 38.3)	7.04 (± 2.15)

**Table 6.** Derived physical properties of the silicone rubber "TM1" compared to commercially available maxillofacial silicone elastomers.<sup>94-97</sup>

The Shore A hardness of the produced slab was the first property to be assessed. Ten random spots were sampled for hardness using a durometer, and the mean value of the ten measurements taken as the material's hardness. The standard deviation of the values was also calculated to account for the variance in the hardness of the rubber. A Shore durometer of 25.6 was obtained for TM1, classifying the material as suitable for use in maxillofacial applications.<sup>92,98-100</sup> There is some evidence that the Shore hardness of a silicone rubber depends on its percentage vinyl concentration,<sup>101</sup> which is in agreement with the above discussion on the relation of elasticity, which increases with increases in PDMS molecular weight. An increase in Shore hardness has been shown to have a correlation with the elasticity of a material, but not with its viscosity another key property of silicones when being considered for application as medical devices.<sup>102</sup>

Once the hardness of TM1 was assessed the slab was cut into dumbbell shapes according to ASTM D412-16 for tensile strength testing,<sup>76</sup> and into strips according to ASTM D624-00 (2020) for tear resistance testing.<sup>77</sup> Both properties were assessed using a Mecmesin MultiTest-d motorised test stand equipped with a Mecmesin AFG 500N digital force gauge. The cut-to-shape silicone rubber samples were held in clamps attached to the test stand and slowly elongated until the silicone rubber snapped. The slits in the centre of the strips used for tear resistance testing were cut halfway along the length and halfway across the width. The purpose of the slit was to act as a starting point for a tear, whereas the elongation was used to test the material's resistance to the propagation of a tear. 10 strips were prepared in line with the testing standard. The use of a dumbbell shape in the tensile strength testing is so that the material always broke in roughly the same place along the material (the narrow section), and was used to assess how much the material could be stretched before failure. 6 dumbbells were prepared in line with the testing standard. The max elongation in mm and the force applied in N was recorded, and used to calculate the tensile strength and tear resistance of the material. The tensile strength (MPa) and tear resistance (kN/m) were calculated based on the dimensions of the test materials and the measurements recorded.

### **Doping of silicones**

Once the physical properties of TM1 had been established, the effects of adding potential antimicrobial agents during the curing process was explored. The initial loading of dopant was decided to be 5 wt% based on work previously conducted at Technovent, as 5 wt% was seen to be the dose required to observe an antimicrobial effect in the case of other dopants. The initial dopants tested were triclosan, triclosan acetate, triclosan benzoate, triclosan laurate, triclosan undecenoate, 3-dodecyl-1-methylimidazolium bromide, 3-dodecyl-1-methylbenzimidazolium bromide, 3-dodecyl-1-methylimidazol-2-ylidene silver(I) bromide, and 3-dodecyl-1-methylbenzimidazol-2-ylidene silver (I) bromide. Upon the preparation of silicone formulations of these above dopants, and the subsequent curing and physical testing of doped slabs where possible, a second batch of dopants was prepared based on the initial findings. This second batch of dopants contained 3-decyl-1-vinylmethylimidazolium bromide, 1-methyl-3-(undec-10-enyl)imidazolium bromide, CuGTSB, CuGTSH, and CuGTSO. The dopants were again incorporated into the two component system at 5 wt%. The effects of 5 wt% doping on the work time of TM1 is summarised below in Table 7.

### Effect of 5 wt% doping on work time of TM1

Dopant (5 wt%)	Work time (minutes)
TM1	25
Triclosan	20
Triclosan acetate	25
Triclosan benzoate	20
Triclosan laurate	60
Triclosan undecenoate	45
3-dodecyl-1-methylimidazolium bromide	15
3-dodecyl-1-methylbenzimidazolium bromide	25
3-dodecyl-1-methylimidazol-2-ylidene silver(I) bromide	15
3-dodecyl-1-methylbenzimidazol-2-ylidene silver(I) bromide	15
3-decyl-1-vinylimidazolium bromide	60
1-methyl-3-(undec-10-enyl)imidazolium bromide	30
CuGTSB	15
CuGTSH	15
CuGTSO	15

**Table 7.** The work time of 5 wt% doped TM1 silicone rubber based on the nature of the dopant.

The work times of the 5 wt% doped silicones was assessed in much the same manner as the work time of TM1. A total mass of 10 g (47.5% Part A, 47.5% Part B, 5% dopant) was employed, with decreases in the total masses of Part A and Part B by comparison with the basic TM1 in order to incorporate the mass of dopant. As previously described, the PDMS mixture was moved around the test vessel, with the viscosity checked on an *ad-hoc* basis, initially roughly every 5 minutes then increasing in frequency as the mixture appeared to be solidifying. The values for the work times of each doped silicone are displayed below. As can be seen, the first set of dopants appeared to have little to no influence on the cure time of TM1. However, both Ag-NHCs appeared to turn the mixture brown over time (illustrated below in Figure 17), and no further curing occurred past the initial increase in viscosity. The apparent inhibition of the curing process by Ag-NHCs is explored later in this chapter. The second set of dopants produced similar results, with

many of the dopants appearing to solidify the silicone to a point beyond workability in a roughly similar amount of time as un-doped TM1.



**Figure 17.** The observed darkening of TM1 doped with 3-dodecyl-1-methylimidazol-2-ylidene silver(I) bromide over time (L to R: 10 minutes, 3 hours, overnight).

#### Effect of 5 wt% doping on cure time

Dopant (5 wt%)	Room temperature cure time (minutes)	100 °C cure time (minutes)
TM1	180	10
Triclosan	180	15
Triclosan acetate	180	15
Triclosan benzoate	180	20
Triclosan laurate	195	10
Triclosan undecenoate	300+ (overnight)	20
3-dodecyl-1-methylimidazolium bromide	180	45
3-dodecyl-1-methylbenzimidazolium bromide	230	15
3-dodecyl-1-methylimidazol-2-ylidene silver(I) bromide	No cure	No cure
3-dodecyl-1-methylbenzimidazol-2-ylidene silver(I) bromide	No cure	No cure
3-decyl-1-vinylimidazolium bromide	No cure	No cure
1-methyl-3-(undec-10-enyl)imidazolium bromide	No cure	No cure
CuGTSB	No cure	No cure
CuGTSH	No cure	No cure
CuGTSO	No cure	No cure

**Table 8.** Room temperature and 100 °C cure time of 5 wt% doped TM1 silicone rubber. A value of "No cure" is entered if the material does not appear to solidify.

The cure time of the doped silicones was assessed at room temperature and at 100 °C. The cure times of each doped silicone at each temperature are listed above. As can be seen, for the first set of dopants, the cure time was unaffected by the dodecyl-substituted imidazolium salts and most of the triclosan esters. The one exception to this is triclosan undecenoate. The 5 wt% triclosan undecenoate-doped TM1 was removed from the oven after 30 minutes, only to find that the silicone had not set. The test vessel was replaced into the oven and checked every subsequent 10 minutes in order to determine whether the silicone had set. The silicone was found to have set by after 1 hour at 100 °C, which at least doubled the cure time of TM1 in the presence of triclosan undecenoate. This increase in cure time not seen with the other triclosan esters is almost certainly to do with the pendant alkene group of triclosan undecenoate taking part in the hydrosilylation reaction as an unsaturated bond source. It should also be noted that 5 wt% triclosan undecenoate doped TM1 cured at room temperature did eventually cure slowly, but retained a tacky feel to it. The Ag-NHC species appeared to darken the TM1 mixture over time. The TM1 mixture doped with Ag-NHCs showed no curing past the initial work time, but continued to darken until completely dark brown (see above in Figure 17). This process was seen to happen at room temperature and at 100 °C, with the darkening predictably occurring more rapidly at elevated temperature. The potential explanation for this darkening is the precipitation of silver species due to degradation of the Ag-NHC species, either by light, temperature, or a combination of the two factors.<sup>103–105</sup> The second batch of dopants appeared to have the same work time as basic TM1 when doped into silicone. The doped silicones appeared to mostly cure at 100 °C in the same amount of time as TM1, but retained a tackiness to the touch. The room temperature cure time also appeared to be similar to that of standard TM1, but again, retained tackiness, suggesting that the material may not fully cure in the presence of the second batch of dopants. A second room temperature and 100 °C test for TM1 was conducted to rule out any aging of the bases or Part A and Part B used as a reason for the tackiness produced. The new control TM1 matched closely with the first TM1 produced, and had no tackiness to the touch when cured at room temperature or elevated temperature (see Figure 15).

### **Production of 5 wt% TM1 slabs**

Doped TM1 slabs were prepared in much the same way as the base TM1 slab, with the Part A and Part B being vacuum mixed for 2 minutes to remove air, then spread using a spatula onto an aluminium mould prepared with release agent. The quantities used in preparing the TM1 mixture (28.5 g Part A, 28.5 g Part B, 3 g dopant) were lesser than those used for preparing the control TM1 slab for two reasons: 80 g of TM1 mix

overflowed from the mould when placed within suggesting that 80 g was more than required to fill the mould completely, and that the lower total mass meant the use of less dopant, meaning smaller batches of dopant could be prepared. As previously described, the silicone was allowed to settle in the mould in a vice at room temperature for 1 hour before being transferred to an oven set at 100 °C and left to cure for an hour. Once cooled the cured slab was removed from the mould as described previously. The appearance of the doped silicones varied slightly depending on the nature of the dopant. The first series of dopants, excluding the Ag-NHCs, produced cured silicone slabs with a solid, non-tacky feel to them. The silicone rubbers produced with solid dopants had a similar colouration to TM1, but had flecks of white of various sizes and dispersity throughout the material, with 3-dodecyl-1-methylbenzimidazolium bromide producing an almost entirely opaque silicone flecked with small particles. Triclosan laurate and triclosan undecenoate, the liquid dopants, produced homogenously white opaque silicone rubber. The surface of the triclosan acetate-doped TM1 appeared to shed triclosan acetate as a powder when touched, whereas the surface of the triclosan laurate-doped TM1 appeared to be slick with released dopant. The doped slabs were then subject to the same physical testing as the basic TM1 material. The second series of dopants did not produce cured silicone slabs, even after 3 hours or more curing at 100 °C, and potentially caused some inhibition to the catalyst in a manner similar to the Ag-NHCs. Images of CuGTSB- and 3-decyl-1-vinylimidazolium bromide-doped TM1 in an uncured state in the mould are displayed below.



**Figure 18.** Uncured slabs of 5 wt% CuGTSB-doped TM1 (L) and 5 wt% 3-decyl-1-vinylimidazolium bromide-doped TM1 (R) after 1 hour at 100 °C, far longer than the usual cure time required for undoped TM1 slabs at the same temperature.

## Physical properties of 5 wt% doped TM1

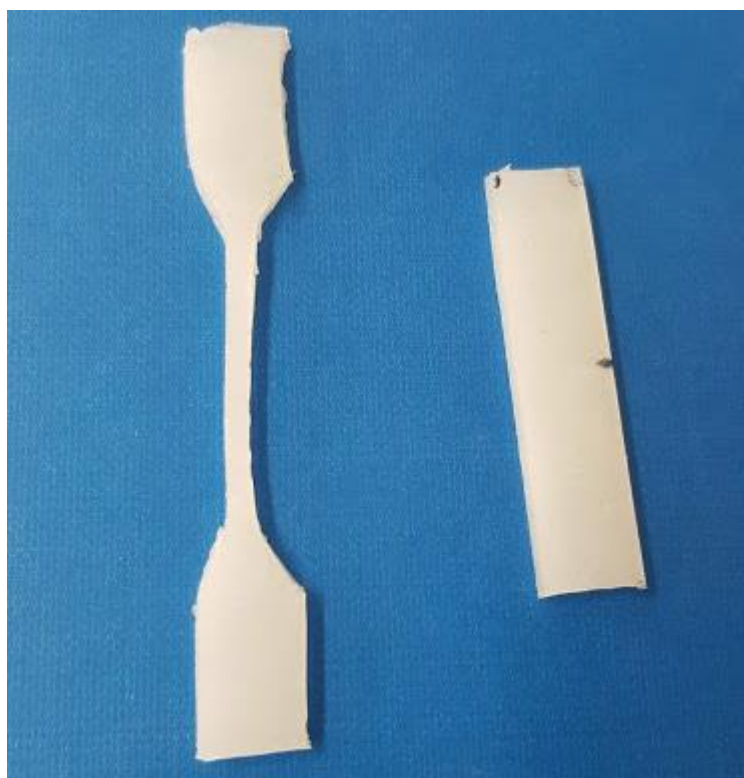


**Figure 19.** Examples of a dumbbell and a strip used for testing tensile strength and tear resistance respectively. The samples were cut from 5 wt% triclosan laurate-doped TM1.

### Doped silicone hardness

The Shore A hardness of the 5 wt% doped TM1 samples was tested in the same manner as the base TM1 as previously described. The Shore A hardness of each doped material alongside the control is summarised in the table below.

Dopant (5 wt%)	Hardness (Durometer)
TM1	25.6 ( $\pm$ 2.55)
Triclosan	26.5 ( $\pm$ 2.32)
Triclosan acetate	25.8 ( $\pm$ 1.32)
Triclosan benzoate	29.5 ( $\pm$ 2.79)
Triclosan laurate	22.0 ( $\pm$ 1.64)
Triclosan undecenoate	23.1 ( $\pm$ 1.52)
3-dodecyl-1-methylimidazolium bromide	23.7 ( $\pm$ 2.26)
3-dodecyl-1-methylbenzimidazolium bromide	23.2 ( $\pm$ 2.53)

**Table 9.** Shore A hardness of TM1 silicone rubber and 5 wt% doped TM1 materials. An average of 10 measurements was taken for each sample.

As can be seen, the Shore durometer values for most of the doped silicones is rather similar, and also similar to the hardness of the control. The standard deviation of these values cause an overlap of hardness values in all cases with that of the control. Despite this, the mean hardness of 4 of the doped materials were lower than TM1, in particular those of the silicones doped with liquid dopants were the two with the lowest mean hardness values. Triclosan acetate- and triclosan-doped silicone had very similar mean hardness values as the base TM1, with 5 wt% triclosan-doped TM1 having a slightly higher hardness. 5 wt% triclosan benzoate-doped silicone has the highest mean hardness by some way (29.5 Shore durometer), but the standard deviation still overlaps with the hardness values of the control material. All silicones produced are classified as soft silicones suitable for maxillofacial applications.<sup>92,98–100</sup>

### Tensile strength of doped silicones

The tensile strength of the doped silicone rubbers was tested in the same manner as the TM1 control using 6 dumbbell-shaped pieces of each experimental material. The values observed for max load (N) and displacement (mm) at failure for each material were recorded, allowing for the tensile strength (MPa) and maximum elongation (%) for each silicone rubber sample to be calculated and recorded in the table below.

Dopant (5 wt%)	Tensile strength (MPa)	Maximum elongation (%)
TM1	1.78 ( $\pm$ 0.263)	1016 ( $\pm$ 129)
Triclosan	2.26 ( $\pm$ 0.427)	1247 ( $\pm$ 148)
Triclosan acetate	1.81 ( $\pm$ 0.420)	1016 ( $\pm$ 177)
Triclosan benzoate	1.86 ( $\pm$ 0.614)	1057 ( $\pm$ 290)
Triclosan laurate	1.84 ( $\pm$ 0.429)	1048 ( $\pm$ 52)
Triclosan undecenoate	2.71 ( $\pm$ 0.509)	1652 ( $\pm$ 202)
3-dodecyl-1-methylimidazolium bromide	1.65 ( $\pm$ 0.627)	1010 ( $\pm$ 202)
3-dodecyl-1-methylbenzimidazolium bromide	0.756 ( $\pm$ 0.400)	882 ( $\pm$ 278)

**Table 10.** Calculated tensile strength and elongation at failure (%) of TM1 silicone rubber and 5 wt% doped TM1 materials. An average from 6 measurements was taken for each sample.

The calculated values for elongation and tensile strength are based on the displacement and max load measured respectively, and so follow the same trend, but take into account the size of the dumbbell shape, particularly the central narrow section. The displacement

and therefore elongation values for most of the doped silicones match well with those of TM1. The elongation of 5 wt% triclosan undecenoate TM1 is far superior to that of control TM1, with a much longer displacement at failure. The mean elongation of triclosan-doped TM1 is also greater than basic TM1, but the standard deviation of the displacement of each material match overlap. In all cases besides that of 5 wt% triclosan laurate, the standard deviation in displacement is larger, suggesting a larger difference in tensile strength within each sample for doped silicones. This difference may be small (triclosan- and triclosan acetate-doped silicone), medium (triclosan undecenoate- and 3-dodecyl-1-methylimidazolium bromide-doped silicone), or large (triclosan benzoate- and 3-dodecyl-1-methylbenzimidazolium bromide-doped silicone), where large standard deviations in displacement are greater than double that of TM1, showing larger variance within each doped sample than TM1. The exception to this is the 5 wt% triclosan laurate-doped TM1, which has a standard deviation of  $\pm 52\%$  for its elongation, indicating that the composition of the material is far more consistent throughout than even the control. The mean tensile strength (MPa) of the doped samples match that of regular TM1 in the case of doping with 5 wt% triclosan acetate, triclosan benzoate, triclosan laurate, and 3-dodecyl-1-methylimidazolium bromide. The mean tensile strength of 3-dodecyl-1-methylbenzimidazolium bromide-doped TM1 is far lower than the control, suggesting a weakening of the material by incorporation of the benzimidazolium salt. The salt is qualitatively much finer than the other dopants, and this may have hampered the strength of the rubber formed due to the disruption of the formation of the silicone network.<sup>85</sup> The mean tensile strength of triclosan-doped TM1 is slightly higher than that of un-doped TM1, but as with the elongation at failure, the standard deviations of each material's tensile strength cause the values to overlap. This is again not the case with 5 wt% triclosan undecenoate TM1, as the tensile strength of this material is higher than that of the control TM1, and there is no overlap in values due to standard deviation.

Overall, the doping of TM1 with 5 wt% of the first series of dopants compounds had little effect on the physical properties of the material, with the exception of 3-dodecyl-1-methylbenzimidazolium bromide and triclosan undecenoate. The reasoning for the potential weakening of the material by the benzimidazolium salt is discussed briefly above. The strengthening of the material by inclusion of triclosan undecenoate is hypothesised to be to do with the alkene group of the undec-10-ene chain becoming involved in the hydrosilylation reaction during curing. The relatively small triclosan undecenoate (by comparison with the PDMS polymers) potentially afforded additional elasticity to the cured rubber, therefore increasing its tensile strength.<sup>85</sup> The success of the physical testing of triclosan undecenoate-doped TM1 informed the preparation of 3-

decyl-1-vinylmethylimidazolium bromide and 1-methyl-3-(undec-10-enyl)imidazolium bromide for use as dopants. The lack of success with these other alkene-containing substances may be due to the cationic nature of the imidazolium salts, and the difficulty of incorporating these polar groups into the hydrosilylation process.<sup>106–108</sup> More research however is needed in order to explore why this phenomenon occurs.

#### Tear resistance of doped silicones

Dopant (5 wt%)	Tear resistance (kNm <sup>-1</sup> )
TM1	12.3 (± 2.34)
Triclosan	14.2 (± 3.01)
Triclosan acetate	13.0 (± 2.74)
Triclosan benzoate	12.5 (± 2.62)
Triclosan laurate	12.8 (± 2.70)
Triclosan undecenoate	14.1 (± 1.77)
3-dodecyl-1-methylimidazolium bromide	10.3 (± 3.11)
3-dodecyl-1-methylbenzimidazolium bromide	4.51 (± 1.36)

**Table 11.** Calculated tear resistance of TM1 silicone rubber and 5 wt% doped TM1 materials. An average from 10 measurements was taken for each sample.

The tear resistance of a material is defined as its ability to resist the propagation of a tear through the material. The tear was simulated in the same manner as with TM1, in that an incision was made halfway up each of the ten strips tested per material. The max load (N) at failure and the displacement (mm) of the sample were measured. The tear resistance (kN/m) was calculated from the max load and the thickness of the test strips. The tear resistance values of the silicone rubbers are listed below. As can be seen, the tear resistance of most of the doped silicones are similar, with the exception of 5 wt% 3-dodecyl-1-methylbenzimidazolium bromide TM1, which is significantly easier to tear. The mean tear resistances calculated are slightly higher for all other dopants except 3-dodecyl-1-methylimidazolium bromide, where the tear resistance is slightly lower than that of normal TM1. The materials with the highest mean tear resistances are also those with the highest tensile strengths, with triclosan- and triclosan undecenoate-doped TM1 being the most and second most tear resistant materials respectively. The exceptional increase in tensile strength seen in triclosan undecenoate-doped silicones is not reflected in the same material's tear resistance. The standard deviations of the tear resistances show overlap for all doped-silicones with that of TM1, with the exception of the benzimidazolium-doped silicone, therefore indicating that 5 wt% doping has little effect on the tear resistance of TM1. The decrease in tear resistance of the material by

doping with 5 wt% 3-dodecyl-1-methylbenzimidazolium bromide is likely due to a similar phenomenon as the decrease in tensile strength, due to the fine powder of the benzimidazolium salt taking up more space in the overall structure of the material, weakening the material by interfering with the bonding of the polymer in the elastomer.

### Investigation into inhibition of curing by Ag-NHCs

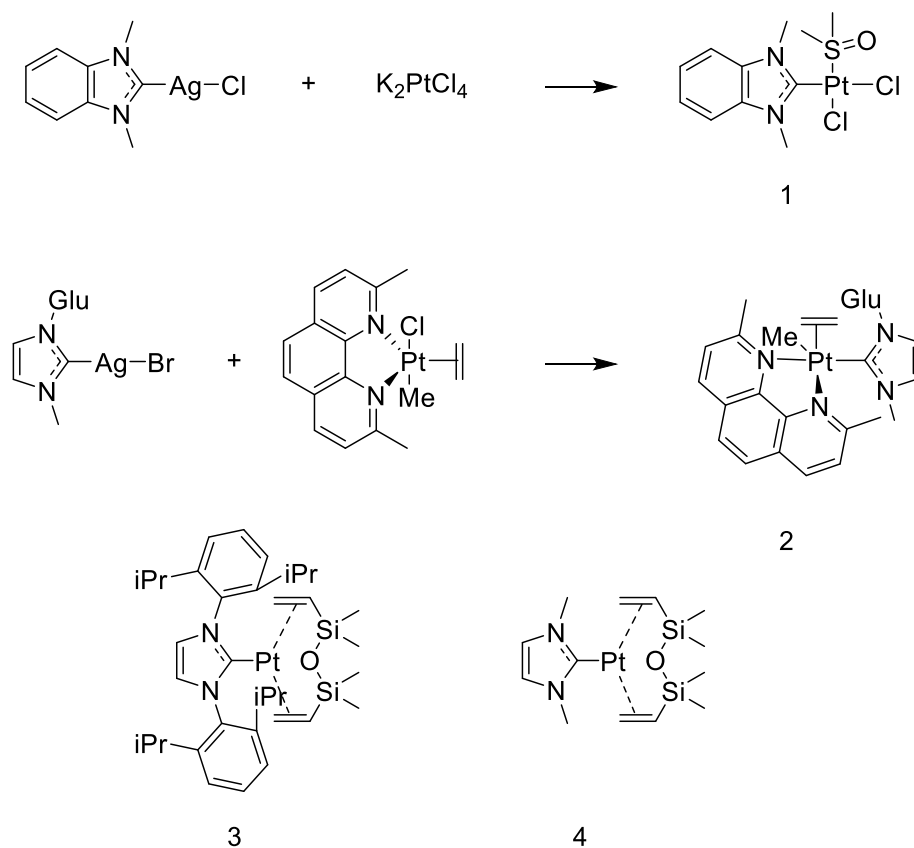


**Figure 20.** Transmetalation of Pt onto Ag NHCs (1,<sup>109</sup> 2<sup>110</sup>), and examples of Pt(0) complexes with NHC ligands from recent literature (3,<sup>111</sup> 4<sup>112</sup>).

The lack of curing of TM1 when doped with the Ag-NHCs from the first set of dopants showed that not all possible antimicrobial dopants are suitable for inclusion. The most obvious cause of the inhibition is interference of the dopant with the platinum hydrosilylation catalyst.<sup>106–108</sup> The catalyst used in heat curing of TM1 is a platinum cyclovinylmethylsiloxane complex, a Pt(0) species stabilised by platinum-alkene bonds. Ag-NHCs are well known as transmetalation agents, with many examples available in the literature.<sup>113–119</sup> Recent examples in the literature include work by Schobert *et al.*<sup>109</sup> who report the reaction of N,N-dialkylbenzimidazol-2-ylidene AgCl-NHCs with  $K_2PtCl_4$  in DMSO to form cis-PtCl<sub>2</sub>(NHC)(DMSO) complexes, whereas Ruffo used glucoconjugated AgBr-NHCs to form glucoconjugated Pt(II)-NHCs from a 2,9-dimethyl-1,10-

phenanthrolinePt(II) complex. NHCs have also been shown to be appropriate ligands for Pt(0), as evidenced in work by Markó et al.<sup>120–123</sup> and others.<sup>111,112,124</sup> Literature preparations for Pt(0)-NHC complexes via transmetalation are uncommon, however the combination of NHCs being appropriate ligands for Pt(0) and Ag-NHCs being potent carbene transfer agents, it is conceivable that a transmetalation of Pt(0) to 3-dodecyl-1-methylimidazol-2-ylidene is possible. In the case of silicone rubber formation the Ag-NHC dopant may lead to the formation of catalytically less active or inert Pt-NHC complexes, halting the curing process. A test reaction was conducted in order to probe this potential poisoning of the catalyst. The substrates used were non-polymeric with no crosslinker present in order to simplify the analysis of the reaction mixture, and based on literature known hydrosilylation procedures with Pt(0) catalysts.<sup>120–123,125</sup> The Pt(0) source used was Karstedt's catalyst (structure illustrated below alongside the Pt cyclovinylmethylsiloxane complex) due to the similar nature of the complexes, availability, and a more well-defined Pt composition than the cyclovinylmethylsiloxane catalyst (2-2.1 wt% Karstedt vs 2-2.3 wt% cyclovinylmethylsiloxane).

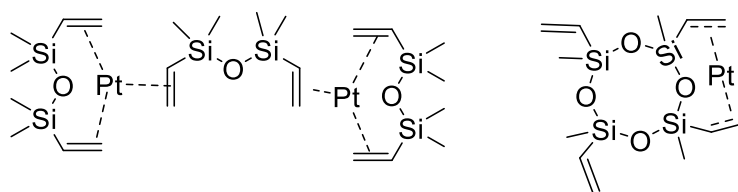


**Figure 21.** Illustrations of Karstedt's catalyst and platinum cyclovinylmethylsiloxane complex catalysts employed in hydrosilylation reactions.<sup>85</sup>

Styrene was selected as a substrate due to the simplicity of its structure, whereas the 1,1,1,3,5,5,5-heptamethyltrisiloxane was used as a hydride source in order to provide steric bulk to the reaction in order to reduce the reaction rate so that the reaction may be monitored over time. A 1:1 mixture of the substrates was dissolved in *o*-xylene to simulate the non-polar environment afforded by the PDMS polymers when curing silicone rubber. Dodecane was added to provide a constant peak in the analysis that would not interfere with the reaction in a competitive manner. The reaction was heated to 70 °C and allowed to thermally equilibrate for 2 hours to ensure a homogeneous temperature throughout. Samples were passed through a charcoal column in order to halt the catalysis by adsorbing the Pt from the catalyst onto the charcoal surface. The reaction was monitored for 3 hours to allow for complete conversion of the substrates. A control reaction was performed without the Ag-NHC to provide a chromatogram for comparison.

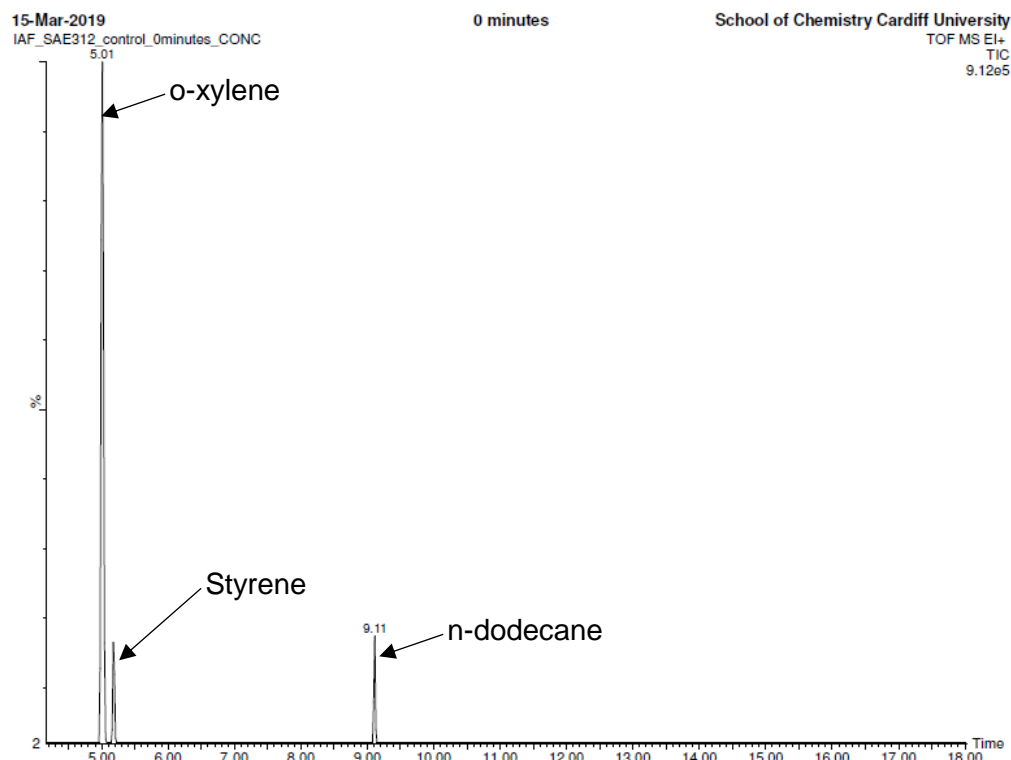


**Figure 22.** Composition of the test hydrosilylation control experiment in the absence of Ag-NHC before the addition of the catalyst presented as a GC-MS chromatogram.

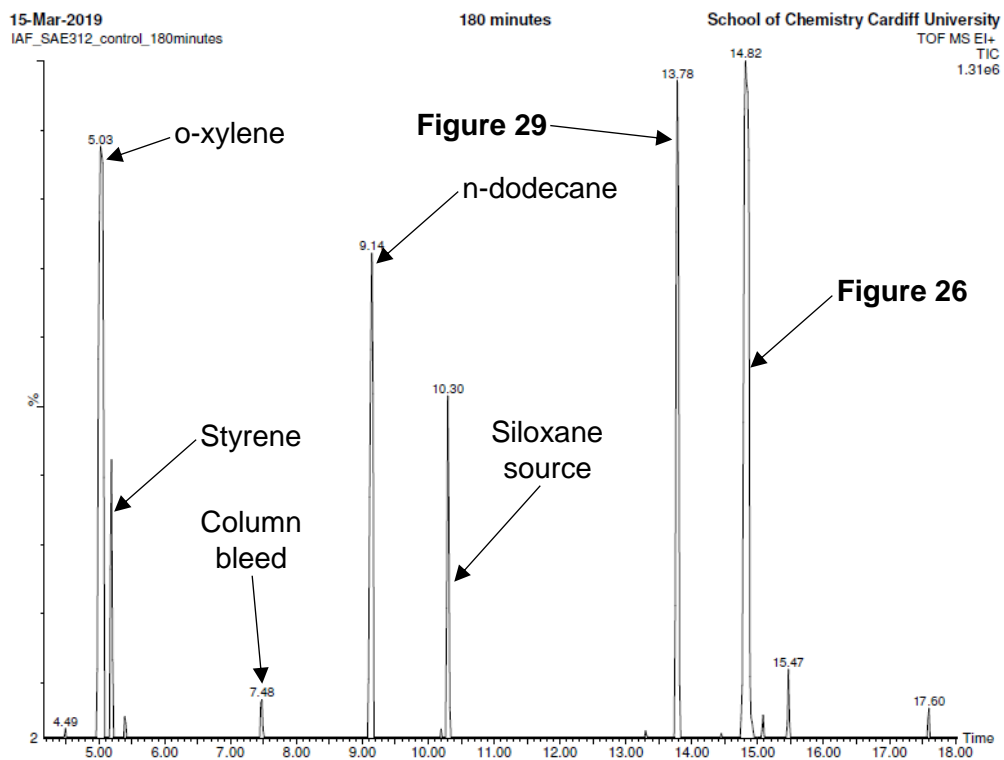


**Figure 23.** Composition of the test hydrosilylation control experiment in the absence of Ag-NHC 180 minutes post-addition of catalyst presented as a GC-MS chromatogram.

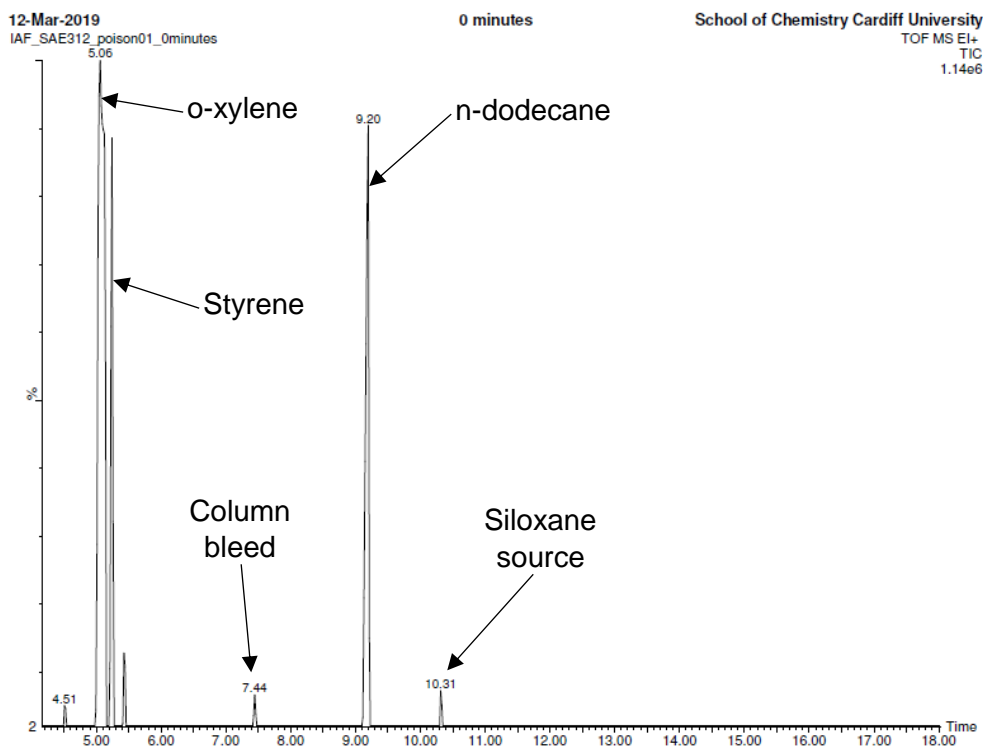


**Figure 24.** Composition of the test hydrosilylation experiment in the presence of 0.5 equivalents of Ag-NHC before the addition of the catalyst presented as a GC-MS chromatogram.

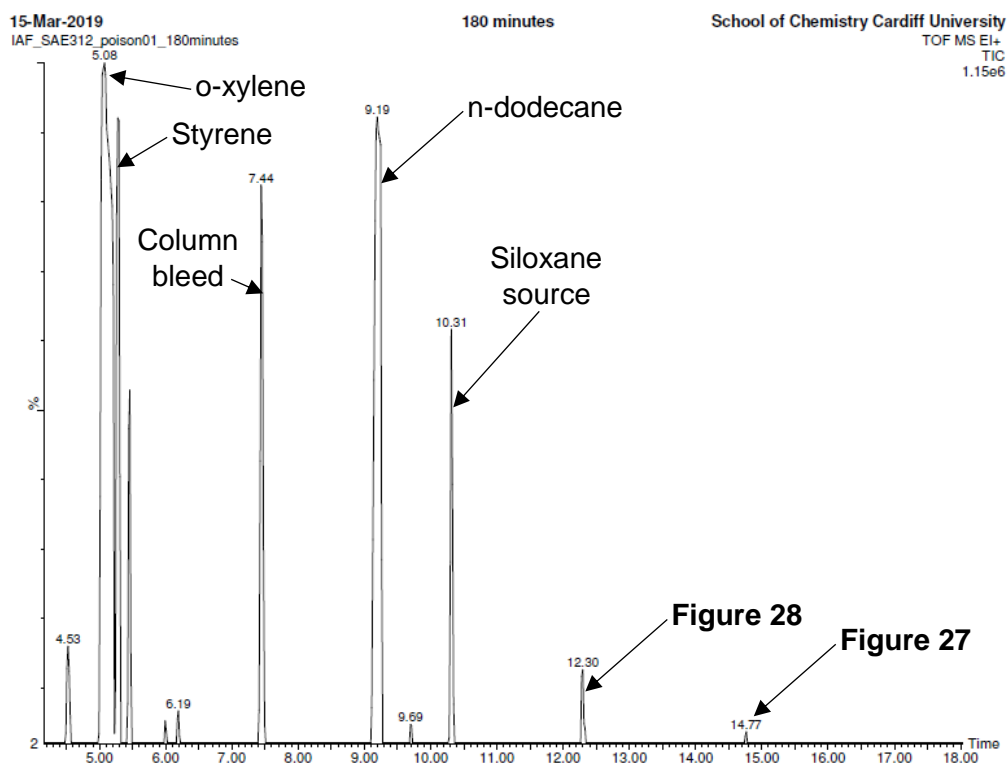


**Figure 25.** Composition of the test hydrosilylation experiment in the presence of Ag-NHC 180 minutes post-addition of catalyst presented as a GC-MS chromatogram.

Many common elutions are observed in the chromatograms both the control and experimental reactions. The first at roughly 5.00 minutes belongs to the solvent, *o*-xylene, with a peak observed at 106 m/z. This peak is common for the 0 minute and 180 minute chromatograms in the experimental and control reactions as expected. The second common peak for all chromatograms is seen at roughly 5.20 minutes. The mass spectra of each of these elution times contain a species with a principal peak at 104 m/z corresponding with styrene, one of the substrates. This area of the chromatogram for the 180-minute sample in the presence of Ag-NHC is more complicated, but the mass spectra derived from this area match well with those reported for the other chromatograms. A common peak is observed at roughly 7.4 minutes. The m/z for the peaks seen here are consistent with that observed due to septum bleed or column bleed contaminants. The next common peak is seen between 9.10-9.20 minutes belongs to the n-dodecane internal standard. This is confirmed by the mass spectra containing peaks at 170 m/z, with regular peaks every 14 m/z corresponding to the loss of methylene groups from the chain upon fragmentation. The common peak observed at roughly 10.3 minutes is likely due to a siloxane source. A peak at 222 m/z matches that of 1,1,1,3,5,5,5-heptamethyltrisiloxane, but the common peak could also similarly be from other siloxane sources such as the septa at the inlet or the column itself, as with the peak observed at 7.4 minutes. These common peaks are not observed in the control sample taken at 0 minutes, but the intensity of the xylene, styrene, and dodecane peaks in this chromatogram are not as intense, and the intensity of the potential contaminant peaks are far less intense than the three listed when observed in the other chromatograms. Both 180-minute chromatograms have a common elution at roughly 14.8 minutes. The spectra however look rather different, with a large peak at 309 m/z in the control reaction similar to the mass of the hydrosilylation product (though 2 m/z out for the  $[M^+ - CH_3]$  ion), but may also be due to column bleed (Figure 26). The spectrum for the poisoned reaction has a much larger number of peaks, and appears to correspond to column bleed. Many of the unique peaks in the poisoned reaction are similar in that they correspond to column bleed. This includes the large, distinct peak recorded at 12.30 minutes. All peaks with lower intensity than this correspond to column or septum bleed, solubilised in the carrier solvent. The peaks previously described as common peaks are broad in the poisoned 180-minute spectrum due to the increased concentration.

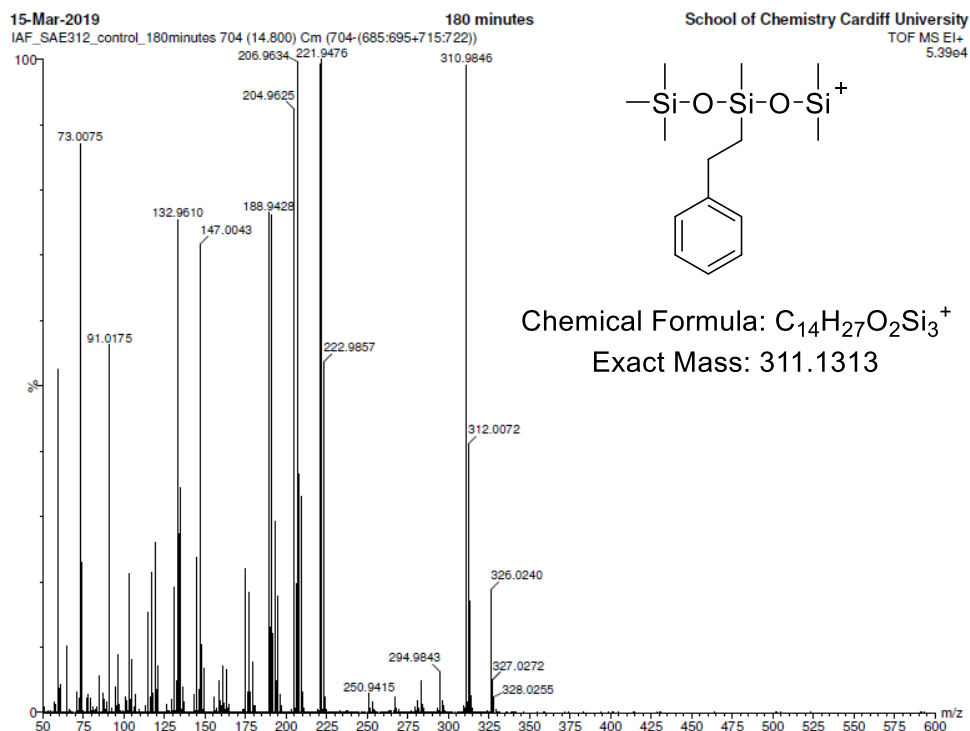


**Figure 26.** Mass spectrum of the elution at 14.8 minutes from the chromatogram of the control reaction in the absence of Ag-NHC after 180 minutes. The potential hydrosilylation product may be represented by the peaks at 310.9846 m/z.

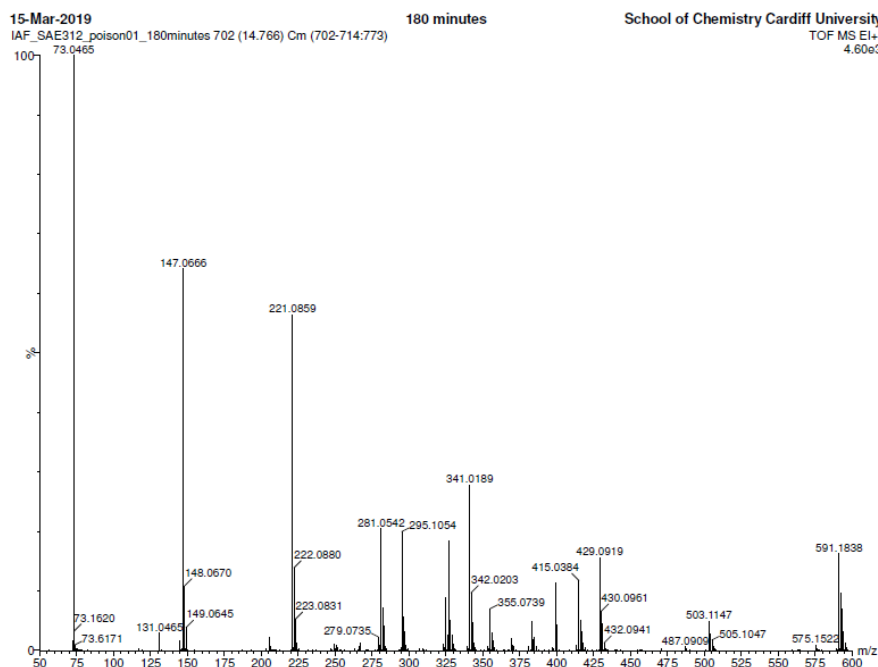


**Figure 27.** Mass spectrum of the elution at 14.8 minutes from the chromatogram of the reaction in the presence of Ag-NHC after 180 minutes. The spectrum is markedly different to that seen at the same elution time in the control reaction (above), and likely caused by column bleed.

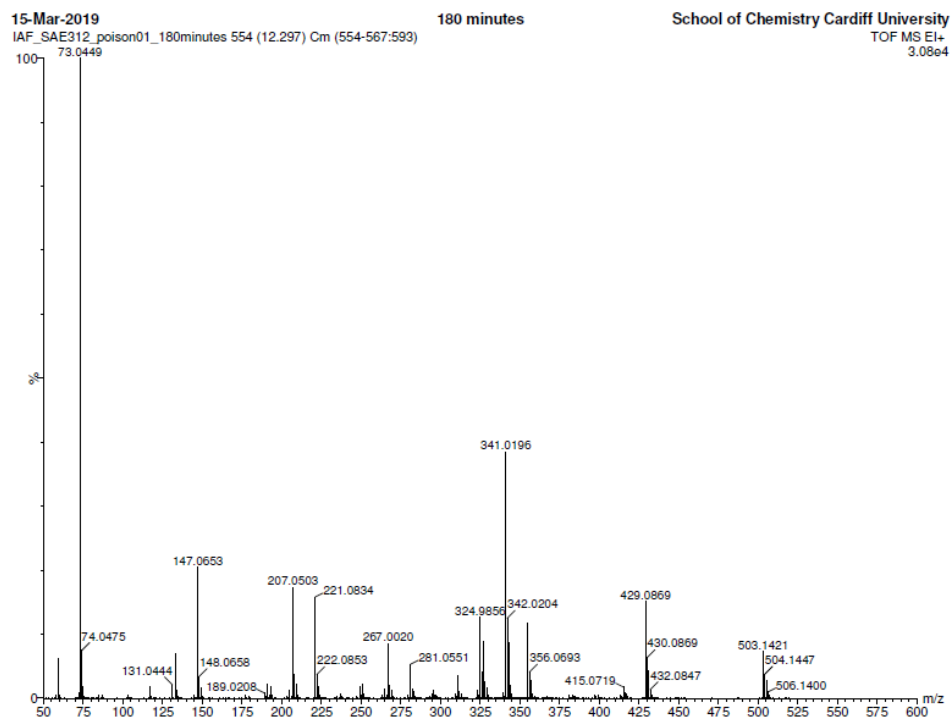


**Figure 28.** Mass spectrum of the elution at 12.3 minutes from the chromatogram of the reaction in the presence of Ag-NHC after 180 minutes. The spectrum is similar to that seen at 14.8 minutes in the same reaction (above), and likely caused by column bleed.

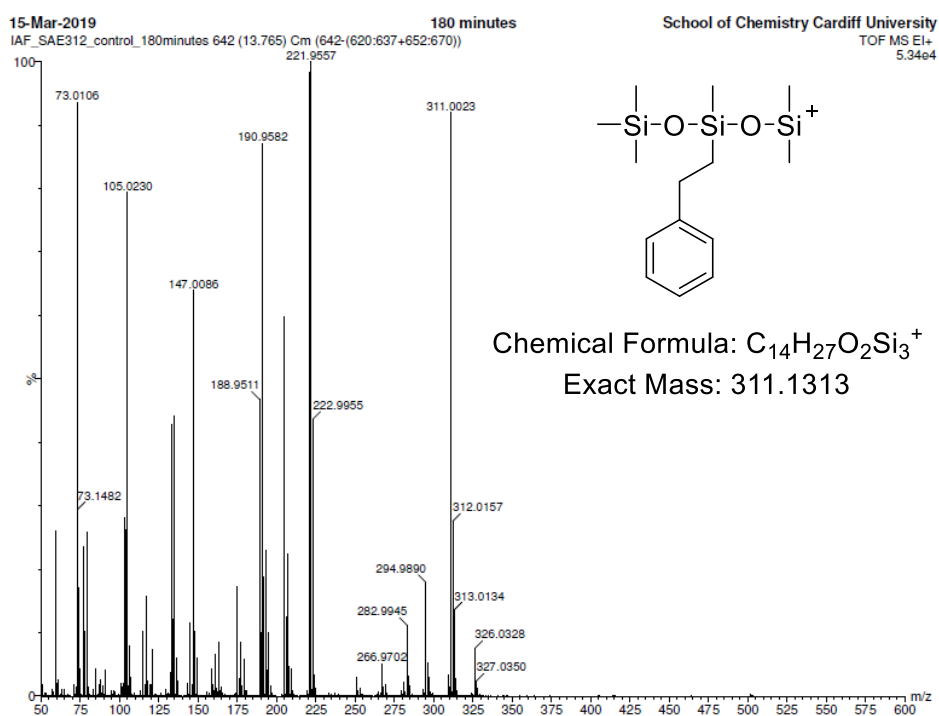


**Figure 29.** Mass spectrum of the elution that occurs at 13.8 minutes in the control reaction that is absent in the reaction containing Ag-NHC. The spectrum contains distinct peaks at 311.0023 m/z and 221.9557 m/z which may be attributed to the  $[M^+ - CH_3]$  and the  $[SiMe(OSiMe_3)_2]^+$  ions of the hydrosilylation product.

## Transmetalation reaction to probe catalyst poisoning

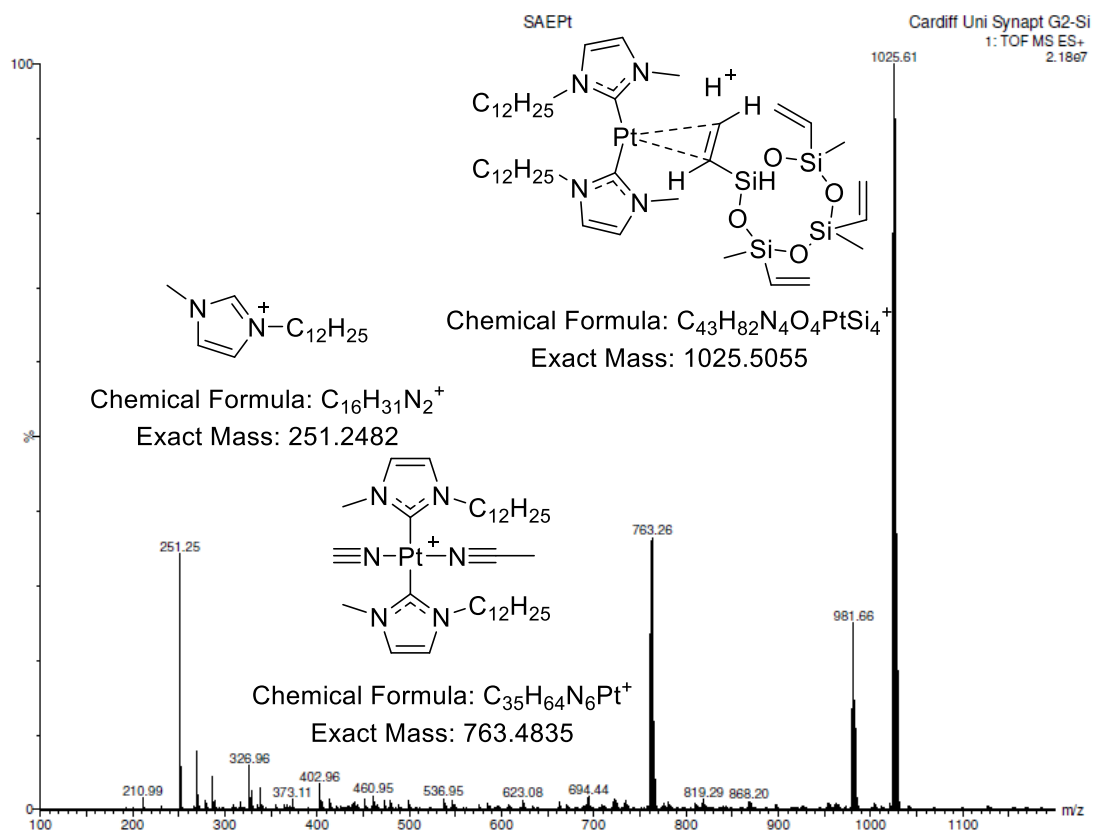


**Figure 30.** Low resolution mass spectrum depicting the species present upon refluxing an Ag-NHC in toluene in the presence of a Pt(0)-cyclovinylnmethylsiloxane.

The reaction produced the same brown colour as formed in the silicone rubber upon heating. There is a peak clearly corresponding to the protonated NHC (the imidazolium cation) at 251.25 in the spectrum, but there is no evidence of any AgBrNHC species (436.06 m/z) or the typically observed  $[\text{Ag}(\text{NHC})_2]^+$  (607.35 m/z) observed, suggesting that there is not silver present. None of the presented peaks at 763.26 m/z, 981.66 m/z, or 1025.61 m/z have isotope patterns that match that of Ag either, further supporting that there are no Ag species present in the filtered reaction with detectable ions. The  $\text{M}^+$  peak observed has a similar mass to a  $[\text{Pt}(\text{0})(\text{NHC})_2(\text{cyclovinylnmethylsiloxane}) - \text{CH}_3]^+$  ion. This species could feasibly form under ionisation, and is therefore potentially the poisoned catalyst produced in upon reaction of Pt in cyclovinylnmethylsiloxane with a model Ag-NHC (**7Ag**). The peak at 981.66 is 44 m/z less and has the same isotope pattern. Another indication of catalyst inhibition is the species observed at 763.26 m/z, which may be assigned as  $[\text{Pt}(\text{NHC})_2(\text{MeCN})_2 - \text{CH}_3]^+$ . Further analysis is required to determine the species that forms during the reaction, but it is clear from the mass spectrum that all Ag-NHC in the reaction is consumed.

## Surface morphology of silicone rubbers

The surface morphology of the TM1 silicone rubbers produced was probed by SEM and EDX.<sup>94,126–129</sup> The samples were cut to shape and mounted on carbon tape. The silicones were then sputter coated with Au/Pd in order to prevent charging on the surface when imaging, as silicone rubber is a poorly conductive material.<sup>130–133</sup> Images of each silicone were recorded at 2 kx, 5 kx, and 50 kx magnification using secondary electron and backscatter detection in order to glean as much information as possible from the images captured. The typical morphology of TM1 is uneven, which is seen at all magnifications. The uneven surface is likely due to the relatively uneven nature of the mould used when considered at a  $\mu\text{m}$ -scale, as well as microscopic damage caused to the surface when removing the silicone from the mould. The general morphology of most of the doped silicones is similar, bar a few examples. The morphology of 5 wt% triclosan laurate TM1 is typically similar to TM1 despite its opaque appearance, besides an observed 100  $\mu\text{m}$  across hole at one location on the sample (Figure 31).

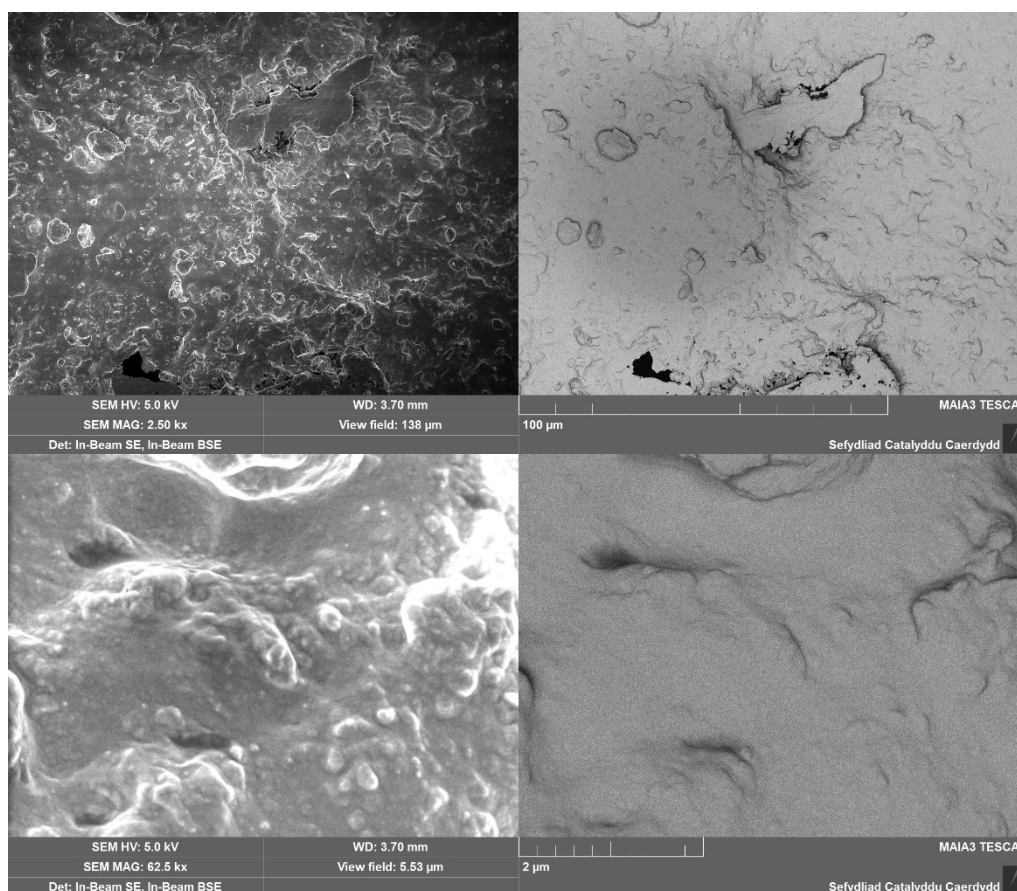


**Figure 31.** SEM images of 5 wt% triclosan laurate doped TM1 silicone rubber. The top images are taken at 2 kx magnification, whereas the bottom images are at 50 kx magnification. The left hand side images are captured with secondary electron detection, whereas the right hand side are captured with back-scattered electron detection.

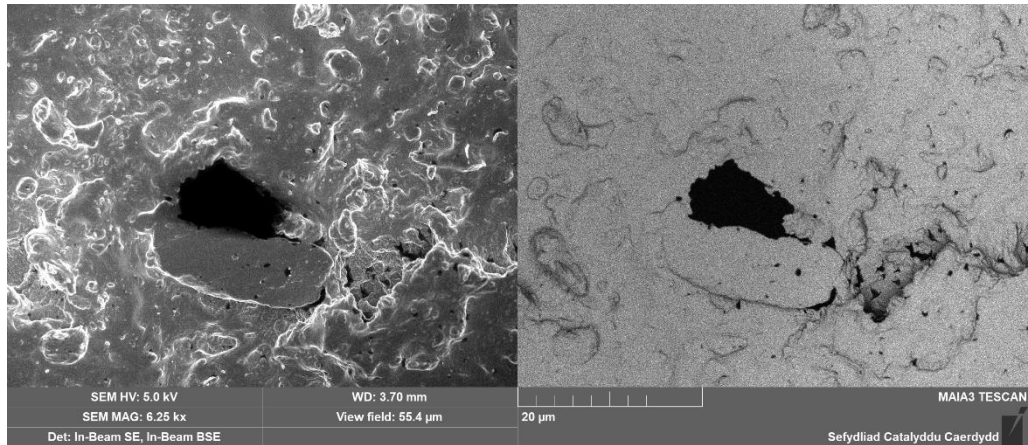


**Figure 32.** The hole previously described observed at 5 kx magnification on a sample of 5 wt% triclosan laurate doped TM1 silicone rubber. The left image was captured with secondary electron detection, whereas the right image was captured with back-scattered electron detection.

The surface of 5 wt% triclosan undecenoate TM1 is smoother than regular TM1, and may go some way to explaining its increased tensile strength due to less microscopic defects.<sup>134–138</sup>

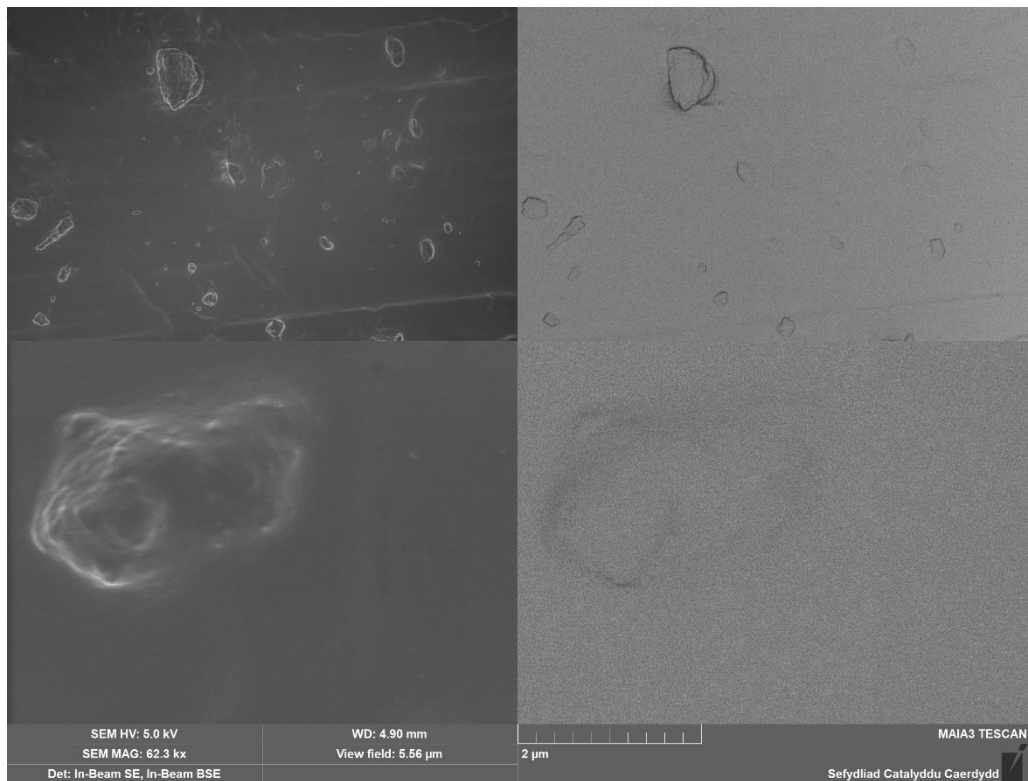


**Figure 33.** The smooth surface of 5 wt% triclosan undecenoate doped TM1 silicone rubber imaged at 2 kx (top) and 20 kx (bottom) magnification. The left image was captured with secondary electron detection, whereas the right image was captured with back-scattered electron detection.

The surface of 5 wt% 3-dodecyl-1-methylbenzimidazolium bromide TM1 is similar to that of TM1, but pock-marked with many holes, which can be as large as 100  $\mu\text{m}$  across. There are also a large number of smaller holes throughout the material that explain in part the silicone's low tensile strength and tear resistance.

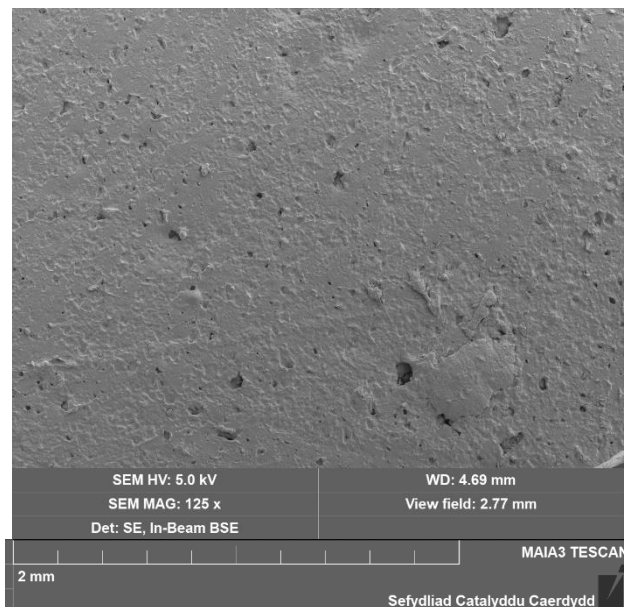


**Figure 34.** The pock-marked surface of 5 wt% benzimidazolium bromide salt doped TM1 silicone rubber imaged at 100 x (top) magnification. The image was captured with secondary electron detection.

There are also large sections with bizarre structures observed that appear to sit below the surface of TM1. The images discussed are shown below. All other images for TM1 materials are supplied in the appendix.

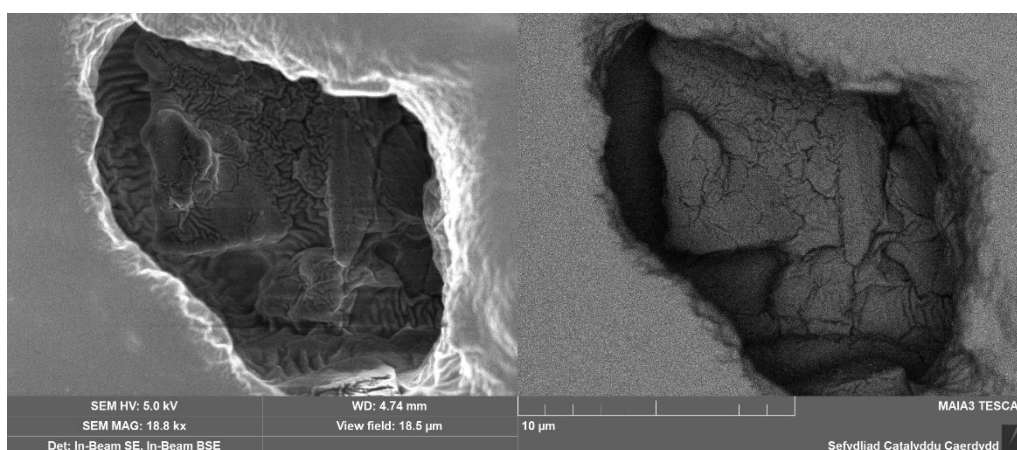


**Figure 35.** The structures observed occupying the holes of 5 wt% benzimidazolium bromide salt doped TM1 silicone rubber imaged at 15 kx (top) magnification. The images were captured with secondary electron detection (left), and back-scattered electron detection (right).

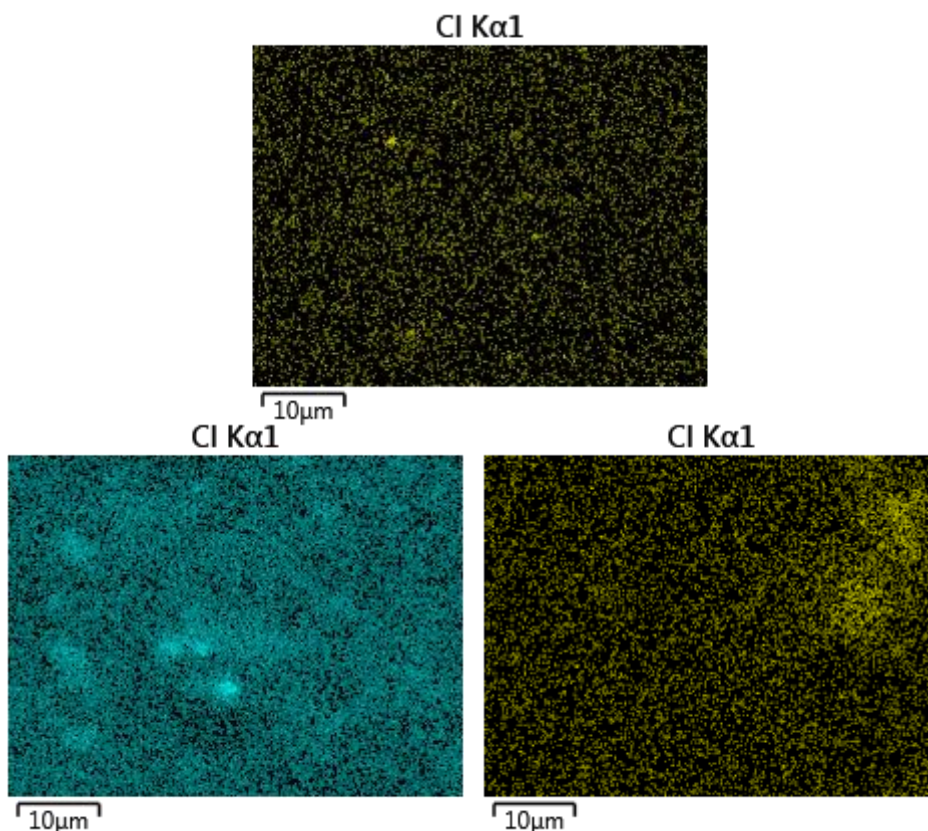


**Figure 36.** EDX mapping of Cl in TM1 (top, yellow), 5 wt% triclosan laurate doped TM1 (left, blue), and 5 wt% triclosan acetate doped TM1 (right, yellow). The presence of Cl species on the surface of TM1 is likely due to handling the sample and NaCl picked up from the environment. The values estimated by software calculation for wt% of Cl is as follows: TM1 = 0.51 wt%, triclosan laurate doped TM1 = 4.82 wt%, and triclosan acetate doped TM1 = 3.82 wt%.

The images taken were also subjected to analysis by EDX in order to determine the distribution of the dopant throughout the material. Though the atomic weights of the constituent atoms of the dopants are typically low, mostly consisting of carbon, nitrogen, and hydrogen atoms and are therefore difficult to distinguish using X-rays, there are distinct atoms that can be used to determine the localisation of the dopants. In the case of the triclosan species, chlorine atoms may be used, whereas bromine may be used as a distinguishing feature for the imidazolium and benzimidazolium bromide salts. All EDX analysed images show a relatively even distribution of these marker halides throughout suggesting that small amounts of the dopant are spread throughout the materials. All spectra show a distribution of chlorine throughout, suggesting some depositing of sodium chloride on the materials. The effective calculated concentration of chlorine is  $\geq 4$  times that found in TM1 in all triclosan- and triclosan ester-doped TM1. The bizarre structures discussed above observed in 5 wt% 3-dodecyl-1-methylbenzimidazolium bromide-doped

TM1 are found to contain a much higher percentage of bromine than the rest of the material, suggesting that the structures observed are large crystals of the benzimidazolium salt.

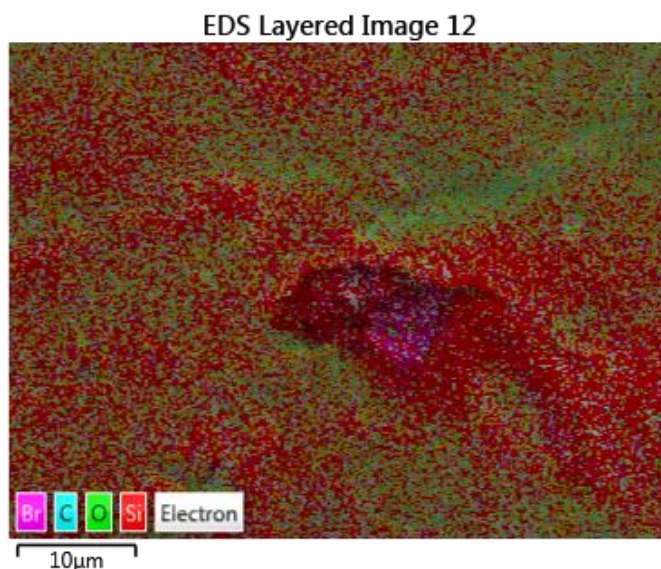


**Figure 37.** EDX mapping of 5 wt% 3-dodecyl-1-methylbenzimidazolium bromide doped TM1. The structure in the centre holds the majority of the Br species in the image. This suggests that the holes in the structure are caused by relatively large aggregates of the benzimidazolium salt

### Antimicrobial efficacy of doped silicones

The antimicrobial efficacy of the doped silicones was assessed using the Kirby-Bauer method.<sup>29,40–47</sup> The Kirby-Bauer method is also known as the disk diffusion method is a standard antimicrobial testing method that produces results rapidly. The test organisms were prepared in the same manner as when used for MIC testing (see Chapter 2). The bacteria used in this study were: *Staphylococcus aureus* NCIMB 9518, *Staphylococcus aureus* NCTC 6571, *Staphylococcus epidermidis* ATCC 14990, *Staphylococcus epidermidis* RP62A, *Pseudomonas aeruginosa* ATCC 15692, and *Escherichia coli* NCTC 12923. The bacteria were selected due to the panel containing common organisms responsible for nosocomial infections, and a mixture of Gram positive and Gram negative species. The test silicone materials doped with antimicrobial agents were placed onto agar inoculated with test organisms using forceps. Silicones must not move around once placed, as this may cause the zone of inhibition to smear and become poorly defined. The diameter of the area around a silicone disc where there was no bacterial growth was measured and defined as the zone of inhibition. The zones were measured against each organism in triplicate for each material.

Sample	Zone of Inhibition (mm) vs Gram positive (+) bacteria (average of 3 values)			
	<i>S. aureus</i> NCTC 6571	<i>S. aureus</i> NCIMB 9518	<i>S. epidermidis</i> ATCC 14990	<i>S. epidermidis</i> RP62A
TM1	13.3	10	14.3	12.3
Triclosan 5 wt% TM1	64	48	>90	>90
Triclosan acetate 5 wt% TM1	52	43.7	58.3	56
Triclosan benzoate 5wt % TM1	17.7	11	18.7	19.3
Triclosan laurate 5 wt% TM1	24.3	15.7	28	20
Triclosan undecenoate 5 wt% TM1	28	22	33	34
1-methyl-3-imidazolium bromide 5 wt% TM1	25	25.3	30	26.3
1-methyl-3-benzimidazolium bromide 5 wt% TM1	17	17	23	24

**Table 12.** Zones of inhibition of novel silicone rubber materials against 4 Gram positive bacteria measured in mm. The zones of inhibition are a measure of the diameter of an area where no visible growth had occurred on the agar. Values were measured in triplicate, and a mean value was taken.

Sample	Zone of Inhibition (mm) vs Gram negative (-) bacteria (average of 3 values)	
	<i>E. coli</i> NCTC 12923	<i>P. aeruginosa</i> ATCC 15692
TM1	6	6
Triclosan 5 wt% TM1	51	6
Triclosan acetate 5 wt% TM1	23	6
Triclosan benzoate 5wt % TM1	6	6
Triclosan laurate 5 wt% TM1	6	6
Triclosan undecenoate 5 wt% TM1	11.3	6
1-methyl-3-imidazolium bromide 5 wt% TM1	13.7	6
1-methyl-3-benzimidazolium bromide 5 wt% TM1	9.7	6

**Table 13.** Zones of inhibition of novel silicone rubber materials against 2 Gram negative species of bacteria measured in mm. The zones of inhibition are a measure of the diameter of an area where no visible growth had occurred on the agar. Values were measured in triplicate, and a mean value was taken.

As can be seen, there is a greater zone of inhibition for Gram positive species than Gram negative species in all cases. This difference may be explained by the secondary membrane of the Gram negative bacteria protecting intracellular processes from the antimicrobial agents present in the silicones.<sup>139</sup> The most effective dopant is 5 wt% triclosan, as the zone of inhibition is exceptionally large against all species except *P. aeruginosa*. *P. aeruginosa* is well known as a hardy organism due to a mixture of multidrug efflux pumps with chromosomally encoded antimicrobial resistance genes, a membrane with low permeability, and the typically low permeability of the species' cell envelope.<sup>140,141</sup> The next most effective is 5 wt% triclosan acetate, followed by 5 wt% triclosan undecenoate, triclosan laurate, 3-dodecyl-1-methylimidazolium bromide, 3-dodecyl-1-methylbenzimidazolium bromide, then triclosan benzoate. In all cases, the doped silicones show a greater zone of inhibition than basic TM1, with the previously noted exception of *P. aeruginosa*. The zone of inhibition of the triclosan and imidazolium derivative-doped TM1 appears to decrease with an increase in molecular weight of the dopant. With an increase in molecular weight, the number of moles of dopant that make up the 5 wt% is lower. The decrease in zone of inhibition may therefore be partially due to less molecules of antimicrobial agent being present per 5 wt% doping. The one dopant that does not follow this trend is triclosan benzoate. Triclosan benzoate has a molecular weight between triclosan acetate and triclosan undecenoate, but its zone of inhibition is the smallest of all 5 wt% doped silicones. Triclosan is a known antimicrobial agent, and benzoates are used frequently as preservatives that inhibit microbial growth in foods,<sup>27,142–144</sup> but the combination of the two components leads to an ineffective dopant. The doped silicones typically have the largest zones of inhibition against the *S. epidermidis* strains, followed by *S. aureus* strains, *E. coli*, and then *P. aeruginosa*. The efficacy of the doped silicones is similar against both strains of *S. epidermidis*, with 5 wt% triclosan acetate, triclosan laurate, and 3-dodecyl-1-methylimidazolium bromide having a slightly larger zone of inhibition against *S. epidermidis* ATCC 14990, and triclosan benzoate, triclosan undecenoate, and 3-dodecyl-1-methylbenzimidazolium bromide having slightly larger zones of inhibition against *S. epidermidis* RP62A. The zones of inhibition exhibited by the doped silicones are almost universally larger against *S. aureus* NCTC 6571 than they are against *S. aureus* NCIMB 9518, with the exception of 3-dodecyl-1-methylbenzimidazolium bromide, which has a zone of inhibition 0.333 mm greater against *S. aureus* NCIMB 9518 than against *S. aureus* NCTC 6571. *E. coli* growth is only inhibited by 5 wt% triclosan TM1, 5 wt% triclosan acetate TM1, 5 wt% triclosan undecenoate TM1, 5 wt% 3-dodecyl-1-methylimidazolium bromide, and 5 wt% 3-dodecyl-1-methylbenzimidazolium bromide. Only triclosan- and triclosan acetate-doped TM1 have a zone of inhibition greater than 20 mm against *E. coli*.



**Figure 38.** Zone of inhibition assay of 5 silicone rubber materials: TM1 (C), triclosan undecenoate doped TM1 (u10), triclosan benzoate doped TM1 (Bz), triclosan laurate doped TM1 (C12), and triclosan acetate doped TM1 (Ac) against *S. aureus* NCIMB 9518. The zones exhibited by triclosan acetate doped TM1 are most visible in this image, and are circled to draw attention to them.



**Figure 39.** Zone of inhibition assay of 5 silicone rubber materials: TM1 (C), triclosan undecenoate doped TM1 (u10), triclosan benzoate doped TM1 (Bz), triclosan laurate doped TM1 (C12), and triclosan acetate doped TM1 (Ac) against *P. aeruginosa* ATCC 15692. No zones of inhibition were observed, leading to a value of 6 mm (the diameter of the silicone disc) to be recorded.

## Conclusion

A novel silicone rubber material, TM1, was prepared. The work time, cure time (at room temperature and elevated temperature), Shore A hardness, tensile strength, elongation at failure (%), and tear resistance, and surface morphology of the material was described as a means of characterising the formulation. A work time of 25 minutes was found for TM1, with cure times of 180 minutes at room temperature and 10 minutes at 100 °C. The Shore A hardness of TM1 was found to be 25.6 durometer ( $\pm 2.55$ ). TM1 was found to have a tensile strength of 1.78 MPa ( $\pm 0.263$ ), with a maximum elongation of 1016% ( $\pm 129$ ) at breakage, along with a calculated tear resistance of 12.3 kNm<sup>-1</sup> ( $\pm 2.34$ ). These values are comparable to other maxillofacial silicone rubbers used in medical and industrial settings. 6 new (to this work) antimicrobial dopant molecules (triclosan acetate, triclosan benzoate, triclosan laurate, triclosan undecenoate, 3-decyl-1-vinylimidazolium bromide, and 1-methyl-3-(undec-10-enyl)imidazolium bromide) were synthesised with good to quantitative yields. The incorporation of the new molecules, triclosan, as well as 7 molecules previously described in this work (3-dodecyl-1-methylimidazolium bromide, 3-dodecyl-1-methylbenzimidazolium bromide, 3-dodecyl-1-methylimidazol-2-ylidene silver(I) bromide, 3-dodecyl-1-methylbenzimidazol-2-ylidene silver(I) bromide, CuGTSB, CuGTSH, and CuGTSO) into the TM1 base mixture before curing was attempted in order to develop new antimicrobial silicone rubbers.

Typically, the addition of the dopant molecules had very little impact on the work time of the silicone rubber. The addition of dopants did however impact the cure time of TM1 at room temperature and elevated temperature, with metal complex dopants and terminal alkene-containing imidazolium bromide salts causing the curing process to fail. In the case of the 2 Ag-NHC dopants, the silicone failed to cure and showed significant discolouration. The curing of TM1 doped with CuGTSB, CuGTSH, CuGTSO, 3-decyl-1-vinylimidazolium bromide, and 1-methyl-3-(undec-10-enyl)imidazolium bromide appeared to succeed on a small scale with some residual tackiness, but failed to cure into slabs that were able to be removed from the mould when slab production was attempted. Triclosan undecenoate, another dopant with a terminal alkene group did not halt the curing process entirely, but slowed the curing process by comparison with TM1 with no dopant. 7 dopants allowed for TM1 to be cured into slabs which could be used for physical testing: triclosan, triclosan acetate, triclosan benzoate, triclosan laurate, triclosan undecenoate, 3-dodecyl-1-methylimidazolium bromide, and 3-dodecyl-1-methylbenzimidazolium bromide. The Shore A hardness of all 5 wt% doped TM1 silicone rubbers were similar to those of base TM1. Triclosan benzoate doped TM1 had a reasonably higher mean hardness than that of the base material, but the standard

deviation of the hardness values overlapped. The tensile strength of TM1 was improved by doping with triclosan, and significantly improved by addition of triclosan undecenoate (from 1.78 MPa ( $\pm$  0.263) to 2.71 MPa ( $\pm$  0.509)). The maximum elongation at failure was also significantly improved by doping TM1 with triclosan undecenoate, with the maximum elongation increasing from 1016% ( $\pm$  129) to 1652% ( $\pm$  202). 3-dodecyl-1-methylbenzimidazolium bromide was found to significantly decrease the tensile strength and elongation at failure of TM1. The same trend was not observed in the enhancement of tear strength for the most part, with only a slight increase observed in tear resistance for TM1 doped with triclosan and its esters. A significant decrease in tear resistance was observed when TM1 was doped with 3-dodecyl-1-methylbenzimidazolium bromide, in keeping with its lower tensile strength.

The discolouration of TM1 when doped with Ag-NHCs was investigated by means of a test hydrosilylation. It was seen by GC-MS that the hydrosilylation product from the reaction of styrene and 1,1,1,3,5,5,5-heptamethyltrisiloxane was formed when catalysed with a Pt(0) catalyst, but did not form when the reaction was conducted in the presence of 3-dodecyl-1-methylimidazol-2-ylidene silver(I) bromide. This suggests that the Ag-NHC species interferes with the reaction, most likely by transmetalation of the NHC onto the Pt component of the catalyst, deactivating or significantly lowering the efficacy of the catalyst in performing the hydrosilylation reaction.

The doped TM1 materials showed some efficacy by zone of inhibition assay against Gram positive *S. aureus* and *S. epidermidis* strains, as well as some success against a Gram negative *E. coli* strain. None of the doped samples produced zones of inhibition against the Gram negative *P. aeruginosa*. The zones of inhibition for triclosan, and to a lesser extent triclosan acetate, were significantly larger than those produced by the other doped samples against the Gram positive *Staphylococcus* strains as well as against *E. coli*. Only triclosan-, triclosan acetate-, triclosan undecenoate-, 3-dodecyl-1-methylimidazolium bromide-, and 3-dodecyl-1-methylbenzimidazolium bromide-doped TM1 produced a zone of inhibition against *E. coli*. The findings discussed suggest that silicone materials doped with antimicrobial agents before curing may be suitable for producing silicone rubber devices that prevent bacterial growth and contamination. There is a need however to carefully select dopants that do not interfere with the curing process of the silicone rubber by interacting with the catalyst and inhibiting the crucial hydrosilylation reaction used to produce 3D silicone networks. A potential solution to the problem of the narrow range of antimicrobial dopants available would involve the development of a poisoning resistant, highly active hydrosilylation catalyst.<sup>106</sup>

## References

- 1 A. Mitra, S. Choudhary, H. Garg and J. H.G., *J. Clin. Diagn. Res. JCDR*, 2014, **8**, ZE08-ZE13.
- 2 H.-C. Flemming, *Appl. Microbiol. Biotechnol.*, 2002, **59**, 629–640.
- 3 C. B. Shah, M. W. Mittelman, J. W. Costerton, S. Parenteau, M. Pelak, R. Arsenault and L. A. Mermel, *Antimicrob. Agents Chemother.*, 2002, **46**, 1674–1679.
- 4 H. Hanna, R. Benjamin, I. Chatzinikolaou, B. Alakech, D. Richardson, P. Mansfield, T. Dvorak, M. F. Munsell, R. Darouiche, H. Kantarjian and I. Raad, *J. Clin. Oncol.*, 2004, **22**, 3163–3171.
- 5 S. Silva, M. Negri, M. Henriques, R. Oliveira, D. W. Williams and J. Azeredo, *J. Med. Microbiol.*, 2010, **59**, 747–754.
- 6 B. Gottenbos, H. C. van der Mei, F. Klatter, P. Nieuwenhuis and H. J. Busscher, *Biomaterials*, 2002, **23**, 1417–1423.
- 7 U. Samuel and J. P. Guggenbichler, *Int. J. Antimicrob. Agents*, 2004, **23**, 75–78.
- 8 J. R. Johnson, M. A. Kuskowski and T. J. Wilt, *Ann. Intern. Med.*, 2006, **144**, 116–126.
- 9 A. Salvarci, M. Koroglu and B. Erayman, *Urology*, 2016, **88**, 66–75.
- 10 E. Ozkan, F. T. Ozkan, E. Allan and I. P. Parkin, *RSC Adv.*, 2015, **5**, 8806–8813.
- 11 A. Piecuch, E. Obłąk and K. Guz-Regner, *J. Surfactants Deterg.*, 2016, **19**, 275–282.
- 12 W. D. Morain and L. M. Vistnes, *Plast. Reconstr. Surg.*, 1977, **59**, 216–222.
- 13 J. M. Schierholz and G. Pulverer, *Biomaterials*, 1998, **19**, 2065–2074.
- 14 D. T. Ciccognani, G. Polson, D. Lei, K. DiNicola, R. Shalvoy, J. Arresse and G. Pierard, *J. Cosmet. Sci.*, 2004, **55**, 217–218.
- 15 M. L. Blanscet, P. A. Tordik and G. G. Goodell, *J. Endod.*, 2008, **34**, 1246–1248.
- 16 A. Kottmann, E. Mejía, T. Hémerly, J. Klein and U. Kragl, *Chem. – Asian J.*, 2017, **12**, 1168–1179.
- 17 S. Perni, C. Piccirillo, A. Kafizas, M. Uppal, J. Pratten, M. Wilson and I. P. Parkin, *J. Clust. Sci.*, 2010, **21**, 427–438.
- 18 E. Ozkan, E. Allan and I. P. Parkin, *RSC Adv.*, 2014, **4**, 51711–51715.
- 19 S. K. Sehmi, S. Noimark, J. Weiner, E. Allan, A. J. MacRobert and Ivan. P. Parkin, *ACS Appl. Mater. Interfaces*, 2015, **7**, 22807–22813.
- 20 Y. Lin, Q. Liu, L. Cheng, Y. Lei and A. Zhang, *React. Funct. Polym.*, 2014, **85**, 36–44.
- 21 X. Cui, C. Qiao, S. Wang, Y. Ding, C. Hao and J. Li, *Colloid Polym. Sci.*, 2015, **293**, 1971–1981.
- 22 A. Vaterrodt, B. Thallinger, K. Daumann, D. Koch, G. M. Guebitz and M. Ulbricht, *Langmuir*, 2016, **32**, 1347–1359.
- 23 P. Ferreira, Á. Carvalho, T. R. Correia, B. P. Antunes, I. J. Correia and P. Alves, *Sci. Technol. Adv. Mater.*, 2013, **14**, 055006.
- 24 T. Kawahara, Y. Takeuchi, G. Wei, K. Shirai, T. Yamauchi and N. Tsubokawa, *Polym. J.*, 2009, **41**, 744–751.
- 25 H.-S. Yang and E.-S. Park, *Macromol. Mater. Eng.*, 2006, **291**, 621–628.
- 26 K. Taptim and N. Sombatsompop, *J. Vinyl Addit. Technol.*, 2013, **19**, 113–122.
- 27 A. A. Al-Juhni and B. Z. Newby, *Prog. Org. Coat.*, 2006, **56**, 135–145.
- 28 A. Fazly, C. Jain, A. C. Dehner, L. Issi, E. A. Lilly, A. Ali, H. Cao, P. L. Fidel, R. P. Rao and P. D. Kaufman, *Proc. Natl. Acad. Sci.*, 2013, **110**, 13594–13599.
- 29 K. De Prijck, N. De Smet, K. Honraet, S. Christiaen, T. Coenye, E. Schacht and H. J. Nelis, *Mycopathologia*, 2010, **169**, 167–174.
- 30 M. Chan, G. Hidalgo, B. Asadishad, S. Almeida, N. Muja, M. S. Mohammadi, S. N. Nazhat and N. Tufenkji, *Colloids Surf. B Biointerfaces*, 2013, **110**, 275–280.
- 31 C.-M. Phan, L. N. Subbaraman and L. Jones, *J. Biomater. Sci. Polym. Ed.*, 2014, **25**, 1907–1919.
- 32 R. Dastjerdi, M. Montazer and S. Shahsavan, *Colloids Surf. Physicochem. Eng. Asp.*, 2009, **345**, 202–210.

- 33 A. Goyal, A. Kumar, P. K. Patra, S. Mahendra, S. Tabatabaei, P. J. J. Alvarez, G. John and P. M. Ajayan, *Macromol. Rapid Commun.*, 2009, **30**, 1116–1122.
- 34 P. Kaali, E. Strömberg, R. E. Aune, G. Czél, D. Momcilovic and S. Karlsson, *Polym. Degrad. Stab.*, 2010, **95**, 1456–1465.
- 35 M. Cazacu, C. Racles, A. Airinei, A. Vlad and I. Stoica, *Polym. Adv. Technol.*, 2012, **23**, 122–129.
- 36 A. L. R. Pires and Â. M. Moraes, *J. Appl. Polym. Sci.*, 2015, DOI:10.1002/app.41686.
- 37 M. Gosau, L. Prantl, M. Feldmann, A. Kokott, S. Hahnel and R. Bürgers, *Biofouling*, 2010, **26**, 359–365.
- 38 S. Ghamrawi, J.-P. Bouchara, O. Tarasyuk, S. Rogalsky, L. Lyoshina, O. Bulko and J.-F. Bardeau, *Mater. Sci. Eng. C*, 2017, **75**, 969–979.
- 39 S. Ghamrawi, J.-P. Bouchara, A. Corbin, S. Rogalsky, O. Tarasyuk and J.-F. Bardeau, *Mater. Today Commun.*, 2020, **22**, 100716.
- 40 M. A. Pigno, M. C. Goldschmidt and J. C. Lemon, *J. Prosthet. Dent.*, 1994, **71**, 295–300.
- 41 S. Patil, J. Claffey, A. Deally, M. Hogan, B. Gleeson, L. M. M. Mendez, H. Mueller-Bunz, F. Paradisi and M. Tacke, *Eur. J. Inorg. Chem.*, 2010, 1020–1031.
- 42 S. Patil, A. Deally, B. Gleeson, H. Mueller-Bunz, F. Paradisi and M. Tacke, *Metallomics*, 2011, **3**, 74–88.
- 43 S. Patil, K. Dietrich, A. Deally, B. Gleeson, H. Müller-Bunz, F. Paradisi and M. Tacke, *Helv. Chim. Acta*, 2010, **93**, 2347–2364.
- 44 S. Patil, A. Deally, B. Gleeson, F. Hackenberg, H. Müller-Bunz, F. Paradisi and M. Tacke, *Z. Für Anorg. Allg. Chem.*, 2011, **637**, 386–396.
- 45 F. Hackenberg, A. Deally, G. Lally, S. Malenke, H. Müller-Bunz, F. Paradisi, S. Patil, D. Quaglia and M. Tacke, *Int. J. Inorg. Chem.*, 2012, Article ID 121450, 13 pages, DOI: 10.1155/2012/121540.
- 46 F. Hackenberg, A. Deally, G. Lally, S. Malenke, H. Müller-Bunz, F. Paradisi, S. Patil, D. Quaglia and M. Tacke, *Int. J. Inorg. Chem.*, 2012, **2012**, 1–13.
- 47 S. Patil, A. Deally, B. Gleeson, H. Müller-Bunz, F. Paradisi and M. Tacke, *Met. Integr. Biometal Sci.*, 2011, **3**, 74–88.
- 48 M. Herla, K. Boening, H. Meissner and K. Walczak, *Materials*, 2019, **12**, 3518.
- 49 A. Bhargava, V. Pareek, S. Roy Choudhury, J. Panwar and S. Karmakar, *ACS Appl. Mater. Interfaces*, 2018, **10**, 29325–29337.
- 50 Woodruff Tracey J., Zota Ami R. and Schwartz Jackie M., *Environ. Health Perspect.*, 2011, **119**, 878–885.
- 51 Philippat Claire, Wolff Mary S., Calafat Antonia M., Ye Xiaoyun, Bausell Rebecca, Meadows Molly, Stone Joanne, Slama Rémy and Engel Stephanie M., *Environ. Health Perspect.*, 2013, **121**, 1225–1231.
- 52 Q. Zhong, M. Peng, J. He, W. Yang and F. Huang, *Sci. Total Environ.*, 2020, **703**, 134720.
- 53 D. Stickler, G. Jones and A. Russell, *The Lancet*, 2003, **361**, 1435–1437.
- 54 G. J. Williams and D. J. Stickler, *J. Med. Microbiol.*, 2008, **57**, 1135–1140.
- 55 D. J. Stickler, *Nat. Clin. Pract. Urol.*, 2008, **5**, 598–608.
- 56 D. M. Siddiq and R. O. Darouiche, *Nat. Rev. Urol.*, 2012, **9**, 305–314.
- 57 D. J. Stickler, *J. Intern. Med.*, 2014, **276**, 120–129.
- 58 V. Zumstein, P. Betschart, W. C. Albrich, M. T. Buhmann, Q. Ren, H.-P. Schmid and D. Abt, *Swiss Med. Wkly.*, 2017, 147:w14408, DOI:10.4414/smw.2017.14408.
- 59 K. Belfield, X. Chen, E. F. Smith, W. Ashraf and R. Bayston, *Acta Biomater.*, 2019, **90**, 157–168.
- 60 T. A. Gaonkar, L. A. Sampath and S. M. Modak, *Infect. Control Hosp. Epidemiol.*, 2003, **24**, 506–513.
- 61 M. C. McBride, R. Karl Malcolm, A. David Woolfson and S. P. Gorman, *Biomaterials*, 2009, **30**, 6739–6747.
- 62 R. P. C. Jordan, S. Malic, M. G. J. Waters, D. J. Stickler and D. W. Williams, *Microbiol. Discov.*, 2015, 3:1, DOI:10.7243/2052-6180-3-1.

- 63 L. Riber, M. Burmølle, M. Alm, S. M. Milani, P. Thomsen, L. H. Hansen and S. J. Sørensen, *Plasmid*, 2016, **87–88**, 72–78.
- 64 S. Mishra, K. Karmodiya, P. Parasuraman, A. Surolia and N. Surolia, *Bioorg. Med. Chem.*, 2008, **16**, 5536–5546.
- 65 United States, US5968207A, 1999.
- 66 FR2839448A1, 2003.
- 67 United States, US6384173B1, 2002.
- 68 S. Choi, J. Jepperson, L. Jarabek, J. Thomas, B. Chisholm and P. Boudjouk, *Macromol. Symp.*, 2007, **249–250**, 660–667.
- 69 H.-X. Wu, L. Tan, Z.-W. Tang, M.-Y. Yang, J.-Y. Xiao, C.-J. Liu and R.-X. Zhuo, *ACS Appl. Mater. Interfaces*, 2015, **7**, 7008–7015.
- 70 Q. Xie, H. Zeng, Q. Peng, C. Bressy, C. Ma and G. Zhang, *Adv. Mater. Interfaces*, 2019, **6**, 1900535, DOI:10.1002/admi.201900535.
- 71 World Intellectual Property Organization, WO1999010310A1, 1999.
- 72 United States, US3784698A, 1974.
- 73 World Intellectual Property Organization, WO1999031036A2, 1999.
- 74 N. I. Malek, Z. S. Vaid, U. U. More and O. A. El Seoud, *Colloid Polym. Sci.*, 2015, **293**, 3213–3224.
- 75 Y. Zhang, C. U. Pittman, A. Arockiasamy and R. L. King, *J. Appl. Polym. Sci.*, 2011, **121**, 2430–2441.
- 76 D11 Committee, *Test Methods for Vulcanized Rubber and Thermoplastic Elastomers Tension*, ASTM International.
- 77 D11 Committee, *Test Method for Tear Strength of Conventional Vulcanized Rubber and Thermoplastic Elastomers*, ASTM International.
- 78 Q. Q. Baltazar, J. Chandawalla, K. Sawyer and J. L. Anderson, *Colloids Surf. Physicochem. Eng. Asp.*, 2007, **302**, 150–156.
- 79 L. Wang and E. Y.-X. Chen, *Green Chem.*, 2015, **17**, 5149–5153.
- 80 Z. Taşçı, A. Kunduracioğlu, İ. Kani and B. Çetinkaya, *ChemCatChem*, 2012, **4**, 831–835.
- 81 2012.
- 82 M. S. Zayas, J. C. Gaitor, S. T. Nestor, S. Minkowicz, Y. Sheng and A. Mirjafari, *Green Chem.*, 2016, **18**, 2443–2452.
- 83 S.-C. Luo, S. Sun, A. R. Deorukhkar, J.-T. Lu, A. Bhattacharyya and I. J. B. Lin, *J. Mater. Chem.*, 2011, **21**, 1866–1873.
- 84 S. K. Tipparaju, S. P. Muench, E. J. Mui, S. N. Ruzheinikov, J. Z. Lu, S. L. Hutson, M. J. Kirisits, S. T. Prigge, C. W. Roberts, F. L. Henriquez, A. P. Kozikowski, D. W. Rice and R. L. McLeod, *J. Med. Chem.*, 2010, **53**, 6287–6300.
- 85 P. Mazurek, S. Vudayagiri and A. L. Skov, *Chem. Soc. Rev.*, 2019, **48**, 1448–1464.
- 86 T. Aziz, M. Waters and R. Jagger, *J. Dent.*, 2003, **31**, 67–74.
- 87 T. Aziz, M. Waters and R. Jagger, *J. Biomed. Mater. Res. B Appl. Biomater.*, 2003, **65B**, 252–261.
- 88 T. Payne, S. Mitchell, R. Bibb and M. Waters, *J. Mech. Behav. Biomed. Mater.*, 2015, **41**, 357–374.
- 89 S. Rezaei and B. Pourabbas, *Polym. Compos.*, 2015, **36**, 1365–1370.
- 90 T. Q. Trung and N.-E. Lee, *Adv. Mater.*, 2016, **28**, 4338–4372.
- 91 J. H. Lai, L. L. Wang, C. C. Ko, R. L. DeLong and J. S. Hodges, *Dent. Mater.*, 2002, **18**, 281–286.
- 92 D. H. Lewis and D. J. Castleberry, *J. Prosthet. Dent.*, 1980, **43**, 426–432.
- 93 S. K. Jindal, M. Sherriff, M. G. Waters and T. J. Coward, *J. Prosthet. Dent.*, 2016, **116**, 617–622.
- 94 S. Tetteh, R. J. Bibb and S. J. Martin, *Materials*, 2018, **11**, 925.
- 95 Y. M. Haider, Z. S. Abdullah, G. H. Jani and N. Mokhtar, *Int. J. Dent.*, 2019, Article ID 2948457, 6 pages, DOI:10.1155/2019/2948457.
- 96 H. A. Abdullah and F. M. Abdul-Ameer, *Saudi Dent. J.*, 2018, **30**, 330–336.
- 97 M. M. Hatamleh and D. C. Watts, *Dent. Mater.*, 2010, **26**, 185–191.

- 98 M. C. Goiato, M. F. Haddad, D. M. dos Santos, A. A. Pesqueira and A. Moreno, *Braz. Oral Res.*, 2010, **24**, 303–308.
- 99 A. M. Guiotti, M. C. Goiato and D. M. dos Santos, *J. Craniofac. Surg.*, 2010, **21**, 323–327.
- 100 D. N. Mancuso, M. C. Goiato, B. C. R. Zuccolotti, A. Moreno and D. M. dos Santos, *Prim. Dent. Care J. Fac. Gen. Dent. Pract. UK*, 2009, **16**, 127–130.
- 101 E. Delebecq and F. Ganachaud, *ACS Appl. Mater. Interfaces*, 2012, **4**, 3340–3352.
- 102 Y. Kitagawa, K. Yoshida, K. Takase, A. Valanezhad, I. Watanabe, K. Kojio and H. Murata, *Odontology*, 2020, **108**, 366–375.
- 103 E. A. Baquero, G. F. Silbestri, P. Gómez-Sal, J. C. Flores and E. de Jesús, *Organometallics*, 2013, **32**, 2814–2826.
- 104 G. C. Fortman and S. P. Nolan, *Chem. Soc. Rev.*, 2011, **40**, 5151–5169.
- 105 K. M. Lee, H. M. J. Wang and I. J. B. Lin, *J. Chem. Soc. Dalton Trans.*, 2002, 2852–2856.
- 106 J. Li, C. Niu, J. Peng, Y. Deng, G. Zhang, Y. Bai, C. Ma, W. Xiao and G. Lai, *Appl. Organomet. Chem.*, 2014, **28**, 454–460.
- 107 T. Galeandro-Diamant, M.-L. Zanota, R. Sayah, L. Veyre, C. Nikitine, C. de Bellefon, S. Marrot, V. Meille and C. Thieuleux, *Chem. Commun.*, 2015, **51**, 16194–16196.
- 108 D. Wang, J. Klein and E. Mejía, *Chem. – Asian J.*, 2017, **12**, 1180–1197.
- 109 T. Rehm, M. Rothemund, A. Bär, T. Dietel, R. Kempe, H. Kostrhunova, V. Brabec, J. Kasparkova and R. Schobert, *Dalton Trans.*, 2018, **47**, 17367–17381.
- 110 A. Annunziata, M. E. Cucciolito, R. Esposito, P. Imbimbo, G. Petruk, G. Ferraro, V. Pinto, A. Tuzi, D. M. Monti, A. Merlino and F. Ruffo, *Dalton Trans.*, 2019, **48**, 7794–7800.
- 111 B. P. Maliszewski, N. V. Tzouras, S. G. Guillet, M. Saab, M. Beliš, K. V. Hecke, F. Nahra and S. P. Nolan, *Dalton Trans.*, 2020, **49**, 14673–14679.
- 112 T. Iimura, N. Akasaka, T. Kosai and T. Iwamoto, *Dalton Trans.*, 2017, **46**, 8868–8874.
- 113 S. Hameury, P. de Fremont, P.-A. R. Breuil, H. Olivier-Bourbigou and P. Braunstein, *Dalton Trans.*, 2014, **43**, 4700–4710.
- 114 R. A. Haque, M. Z. Ghadhayeb, S. Budagumpi, A. W. Salman, M. B. K. Ahamed and A. M. S. A. Majid, *Inorganica Chim. Acta*, 2013, **394**, 519–525.
- 115 F. Quintin, J. Pinaud, F. Lamaty and X. Bantreil, *Organometallics*, 2020, **39**, 636–639.
- 116 U. F. M. Haziz, R. A. Haque, S.-Z. Zhan and M. R. Razali, *J. Organomet. Chem.*, 2020, **910**, 121137.
- 117 A. G. Tennyson, V. M. Lynch and C. W. Bielawski, *J. Am. Chem. Soc.*, 2010, **132**, 9420–9429.
- 118 R. A. Haque, A. W. Salman, S. Budagumpi, A. A.-A. Abdullah and A. M. S. A. Majid, *Metallomics*, 2013, **5**, 760–769.
- 119 J. Lemke, A. Pinto, P. Niehoff, V. Vasylyeva and N. Metzler-Nolte, *Dalton Trans.*, 2009, 7063–7070.
- 120 G. De Bo, G. Berthon-Gelloz, B. Tinant and I. E. Markó, *Organometallics*, 2006, **25**, 1881–1890.
- 121 G. Berthon-Gelloz, O. Buisine, J.-F. Brière, G. Michaud, S. Stérin, G. Mignani, B. Tinant, J.-P. Declercq, D. Chapon and I. E. Markó, *J. Organomet. Chem.*, 2005, **690**, 6156–6168.
- 122 I. E. Markó, S. Stérin, O. Buisine, G. Berthon, G. Michaud, B. Tinant and J.-P. Declercq, *Adv. Synth. Catal.*, 2004, **346**, 1429–1434.
- 123 I. E. Markó, S. Stérin, O. Buisine, G. Mignani, P. Branlard, B. Tinant and J.-P. Declercq, *Science*, 2002, **298**, 204–206.
- 124 T. Iimura, N. Akasaka and T. Iwamoto, *Organometallics*, 2016, **35**, 4071–4076.
- 125 A. M. Ruiz-Varilla, E. A. Baquero, G. F. Silbestri, C. Gonzalez-Arellano, E. de Jesús and J. C. Flores, *Dalton Trans.*, 2015, **44**, 18360–18369.

- 126U. Ajdnik, L. F. Zemljič, M. Bračič, U. Maver, O. Plohl and J. Rebol, *Materials*, 2019, **12**, 847.
- 127S. Kanugala, S. Jinka, N. Puvvada, R. Banerjee and C. G. Kumar, *Sci. Rep.*, 2019, **9**, 6198.
- 128C. Ceresa, F. Tessarolo, D. Maniglio, E. Tambone, I. Carmagnola, E. Fedeli, I. Caola, G. Nollo, V. Chiono, G. Allegrone, M. Rinaldi and L. Fracchia, *Molecules*, 2019, **24**, 3843.
- 129C. Ceresa, L. Fracchia, M. Williams, I. M. Banat and M. A. Díaz De Rienzo, *J. Biotechnol.*, 2020, **309**, 34–43.
- 130Stokroos, Kalicharan, V. D. Want and Jongebloed, *J. Microsc.*, 1998, **189**, 79–89.
- 131K. H. Kim, Z. Akase, T. Suzuki and D. Shindo, *Mater. Trans.*, 2010, **51**, 1080–1083.
- 132H.-J. Ensikat and M. Weigend, *J. Microsc.*, 2014, **256**, 226–230.
- 133Seog-Hyeon Kim, E. A. Cherney, R. Hackam and K. G. Rutherford, *IEEE Trans. Dielectr. Electr. Insul.*, 1994, **1**, 106–123.
- 134Y. Wang, G. Cherry and M. A. Minor, *Soft Robot.*, 2018, **5**, 272–290.
- 135A. Ghosh, R. S. Rajeev, S. K. De, W. Sharp and S. Bandyopadhyaya, *J. Elastomers Plast.*, 2006, **38**, 119–132.
- 136H. Yamaguchi, J. Tatami, T. Yahagi, H. Nakano, M. Iijima, T. Takahashi and T. Kondo, *J. Mater. Sci.*, 2020, **55**, 7359–7372.
- 137Y. Jia, B. Xiang, W. Zhang, T. Liu and S. Luo, *Polym. J.*, 2020, **52**, 207–216.
- 138A. A. Al-Dharrab, S. B. Tayel and M. H. Abodaya, *ISRN Dent.*, 2013, Article ID 582051, 9 pages, DOI:10.1155/2013/582051.
- 139A. H. Delcour, *Biochim. Biophys. Acta*, 2009, **1794**, 808–816.
- 140N. Mesaros, P. Nordmann, P. Plésiat, M. Roussel-Delvallez, J. Van Eldere, Y. Glupczynski, Y. Van Laethem, F. Jacobs, P. Lebecque, A. Malfroot, P. M. Tulkens and F. Van Bambeke, *Clin. Microbiol. Infect.*, 2007, **13**, 560–578.
- 141K. Poole, *Clin. Microbiol. Infect.*, 2004, **10**, 12–26.
- 142H. Mohammadzadeh-Aghdash, N. Akbari, K. Esazadeh and J. Ezzati Nazhad Dolatabadi, *Food Chem.*, 2019, **293**, 491–498.
- 143D. Błędzka, J. Gromadzińska and W. Wąsowicz, *Environ. Int.*, 2014, **67**, 27–42.
- 144N. Beales, *Compr. Rev. Food Sci. Food Saf.*, 2004, **3**, 1–20.

## **Chapter 5: Concluding remarks**

The research presented in Chapters 2, 3, and 4 of this thesis highlights the potential of metallodrugs with NHC and BTSC ligands as antibacterial and anthelmintic agents. The activity of the most effective agents described was potent enough against species that are clinically relevant to human health warrants further investigation of these compounds as potential medicines. The below discussion is presented as a summary of the work presented in this thesis, as well as to act as a critical evaluation of the results and methodology described, and to comment on the future direction of the work.

### **Surface and antimicrobial activity of Ag-NHCs and imidazolium salts**

The antimicrobial efficacy of the Ag-NHCs and imidazolium salts described was found to rely mostly on the length of the N-substituted alkyl chain on the NHC ligand, with longer alkyl chains typically providing an increased antibacterial efficacy to an Ag-NHC or imidazolium salt. This is in agreement with the literature, where the importance of high lipophilicity is reported to be a crucial property in effective antimicrobial Ag-NHCs,<sup>1-8</sup> and is also in agreement with the understanding of the mechanisms behind the antimicrobial efficacy of surfactants.<sup>9-11</sup> The Gram negative bacteria tested (*Escherichia coli* and *Pseudomonas aeruginosa*) were found to be more resistant to the tested compounds than the Gram positive bacteria tested (*Staphylococcus aureus* and *Staphylococcus epidermidis*). More repeats are required for the MIC testing in order to completely confirm the results reported, and further investigation into the antimicrobial effects of the reported compounds could be conducted by broth microdilution in order to establish minimum bactericidal concentrations (MBCs)<sup>12-14</sup> and minimum biofilm eradication concentrations (MBECs).<sup>15-17</sup> Testing of a broader panel of bacterial species would also help to establish whether the compounds are broad spectrum antibacterial agents, particularly against other clinically relevant ESKAPE pathogens.<sup>18-20</sup> The surface activity of the imidazolium salts was determined by conductivity, a suitable and non-perturbing method with which to measure the CMC due to the cationic nature of the surfactants. CMC values recorded for the known 3-alkyl-1-methylimidazolium bromide salts using this method also agree with reported literature values.<sup>21-25</sup> It would be useful to investigate the CMC via other methods such as drop volume tensiometry in order to verify the reported CMC.<sup>26-28</sup> It would also be useful to probe the mechanism of action of the Ag-NHCs using <sup>13</sup>C-C2-enriched NHC ligands, and as with any new metallodrug it is important to establish the cytotoxicity of the Ag-NHCs and their (benz)imidazolium salt precursors with regard to mammalian cells.

### **Bisthiosemicarbazone complexes and their anthelmintic properties**

The synthesised CuBTSC complexes were found to be effective anthelmintic agents against larval schistosomules and adult *Schistosoma mansoni* worms to the same degree as the positive control Auranofin (at 10  $\mu$ M and 20  $\mu$ M concentrations respectively). The reported MGTSA complexes of Ni, Mn and Co, along with the long chain-substituted ZnGTSA complexes were found to be poor anthelmintic agents. The discovery of the excellent activity of the CuBTSC complexes along with ZnGTSM and ZnATSM is a promising step in the development of treatments for schistosomiasis, a neglected tropical disease that often has debilitating consequences for people in the developing world.<sup>29-31</sup> Of particular interest is the fact that the active CuBTSC and ZnBTSC complexes are effective against both larval and adult schistosomes, whereas the current *de facto* treatment used for schistosomiasis, praziquantel, is only effective against mature adult worms, and therefore requires multiple doses in order to treat an inflicted patient.<sup>32-34</sup> The next step in the development of these MBTSCs as potential treatments for schistosomiasis include determining minimum effective concentrations of the complexes against schistosomules and adult worms, as well as determining the cytotoxicity of the complexes towards mammalian cells. Increasing the lipophilicity of the MBTSCs by introducing pendant alkyl chains of  $-C_4H_9$ ,  $-C_6H_{13}$ , and  $-C_8H_{17}$  appeared to decrease the anthelmintic activity of the complexes. Simple increasing lipophilicity at the pendant nitrogen atoms is therefore unlikely to produce effective metallodrugs during further development of novel MBTSCs as antischistosomal agents. MBTSCs do however have the potential to be excellent candidates for the development of new anthelmintic drugs to replace praziquantel.

### **Development of antimicrobial doped silicone rubbers**

A novel silicone rubber formulation, TM1, was prepared and found to have tensile strength, tear resistance, hardness, and a maximum elongation that was comparable with commercially available (M511 Maxillofacial Rubber,<sup>35</sup> A-2186 Platinum RTV Silicone Elastomer,<sup>36</sup> RT Vulcanized VST-30 silicone,<sup>37</sup> and Cosmesil Z004<sup>38</sup>). Doping the silicones with antimicrobial agents at 5 wt% was possible in the case of triclosan, the triclosan esters, and the dodecyl-substituted (benz)imidazolium bromide salts, but was inhibited by Ag-NHCs and CuGTSA. The dopants provided good to excellent antimicrobial properties to the silicone rubber material, and were more effective against the Gram positive bacteria than the Gram negative bacteria. The resistance of these materials to colonisation by other clinically relevant bacteria is important to establish in the further development of these doped rubbers as potential materials for medical

devices.<sup>18–20</sup> The persistence of the antimicrobial effect over time *in situ* is also important to establish<sup>39–41</sup> as well as measuring the rate of release of the antimicrobial dopant from the silicone matrix.<sup>42–44</sup> A new curing system (such as condensation curing)<sup>45–47</sup> or a new Pt catalyst that is more resistant to poisoning by nucleophiles is required in order to develop Ag-NHC- or CuGTSA-doped silicone rubber.

## References

- 1 S. Patil, J. Claffey, A. Deally, M. Hogan, B. Gleeson, L. M. M. Mendez, H. Mueller-Bunz, F. Paradisi and M. Tacke, *Eur. J. Inorg. Chem.*, 2010, 1020–1031.
- 2 S. Patil, K. Dietrich, A. Deally, B. Gleeson, H. Müller-Bunz, F. Paradisi and M. Tacke, *Helv. Chim. Acta*, 2010, **93**, 2347–2364.
- 3 S. Patil, A. Deally, B. Gleeson, H. Müller-Bunz, F. Paradisi and M. Tacke, *Appl. Organomet. Chem.*, 2010, **24**, 781–793.
- 4 S. Patil, A. Deally, B. Gleeson, F. Hackenberg, H. Müller-Bunz, F. Paradisi and M. Tacke, *Z. Für Anorg. Allg. Chem.*, 2011, **637**, 386–396.
- 5 F. Hackenberg, A. Deally, G. Lally, S. Malenke, H. Müller-Bunz, F. Paradisi, S. Patil, D. Quaglia and M. Tacke, *Int. J. Inorg. Chem.*, 2012, Article ID 121450, 13 pages, DOI: 10.1155/2012/121540.
- 6 F. Hackenberg, G. Lally, H. Müller-Bunz, F. Paradisi, D. Quaglia, W. Streciwilk and M. Tacke, *Inorganica Chim. Acta*, 2013, **395**, 135–144.
- 7 W. Streciwilk, J. Cassidy, F. Hackenberg, H. Müller-Bunz, F. Paradisi and M. Tacke, *J. Organomet. Chem.*, 2014, **749**, 88–99.
- 8 C. O’Beirne, N. F. Alhamad, Q. Ma, H. Müller-Bunz, K. Kavanagh, G. Butler, X. Zhu and M. Tacke, *Inorganica Chim. Acta*, 2019, **486**, 294–303.
- 9 H. Heerklotz, *Q. Rev. Biophys.*, 2008, **41**, 205–264.
- 10 N. A. Falk, *J. Surfactants Deterg.*, 2019, **22**, 1119–1127.
- 11 C. Zhou and Y. Wang, *Curr. Opin. Colloid Interface Sci.*, 2020, **45**, 28–43.
- 12 J. Pernak, I. Goc and I. Mirska, *Green Chem.*, 2004, **6**, 323–329.
- 13 R. Wesgate, P. Grasha and J.-Y. Maillard, *Am. J. Infect. Control*, 2016, **44**, 458–464.
- 14 A. R. Schug, A. Bartel, A. D. Scholtzek, M. Meurer, J. Brombach, V. Hensel, S. Fanning, S. Schwarz and A. T. Feßler, *Vet. Microbiol.*, 2020, **248**, 108791.
- 15 D. D. Tassew, A. F. Mechesso, N.-H. Park, J.-B. Song, J.-W. Shur and S.-C. Park, *J. Vet. Med. Sci.*, 2017, **79**, 1716–1720.
- 16 J. Sun and X. Song, *J. Periodontol.*, 2011, **82**, 626–631.
- 17 T. Shimizu and K. Harada, *Microbiol. Immunol.*, 2017, **61**, 17–22.
- 18 H. W. Boucher, G. H. Talbot, J. S. Bradley, J. E. Edwards, D. Gilbert, L. B. Rice, M. Scheld, B. Spellberg and J. Bartlett, *Clin. Infect. Dis.*, 2009, **48**, 1–12.
- 19 V. Tiwari, K. Meena and M. Tiwari, *Infect. Genet. Evol.*, 2018, **66**, 57–65.
- 20 Y. Ma, C. Wang, Y. Li, J. Li, Q. Wan, J. Chen, F. R. Tay and L. Niu, *Adv. Sci.*, 2020, **7**, 1901872
- 21 T. Inoue, H. Ebina, B. Dong and L. Zheng, *J. Colloid Interface Sci.*, 2007, **314**, 236–241.
- 22 Q. Q. Baltazar, J. Chandawalla, K. Sawyer and J. L. Anderson, *Colloids Surf. Physicochem. Eng. Asp.*, 2007, **302**, 150–156.
- 23 M. Ao and D. Kim, *J. Chem. Eng. Data*, 2013, **58**, 1529–1534.
- 24 A. Cornellias, L. Perez, F. Comelles, I. Ribosa, A. Manresa and M. T. Garcia, *J. Colloid Interface Sci.*, 2011, **355**, 164–171.
- 25 F. Geng, J. Liu, L. Zheng, L. Yu, Z. Li, G. Li and C. Tung, *J. Chem. Eng. Data*, 2010, **55**, 147–151.
- 26 M. Anouti, J. Jones, A. Boisset, J. Jacquemin, M. Caillon-Caravanier and D. Lemordant, *J. Colloid Interface Sci.*, 2009, **340**, 104–111.
- 27 S. Horiuchi and G. Winter, *Eur. J. Pharm. Biopharm.*, 2015, **92**, 8–14.
- 28 M. T. Garcia, I. Ribosa, L. Perez, A. Manresa and F. Comelles, *Langmuir*, 2013, **29**, 2536–2545.
- 29 D. G. Colley, A. L. Bustinduy, W. E. Secor and C. H. King, *Lancet Lond. Engl.*, 2014, **383**, 2253–2264.
- 30 D. P. McManus, D. W. Dunne, M. Sacko, J. Utzinger, B. J. Vennervald and X.-N. Zhou, *Nat. Rev. Dis. Primer*, 2018, **4**, 1–19.

- 31 J. Cao, W.-J. Liu, X.-Y. Xu and X.-P. Zou, *World J. Gastroenterol.*, 2010, **16**, 723–727.
- 32 G. A. Dziwornu, H. D. Attram, S. Gachuhi and K. Chibale, *RSC Med. Chem.*, 2020, **11**, 455–490.
- 33 D. J. Gray, A. G. Ross, Y.-S. Li and D. P. McManus, *BMJ*, 2011, 342:d2651 DOI:10.1136/bmj.d2651.
- 34 P. Andrews, H. Thomas, R. Pohlke and Jür. Seubert, *Med. Res. Rev.*, 1983, **3**, 147–200.
- 35 S. Tetteh, R. J. Bibb and S. J. Martin, *Materials*, 2018, **11**, 925.
- 36 Y. M. Haider, Z. S. Abdullah, G. H. Jani and N. Mokhtar, *Int. J. Dent.*, 2019, Article ID 2948457, 6 pages, DOI:10.1155/2019/2948457.
- 37 H. A. Abdullah and F. M. Abdul-Ameer, *Saudi Dent. J.*, 2018, **30**, 330–336.
- 38 M. M. Hatamleh and D. C. Watts, *Dent. Mater.*, 2010, **26**, 185–191.
- 39 D. Stickler, G. Jones and A. Russell, *The Lancet*, 2003, **361**, 1435–1437.
- 40 T. A. Gaonkar, L. A. Sampath and S. M. Modak, *Infect. Control Hosp. Epidemiol.*, 2003, **24**, 506–513.
- 41 T. A. Gaonkar, L. Caraos and S. Modak, *Infect. Control Hosp. Epidemiol.*, 2007, **28**, 596–598.
- 42 J. Kamalipour, M. Masoomi, H. A. Khonakdar and S. M. R. Razavi, *Colloids Surf. B Biointerfaces*, 2016, **145**, 891–898.
- 43 S. Kockisch, G. D. Rees, J. Tsibouklis and J. D. Smart, *Eur. J. Pharm. Biopharm.*, 2005, **59**, 207–216.
- 44 D. Steinberg, T. Tal and M. Friedman, *J. Biomed. Mater. Res. B Appl. Biomater.*, 2006, **77B**, 282–286.
- 45 J. Cervantes, R. Zárraga and C. Salazar-Hernández, *Appl. Organomet. Chem.*, 2012, **26**, 157–163.
- 46 M. Navarro, A. Michiardi, O. Castaño and J. A. Planell, *J. R. Soc. Interface*, 2008, **5**, 1137–1158.
- 47 D. Wang, J. Klein and E. Mejía, *Chem. – Asian J.*, 2017, **12**, 1180–1197.

## Appendices

### Molar concentrations of antimicrobial agents (Chapter 2)

NHC/ Salt	Concentration ( $\mu\text{g/mL}$ )							
	100	50	25	12.5	6.25	3.125	1.5625	0.78125
	Molar concentration (mM)							
1	0.307	0.154	0.0769	0.0384	0.0192	0.00961	0.00480	0.00240
2	0.262	0.131	0.0656	0.0328	0.0164	0.00819	0.00410	0.00205
3	0.229	0.114	0.0571	0.0286	0.0143	0.00714	0.00357	0.00179
4	0.283	0.142	0.0708	0.0354	0.0177	0.00884	0.00442	0.00221
5	0.244	0.122	0.0611	0.0305	0.0153	0.00763	0.00382	0.00191
6	0.215	0.108	0.0538	0.0269	0.0135	0.00673	0.00336	0.00168
7	0.363	0.182	0.0908	0.0454	0.0227	0.0114	0.00568	0.00284
8	0.302	0.151	0.0755	0.0377	0.0189	0.00943	0.00472	0.00236
9	0.258	0.129	0.0645	0.0323	0.0161	0.00807	0.00403	0.00202
10	0.330	0.165	0.0824	0.0412	0.0206	0.0103	0.00515	0.00258
11	0.278	0.139	0.0696	0.0348	0.0174	0.0087	0.00435	0.00217
12	0.241	0.120	0.0601	0.0301	0.0150	0.00752	0.00376	0.00188
1Ag	0.231	0.116	0.0579	0.0289	0.0145	0.00723	0.00362	0.00181
2Ag	0.205	0.102	0.0512	0.0256	0.0128	0.00640	0.00320	0.00160
3Ag	0.183	0.0919	0.0459	0.0230	0.0115	0.00574	0.00287	0.00144
4Ag	0.217	0.109	0.0543	0.0271	0.0136	0.00679	0.00340	0.00170
5Ag	0.194	0.0968	0.0484	0.0242	0.0121	0.00605	0.00303	0.00151
6Ag	0.175	0.0875	0.0438	0.0219	0.0109	0.00547	0.00273	0.00137
7Ag	0.262	0.1309	0.0654	0.0327	0.0164	0.00818	0.00409	0.00204
8Ag	0.228	0.114	0.0571	0.0285	0.0143	0.00713	0.00357	0.00178
9Ag	0.202	0.101	0.0506	0.0252	0.0126	0.00632	0.00316	0.00158
10Ag	0.244	0.122	0.0610	0.0305	0.0152	0.00762	0.00381	0.00190
11Ag	0.214	0.107	0.0536	0.0268	0.0134	0.00670	0.00335	0.00168
12Ag	0.191	0.0957	0.0479	0.0239	0.0120	0.00598	0.00299	0.00150

**Table 1.** MIC values of Ag-NHCs expressed in mM concentrations (to 3 significant figures) relative to the  $\mu\text{g/mL}$  concentrations reported in Chapter 2.

**MIC testing of Ag-NHCs and (benz)imidazolium salts against bacteria (Chapter 2)**

NHC/ Salt	MIC Value ( $\mu\text{g/mL}$ )					
	<i>S. aureus</i> NCIMB 9518 (+)	<i>S. aureus</i> NCTC 6571 (+)	<i>S.</i> <i>epidermidis</i> RP62A (+)	<i>S.</i> <i>epidermidis</i> ATCC 14990 (+)	<i>E. coli</i> NCTC 12923 (-)	<i>P.</i> <i>aeruginosa</i> ATCC 15692 (-)
1	50	25	25	12.5	R	R
2	3.125	3.125	1.5625	1.5625	25	R
3	1.5625	1.5625	0.78125	0.78125	50	R
4	50	50	25	25	R	R
5	3.125	3.125	1.5625	1.5625	25	R
6	1.5625	1.5625	0.78125	0.78125	50	R
7	R	R	R	100	R	R
8	3.125	3.125	1.5625	1.5625	25	R
9	0.78125	0.78125	0.78125	0.78125	25	100
10	100	100	100	50	R	R
11	1.5625	1.5625	0.78125	0.78125	50	R
12	0.78125	0.78125	0.78125	0.78125	50	R
1Ag	25	25	3.125	3.125	12.5	6.25
2Ag	1.5625	1.5625	0.78125	0.78125	6.25	6.25
3Ag	1.5625	1.5625	0.78125	0.78125	12.5	6.25
4Ag	25	25	50	25	25	25
5Ag	1.5625	1.5625	0.78125	0.78125	12.5	25
6Ag	1.5625	1.5625	0.78125	0.78125	25	25
7Ag	25	25	25	25	50	25
8Ag	3.125	3.125	1.5625	0.78125	25	25
9Ag	0.78125	0.78125	0.78125	0.78125	25	50
10Ag	50	100	100	50	100	100
11Ag	1.5625	1.5625	0.78125	0.78125	12.5	25
12Ag	0.78125	1.5625	0.78125	0.78125	6.25	12.5

**Table 2.** MIC values of Ag-NHCs and (benz)imidazolium salts against Gram positive (+) and Gram negative bacteria (-) summarised.

NHC/ Salt	MIC Value ( $\mu\text{g/mL}$ )					
	<i>S. aureus</i> NCIMB 9518 (+)	<i>S. aureus</i> NCTC 6571 (+)	<i>S.</i> <i>epidermidis</i> RP62A (+)	<i>S.</i> <i>epidermidis</i> ATCC 14990 (+)	<i>E. coli</i> NCTC 12923 (-)	<i>P.</i> <i>aeruginosa</i> ATCC 15692 (-)
1	0.154	0.076854	0.076854	0.038427	R	R
2	0.00819	0.00819	0.00410	0.00410	0.0655	R
3	0.00357	0.00357	0.00179	0.00179	0.114	R
4	0.142	0.142	0.0708	0.0708	R	R
5	0.00763	0.00763	0.00382	0.00382	0.0611	R
6	0.00336	0.00336	0.00168	0.00168	0.108	R
7	R	R	R	0.363	R	R
8	0.00943	0.00943	0.00472	0.00472	0.0755	R
9	0.00202	0.00202	0.00202	0.00202	0.0645	0.258
10	0.330	0.330	0.330	0.165	R	R
11	0.00435	0.00435	0.00217	0.00217	0.139	R
12	0.00188	0.00188	0.00188	0.00188	0.120	R
1Ag	0.0769	0.0769	0.00961	0.00961	0.0384	0.0192
2Ag	0.00410	0.00410	0.00205	0.00205	0.0164	0.0164
3Ag	0.00357	0.00357	0.00179	0.00179	0.0286	0.0143
4Ag	0.0708	0.0708	0.142	0.0708	0.0708	0.0708
5Ag	0.00382	0.00382	0.00191	0.00191	0.0305	0.0611
6Ag	0.00336	0.00336	0.00168	0.00168	0.0538	0.0538
7Ag	0.0908	0.0908	0.0908	0.0908	0.182	0.0908
8Ag	0.00943	0.00943	0.00472	0.00236	0.0755	0.0755
9Ag	0.00202	0.00202	0.00202	0.00202	0.0645	0.129
10Ag	0.165	0.330	0.330	0.165	0.330	0.330
11Ag	0.00435	0.00435	0.00217	0.00217	0.0348	0.0696
12Ag	0.00188	0.00376	0.00188	0.00188	0.0150	0.0301

**Table 3.** Milimolarities determined for the MIC values of Ag-NHCs and (benz)imidazolium salts against Gram positive (+) and Gram negative bacteria (-) summarised.

### Square root of scan rates versus cathodic peak current (Chapter 3)

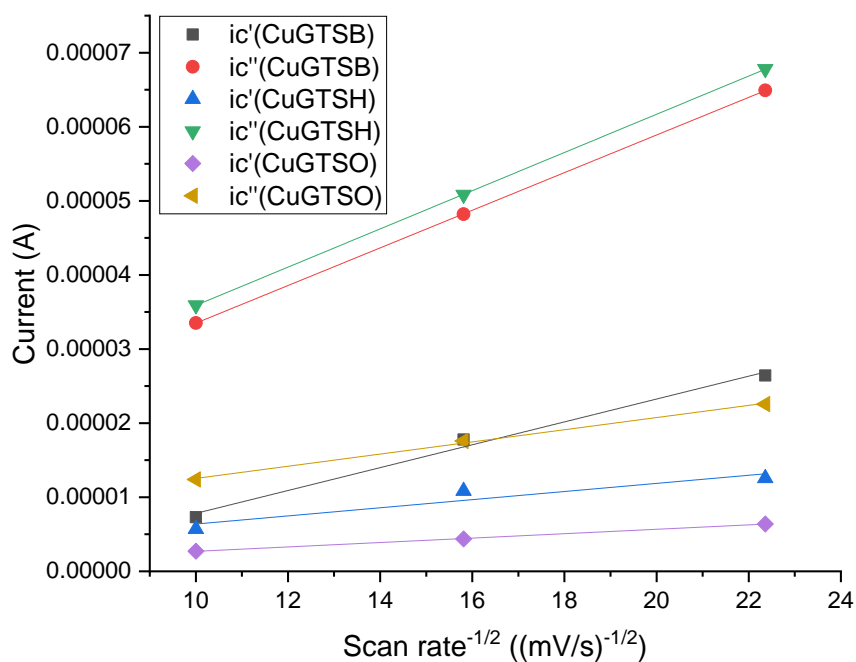


**Figure 1.** Plot of scan rate versus cathodic peak currents for CuGTSA complexes. A truly linear relationship means the redox processes are reversible, whereas deviations from linearity confirm quasi-reversibility.

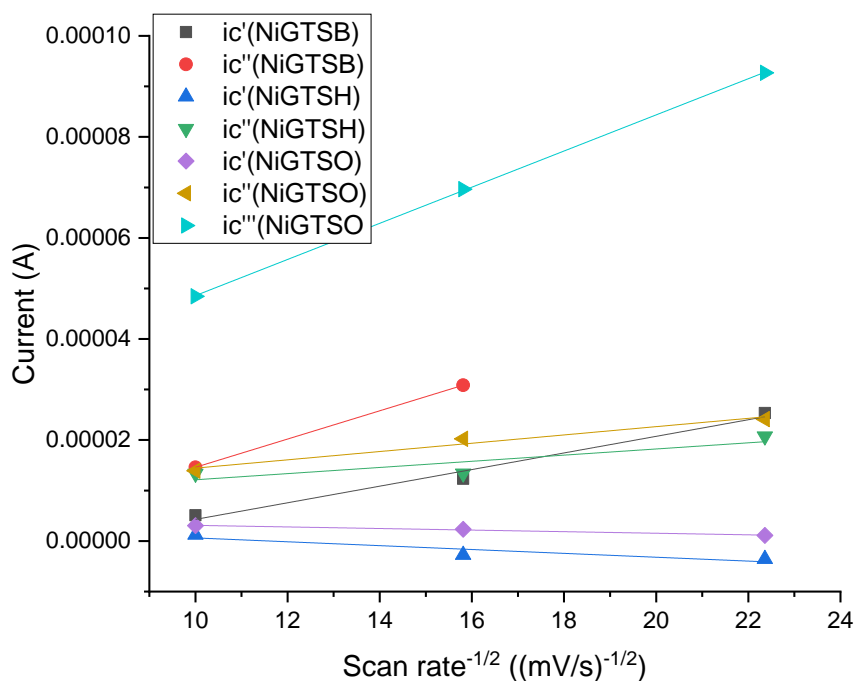


**Figure 2.** Plot of scan rate versus cathodic peak currents for NiGTSA complexes. A truly linear relationship means the redox processes are reversible, whereas deviations from linearity confirm quasi-reversibility.

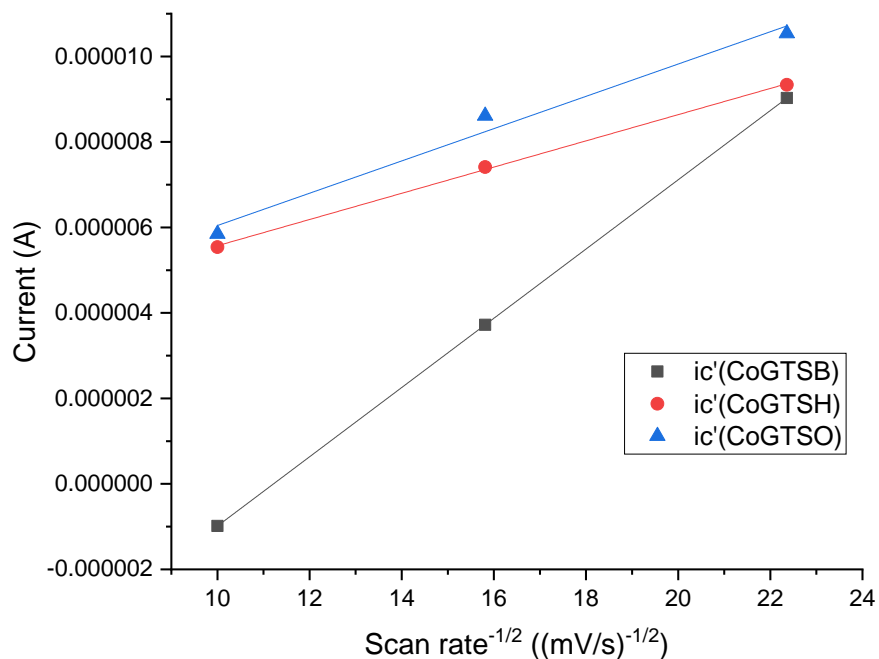


**Figure 3.** Plot of scan rate versus cathodic peak currents for CoGTSA complexes. A truly linear relationship means the redox processes are reversible, whereas deviations from linearity confirm quasi-reversibility.

#### SEM/EDX of TM1 silicone rubbers (Chapter 4)

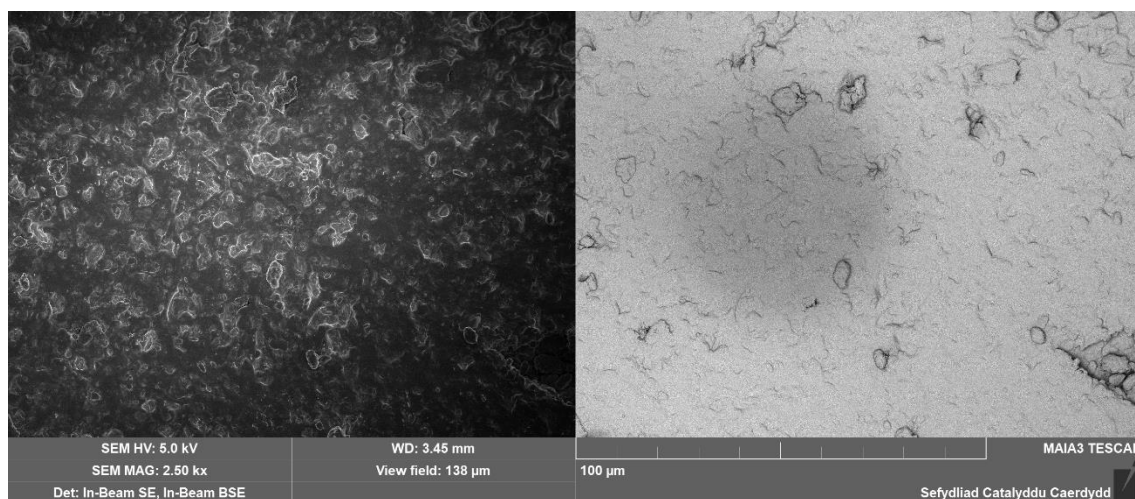


**Figure 4.** SEM images of TM1 silicone rubber. The images are recorded at 2 kx magnification. The left hand side image is captured with secondary electron detection, whereas the right hand side is captured with back-scattered electron detection.

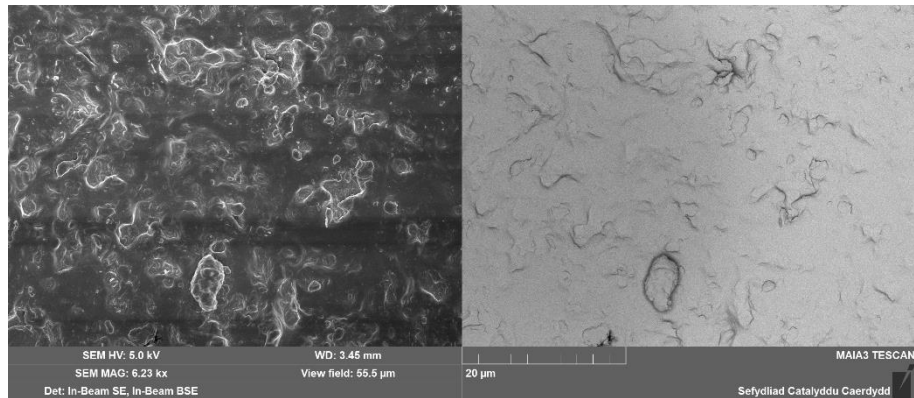


**Figure 5.** SEM images of TM1 silicone rubber. The images are recorded at 5 kx magnification. The left hand side image is captured with secondary electron detection, whereas the right hand side is captured with back-scattered electron detection.

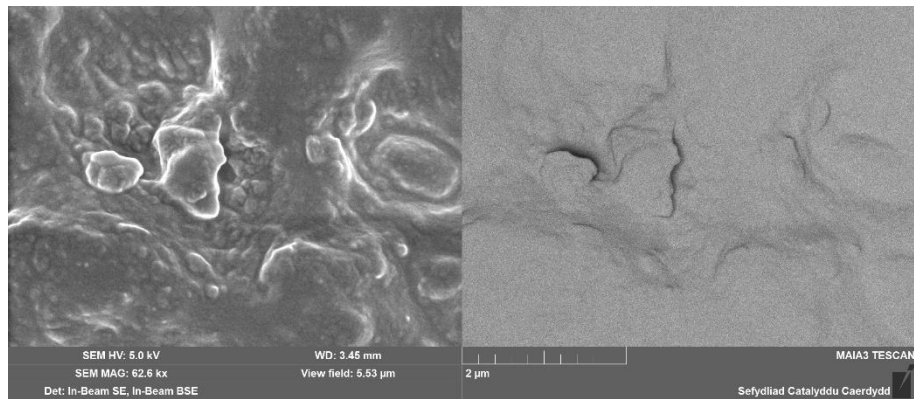


**Figure 6.** SEM images of TM1 silicone rubber. The images are recorded at 50 kx magnification. The left hand side image is captured with secondary electron detection, whereas the right hand side is captured with back-scattered electron detection.

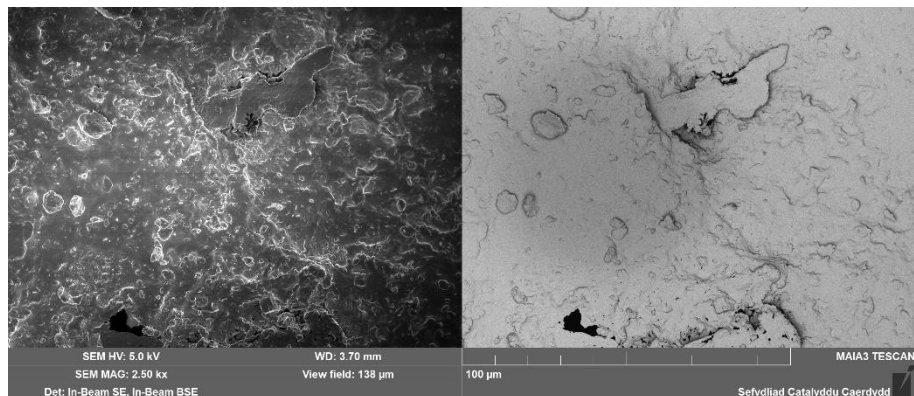


**Figure 7.** SEM images of 5 wt% triclosan laurate doped TM1 silicone rubber. The images are recorded at 2 kx magnification. The left hand side images is captured with secondary electron detection, whereas the right hand side is captured with back-scattered electron detection.

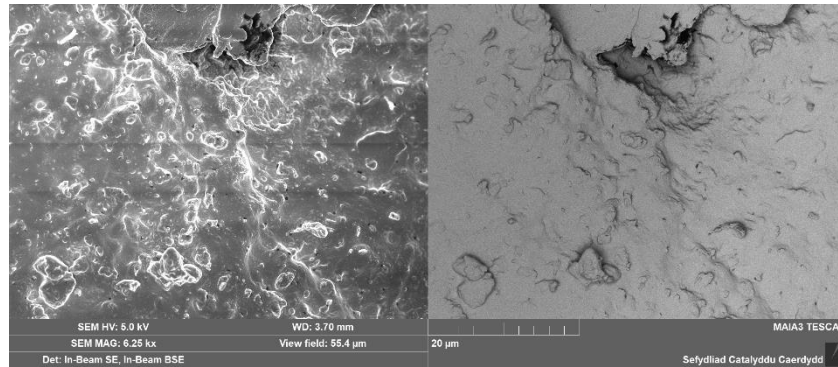


**Figure 8.** SEM images of 5 wt% triclosan laurate doped TM1 silicone rubber. The images are recorded at 5 kx magnification. The left hand side images is captured with secondary electron detection, whereas the right hand side is captured with back-scattered electron detection.

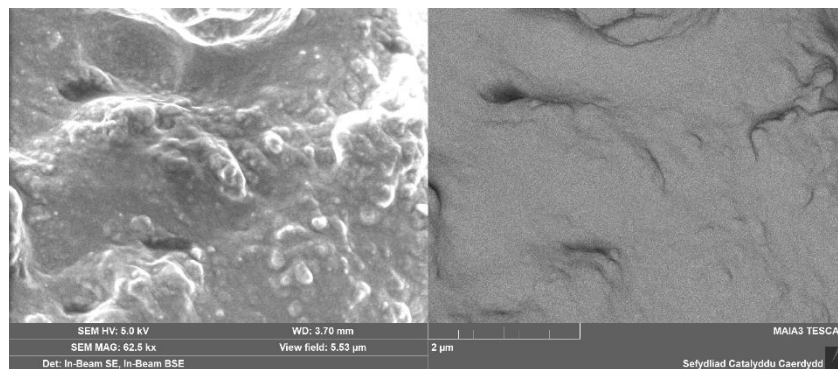


**Figure 9.** SEM images of 5 wt% triclosan laurate doped TM1 silicone rubber. The images are recorded at 50 kx magnification. The left hand side image is captured with secondary electron detection, whereas the right hand side is captured with back-scattered electron detection.

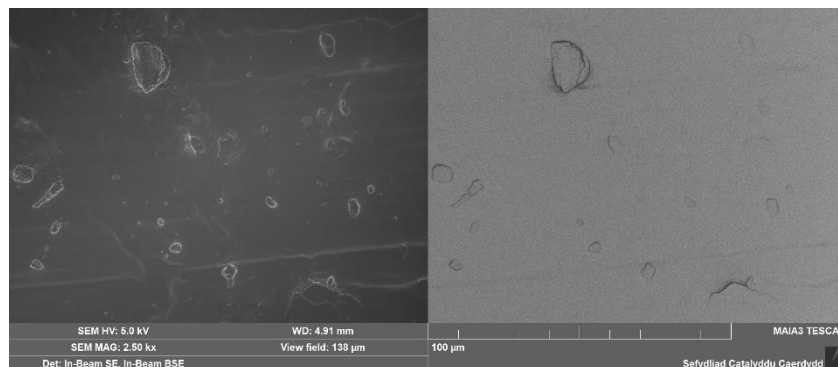


**Figure 10.** SEM images of 5 wt% triclosan undecenoate doped TM1 silicone rubber. The images are recorded at 2 kx magnification. The left hand side images is captured with secondary electron detection, whereas the right hand side is captured with back-scattered electron detection.

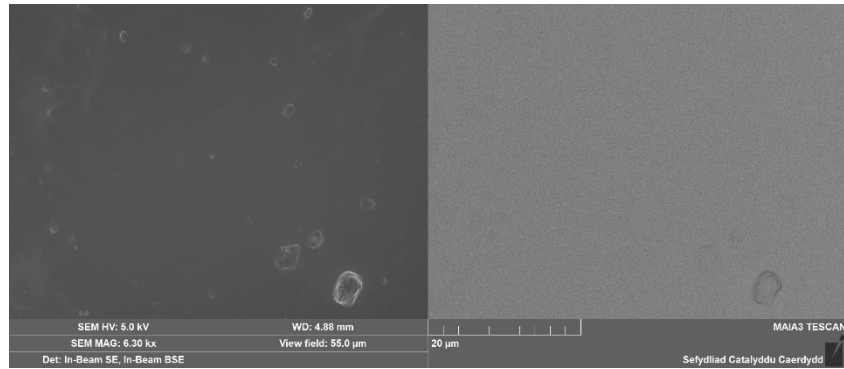


**Figure 11.** SEM images of 5 wt% triclosan undecenoate doped TM1 silicone rubber. The images are recorded at 5 kx magnification. The left hand side images is captured with secondary electron detection, whereas the right hand side is captured with back-scattered electron detection.

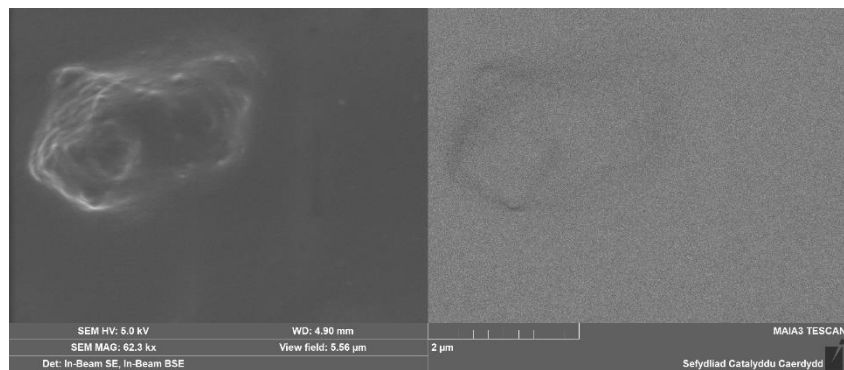


**Figure 12.** SEM images of 5 wt% triclosan undecenoate doped TM1 silicone rubber. The images are recorded at 50 kx magnification. The left hand side images is captured with secondary electron detection, whereas the right hand side is captured with back-scattered electron detection.

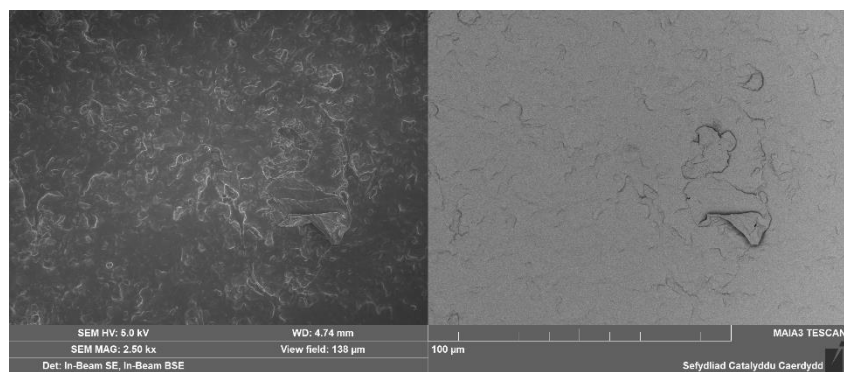


**Figure 13.** SEM images of 5 wt% triclosan benzoate doped TM1 silicone rubber. The images are recorded at 2 kx magnification. The left hand side images is captured with secondary electron detection, whereas the right hand side is captured with back-scattered electron detection.

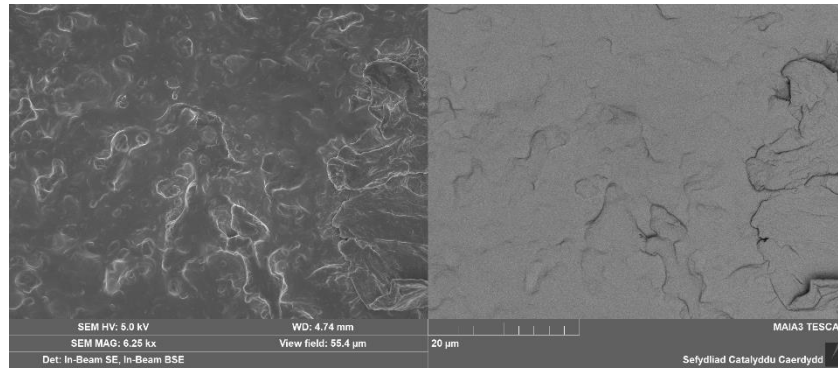


**Figure 14.** SEM images of 5 wt% triclosan benzoate doped TM1 silicone rubber. The images are recorded at 5 kx magnification. The left hand side images is captured with secondary electron detection, whereas the right hand side is captured with back-scattered electron detection.

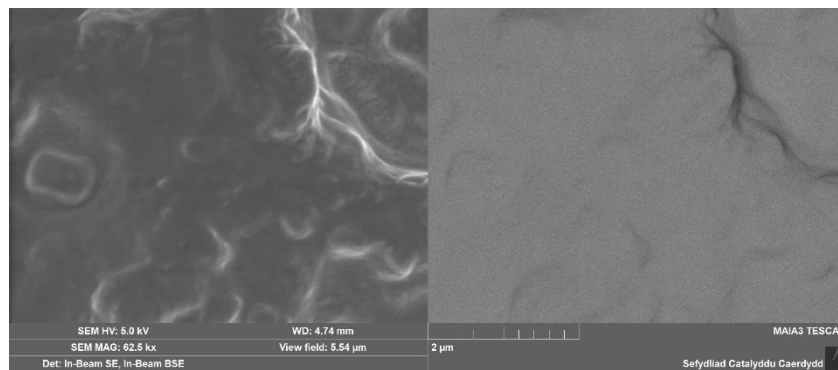


**Figure 15.** SEM images of 5 wt% triclosan benzoate doped TM1 silicone rubber. The images are recorded at 50 kx magnification. The left hand side images is captured with secondary electron detection, whereas the right hand side is captured with back-scattered electron detection.

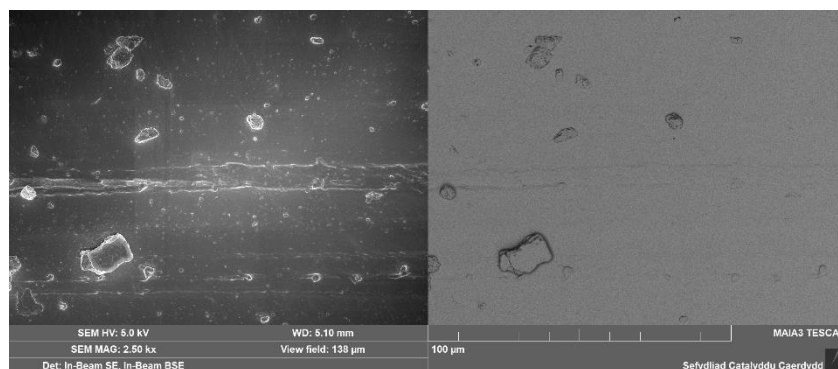


**Figure 16.** SEM images of 5 wt% triclosan acetate doped TM1 silicone rubber. The images are recorded at 2 kx magnification. The left hand side images is captured with secondary electron detection, whereas the right hand side is captured with back-scattered electron detection.

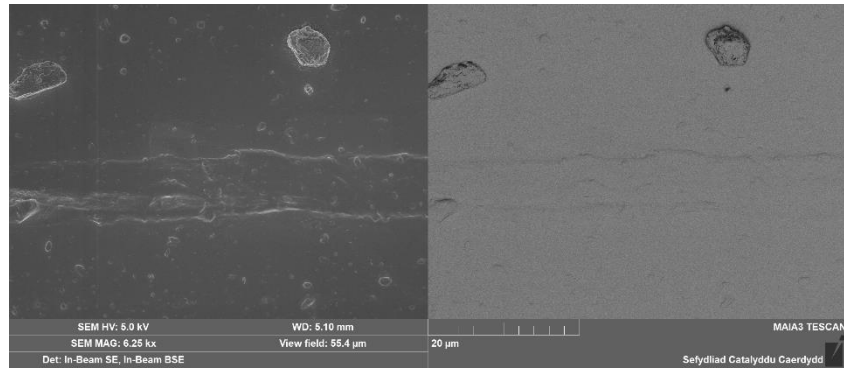


**Figure 17.** SEM images of 5 wt% triclosan acetate doped TM1 silicone rubber. The images are recorded at 5 kx magnification. The left hand side images is captured with secondary electron detection, whereas the right hand side is captured with back-scattered electron detection.

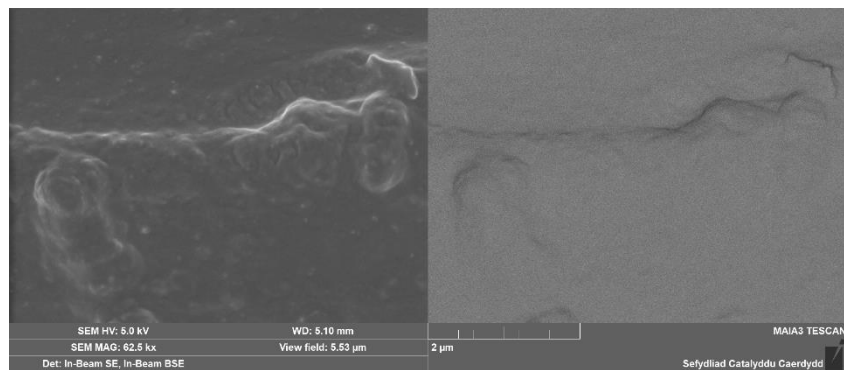


**Figure 18.** SEM images of 5 wt% triclosan acetate doped TM1 silicone rubber. The images are recorded at 50 kx magnification. The left hand side images is captured with secondary electron detection, whereas the right hand side is captured with back-scattered electron detection.

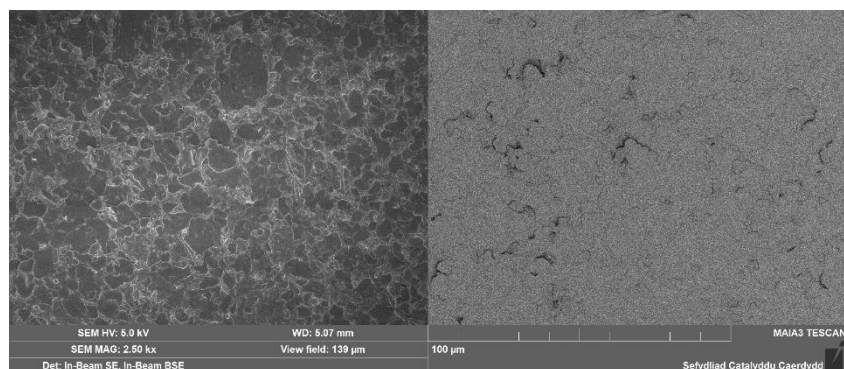


**Figure 19.** SEM images of 5 wt% triclosan doped TM1 silicone rubber. The images are recorded at 2 kx magnification. The left hand side images is captured with secondary electron detection, whereas the right hand side is captured with back-scattered electron detection.

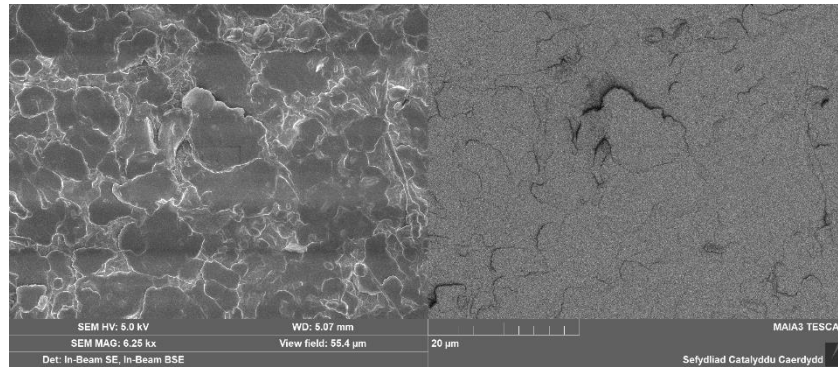


**Figure 20.** SEM images of 5 wt% triclosan doped TM1 silicone rubber. The images are recorded at 5 kx magnification. The left hand side images is captured with secondary electron detection, whereas the right hand side is captured with back-scattered electron detection.

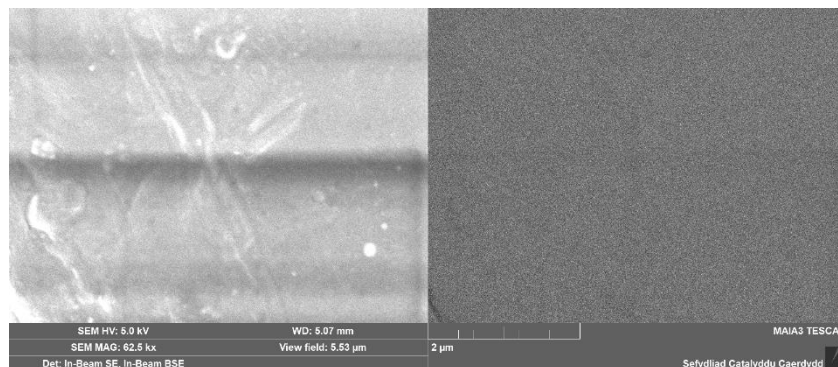


**Figure 21.** SEM images of 5 wt% triclosan doped TM1 silicone rubber. The images are recorded at 50 kx magnification. The left hand side images is captured with secondary electron detection, whereas the right hand side is captured with back-scattered electron detection.

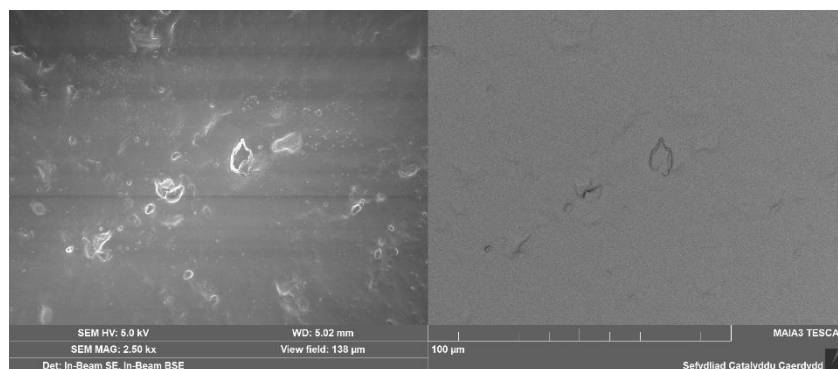


**Figure 22.** SEM images of 5 wt% 3-dodecyl-1-methylimidazolium bromide doped TM1 silicone rubber. The images are recorded at 2 kx magnification. The left hand side images is captured with secondary electron detection, whereas the right hand side is captured with back-scattered electron detection.

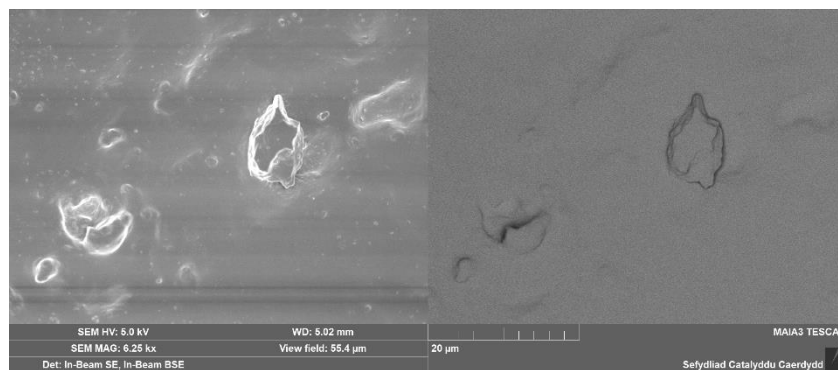


**Figure 23.** SEM images of 5 wt% 3-dodecyl-1-methylimidazolium bromide doped TM1 silicone rubber. The images are recorded at 5 kx magnification. The left hand side images is captured with secondary electron detection, whereas the right hand side is captured with back-scattered electron detection.

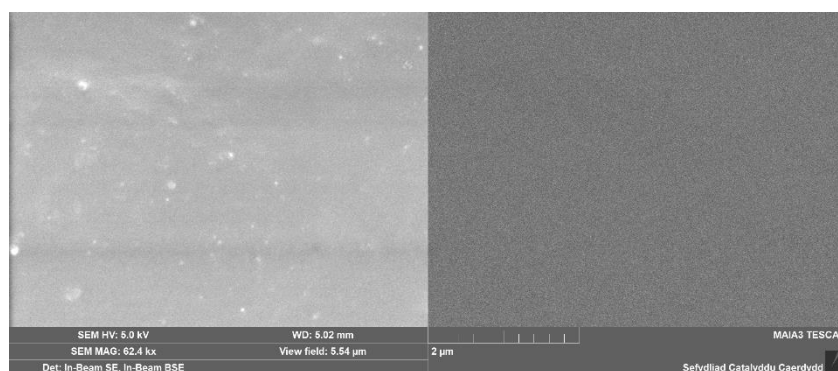


**Figure 24.** SEM images of 5 wt% 3-dodecyl-1-methylimidazolium bromide doped TM1 silicone rubber. The images are recorded at 50 kx magnification. The left hand side images is captured with secondary electron detection, whereas the right hand side is captured with back-scattered electron detection.

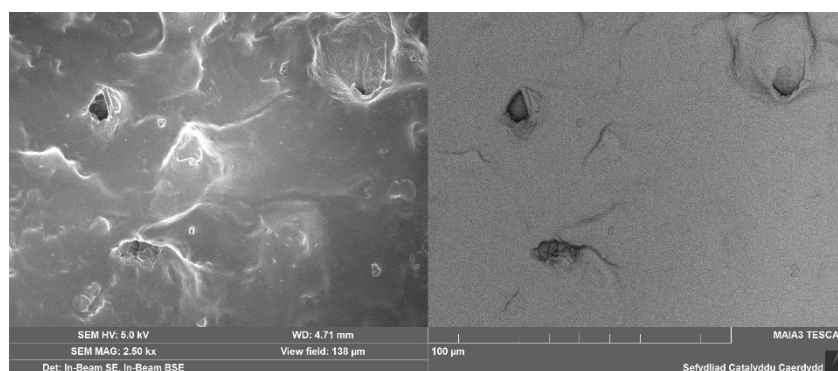


**Figure 25.** SEM images of 5 wt% 3-dodecyl-1-methylbenzimidazolium bromide doped TM1 silicone rubber. The images are recorded at 2 kx magnification. The left hand side images is captured with secondary electron detection, whereas the right hand side is captured with back-scattered electron detection.

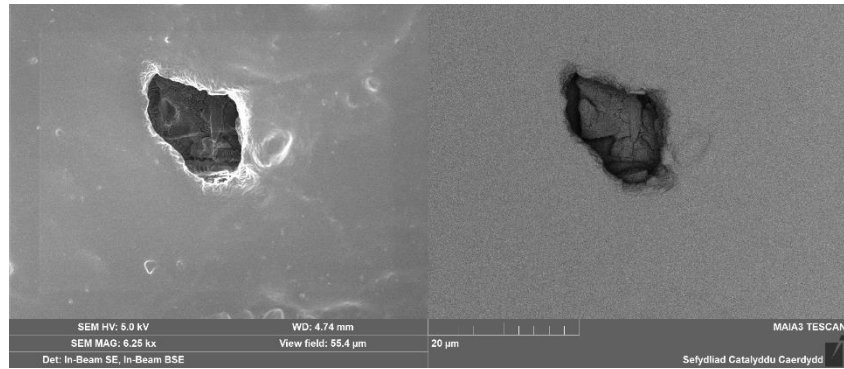


**Figure 26.** SEM images of 5 wt% 3-dodecyl-1-methylbenzimidazolium bromide doped TM1 silicone rubber. The images are recorded at 5 kx magnification. The left hand side images is captured with secondary electron detection, whereas the right hand side is captured with back-scattered electron detection.

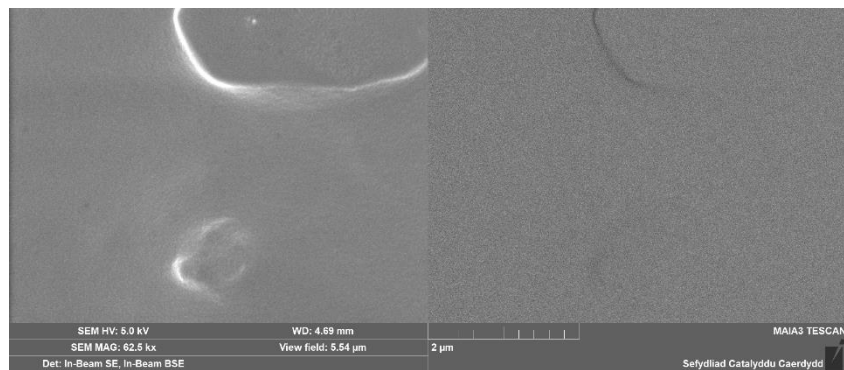


**Figure 27.** SEM images of 5 wt% 3-dodecyl-1-methylbenzimidazolium bromide doped TM1 silicone rubber. The images are recorded at 50 kx magnification. The left hand side images is captured with secondary electron detection, whereas the right hand side is captured with back-scattered electron detection.



**Figure 28.** EDS layered image showing elemental distribution recorded from EDX analysis of TM1.

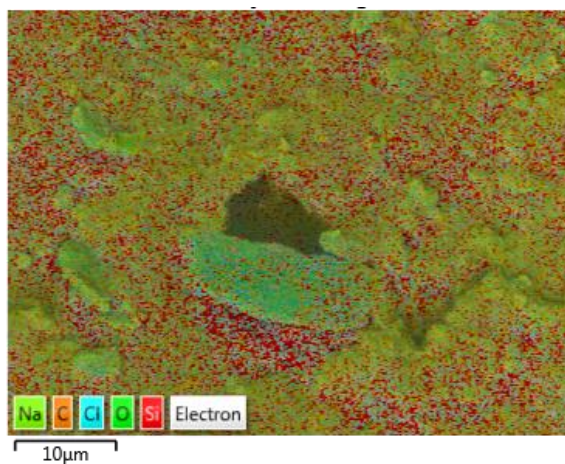


**Figure 29.** EDS layered image showing elemental distribution recorded from EDX analysis of 5 wt% triclosan laurate doped TM1.

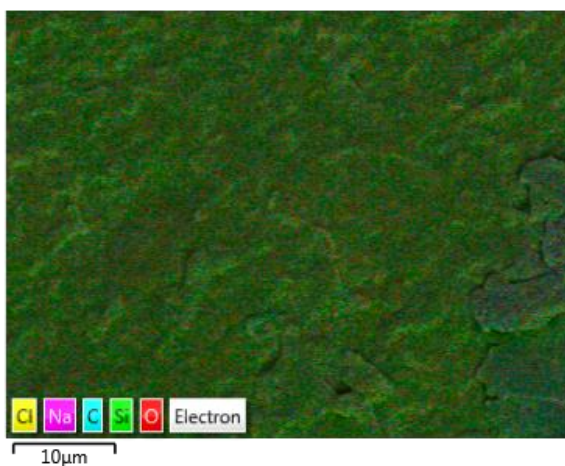


**Figure 30.** EDS layered image showing elemental distribution recorded from EDX analysis of 5 wt% triclosan benzoate doped TM1.

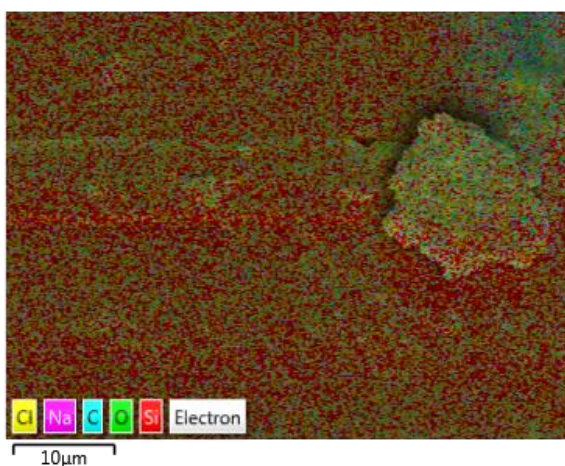


**Figure 31.** EDS layered image showing elemental distribution recorded from EDX analysis of 5 wt% triclosan acetate doped TM1.

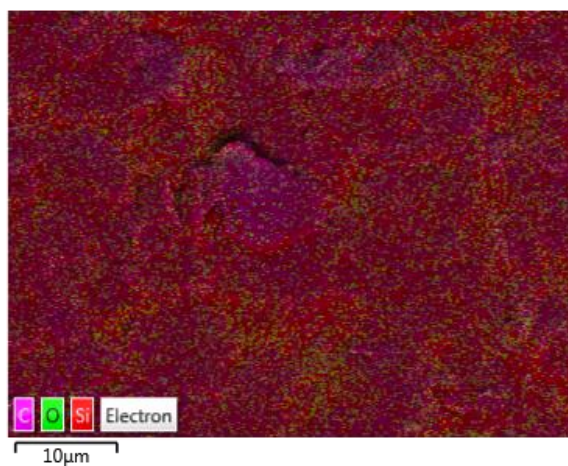


**Figure 32.** EDS layered image showing elemental distribution recorded from EDX analysis of 5 wt% triclosan doped TM1.

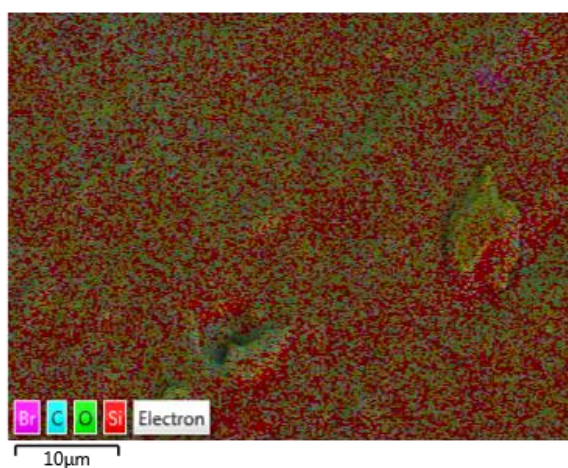


**Figure 33.** EDS layered image showing elemental distribution recorded from EDX analysis of 5 wt% 3-dodecyl-1-methylimidazolium bromide doped TM1.

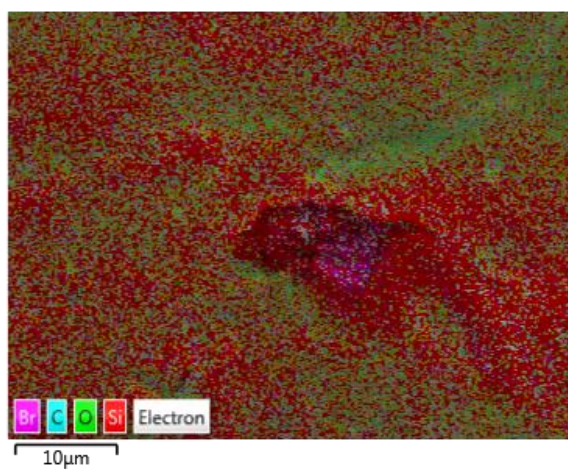


**Figure 34.** EDS layered image showing elemental distribution recorded from EDX analysis of 5 wt% 3-dodecyl-1-methylbenzimidazolium bromide doped TM1.